Surface Modified Minerals for Radionuclide Sequestration

By

Hayley Sarah Gillings

A doctoral thesis submitted in partial fulfilment of the requirements for the award of

Doctor of Philosophy

Loughborough University

Abstract

This thesis is concerned with experiments designed to identify materials to increase the utility of the Sellafield Ion Exchange Plant (SIXEP) process. Clinoptilolite, ZSM-5, vermiculite and kaolinite have been surface modified by grafting with APTES, TMSPE and TMSPETT ligands using varying grafting times (1-24 h), ligand concentrations (1-3 mmol) and solvents with different polarities (with dielectric constant between 1.9 – 80). Materials before and after grafting were analysed using long and short range techniques including elemental analysis (CHN), powder X-ray diffraction (PXRD), scanning electron microscopy (SEM), solid state nuclear magnetic resonance (SSNMR) and infra-red (FTIR) spectroscopy. The amount of graft placed on the surface increased with reaction time for all materials as the amount of carbon per unit mass of the support, determined by CHN analysis, increased with time. C-H stretches were consistently observed in the FTIR of the grafted materials but no change was observed to the long range order in the PXRD pattern. ^{13}C SSNMR showed that small solvent molecules such as acetone can become trapped in the material supports during grafting and long drying times are required to ensure that trapped solvent molecules do not contaminate the CHN analyses of the materials after grafting. Clinoptilolite and vermiculite consistently achieved higher grafting levels than ZSM-5 or kaolinite, with clinoptilolite (NDA) showing the greatest carbon content of 56.16 mmol of APTES per gram of clinoptilolite using hexane as the solvent. Despite a similar molecular weight, TMSPE consistently showed lower levels of grafting than APTES. APTES grafting levels were increased by using citric, phosphoric and nitric acid (1-3 mol L^{-1}) to pre-treat the surface of the materials over different time periods (1-24 h) to improve the level of APTES graft. While the carbon content was higher for acid treated clinoptilolite (NDA) after grafting, in the case of the citric acid treatment, this increase maybe due to the formation of iron (III) citrate from the dissolution of poorly crystalline iron impurities in the clinoptilolite (NDA).

Ungrafted and grafted clinoptilolite, ZSM-5, vermiculite and kaolinite samples were investigated for their ability to sequester caesium, strontium, uranium and plutonium species. Absorption/desorption experiments were initially conducted on the ungrafted compounds using caesium and strontium cations to establish a baseline for the most abundant species in pond liquor. Caesium and strontium cations are trapped within the cages of clinoptilolite in an ion exchange reaction which places these ions on sites of the appropriate size and geometry for these species. Once ion exchanged, neither ion is desorbed from the clinoptilolite readily and they remain trapped inside the cage, irrespective of concentration of other species in solution. While vermiculite is also successful at removing both

caesium and strontium cations, it is less successful in retaining them during desorption, with typically one third of the trapped ions being released back into solution. ZSM-5 and kaolinite have contrasting behaviour, due to few exchangeable cations, meaning caesium and strontium uptake is poor. Samples of clinoptilolite with different particle sizes and potassium content were compared and showed that smaller particles facilitated faster exchange. Grafting had a variable effect on the caesium/strontium cation uptake and release during absorption/desorption presumably as a result of the donors on grafted ligand interacting weakly with the large cations. Experiments using distilled water and synthetic liquor (carbonated sodium hydroxide), demonstrated uranium and plutonium species were extracted by all materials after grafting at concentrations in the SIXEP range. The most successful ligand/graft combination for plutonium at pH 7 was APTES grafted on clinoptilolite (10.79% carbon).

Acknowledgements

There are so many people I would like to thank that without their help, influence and support then neither this thesis or I would be where it is today. As always words are rarely enough but I hope that everyone involved understands the deep appreciation I have for them.

To Dr Sandie Dann whom without her help and unwavering support this thesis and work would never have been possible. Your help and support over the years has been invaluable, thank you for giving me this opportunity and believing in me even when I did not. Next I would like to thank Prof. Peter Warwick. Thank you for your help and advice. I am unable to express how grateful I am to have had your input in this work and I only wish that you had been on this journey from the start, it would have been a much richer one.

I have been lucky enough to have worked with some amazing people throughout my time at Loughborough. A special mention however must go to the long suffering Mrs Pauline King who is one in a million, without whom the PXRD and CHN in this thesis would quite honestly not exist. I am truly sorry for the hundreds of CHN samples and cannot express my gratitude for the many times you fixed the diffractometer when we had fallen out. I thank you from the bottom of my heart for all the help you have given, it has always been appreciated. To Dr Les Mustoe for accepting me to Loughborough on SEFS and for all your help and support since, you are a true gentleman. For all the help with the NMR analysis, for a boundless supply of information and all the chats I would like to thank Dr Mark Edgar. To Mr Stuart Pinkney, your help with all that is technical has never gone unnoticed and it always a pleasure to see you.

Throughout my time at Loughborough I have had the pleasure of being part of the chemistry department and many people have provided support throughout my undergraduate and PhD studies. I would like to thank Dr Caroline Kirk, Dr George Weaver and Dr Sian Williams for all the help, talks and understanding, sometimes a friendly face and a chat can be more reassuring than is understood. Thanks must go to Mr Callum Crane for all the help, support, lunches and endless chats; Ms Christine Bagley for all the advice and support and Dr Paul Kelly for many amusing anecdotes during the long hours.

I would like to thank the members (and associated) of the Graham Oldham building, both past and present. To Ms Joan Sutherland for all her help with well everything and for listening I thank you. To

Dr Sneh Jain you are deeply missed, your kindness knew no bounds, thank you for all your help and for just being you.

To Mr Dimitris Kosmidis and Miss Joanna Kulazewska we are the survivors! Thank you for your support, together we can make it!!! To past members of the radiochemistry group Joel Gardner, Julie Turner, Stephen Pendelton, James Holt, Matt Druce and Matt Issacs thank you for the support and good times. A special mention must go to John Hinchcliffe whom was full of advice and could always raise a chuckle, thank you. To the latest additions to the GO Stephen Yeandel, Dave Case, Michael Watts and Adam McSloy for the good times shared, interesting conversations and support.

I would also like to thank the many members of the inorganic chemistry group for all the help, support and most importantly laughter provided over the years; Dr Mark Elsegood, Dr Martin Smith, Tom Noble, Rose Ikyereve, Jade Markham, Simon Sharp, Paul Brack, Richard Wilson and Lloyd Davis.

I would like to say a special thank you to all the friends I have been lucky enough to have met. To Shelina Kassam for always being the kindest of people and the best friend anyone could ask for. To Dr Alex Hill for the endless calls to lunch, the lab chats and for always being a good friend. To my friends Craig Buck, Carl Cooper, Sally Hodgeson, John Hodgeson, Jim Dobrzanski and Roz Dobrzanski, thank you. To Dr Iain Kirkpatrick and Prof. Stephen Fletcher for the endless information imparted, the chats and the tea.

To my extended family whom have given me the most precious gift; Jane, Dave, Nicholas, Claire, Richard and Simon. A very special mention must go to Richard for keeping us moving and Jane without whom it would never have been organised.

To my family Mum, Dad, Claire, Lauren, Caz, Auntie Carol and Uncle Dave words will never be enough to even start to tell you how much you have heled me and how much you mean to me. Your faith and support in everything I have ever done is overwhelming and humbling. I am lucky enough to have what I consider two sets of parents, who were proud before I even started, two sisters who always have my back and always seem to know when I need catching. You have all made me know I am today and I am stronger just knowing you are there. To my puppies Dylan Bob and Lola Bear although you will never understand you have always made things a little easier. To Princess Poppy puppy who came into our lives smiling then never stopped and made us a little family.

To everyone that saw the beginning but not the end. To Les, Nan and Abbie thank you for shaping me into who I am, tempus fugit.

Finally, I would like to thank Ollie, you have been my rock, my support and my everything. I can honestly say that without you I would not be where I am today or the person I am today. You have and will always be loved more than you understand. Throughout the ups, downs, late nights and early mornings your understanding whilst embarking on your own PhD journey has been nothing short of amazing. Thank you is just not enough. Here is to new beginnings.

List of abbreviations

AERE - Atomic Energy Research Establishment

AGR - Advanced gas-cooled reactor

BFS - Blast furnace slag

CHN – Carbon, hydrogen and nitrogen analysis

CoRWM – Committee on Radioactive Waste Management

CP – Cross polarisation

CSA – Chemical shift anisotropy

DP – Direct polarisation

DPM – Disintegrations per minute

e^- - Electron

FTIR – Fourier transform infrared spectroscopy

GDF – Geological disposal facility

HLW – High level waste

ICDD - International centre for diffraction database

ILW – Intermediate level waste

LLW – Low level waste

LSC – Liquid scintillation counting

MAGNOX – **Mag**nesium **N**on-**Ox**idising (a magnesium and aluminium alloy cladding for uranium)

MRWS – Managing Radioactive Waste Safely

MSA – Magic angle spinning

MCA – Multi channel analyser

NDA – Nuclear Decommissioning Authority

NNL – National Nuclear Laboratory

NIREX - Nuclear Industry Research Executive

NMR – Nuclear magnetic resonance

NRVB - Nirex reference vault backfill

OPC - Ordinary Portland cement

PFA - Pulverised fuel ash

PFSP - Pile fuel storage pond

PMT – Photomultiplier tube

PTW – Permeable treatment wall

PWR – Pressurised water reactor

PXRD – Powder X-ray diffraction

RWM – Radioactive Waste Management

SEM – Scanning electron microscopy

SIXEP - Sellafield ion exchange effluent plant

SSB – Spinning side bands

SSNMR – Solid state nuclear magnetic resonance

UK – United Kingdom

VLLW – Very low level waste

Table of Contents

Chapter One – Introduction

1.0 Introduction to chapter one.

The safe management of radioactive waste is crucial for the future of the nuclear industry and one of the largest technical challenges faced by countries using nuclear power. Part of the clean-up process used in the treatment of such waste in the United Kingdom (UK) involves removal of radioactive species from the alkaline liquor used in storage pond facilities containing spent pile materials and reactor debris. This thesis focuses on the synthesis and characterisation of modified and replacement functional materials for use in the Sellafield Ion Exchange Effluent Plant (SIXEP); the last stage in the aqueous clean-up process before discharge of the neutralised liquor into the sea. This chapter covers the background to the legacy nuclear waste problem and the storage methodologies which led to large volumes of aqueous waste. The text also describes the materials such as clinoptilolite used in effluent treatment and the proposed storage options of radioactive species remediated from the waste. Finally, it describes the group of materials that will be investigated, and the surface-modification process carried out, to produce possible alternatives or additives to improve the existing clean-up process.

1.1 Introduction to the nuclear waste problem

The UK has accumulated a large volume of legacy nuclear waste and much of this waste is located at Sellafield. Due to the waste being generated from both military and domestic applications, it is varied in nature. The first nuclear waste produced from an energy generation source dates back to 1947, when the first reactor was built at the Atomic Energy Research Establishment (AERE), Harwell, to establish the validity of commercial power reactors.[1] Since then the UK has had an active nuclear energy program. However, before any large-scale domestic applications were instigated, it was the defence sector that generated the initial waste from a nuclear source in the UK as a result of the development of a nuclear deterrent during World War II.[2] In 1941, after research into the viability of an atomic bomb, the Prime Minister, Winston Churchill, authorised the development of an atomic weapon under the title 'Tube Alloys'.[2] In 1943, an agreement with the US President, Franklin D Roosevelt, led to the Manhattan project; a joint US/UK research project into the first atomic weapons[1]. From this initiative, it was realised that the technology used to generate plutonium for nuclear weapons could also be used for the production of energy for domestic purposes.[1]

Subsequently, nuclear waste has been generated from reactors used for domestic energy production for a long period of time; the first MAGNOX nuclear reactor became operational in 1956 when the UK government announced that Britain was home to the first power station in the World to produce electricity from atomic energy on a full industrial scale.[1] The height of the UK's nuclear power generation occurred in the late 1990's with 25% of the energy being provided by nuclear power.

Currently 16% of the UK's energy is produced from nuclear power, which is lower on average than the 25-30% produced globally.[3] The different reactors and their locations can be seen in Tables 1.1 and 1.2. Establishing the nuclear industry itself was the original focus of the project and much less consideration was given to the waste generated by those activities. The swiftness at which both nuclear weapons and domestic energy programs progressed, meant the quantity of waste being generated, and the consequences of that waste, were not fully realised for many years. This led to a legacy waste problem, which now needs to be addressed to ensure the future of a nuclear power industry in the UK.[4] However despite the challenges of the resulting nuclear waste, energy from nuclear power sources has been receiving renewed interest recently as a method of low carbon energy production since the Paris Agreement,[5] particularly as concerns over environmental damage caused by fracking to extract new oil and gas sources have grown.[6]

Reactor	Commenced operation	Operational until
Calder Hall 1	1956	2003
Calder Hall 2	1957	2003
Calder Hall 3	1958	2003
Calder Hall 4	1959	2003
Chapelcross 1	1959	2004
Chapelcross 2	1959	2004
Chapelcross 3	1959	2004
Chapelcross 4	1960	2004
Berkeley 1	1962	1989
Berkeley 2	1962	1988
Bradwell 1	1962	2002
Bradwell 2	1962	2002
Hunterston A1	1964	1990
Hunterston A2	1964	1989
Dungeness A1	1965	2006
Dungeness A2	1965	2006
Hinkley Point A1	1965	2000
Hinkley Point A2	1965	2000
Trawsfynydd 1	1965	1993
Trawsfynydd 2	1965	1993
Sizewell A1	1966	2006
Sizewell A2	1966	2006
Oldbury 1	1967	2012
Oldbury 2	1968	2011
Wylfa 1	1971	2015
Wylfa 2	1971	2012

Table 1.1 - Nuclear Reactors in the UK and their Operational Timescales[1]

Reactor	Type	Commenced operation	Expected Operation
Hinkley Point B1	AGR	1976	2016
Hinkley Point B2	AGR	1976	2016
Hunterston B 1	AGR	1976	2016
Hunterston B 2	AGR	1977	2017
Dungeness B1	AGR	1983	2018
Hartlepool 1	AGR	1983	2019
Heysham I-1	AGR	1983	2019
Hartlepool 2	AGR	1984	2019
Heysham I-2	AGR	1984	2019
Dungeness B2	AGR	1985	2018
Heysham II-1	AGR	1988	2023
Heysham II-2	AGR	1988	2024
Torness 1	AGR	1988	2023
Torness 2	AGR	1989	2023
Sizewell B	PWR	1995	2035

The last serious attempt to develop a long-term solution to the problem of the legacy waste was undertaken by NIREX (Nuclear Industry Research Executive) in the late 1980's when they were investigating a possible underground repository site in Cumbria, near Sellafield. Sellafield is expected to generate approximately 60% of the nuclear waste in the UK in the future, so proximity of the repository to the source of the waste was considered an important part of the solution to this problem. On the 17th of March 1997, the inspectors investigated the site for suitability of the underground repository and rejected NIREX's proposal due to the poor understanding of the geology and hydrogeology of the site.[7] This highlighted the need for greater understanding of the fundamental chemistry and overall geology of any site before its use could be agreed for radioactive waste management purposes.

In 2001, the UK government produced the Managing Radioactive Waste Safely (MRWS) initiative managed by Radioactive Waste Management (RWM), to begin to deal with the UK's waste legacy.[7]

The proposal aimed to provide a long term scientific solution that would protect people and the environment in a cost-effective manner that must be transparent to the public. The Nuclear Decommissioning Authority (NDA) was created in 2003 to manage the funding, planning and implementation of the legacy waste management processes and decommissioning of nuclear installations in the UK. The NDA is responsible for the clean-up and decommissioning of 17 of the UK's nuclear sites and implementing the high level waste (HLW) and low level waste (LLW) strategy.[7] This encompasses the first generation MAGNOX power stations, research facilities, fuel processing plants and the highly complex Sellafield site. A report by Nirex summarised proposed methods for dealing with nuclear waste including; deep geological disposal, near surface storage, long term storage above ground, deep borehole disposal, disposal at sea, sub-sea bed disposal, disposal in ice sheets, disposal in subduction zones, rock melting, direct injection and disposal in space. The international community has since agreed that the best way to ensure long term safe disposal of the highly hazardous waste is via a geological disposal facility (GDF).[8–11]

In 2006, CoRWM (Committee on Radioactive Waste Management) recommended geological disposal and secure interim storage as the long-term solution for the UK's waste. In 2008, the Government officially adopted Deep Geological Disposal and research is being conducted to the viability of volunteered sites.[11]

1.2 Nuclear fuel cycle

The nuclear fuel cycle in its simplest form is the life of the fuel from the mining process to the final waste produced after the fuel has been used. Nuclear energy is produced by the fission of a material such as uranium, which can sustain a chain reaction. Fission can be spontaneous or induced by the introduction of neutrons into the system. There are two main types of nuclear fuel cycles, one that utilises ^{235}U and the other which utilises ^{232}Th. ^{235}U is a fissile isotope, whereas ^{232}Th is transmuted by neutron activation to ^{233}U which is fissile. Most reactors throughout the UK and Europe utilise ^{235}U. [4], [8], [12]

The UK's operating nuclear reactors are predominately advanced gas-cooled reactors (AGR), these reactors use graphite as a moderator and carbon dioxide as a coolant gas as seen in Figure 1.1. These are second generation reactors replacing the first-generation Magnox reactors. Sizewell B, the last reactor to be opened, is a pressurised water reactor (PWR). AGR use enriched uranium as the fuel source. Natural uranium ore contains approximately 99.28% ^{238}U and 0.71% ^{235}U by mass. In order to be used as a fuel, the uranium must be enriched to 2-5% ^{235}U for AGR. AGR uses thermal neutrons as they are more efficient than fast neutron reactors, therefore graphite is required as a moderator to lower the kinetic energy of the neutrons and increase the probability of a fission occurring. In thermal

reactors, moderators of low atomic numbers such as graphite or water are used to slow down neutrons via elastic scattering.

$$^{235}_{92}U + neutron \rightarrow 2.5\ neutrons + fission\ products + energy$$
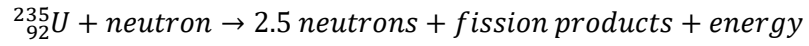
The majority of operational nuclear reactors are AGR type and utilise uranium dioxide pellets where the ^{235}U is split by thermal neutrons according to Equation 1.1. The reaction is self- sustaining as for every atom split 2.5 neutrons are generated, along with the associated fission products and thermal energy. The thermal energy is used to generate steam which turns a turbine and generates electricity.
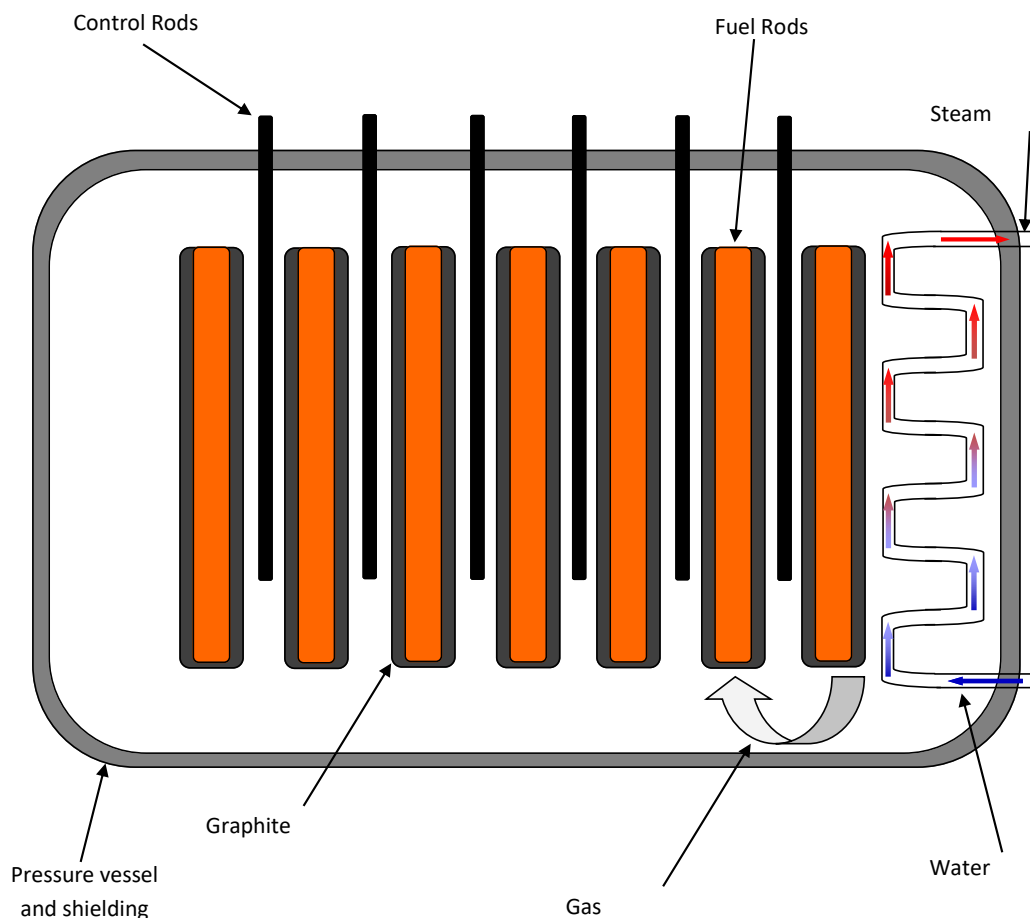
Figure 1.1 - Schematic Diagram of an Advanced Gas Cooled Reactor (AGR)

A flux of neutrons is generated and fission of ^{235}U occurs, this produces energy and more neutrons. Of the neutrons produced on average only one produces a further fission, the rest are absorbed by the control material, shielding and other materials such as the fertile ^{238}U which is the predominant material in fuel rods. ^{238}U absorbs a neutron and transmutes into ^{239}Np which then decays to ^{239}Pu, shown in Equation 1.2.[13]

$$^{238}_{92}U + Neutron \rightarrow {}^{239}_{92}U \xrightarrow{\beta-} {}^{239}_{93}Np \xrightarrow{\beta-} {}^{239}_{94}Pu$$
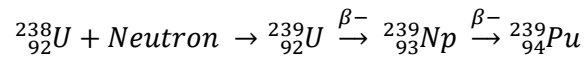
Equation 1.2

Once the fuel rods have reached the end of their useful life, they still contain approximately 1 % ^{235}U. Due to the exothermic nature of radioactive decay, the fuel rods produce heat and are kept cool by storing them in fuel storage ponds, Figure 1.2, which are highly caustic to limit the solubility of the actinides contained in the fuel rods.[4,8,14]
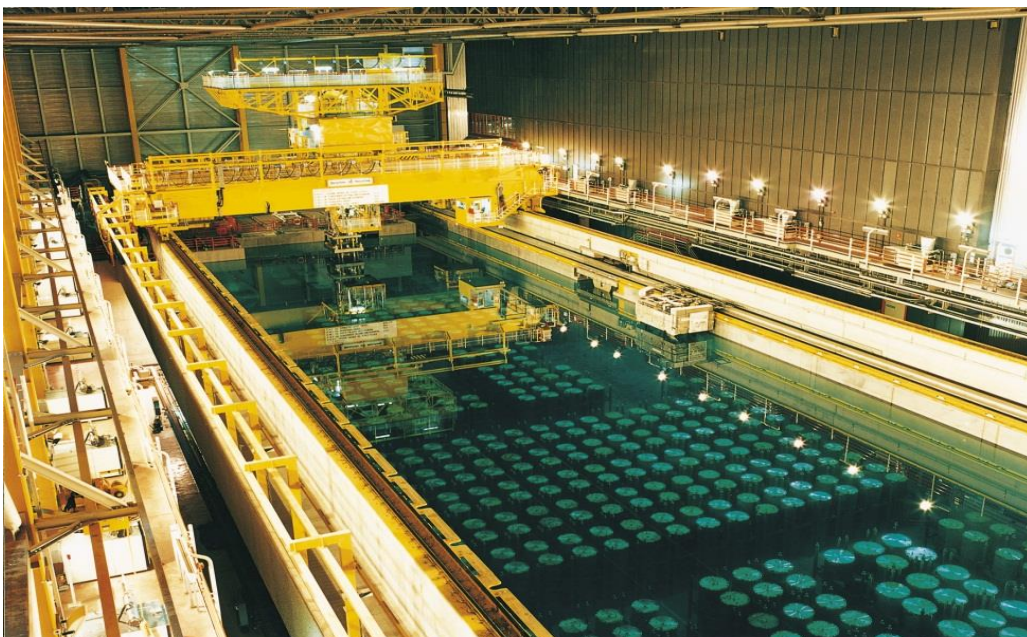
Figure 1.2 - Fuel storage pond[15]

1.3 Sellafield storage ponds

The first fuel storage pond in the UK was the Pile Fuel Storage Pond (PFSP) built in 1949/50. It was designed to house waste from both the Windscale piles that were part of the atomic weapons project. The pond was designed to receive and regulate the temperature of fuel and isotopes from the reactors. However in 1957; the Windscale fire in reactor 1 closed the plant. The storage pond usage changed to store ILW, and with the commissioning of the Magnox fuel ponds, the PFSP was closed in 1962.[4,8] The first fuel pond has recently been decommissioned; the inventory of the pond has been investigated and was found to contain a wide variety of materials highlighting the problems with legacy waste. The pond contained fuel from reactors in rods and flat bars; fuel cladding consisting of Magnox, aluminium and zircalloy; isotope cartridges and reactor furniture (originally non-active material that becomes active in the presence of the fuel) from the piles, Calderhall and Chapelcross. Due to the pond being exposed to the elements, the bottom of the ponds contain sludge, consisting of approximately 300 m^3 of bio-organic material, metal corrosion products, spent fuel and windblown debris. Ponds that have been built more recently are not open to the elements and bio-organics and windblown debris cannot enter the new storage ponds. Spent fuel is discharged to skips which are placed into the ponds. All waste is now inventoried, but there is still a wide variety of waste. The ponds are kept at a high pH of 11-11.5 using a sodium hydroxide solution made from demineralised water.[8]

Fission products from the fission of uranium in fuel rods are present in the storage ponds. In addition to the neutrons and energy produced when the ^{235}U nucleus splits, two asymmetric fission products are produced. Caesium and strontium are two such fission products and are therefore present in used fuel rods. Normally one light element with a mass number of approximately 90 and one heavy element with a mass number of approximately 140 are produced per fission. Fission products are produced in a 200% yield, as two isotopes are produced per fission, and can be highly mobile. Many of these fission products also decay generating a large number of isotopes present in nuclear waste as shown in figure 1.3.
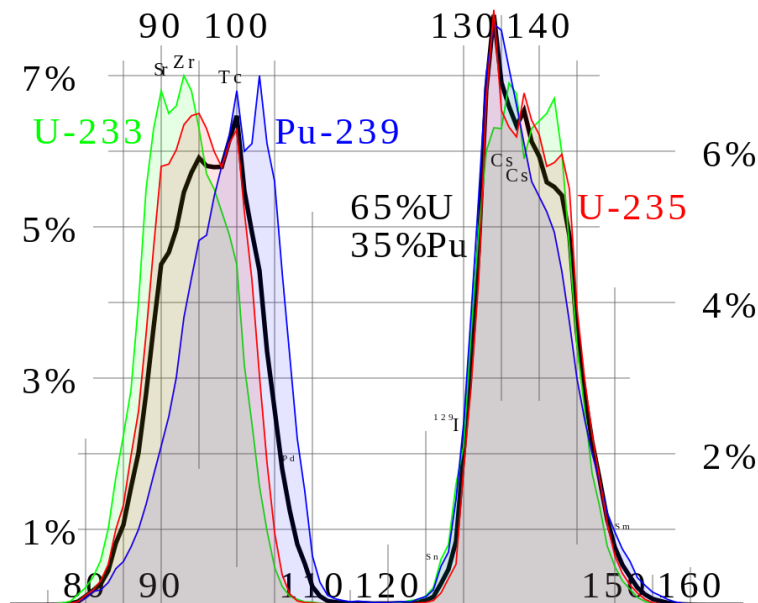
Figure 1.3: fission product yield [135]

Activation products from neutron capture are also found in the storage ponds. Activation products are heavier than the parent element and are found not only in the fuel rods but also the surrounding structure. Activation products come from the neutron capture where a neutron collides with an atomic nucleus and they combine to form a heavier nucleus. Therefore, heavier elements which are activation products of ^{238}U such as americium, plutonium and curium are all found in the storage ponds. Lighter activation products are also found in the ponds that are generated from materials in the surrounding structure of the reactor.[8]

The pond liquor is continuously circulated to prevent the built up of soluble isotopes. Over time, the various materials present in the ponds breakdown and cause the concentration of the radioactive species in the liquor to increase. The concentration is monitored and the ponds partially drained to remove some of this solution with high activity and then backfilled with sodium hydroxide solution.

The Sellafield storage ponds contain a wide variety of materials and isotopes from many different sources. The high pH and variety of materials makes this waste some of the most hazardous waste produced. The liquor removed from the storage ponds is sent to SIXEP for treatment to reduce the alkalinity and remove the radioactive ions and the remaining neutralised solution at pH 7-7.5 after the process is complete is discharged into the sea.[10]

1.4 SIXEP process

The SIXEP concept was developed in the 1970s and construction of the plant began in 1979 before being commissioned for operation in 1985. The process is based on ion-exchange to remove radioactive caesium and strontium cations from the waste stream, using the natural zeolite, clinoptilolite. Although other active species are also removed during the process through settling of particulate matter and sand filtration, the primary purpose of the various pre-treatments and filtration beds is to deliver a solution of pH 7-7.5 to the zeolite so ion exchange proceeds efficiently in the zeolite.

The SIXEP process works by passing liquor from the ponds through a system of tanks, filters and exchangers to remove activity, reduce alkalinity and minimise the activity of discharges from the Sellafield site, as shown in Figure 1.4. The liquor is drained from the ponds and enters the reception tank; here the solids and particulate materials are allowed to settle. The liquid is removed from the top of the reception tank and passed through a series of sand beds. The sand is coated in a polyelectrolyte, to remove the bulk of the remaining solid, but does not remove colloids. The sand beds are then backwashed into sludge tanks. The pH of the process through the reception tank and sand beds is closely monitored and controlled to be consistently pH 11-11.5, as the liquid enters the carbonation tower the pH is reduced to 7 by bubbling carbon dioxide gas through the liquor. This neutralisation process is essential to prevent degradation of the zeolite in the ion exchange bed, since it can dissolve in basic solutions. The solution is then sent to the clinoptilolite ion exchanger where it is run through a lead bed then a trail bed. This removes caesium and strontium cations from the solution, which is then sent to the final proportional tank, which is sampled every day to detect break though of active species. Water from this tank is then discharged into the sea. When breakthrough occurs, typically at between 55-84 days, the lead bed is replaced by the trail bed, and the spent ion exchanger from the lead bed is sent to the waste tank, both the waste ion exchanger and sludge are sent for interim storage. The SIXEP process has proven to be very successful with the removal of activity in excess of 85875 TBq of beta and nearly 80 TBq of alpha. [8,10,16]
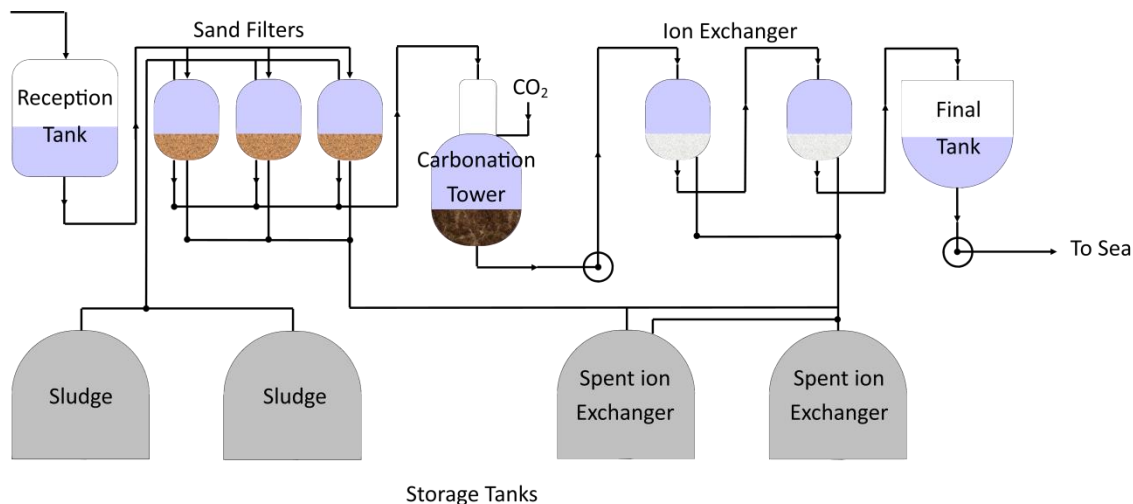
Figure 1.4 - Schematic Diagram of the SIXEP Process

One problem faced by the SIXEP process is the variety of ions in solution. Clinoptilolite removes caesium and strontium cations by ion exchange; however there are competing group one and two ions such as magnesium, calcium, barium, sodium and potassium also found in the waste stream. Sodium has the highest concentration of 100 to 250 ppm; this arises from the sodium hydroxide solution that is used to keep the pH levels in the pond greater than 11. The remaining ions are found in relatively low concentrations in the waste stream when they reach the clinoptilolite. The magnesium found in the ponds from the Magnox cladding is mostly in solid form and is filtered out by the sand beds. Americium is mostly bound to the magnesium solids or forms carbonates and is removed before the clinoptilolite beds. The remaining problematic isotopes are present in too higher oxidation states or as large hydroxylated species and are unlikely to be ion exchanged readily. A small amount of the uranium is removed by the clinoptilolite, by flocculation at lower pH rather than exchange, but the plutonium neither forms solids in the sand bed nor is removed by ion exchange via the zeolite.[10] Often these species breakthrough into the waste tank before the clinoptilolite beds are fully exhausted, resulting in a change of the clinoptilolite beds. Incorporation of a substrate into the SIXEP process that would remove the uranium and plutonium species would prolong the lifetime of the clinoptilolite beds and hence reduce the amount of waste generated by SIXEP. This hypothesis is the idea that is tested during this thesis by modification of materials already present in the process and the introduction of other industrially viable solids already utilised elsewhere. The ability to remove the actinide species from solution depends on understanding what form those species are in when they reach the clinoptilolite beds. At this point, the originally alkaline liquor has been neutralised using carbonation and hence there is the potential for a variety of species in solution. Uranium is present in the storage ponds, but is largely removed by the process before the clinoptilolite

ion exchangers due to the high pH, however the work in this thesis has utilised uranium as a surrogate for plutonium to allow a method to be developed to allow the safe use of plutonium, and so its speciation is discussed here.

The un-complexed uranium (VI) ion normally exists in solution as uranyl ion species, UO_2^{2+}.   By changing the pH, a range of uranium hydroxyl species can also be formed and these are shown in the Pourbaix diagram (Figure1.5) together with reduced species of uranium.[17]

Figure 1.5 – Pourbaix diagram of uranium[18]
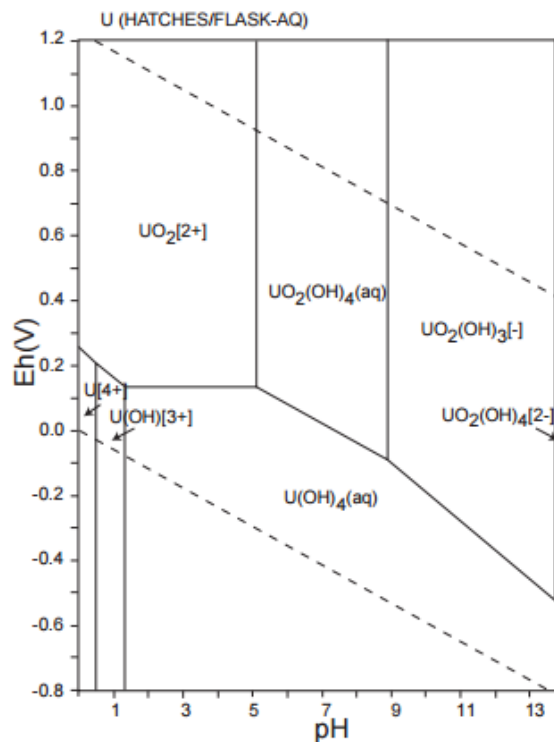
The hydrolysis of uranium is well documented in the literature; the general mechanism for the hydration of the uranyl ion is shown in Equation 1.6.

$$xUO_2^{2+} + yH_2O = (UO_2)_x(OH)_y^{2x-y} + yH^+$$
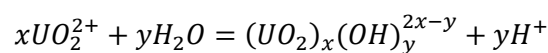
Equation 1.3

At lower pH values and uranium concentration the formation of monomeric uranium hydroxide species is typical, as shown in the Figure 1.6. [19]
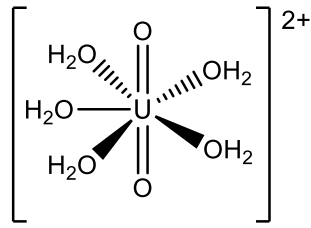
Figure 1.6 – monomeric uranium species

This shows that as the pH increases more hydroxyl species are added and anionic species are favoured. If the uranium concentration is sufficiently increased then polymeric uranium species are formed, the structures of which are shown in Figure 1.7.
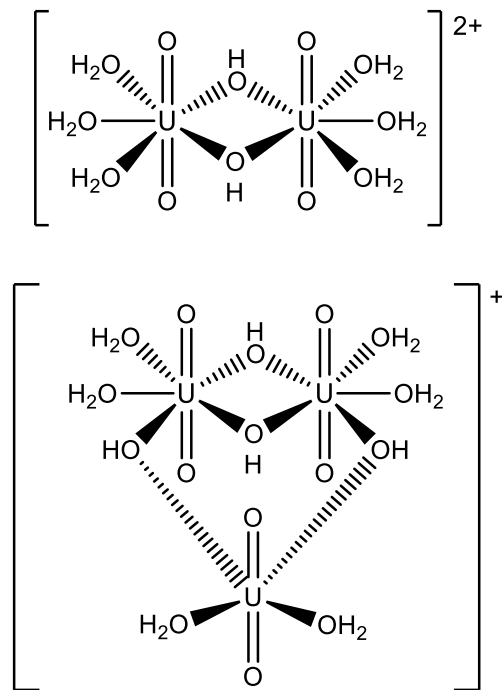
Figure 1.6 – Polymeric Uranium Species formed at Low pH.

Camacho et al showed, using a sample of clinoptilolite from Sweetwater, Wyoming that was a mixture of zeolite and mineral impurities, that the ability of the sample to remove uranium species was dependent on pH and feed concentration; since this sample was a mixture, it cannot be certain whether it is the zeolite or the impurities interacting with uranium in this case. The optimum pH for removal of uranium (IV) species was pH 6. The fall in uptake above pH 6 was attributed to the

formation of the stable precipitation product $UO_2(OH)_2$ which competed with the interaction between the Sweetwater mineral sample and the cationic species.[20] Cationic species $(UO_2)(OH)^+$ and $(UO_2)^2(OH)_2^{2+}$ disappear between pH 5 and 6 according to Misaelides et al, and $(UO_2)_3(OH)_5^+$ becomes gradually more limited until no major hydrolysis product exists above pH 9.[21] This study did not take into account the presence of carbonate as the objective was focussed on the removal of uranium from groundwater rather than from alkaline liquor from holding ponds which had been neutralised by carbonation. The solubility of uranium species decreases as the solution becomes more basic, however there has been some uncertainty surrounding the solubility and speciation under hyperalkaline conditions. A possible explanation for this is colloid formation; a study has confirmed the presence of stable uranium colloidal nanoparticles of the order or 20 nm which form at relatively low concentrations of uranium of 2.5×10^{-5} mol L^{-1}.

Maher et al reported that Pu(V) is the dominate plutonium oxidation state in the SIXEP liquor, where greater than 90% of the alpha activity associated with the plutonium species is particulate (> 1 µm) in nature. The particulate matter results from interaction of the plutonium species with $Mg(OH)_2$ and $MgCO_3$ phases derived from the Magnox cladding found in the ponds. Of the remaining plutonium species, 40% are in the colloidal range (100-200 nm).[22]

The plutonium specific activity in the bulk storage tank liquor is 3.66 +/- 0.18 Bq ml^{-1} and contains about 0.41 +/- 0.18 Bq ml^{-1} of soluble activity which passes through SIXEP into the ion exchanger beds. An improvement in the reduction of the specific activity of plutonium is the major driving force behind the work in this thesis. Plutonium speciation in the fuel storage ponds was carried out using PHREEQC by Gregson and Taylor coupled with some experimental results.[23] Filtration was shown to remove the majority of the plutonium activity indicating the particulate nature of the plutonium. After removal of the colloidal species, the dominant soluble species remaining between pH 3 and 10 were identified as Pu (V) when open to the air. In the highly alkaline ponds (pH =11) themselves there was evidence to suggest that the dominate species was $Pu(OH)_4$. Modelling results confirmed the analytical results from the liquor where PHREEQC calculations using the HATCHES database with nanomolar concentrations of plutonium in the presence of carbonate (10 mM) generate the Pourbaix diagram given below in Figure 1.7.[23]
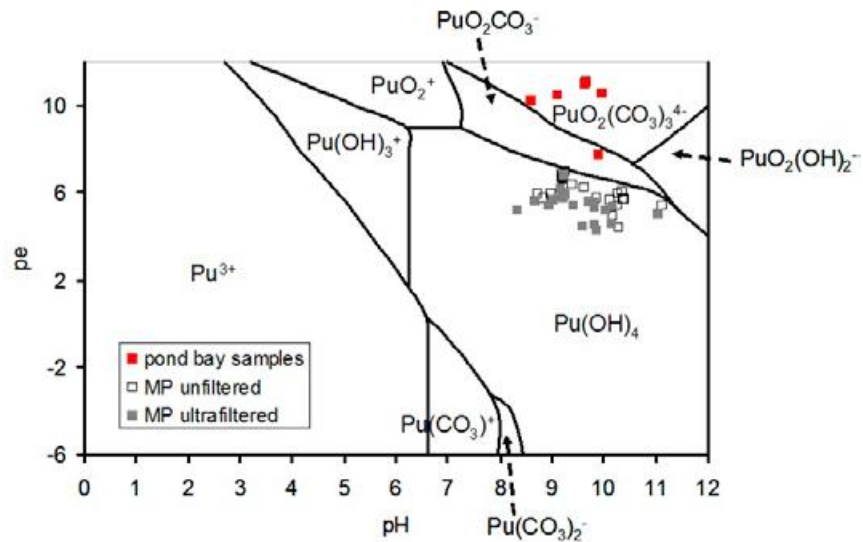
Figure 1.7 Plutonium poirbaix diagram[23]

Although it has been suggested by Owens et al that the SIXEP process is not effective at removing all the plutonium species from solution because not all of the species are cationic, the suggestion from the Pourbaix diagram is that at pH 7, the plutonium should be present as PuO_2^+ at high pE levels. At lower pE levels, plutonium could be present as $Pu(OH)_4$ (0<pE<9) and possibly as the trivalent cationic species $PuCO_3^+$ at pE <0. [24]

Ewing also published a Pourbaix diagram that predicted the speciation of plutonium in fuel ponds.
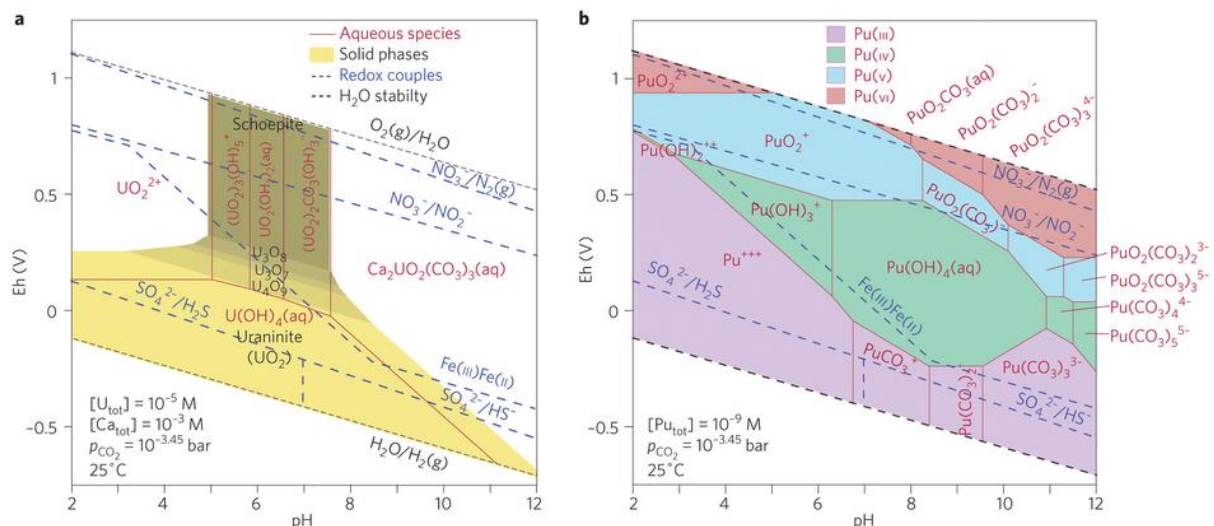
Figure 1.8: Plutonium speciation diagrams[25]

This second modelling study also predicts that the major Pu species at pH 7 are $Pu(OH)_4$ and PuO_2^+ i.e. Pu(IV) and Pu(V) depending on pE levels. The likely levels of oxygenation present in the SIXEP process after the carbonation step is unclear and it is not immediately obvious in which pE region the clinoptilolite beds will operate. The author suggested that SIXEP does not efficiently remove actinide is because species maybe anionic rather than cationic. However, as previously discussed, ion exchange in zeolites is controlled by size and charge of the species meaning clinoptilolite is unlikely to be selective for the cationic plutonium species either.

1.5 Managing nuclear legacy

1.5.1 Nuclear Waste

Nuclear or radioactive waste is classified as material that has no further use or is contaminated by radioactivity that is above threshold levels defined by UK legislation. Nuclear or radioactive waste encompasses a wide range of wastes ranging from those which have high levels of radioactivity to those which are mildly contaminated. These wastes are classified into high level waste HLW, intermediate level waste ILW and low level waste LLW. The waste is classified by the type and amount of radioactivity present and if they are heat generating.[26]

1.5.2 Types of waste

High level waste is defined as wastes that are heat generating and have high levels of radioactivity. HLW arises from the nuclear fuel cycle from operations such as reactor operations, reprocessing and decommissioning. The majority of the waste when categorised by activity is high level waste. Intermediate level waste has higher levels of activity than is permitted for low level waste but is not heat generating like HLW. Low level waste is defined by the limit of 4 GBq per tonne of α or 12 GBq of β/γ. The majority of the waste produced is LLW by volume with 93.9% of the waste being classified as LLW, as seen in Figure 1.9.[27]
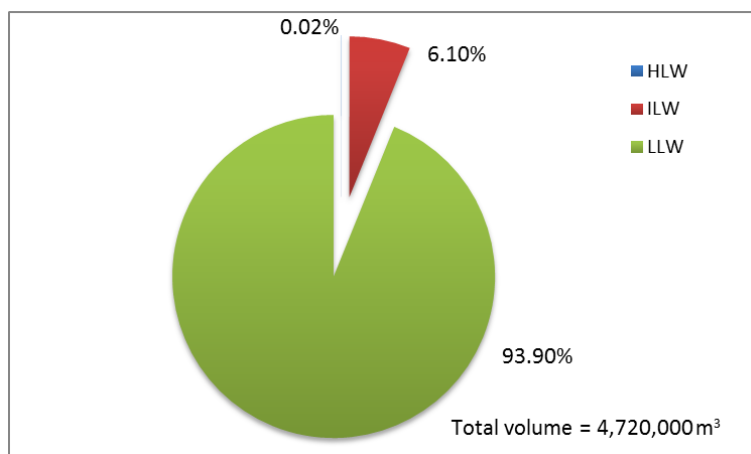
Figure 1.9 Diagram showing the types of waste by volume[27]

A total activity of 84,000 PBq was the reported activity for UK waste in 2010. HLW contributes 95% to the overall activity total, ILW contributes ca. 5% to the overall activity with LLW contributing 0.00005% to the overall activity.[27]

Table 1.3 - Categorisation of Nuclear Waste and Waste Volume[27]

Waste Type	As of 1st April 2010	Volume / m³	Mass / Tonnes	Number of packages
HLW	Total	1620	3300	
	Not yet conditioned	850	1300	0
	Already Conditioned	766	2000	5108
ILW	Total	94300	110000	
	Not yet conditioned	69800	68000	1091
	Already Conditioned	24500	46000	46571
LLW	Total	66000	76000	
	Not yet conditioned	44300	45000	0
	Already Conditioned	21700	30000	1288

In Table 1.3 conditioned refers to waste encapsulated in cementitious media, polymer or glass. Waste denoted as not yet conditioned refers to untreated or partially treated waste. Table 1.4 shows the increase of waste and waste packages since 1994.

Table 1.4 - Increase in Waste since 1994[27]

Date	Number of packages			
	HLW	ILW	LLW	Total
1st April 1994	529	4466	-	4995
1st April 1998	1633	17027	-	18660
1st April 2001	2281	21654	23	23958
1st April 2004	3037	31557	123	34717
1st April 2007	4319	40797	8527	53643
1st April 2010	5108	47662	1288	54058

The spent zeolite material waste generated by the SIXEP process falls predominately into the category of ILW once it has been exhausted as an ion exchange reagent for strontium and caesium cations. The hydrated nature of the zeolite causes a problem of its own when it comes to creating a waste form from this material, since the normal process for the disposal of solid waste using cement encapsulation can be affected by the moisture which is inherent to any zeolite material. The current method proposed for disposal of this waste is dehydration and vitrification in borosilicate glass.

1.5.3 Geological Disposal Facility

As previously discussed in this section, whilst a range of disposal options have been discussed, the international community have agreed that a deep geological disposal facility (GDF), Figure 1.10, is the best option for long term storage of solid nuclear waste. This option uses a multi barrier approach that utilises both natural and engineered barriers to limit the leakage of spent nuclear waste into the environment.

The GDF has to incorporate a wide range of different isotopes and encapsulation within the waste form will not be enough to prevent some of the highly mobile isotopes from leaching out. Isotopes

such uranium and plutonium will need physical and geochemical barriers such as alkaline cementitious material. A key feature of the GDF will be the surrounding geology; by selecting a suitable host site the use of geochemically reducing conditions, rather than oxidising conditions, will retard the movement of radionuclides. The UK government is currently looking to a GDF for the disposal of higher activity radioactive waste. The current policy is based on a community volunteering to host the GDF but it is noteworthy that the volunteer site needs to have suitable geology to be able to safely house the waste. The government released a MRWS consultation document on 25 June 2007, covering the technical aspects of geological disposal and outlining the voluntarism approach and evaluation of potential disposal sites. The consultation process closed on 2 November 2007, with one hundred and eighty-one responses being received. The government published the results on the 10 January 2008.
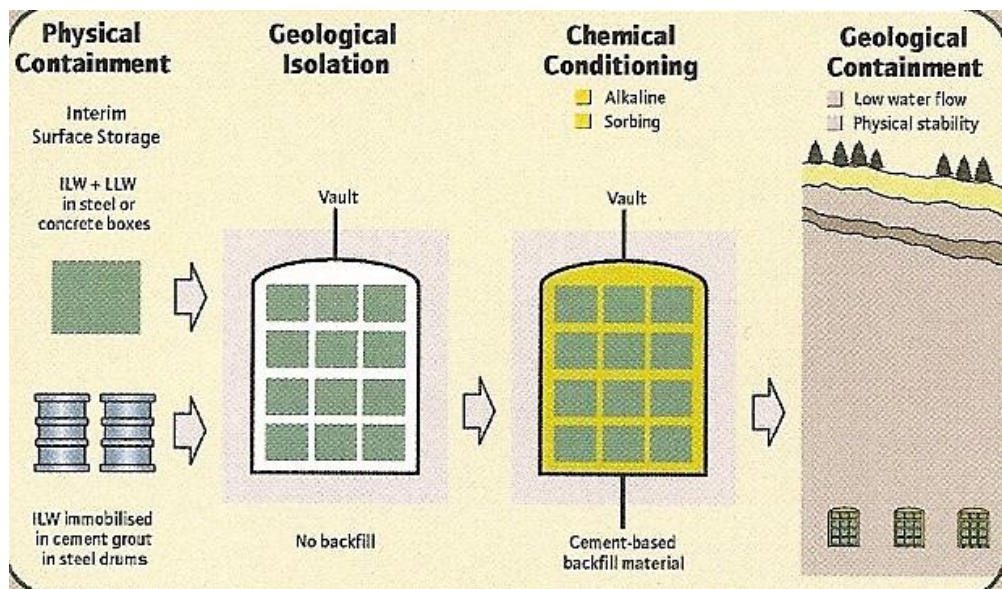
Figure 1.10 - Schematic of the multi-barrier concept[28–30]

Some of the barriers that will be present in the deep geological disposal facility are depicted in Figure 1.11. This includes the actual waste form itself; by combination of the waste with other materials to condition the waste, the movement of isotopes can be retarded e.g. by the vitrification of HLW in glass. The next barrier present is the container within which the conditioned waste is placed. An example of a container that is often used is a steel drum. The steel drum must be corrosion resistant and must be suitable for long term storage and prevent the migration of materials through the repository. The waste containers will then be surrounded by a buffer or backfill material. The buffer/backfill provides a chemical and physical barrier in the GDF.[8,28]
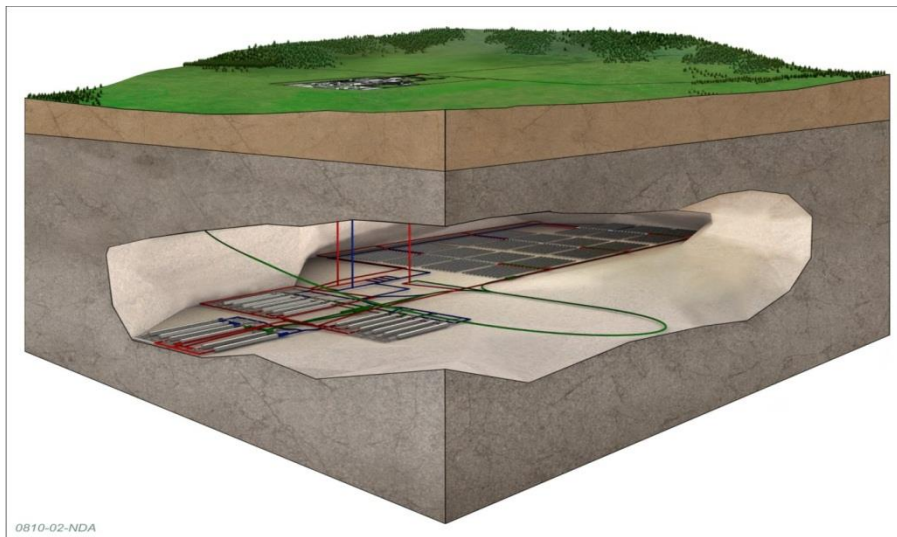
The backfill and

encapsulation material currently being investigated is cement. It is important to note the difference between cement and concrete, cement is a binder that hardens independently, whereas concrete is a mixture of a binder such as cement and aggregate such as crushed limestone.

Figure 1.12 - Cross-section of a filled barrel proposed for the GDF

There are four types of cementious media that are currently being investigated for use within the repository. Nirex Reference Vault Backfill (NRVB), ordinary Portland cement (OPC), 3:1 pulverised fuel ash (PFA):OPC and 9:1 blast furnace slag (BFS):OPC. The preferred medium at the current time is NRVB; NRVB was designed for use in the repository to maintain high alkalinity, be homogeneous and have good flow to allow good packing around materials. The high pH of the repository can be partly attributed to the ions present in the cementious media. The pH of the cement pore water is high due to species like calcium hydroxide ($Ca(OH)_2$), which causes the pH to be approximately 12.5.[28] An example of a cementious filled steel barrel can be seen in figure 1.12.[15]

The geology of the host rock that is selected will also form a physical barrier. By selecting the chemical geology of the host rock carefully, the migration of the radionuclides can be retarded. The near field geology of the site where the repository is built, which surrounds the host rock, can also be a physical barrier. The alkaline disturbed zone is the area around the GDF where the alkalinity is high due to leaching of potassium and sodium hydroxides from the cement. The area referred to as the far field is

beyond the alkaline disturbed zone but is close enough for the potential to see some migration from radionuclides, normal environmental conditions should be prominent

1.6 Materials of interest

Zeolites and layered materials (clays) have been investigated in this work to replace/improve utility of the ion-exchange medium currently used in the SIXEP process. These materials have been chosen as they are both cheap and readily available and suitable for industrial scale applications. As well as looking at alternative materials to clinoptilolite for ion exchange, the option of using both clinoptilolite and these alternative materials as a support for chelating ligands to remove highly charged and/or hydroxyl radionuclides species from solution has been investigated. As previously discussed in section 1.4, clinoptilolite does not ion exchange these type of species as the specific ion exchange sites are selective for caesium and strontium cations only and the other species are very different in terms of size.[20,31–35]. This section gives a brief overview of the materials used and their properties in relation to the type of material under study. The need for a range of materials which can be applied to varying environments to remove radionuclides is important in the clean-up of nuclear waste due to the varied composition of the liquor in waste ponds and the possibility of spills in different environmental conditions. To address this need, a range of materials have been studied in this work. A natural zeolite, clinoptilolite, one synthetic zeolite, ZSM-5, a 2:1 clay, vermiculite and a 1:1 clay, kaolinite have been investigated. The natural zeolite clinoptilolite is currently used in the UK nuclear industry to reduce the activity of the aqueous waste stream forming part of the SIXEP process. This zeolite was selected for investigation with the aim of modifying the surface allowing additional radionuclides to be removed, without the need to alter the process already in place. The NNL/NDA provided a sample of the zeolite used in the SIXEP plant which is taken directly from a mineral source (in the Mojave desert in California).[10] As this material is a natural material taken from the ground, it is subject to significant variation in particle size and absolute composition; as well as the required zeolite, a number of other phases are present in the sample such as quartz which are identified in the experimental section. In the plant this material is used with very little pre- treatment except washing to remove fine particulates and particle sizing to prevent clogging of SIXEP. A second sample of clinoptilolite was sourced from IMERYS minerals, that was also sourced from the Mojave desert. This sample had been processed to remove some of the impurities by sieving and as a result has a narrower particle size distribution. The sample has also been processed by exchanging with potassium in order to replace the exchangeable cations within the structure. The two types of clinoptilolite have been selected to investigate whether the processing alters the grafting ability of clinoptilolite by removal of the larger particles. ZSM-5 was selected as it has shown an ability to be surface modified and is used in other

commercial applications such as alcohol conversion and fluid catalytic cracking. Two clay minerals have been studied as an alternative to clinoptilolite for removal of the highly charged/hydroxyl species; vermiculite and kaolinite. Vermiculite has been selected for investigation as it able to undergo ion exchange and has been used to remove ions from solution, such as Na, Mg, Ca, Sr and Ba.[36,37] Kaolinite has been used as a blank; as no exchangeable cations are available in kaolinite, it cannot undergo the same type of reactions as any of the other species and therefore the only sequestration it can undertake should be via the grafting process.

1.6.1 Zeolites

1.6.1.1 Background

Zeolites are microporous crystalline materials comprised of aluminium, silicon and oxygen, with charge balancing exchangeable cations. They can be natural or synthetic in origin with greater than 40 naturally occurring zeolites and over 150 synthetic zeolites characterised. The term zeolite means 'boiling stone'; named by Swedish mineralogist Axel Fredrick Cronstedt, from the Greek words 'zein' meaning boiling and 'lithos' meaning stone. Cronstedt observed that the mineral stilbite released large amounts of steam when heated, from water absorbed into the mineral[38].

Zeolites and their uses in chemistry are growing and the number of new frameworks has been increasing steadily. In 1970 before the International Zeolite Association (IZA) approved the general collection of zeolitic materials, The Atlas of Zeolite Frameworks, there were only 27 known zeolites. In the 2001 5th edition of the Atlas of Zeolite Frameworks there were 133 known and by the 2007 6th edition, 176 approved and named frameworks were included. In 2015, there were approximately 229 natural and synthetic zeolites known. [39]

1.6.1.2 Nomenclature and classification

Zeolitic materials have proved challenging to name and classify due to the composition, framework topology, secondary building blocks (SBU), framework density, crystal symmetry, channel system and unit cell constant. For example zeolite Y can have different Si:Al ratios ranging from 2.3 to 4.86 meaning different chemical compositions for nominally the same zeolite.[40–48] R. M. Barrer worked on nomenclature of zeolites in 1978, but the rapidly expanding field has since generated too many new frameworks simultaneously to maintain the Barrer nomenclature.[49] Zeolitic materials are now classified by the parameters mentioned previously. Zeolites with similar morphologies and properties are classified in the same group. There are three classification systems, the first is based on framework topology, each framework is given a three-letter code by the International Zeolite Association (IZA)

e.g. FAU for zeolites X and Y to indicate their faujasite framework topology.[38] The second is based on secondary building units (SBU); this method is based more on the morphology of the zeolites referring to key building blocks such as single and double six rings. The third classification scheme is based on the Breck system (1974) with historical concepts including how zeolites were found, playing an important part in the naming and classification.[50] This third concept is widely used by geologists and by Occelli and Kesster in their book Synthesis of Porous Materials published in 1997. [51]

A general formula for zeolites is shown below[39]:

$$M_{2/n}: Al_2O_3: xSiO_2: yH_2O$$
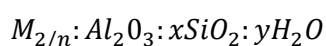
M = charge-balance cation

n = charge of the cation

x/y = number of SiO_2 /water molecules

1.6.1.3 Structure

Zeolites have a three-dimensional framework that is created by AlO_4 and SiO_4 oxygen sharing tetrahedra, figure 1.13. The tetrahedra are the building blocks of the zeolites and pack together to form three dimensional lattices. By replacing silicon with aluminium an overall negative charge can be created. This charge is then balanced with a cation such as sodium which is incorporated within the lattice.[52,53]

The microporous structure with pores allows cations, such as Na^+, Cs^+, and, Sr^{2+} or water to be accommodated. The trapped ions are held weakly by the zeolite, and as result can readily be exchanged. The affinity of a zeolite for a particular ion is largely controlled by the structure of the zeolite, the coordination number of the site which affects size, and the aluminium to silicon ratio.[49,50]

Oxygen

Silicon

Aluminium
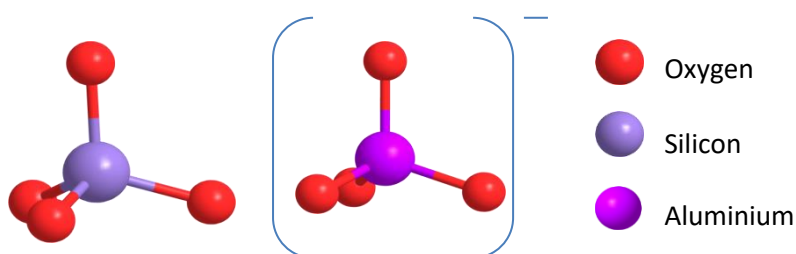
Figure 1.13 - SiO₄ and AlO₄ tetrahedra

Zeolites are formed from SBU; primary building blocks are the SiO_4 and AlO_4 tetrahedra which are vertex-sharing through oxygen bridges. SBUs are small molecules and form from soluble silicate anions from alkaline solutions and lead to the growth of zeolitic structures.[54] A selection of SBUs are shown in figure 1.14.

3   4   5   6

Spiro-5   4-4   6-6   8-8

4-1   4=1   4-2   4-4-1

5-1   5-2   5-3

6-2   2-6-2   6-1
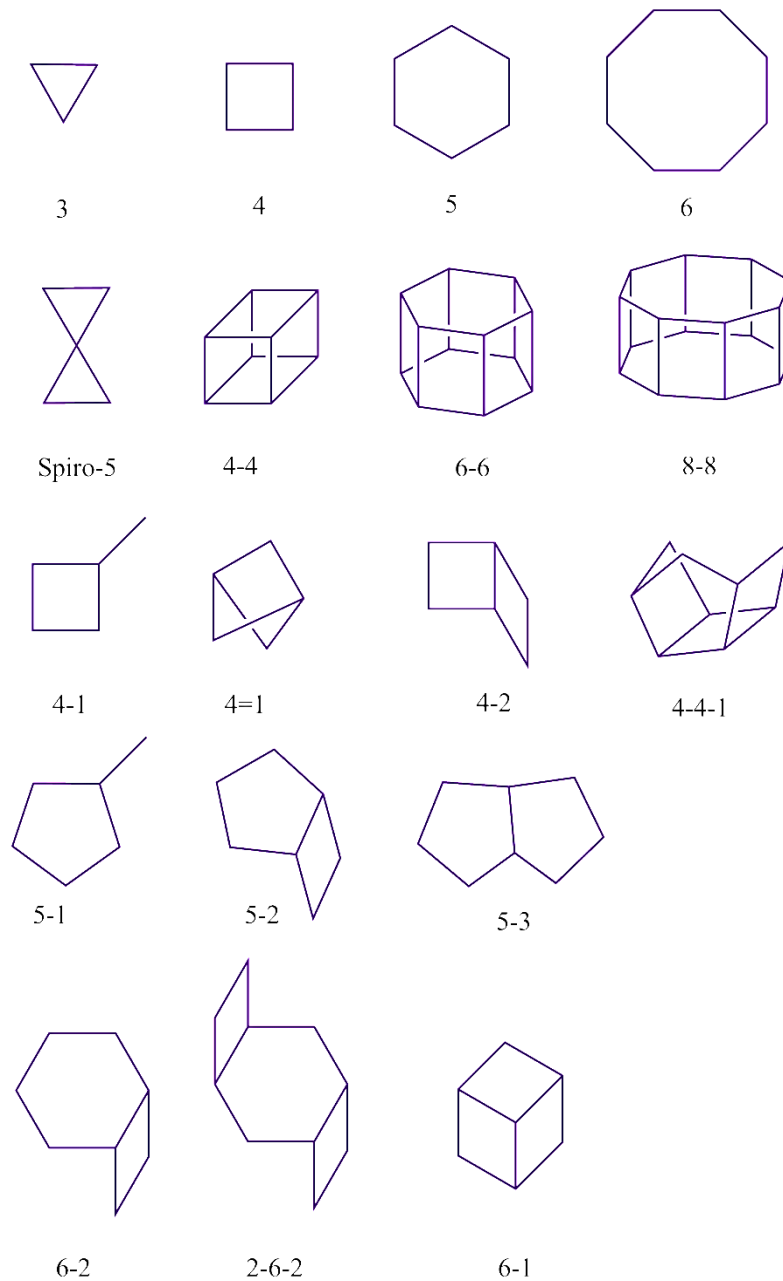
Figure 1.14 - Schematic Diagram of Secondary Building Blocks; solid black lines represent T-O-T links.

The channels or pores in a zeolite are created by the way the building blocks connect. The size and shape of these pores depends on the configuration of the SBUs and ratio of the silicon and aluminium ions[39,49,50]. Pores are assigned a ring size calculated by the number of T-atoms in the ring. T-atoms are

the central atoms, usually silicon or aluminium. Small pores have 8 T-atoms, medium pores 10 T-atoms and large pores 12 T-atoms. Pore size is usually determined by selecting molecules of a set size and investigating whether these molecules can be absorbed by the zeolite. Methane, cyclohexane, n-hexane and mesitylene are commonly used to determine pore size. Methane is absorbed by small pores, methane and n-hexane are absorbed by medium pores which also absorbs cyclohexane slowly and large pores absorb all the compounds.[55]

Each silicon atom has a +4 charge; it is connected to four vertex shared oxygens which have a -2 charge. As each oxygen atom is connected to 2 T-atoms the effective charge contribution from each oxygen atom is -1. SiO_4 tetrahedra are therefore neutral, whilst aluminium has a +3 charge, and hence AlO_4 tetrahedra have a net negative charge of -1. This charge is balanced with a cation for example sodium so the structure has no overall charge. As the cation is only weakly held by the zeolite framework they are exchangeable. Zeolites will show a preference for specific cations due to the size of the pores and the coordination number of the site; zeolites with large pores will preferentially exchange smaller cations for larger cations as there is less distance between the positive cation and the negative framework. Due to this selectivity zeolites have found many uses as ion exchangers in a variety of industries.[49,50,56–59] As well as being used as ion exchangers, zeolites are also used as molecular sieves in industrial processes due to their pores and channels; they allow ions smaller than their pore size and water to move freely through them whist restricting larger molecules, for example para xylene can move freely through ZSM-5 whilst ortho and meta xylene are too bulky.[49,60–63]

Cations have two roles within the zeolitic structure; these are to charge balance and to act as a spacer to prevent the collapse of the cages. The size of the cations absorbed by the zeolite cages are smaller than the pore they inhabit. This means that the cage must partially 'collapse' to allow coordination of the framework oxide anions to the cation. The 'collapsing' of the cage is referred to tilting. [64]

Two aluminium tetrahedra joined through an oxygen atom are energetically unfavourable due to electrostatic repulsion between the two negatively charged tetrahedra. Due to this issue, zeolites generally have ordered structures with the highest Si:Al ratio being 1:1. This is known as Löwenstein's rule and is applicable under the low temperature and pressure conditions under which zeolites are normally made. Disordered and aluminium rich frameworks have been prepared using high temperature and/or high pressure including naturally by geological means.[57,64–68]

1.6.1.4 Applications

Due to the vast array of zeolites they have found many applications, the four main uses are: ion exchangers, absorbents, catalysts and desiccants, as explained below. The application of the zeolite depends on framework structure and pore size. The structure and ion exchange capacity varies with the silicon aluminium ratio of the structure which can range from 1 to 5. [66,45,48]

1.6.4.1.1 Ion exchange

Zeolites provide a more ubiquitous alternative to classical organic ion exchangers which are less stable to temperature and pH. Zeolite frameworks with high aluminium to silicon ratio (ideally 1:1) are most desirable as they have a highly-charged framework and therefore have more charge balancing ions available for ion exchange. Ion exchange using zeolites has been used in a wide variety of industries from the clean-up of nuclear waste to softening of water in washing detergents. Zeolites are versatile ion exchangers; they are stable in a wide range of conditions and can remove several ions. By selectively choosing the zeolite based on the pore size and Si:Al ratio, zeolites can be tailored to preferentially remove specific ions from solutions containing a mixture of species.[10,56–59,63,68,69]

Clinoptilolite is used in the SIXEP processing plant in the UK to remove cations from aqueous waste before discharge.[22] One of the main concerns about the aqueous waste stream from the holding ponds is that caesium and strontium cations have high abundance, high solubility and short lifetimes. Clinoptilolite preferentially removes caesium and strontium cations from the nuclear waste streams owing to the size and coordination number of the sites in clinoptilolite being more appropriate for these two ions than the others ions in the liquor.[31,32] Clinoptilolite reduces the activity of the aqueous waste stream to a level which allows safe discharge to sea, leaving the activity trapped in the zeolite as solid waste. This process concentrates the activity into a smaller volume. The natural zeolitic clinoptilolite chosen to be used in SIXEP was carefully selected to be the most stable to radiation damage and the have the best selectively for caesium and strontium by trialling deposits from different locations across the World.[10] Enough clinoptilolite was purchased for the site after the selection process to ensure availability into the middle of the 21st century. However, this material is subject to significant geological variation even across the single site from where it is extracted. Additional minerals such as quartz and feldspar of varying quantities are present batch to batch which contributes to a variation in residence time that the zeolite spends in SIXEP; less clinoptilolite means less time before breakthrough of the active species as the material becomes saturated. The variation in the pond liquor from batch to batch as different components in the liquor etch also cause variation

in the residence time leading to a window of 30 days between the shortest and longest times.[4] Variation in the formula of clinoptilolite depending on the geological variation where it is found in the World and/or the type of ions present in solution both affect the utility. Although clinoptilolite has the highest affinity for caesium and strontium, it has been reported to remove other cations from solution in the absence of caesium and strontium. Ćurković et al. report the removal of Pb^{2+} and Cd^{2+} by ion exchange using clinoptilolite while Erdem et al. report the removal of Co^{2+}, Cu^{2+}, Zn^{2+} and Mn^{2+}. Motsi et al. report the use of ion exchange using clinoptilolite in the removal of Fe^{3+}, Cu^{2+}, Zn^{2+} and Mn^{2+} to clean-up the metal contaminated washings of a Cornish mine. Clinoptilolite is an unusual member of the zeolite family since it has never been made pure synthetically. Many synthetic zeolites are also used for ion exchange; Ríos report the use of faujasite and phillipsite for the removal of Fe^{3+}, As^{3+}, Cr^{3+}, Pb^{2+}, Zn^{2+}, Cu^{2+}, and Ni^{2+} from a Welsh mine waste stream for example. One of the most common uses for zeolites is as water softeners in cleaning; the sodium in the framework exchanges for calcium to soften the water and improve the efficacy of the detergent e.g. Zeolite A replaced phosphates in washing powder to reduce environmental damage caused by algae blooms.[57,59,68,70]

1.6.4.1.2 Absorbents

Due to the framework structure of zeolites, small molecules can be absorbed; the type of molecule adsorbed by the framework depends on the Si:Al ratio and the pore geometry. The Si:Al ratio causes the framework to be either hydrophilic or hydrophobic. Frameworks with high Si:Al ratios are hydrophobic, whereas a low Si:Al ratio causes the framework to be hydrophilic. By selectively choosing the best zeolite, the separation of gases and pollutants from water can be carried out.[37,47,71,72]

Zeolites are used to separate gases; they show high selectivity which can be tuned by selecting different pore sizes. Dehydrated zeolites show the best adsorption capacity, dehydrated chabazite absorbs water, methanol, ethanol, formic acid, n-propane, n-butane and n-heptane but excludes acetone, ether, benzene and branched alkanes such as isobutene.[73–75] Chabazite has a channel size of approximately 5 Å, and therefore excludes molecules larger than the pore opening.[76] The absorption of molecules is related to the temperature, pressure, particle size and the nature of the gas and solid. Once they have been used most zeolitic materials can be regenerated by heating or by passing a stream of gas such as nitrogen over them flushing the molecules out. Higher pressure and temperatures show a much quicker uptake of molecules by the zeolite. Zeolite Y membranes have shown selective separation of CO_2.[75,77]

It is possible to modify zeolites to target specific species; clinoptilolite was modified by Mendoza-Barron *et al.* to remove arsenic from water.[78] The use of surface modified zeolites to separate gases

using grafted organic ligands is an area of current interest. Faujasite has been modified to separate CO_2 from CH_4. MCM-41 and MCM-48 have been modified to remove CO_2 from CO_2 NH_2 mixtures.[62,70,77,79–81] Other zeolites have been modified for gas separation, ZSM-5 and EMT zeolites have also been used in this field. Alkyl silanes are often used for the modification of zeolites as the reaction of substitution of an OH group with the R-Si-O-R group is well known.[69,71,73,75,82,83]

Zeolites have also been used in the clean-up after the Chernobyl and Fukushima nuclear disasters as absorbent to stop the spread of radioactivity. Clinoptilolite has been used to prevent the spread of ^{137}Cs and a zeolite wall containing clinoptilolite to stop the migration of ^{90}Sr into the sea has been used at Fukushima. Clinoptilolite tuffs, deposits of zeolites formed from volcanic debris which are consolidated by heat and compaction, were found to reduce the uptake of ^{137}Cs by plants at Chernobyl. [31,37,84]

1.6.1.4.3 Catalysts

Zeolites have catalytic properties defined by their acidity and shape selective features, due to the rigidity of their structure. As previously discussed zeolitic channels and pore sizes are defined by the number of T-atoms and secondary building blocks which determine the framework type and overall structural arrangement. By selecting a zeolite with the desired pore size, molecules can enter the pores and are held in close spacial proximity facilitating the desired reaction. By selectively choosing a zeolite by the pore size, molecules which are the wrong size or shape cannot enter the framework excluding them from the competing in desired reaction. [47,80,85–87]

As well as size and shape selective catalysts zeolites have also been used as acid catalysts. Zeolites have shown selectivity towards specific molecules which has allowed them to be utilised as acid catalysts. Zeolites have active acid sites, both Brønsted acid and Lewis acid sites, which allow zeolites to catalyse reactions, as shown in figure 1.15. The Brønsted acid sites are the hydrogen atoms which are bonded to the bridging oxygen of the tetrahedral atoms of the framework and Lewis acid sites are electron deficient sites which contain an empty orbital which can accept a pair of electrons, for example a AlO^+ species. Examples of zeolites being used as acid catalysts can be found in the petroleum industry where acidified ZSM-5, denoted H-ZSM-5, is used as an additive to improve the octane number of the petroleum produced. H-ZSM-5 is also used in the cracking of n-hexane.[47,71,88]

Brønsted acid
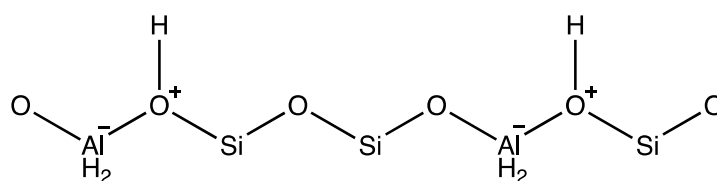
Lewis acid
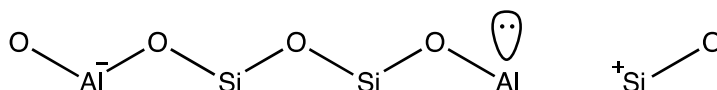
Metal replacement

Figure 1.15 – Schematic of acidic sites present in zeolites

Zeolitic materials have also been used as supports for other metals which act as catalysts. By replacing either the Si^{4+} atom with other species such as Ti^{4+} and Ge^{4+} or replacing the Al^{3+} atom with species such as Fe^{3+}, B^{3+}, Ga^{3+} and Cr^{3+} these catalytic species can be fixed into a stable framework allowing them to be used in a wide range of situations.[86]

The use of zeolites as catalyst in industrial processes have increased with the discovery or synthesis of new zeolites. For example, zeolite Y is used as a catalyst in the cracking of crude oil and petroleum, ZSM-5 is used in the production of caprolactam. Zeolites have also been modified to increase their ability as catalysts, ZSM-5 has been surface modified with alkyl chains for the catalysis of cracking n-dodecane. Modified MCM-41 is used in the basic catalysis of perfumes and in the oxidation of hydroquinones.[47,62,69,81]

The use of zeolites as catalysts has reduced the need for redox catalysts, liquid acid catalysts and expensive metal catalyst. By reducing the need for previously standard catalyst and increasing the use of zeolites and the larger family of molecular sieves there has been a reduction in toxic pollutants released into the environment and a reduction in cost and energy used in the catalytic industry.

1.6.1.4.4 Desiccants

Most zeolites contain water molecules within the structure; the water molecules are coordinated to the exchangeable cations within the lattice. Water molecules are able to move freely throughout the zeolite framework, and can be removed through heating the zeolite or using a vacuum. Once the water molecules have been removed, the cations within the zeolite move closer to the framework, to sites of lower coordination. The cations need to move to sites of lower coordination once dehydrated because when the cations have fewer coordinated bonds to water molecules they can become under-bonded as the coordination sphere is smaller. This process is reversed once the cations become rehydrated, the coordination number of the ion increases and the ions shift back to alternative sites further away from the framework.[63] Zeolites remove water from the environment and have proved better absorbents than clays, silica gels, and calcium based absorbents especially at low humidity. Zeolites can also be stable at higher temperatures and therefore require more heat to remove the water and hence have a wider range of applications. The absorption process is reversible which allows the absorbents to be reusable. They do not show a reduction in capacity even after many regenerations due to the stability of the framework, this stability allows water to be absorbed and desorbed without damage to the crystal structure. An example of this is Zeolite A which is used as a desiccant in organic solvents to remove water and prevent the solvents from becoming wet when stored in ambient conditions. Due to the stability of zeolites and the regeneration ability the use of zeolites as desiccants is increasing replacing some of the previously used desiccants such as silica gels.

1.6.2 Materials Utilised in this Investigation

1.6.2.1 Clinoptilolite

Two sources of the natural zeolite, clinoptilolite, have been used in the experimental work discussed within this thesis. A sample of clinoptilolite was provided by the NNL/NDA which is currently used in the SIXEP plant at Sellafield. The second clinoptilolite sample was sourced from Imerys minerals. The differences between these samples have been discussed above in section 1.6.

Clinoptilolite means 'oblique feather stone' in Greek and is one of the most common natural zeolites which is formed from the devitrification of volcanic glass tuffs.[89] The glass tuffs are formed by volcanic materials cooling and the formation of the clinoptilolite depends on the location and the duration and intensity of the thermal water flow. Tuffs that are close to the thermal water form fully altered stable materials, whereas ones further away are often poorly formed and most break down into clay minerals.[31] Inevitably, these two extreme situations are rare and mostly a continuum between them makes up extensive zeolite deposits generating different quantities of clay minerals and clinoptilolite in different areas, even within the same pit. While pure clinoptilolite should be colourless, it often

appears coloured due to the presence of impurity phases, for example, iron oxide occlusions gives clinoptilolite a red-brown colour.
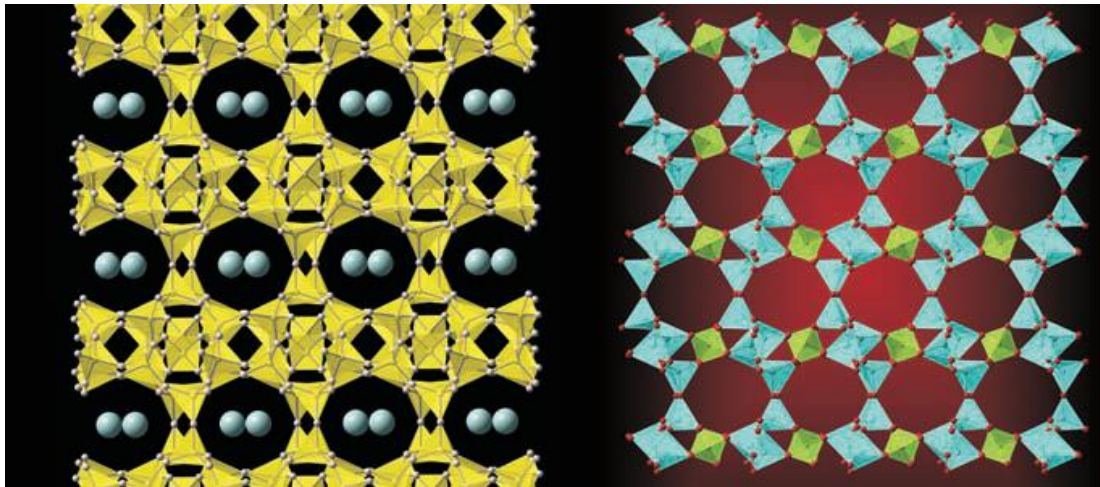
Figure 1.16 – ATOMS picture of clinoptilolite - blue triangles are SiO_4 tetrahedra and AlO_4 tetrahedra[90]

Clinoptilolite (($Ca,K,Na)_{2-3}Al_3(Al,Si)_2Si_{13}O_{36} \bullet 12(H_2O)$) is closely related to heulandite (($Ca,Na)_{2-3}Al_3(Al,Si)_2Si_{13}O_{36} \bullet 12(H_2O)$), and differs only in presence of significant amounts of potassium.[66] The structure of clinoptilolite and heulandite consists of corner-sharing tetrahedra generating a microporous framework where every oxygen is connected to either a silicon or an aluminium ion with a ratio of [Al + Si] : O of 1:2. There is a negative charge caused by the replacement of silicon with aluminium which is balanced with alkali and alkaline earth metal cations, commonly sodium, potassium and calcium. Since there are potassium, sodium and calcium rich clinoptilolite tuffs, they are distinguished by the predominant ion being added as a suffix i.e. clinoptilolite-K, clinoptilolite-Na, and clinoptilolite-Ca. Due to the wide variety of ions in volcanic tuffs across the World, clinoptilolite can also contain other cations such as iron and magnesium. Clinoptilolite is monoclinic and crystallises in the space group C2/m, containing alternate rings of eight and ten T-atoms. The rings form sheets and stack to form channels throughout the crystal structure. The size of the channels controls the size of the ions or molecules that can enter, allowing clinoptilolite to be used as a molecular sieve.[89] Figure 1.16 shows the channels of the zeolite with and without exchangeable cations. Due to its versatile nature, large pore spaces and temperature stability, clinoptilolite has many uses in industry, from ion exchangers for Cs^{2+}, Sr^{2+} and NH_4^+, to feed additives for livestock as it absorbs toxins created by mould and helps the animals absorb food. It is also used as a chemical sieve, a gas absorber, water filters, in construction materials and odour control agents e.g. in cat litter.[31–35,57,66,68,91,92] Clinoptilolite has highly

variable amounts of water in the channels due to its absorptive capacity; the water is weakly held within the framework.

Clinoptilolite is found in many locations throughout America such as Arizona, Nevada, Washington, Oregon, Idaho, New Mexico, Texas, Utah, Wyoming and California. Clinoptilolite is also found in Australia, Austria, Bulgaria, Canada, China, Cuba, Germany, Hungary, India, Italy, Japan, New Zealand, Slovakia, and South Africa, some locations are shown in Figure 1.17. Clinoptilolite is often found with other minerals such as cristobalite, quartz, feldspar and illite. The percentage of clinoptilolite in the host rock can vary from 50-90% and not all deposits are of a high enough quality to be used for ion exchange applications.[35,42,93–98]

Figure 1.17 - Map of the World showing Geological Deposits of Clinoptilolite as Red Octahedra.

1.6.2.2 ZSM-5

The synthetic zeolite, ZSM-5, has been selected to be investigated in this work due to its high silicon to aluminium ratio and previous literature that shows the ability of this zeolite to be modified with organic ligands for sequestration of different species.[69]

ZSM-5 or zeolite socony mobil-5, has a MFI framework and was patented by Mobil oil company in 1975. It a pentasil zeolite with layers created by connecting five-membered rings. The pentasil building block can be seen in Figure 1.18. The pentasil building blocks connect to form chains that then join to form layers, Figure 1.19, these connect to build a three-dimensional structure. The structure can be seen in Figure 1.16. ZSM-5 has high silica content and low alumina content and the ratio of Si:Al varies depending on the Si:Al ratio of the starting mixture. Lin *et al.* reported ratios of approximately 20-120.[99,100] ZSM-5 is synthesised using tetrapropylammonium ion ($N(C_3H_7)_4^+$ as an organic template to form the pores, which is removed by calcination after synthesis.
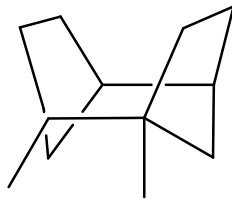
Figure 1.18 - Pentasil building block
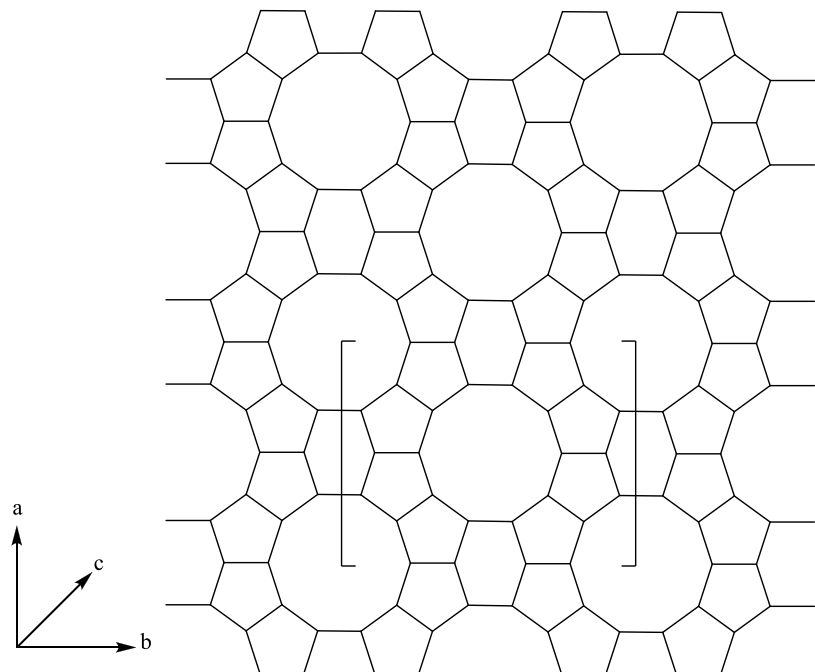
Figure 1.15 Pentasil layer

The structure of many zeolites are cubic with the channels being the same in all three lattice directions, but ZSM-5 has a more complex structure that can be seen in figure 1.20. The horizontal channels are woven around the vertical channels creating a zig-zag structural arrangement.
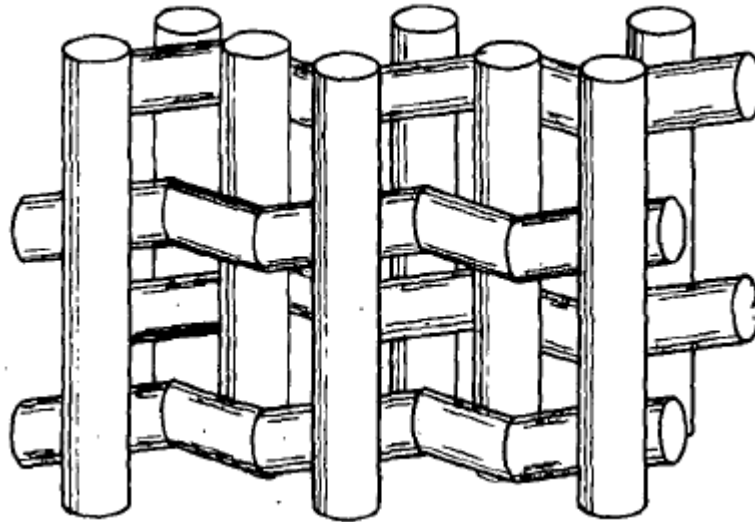
ZSM-5 has many uses; its primary function was designed for use in the petroleum industry where it is used as a heterogeneous catalyst for hydrocarbon isomerisation. ZSM-5 is also used in the catalysis of methanol into longer chain hydrocarbons for fuel use. ZSM-5 is also used as an acid catalyst when the charge balancing ion is a proton.[69,71] H-ZSM-5 is used to convert meta-xylene to para-xylene, para-xylene can diffuse rapidly through the structure whereas meta-xylene diffuses slower and becomes tapped in the structure where it is transformed into para-xylene.

1.6.2.3 Natural Clay Materials

Clay minerals are aluminium phyllosilicates, which contain variable amounts of iron, magnesium with alkali and alkali earth metal cations. Phyllosilicates are sheet silicates which are formed with a 2:5 ratio of (Si+Al):O to form flat hexagonal sheets. Clay minerals particles are typically less than 2 micrometres in size as they form from weathering of rocks and compression at high temperatures and are found in fine grained metamorphic and sedimentary rock.[96,101–103]

Clay minerals have characteristic two-dimensional sheets of corner sharing SiO_4 and AlO_4 tetrahedra. These sheets have the chemical composition $(Al,Si)_3O_4$, where each tetrahedron shares 3 of its corner oxygen atoms forming a hexagonal array. The fourth oxygen is unshared and all of the tetrahedra point in the same direction on the same side of the sheet. The tetrahedral sheets are bound to octahedral sheets. The unshared vertex from the tetrahedral sheet forms part of one side of the octahedral sheet but an additional oxygen atom is located above the gap in the tetrahedral sheet at the centre of the six tetrahedra, this can be seen in figures 1.16 and 1.17. This oxygen atom is bonded

to a hydrogen atom forming an OH group in the clay structure. If the clays are layered with one tetrahedral sheet and one octahedral sheet alternately, it is termed a 1:1 clay. If there are two tetrahedral sheets with the unshared vertex of each sheet pointing towards each other and forming each side of the octahedral sheet it is termed a 2:1 clay. The clay can have an overall negative charge depending on the composition; this charge is balanced by an interlayer cation such as sodium.[104–106]

The layered structure of clays means they disperse evenly through aqueous solutions and can remove and release ions in solution. Clay minerals have charged layers so they are also able to exchange ions in a similar way to zeolites although the layered arrangement is less restrictive than the zeolite structure. Clays are often used to prevent contaminants from dispersing. Many types of clay swell in water and can experience swelling and shrinking depending on the cation present. If the interlayer cation is originally sodium and is replaced by a larger cation such as caesium, the interlayer space will swell to accommodate the larger cation.[36,107,108] This is reversible and hence the swelling and shrinking of the structure. Donat et al reported the clay sepiolite removes uranium from solution and Smith et al report the use of bentonite to remove cobalt from solution.[109]

Two clays were selected for study, these were a 2:1 clay, vermiculite and a 1:1 clay kaolinite. Vermiculite has exchangeable cations whereas kaolinite does not contain exchangeable cations. The two clays were selected to allow two different clays with different properties to be investigated.

1.6.2.4 Vermiculite

Vermiculite is a 2:1 layered clay with an octahedral sheet between two tetrahedral sheets, shown in Figure 1.21. Vermiculite has the general formula $(Mg,Fe,Al)_3((Al,Si)_4O_{10})(OH)_2.4H_2O$ and is brown/yellow in colour. It has a high ion exchange capacity, exchanging its interlayer cations. It was discovered in 1824 in Massachusetts, America, and is not often found in large quantities, this could be because vermiculite is a weathering or hydrothermal alteration product of biotite or phlogopite.[37,103,107,110] Vermiculite is a high capacity ion exchanger and readily forms complexes with organic materials.
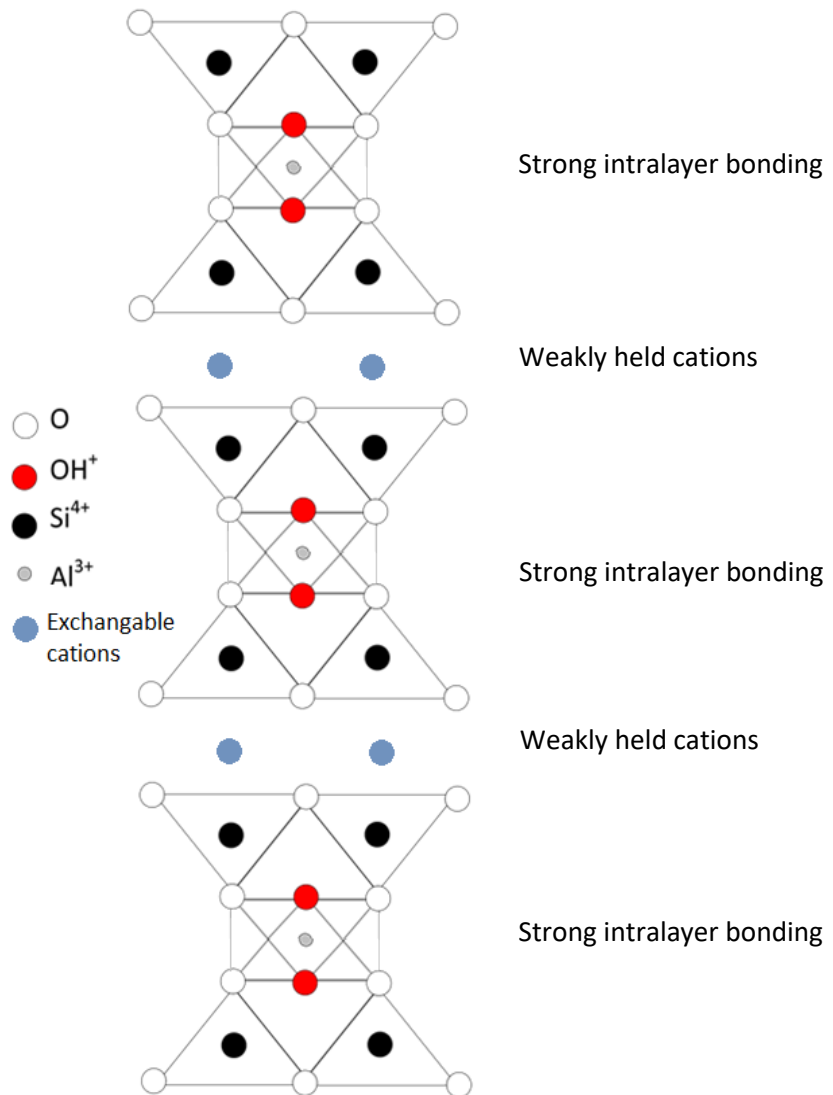
Figure 1.21 Structure of Vermiculite

Vermiculite has found many uses due to its unique properties. Vermiculite is treated and dried. It is then expanded in a process called exfoliating by heating the mineral. After this process vermiculite becomes a light weight, absorbent, compressible, non-combustible and non-reactive material. This has led to it finding uses in insulation, as a concrete additive, as a fireproofing material and as an absorbent packing material. The use of vermiculite for high temperature insulations and as friction linings has arisen due to its thermal stability and mixing ability with other materials. Vermiculite is added to concrete to allow easier handling of the material, improve fire resistance and coverage. Vermiculite is also used as a soil additive, where it absorbs nutrients and prevents them from being washed out of the soil.[10,12,36,63,96]

Kaolinite is a 1:1 clay mineral with alternating tetrahedral and octahedral sheets; this can be seen in Figure 1.22. It has the general formula $Al_2Si_2O_5(OH)_4$, and is generally white in colour, though may have a red/brown tint that arises from iron impurities in the clay. Kaolinite varies very little in composition; it does not absorb water and therefore does not show the expansion of vermiculite when in contact with water. It is formed as a secondary mineral from the weathering of other alumina-silicate minerals. It is distinguished from the other clay minerals by the fact that no exchangeable cations lie between the layers.[111,112]
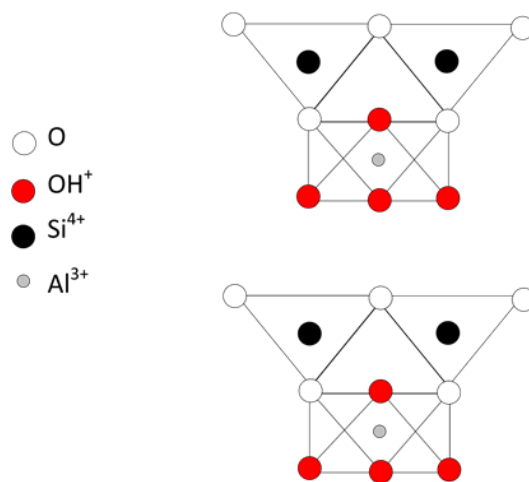
Figure 1.22 Structure of Kaolinite

Kaolinite is one of the main components of kaolin (China Clay), and gives it its distinctive white colour. Kaolinite is found throughout the world, from Australia to the United Kingdom, including the china-clay pits in Devon and Cornwall. It is a common mineral and is often found with quartz, feldspar and muscovite. Kaolinite has a wide range of uses, one use is in the paper industry as a filler and as coating due to its colour and chemical inertness, it also improves the surface smoothness and appearance. Kaolinite like vermiculite is also used as an additive to concrete to improve strength and durability. Kaolinite has also found uses in agriculture as a carrier in fertilisers and pesticides due to its small particle size, inert chemical properties and ability to be used in a spray. The use of kaolinite in agriculture limits the damage of plants due to excess water, and allows the event spread of fertilisers over crops. Kaolinite is used in paints as an additive to improve the texture and reduce the use of expensive pigments. Kaolinite is used in paints due to its small particle sizes; it improves the processing, storage and application properties of the paint. Due to the chemical inertness of kaolinite it has also found use in the cosmetic industry.[10,37,44,68,70,96,102,109,113–115]

1.6.3. Properties relevant to this Investigation

1.6.3.1. Ion exchange

Ion exchange is a common procedure used for the removal of ions from aqueous waste streams including those containing radioactive species. Ion exchange in its simplest form is the exchange of ions between a complex and an electrolyte, or between two electrolytes.[10,57,116] The process is most successful for large, low charged ions that have a small hydration radius. This means that while species such as potassium and sodium cations exchange relatively readily, lithium is not easily exchanged due to a large hydrated radius. In terms of the species present in the SIXEP plant, caesium and strontium cations are the most abundant and are good candidates for ion exchange due to their large size and low charge.[10,56,92,113] However, uranium and plutonium speciation is complex with the highly charged cations actually being present as oxo (e.g UO_2^{2+}) or hydroxyl species (e.g $Pu(OH)_4^+$) rather than the uncoordinated cations.[9–11,23,85,117,118] The efficacy of ion exchange reagents is also affected by the size/coordination number of the site and its availability in a structure; open channels and layers are easier than condensed structures. For this reason clays and zeolites are some of the most well-known ion exchangers in inorganic solid state chemistry. Mixed oxide ion exchangers, zeolites, clays and acid phosphates use a network of channels, cages of layers to accommodate ions whereas some materials such as hydrous oxides only exhibit ion exchange on the surface of the material. The overall framework of zeolite is largely unaffected by the exchange of ions due to its rigid three-dimensional structure. Clays and other layered ion exchangers undergo swelling or shrinking due to cation ion exchange of different size ions. Ion exchange plays an important part in the nuclear fuel cycle from start to end, and remains an area of interest in the clean-up of nuclear waste streams; selective removal of ions from radioactive waste effluent streams, reprocessing of nuclear waste and purification of ore.[14,119,120]

Ion exchange was originally seen in soils, where the ion exchange materials were found to be clays, zeolites, glauconites and humic acid. The first commercial ion exchangers available were amorphous aluminosilicate gels, which were unsuitable for use with acidic solutions. Organic ion exchange resins were developed which were stable and uniform under acidic conditions and could be controlled by the synthesis procedure used.[56] These resins were however not suitable for use in the nuclear industry, which require ion exchangers that were stable to radiolysis and heat. Alongside the developments of new nuclear facilities, zeolite chemistry had seen a rapid expansion with research by R.M. Barrer developing zeolites specifically for use as catalysts and sorbents in different conditions.[49] As a result of advances in zeolite chemistry, zeolite A replaced phosphates in detergents to act as an environmentally friendly water softener by removal of the hard water ions via ion exchange. This meant that the amount of zeolite A used rapidly exceeded the tonnage of all organic resins used in any application.[48,50,53,54,56,121,122]

Inorganic ion exchangers are highly selective for some metal ions, have good radiation stability and are more compatible with encapsulation processes than their organic counterparts. These factors are considered more important in the radiochemical context than some of the other properties of organic exchangers which include greater exchange capacity and low pH stability. As previously discussed, clinoptilolite is used in the removal of caesium and strontium cations from nuclear waste due to its high selectivity for those ions over many others cationic species present in waste ponds. Inorganic ion exchangers are also often used in the treatment of nuclear waste effluents; e.g. fuel pond water or floor drain waters in nuclear power plants. The use of inorganic ion exchangers in nuclear waste streams has allowed a significant reduction in the volume of waste, reducing the cost and the release of harmful metals into the environment.[4,8,10,14,16,23,63,70,123]

While this thesis concentrates on the SIXEP process which restricts the materials of interest, there are many other types of inorganic ion exchangers that have been used in radiochemical environments[10,31]. Ferrocyanides (FCN) have been used for a long time in the treatment of radioactive wastes, but these species have to be supported on a silica matrix due to their fine powdery consistency not being compatible for use in columns or under flow conditions. Potassium nickel ferrocyanide has been investigated for the separation of radiocaesium from high pH solutions of 11.5 and has shown good uptake under these conditions. The sample showed good radiation resistance and the uptake of the material was similar to the pure ferrocyanides. [124]

A group of inorganic ion exchange materials produced specifically for nuclear waste remediation are CsTreat, CoTreat, CsFloc and CoFloc which are selective for radiocobalt and radiocaesium, depending on the prefix, from nuclear waste.[10,56,57] The exact composition of these materials is difficult to determine as they remain commercially sensitive, but they are described as 'inorganic titanosilicates'. Kinetic analysis indicated that the uptake of species in these materials was controlled by diffusion. Caesium removal was unaltered by the addition of competing ions, however the cobalt uptake clearly decreased by increasing the calcium cation content of the solution; calcium rich solutions are often used in nuclear waste experiments to mimic the effects of encapsulation in concrete where portlandite ($Ca(OH)_2$) is common. In a similar vein to CsTreat and CoTreat, SrTreat is a inorganic titanium oxide ion exchanger that has been designed to remove strontium cations from radioactive waste streams effectively. In 1996, this material was introduced in an industrial plant in Murmansk, Russia. It is able to be used in high pH waste streams such as the aqueous streams from nuclear fuel storage ponds. CoTreat and a chelating aminophosphonate resin were investigated for ion exchange removal of metals and was found to be efficient in removing transition metals, alkali-earth cations (strontium and calcium) and arsenic from solution.

As well as the clinoptilolite that is used in the SIXEP plant, a number of other zeolites have been used in the treatment of radioactive waste. The zeolite, mordenite, was investigated via a batch methodology for the sorption of caesium. [137]Cs was used as a radiotracer with an inactive caesium carrier to investigate concentration, pH, temperature and particle size. A sorption of 19 kg Cs/kg was achieved. A higher temperature caused a sorption decrease, suggesting the reaction is exothermic.[115] A synthesised analogue of heulandite was used to investigate the study of Th(IV), Eu(III), Sm(II), and Fe(III)) recovery from aqueous waste via batch experiments.[125] Metal ion concentration, pH, mass of sorbent, time and temperature were all investigated. It was found that the pH had a large influence on the sorption due to the formation of different metal species. Heulandite showed maximum sorption affinity for Eu(III) and Fe(III). A permeable treatment wall (PTW) consisting of natural zeolite was investigated for the removal of strontium-90 from groundwater at the West Valley Demonstration Project (WVDP), Buffalo, NY. The removal was investigated in the presence of competitive ions Na^+, K^+, Ca^{2+}, Mg^{2+}, Sr^{2+}. The PTW is a viable method for the removal of radioactive strontium from groundwater.[31,57]

Zeolite A and hydrotalcite were investigated for their utility for the removal of uranium species from solution using batch experiments. The concentration, pH, solid/liquid ratio and temperature for the removal of UO_2^{2+} by NaA from an aqueous solution were studied.[121] The rate of removal was believed to be controlled by the chemical sorption process which is due to the diffusion of the ions through the channels. However as no change to the structure of the zeolite was seen after ion exchange the probability that this really an ion exchange process is low; the size of the ring window in zeolite A should not allow passage of the large uranyl species and the cell parameter of zeolite A is sensitive to ion exchange.[10,21,33,56] The removal of uranium by calcined hydrotalcite was investigated in acidic and basic aqueous systems. The uptake of uranium was found to be preferred in the acidic environment with the calcined hydrotalcite having an uptake of 5 to 200 mol mL^{-1}. The removal of uranium from solution is important due to its toxicity and mobility.[94] Under standard environmental conditions uranium exists as a mobile hexavalent ion and migrates as the hydrated uranyl ion. Two types of chabazite from Italy and Scotland were investigated using a batch method for their potential to remove uranium from solution under acidic pH 3-4 conditions using the natural and sodium exchanged versions.[10,63,126] The samples were shown to be able to remove between 23-34 mg/g of uranium from solution. The mechanism for the removal of the uranium was found to be surface sorption processes such as adsorption and surface precipitation rather than ion exchange. The removal of [137] Cs, [90] Sr, [90] Y, [144] Ce, [238] U and [239] Pu species from aqueous solutions containing the zeolite was investigated. Two types of interactions; exchange and adsorption, which were dependant on the type, nature, and size of the ion. It is postulated that in the case of cerium, yttrium, uranium and plutonium at between pH

4.5 and 7 the interaction is due to attraction between positively charged elements and the negatively charged zeolite surface whereas for caesium and strontium, the process is ion exchange. These results are in good agreement with previous hypothesis that uranium and plutonium are unlikely to be present as uncoordinated cations due to their high charge.[10]

Removal of ions from real world situations have been carried out using zeolites, albeit not always intentionally. An example of this was the hyperalkaline high level waste leak from underground storage tanks at the US Department of Energy's Hanford site.[10,12,16,58] The solution on contact with sediments caused the surrounding silicate minerals to dissolve and precipitate new aluminosilicate minerals including zeolites. These phases have been identified as cancrinite, sodalite, LTA zeolite, and allophane. An investigation into caesium incorporation into these phases and determination the resistance of incorporated Cs^+ to ion exchange and mobility. The exchange of caesium in sodalite and cancrinite was 20% and <55% respectively, the exchange of caesium in LTA zeolite and allophane was 94–99%.

A Chinese sample of clinoptilolite was treated with sodium hydroxide in a hydrothermal reaction to transform the sample into modified zeolite Na–Y. The two samples, clinoptilolite and Na-Y, were exchanged with potassium, calcium and magnesium ions. The clinoptilolite sample showed preference for the ions in the order $K^+ > Ca^{2+} > Mg^{2+}$, the treated Na-Y sample showed a reverse order preference of $Mg^{2+} > Ca^{2+} > K^+$, reflecting the change in the ring size and coordination numbers in the two zeolites.[100] An Iranian clinoptilolite sample was investigated for the abilities to take up barium, calcium, potassium and sodium cations from aqueous radioactive waste. A pre-treatment of the zeolite to create sodium and ammonium exchanged forms, showed that the uptake of the ions could be increased between 7 to 100 times when compared to the untreated sample. All of the samples showed a selectivity of the ions in the following order of $K^+ > Ba^{2+} > Ca^{2+} > Na^+$. [31]

Zeolite composites have been investigated for the removal of actinides. A novel chitosan/ clinoptilolite composite was investigated for the removal of UO_2^{2+} and Th^{4+} ions by variation of contact time, metal ion concentration, sorbent mass and temperature.[33,127] The adsorption capacity for thorium was 328.32 mg/g, and uranium was 408.62mg/g. Under the addition of competing ions, a selectivity series of $Cu^{2+} > UO_2^{2+} > Fe^{2+} > Al^{3+}$, and $Cu^{2+} > Th^{4+} > Fe^{2+} > Al^{3+}$ was observed. A natural clinoptilolite was Na exchanged and investigated for the removal of thorium from aqueous solutions. Concentration, time, solid:liquid ratio, temperature and pH on the removal efficiency were investigated via batch experiments. The pH of the solution strongly influenced the sorption, with the highest sorption occurring at pH 4.

The sorption properties of manganese oxide coated sand (MOCS) for uranium in aqueous solution were studied via batch methods. Contact time, salt concentration, competitive ions, temperature and uranium concentration were investigated. The mechanism for the removal was found to be surface adsorption and pore diffusion with 1.75 mg/g removal achieved.[128]

1.6.3.2 Use of Zeolites and Clays as Solid Supports

Aluminosilicates such as zeolites and clays also have the ability to act as inorganic supports.[62] Both zeolites and clays have a high surface area and porosity and good availability of surface hydroxyl groups that act as reaction sites. These hydroxyl groups can anchor organic ligands hosting functional groups which can immobilise metal ions. This process that is known as surface functionalisation or modification, has been used to selectively sequester many metal ions from solution including Fe(II),Cu(II), Ni(II), Cd(II) and Pb(IV) onto both clays and zeolites. [57,129]

Much of the work in this area has been concentrated on mesoporous materials rather than their microporous counterparts. For example, mesoporous silica modified with 2-aminothiazole was shown to selectively remove Hg(II) in solutions containing a mixture of species.[116] The reason that these mesoporous materials are favoured in this context is that the level of surface modification possible is much higher than for their microporous counterparts. The highly crystalline microporous materials tend to be grafted to much lower level of less than 5%. Surface roughening of the materials using different mild acids such as citric acid has however significantly improved the amount of sites available for modification. [130,131]

Gopalan et al reported that actinide species could be selectively complexed through the use of carefully chosen ligands.[132] Polyhydroxamate chelators were designed and evaluated for the purpose of removal of actinides from waste waters using the polymer as a solid support to form an extraction system. In a similar way to that described for ion exchange reagents, this acted to concentrate the activity and reduce the volume of waste by having all the species captured in one place on the polymer. These polymers have a hydrophilic backbone for use in aqueous media and are available in a number of different molecular weights. As well as the water soluble materials, Gopalan also produced a group of materials that were water insoluble. These chelating species were shown to have good selectivity for plutonium in a 0.1 M nitric acid solution, removing more than 90% of the Pu(IV). These authors found that a mixture of nitrogen and oxygen chelating groups were important for the sequestration of the actinide. The same researchers, also carried out a similar study on the UO_2^{2+} species and its propensity for removal using similar ligands over the range pH 2-7. Between pH 3 and 7, ca 85% of the uranyl placed in solution was sequestered using these type of ligands. Silica has been

used as a support by several researcher in order to anchor different polymeric groups for the extraction of harmful ions.[133] Panahi and co-workers, grafted silica gel with an iminodiacetic acid polymer to produce a material capable of extracting divalent copper from water.[134]

By copolymerisation of N,N-dimethylacrylamide (DMAA) and a functional monomer containing a chelating group, 1-(N,N-bis-carboxymethyl)amino-3-allylglycerol, onto the silica surface that had been previously modified with (3-mercaptopropyl) trimethyloxysilane, the surface modified silica was generated. Functionalisation of silica was carried out by Holt et al in order to investigate the utility of the anchored 3-aminorpropyltriethoysilane (APTES) ligand for the removal of Co(II), Ni(II) Cu(II), Cd(II) and U(VI) species from solution. By using different forms of silica with varying particle size and available silanol groups between 1.51×10^{-3} mol g^{-1} and 1.63×10^{-3} mol g^{-1} of APTES was placed on the surface. Solutions containing the uranyl ion, UO_2^{2+}, showed a 10 fold reduction in the species remaining in solution after four weeks in contact with the modified silica from 17 ppm to 1.6 ppm at pH 4.7 using 50mg of material in 45 mL of solution.[135]

1.7 Aim

This research project aims to use the process of surface modification via functionalisation of the surface silanol groups using different polymers to improve the utility of the clinoptilolite used in the SIXEP process.   While sand beds are used in the SIXEP process, the pH range identified for extracting high quantities of ions (typically pH 4) using ligand modified sand is not compatible with this process. The sand beds receive solutions at between pH 11 and 11.7. Therefore instead of looking at modification of the silica, the focus here is on the clinoptilolite beds where the pH is 7 and the ligands should be more appropriate for good functionality of the ligands.   Although it is the modification of clinoptilolite which will be of most interest to the Nuclear Decommissioning Authority that commissioned this project due to a 30+ years of remaining material in storage, other zeolites and clays have been investigated for removal of plutonium, uranium, caesium and strontium from solution.

The objectives of this work are focussed on improving the sequestration capability of the SIXEP process by either improving the functionality of clinoptilolite through surface modification using chelating polymers or addition of other organic-inorganic hybrid prepared from zeolites or clays to the plant.

Functionalisation of the clinoptilolite to sequester uranium and plutonium must be achieved without reduction in the caesium and strontium cation exchange capability, thus active experiments on all four species are carried out to determine the removal with and without the presence of the ligands to ensure that the uptake of non-actinides is maintained.

If successful, increased functionality will increase the residence times of the clinoptilolite beds and reduce the waste generated.

Summary of key research steps

1. Prepare a family of surface-modified aluminosilicates from the zeolite and clay group using several ligands with varying numbers of nitrogen and oxygen donors

2. Characterise the materials prepared in (1) to determine the amount of ligand sequestered and compare the performance of free and anchored ligands.

3. Undertake absorption/desorption experiments under batch conditions to examine the makeup of caesium, strontium, uranium and plutonium species of concentrations of relevant to the SIXEP process.

Chapter Two – Analysis Techniques

2.0 Introduction

The characterisation of inorganic-organic hybrid materials requires various techniques to allow structure and composition to be determined. Techniques used to examine the inorganic host material are not always ideal for evaluating the organic grafting ligands and the amount of ligand grafted; therefore, techniques which allow inorganic/organic materials such as SSNMR have been used to evaluate the solid-ligand interface. Radiometric techniques have been used to determine the sequestering ability of the materials, for both ion exchange and uptake by the grafted ligands. The techniques used to investigate these materials are briefly discussed below.

2.1 Material Characterisation

2.1.1 Nuclear Magnetic Resonance Spectroscopy (NMR)

NMR allows short-range structural information about samples to be determined. Both solution and solid state NMR have been used in the characterisation of the materials prepared in this work.

The fundamentals of NMR are the same for all techniques used. NMR spectroscopy uses the basic principle of the atomic nucleus involved in the measurement has a nuclear spin (I), which has values of ½, 1, 1 ½, 2, etc. The value of the nuclear spin is dependent on the mass number and atomic number of the nucleus.[136,137] This can be seen in Table 2.1.

Table 2. 1 - Table relating the nuclear spin to atomic properties of the nucleus

Mass number	Atomic number	Nuclear spin
Odd	Even or Odd	½, 1 ½, 2 ½, etc.
Even	Even	0
Even	Odd	1, 2, 3, 4, etc.

From the above table it can be determined that ^{12}C which has an even mass number and even atomic numbers has a zero spin, and is therefore NMR inactive. Whereas ^{2}H has an even mass number but an odd atomic number and therefore has a spin of 1. The nuclear magnetic moment (μ) of the nucleus is directly proportional to the spin, shown in equation 2.1.

$$\mu = \frac{\gamma I h}{2\pi}$$

Where, γ = magnetogyric ratio which is a constant for each nucleus. The spin of each nuclei can interact with other nuclei through chemical bonds or spatial proximity; the interactions are dependent on orientation of the spin. When a magnetic field is applied to a sample the nuclear moments orient themselves, the total possible number of orientations is $2I+1$; this is termed as the magnetic quantum number, m_I. The selection rules for NMR transitions are that m_I can only change by one unit, therefore the orientations seen are I, I ± 1 and –I. So for a nucleus with I = 3/2 the possible orientations are: 3/2, 1/2, -1/2 and -3/2. For a nucleus with spin ½ the orientations seen are 1/2 and -1/2. An example of the energy levels for a nucleus with spin 3/2 can be seen in figure 2.2.[137]
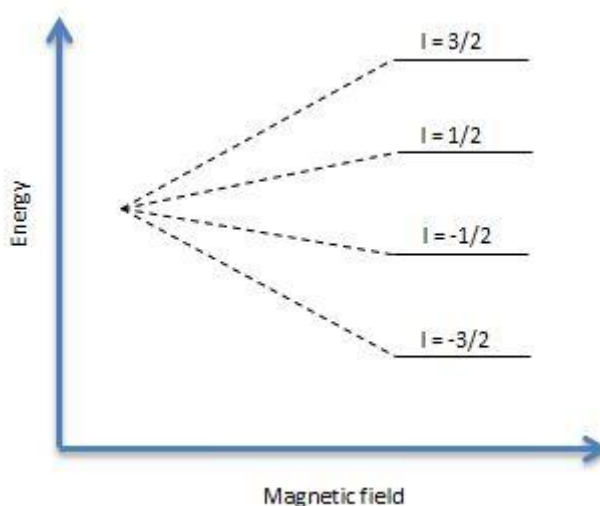
Figure 2.2 - An example of the possible energy levels that can be seen in NMR for a nucleus with spin 3/2

The more stable state (+ 1/2) is the lower energy state and is termed α, the higher energy state is termed β. The transitions of α→β correspond to the adsorption of energy, causing the lower energy state to transfer to the higher energy state. The transition β→α is conversely the emission of energy when the higher energy state switches to the lower energy more stable state. If the number of α and β were equal than no spectrum would be seen. However, β ‹ α causing a net absorption of energy which give rise to the signal recorded. In NMR the sensitivity is intrinsically low due to tiny population differences between the spin states, when compared to other techniques such as IR and UV. The sensitivity of the nuclide is determined by the magnetogyric ratio (ϒ) and abundance of the nuclide.

Nuclei are termed quadrapolar if the spin quantum number (I) is greater than a half. In SSNMR only one nucleus can be studied at a time. Given that the NMR signal is directly proportional to the number of nuclei present by using a stronger magnet more sensitivity is gained. The differences in the energy between the states are governed by Equation 2.2.[136]

$$\Delta E = \frac{\gamma h B_o}{2\pi}$$

Where, B_o is the strength of the applied magnetic field. B_o is the strength of the applied magnetic field but the magnetic field actually experienced by the nucleus is B_{eff}. The magnetic field experienced by the nucleus is not the same as B_o as the nucleus experiences shielding due to the surrounding electrons which can induce a magnetic field. This effect is termed shielding and is defined by the equation 2.2.

$$B_{eff} = B_o(1 - \sigma)$$

Where, σ is the shielding constant. The shielding constant is dependent on the surrounding environment; this can cause a shift in the observed frequency. The equation 2.2 shows that the B_{eff} is strongly influenced by the shielding. When the degree of shielding increases the B_{eff} will decrease which will cause the observed peak being observed as a lower chemical shift (ppm). For a decreased shielding effect the observed peak will be observed at a higher chemical shift (ppm). This effect is shown in figure 2.3. An example of this is when the nucleus is close to an electron withdrawing group such as oxygen, this causes a shift downfield in the spectrum as the nucleus is deshielded, therefore the peak is seen at a higher ppm value. [137,138]
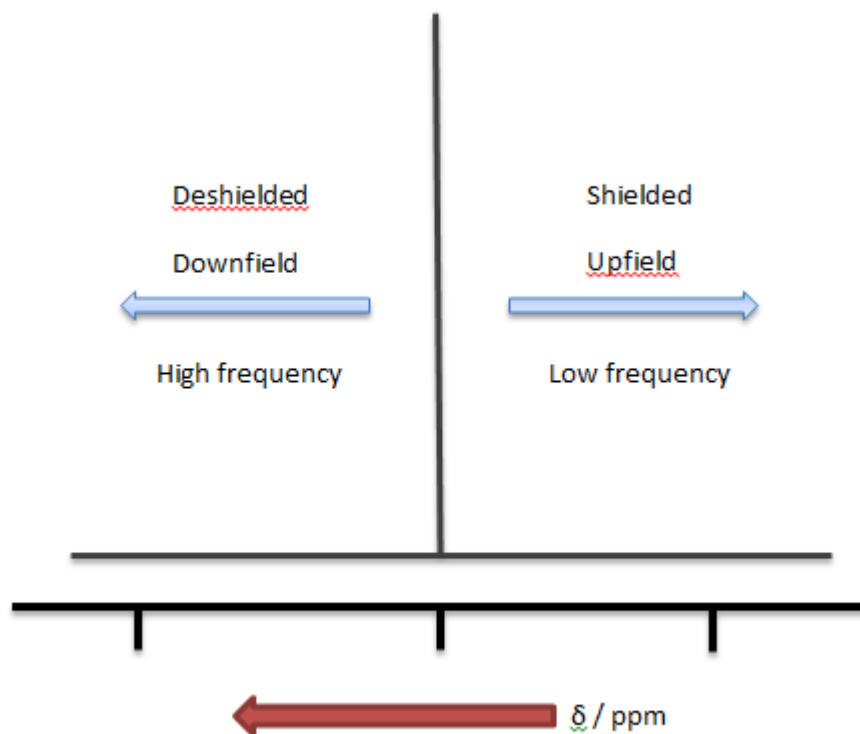
Figure 2.3 - Diagram showing the chemical shift due to the effect of shielding in NMR

When a sample is subjected to a magnetic field the spin of the nuclei undergoes a net magnetisation, as seen in Figure 2.4. This causes the individual magnetic moments of the sample to preferentially align to the applied field.
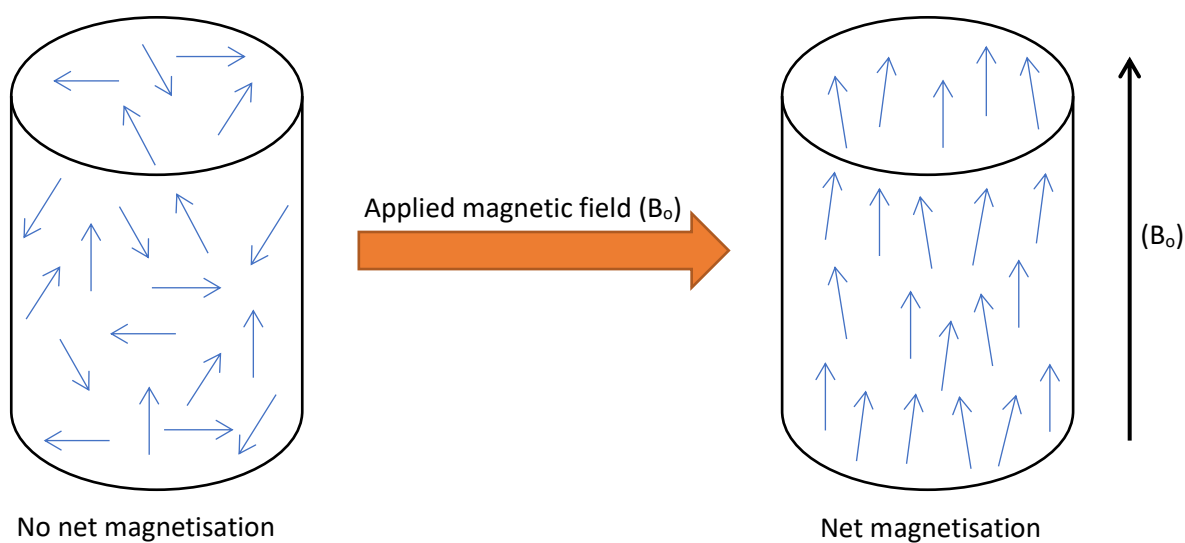
Figure 2.4 - Figure showing magnetic effect on nuclear spin when a magnetic field is applied

The external magnetic field is applied to a sample via an electromagnetic wave; in this case a radio wave is used to align the spin moments of the sample to either α or β. The net magnetisation of the sample is then measured as a spectrum using an alternating radio frequency. By alternating the frequency of the radio waves the sample is allowed to relax to a lower energy state and the resonance this creates is detected and converted to an NMR spectrum.[137]

The peaks associated with different groups are due to the different surrounding atoms; for example a hydrogen atom near an electron withdrawing atom will require a higher frequency to flip orientation than a hydrogen atom near an electron donating atom. Therefore due to the Equation 2.4, a peak associated with a hydrogen atom near an electron donating atom would be seen at a higher ppm value and the reverse is true for a hydrogen atom near an electron donating group, a lower ppm would be observed. As NMR frequencies are difficult to measure the output is record as a chemical shift δ in ppm, this also allows spectra from different magnets to be compared.

$$Chemical\ shift\ (ppm) = \frac{Peak\ position\ (Hz)}{Spectrometer\ frequency\ (MHz)}$$

<div align="right">**Equation 2.4**</div>

2.1.2 Solid State NMR

Solid state NMR (SSNMR) is used to determine structural information about materials which are not suitable for solution NMR, such as solids which are not soluble. In solution NMR sharp peaks are observed due to the averaging of the directionally dependant interactions due to the Brownian motion (random movement of the molecules within liquids). In SSNMR broad peaks are observed due to the interactions not being averaged by this random movement. Two of the most observed directionally dependent interactions are dipole coupling and chemical shift anisotropy (CSA); other influencing effects include anisotropic J-coupling.

In a solid sample the dipole-dipole couplings can be seen between hydrogens within molecules and with neighbouring molecules via hydrogen bonding. This is a large influencing factor as the Brownian motion is not possible. Dipole interactions (D) are influenced by three terms; the distance between the nuclei (D α $1/r^3$), the nuclei involved in the interactions and their gyromagnetic ratios (D α γ_A-γ_B) and the angle of the interaction relative to the applied magnetic field (D α $3cos^2\theta$-1). To suppress the influence of the (D α $3cos^2\theta$-1) interaction magic angle spinning (MAS) is used. This is used to remove the dipolar couplings and other anisotropic interactions. In solution NMR the random movement of

the molecules within liquids averages the $(3\cos^2\theta-1)$ term to zero. The first two terms are hard to influence and therefore the dipolar interactions relating to the third term are removed to provide more defined peaks in the spectra. In order to produce improved data from SSNMR techniques such as magic angle spinning (MAS) and cross polarisation (CP) are used.[136,139]

2.1.2.1 Magic angle spinning

The magic angle spinning utilises spinning the sample and the angle 54.74 ° to replicate the random movement of molecules within solution NMR. At this angle, the term $(3\cos^2\theta-1) =1$, however if the rate of spinning is greater than or equal to the magnitude of the anisotropic interactions the term $(3\cos^{preffer}\theta-1) =0$. To achieve this the sample is tightly packed into a rotor, moved to the angle 54.74 ° and spun at a high rate ranging from 1-35 KHz. Most solid state samples consist of powders and so the probability of the atom being at the magic angle is low. However, due to the spinning of the sample non-orientated spin-pairs which are not aligned to the magic angle will produce a cone shape when spun; the geometric average of this cone is the magic angle. Therefore the spins not aligned to the magic angle experience effective MAS, achieving the same effect as aligned spins if the spinning speed is sufficient, explaining why such high spin speeds are used. A schematic of MAS can be seen in figure 2.5.

B_o

Cap

Roto

54.4
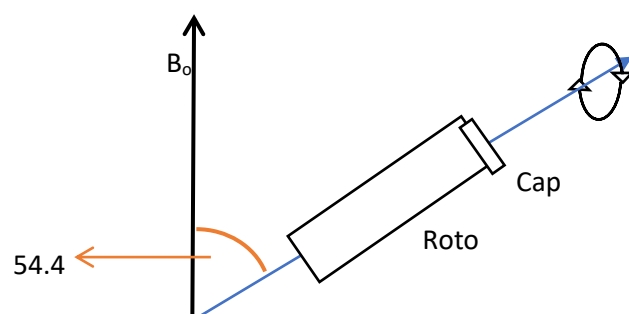
Figure 2.5 - Diagram showing the MAS in SSNMR

Chemical shift anisotropy cannot be removed by decoupling, only by magic angle spinning. The contribution by CSA can be large for molecules with low symmetry. To reduce the magnitude of the anisotropic interactions the sample is spun at a high speed. If the speed is less than the magnitude of the anisotropic interactions then they are not high enough to remove the CSA. This causes a series of spinning side bands (SSB) to be seen, the SSB are separated by multiples of the spinning speed. Increasing the speed of the sample can cause the SSB to be 'spun out', however this is not always possible depending on the nature and stability of the sample and suppression pulse programs may be used.[139]

2.1.2.2 Cross polarisation

Cross polarisation is used to allow less sensitive nuclei to be studied. It allows the polarisation of abundant nuclei such as ^{1}H to be used to enhance the signal to noise ratio of low abundant spins such as ^{13}C. NMR spectra are built up using many scans, by adding the scans together signal noise is increased and the background noise averages. The time between scans is dependent on the relaxation time of the nucleus being studied. The relaxation time is important as scanning too rapidly will result in over saturation of the magnetisation resulting in no signal, whereas long relaxation times results in wasted instrument time. The relaxation time for a solid crystalline material containing ^{1}H and ^{13}C are 10-300 s and 60-3000 s respectively. This is compared to an amorphous or poorly crystalline solid where the relaxation times of ^{1}H and ^{13}C are 1-60 s and 2-60 s respectively. By using cross polarisation to study ^{13}C shorter relaxation times can be used when compared to direct polarisation (DP).

CP works by transferring the nuclear magnetisation from ^{1}H to ^{13}C. For the transfer of energy to occur the nuclei must be dipolar coupled to each other.

A magnetic field is applied to the ^{1}H within the sample creating an applied magnetic field. This is then subjected to a 90° pulse. The energy is then transferred to the ^{13}C in the sample via a ramped program. The purpose of the ramped program is to cover a range of frequencies allowing transfer via all possible ^{1}H – ^{13}C bonds, as the frequency required is different depending on the environment and nature of the H – C bond. After the CP step has occurred the protons are decoupled, preventing any further energy transfer and the spectra for ^{13}C is collected. The last two steps after the CP occur simultaneously. This process can be seen as a schematic in figure 2.6. As the protons with in the sample relax faster that carbon nuclei this allows more scans over a much shorter period generating a better signal to noise ratio.
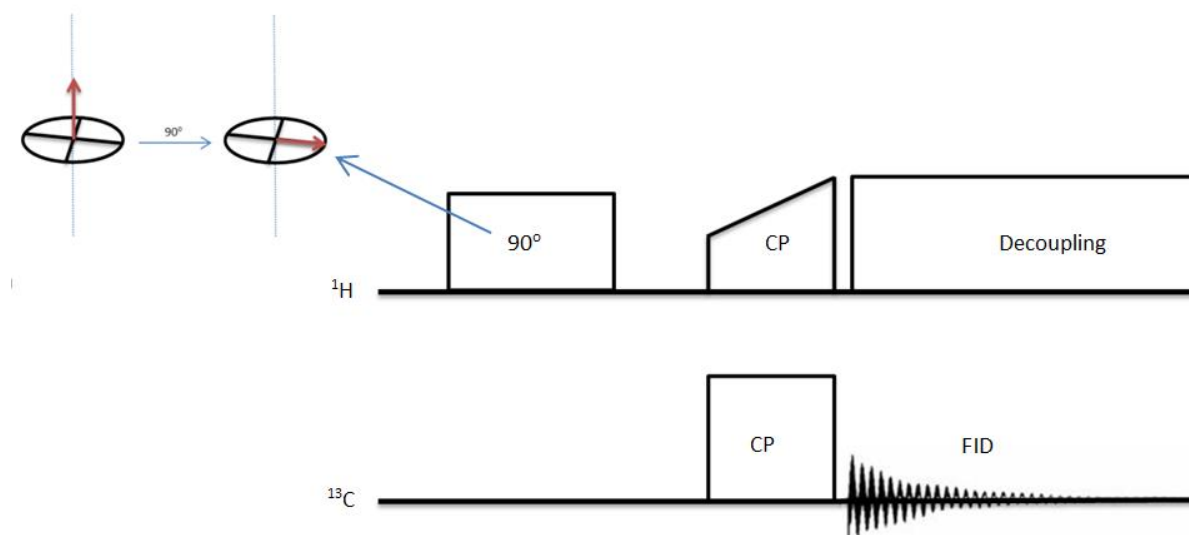
Figure 2.6 - Schematic of a cross polarisation NMR experiment with decoupling

By using cross polarisation the nature of the ligand after grafting can be determined. Liquid samples cannot be seen in CP experiments as the dipolar interactions are averaged to zero and therefore the energy transfer cannot occur.[136,137,139138]

2.1.2.3 SSNMR experimental parameters

Solid-state NMR spectra were recorded on Bruker Advance 500MHz NMR spectrometer, equipped with a 4mm MAS HX probe, 100W proton amplifier and 500W X amplifier. Cross-polarisation used a 1H pulse of 2 us (at −5.5 dB), a ramped proton CP pulse of 2ms (at −4.0 dB) and a carbon CP pulse of 2ms (at −3.1 dB). TPPM15 proton decoupling was applied during the 30ms acquisition time. FIDs contain 3k data points which were Fourier transformed into 16k data points; an exponential function of 20 Hz was applied to the FID using Bruker TOPSPIN (1.3) software. Spectra were referenced to external TMS (^{1}H, ^{13}C, ^{29}Si) and the magic angle was set up using KBr. Magic angle spinning of 10kHz was used. CP-MAS ^{29}Si a relaxation delay of 5s was used between each scan, DP-MAS ^{29}Si a relaxation of 10s was used. Direct polarisation was used for ^{1}H and ^{27}Al spectra (4us at 1dB).

2.2 Elemental analysis

Elemental analysis is used to determine the carbon, nitrogen and hydrogen content of a sample. This is done by accurately weighing approximately 2 mg a sample into an into a disposable tin capsule. The sample is then inserted into a nickel sleeve which is introduced into a high temperature furnace at 975 °C where combustion in a pure oxygen environment under static conditions occurs. To ensure complete combustion of the sample has occurred, a blast of oxygen is passed over the sample at the end of the combustion cycle. An initial exothermic reaction occurs raising the temperature of combustion to over 1800°C. The combustion products are passed through specialist reagents to produce carbon dioxide, water, nitrogen gas and nitrogen oxides. Halogen, sulphur and phosphorus impurities are removed by the reagents and the gases are passed over a pure copper wire at 620°C to remove excess oxygen from the mixture and reduce the nitrogen oxides into nitrogen gas. The gases enter a mixing chamber and are thoroughly mixed to ensure a homogenous mixture of the combustion products at constant temperature and pressure. The gas is then passed through a series of high precision thermal conductivity detectors containing a pair of thermal conductivity cells with a trap between each. The first detector measures the water content allowing the hydrogen content of the sample to be determined. The difference in signal between the two cells is proportional to the water concentration from the hydrogen in the sample. The second trap measures the carbon dioxide content which corresponds to the carbon in the sample. The last trap measures nitrogen content within the sample against a helium reference. The results are calculated and presented as a percentage of the total mass of the original sample.[140]

CHN results reported in this thesis were made using an Exeter Analytical CE-440 analyser configured and optimised for C, H and N analysis.

2.3 Powder X-Ray Diffraction (PXRD)

2.3.1 Principles of PXRD

X-ray diffraction is a key technique in the characterisation of solids. It is used to identify unknown materials, assess the purity of samples, follow solid-state reactions to completion and solve crystal structures. X-ray diffraction works by the interaction of X-rays with the electron cloud of the atoms/ions in crystalline materials, causing scattering of the X-rays. The scattered X-rays are detected and a diffraction pattern produced, the pattern is unique to each powdered crystallite and from this unique pattern compounds can be identified and compared to the international centre for diffraction database (ICDD). By analysing the scattered X-rays information on the separation and arrangements of atoms and ions can be determined.[141]

2.3.2 PXRD experiments

An X-ray experiment in its simplest terms requires a sample, an X-ray source and a detector. The X-rays interact with the sample are scattered and are observed by a suitable detector. This can be seen in the simple schematic of a reflectance diffractometer figure 2.7.
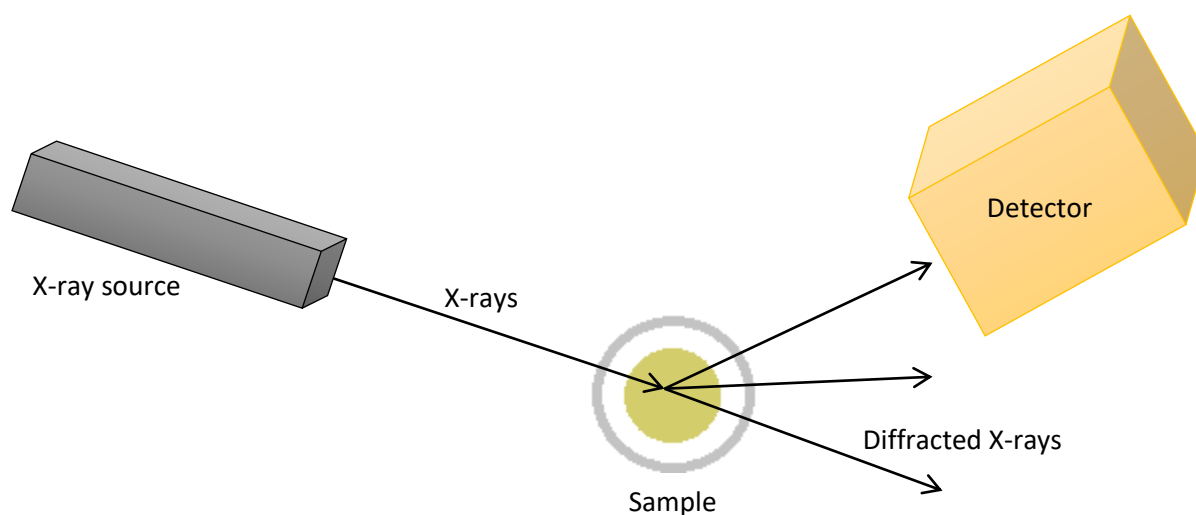
Figure 2.7 - Simple schematic of a PXRD in reflectance mode geometry

In reality, PXRD is a much more complex technique. However, to give a brief overview a simplistic system is discussed below. Its use in the nature of this work has been primarily for identification of materials and to show that the phases and long range order of the samples remains the same after treatment.[141]

2.3.3 Generation of X-rays

Powder X-ray diffractometers use X-ray radiation generated by an X-ray tube, an example is shown in figure 2.8. An electron beam is created by heating a tungsten filament in a vacuum (thermionic emission) and accelerated using a high voltage (30000 V) towards a metal target, such as copper, causing a core electron to be ejected from the 1s shell of the metal target. The electrons within the metal atoms then rearrange filling the ejected core electron with electrons from higher shells. This rearrangement releases energy in the form of X-rays, shown in figure 2.8. The X-rays pass from the tube through a beryllium window and a single wavelength X-ray is selected by filtering the beam through a single crystal monochromator.
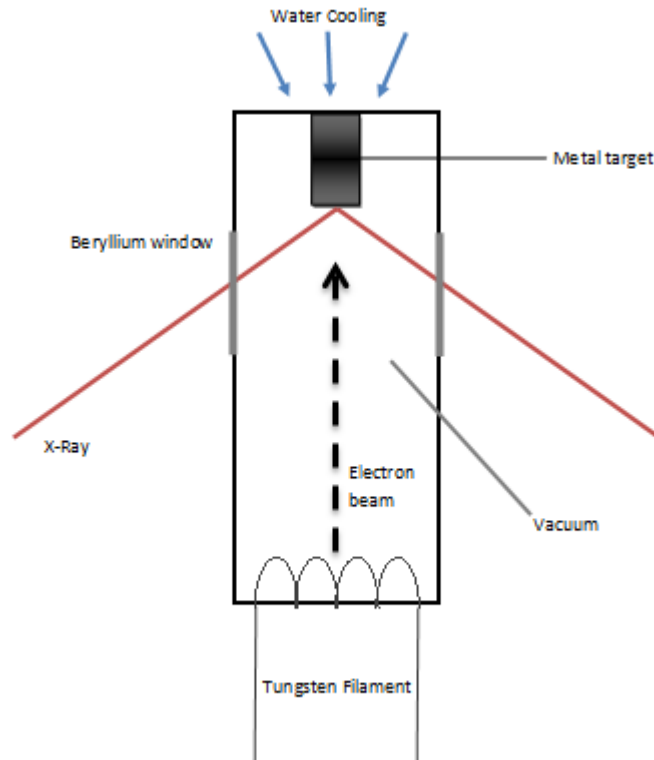
Figure 2.8 – Diagram showing the generation of X-rays using a tungsten filament

As discussed above, when a metal target is impacted by a high energy electron beam it ejects core electrons from energy levels close to the nucleus. Quantised vacancies are created and electrons from higher energy levels fill the vacancy. The difference in energy between the two levels is emitted as an X-ray of a precise energy dictated by Planck's equation, shown below;

$$E \ = \ h\nu$$

Where E = Energy Difference

h = Planck's constant

ν = Frequency Emitted

<div align="right">**Equation 2.5**</div>

This means by using different metal targets, X-rays of different energies can be produced. The X-rays have different energies dependant on the process of relaxation. An example of this is shown in figure 2.9. The $K_{\alpha 1}$ radiation produced from the relaxation of a 2p electron to a 1s transition in copper has a wavelength of 1.54 Å.
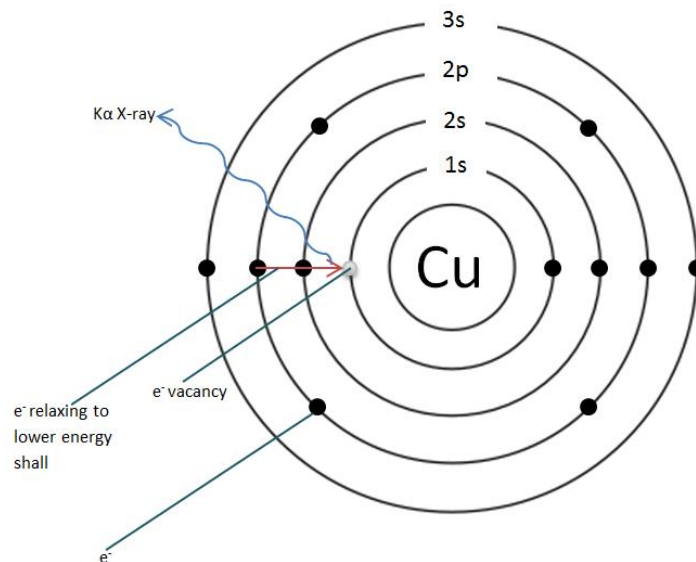
Figure 2.9 – Generation of X-rays using a copper source

Figure 2.10 shows the output from an X-ray tube, the background radiation (Bremsstrahlung or braking radiation) is emitted over the whole spectrum. The sharp lines are generated from the quantised transitions. The type of X-ray generated is described by its spin state of the electron and the vacancy filled, e.g. $K_{\alpha 1}$, $K_{\alpha 2}$, $K_{\beta 1}$, and $K_{\beta 2}$. The α/β refers to the higher energy level that the electron transfers from, α notates an electron transferring from 2p to 1s and β notates an electron transferring from 3p to 1s. The subscript 1 and 2 denotes the spin state of the electron. An example of this is α radiation which is a mixture of two wavelengths, α1 and α2. α1 means that the spin state of the electron filling the vacancy is the same as the one that has been ejected, whereas, α2 means that they have the opposite spin state.[141]
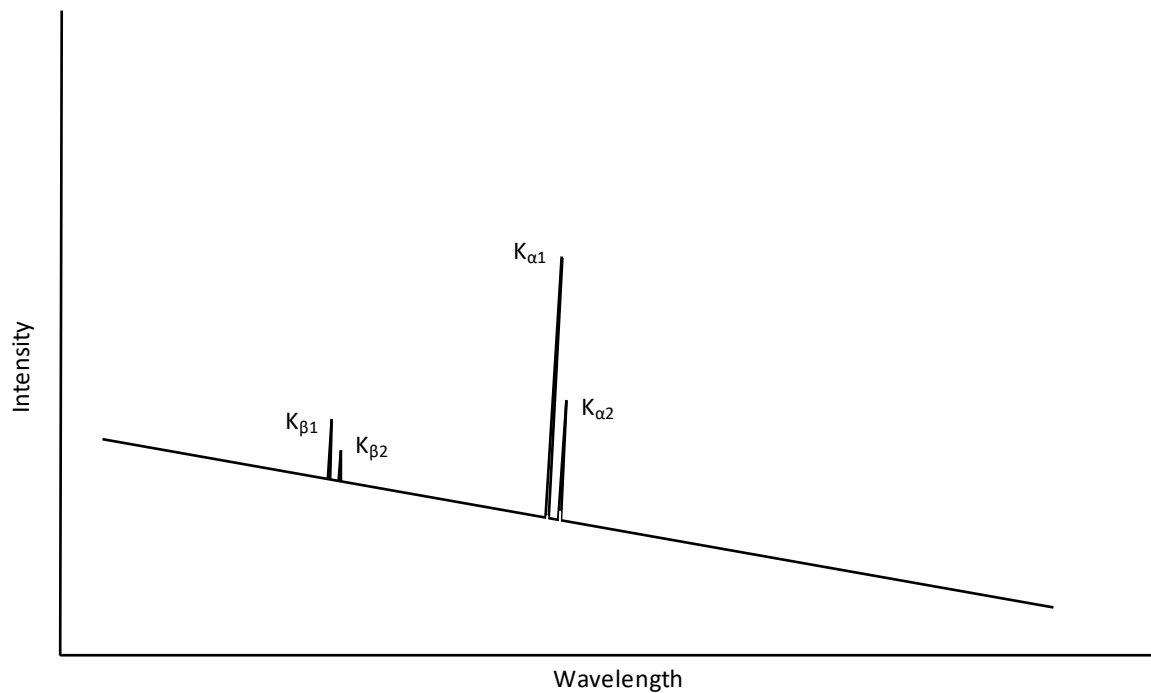
Figure 2.10 – The output from an X-ray tube

2.3.4 Powder X-Ray Diffraction Data Collection and Analysis

The diffraction pattern is generated when X-rays interact with atoms within a solid sample. This results in scattering of the X-rays which is detected and translated into an X-ray pattern of intensity vs. 2θ. When the X-ray beam interacts with the sample it is diffracted in all possible directions simultaneously in accordance with the Bragg equation. Each lattice spacing with in the crystalline sample generates a cone of diffraction, as seen in figure 2.11. Each cone is actually a set of closely spaced dots; each dot denotes a diffraction of a single crystallite from the sample. As each sample contains many crystallites the dots join together to form a continuous cone.[141]
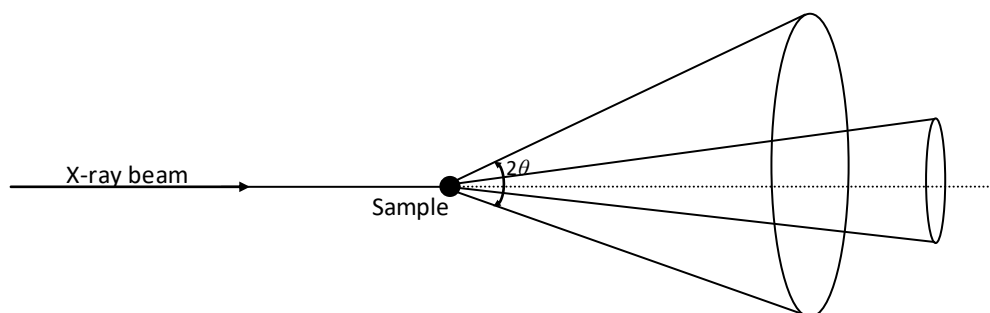
Figure 2.11 - Cones of diffraction generated by a sample

To analyse the sample the position of the cones is measured using a radiation detector. Radiation detectors are used due to their resolution and storage capability. A schematic of a powder X-ray diffractometer is shown in figure 2.12. The X-rays produced are aligned with the sample through a slit at the end of the X-ray tube. Once the X-rays interact with the sample they are scattered in all directions, the scattered X-rays are measured by scanning the detector around the sample along the measuring circle. The detector cuts through the diffraction cones allowing the angle of the X-rays to be measured. The X-ray diffraction pattern produced displays intensity as a function of the detector angle 2θ. The X-ray pattern produced is generated from the arrangement of atoms within the unit cell. There are several factors influencing the intensity of the reflections, these are: crystal class, lattice type, symmetry, unit cell parameters and the type and distribution of atoms. Due to these multiple factors, each material has a different diffraction pattern in relation to the intensities and positions of the observed reflections. This is due to the degree of scattering being dependent on the number of electrons present in the atom, meaning that the scattering of a sample will be dependent on the atoms present, the ratio of the atoms present and the ordering of the atoms within the sample. Therefore, in a mixture of compounds, each compound will have its own set of reflections; the relative intensities of the set of reflections depend somewhat on the amount of each phase present.[141]
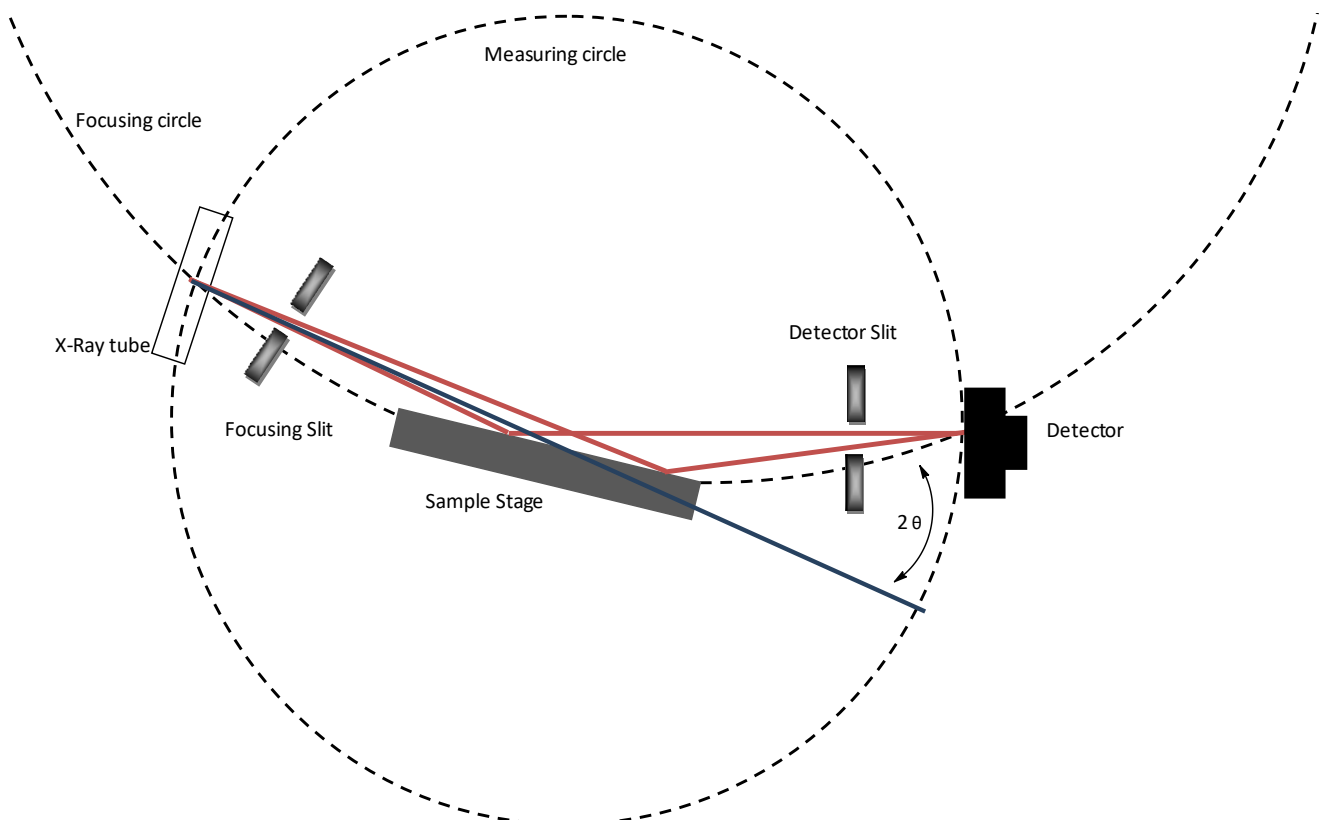
Figure 2.12 - Schematic of a PXRD instrument

2.3.4.1 Miller indices and Bragg's Law

A primary use of PXRD is in the identification of crystalline and polycrystalline compounds, which have long range order. Long range order is defined as a single repeating unit, where the simplest repeating unit representing the symmetry of the sample is termed the unit cell. The translational symmetry of the sample where multiple unit cells exists is termed Miller planes. The Miller planes are described using Miller indices (h, k, l) by their positions within the 3D lattice. Miller indices are assigned to observed reflections and from this cell constants are determined using an equation relating diffraction angle to Miller indices. In three-dimensional lattices there are planes of atoms, these planes show the translational symmetry of the structure. Each plane belongs to a series of parallel equally spaced planes, each lattice point lies on one of these planes. The X-rays produced interact with these planes of atoms. Miller indices are used to describe these planes, they are denoted by the labels *h, k* and *l,* which are integers and can be positive negative or zero.

The miller indices are given by the reciprocals of fractional intercepts, a/*h*, b/*k* and c/*l*. The 2, 4, 1 plane is shown in figure 2.13. It intersects half way along a, a quarter of the way along b and all the way along c.
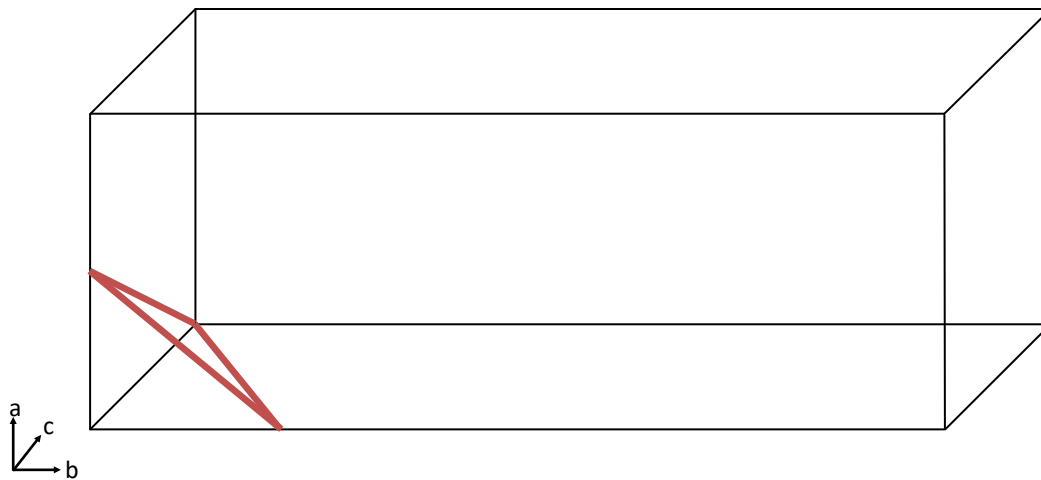
Figure 2.13 - Schematic showing a Miller plane

The d $_{(hkl)}$ spacing is the separation between the planes (often referred to as d spacing) and the perpendicular distance from the origin to the nearest plane. The d $_{(hkl)}$ spacing is related to the wavelength and angle of incidence of the X-ray beam via Bragg's law, equation 2.6.

$$2. d_{hkl}. sin\theta = n\lambda$$

Where n = an integer, normally 1

λ = the X-ray wavelength

θ = angle of incidence

Powdered X-ray samples are termed polycrystalline as they contain many crystallites all in random orientations. When subjected to an X-ray beam it diffracts in all possible directions at once as governed by Bragg's equation. This means each set of lattice points gives arise to a diffraction cone, which is observed at a set 2θ value.
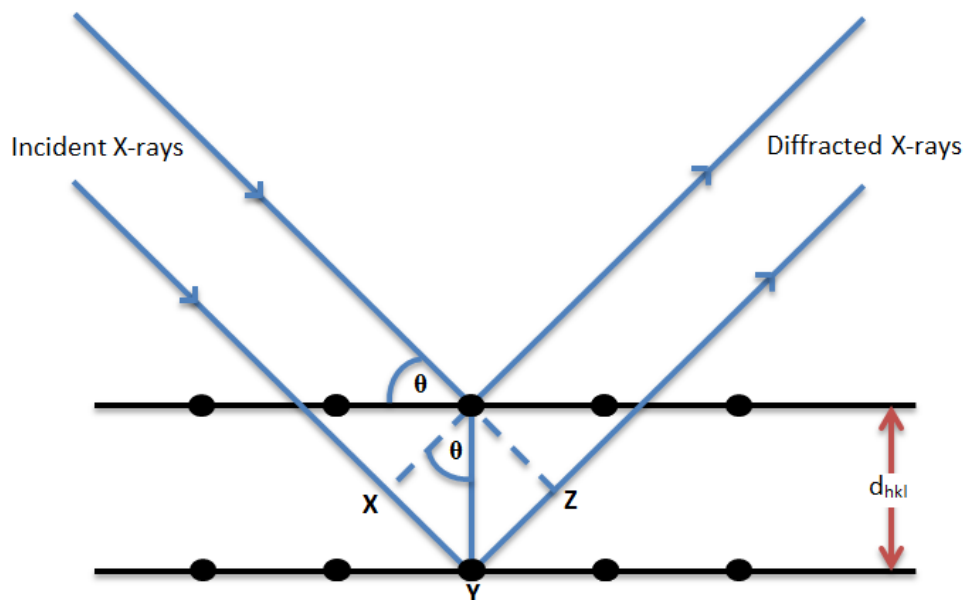
Figure 2.14 - Figure showing the diffracted X-ray beams obeying Bragg's law

Bragg's law describes the reflection of X-rays from the Miller planes separated by d spacing in a sample. Figure 1.14 shows two Miller planes separated by d_{hkl}. The incident X-rays interact with the atoms within the sample. The diffracted X-rays must be in phase with each other, termed constructive interference to generate intensity and be present in the diffraction pattern. If the diffracted X-rays are out of phase, termed destructive interference, the X-rays cancel each other out and are not seen in the X-ray diffraction pattern. The distance the top and bottom X-rays in figure 2.14 have to travel in relation to each other depends on the distance XYZ. If the distance relates to a whole wavelength then the X-rays are in phase, if not then the X-rays will have deconstructive interference. The distance

between XYZ, d spacing and angle of incidence θ, relate to Bragg's Law as such that the equation can be defined as shown previously. When the Bragg's Law, equation 2.6, is satisfied constructive interference is seen and the reflections are present in the X-ray diffraction pattern.[141]

2.3.4.2 Preferred Orientation

Preferred orientation in powder X-Ray diffraction is a phenomenon where intensities and positions of reflections differ in observed and reference patterns. This can be attributed to the packing of powdered polycrystalline material. As previously discussed in section 2.3 powder X-Ray diffraction relies on the average of a large number of randomly oriented crystallites. The discrepancy occurs when the crystallites are aligned in epitaxial alignment, and as they are not oriented at random certain reflections show increased intensity. The most affected reflections are typically low angle. A schematic showing the difference between epitaxial alignment and random orientation is given below in figure 214.
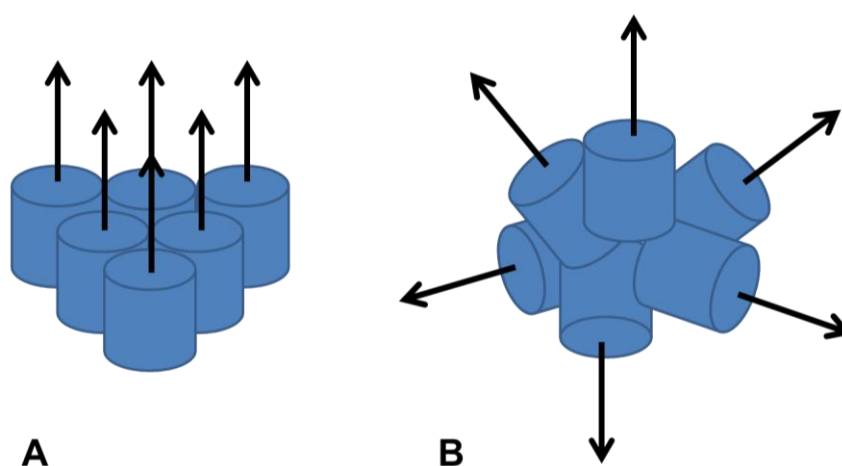
Figure 2.6 – Schematic of crystallites in a A) epitaxial and B) random orientation

2.3.5 PXRD experimental parameters

A Bruker D8 powder diffractometer with $Cu_{K\alpha1}$ (1.5406Å), using a 2θ range of 5° - 65°, with a step size of 0.014° with a step time of 1s was used. Continuous scanning was used for the collection of the X-ray data presented here in this work. The samples were mounted in Perspex sample holders. The detector used in the collection of the data was a Lynxeye position sensitive detector that allows a range of scattering angles to be measured increasing signal detection and reducing noise. The collected data were then analysed in the EVA program using the ICDD to identify the phases present and determine sample purity.

2.4 Scanning electron microscopy

Scanning electron microscopy (SEM) is used to record high resolution images of material surfaces. SEM generates an electron beam which is passed through a series of electromagnetic lenses and coils which control the position, size and shape of the electron beam directed at the sample surface. SEM is carried out under vacuum as the electron beam would otherwise interact with other molecules causing the beam to attenuate. The electrons emitted in the beam are accelerated at approximately 20 KV down the SEM column. The electromagnetic lenses are coiled copper wire around iron poles which create a magnetic field controlling the electron beam. A simple schematic of this can be seen in figure 2.15. The focused beam of electrons is scanned across the surface to build up an image. The electron beam interacts with the atoms in the sample producing signals which allow the image to be created.

The electron beam interacts with the surface of the material and there are three types of resultant emissions; backscattered electrons, secondary electrons and X-rays. Backscattered electrons are high in energy, give compositional information about the material but produce lower resolution images. Secondary electrons are lower in energy and only interact with a few nm of the surface, so are surface sensitive; therefore they produce higher resolution images of the topography of the surface. The secondary electrons are detected using a photomultiplier tube. Different detectors are used which have different sensitivities with regard to different energies and particle emission from the sample. The signals are then processed and an output of a visual display of the surface.

For samples to be suitable for SEM imaging they must be electronically conductive. To make the sample conductive it is coated with a conducting material, such as gold. One method of coating the material is low-vacuum sputter coating. If the material is poor at conducting then an effect called charging occurs. Charging is when the surface accumulates charge and can then repel the electrons, distorting the image, by appearing as bright spots. Coating a low or non-conductive material in a conductive media such as a metal can reduce the charging of surfaces.[142]

The measurements in this work were carried out on a JEOL JSM-7800F FE-SEM instrument.

Electron beam
generation

Condenser
lens

Objective
lens

Objective
lens

Output

Aperture

Detector
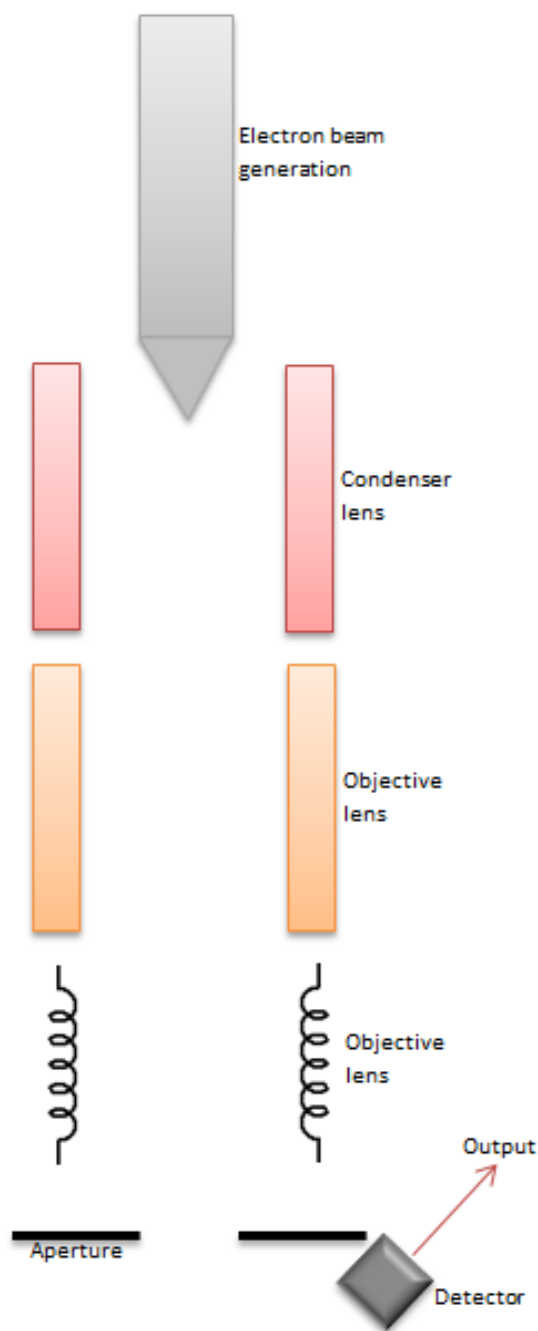
Figure2.15 - Schematic of SEM

2.5 Infra-red spectroscopy

Infra-red spectroscopy (IR) uses infrared wavelengths to excite molecules and induce vibrations. Infra-red wavelengths are located outside the red of visible spectrum and are low energy. Due to the low energy of infrared wavelengths they do not contain enough energy to excite electrons but can induce vibrational excitation of covalent bonds. Infra-red spectroscopy is an absorption technique; where the molecules absorb the energy and this causes the bonds to vibrate. There are two types of vibrations

seen these are stretching and bending. For a molecule to be infra-red active there must be a change in the electric dipole moment of the molecule, where the atoms are displaced relative to one another. This can be a change from a zero dipole or an existing dipole within the molecule, and does not have to be a permanent dipole. Vibrations arise from stretching of bond lengths and the bending of bond angles causing a shift in the dipole moment of the molecule. There are two types of stretching; symmetric where the bonds move in opposite directions, and asymmetric where the bonds move in the same direction. Bending modes can occur both in and out of the plane of the molecule. The bending and stretching vibrations can be seen in figure 2.16.
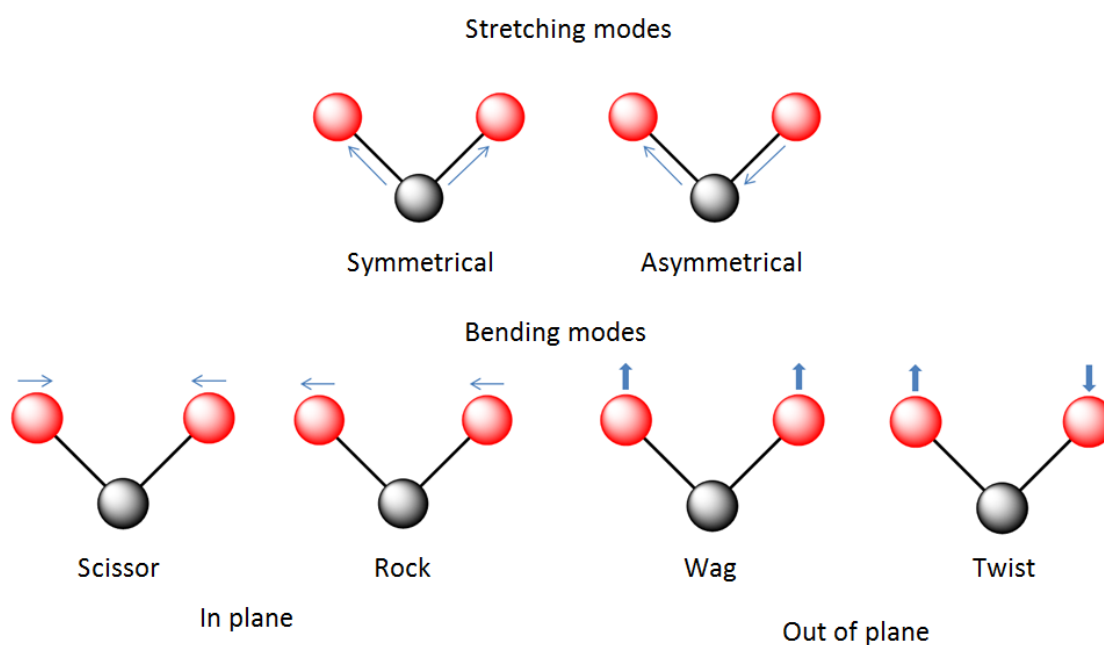
Infrared spectroscopy is used to help determine the structure of functional groups present.

Figure 2.16 – Modes of stretching and bending seen in FTIR

Molecules are continuously moving, the bending and stretching of molecules have characteristic frequencies, and they absorb light at these frequencies. The common range for IR experiments is 650-4000 cm^{-1}, where the sample is subjected to a source of infrared light and produces a spectrum showing peaks corresponding to functional groups, a common example of this is the C=O stretching band present at 1750 cm^{-1}. IR data is seen as a plot of transmittance (%) against wavenumber (cm^{-1}) providing an IR spectrum, where the observed peaks are seen as a decrease in transmittance.

IR spectroscopy has been used in this work to identify peaks that correspond to the ligands grafted to the surface. In some cases, due to the low percentage of ligand grafted it is not visible in the IR spectra and more accurate techniques have been used to determine the presence of the ligands.[97,102,141]

FTIR spectra were collected between 4000-400 cm^{-1} in transmission mode using a Shimazdu 8400S FTIR spectrometer, using an attenuated total reflection (ATR) Spectra single reflection monolithic diamond attachment.

2.6 Radiochemical analysis

Solutions containing radioactivity were measured by gamma counting (section 2.6.1) or by liquid scintillation counting (section 2.6.2). The results from measurements using either technique are usually reported in disintegration per second (Bq) or disintegrations per minute (DPM). If reported in dps or dpm, the counting efficiency of the instrument for the particular radioisotope of interest must be pre-determined and used to convert cps of cpm to dps or dpm by dividing the cps or cpm value by the counting efficiency. However, as in the experiments reported in this thesis, if the geometry (same vial, same volume of liquid) and density of the liquid to be counted are kept constant, the results of measurements from gamma counting and from the use of LSC can be used relatively and the counting efficiency can be assumed to be constant when using the same radionuclide. It is then acceptable to use cps or dps in calculations.

2.6.1 Gamma counting

Gamma spectroscopy is used in the analysis of radionuclides which when decay produces gamma emissions. Gamma spectroscopy differs from liquid scintillation counting as no scintillation media is required; the sample is placed in a polypropylene tube to give the best efficiency. Each isotope produces gamma emissions of specific energies and intensities. Gamma rays are commonly detected using sodium iodide scintillation counters or high purity germanium detectors. Sodium iodide (NaI) scintillation counters utilise light which is produced after a gamma ray is emitted and interacts with the NaI crystal. There are three possible types of interactions; the photoelectric effect, Compton scattering and pair production. The photoelectric effect occurs when an incident gamma photon ejects an inner electron from the K or L shell; an electron from a higher shell drops down to fill the vacancy and emits an X-ray. Compton scattering is when a gamma photon hits an electron and ejects it, the energy of the emitted electron depends on the scattering angle θ. If θ is small then the energy is small, the maximum energy of the Compton electron is that of the original gamma photon. Pair production occurs when a gamma emission is greater than 1.022 MeV. The gamma photon splits into an electron

and a positron pair. The positron is short lived and takes part in an annihilation reaction shown the equation 2.7, where a position and an electron combine to give 2 gamma photons of 0.511 MeV. The two photons are produced at 180º to each other. The NaI crystal is the scintillator and produces light, this is detected by a photomultiplier tube which multiplies the signal and sends an electrical signal to be processed. The intensity of the light produced by the NaI crystal is proportional to the energy of the interacting gamma ray.

$$e^+ + e^- = 2\Upsilon$$
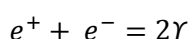
<div align="right">**Equation 2.7**</div>

Gamma spectroscopy measurements were made using a Cobra Auto Gamma II counter. 2 ml of each sample was weighed in to a 4 ml polypropylene gamma tube and counted for 5 minutes. The background was measured using 2 ml of distilled water and subtracted from each sample.

2.6.2 Liquid scintillation counting

Liquid scintillation counting (LSC) is an analytical technique predominately used to measure the activity of radioactive samples that produce alpha (α) or beta (β) decay. When a radioactive particle decays via α decay a helium nucleus is ejected, whereas when particle decays via β decay an antineutrino and an electron are ejected. In β decay the energy is split between the electron and antineutrino. It is only the electron that is counted as the antineutrino does not interact significantly with matter. Liquid scintillation counting turns nuclear emissions into light energy; it is this light energy that is counted to produce a spectrum.

In LSC, the sample is added to a solution which contains a solvent and a solute. As an alpha or beta particle passes through the solvent the particle loses energy by interacting with the solvent molecules causing electronic excitation of these molecules figure 2.17.
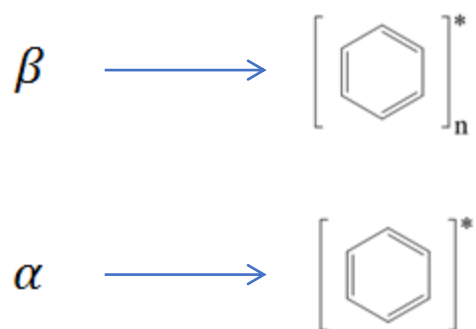
Figure 2.17 – α and β particles exciting scintilant molecules

The excited molecules pass on their excitation energy to the solute molecules which themselves become electronically excited. The solute molecules return to the ground state by emitting photons of light (scintillate). These light flashes are converted to electrical pulses by photomultiplier tubes and are then recorded as counts in a multi-channel analyser as shown in Figure 2.18. Thus one light flash is converted to one electrical pulse which is then recorded as one count. Since beta particles are emitted from the nucleus with a range of energies, they produce a range of intensities of flashes of light i.e. the more energetic the beta particle the more intense is the flash of light emitted. The range of energies of beta particles emitted from a radionuclide (eg. $0 - 18.6$ keV for ^{3}H, $0 - 156$ keV for ^{14}C) results in a range of intensities of the light flashes and a range of magnitudes of electrical pulses. The MCA sorts these pulses into channels according to their magnitude and the result is the production of a pulse height spectrum. Beta particles produce a pulse height spectrum which is a continuum up to the maximum energy of the beta particle whereas alpha particles, which are roughly mono energetic, produce a pulse height spectrum which is roughly Gaussian in shape. The simplistic schematic figure 2.18 shows a simplified scintillation process.
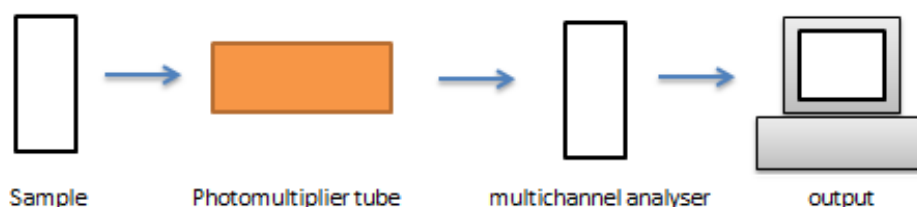
Figure 2.18 - Schematic of a LSC counter

The sample decays releasing nuclear emission, either α or β, this is absorbed by the scintillation molecule and released as flashes of light (photons). The photons are detected by the cathode of the photomultiplier tube and converted into an electrical pulse which is proportional to the number of photons produced. This electrical signal enters the multichannel analyser (MCA) which converts the

analogue signal into a digital signal and stores the electrical pulses from the PMT and builds up a digital profile of the energy distribution. In liquid scintillation counters there are two PMTs which are connected to a coincidence circuit. A coincidence circuit is important as it allows only true pulses to be counted. The coincidence circuit was introduced in the early 1950s to reduce background noise. It works by having two or more inputs but only one output. In LSC output only occurs when two signals are received within a specified time frame. Therefore both PMTs have to be simulated at the same time to produce an output from the coincidence circuit. A schematic of this can be seen in figure 2.19.
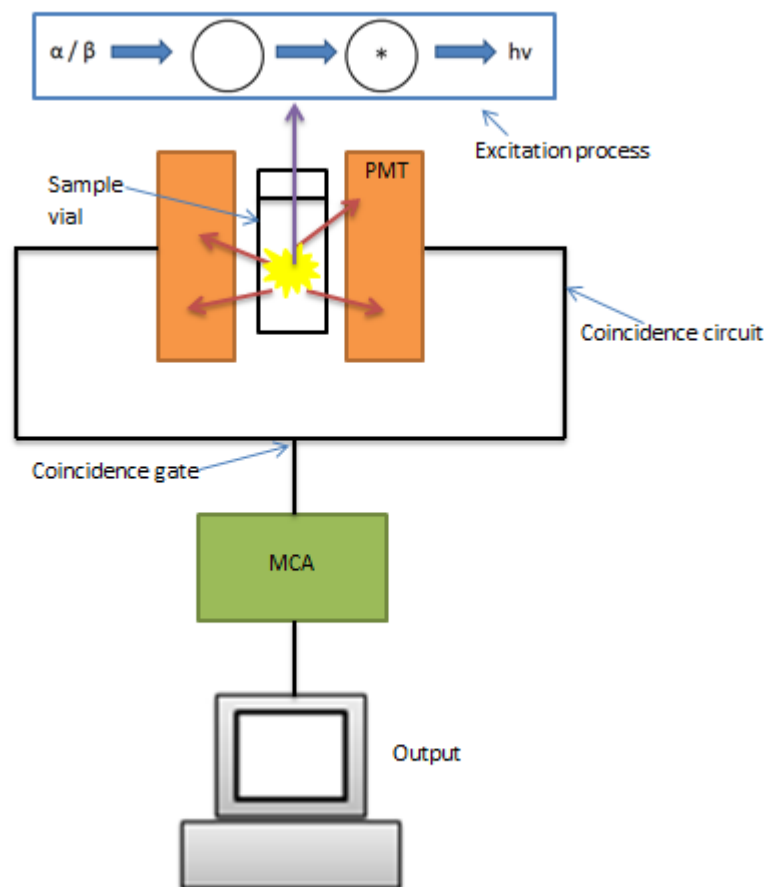
Figure 2.19 - Schematic showing a coincidence circuit with both PMTs

One problem with scintillation counting is quenching. Quenching of samples can occur via colour quenching, chemical quenching or physical quenching. Colour quenching occurs when the sample is coloured and this shifts the energy profile of the decay down the spectrum to a lower energy. Chemical quenching occurs when other molecules are present which absorb the energy. Physical quenching occurs when there is self-absorption of the decay or photon. Quenching reduces the measured emission (loss of efficiency) or a shift to a lower energy in the spectrum. A quench correction curve

can be plotted showing the relationship between counting efficiency and the quenching of the sample to allow correction for quenching.[143,144]

For this work 2 cm^3 of sample was added to a scintillation vial with 10 cm^3 of scintillation fluid, thoroughly mixed using a vortex mixer for 30 seconds per sample. The sample was then allowed to settle for 30 minutes to allow any bubbles to dissipate before placing in the counter. The samples were counted on a Perkin Elmer Tricarb 2500 tr. The calculations used to calculate the amount of activity removed are the same as previously shown for gamma spectroscopy.

Chapter 3-Chemical characterisation

3.0 Introduction to chapter 3

In this chapter, clinoptilolite (NDA), clinoptilolite (Imerys), ZSM5, vermiculite and kaolinite are characterised by short and long range techniques and elemental analysis performed before and after attempts are made to modify the surfaces of the materials for sequestration of actinides using three different ligands. The ligands selected contain oxygen and nitrogen donors that should be suitable for chelation of hard acid actinide species and have been previously designed for this purpose.[132,133] Experimental parameters of reaction time, ligand concentration and polarity of solvent are varied in order to optimise the amount of ligand anchored on the surface of the substrate.

3.1 Characterisation of unmodified materials

The characterisation of the materials was performed using different techniques which focus on the inorganic solid support and the organic chelating ligand. The techniques were used to provide a baseline analysis to allow comparison of the different materials before and after modification by the ligands. Theoretical formulae for the materials under investigation are given in Table 3.1; it should be noted that the natural materials are subject to geological variation in both the chemical formulae and the presence of other materials in the pit. The insoluble nature of all materials in all solvents except concentrated acid, negates easy separation of impurity phases such as quartz found in the minerals, which means purification is relatively limited.

Table 3.1 – Material Formulae [89,91,145]

Material	Source	Formula
Clinoptilolite	NDA/NNL	$(Ca,K,Na)_{2-3}Al_3(Al,Si)_2Si_{13}O_{36} \bullet 12(H_2O)$
Clinoptilolite	IMERYS minerals	$(Ca,K,Na)_{2-3}Al_3(Al,Si)_2Si_{13}O_{36} \bullet 12(H_2O)$
ZSM-5	Acros Organics	$Na_x(Si_{96-x}Al_x)O_{192}.16H_2O$, $0<x<27$.
Kaolinite	IMERYS minerals	$Al_2Si_2O_5(OH)_4$
Vermiculite	IMERYS minerals	$(Mg,Fe,Al)_3((Al,Si)_4O_{10})(OH)_2.4H_2O$

Sieving, which is perhaps the only real routine purification method, uses the idea that the morphology and size of some mineral particles tend to be larger than others, but this is not always the case. As a result, these materials have been used without purification. The information provided by the NDA appears to suggest that the key difference between the original NDA clinoptilolite material and that supplied by Imerys is that the latter has been sieved and potassium exchanged.

3.1.1 Phase identification by PXRD

3.1.1.1 Clinoptilolite (NDA)

The powder X-ray diffraction pattern of the sample of clinoptilolite provided by the NDA is shown in Figure 3.1. The reference pattern for clinoptilolite (ICDD reference: 00-047-1870) is shown in orange. In addition to clinoptilolite, additional natural mineral phases are also present. Quartz (α-SiO$_2$) is a very common impurity found in mineral samples due to the high proportion of silicate minerals in the Earth's crust. This material is also found in the clinoptilolite provided by the NDA and it is indicated by blue vertical tick marks (ICDD reference pattern 01-079-0563). One or two additional reflections are also seen in the pattern, which are broad and not easily matched definitively to a particular phase. Clinoptilolite tuffs typically coexist with other silicates and clay minerals of varying crystallinity in vast deposits, so weak additional reflections are expected.[10,20,31–35,37,43,57,59,63,68,71,89,91,92,109,113,115,145] In the course of this work, additional phases were sometimes identifiable in the X-ray pattern but were not consistently observed. This includes clay minerals such as kaolinite ($Al_2Si_2O_5(OH)_4$) and feldspars ($MAlSi_3O_8$, M= K, Na) As the intensity of reflections in diffraction is based on crystallinity and not quantity of material, the relative proportions of each mineral cannot easily be determined by the technique. It is accepted that the presence of these phases is problematic as they could be surface-grafted in a similar way to clinoptilolite; they contain available silicate groups which could be grafted, thus making it unclear whether clinoptilolite or other phases are surface-modified. Techniques such as SSNMR that are used for characterisation of the ligand graft cannot distinguish between the silicon sites in the different minerals, so their presence is not ideal. As previously discussed in the introduction to this chapter, those impurities are not easily removed, so the removal of the phases is not an option for this research. However, as this is the actual material used in the SIXEP process, if any improvement in the uptake of radioactive species is shown through modification, it would still prove useful to the NDA as enough of this material is left in storage for another 30-50 years use in SIXEP.[10,146]
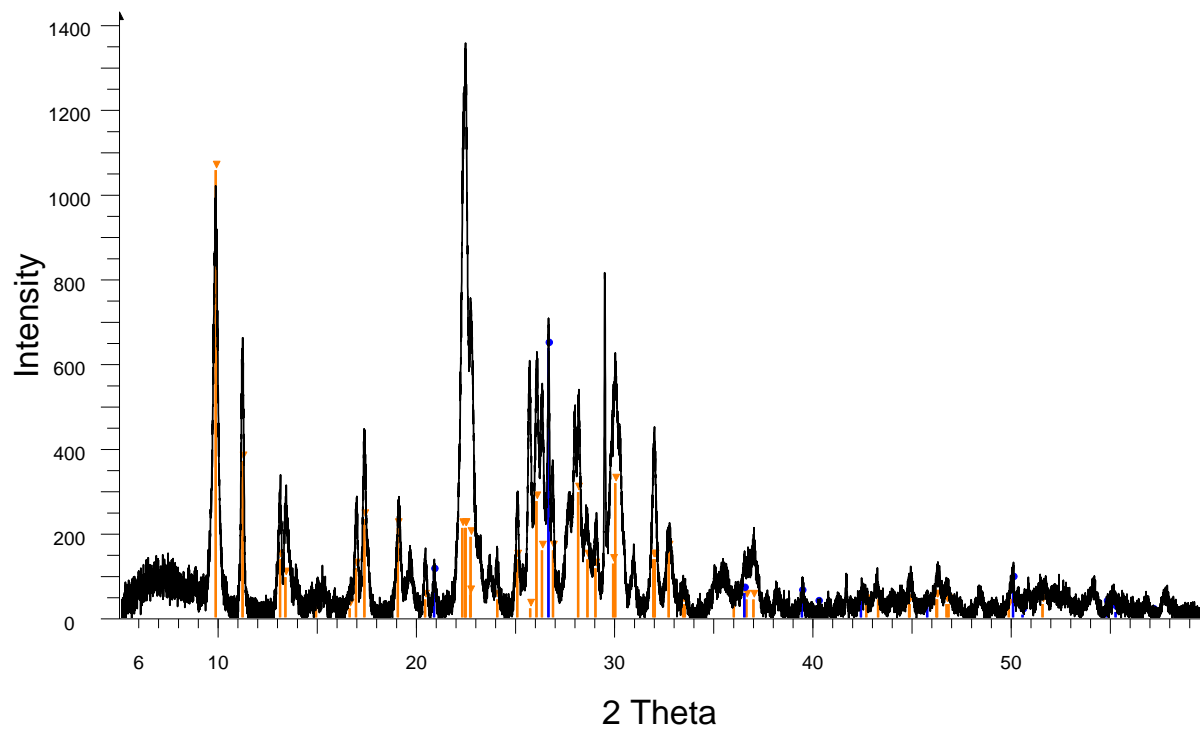
Figure 3.1 Powder X-ray Diffraction Pattern of NDA Clinoptilolite; orange tick marks clinoptilolite (ICDD reference 00-047-1870) and blue tick marks, quartz (ICDD reference 00-46-1045).

3.1.1.2 Clinoptilolite (Imerys)

The X-ray diffraction pattern collected on the sample of clinoptilolite sourced from Imerys minerals is shown in Figure 3.2. The pattern for clinoptilolite is indicated by orange vertical tick marks (ICDD reference pattern 00-047-1870). This sample of clinoptilolite has been processed by sieving to remove most of the impurity phases associated with the natural unaltered sample from the NNL/NDA. The sample does still have quartz present shown as blue tick marks (reference pattern 00-046-1045). The sample also has smaller particle size than the clinoptilolite sourced from the NDA. The small particular size is further evidenced by the Scanning Electron Microscopy characterisation in section 3.1.3. Grafting experiments will be carried out on both clinoptilolite samples to determine if the processed clinoptilolite provides a better base material for the grafting than the unprocessed sample.

3.1.1.3 ZSM-5

The PXRD pattern for ZSM-5 is shown below in Figure 3.3. The sample purchased from Acros organics was analysed for impurities, but none were seen in the pattern. The ZSM-5 pattern is shown in black (ICDD reference pattern 00-042-0023), and no remaining reflections were present in the pattern after the data was compared with the ZSM-5 pattern. A sample of ZSM-5 with a 400 to 570 molar ratio of SiO_2/Al_2O_3 was purchased to allow all the experiments to be carried out on one batch and not multiple batches of synthesised material. This was to allow the comparison of samples during the optimisation process without the concern of differences due to the synthesis process. As the purchased material showed no signs of impurities in the PXRD pattern this sample was used for the modification steps outlined later in this thesis.
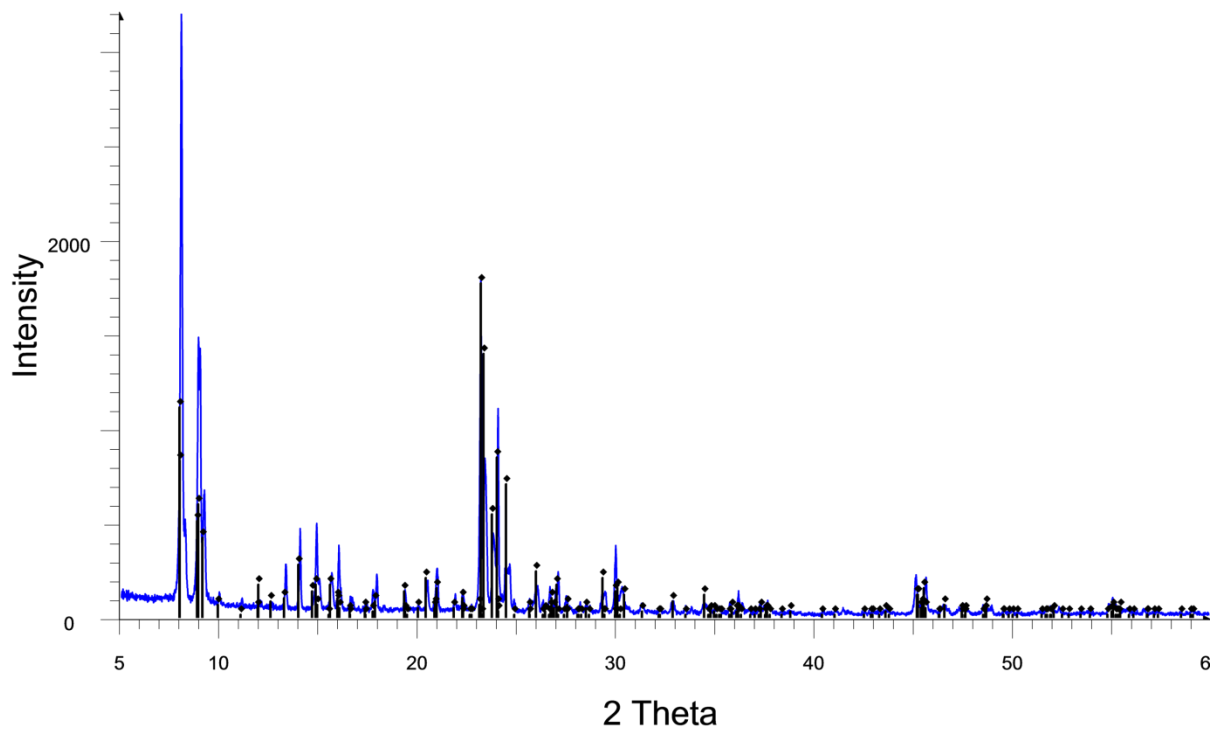
Figure 3.3: Powder X-ray Diffraction Pattern of ZSM5, black tick marks show ZSM-5 (ICDD reference 00-042-0023 for Na$_{0.3}$Si$_{96.7}$Al$_{0.3}$O$_{192}$.16H$_2$O).

3.1.1.4 Vermiculite

A typical powder diffraction pattern of the vermiculite used in the experiments described in this thesis is shown in Figure 3.4. Due to the geological nature of the sample, some associated impurity phases which are commonly found within vermiculite mineral deposits are sometimes observed such clinochlore (Mg$_5$Al$_2$(Si$_3$Al)O$_{10}$(OH)$_8$, (ICDD reference 00-029-0853) and kalifersite ((K,Na)$_5$Fe$_7$(Si$_{20}$O$_{50}$)(OH)$_8$, (ICDD reference 00-052-1646). The intensity of the reflections of the major vermiculite phase rarely matched those give in the data base file (ICDD 01-077-0022) as a result of preferred orientation of the crystals of vermiculite which tend to line up in the direction of the layers; as X-ray diffraction is dependent on the crystals being randomly oriented, the favourable alignment of the crystals results the 00l reflections showing enhanced intensity.
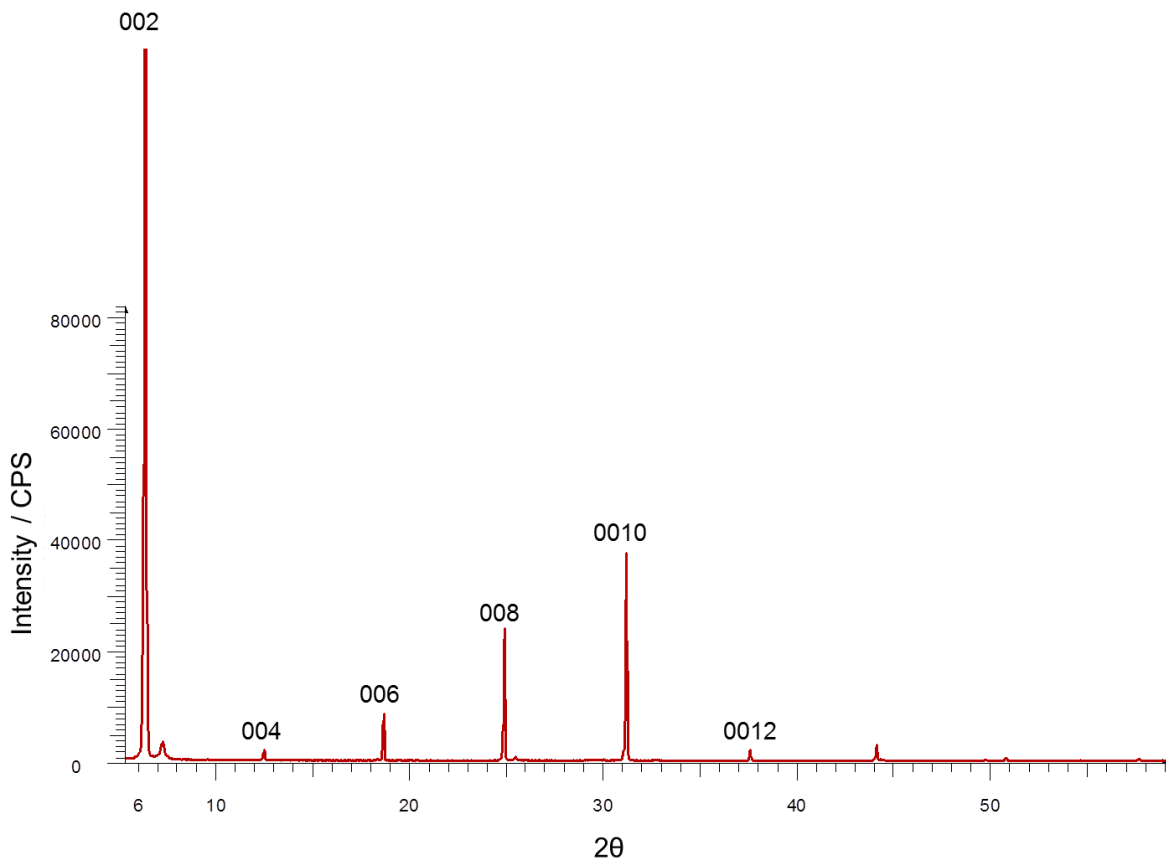
3.1.1.5 Kaolinite

The PXRD pattern taken from the sample of kaolinite is shown below in Figure 3.5. The sample was found to be mostly kaolinite shown in blue (ICDD reference pattern 01-075-1593) but with two different forms of halloysite impurities. Due to the geological nature of the sample, these impurities are typically found alongside kaolinite in the mineral deposits. The relative intensities of kaolinite and halloysite would indicate only small quantities of halloysite present in the kaolinite sample, although some caution is necessary as both phases are layered and can show preferred orientation. Halloysite ($Al_2Si_2O_5(OH)_4$-$2H_2O$) (ICDD reference pattern 00-009-0451 in red and ICDD reference pattern 00-002-0058 in pink) has a similar formula to kaolinite but with added interlayer water.
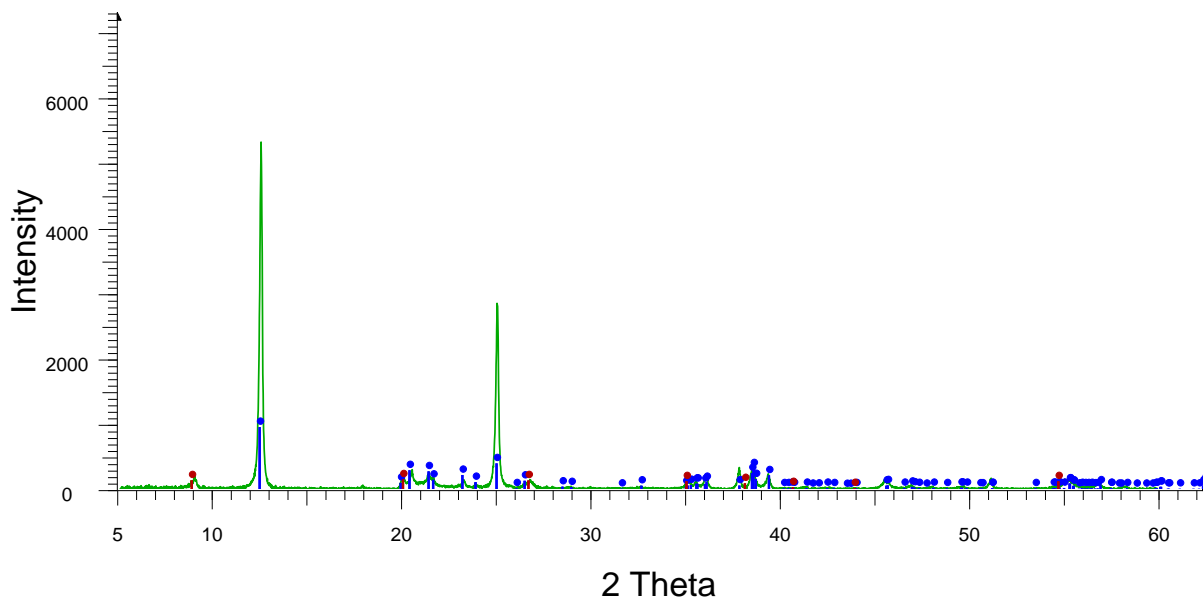
Figure 3.5: Powder X-ray Diffraction Pattern of Kaolinite, blue tick markers indicate kaolinite (ICDD reference pattern 01-075-1593), red and pink markers show halloysite (ICDD reference pattern 00-009-0451 and ICDD reference pattern 00-002-0058 respectively).

3.1.2 Elemental composition by XRF

Elemental analysis was carried out by XRF, the major components of each material are presented in table 3.2.

Table 3.2 Elemental composition by XRF

Material	Atomic %									
	Al		Si		K		Ca		Fe	
	At %	error	At %	error	At %	error	At %	error	At %	error
Clino (NDA)	13.56	0.16	77.38	0.10	5.98	0.09	1.59	0.01	2.31	0.01
Clino (Imerys)	13.63	---	76.95	3.92	7.80	1.41	1.95	1.78	2.82	0.67
ZSM-5	5.82	---	94.91	7.34	---	---	0.53	0.45	0.05	0.05
Vermiculite	19.88	3.16	56.45	2.62	---	---	1.11	0.02	22.46	0.57
Kaolinite	32.47	0.19	61.45	0.09	5.45	0.12	---	---	1.54	0.03

The clinoptilolite samples have a similar composition as is expected, the material from Imerys minerals was determined to contain a larger amount of potassium indicating potassium exchange has taken

place. The ZSM-5 was determined to be largely aluminium and silicon. The two clays were in good agreement with the expected values and vermiculite shown to be iron rich.

The silicon aluminium ratio's for all materials is given in table 3.3

Table 3.3 Silicon aluminium ratio for unmodified materials

Material	Si:Al ratio
Clino (NDA)	5.70
Clino (Imerys)	5.65
ZSM-5	16.31
Vermiculite	2.84
Kaolinite	1.89

Although these results are reasonable, there are some discrepancies which are attributed to using XRF as a quantitative technique. Other methods were previously attempted namely microwave assisted acid digestion using hydrofluoric acid followed by analysis by inductively coupled plasma mass spectroscopy. However due to the stability of the materials a method for successfully dissolving the materials allowing accurate silicon determination was not achieved and so results are not presented in this thesis.

3.1.3 Structure by SSNMR

SSNMR was used to characterise the substrates before and after grafting with the ligands. Before grafting, no signals were observed in the ^{13}C SSNMR of any of the samples. The ^{29}Si SSNMR of all samples are shown in Figure 3.6
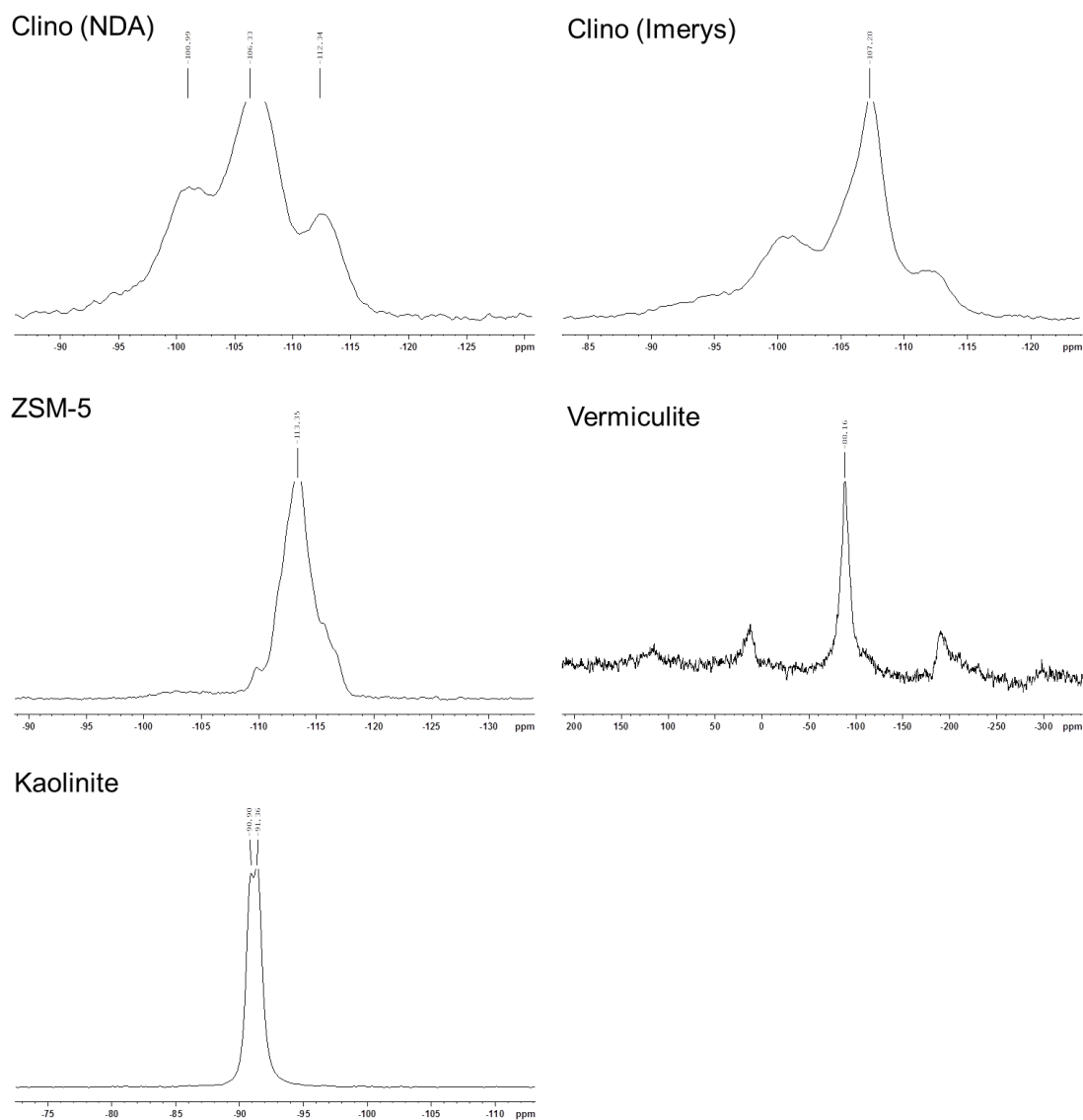
Figure 3.6- ^{29}Si NMR spectra for unmodified materials

^{29}Si SSNMR spectra of zeolites give characteristic spectra with signals between -90 and -115 ppm (referencing against tetramethylsilane) depending on the number of Si-O-Al linkages. In a purely silicon framework of vertex-sharing tetrahedra, each silicon tetrahedron is surrounded by four silicon tetrahedra and the signal is at ca -110-115 ppm. This is the spectrum observed for ZSM5, which is expected as the Si:Al ratio is high and hence the majority of Si will be surrounded by four other silicon tetraedra. The spectrum for both clinoptilolite samples show a greater number of signals being a mixture of 100 ppm (Si$_2$Al$_2$), 105 ppm (Si$_3$Al) and 110 ppm (Si$_4$AlO) nuclei. As the clinoptilolite samples

are made geologically, the framework can be disordered rather than being ordered as might be expected from a synthetic sample prepared under less extreme conditions, governed by Lowenstein's rule. The spectrum of kaolinite is in full agreement with previous SSNMR studies on kaolinite by Rocha and coworkers[147] giving a broad resonance centred around 90 ppm. The spectrum of vermiculite is of poorer quality than the rest of the spectra as a result of a significant quantity of iron oxide in the sample that affects the quality of the data since iron(III) has unpaired electrons. The signal itself is centred at 90 ppm and two spinning side bands are also present which are equidistant from the central band.[139,147]

3.1.4 Morphology and particle size by SEM

Scanning electron micrographs of all four mineralogical samples showed a mixture of particles sizes and morphologies consistent with samples derived from a geological origin and are shown in Figure 3.6. The clinoptilolite (NDA) sample appears to be less uniform than the same material which was processed by Imerys, indicating that the particle sieving was successful in creating better uniformity in the sample. The image of the sample of ZSM-5 in Figure 3.7 is notably different to the others with the crystals being more uniform and characteristically smooth in shape, indicative of the much faster synthetic process followed by calcination to remove the template rather than the much slower evolution/growth of the materials produced by nature.

Table 3.4 Particle size determined by SEM images

Sample	Average size / μm	Error $\pm$ / μm
Clino NDA	2.46	0.93
Clino Imerys	0.64	0.29
ZSM-5	2.55	0.92
Vermiculite	17.64	12.95
Kaolinite	5.61	0.66

The particle size analysis of the unmodified materials is shown in table 3.4. The two clay samples were determine to have the largest particle sizes. The NDA clinoptilolite samples differ with the NDA being larger as it is unprocessed.
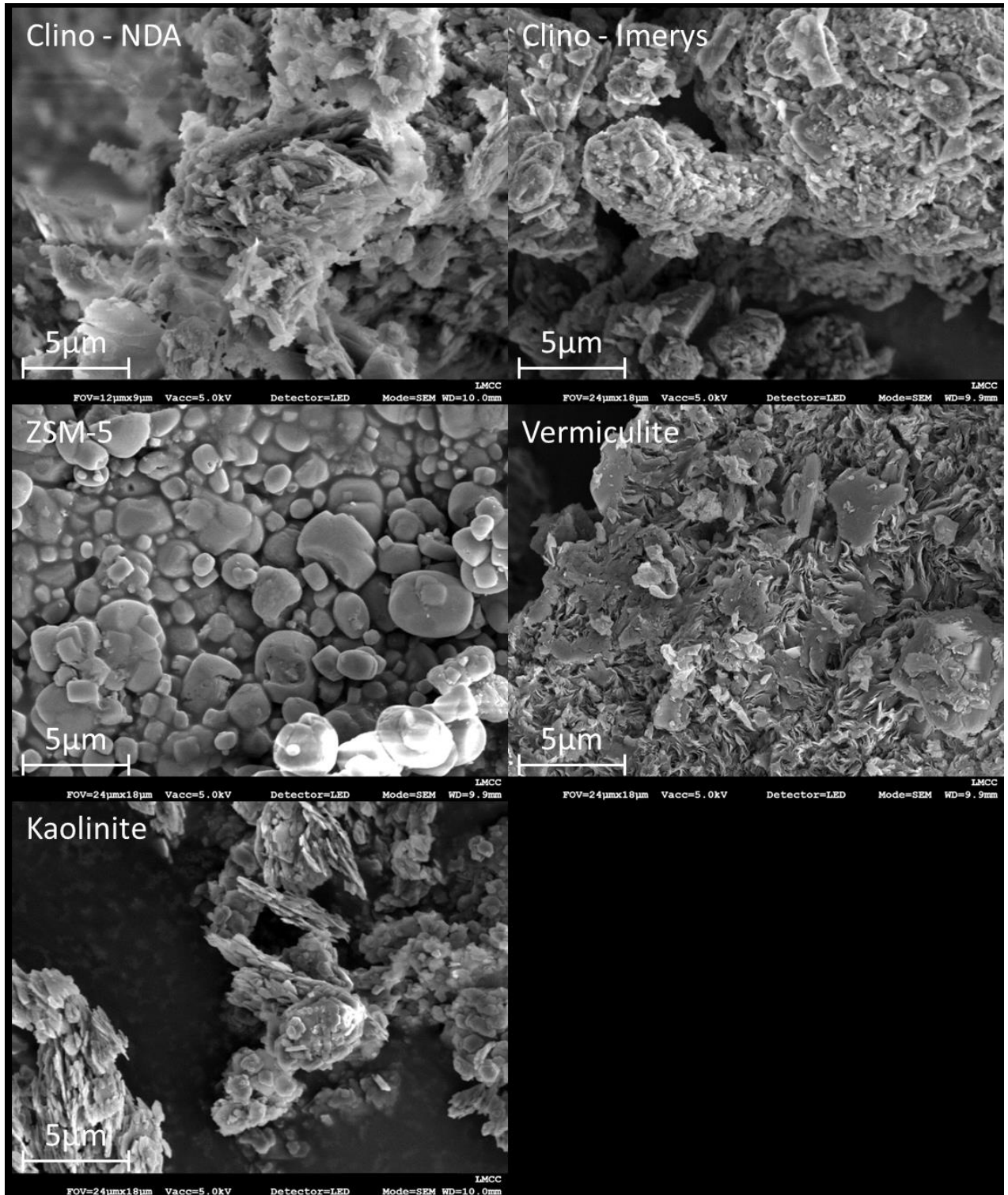
Figure 3.7: SEM micrographs of the materials selected for grafting experiments.

For comparison optical images of the materials used are shown below in figure 3.8.

Figure 3.8: Images of the materials selected for grafting experiments.

As can be seen the particle size of the two clinoptilolite samples are vary with the unprocessed clinoptilolite (NDA) sample having larger particles.

3.1.5 CHN analysis to determine carbon content.

The carbon content of the solid supports was determined before any modification experiments were carried out to allow the amount of ligand on the solids to be determined. The result of the CHN analyses are summarised in Table 3.5

Table 3.5: CHN analysis on unmodified samples; esd in parentheses

Material	C%	H%	N%
Clinoptilolite (NDA)	0.03(3)	0.84(3)	0.01(3)
Clinoptilolite (IMERYS)	0.07(3)	0.53(3)	0.03(3)
ZSM-5	0.04(3)	0.07(3)	0.05(3)
Vermiculite	0.39(3)	0.82(3)	0.17(3)
Kaolinite	0.07(3)	0.53(3)	0.03(3)

The variation in carbon, hydrogen and nitrogen between different samples is relatively small and within acceptable variation of the instrument. This is perhaps slightly surprising given the natural origins of the samples although the carbon content of the materials is expected to be low by the nature of the compounds; as cationic clays/zeolites, incidence of carbon containing species between the layers and within the cages is unusual. The amount of carbon was selected to investigate the success of the grafting experiments since the nitrogen content of the ligands is low compared to carbon. The amount of hydrogen in the materials was considered to be unreliable as the amount of water that may be found in the cages or layers of the material can vary considerably with the cations occluded within them.

The amount of ligand grafted is calculated from the measured difference in carbon according to Equation 3.1 given.

$$\% \; difference \; in \; C\% = X$$

$$\frac{X}{100} \; x \; mass \; of \; sample \; (mg) = Y$$

$$\frac{Y}{1000} = mass \; (g)$$

$$\frac{mass \; (g)}{RMM \; (12.0)} = moles \; of \; C$$

$$\frac{mass \; of \; ligand}{mass \; of \; carbon \; (12.0)} \; x \; moles \; of \; C = moles \; of \; ligand \; grafted$$

$$\frac{moles \; of \; ligand \; grafted}{mass \; of \; sample \; analysed \; (g)} = moles \; / \; g$$

Equation 3.1

In using this equation, an assumption is made that all of the carbon is within the grafted ligand and the ligand grafted remains intact. The moles of ligand grafted is then compared as the calculation accounts for the weight of sample used for analysis. For comparative purpose, the results are presented as moles of ligand grafted per gram of support material.

3.1.6 Functional group identification by FTIR

FTIR of the solid support materials was carried out before and after modification to allow the materials to be compared. This allowed the structure of the solid support to be monitored after modification to see if any changes had occurred. Selected IR bands are summarised in Table 3.6

Table 3.6 Summary of IR bands exhibited by materials before grafting

	Observations / cm^{-1}							
Zeolites	**NH$_2$ Stretch**	**O-H Asymmetric stretch**	**CH$_2$ Stretch**	**Si-O Stretch / H$_2$0**	**Si - O Asymmetric stretch**	**T- O Symmetric stretch**	**Double rings**	**T-O bend**
Literature values[50]	3300-3500	3200-3400	2900-3100	1600-1700	1250-950	820-650	650-500	500-420
Clinoptilolite (NDA)		3411		1636	1033	736	574	431
Clinoptilolite (Imerys)		3379		1632	1018	786	586	432
ZSM-5		3332		1643	1064	802	547	432
Clays[102,148,149]	**Si-O-Si stretch**	**OH Stretch**	**CH$_2$ Stretch**	**Si-O Stretch / H$_2$0**	**Si-O Symmetric stretch**	**Si-O-Si stretch**	**Al-OH bend**	**Si-O-Al /Si-O-Si bend**
Literature values	3650-3695	3620-3550	2900-3100	1600-1700	1200-1400	1150-1050	950-600	550-500
Vermiculite		3654		1651	1273	972	748	532
Kaolinite	3687	3618		1627	1273	1002	756	532

The materials all show IR absorptions associated with Si/Al-O vertex-sharing tetrahedra which is expected due to the structures of the materials. C-H stretches are included in this table as a number of synthetic zeolites, including ZSM-5, are synthesised using an organic template. Typically, large alkyl ammonium cations are used as the template for the cages which are then removed by calcination after synthesis to empty the cages and allow their properties of e.g. ion exchange or catalysis to be realised. Full characterisation of the templated material often includes identification of the C-H and N-H bands associated with their templates. There is also O-H stretch present which could be an indicator of Brønsted acid sites or water within the zeolite or clay solid support.

3.2 Introduction into modification experiments

This part of the study involves surface modification of the support materials characterised in 3.1 for the purpose of extracting high oxidation state actinide species from nuclear waste streams. The idea being that utility of materials such as zeolites and clays which are capable of ion exchange, can be increased by adding chelating species to the surface of the material and remove the actinides in the water through chelation as well as removing the low valent ions through ion exchange. Due to the size and charge of the actinide species, ion exchange would not usually be a reasonable method for extraction of the actinide species. Preliminary experiments were conducted to assess the viability of attaching ligands to the surface. Further experiments were then carried out to optimise the grafting process by exploring different parameters such as reaction time, concentration and solvent polarity. The ligands were selected based on the functional groups present and the ions in solution being targeted after the review of the literature that is described in Chapter 1.
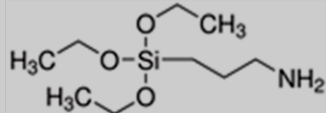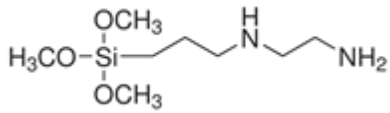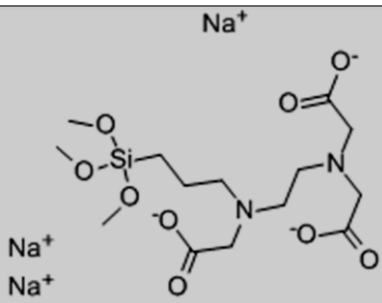
3.2.1 Ligands selected

The ligands that have been selected for use can be seen in Table 3.7, these are (3-aminopropyl)triethoxysilane (APTES), N-[3-(trimethoxysilyl)propyl] ethylenediamine (TMSPE) and N-[(3-Trimethoxysilyl)propyl]ethylenediamine triacetic acid trisodium salt (TMSPETT). APTES and TMSPE both have amine functionalities. Nitrogen donors are termed hard donors by hard-soft acid base theory (HSAB). This should allow the removal of uranium in solution. Uranium forms UO_2^{2+} in solution, with an atomic radius of 1.8 Å and an overall charge of +2.[150,17,19,37] Light ions in the s and p-block, ions formed in early d-block and f-block ions are also considered hard by hard-soft acid base theory. Therefore, ligands with nitrogen donors should facilitate the removal of uranium from solution.[69]

The more electronegative an ion the harder it is considered to be in HSAB theory, hence oxygen is a harder base than nitrogen. Plutonium forms PuO_2^+ in solution and has a smaller radius of 1.15 Å than uranium, and is designated harder than uranium.[150] Therefore TMSPETT was selected with oxygen donors to facilitate the removal of plutonium from solution. The ligands were selected as they have already shown the ability to remove metal ions such as Cd^{2+}, Cu^{2+}, Ni^{2+}, Pb^{2+} and Zn^{2+} from solution.[151]

Due to the very low concentration of the actinides in the SIXEP liquor, a relatively small amount of surface alteration is theoretically needed to remove the long-lived actinide species entirely from solution.[7,10,14,95]

Table 3.7: Ligands chosen for the grafting experiments and their chemical structure.

Ligand	Chemical structure
(3-Aminopropyl)triethoxysilane (APTES) **RMM 221.37 gmol^{-1}, ρ 0.946 gmL^{-1}**	
N-[3-(trimethoxysilyl)propyl] ethylenediamine (TMSPE) RMM 222.36 gmol^{-1}, ρ 1.028 gmL^{-1}	
N-[(3-Trimethoxysilyl)propyl]ethylenediamine triacetic acid trisodium salt (TMSPETT) **RMM 462.41 gmol^{-1}, ρ 1.26 gmL^{-1}**	

3.3 Preliminary grafting experiments

Preliminary experiments to test the ability of the surface of the zeolite for grafting ability were conducted on both clinoptilolite samples using a method previously described by Holt .[135]

2g of clinoptilolite was weighed out and placed into a 100 mL round bottom flask fitted. 3 mL (1.28 x 10^{-2} moles) of APTES was measured out using a 5 mL plastic syringe and placed into a beaker containing 15 mL of acetone. The resulting solution was then placed into the round bottom flask and a reflux condenser added. The sample was allowed to reflux for a period of 2h. The mixture was then filtered under vacuum using a number 3 sintered glass crucible. The separated solid was then washed with 3 x 20 mL of deionised water and left to air dry. The solid was then transferred to a watch glass and placed inside a carbolite oven at 80°C and allowed to fully dry. The sample was then analysed by powder X-ray diffraction, infrared spectroscopy and elemental analysis. Diffraction patterns were collected for 2θ values between 5 and 60 using a Bruker D8 ADVANCE diffractometer in reflectance geometry operating with monochromated Cu$_{K\alpha1}$ radiation. The collected diffraction patterns were analysed using the Bruker Eva software with the PDF MaintEX library version 9.0.133 to determine the phases present. Elemental analysis was carried out using an Exeter Analytical CE-440 analyser

The proposed mechanism can be seen in Figure 3.9, where the $SiOCH_2CH_3$ group of the ligand is replaced by the oxygen of the OH group on the surface of the silicate.
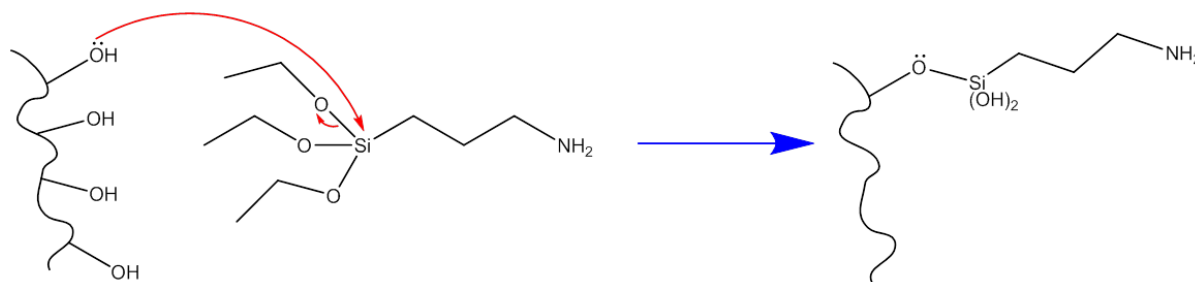
Figure 3.9: Proposed reaction mechanism for the incorporation of APTES on a silicate surface via silanol groups

The CHN results given below in Table 3.5 obtained from these experiments show that there is an increase in the organic content (carbon, hydrogen and nitrogen) of the sample after the reaction had occurred.

Table 3.8 CHN analyses of APTES grafted clinoptilolite; esd given in parentheses

Material	Reaction time / hr	C%	H%	N%	Difference in C%	mmols of ligand / g
Clinoptilolite (NDA)	Unreacted	0.03(3)	0.84(3)	0.01(3)		
Clinoptilolite (NDA)	2	1.83(3)	1.12(3)	0.46(3)	1.80	22.62
Clinoptilolite (Imerys)	Unreacted	0.07(3)	0.53(3)	0.03(3)		
Clinoptilolite (Imerys)	2	1.29(3)	0.95(3)	0.32(3)	1.22	18.72

^{13}C SSNMR analysis was carried out on the samples after grafting and an example of the spectrum is given in Figure 3.10. The spectrum indicates that a carbon based compound is present, however, there was also some residual solvent in the sample. The SSNMR confirms that the ligand is present as a solid and not in the pores as a liquid. There are three resonances at 43, 22 and 11ppm corresponding to the CH_2 and CH_3 groups present in the molecule in agreement with previous work.[135,138] The solvent resonances can be seen at 30 and 164 ppm which indicate the acetone solvent used in the reaction has not being fully removed.
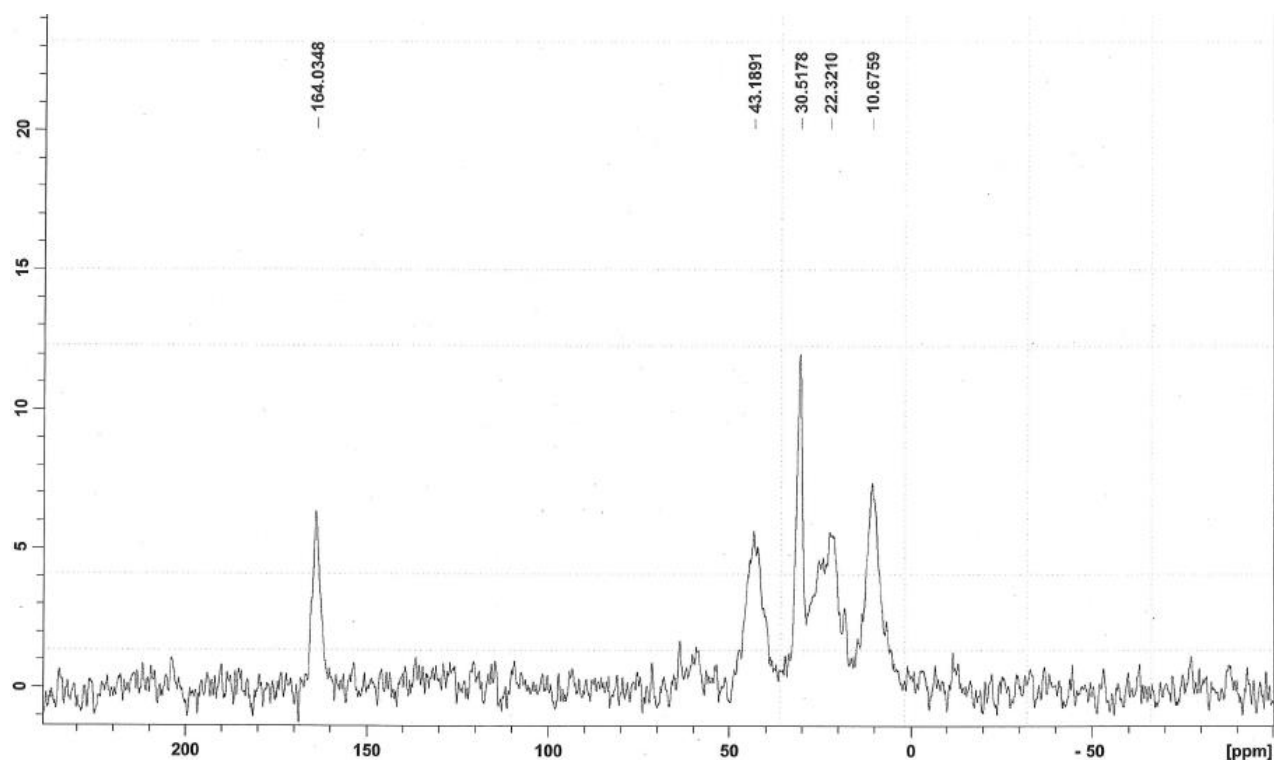
Figure 3.10: ^{13}C SSNMR spectrum of APTES grafted clinoptilolite (NDA).

This result meant that the drying process was increased to twenty-four hours to ensure the removal of the solvent from the pores and layers in future experiments. A blank SSNMR spectrum is shown in Figure 3.11. This shows an example where the ligand does not appear to have grafted and the small carbon increase seen in the CHN is due to residual solvent in the sample, which can be seen at about 30 ppm (CH$_3$) and 164 ppm (C=O). This clearly indicates a difference in the spectra when the ligand is successfully grafted and/or grafted to a sufficiently high level to observe a spectrum. Further work on changing the reaction parameters in terms of time, type of solvent and concentration of ligand followed to increase the amount of ligand functionalisation taking place. Liquids do not give SSNMR signals unless coordinated to the solid, so the acetone must be interacting with the framework.
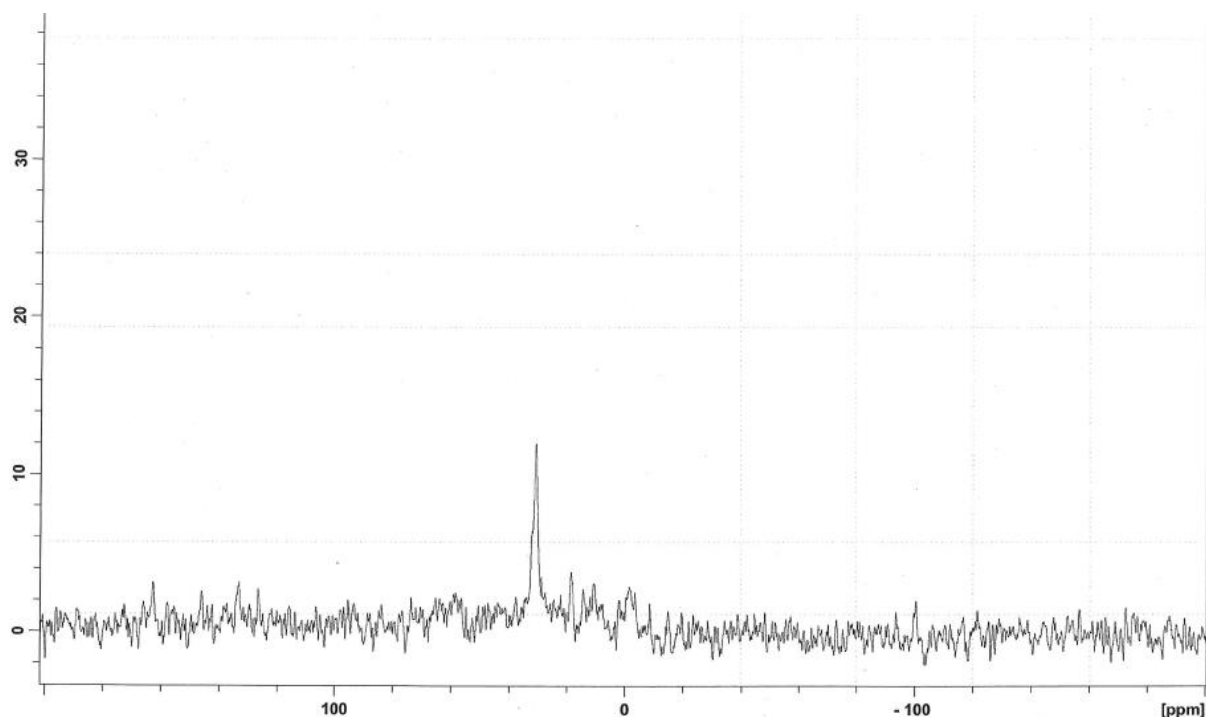
Figure 3.11: ^{13}C SSNMR spectrum of clinoptilolite (IMERYS) where no appreciable ligand grafting was detected.

Raman data were also collected on the clinoptilolite NDA and modified clinoptilolite. Since the framework bonds of aluminosilicate species are strongly polarised, IR stretches of the framework are extremely strong resulting in spectra where cage species and/or grafted species are difficult to detect. Due to a different set of selection rules based on polarizability, framework bands are weak in Raman spectroscopy and occluded/grafted species are more easily identified. However, it can be seen from Table 3.6 that no changes were seen in the Raman data for the reacted and unreacted material, showing that the overall structure of the material remains unchanged. The peaks observed in the Raman correspond to the framework structure of the T-O-T bonds relating to the Si-O-Si bonds and the Si-O-Al bonds. The additional band seen in the clinoptilolite NDA sample is attributed to other phases present in the sample.

Clinoptilolite NDA	Clinoptilolite NDA + APTES	Clinoptilolite Imerys	Clinoptilolite Imerys + APTES
415	409	412	409
569	570	566	569
651	652		

FTIR analysis carried out on the clinoptilolite after grafting showed little change except the appearance of a weak band at 2932 cm^{-1} that lies in the C-H region.

The Raman and FTIR data are supported by the PXRD pattern shown in Figure 3.12, which shows no change to the patterns. The long-range order of the sample after modification is unlikely to change as the small number of silanol groups that are functionalised are likely to do so in a random fashion across the framework rather than in an ordered way that will change the PXRD pattern. This is in full agreement to previous studies on surface modified clays and zeolites. [4,8–10,12,33–36,47,55,56,59,62,63,71,75,79–83,87,88,92,99,100,113–115,120,122,127,129,148,149,152–160]
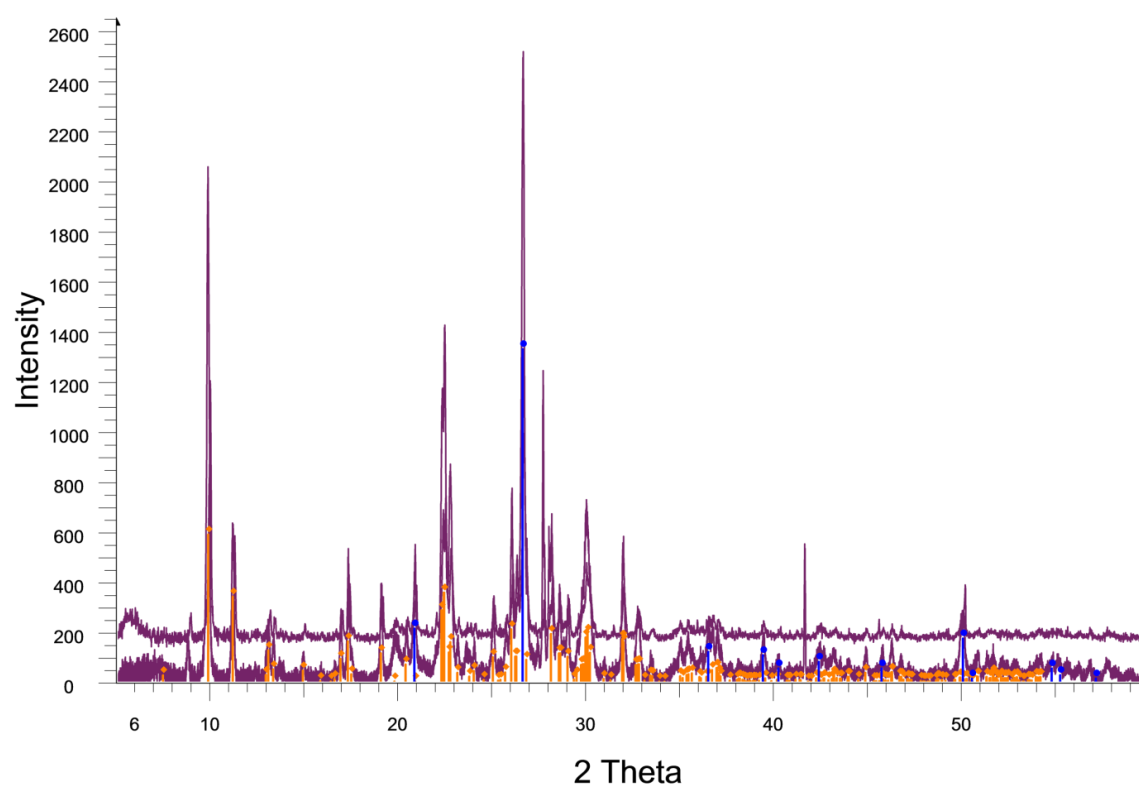
Figure 3.12: Example PXRD pattern of APTES grafted clinoptilolite (Imerys), showing no changes to the pattern, in agreement with the hypothesis that there is no change to the long range order.

The results from the preliminary experiments show that the ligand is present as a coordinated ligand, indicating that some grafting has occurred. The results support the idea that the grafting of the ligand does not affect the long-range order of the sample and that in theory the zeolite should still be able to undergo ion exchange. The results also show that both the samples require longer drying times to full remove any solvents present. This can be attributed to the solvent entering the pores of the zeolites requiring longer drying times to remove all the solvent, whereas the reported method by Holt used silicon dioxide of varying particle size but with no pores.[135]

3.4 Surface grafting experiments

This section investigates the differing amount of ligand grafting depending on the reaction conditions. The effect of reaction time, concentration of ligand and polarity of the solvent used was studied for all the materials and ligands to create a range of materials.

3.4.1 Characterisation of modified materials: Investigating reaction time, concentration and solvent effect on APTES grafting

3.4.1.1 Clinoptilolite NDA

3.4.1.1.1 Effect of reaction time

2 g of clinoptilolite (NDA) was accurately weighed out using an analytical balance, and added to a 100 mL round bottomed flask fitted with a reflux condenser. 20 mL of acetone was added to the flask and heated with stirring until reflux occurred. 8 mL (2.14×10^{-2} moles) of APTES was then added to the flask down the condenser using a 10 mL syringe fitted with a long needle. The flask was refluxed for either 1, 2, 4, 8, 16 or 24 hours. The flask was allowed to cool and the reaction mixture separated under vacuum filtration using a büchner flask and sintered glass filter. The separated solid was then washed with acetone (3 x 20 mL) followed by deionised water (3 x 50 mL) and then transferred to a watch glass, placed into an oven at 120 °C and allowed to dry for 24 hours. The sample was then analysed by powder X-ray diffraction, infrared spectroscopy and elemental analysis. Diffraction patterns were collected for 2θ values between 5 and 60 using a Bruker D8 ADVANCE diffractometer in reflectance geometry operating with monochromated $Cu_{K\alpha1}$ radiation. The collected diffraction patterns were analysed using the Bruker Eva software with the PDF MaintEX library version 9.0.133 to determine the phases present. FTIR spectra were collected between 4000-400 cm^{-1} in transmission mode using a shimazdu 8400S FTIR spectrometer. Elemental analysis was carried out using an Exeter Analytical CE-440 analyser.

3.4.1.1.1.1 Carbon content determined by elemental analysis

The results from the CHN analysis can be seen graphically in Figure 3.13 and is presented in tabulated form in Table 3.10. The results show the increase in carbon content with reaction time.
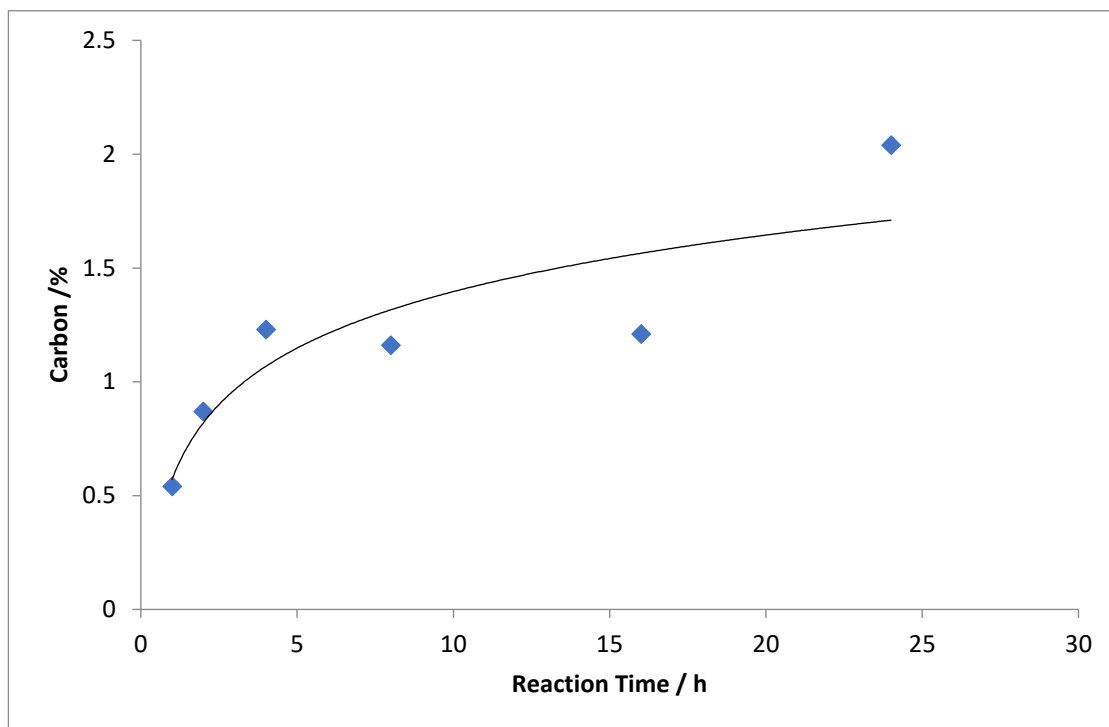
Figure 3.13: Graphical representation of the change in carbon content (%) with reaction time (h)

Table 3.10 Change in carbon content (%) with reaction time (h); esd given in parentheses[140]

Material	Reaction time / hr	C%	H%	N%	Difference in C%	mmol ligand /g
Clinoptilolite	unreacted	0.03(3)	0.84(3)	0.01(3)		
Clinoptilolite	1	0.54(3)	0.90(3)	0.05(3)	0.51	7.83
Clinoptilolite	2	0.87(3)	1.14(3)	0.38(3)	0.84	18.41
Clinoptilolite	4	1.23(3)	1.00(3)	0.71(3)	1.20	12.89
Clinoptilolite	8	1.16(3)	0.98(3)	0.23(3)	1.13	17.34
Clinoptilolite	16	1.21(3)	1.01(3)	0.45(3)	1.18	18.11
Clinoptilolite	24	2.04(3)	1.11(3)	0.45(3)	2.01	30.84

As the reaction time is increased, the proportional percentage of carbon also increased, suggesting that the amount of graft on the surface is also increasing. This process can be attributed to the increased contact time in the solvent allowing more interactions between the available surface sites and the ligand. By allowing more time for the reaction to take place, the probability of the surface sites and the ligand aligning in the appropriate way to allow reaction increases resulting in reaching the observed limit of 2.01% carbon increase and 0.096 mmol of graft in a 24 h period. Further increases in the time were not explored.

3.4.1.1.1.2 Phase identification by PXRD

The PXRD pattern of the clinoptilolite (NDA) samples after reaction with the ligand can be seen below in Figure 3.14.
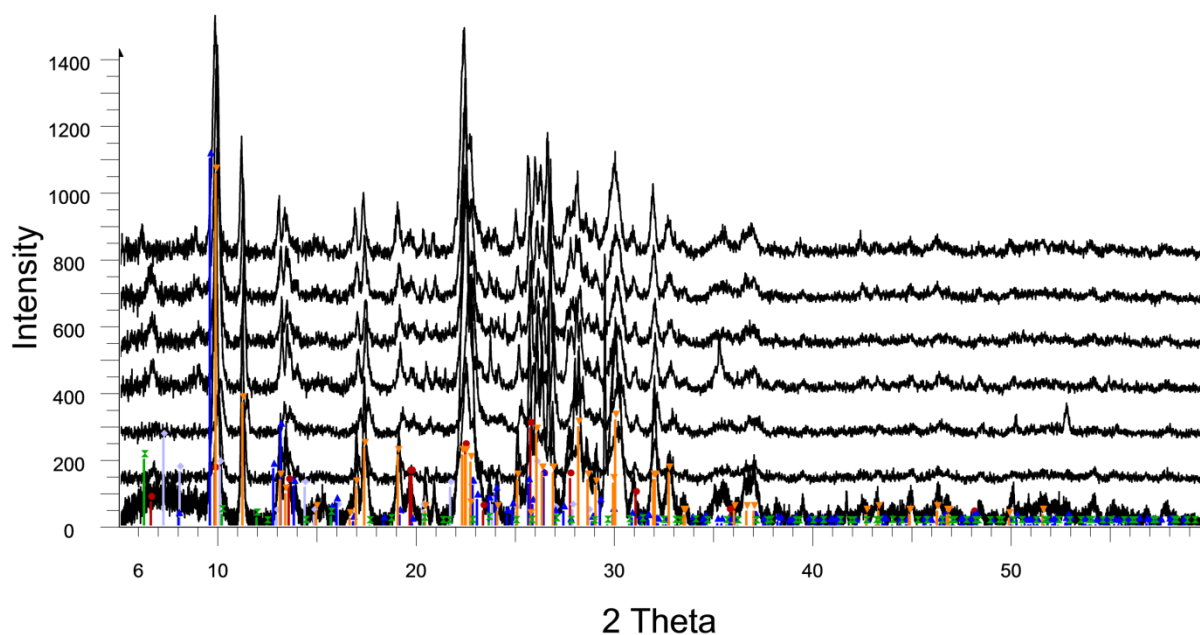
Figure 3.14: PXRD patterns of clinoptilolite (NDA) after 1,2,4,8, 16 and 24h (increasing hours from 2nd to bottom to top) against reference pattern (bottom).

The PXRD pattern shows that there is no change in the long-range order of the samples after grafting. This is expected as the ligand is expected to graft to only a small number of groups on the surface due to the size of the ligand and rigidity of the three-dimensional cage structure preventing any alteration of the long range structure. Clinoptilolite is a stable zeolite and the addition of solvent, heat and organic to the structure would not be expected to cause any structural changes in the quantities used.

3.4.1.1.1.3 Functional group identification by FTIR

Analysis by IR showed very little differences in the spectra before and after grafting as previously observed in the preliminary experiments. The C-H stretch that was observed in the clinoptilolite samples after grafting in the preliminary experiments at $\sim$ 2950 cm^{-1}, was visible at the longer reaction times of 16-24 h in these experiments. Both IR and XRD analyses indicate that no change in the long range order for the zeolite occurs on grafting at these low levels. These experiments led to the reaction time for grafting experiments for APTES to be fixed at 24h.

3.4.1.1.2 Effect of ligand concentration

The methodology described in 3.4.1.1.1 was replicated for these experiments except the ligand concentration was altered by adding 3 ml (1.28 x 10^{-2} moles), 5 ml (2.14 x 10^{-2} moles) or 8 ml (3.41 x 10^{-2} moles) of APTES into the reaction mixture in three different experiments. All other parameters and analyses were the same.

3.4.1.1.2.1 Analyses of clinoptilolite (NDA) after APTES grafting

The results from the CHN analysis are tabulated in Table 3.11. The results show that the amount of ligand grafted increases with the ligand concentration.

Table 3.11: CHN analysis of clinoptilolite with increasing ligand concentration; esd are given in parentheses.

Material	Concentration (moles)	C%	H%	N%	Difference in C%	mmol of ligand /g
Clinoptilolite	unreacted	0.03(3)	0.84(3)	0.01(3)		
Clinoptilolite	1.28 x 10^{-2}	1.12(3)	1.26(3)	0.31(3)	1.09	16.73
Clinoptilolite	2.14 x 10^{-2}	1.83(3)	1.43(3)	0.51(3)	1.80	27.62
Clinoptilolite	3.41 x 10^{-2}	2.04(3)	1.11(3)	0.45(3)	2.01	30.84

By increasing the molar concentration of the ligand available, there are more molecules available for surface grafting. The results show that as the ligand concentration is increased, the extent of the grafting also increases. As the change between 3ml and 5ml is less than between 5ml and 8ml, it may suggest that the effect of increased concentration is reducing. This can be attributed to the available surface sites being in excess at low ligand concentration but becoming occupied with ligand as the

concentration increases until eventually all the available sites are full. In keeping with previous experiments, neither the XRD nor the IR showed any differences before and after the graft, except the appearance of the C-H band in the IR spectrum of the clinoptilolite after grafting. In later experiments, the quantity of APTES was fixed at 8ml (3.41 x 10^{-2} moles).

3.4.1.1.3: Effect of solvent polarity

The methodology described in 3.4.1.1.1 was followed to investigate whether grafting of APTES to clinoptilolite (NDA) was effected by changing the polarity of the solvent used. Methanol, ethanol, dichloromethane, toluene or hexane replaced the acetone in the reaction mixture in the same volume (20 ml).   The reaction time was 24 h and 8 ml of APTES was used.

3.4.1.1.3.1: Analysis of clinoptilolite (NDA) after grafting experiments.

The results from the CHN analysis can be seen graphically in Figure 3.15 and tabulated in Table 3.12. The results show that the amount of ligand grafted decreases as the polarity of the solvent decreases.
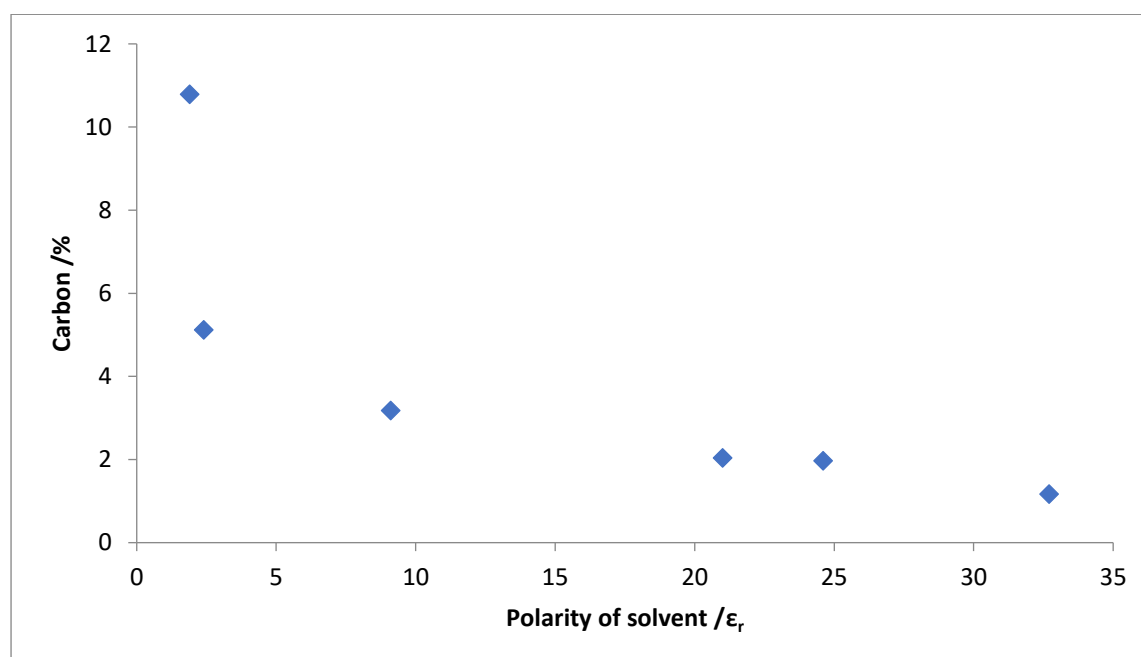
Figure 3.15: Graph of the change in carbon content of clinoptilolite (NDA) after APTES grafting with polarity of the solvent

By decreasing the polarity of the solvent, the amount of graft was increased from 1.14% carbon (0.033 mmol ligand) grafted to 10.76% carbon (0.227 mmol ligand) grafted. The ligand has a polar and a non-polar end. By using a non-polar solvent such as hexane, the polar end of the ligand and the polar surface groups of the zeolite are attracted to each other and the non-polar end group of the ligand is included into the solvent encouraging the ligand to be in a favourable orientation for the grafting reaction to occur.

Table 3.12 Change in carbon content of grafted clinoptilolite as a function of solvent polarity after 24 h; esd are given in parentheses.

Material	Solvent	Dielectric constant	C%	H%	N%	Difference in C %	mmol of ligand /g
Clinoptilolite	unreacted		0.03(3)	0.84(3)	0.01(3)		
Clinoptilolite	Hexane	1.9	10.79(3)	2.80(3)	3.66(3)	10.76	56.16
Clinoptilolite	Toluene	2.4	5.12(3)	1.31(3)	0.52(3)	5.09	26.39
Clinoptilolite	DCM	9.1	3.18(3)	1.80(3)	1.72(3)	3.15	12.12
Clinoptilolite	Acetone	21.0	2.04(3)	1.11(2)	0.45(3)	2.01	6.91
Clinoptilolite	Ethanol	24.6	1.97(3)	1.45(3)	0.79(3)	1.94	7.98
Clinoptilolite	Methanol	32.7	1.17(3)	1.19(3)	0.31(3)	1.14	4.76

In agreement with previous observations, the PXRD patterns show no notable changes indicating no real change to the long range order, see appendix 8.1. Between 2950 and 3000 cm^{-1}, the characteristic C-H band appears in the IR spectrum for all sample. Even though the nitrogen content is now significant, there is no real indication of additional bands appearing between 1650 and 1700 wavenumber; the strongly polar Si-O framework stretch at 1627 cm^{-1} is very broad and may always obscure the more weakly polar N-H stretch that is expected to be less strong see appendix 8.2.

3.4.1.1.4: Summary of Clinoptilolite (NDA)

Increase in ligand grafting was seen with reaction time, ligand concentration and decreased solvent polarity in the case of clinoptilolite (NDA). Of these three the most significant effect was seen with the reaction solvent, where using a non-polar solvent increased the graft to approximately 10%. This can

be attributed to the non-polar solvent encouraging the orientation of the ligand to be more favourable for the grafting reaction to occur. No change is seen in the structure of clinoptilolite (NDA) by PXRD as expected by the low proportion of graft. The only change in the IR is the appearance of a weak IR band in the C-H region of the spectrum at ca. 2950 cm^{-1}

3.4.1.2 Clinoptilolite (Imerys)

3.4.1.2.1 Effect of reaction time

Following the same procedures carried out in sections 3.4.1.1, analogous grafting experiments were carried out on the second sample of clinoptilolite with a smaller particle size and less impurities provided by Imerys. As only clinoptilolite and quartz had been identified in these materials, the location of the graft would be restricted to a smaller number of possible phases.

3.4.1.2.1.1 Analysis of clinoptilolite (Imerys) after grafting

The results from the CHN analysis can be seen graphically in Figure 3.16 and tabulated in Table 3.13. The results show that the carbon content increases with the reaction time in a similar way to that observed for the clinoptilolite sample provided by the NDA. The carbon content after 24 h was however higher for this material. The likely reason for the higher final carbon content being that the smaller particle size leads to a greater surface area and more available silanol groups for functionalisation.
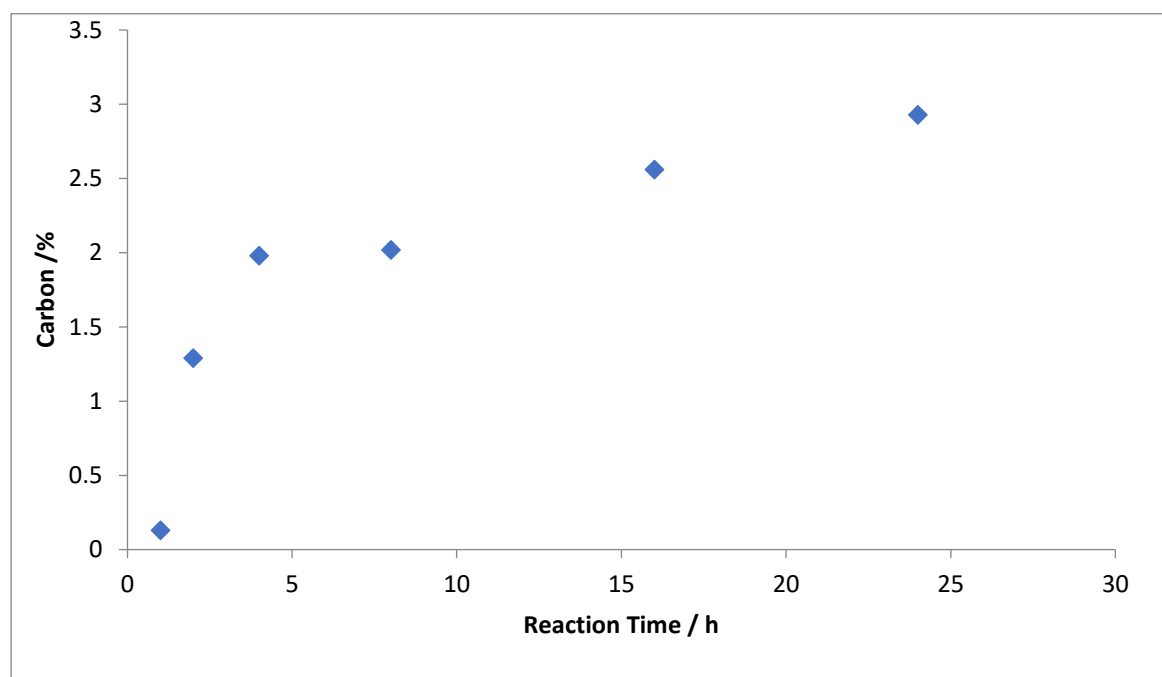
Figure 3.14: Graph of the change in carbon content as a function of reaction time.

By increasing the reaction time the amount of graft can be seen to increase, this can be attributed to the added contact time allowing more interactions between the available surface sites and the ligand. By allowing more time for the reaction, the probability of the surface sites and the ligand aligning to allow reaction increases and gives a greater overall functionalisation. The smaller particle size appears to have allowed significantly greater functionalisation in the case of this sample compared to that used in the NDA plant.

Table 3.13: Change in carbon content (%) with reaction time (h); esd given in parentheses

Material	Reaction time / hr	C%	H%	N%	Difference in C%	mmol of ligand /g
Clinoptilolite	unreacted	0.07(3)	0.53(3)	0.03(3)		
Clinoptilolite	1	0.13(3)	0.46(3)	0.02(3)	0.06	0.92
Clinoptilolite	2	1.29(3)	0.95(3)	0.32(3)	1.22	18.72
Clinoptilolite	4	1.98(3)	0.87(3)	0.52(3)	1.91	29.31
Clinoptilolite	8	2.02(3)	0.78(3)	0.39(3)	1.95	29.92
Clinoptilolite	16	2.56(3)	1.11(3)	0.50(3)	2.49	38.21
Clinoptilolite	24	2.93(3)	1.07(3)	0.63(3)	2.86	43.89

In agreement with previous observations, the PXRD patterns show no notable changes indicating no real change to the long-range order see appendix 8.1. Between 2950 and 3000 cm^{-1}, the characteristic C-H band appears in the spectrum in a similar way to the analogous experiments on the clinoptilolite (NDA) samples see appendix 8.2.

3.4.1.2.2 Effect of ligand concentration

The methodology described in 3.4.1.2.1 was replicated for these experiments except the ligand concentration was altered by adding 3 ml (1.28×10^{-2} moles), 5 ml (2.14×10^{-2} moles) or 8 ml (3.41×10^{-2} moles) of APTES into the reaction mixture in the three different experiments.

3.4.1.2.2.1 Analysis of clinoptilolite (Imerys) after grafting experiments

The results from the CHN analysis are tabulated in Table 3.14. The results show an increase in the amount of ligand grafted with increasing ligand concentration.

The variation in concentration does not seem to make much difference to the amount of ligand grafted over the concentration range studied.

In agreement with previous observations, the PXRD patterns show no notable changes before or after grafting indicating no real change to the long range order see appendix 8.1. Between 2950 and 3000 cm^{-1}, the characteristic C-H band appears in the spectrum in a similar way to the analogous experiments on the clinoptilolite (NDA) samples appendix 8.2.

Table 3.14: CHN analysis of clinoptilolite (Imerys) with increasing ligand concentration; esd are given in parentheses.

Material	Concentration (moles)	C%	H%	N%	Difference in C%	mmol of ligand /g
Clinoptilolite	unreacted	0.07(3)	0.53(3)	0.03(3)		
Clinoptilolite	1.28 x 10^{-2}	3.00(3)	1.15(3)	0.64(3)	2.93	44.96
Clinoptilolite	2.14 x 10^{-2}	3.38(3)	1.03(3)	0.80(3)	3.31	50.79
Clinoptilolite	3.41 x 10^{-2}	2.93(3)	1.07(3)	0.63(3)	2.86	43.89

3.4.1.2.3 Effect of solvent polarity

The methodology described in 3.4.1.2.1 was followed except the acetone solvent was replaced with a range of solvents with different polarities to examine whether ligand grafting was affected by polarity. Methanol, ethanol, dichloromethane, toluene or hexane replaced the acetone in the reaction mixture in the same volume (20 ml). The reaction time was 24 h and 8 ml of APTES was used.

3.4.1.2.3.1 Analysis of Clinoptilolite (Imerys) after grafting.

The results from the CHN analysis can be seen graphically in Figure 3.17 and tabulated in Table 3.15. In contrast to the previous experiments on the NDA sample of clinoptilolite, the Imerys sample does not show such a clear trend in relation to the change in polarity. The reason for this is not immediately clear as the spurious result is for acetone, but could be related to earlier result where the NDA sample of clinoptilolite was shown to absorb acetone readily, possibility due to the large channels in clinoptilolite. The larger surface area of the smaller particle sized Imerys material may have allowed greater acetone take up and more dense packing of the material during drying, meaning not all acetone could be removed from the sample, even during the extended drying period.
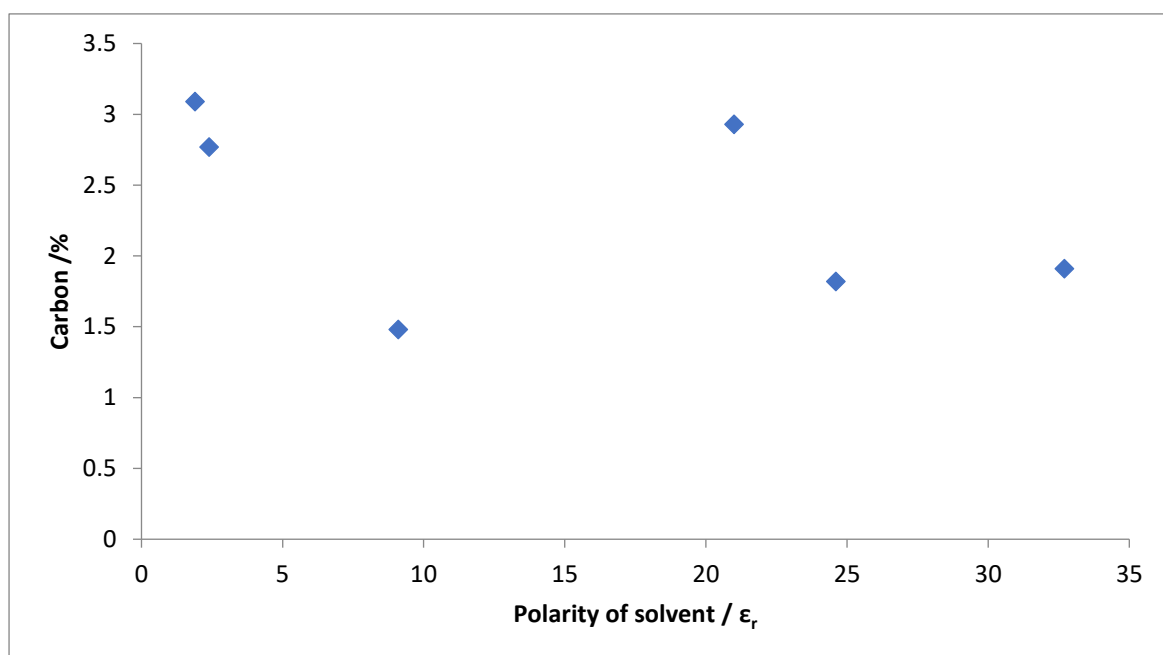
Figure 3.17: Graph of the change in carbon content (%) of clinoptilolite (Imerys) after grafting with the polarity of the solvent

Table 3.15 Change in carbon content of grafted clinoptilolite as a function of solvent polarity after 24 h; esd are given in parentheses.

Material	Solvent	Dielectric constant	C%	H%	N%	Diff in C%	Mmol of ligand
Clinoptilolite	unreacted		0.07(3)	0.53(3)	0.03(3)		
Clinoptilolite	Hexane	1.9	3.09(3)	1.40(3)	1.00(3)	3.02	15.35
Clinoptilolite	Toluene	2.4	2.77(3)	1.27(3)	0.79(3)	2.70	12.12
Clinoptilolite	DCM	9.1	1.48(3)	1.07(3)	0.46(3)	2.41	7.06
Clinoptilolite	Acetone	21.0	2.93(3)	1.07(3)	0.63(3)	2.86	9.67
Clinoptilolite	Ethanol	24.6	1.82(3)	1.05(3)	0.49(3)	1.75	7.52
Clinoptilolite	Methanol	32.7	1.91(3)	1.21(3)	0.64(3)	1.84	9.82

3.4.1.2.4: Summary of clinoptilolite (Imerys) experiments.

An increase in ligand grafting was seen with reaction time and ligand concentration. Solvent polarity had little effect on the amount of grafting observed. A graft of approximately 0.1 mmol is observed and appears to be the grafting limit for clinoptilolite (Imerys) and APTES. No change is seen in the structure of clinoptilolite (Imerys) by PXRD or FTIR see appendices 8.1 and 8.2.

3.4.1.3 ZSM-5

Grafting experiments were carried out using APTES as the ligand on the synthetic zeolite, ZSM-5. This sample has no quartz impurities and hence any modifications due to grafting must be as a result of changes to the zeolite itself.

3.4.1.3.1 Effect of reaction time

Following the same procedures carried out in sections 3.4.1.1, analogous grafting experiments were carried out on the sample of ZSM-5.

3.4.1.3.1.1 Analysis of ZSM-5 after grafting.

The results from the CHN analysis can be seen graphically in Figure 3.18 and tabulated in Table 3.16. The results show that the mmol of ligand grafted increases with the reaction time but the overall values are lower than with either sample of clinoptilolite.
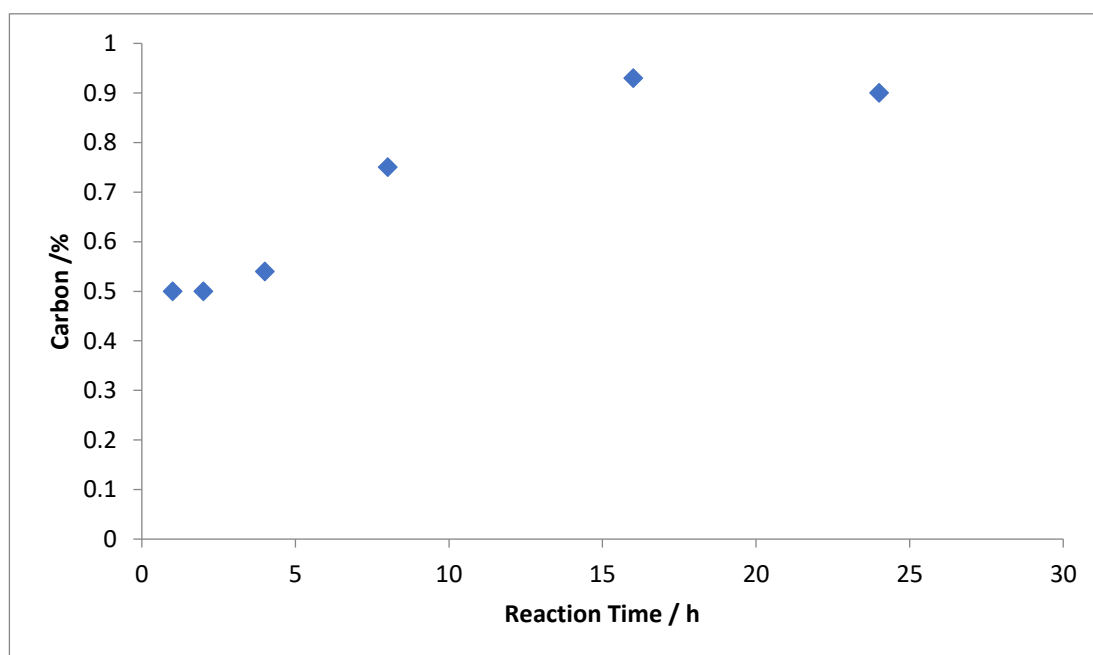
Figure 3.18: Graph of the change in carbon content (%) with reaction time (h) for ZSM-5.

Table 3.16: Change in carbon content (%) with reaction time; esd's given in parentheses.

Material	Reaction time / hr	C%	H%	N%	Difference in C%	Mmol of ligand / g
ZSM-5	unreacted	0.04(3)	0.07(3)	0.05(3)		
ZSM-5	1	0.50(3)	0.16(3)	0.13(3)	0.46	7.06
ZSM-5	2	0.50(3)	0.09(3)	0.15(3)	0.46	7.06
ZSM-5	4	0.54(3)	0.08(3)	0.16(3)	0.50	7.67
ZSM-5	8	0.75(3)	0.16(3)	0.16(3)	0.71	10.90
ZSM-5	16	0.93(3)	0.17(3)	0.19(3)	0.89	13.66
ZSM-5	24	0.90(3)	0.14(3)	0.17(3)	0.86	13.20

In keeping with results from the clinoptilolite samples, increasing the reaction time allows more grafting of the APTES ligand. Since increasing the contact time allows greater opportunity for the appropriate interactions and reaction between the ligand and substrate to take place, this is an expected result. The much lower levels of functionalisation may be as a result of the ZSM5 having less available sites for functionalisation.

The PXRD pattern of the reacted samples can be seen below in Figure 3.19. No change is seen in the pattern that would be consistent with a change to the long range order, such as the appearance of additional reflections particularly at low angle. This is in agreement with what was observed with the clinoptilolite samples and previous work on surface functionalised silicas.[135,160]
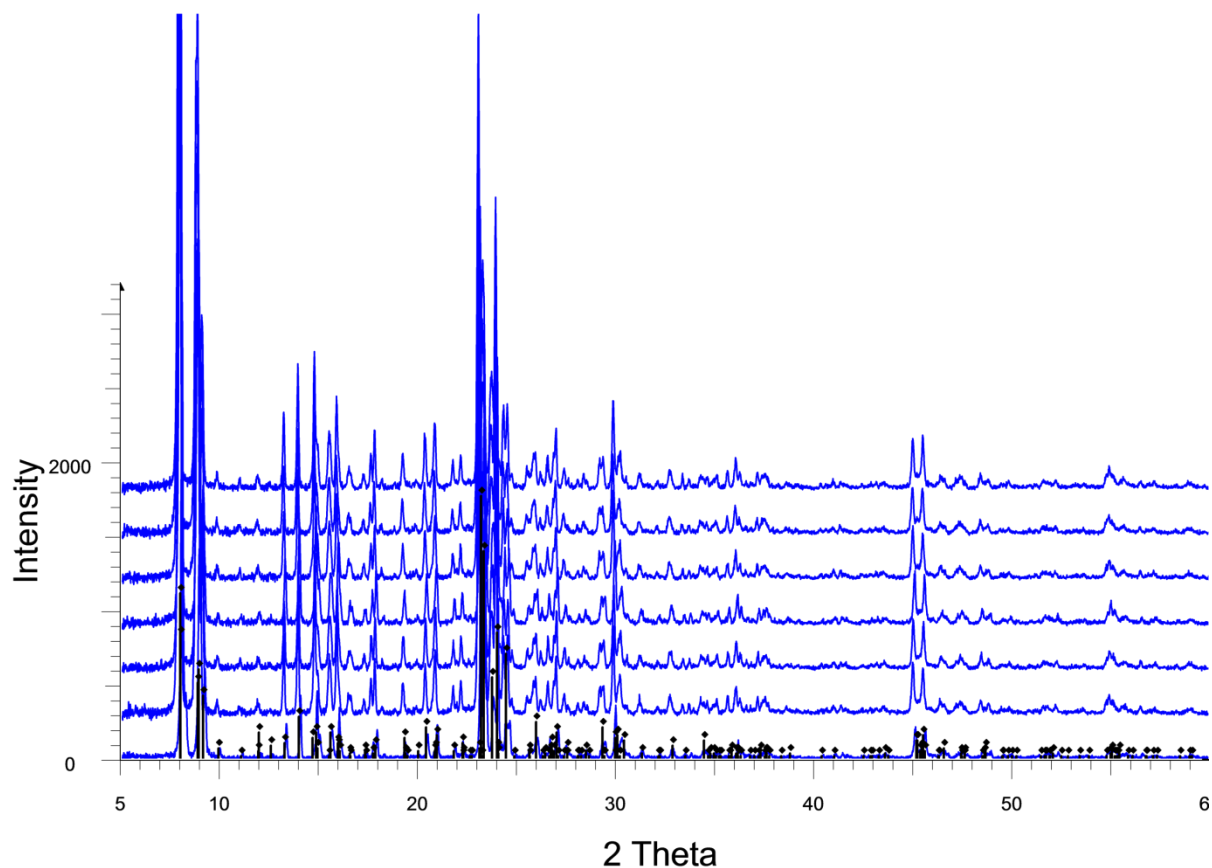
Figure 3.19: PXRD patterns of ZSM-5 after grafting for 0,1,2,4,8,16 and 24 h. Shortest reaction time to the longest reaction time increasing upwards.

ZSM-5 is a zeolite which is used for acid catalysis such as the separation of the different isomers of xylene. It would not be expected to degrade under these mild reaction conditions as those used for acid catalysis are much more extreme. Therefore these results are consistent with what is expected for this compound.

IR analyses of the compounds formed during the grafting process showed little change except the appearance of a band in the C-H stretching region, in agreement with the work carried out on clinoptilolite see appendix 8.2.

3.4.1.3.2 Effect of ligand concentration

The methodology described in 3.4.1.2.1 was replicated using the ZSM-5 as the substrate and the ligand concentration was altered by adding 3 ml (1.28×10^{-2} moles), 5 ml (2.14×10^{-2} moles) or 8 ml (3.41×10^{-2} moles) of APTES into the reaction mixture in the three different experiments. The experiments were carried out over a 24h period.

3.4.1.3.2.1 Analysis of ZSM-5 after experiments to investigate ligand concentration.

The results from the CHN analysis are tabulated in Table 3.17. The results show that the mmol of ligand grafted increases with ligand concentration.

Table 3.14: Change in carbon content (%) and a function of ligand concentration (moles); esd's are given in parentheses

Material	Concentration (moles)	C%	H%	N%	Difference in C%	mmol of ligand /g
ZSM-5	unreacted	0.04(3)	0.07(3)	0.05(3)		
ZSM-5	1.28×10^{-2}	0.85(3)	0.16(3)	0.17(3)	0.81	12.43
ZSM-5	2.14×10^{-2}	0.88(3)	0.2(3)	0.27(3)	0.84	12.89
ZSM-5	3.41×10^{-2}	0.90(3)	0.14(3)	0.17(3)	0.86	13.20

Very little change was observed between the lowest and highest concentration, suggesting that the amount of modification is unaffected by the ligand concentration. Both in these experiments and in those where variable time was used, the maximum graft appears to be only 1% carbon, lower than that observed for the samples of clinoptilolite.

In agreement with previous observations, the PXRD patterns show no notable changes before or after grafting indicating no real change to the long range order see appendix 8.1. Between 2950 and 3000 cm^{-1}, the characteristic C-H band appears in the spectrum in a similar way to the analogous experiments on the clinoptilolite (NDA) samples see appendix 8.2.

3.4.1.3.3 Effect of solvent polarity

The methodology described in 3.4.1.3.1 was followed except the acetone solvent was replaced with a range of solvents with different polarities to examine whether ligand grafting was affected by polarity. Methanol, ethanol, dichloromethane, toluene or hexane replaced the acetone in the reaction mixture in the same volume (20 ml). The reaction time was 24 h and 8 ml of APTES was used.

3.4.1.3.3.1 Analyses of ZSM-5 after grafting

The results from the CHN analysis can be seen graphically in Figure 3.20 and tabulated in Table 3.18. The results show that the mmol of ligand grafted increases with the solvent polarity, albeit at a very much lower level than that observed with clinoptilolite. The total graft for ZSM-5 could not be extended beyond 1%, similar to both concentration and length of time experiments.
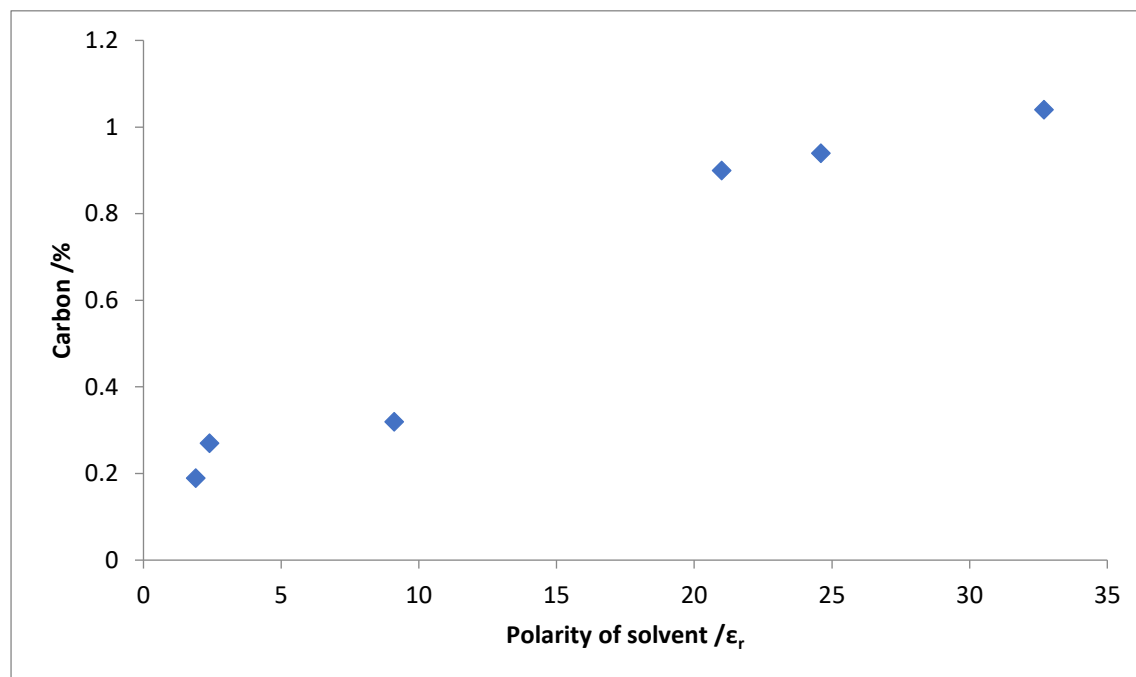
Figure 3.20: Change in carbon content (%) with increasing polarity of solvent

Table 3.18: Change in carbon content (%) with increasing polarity of solvent; esd given in parentheses.

Material	Solvent	Dielectric constant	C%	H%	N%	Difference in C%	mmol of ligand/g
ZSM-5	unreacted		0.04(3)	0.07(3)	0.05(3)		
ZSM-5	Hexane	1.9	0.19(3)	0.02(3)	0.02(3)	0.15	0.31
ZSM-5	Toluene	2.4	0.27(3)	0.06(3)	0.06(3)	0.23	0.92
ZSM-5	DCM	9.1	0.32(3)	0.05(3)	0.09(3)	0.28	1.38
ZSM-5	Acetone	21.0	0.90(3)	0.14(3)	0.17(3)	0.86	2.61
ZSM-5	Ethanol	24.6	0.94(3)	0.18(3)	0.18(3)	0.90	2.76
ZSM-5	Methanol	32.7	1.04(3)	0.20(3)	0.23(3)	1.00	3.53

It can be seen that for ZSM-5 the more polar solvents increase the grafting of APTES. ZSM-5 has a high Si :Al ratio and the surface is less polar due to there being less AlO_3^+ species. Whereas the NH_2 group on the ligand will interact with the polar solvent Therefore the surface and solvent will have a directing effect on the ligand and this can explain the higher grafting amounts seen for the polar solvents.

In agreement with previous observations, the PXRD patterns show no notable changes before or after grafting indicating no real change to the long range order see appendix 8.1. Between 2950 and 3000 cm^{-1}, the characteristic C-H band appears in the IR spectrum that has been observed in the previous grafting experiments see appendix 8.2.

3.4.1.3.4: Summary of ZSM-5 experiments

An increase in ligand grafting was seen with increased reaction time and the polarity of solvent. A graft of approximately 0.05 mmol is observed and appears to be the grafting limit for ZSM-5 and APTES. No change is seen in the structure of ZSM-5 by PXRD and the only changes to the IR appear to be the appearance of a C-H band at 2850-3000 wavenumbers. The proportion of grafting possible for ZSM-5 appears to be significantly less than that observed for the samples of clinoptilolite.

3.4.1.4: Vermiculite

Following the same procedures carried out in sections 3.4.1.1, analogous grafting experiments were carried out on a sample of the clay, vermiculite. In a similar way to the zeolite samples, this clay has exchangeable cations as well as a rigid structure unlikely to change significantly during the reaction; in the clay the rigid aluminiosilicate structure is in layers rather than cages as seen in the zeolite.

3.4.1.4.1 Effect of reaction time

The reaction time for the grafting experiment with APTES was varied between 1 and 24 h in using the same intervals used for the zeolite samples.

3.4.1.4.1.1 Analysis of vermiculite after grafting for varying time intervals.

The results from the CHN analysis can be seen graphically in Figure 3.21 and tabulated in Table 3.19. Similar to the experiments on the zeolite samples, the amount of graft appears to rise with longer reaction times since the carbon content increases. As the starting concentration of carbon in the as-provided sample are ca. 0.38(2)%, the absolute increase is offset by this amount leading to a maximum carbon content of ca. 2%
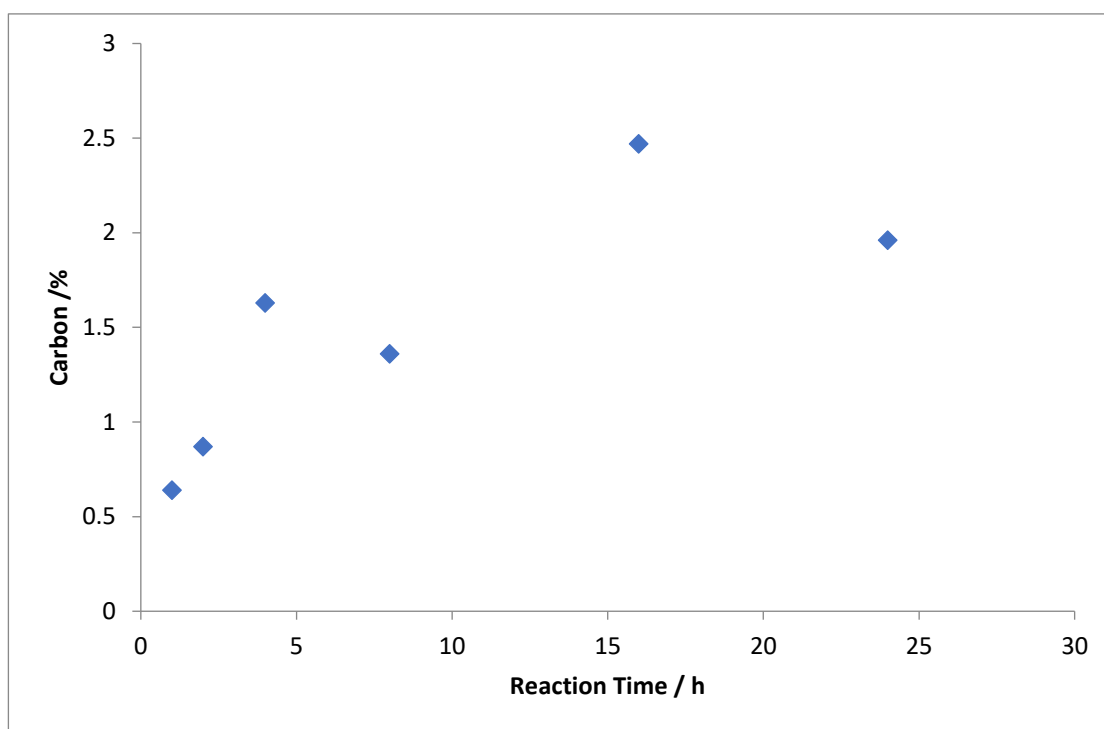
Figure 3.21: Change in carbon content (%) with reaction time (h) for vermiculite.

Table 3.19. Change in carbon content (%) with reaction time (h) for vermiculite; esd's given in parentheses.

Material	Reaction time / hr	C%	H%	N%	Difference in C%	Mmol of ligand
Vermiculite	unreacted	0.39(3)	0.82(3)	0.17(3)		
Vermiculite	1	0.64(3)	1.26(3)	0.47(3)	0.06	0.92
Vermiculite	2	0.87(3)	1.20(3)	0.59(3)	1.22	18.72
Vermiculite	4	1.63(3)	1.18(3)	1.07(3)	1.91	29.31
Vermiculite	8	1.36(3)	1.07(3)	1.09(3)	1.95	29.92
Vermiculite	16	2.47(3)	1.30(3)	1.33(3)	2.49	38.21
Vermiculite	24	1.96(3)	1.36(3)	0.55(3)	2.86	43.89

There is significant variation of the carbon content of these samples which may be due to the variation of the natural material itself as a result of geological variation.

Similar to the results from the PXRD for the clinoptilolite samples, the pattern for vermiculite shows no change to the long-range order, see Figure 3.22
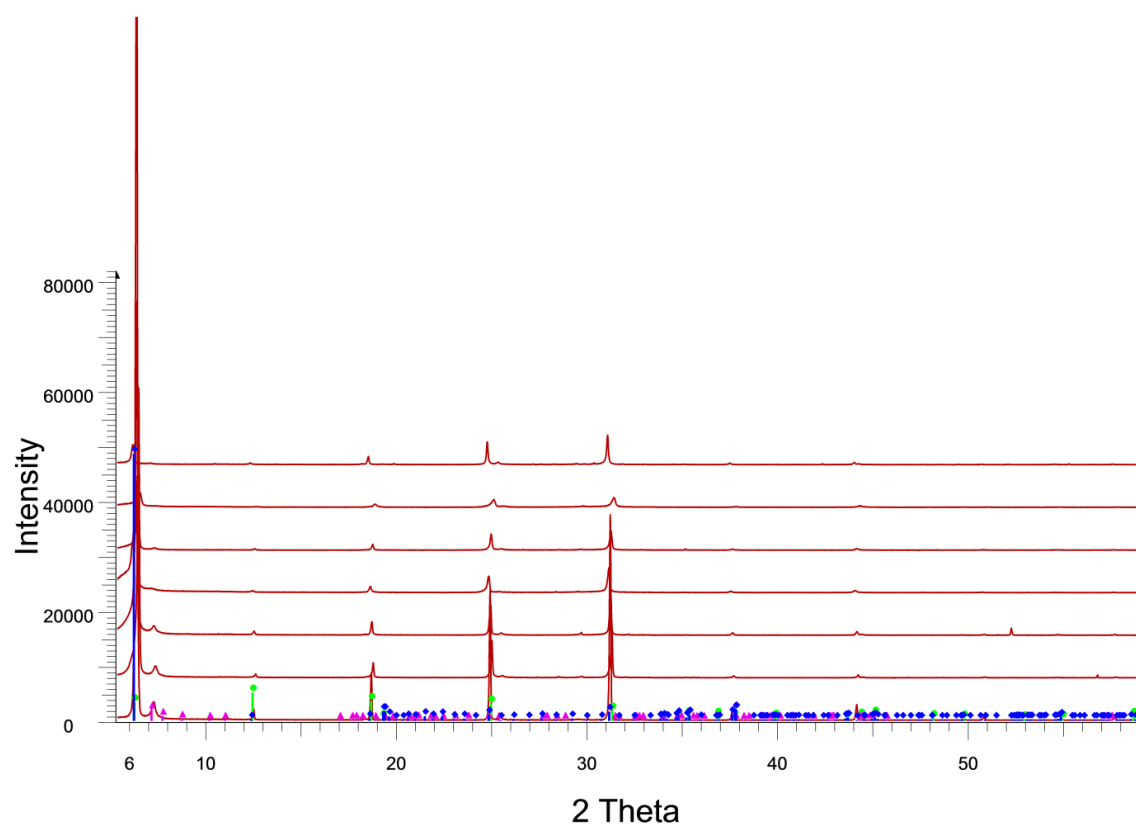
Figure 3.22: PXRD patterns of vermiculite after grafting with APTES over varying time periods. Bottom pattern is the reference before grafting, and the patterns represent 1, 2, 4, 8, 16 and 24h of grafting from penultimate to bottom to top.

The PXRD pattern does show broadening of the reflections which relate to the layers meaning the preferred orientation is less pronounced than others in some cases. This is due to the ligand grafting to the available sites and the ability of vermiculite to swell can possibly allow the ligand to graft between layers.   Inorganic-organic hybrids using various clays and micas such as illite, montmorillionite and muscovite as the inorganic hosts, have also shown broadening of the hk0 reflections on grafting of the organics.

FTIR analysis of the samples showed no changes to the Si/Al-O data but the OH stretch is sometimes absent. An additional band at 2950-3000 cm^{-1} is seen at the higher levels of carbon content, in agreement with the work on the zeolites see appendix 8.2. The FTIR data and PXRD pattern support the idea that the overall structure remains similar but the grafting is likely to be inter-layer as well as surface.

3.4.1.4.2 Effect of ligand concentration

The methodology described in 3.4.1.2.1 was replicated using the vermiculite as the substrate and the ligand concentration was altered by adding 3ml (1.28×10^{-2} moles), 5ml (2.14×10^{-2} moles) or 8 ml (3.41×10^{-2}) of APTES into the reaction mixture in the three different experiments. The experiments were carried out over a 24h period.

3.4.1.4.2.1 Analyses of the vermiculite after grafting

The results from the CHN analysis are tabulated in Table 3.20. The results show that the mmol of ligand grafted no significant change with the ligand concentration.

Table 3.20: Change in carbon content (%) with varying ligand concentration mL: esds are given in parentheses

Material	Concentration (moles)	C%	H%	N%	Difference in C%	mmol of ligand /g
Vermiculite	unreacted	0.39(3)	0.82(3)	0.17(3)		
Vermiculite	1.28×10^{-2}	2.17(3)	1.38(3)	0.64(3)	1.78	27.32
Vermiculite	2.14×10^{-2}	1.79(3)	1.41(3)	0.51(3)	1.40	21.48
Vermiculite	3.41×10^{-2}	1.96(3)	1.36(3)	0.55(3)	1.57	24.09

The effect of ligand concentration on the grafting of APTES and vermiculite shows no significant change. There is a small fluctuation in the results which could be due to the geological nature of the sample, meaning that the sample weighed out for reaction may have a small compositional difference for each sample. This is similar to the results from ZSM-5 where the graft concentration remains low across the range of concentrations used.

In agreement with the previous observations, the PXRD patterns show no notable changes before or after grafting indicating no real change to the long-range order see appendix 8.1. There is some variation in the extent of preferred orientation and the breadth of the hk0 reflections perhaps indicating a disruption to the stacking of the layers as a result of swelling when the ligands are intercalated. Between 2950 and 3000 cm^{-1}, the characteristic C-H band appears in the spectrum in a

similar way to the analogous experiments on the zeolite samples. The O-H bands are also sometimes suppressed, possibly as a result of the intercalation behaviour see appendix 8.2.

3.4.1.4.3 Effect of solvent polarity

The methodology described in 3.4.1.3.1 was followed except the acetone solvent was replaced with a range of solvents with different polarities to examine whether ligand grafting was affected by polarity. 2g of vermiculite replaced the zeolite. Methanol, ethanol, dichloromethane, toluene or hexane replaced the acetone in the reaction mixture in the same volume (20 ml). The reaction time was 24 h and 8 ml of APTES was used.

3.4.1.4.3.1: Analysis of vermiculite samples after solvent polarity experiments

The results from the CHN analysis can be seen graphically in Figure 3.23 and tabulated in Table 3.21. The results show that sample polarity does not seem to have any significant effect.
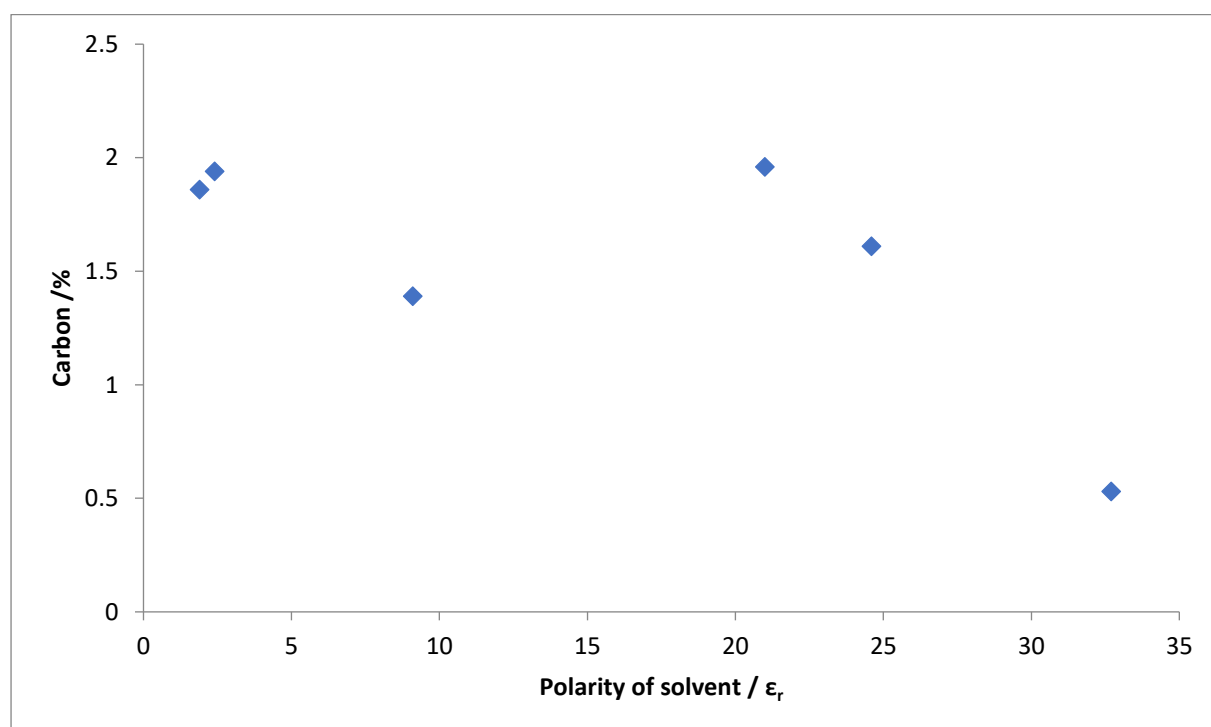
Figure 3.23: Graphical representation of the change in carbon content (%) against the polarity.

These results are similar to those previously observed for ZSM-5 and the Imerys sample of clinoptilolite. The significant change (5-10 fold) change observed for the NDA sample of clinoptilolite not being replicated in any of the other reactions.

PXRD and IR data are similar to those observed for the previous samples of vermiculite in this section showing very minimal changes as a result of the grafting procedure see appendix 8.1 and 8.2.

Table 3.21 Carbon content (%) of grafted vermiculite as a function of solvent polarity; esd's given in parentheses.

Material	Solvent	Dielectric constant	C%	H%	N%	Difference in C%	mmol of ligand /g
Vermiculite	unreacted		0.39(3)	0.82(3)	0.17(3)		6.91
Vermiculite	Hexane	1.9	1.86(3)	1.71(3)	0.45(3)	1.47	7.67
Vermiculite	Toluene	2.4	1.94(3)	1.53(3)	0.50(3)	1.55	5.06
Vermiculite	DCM	9.1	1.39(3)	1.39(3)	0.33(3)	1.00	8.44
Vermiculite	Acetone	21.0	1.96(3)	1.36(3)	0.55(3)	1.57	1.84
Vermiculite	Ethanol	24.6	1.61(3)	0.98(3)	0.12(3)	1.22	1.23
Vermiculite	Methanol	32.7	0.53(3)	1.16(3)	0.08(3)	0.14	6.91

3.4.1.4.4 Summary of Vermiculite experiments

Under the conditions studied, only time in contact with the ligand in the solvent appears to make a significant difference to the amount of ligand grafted, where longer times result in higher quantities of ligand grafted. 0.05 mmol appears to be the observed limit for vermiculite and APTES. A small change is seen in the PXRD and FTIR in the long range order of the sample which can be attributed to the shrink / swell ability of vermiculite.

3.4.1.5 Kaolinite

3.4.1.5.1 Effect of reaction time

Following the same procedures carried out in sections 3.4.1.1, analogous grafting experiments were carried out on the sample of kaolinite using the same parameters over a period of 24 h using APTES as the grafting ligand, acetone as the solvent and refluxing for 1, 2, 4, 8, 16 or 24 h respectively.

3.4.1.5.1.1 Analysis of kaolinite sample after grafting.

The results from the CHN analysis can be seen graphically in Figure 3.24 and tabulated in Table 3.22.

The results show that the mmol of ligand grafted does not change much with the reaction time.
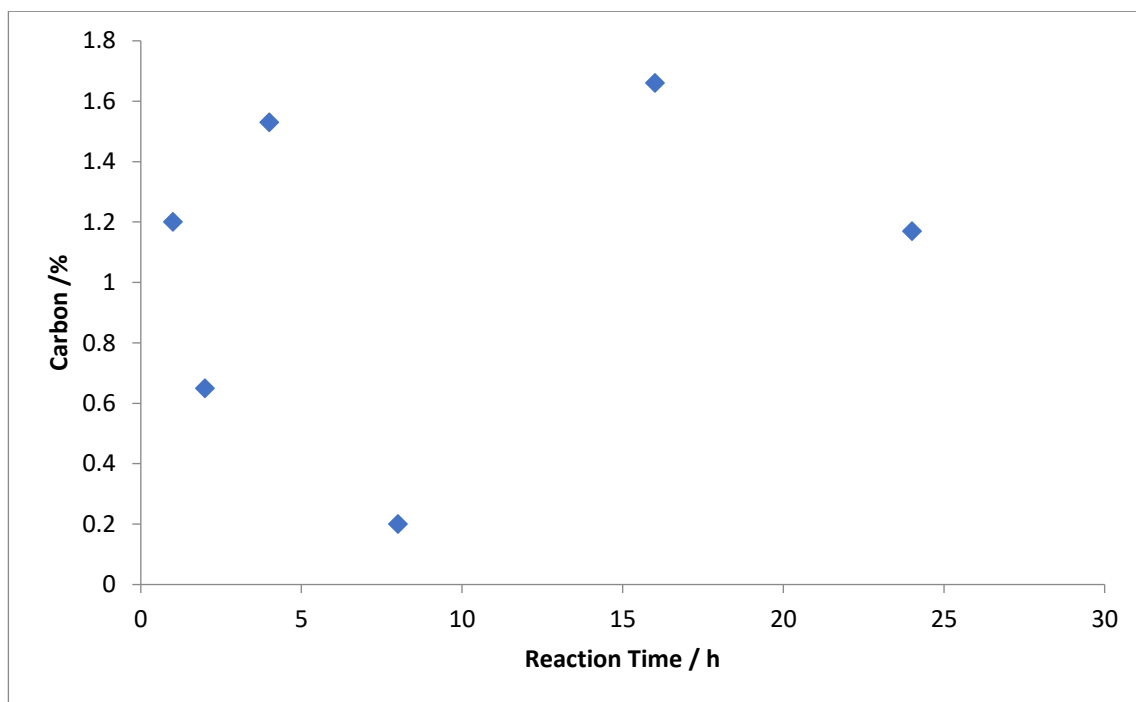
Figure 3.24: Change in carbon content (%) as a function of reaction time for kaolinite

Table 3.22: Change in carbon content (%) as a function of reaction time for kaolinite; esd's are given in parenthesis.

Material	Reaction time / hr	C%	H%	N%	Difference in C%	mmol of ligand /g
Kaolinite	unreacted	0.07(3)	0.53(3)	0.03(3)		
Kaolinite	1	1.20(3)	1.05(3)	1.55(3)	1.13	17.34
Kaolinite	2	0.65(3)	1.27(3)	0.68(3)	0.58	8.90
Kaolinite	4	1.53(3)	1.32(3)	0.44(3)	1.46	22.40
Kaolinite	8	0.20(3)	1.17(3)	0.42(3)	0.13	1.99
Kaolinite	16	1.66(3)	1.54(3)	0.42(3)	1.59	24.40
Kaolinite	24	1.17(3)	1.46(3)	0.32(3)	1.10	16.88

The change of reaction time does not have a correlation to the amount of graft seen. This can be due to the fact that kaolinite does not swell / shrink much and therefore grafting between layers is unlikely, limiting the amount of grafting seen. The sample is also of geological origin and therefore there can be a difference in the composition for each sample weighed out.

The PXRD pattern of the grafted samples can be seen in Figure 3.25. No new reflections appear indicating that there is no change to the long range order which is in agreement with previous work.
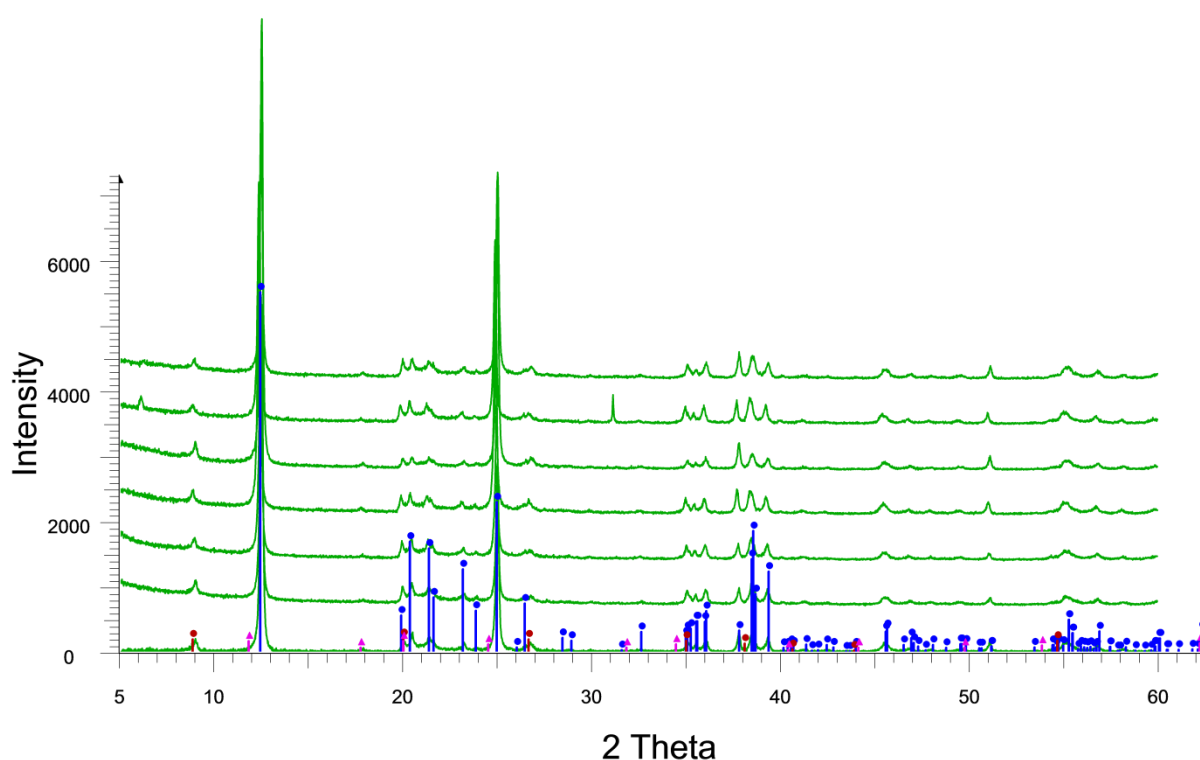
Figure 3.25: PXRD pattern of kaolinite after reaction with APTES over the period 1-24h; bottom pattern pre-treated reference, samples after 1, 2, 4, 8, 16 and 24 h vertically placed with shortest reaction time first.

As kaolinite has a low shrink-swell capacity and so no ligand is expected to enter the layers without pre-treatment, the change seen in preferred orientation and breath of the hk0 seen in the vermiculite samples is not replicated for the kaolinite. FTIR analyses showed the appearance of a band in the C-H stretching region for some of the samples between 2950 and 3000 wavenumbers in agreement with the previous work carried out on the other materials see appendix 8.2.

3.4.1.5.2 Effect of ligand concentration

The methodology described in 3.4.1.2.1 was replicated using vermiculite as the substrate and the ligand concentration was altered by adding 3 ml (1.28 x 10^{-2} moles), 5 ml (2.14 x 10^{-2} moles) or 8 ml (3.41 x 10^{-2} moles) of APTES into the reaction mixture in the three different experiments. The experiments were carried out over a 24h period.

3.4.1.5.2.1 Analysis of kaolinite after grafting

The results from the CHN analysis are given in 3.20. The results show that the mmol of ligand grafted does not change much with the ligand concentration.

Table 3.23: Change in carbon content (%) as a function of concentration; esd's are given in parentheses

Material	Concentration (moles)	C%	H%	N%	Difference in C%	Mmol of ligand
Kaolinite	unreacted	0.07(3)	0.53(3)	0.03(3)		
Kaolinite	1.28 x 10^{-2}	1.64(3)	1.43(3)	0.43(3)	1.57	0.049
Kaolinite	2.14 x 10^{-2}	1.18(3)	1.32(3)	0.26(3)	1.11	0.030
Kaolinite	3.41 x 10^{-2}	1.17(3)	1.46(3)	0.32(3)	1.10	0.040

The concentration of the ligand does not have a pronounced effect on the amount of grafting that occurs. The amount of grafting for kaolinite and APTES appears to be approximately 0.05 mmol, due to the low shrink / swell capacity of kaolinite preventing inter-layer grafting from occurring

In agreement with previous observations, the PXRD patterns show no notable changes before or after grafting indicating no real change to the long range order. Between 2950 and 3000 cm^{-1}, the characteristic C-H band appears in the spectrum in a similar way to the analogous experiments on the other clay and zeolite samples appendix 8.2.

3.4.1.5.3 Effect of solvent polarity

The methodology described in 3.4.1.3.1 was followed except the acetone solvent was replaced with a range of solvents with different polarities to examine whether ligand grafting was affected by polarity.

Methanol, ethanol, dichloromethane, toluene or hexane replaced the acetone in the reaction mixture in the same volume (20 ml). The reaction time was 24 h and 8 ml of APTES was used.

3.4.1.5.3.1 Analyses of the kaolinite samples after grafting

The results from the CHN analysis can be seen graphically in Figure 3.26 and tabulated in Table 3.24. The polarity of the solvent appears to have little effect on the amount of ligand grafted in the case of kaolinite in a similar way to that observed for all samples except the NDA clinoptilolite.
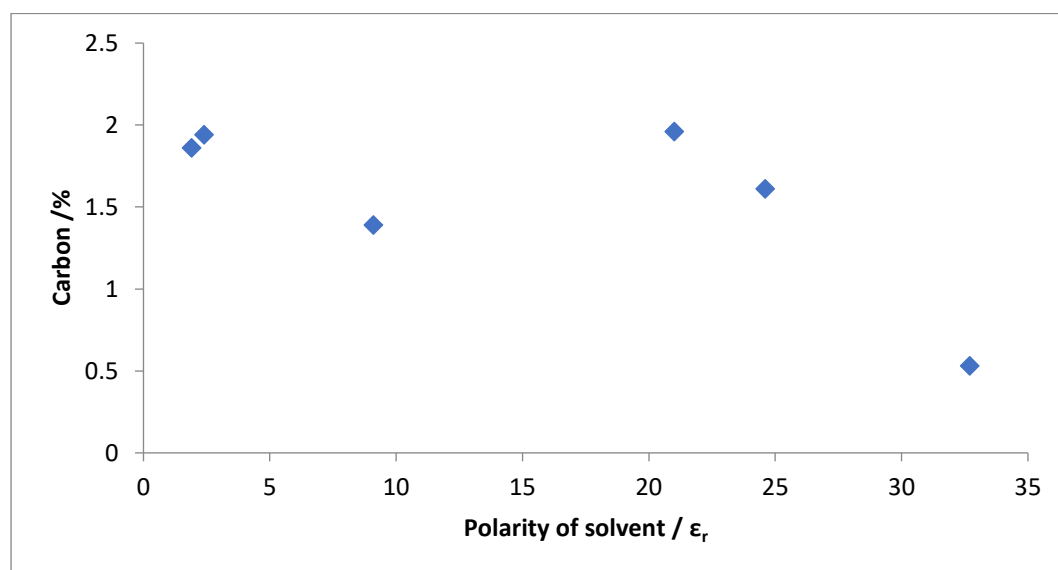
Figure 3.26: Change in carbon content (%) with solvent polarity for kaolinite.

Table 3.24 Change in carbon content (%) with solvent polarity; esd's given in parentheses.

Material	Solvent	Dielectric constant	C%	H%	N%	Difference in C%	mmol of ligand /g
Kaolinite	unreacted		0.07(3)	0.53(3)	0.03(3)		
Kaolinite	Hexane	1.9	0.72(3)	1.31(3)	0.30(3)	0.65	4.60
Kaolinite	Toluene	2.4	1.22(3)	1.41(3)	0.40(3)	1.15	6.14
Kaolinite	DCM	9.1	0.44(3)	1.34(3)	0.14(3)	0.37	2.15
Kaolinite	Acetone	21.0	1.17(3)	1.46(3)	0.32(3)	1.10	4.91
Kaolinite	Ethanol	24.6	1.12(3)	1.39(3)	0.42(3)	1.05	6.45
Kaolinite	Methanol	32.7	0.55(3)	1.25(3)	0.22(3)	0.48	3.38

The polarity of the solvent does not have a noticeable effect on the amount of grafting that occurs. The amount of grafting for kaolinite and APTES appears to reach a maximum at approximately 0.05 mmol, due to the low shrink / swell capacity of kaolinite preventing inter-layer grafting from occurring.

No changes are observed to the PXRD pattern to suggest that long range order is being disrupted by the small amount of surface graft. In the case of the IR, the characteristic C-H stretch appears in the IR pattern at ca. 2950-3000 cm^{-1} see appendices 8.1 and 8.2.

3.4.1.5.4 Summary of Kaolinite experiments

The grafting of kaolinite is relatively consistent at 0.05 mmol regardless of reaction time, ligand concentration and solvent polarity. Kaolinite does not have a large shrink / swell capacity and pre-treatment is required to exude the layers allowing for interlayer grafting. The grafting capacity for kaolinite and APTES is 0.05 mmol. No change is the long range order of the structure is seen in the PXRD or FTIR.

3.4.1.6 Summary of APTES grafting

The overall structure of the clinoptilolite (NDA), clinoptilolite (Imerys), ZSM-5 and kaolinite remains unaltered by the grafting process. Vermiculite does show a small variation after grafting. Clinoptilolite (NDA) shows the largest graft at 0.227 mmol of ligand grafted, with the solvent polarity having the largest effect on the amount of graft of this material. PXRD gives very little information about the

change in the material on grafting; as the proportion of graft is low, there is no change to the long range order. IR consistently shows the appearance of absorptions consistent with C-H stretches once APTES has been grafted suggesting that the ligand has been incorporated into the support material. SSNMR indicates that the ligand is attached to the framework, rather than enclatharated due to the appearance of broads shifted bands in the spectrum consistent with carbon species bound to a silicate host.

3.4.2 Characterisation of materials modified with the TMSPE and TMSPETT ligands: Investigating reaction time, concentration and solvent effects.

Analogous experiments were carried out using varying reaction time, concentration of solvent and type of solvent for TMSPE and TMSPETT ligands.

In all cases, no change was observed to the long-range order of the materials using PXRD and the IR showed very minor changes except the appearance of the C-H stretch at 2950-3000 cm^{-1} see appendices 8.1 and 8.2.

Table 3.25 summarises the changes in carbon content with respect to time for all three ligands. Figure 3.27 compares the quantity of graft on each substrate for each ligand as a function of time. In all cases, there is a general trend that the amount of ligand grafted increases with time in contact with substrate. Logically increasing the contact time in the solvent should allow more time for interactions to occur between the available surface sites and the ligand in the solvent; by allowing more time for the reaction to take place, the probability of the surface sites and the ligand aligning in the appropriate way to allow reaction increases. TMSPETT was the least successful graft in all the materials investigated. A mixture of poor solubility in organic solvents due to the ligand being ionic and bulky nature could be possible causes of the low graft capability on these materials. Of all the substrates, ZSM5 appears to be the least reactive with the lowest levels of grafting followed closely by kaolinite as shown in Figure 3.28

Table 3.25 Change in carbon content with ligand and reaction tim

		APTES					TMSPE					TMSPETT				
		C%	H%	N%	Diff in C%	mmol of ligand / g	C%	H%	N%	Diff in C%	mmol of ligand / g	C%	H%	N%	Diffe in C%	mmol of ligand / g
CLINO NDA	0	0.03 (3)	0.84 (3)	0.01 (3)			0.03 (3)	0.84 (3)	0.01 (3)			0.03 (3)	0.84 (3)	0.01 (3)		
	1	0.54 (3)	0.9 (3)	0.05 (3)	0.51	7.83	0.82 (3)	1.08 (3)	0.39 (3)	0.79	12.18	0.13 (3)	0.84 (3)	0.01 (3)	0.1	9.62
	2	0.87 (3)	1.14 (3)	0.38 (3)	0.84	18.41	2.03 (3)	1.42 (3)	0.56 (3)	2	30.69	0.33 (3)	0.79 (3)	0.09 (3)	0.3	18.59
	4	1.23 (3)	1 (3)	0.71 (3)	1.2	12.89	1.42 (3)	1.37 (3)	0.47 (3)	1.39	21.33	0.61 (3)	1.01 (3)	0.13 (3)	0.58	22.76
	8	1.16 (3)	0.98 (3)	0.23 (3)	1.13	17.34	2.01 (3)	1 .32 (3)	0.71 (3)	1.98	30.38	0.74 (3)	1.11 (3)	0.15 (3)	0.71	20.52
	16	1.21 (3)	1.01 (3)	0.45 (3)	1.18	18.11	2 (3)	1.38 (3)	0.47 (3)	1.97	30.23	0.67 (3)	1.02 (3)	0.14 (3)	0.64	21.48
	24	2.04 (3)	1.11 (3)	0.45 (3)	2.01	30.84	1.92 (3)	1.12 (3)	0.41 (3)	1.89	29.00	1.84 (3)	0.99 (3)	0.27 (3)	1.81	58.02
CLINO Imerys	0	0.07 (3)	0.53 (3)	0.03 (3)			0.07 (3)	0.53 (3)	0.03 (3)			0.07 (3)	0.53 (3)	0.03 (3)		
	1	0.13 (3)	0.46 (3)	0.02 (3)	0.06	0.92	2.05 (3)	1.08 (3)	0.77 (3)	1.98	30.38	0.77 (3)	0.77 (3)	0.17 (3)	0.7	22.44
	2	1.29 (3)	0.95 (3)	0.32 (3)	1.22	18.72	2.79 (3)	1.09 (3)	0.99 (3)	2.72	41.74	3.43 (3)	0.97 (3)	0.72 (3)	3.36	107.71
	4	1.98 (3)	0.87 (3)	0.52 (3)	1.91	29.31	2.11 (3)	1.07 (3)	0.66 (3)	2.04	31.30	1.12 (3)	0.88 (3)	0.24 (3)	1.05	33.66
	8	2.02 (3)	0.78 (3)	0.39 (3)	1.95	29.92	3.23 (3)	1.15 (3)	0.87 (3)	3.16	48.49	1.14 (3)	0.93 (3)	0.22 (3)	1.07	34.30
	16	2.56 (3)	1.11 (3)	0.5 (3)	2.49	38.21	3.08 (3)	1.15 (3)	0.69 (3)	3.01	46.19	0.89 (3)	0.37 (3)	0.16 (3)	0.82	26.29
	24	2.93 (3)	1.07 (3)	0.63 (3)	2.86	43.89	2.75 (3)	0.99 (3)	0.65 (3)	2.68	41.13	0.99 (3)	0.74 (3)	0.13 (3)	0.92	29.49
ZSM-5	0	0.04 (3)	0.07 (3)	0.05 (3)			0.04 (3)	0.07 (3)	0.05 (3)			0.04 (3)	0.07 (3)	0.05 (3)		
	1	0.5 (3)	0.16 (3)	0.13 (3)	0.46	7.06	0.5 (3)	0.03 (3)	0.04 (3)	0.46	7.06	0.22 (3)	0.06 (3)	0(3)	0.18	5.77
	2	0.5 (3)	0.09 (3)	0.15 (3)	0.46	7.06	0.95 (3)	0.06 (3)	0.1 (3)	0.91	13.96	0.18 (3)	0.09 (3)	0.03 (3)	0.14	4.49

	4	**0.54 (3)**	0.08 (3)	0.16 (3)	0.5	7.67	**0.41 (3)**	0.1 (3)	0.12 (3)	0.37	5.68	**0.3 (3)**	0.05 (3)	0.01 (3)	0.26	8.33
	8	**0.75 (3)**	0.16 (3)	0.16 (3)	0.71	10.90	**0.59 (3)**	0.01 (3)	0.1 (3)	0.55	8.44	**0.33 (3)**	0.07 (3)	0.07 (3)	0.29	9.30
	16	**0.93 (3)**	0.17 (3)	0.19 (3)	0.89	13.66	**0.56 (3)**	0.03 (3)	0.13 (3)	0.52	7.98	**0.47 (3)**	0.09 (3)	0.06 (3)	0.43	13.78
	24	**0.9 (3)**	0.14 (3)	0.17 (3)	0.86	13.20	**0.48 (3)**	0.11 (3)	0.13 (3)	0.44	6.75	**0.8 (3)**	0.11 (3)	0.1 (3)	0.76	24.36
VERM	0	**0.39 (3)**	**0.82 (3)**	**0.17 (3)**			**0.39 (3)**	**0.82 (3)**	**0.17 (3)**			**0.39 (3)**	**0.82 (3)**	**0.17 (3)**		
	1	**0.64 (3)**	1.26 (3)	0.47 (3)	0.25	0.92	**1.12 (3)**	1.43 (3)	0.23 (3)	0.73	11.20	**0.47 (3)**	1.2 (3)	0.19 (3)	0.08	2.56
	2	**0.87 (3)**	1.2 (3)	0.59 (3)	0.48	18.72	**0.65 (3)**	1.41 (3)	0.15 (3)	0.26	3.99	**0.49 (3)**	1.12 (3)	0.23 (3)	0.1	3.21
	4	**1.63 (3)**	1.18 (3)	1.07 (3)	1.24	29.31	**0.45 (3)**	1.36 (3)	0.1 (3)	0.06	0.92	**0.45 (3)**	1.03 (3)	0.02 (3)	0.06	1.92
	8	**1.36 (3)**	1.07 (3)	1.09 (3)	0.97	29.92	**1.5 (3)**	1.27 (3)	0.25 (3)	1.11	17.03	**0.48 (3)**	1.21 (3)	0.09 (3)	0.09	2.88
	16	**2.47 (3)**	1.3 (3)	1.33 (3)	2.08	38.21	**1.21 (3)**	1.55 (3)	0.27 (3)	0.82	12.58	**0.42 (3)**	1.02 (3)	0.04 (3)	0.03	0.96
	24	**1.96 (3)**	1.36 (3)	0.55 (3)	1.57	43.89	**1.73 (3)**	1.46 (3)	0.4 (3)	1.34	20.56	**0.99 (3)**	1.32 (3)	0.19 (3)	0.6	19.23
KAO	0	**0.07 (3)**	**0.53 (3)**	**0.03 (3)**			**0.07 (3)**	**0.53 (3)**	**0.03 (3)**			**0.07 (3)**	**0.53 (3)**	**0.03 (3)**		
	1	**1.2 (3)**	1.05 (3)	1.55 (3)	1.13	17.34	**0.82 (3)**	1.08 (3)	0.39 (3)	0.75	11.51	**0.47 (3)**	1.26 (3)	0.08 (3)	0.4	12.82
	2	**0.65 (3)**	1.27 (3)	0.68 (3)	0.58	8.90	**1.96 (3)**	1.47 (3)	0.68 (3)	1.89	29.00	**0.22 (3)**	1.13 (3)	0.04 (3)	0.15	4.81
	4	**1.53 (3)**	1.32 (3)	0.44 (3)	1.46	22.40	**2.85 (3)**	1.58 (3)	0.98 (3)	2.78	42.66	**0.4 (3)**	1.16 (3)	0.12 (3)	0.33	10.58
	8	**0.2 (3)**	1.17 (3)	0.42 (3)	0.13	1.99	**1.36 (3)**	1.36 (3)	0.35 (3)	1.29	19.80	**0.38 (3)**	1.11 (3)	0.14 (3)	0.31	9.94
	16	**1.66 (3)**	1.54 (3)	0.42 (3)	1.59	24.40	**1.96 (3)**	1.47 (3)	0.58 (3)	1.89	29.00	**0.42 (3)**	0.98 (3)	0.03 (3)	0.35	11.22
	24	**1.17 (3)**	1.46 (3)	0.32 (3)	1.1	16.88	**2.25 (3)**	1.51 (3)	0.62 (3)	2.18	33.45	**1.46 (3)**	1.14 (3)	0.25 (3)	1.39	44.56

Clinoptilolite (NDA)

Clinoptilolite (Imerys)

ZSM5

Vermiculite

Kaolinite
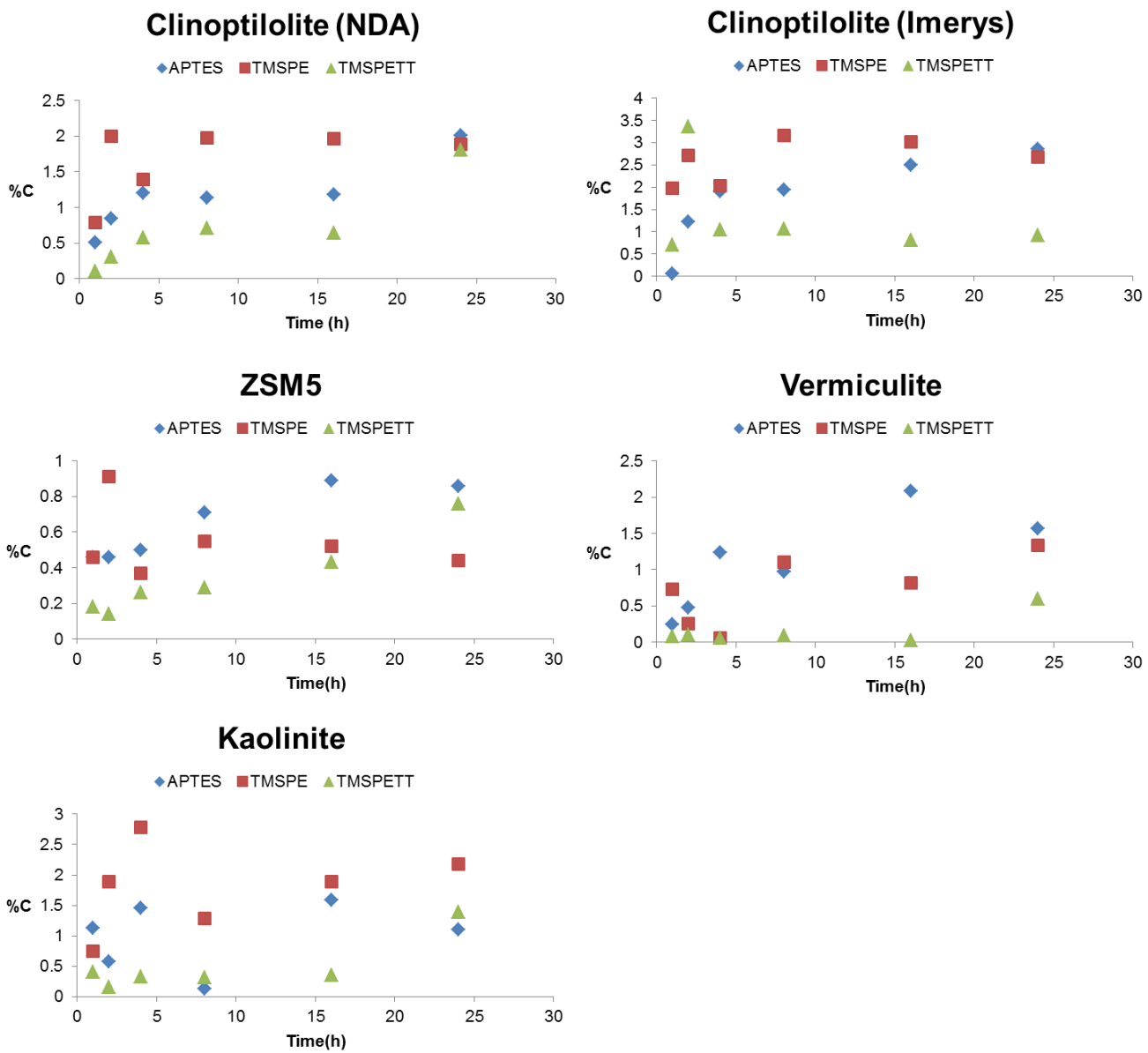
Figure 3.27: Variation in ligand graft as carbon content with time for supports for 5 substrates

Comparison of the different substrates over the 24 h period in Figure 3.26 suggests that ZSM5 is the least effective support. The proportionally better grafting capability of the clinoptilolite from Imerys compared to that provided by the NDA is presumably showing the effect of particle size; the larger surface area giving a better opportunity for the ligand to access suitable sites. In all cases, TMSPETT appears to be the least effective graft.
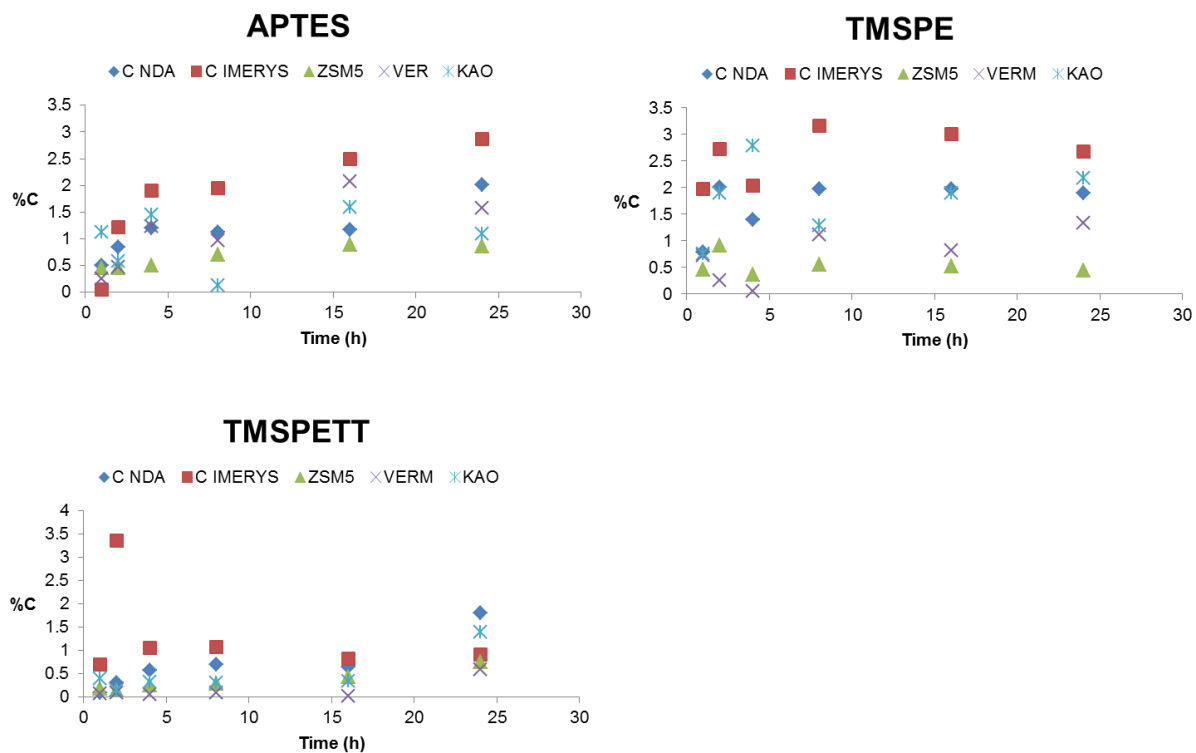
Figure 3.28: Comparison of ligand on substrate as a function of time for APTES, TMSPE and TMSPETT

The attempts to improve the amount of graft on the surface by increasing the ligand concentration are summarised in Table 3.26 and in Figure 3.29. Increasing the ligand concentration does not markedly affect the uptake of the ligand onto the surface. This is in agreement with expectations as it is expected that relatively few surface silanol groups will be available for grafting in these microporous materials. However, due to the very low levels of actinide species in the SIXEP plant, the objective is not about increasing the carbon content to the highest levels possible, but to focus on consistently attaining the 5-7% modification levels sufficient to deal with the actual quantities of actinides present and demonstrating proof of the concept.

Table 3.26: Changes in carbon content with ligand concentration

		APTES					TMSPE						TMSPETT				
	Ligand / mol^{-1}	C%	H%	N%	Difference in C%	mmol of ligand /g	Ligand / mol^{-1}	C%	H%	N%	Difference in C%	mmol of ligand / g	Ligand / mol^{-1}	C%	H%	N%	Difference in C%	mmol of ligand / g
CLINO NDA	0	0.03(3)	0.84(3)	0.01(3)			0	0.03(3)	0.84(3)	0.01(3)			0	0.03(3)	0.84(3)	0.01(3)		
	1.28×10^{-2}	1.12(3)	1.26(3)	0.31(3)	1.09	16.73	1.39×10^{2}	1.72(3)	1.29(3)	0.41(3)	1.69	25.93	8.17×10^{3}	0.19(3)	0.83(3)	0.00(3)	0.16	5.13
	2.14×10^{-2}	1.83(3)	1.43(3)	0.51(3)	1.8	27.62	2.31×10^{2}	1.71(3)	0.96(3)	0.61(3)	1.68	25.78	1.36×10^{2}	0.4(3)	1.01(3)	0.05(3)	0.37	11.86
	3.41×10^{-2}	2.04(3)	1.11(3)	0.45(3)	2.01	30.84	3.70×10^{2}	1.92(3)	1.12(3)	0.41(3)	1.89	29.00	2.18×10^{2}	1.84(3)	0.99(3)	0.27(3)	1.81	58.02
CLINO IMERYS	0	0.07(3)	0.53(3)	0.03(3)			0	0.07(3)	0.53(3)	0.03(3)			0	0.07(3)	0.53(3)	0.03(3)		
	1.28×10^{-2}	3.00(3)	1.15(3)	0.64(3)	2.93	44.96	1.39×10^{2}	2.75(3)	1.12(3)	0.69(3)	2.68	41.13	8.17×10^{3}	0.36(3)	0.67(3)	0.05(3)	0.29	9.30
	2.14×10^{-2}	3.38(3)	1.03(3)	0.8(3)	3.31	50.79	2.31×10^{2}	3.15(3)	1.15(3)	0.81(3)	3.08	47.26	1.36×10^{2}	1.33(3)	0.94(3)	0.32(3)	1.26	40.39
	3.41×10^{-2}	2.93(3)	1.07(3)	0.63(3)	2.86	43.89	3.70×10^{2}	2.75(3)	0.99(3)	0.65(3)	2.68	41.13	2.18×10^{2}	0.99(3)	0.74(3)	0.13(3)	0.92	13.46
ZSM-5	0	0.04(3)	0.07(3)	0.05(3)			0	0.04(3)	0.07(3)	0.05(3)			0	0.04(3)	0.07(3)	0.05(3)		
	1.28×10^{-2}	0.85(3)	0.16(3)	0.17(3)	0.81	12.43	1.39×10^{2}	0.45(3)	0.13(3)	0.13(3)	0.41	6.29	8.17×10^{3}	0.42(3)	0.09(3)	0.02(3)	0.38	12.18
	2.14×10^{-2}	0.88(3)	0.2(3)	0.27(3)	0.84	12.89	2.31×10^{2}	1.07(3)	0.09(3)	0.24(3)	1.03	15.81	1.36×10^{2}	0.43(3)	0.12(3)	0.04(3)	0.39	12.50
	3.41×10^{-2}	0.90(3)	0.14(3)	0.17(3)	0.86	13.20	3.70×10^{2}	0.48(3)	0.11(3)	0.13(3)	0.44	6.75	2.18×10^{2}	0.8(3)	0.11(3)	0.10(3)	0.76	24.36
VERM	0	0.39(3)	0.82(3)	0.17(3)			0	0.39(3)	0.82(3)	0.17(3)			0	0.39(3)	0.82(3)	0.17(3)		
	1.28×10^{-2}	2.17(3)	1.38(3)	0.64(3)	1.78	27.32	1.39×10^{2}	1.59(3)	1.39(3)	0.41(3)	1.2	18.41	8.17×10^{3}	0.41(3)	0.89(3)	0.06(3)	0.02	0.64
	2.14×10^{-2}	1.79(3)	1.41(3)	0.51(3)	1.4	21.48	2.31×10^{2}	1.76(3)	1.36(3)	0.35(3)	1.37	21.02	1.36×10^{2}	0.63(3)	1.02(3)	0.11(3)	0.24	7.69
	3.41×10^{-2}	1.96(3)	1.36(3)	0.55(3)	1.57	24.09	3.70×10^{2}	1.73(3)	1.46(3)	0.4(3)	1.34	20.56	2.18×10^{2}	0.99(3)	1.32(3)	0.19(3)	0.6	19.23
KAO	0	0.07(3)	0.53(3)	0.03(3)			0	0.07(3)	0.53(3)	0.03(3)			0	0.07(3)	0.53(3)	0.03(3)		
	1.28×10^{-2}	1.64(3)	1.43(3)	0.43(3)	1.57	24.09	1.39×10^{2}	2.05(3)	1.32(3)	0.34(3)	1.98	30.38	8.17×10^{3}	0.33(3)	1.16(3)	0.05(3)	0.26	8.33
	2.14×10^{-2}	1.18(3)	1.32(3)	0.26(3)	1.11	17.03	2.31×10^{2}	1.34(3)	1.13(3)	0.4(3)	1.27	19.49	1.36×10^{2}	0.34(3)	1.23(3)	0.06(3)	0.27	8.65
	3.41×10^{-2}	1.17(3)	1.46(3)	0.32(3)	1.1	16.88	3.70×10^{2}	2.25(3)	1.51(3)	0.62(3)	2.18	33.45	2.18×10^{2}	1.46(3)	1.14(3)	0.25(3)	1.39	44.56

APTES

TMSPE

TMSPETT
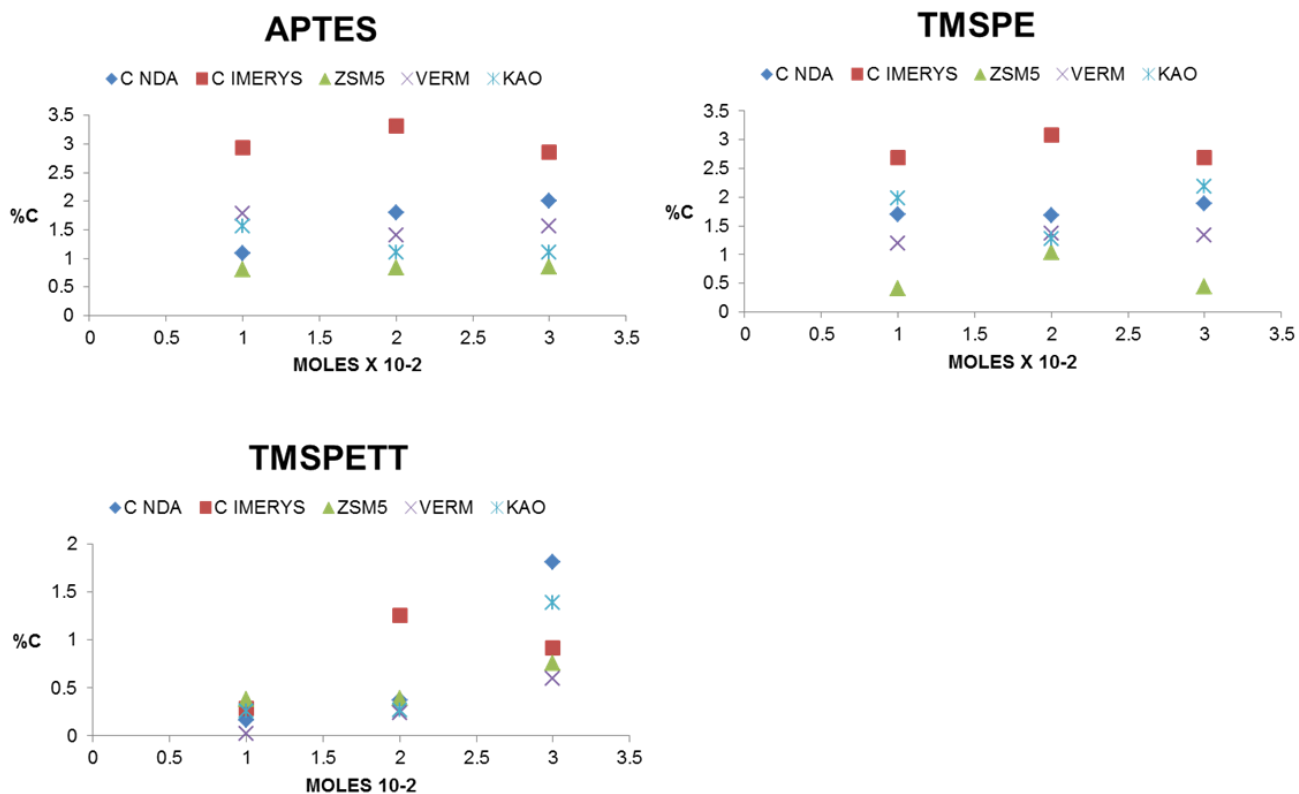
Figure 3.29: Change in carbon content as a function of ligand concentration

The changes in ligand grafting as a function of the polarity of the solvent used to facilitate grafting is summarised in Table 3.27 and Figures 3.30 and 3.31

Increasing the solvent polarity appears beneficial to some materials and not to others. The framework/layers with little/no charge appear relatively unaffected by solvent. So ZSM-5 is a very silicon rich material with few exchangeable cations. The charge on the framework is therefore low and polarity should make little difference. In the case of materials where there is a high charge, the frameworks are more highly charged meaning greater interaction with polar molecules. Unsurprisingly, kaolinite shows very similar behaviours with uncharged layers and no exchangeable cations meaning solvent does strongly affect grafting to any notable extent. The greatest effect of solvent on ligands appears to be in the case of APTES, where the graft favours low polarity solvents.

Table 3.27: Change in carbon content on grafting in the presence of different solvents

	Solvent	Dielectric constant	C%	H%	N%	Diff in C%	Mmol of ligand / g	C%	H%	N%	Diff in C%	Mmol of ligand / g	C%	H%	N%	Diff in C%	Mmol of ligand / g
CLINO NDA	unreacted		0.03 (3)	0.84 (3)	0.01 (3)			0.03 (3)	0.84 (3)	0.01 (3)			0.03 (3)	0.84 (3)	0.01 (3)		
	Hexane	1.9	10.79 (3)	2.8 (3)	3.66 (3)	10.76	56.16	**1.1 (3)**	0.99 (3)	0.47 (3)	1.07	16.42	**0.77 (3)**	0.79 (3)	0.17 (3)	0.74	5.449
	Toluene	2.4	5.12 (3)	1.31 (3)	0.52 (3)	5.09	26.39	**0.87 (3)**	1.16 (3)	0.34 (3)	0.84	12.89	**0.33 (3)**	0.7 (3)	0.05 (3)	0.30	1.603
	DCM	9.1	3.18 (3)	1.8 (3)	1.72 (3)	3.15	12.12	**1.01 (3)**	1.11 (3)	0.42 (3)	0.98	15.04	**0.59 (3)**	1.12 (3)	0.12 (3)	0.56	3.847
	Acetone	21.0	2.04 (3)	1.11 (3)	0.45 (3)	2.01	6.91	**1.92 (3)**	1.12 (3)	0.41 (3)	1.89	29.00	**1.84 (3)**	0.99 (3)	0.27 (3)	1.81	8.655
	Ethanol	24.6	1.97 (3)	1.45 (3)	0.79 (3)	1.94	7.98	**1.26 (3)**	1.1 (3)	0.43 (3)	1.23	18.88	**0.16 (3)**	0.98 (3)	0.01 (3)	0.13	0.321
	Methanol	32.7	1.17 (3)	1.19 (3)	0.31 (3)	1.14	4.76	**1.05 (3)**	1.11 (3)	0.42 (3)	1.02	15.65	**0.6 (3)**	1.05 (3)	0.1 (3)	0.57	3.206
	Water	80.0											**0.59 (3)**	0.95 (3)	0.11 (3)	0.56	4.354
CLINO IMERYS	unreacted		**0.07 (3)**	**0.53 (3)**	**0.03 (3)**			0.07 (3)	0.53 (3)	0.03 (3)			0.07 (3)	0.53 (3)	0.03 (3)		22.413
	Hexane	1.9	3.09 (3)	1.4 (3)	1 (3)	3.02	15.35	**2.68 (3)**	1.1 (3)	1.05 (3)	2.61	40.05	**2.44 (3)**	1.13 (3)	0.53 (3)	2.37	16.989
	Toluene	2.4	2.77 (3)	1.27 (3)	0.79 (3)	2.70	12.12	**2.97 (3)**	1.09 (3)	1.19 (3)	2.90	44.50	**0.47 (3)**	0.75 (3)	0.06 (3)	0.40	1.923
	DCM	9.1	1.48 (3)	1.07 (3)	0.46 (3)	2.41	7.06	**2.17 (3)**	1.21 (3)	0.81 (3)	2.10	32.23	**0.93 (3)**	0.8 (3)	0.14 (3)	0.86	4.488
	Acetone	21.0	2.93 (3)	1.07 (3)	0.63 (3)	2.86	9.67	**2.75 (3)**	0.99 (3)	0.65 (3)	2.68	41.13	**0.99 (3)**	0.74 (3)	0.13 (3)	0.92	4.167
	Ethanol	24.6	1.82 (3)	1.05 (3)	0.49 (3)	1.75	7.52	**1.34 (3)**	1.09 (3)	0.53 (3)	1.27	19.49	**0.26 (3)**	0.67 (3)	0.12 (3)	0.19	3.847

	Methanol	32.7	1.91 (3)	1.21 (3)	0.64 (3)	1.84	9.82	**1.43 (3)**	0.91 (3)	0.58 (3)	1.36	20.87	**0.45 (3)**	0.67 (3)	0.2 (3)	0.38	6.411
	Water	80.0											**0.38 (3)**	0.72 (3)	0.07 (3)	0.31	2.244
ZSM-5	unreacted		**0.04 (3)**	**0.07 (3)**	**0.05 (3)**			**0.04 (3)**	**0.07 (3)**	**0.05 (3)**			**0.04 (3)**	**0.07 (3)**	**0.05 (3)**		
	Hexane	1.9	0.19 (3)	0.02 (3)	0.02 (3)	0.15	0.31	**0.54 (3)**	0.07 (3)	0.18 (3)	0.50	7.67	**0.82 (3)**	0.16 (3)	0.03 (3)	0.78	0.962
	Toluene	2.4	0.27 (3)	0.06 (3)	0.06 (3)	0.23	0.92	**0.36 (3)**	0.12 (3)	0.06 (3)	0.32	4.91	**0.31 (3)**	0.09 (3)	0.06 (3)	0.27	1.923
	DCM	9.1	0.32 (3)	0.05 (3)	0.09 (3)	0.28	1.38	**0.26 (3)**	0.14 (3)	0.06 (3)	0.22	3.38	**0.31 (3)**	0.08 (3)	0.04 (3)	0.27	1.282
	Acetone	21.0	0.9 (3)	0.14 (3)	0.17 (3)	0.86	2.61	**0.48 (3)**	0.11 (3)	0.13 (3)	0.44	6.75	**0.8 (3)**	0.11 (3)	0.1 (3)	0.76	24.362
	Ethanol	24.6	0.94 (3)	0.18 (3)	0.18 (3)	0.90	2.76	**0.44 (3)**	0.08 (3)	0.08 (3)	0.40	6.14	**0.52 (3)**	0.14 (3)	0.08 (3)	0.48	2.564
	Methanol	32.7	1.04 (3)	0.2 (3)	0.23 (3)	1.00	3.53	**0.46 (3)**	0.14 (3)	0.09 (3)	0.42	6.45	**0.43 (3)**	0.12 (3)	0.06 (3)	0.39	1.923
	Water	80.0											**0.71 (3)**	0.11 (3)	0.15 (3)	0.67	4.808
VERM	unreacted		**0.39 (3)**	**0.82 (3)**	**0.17 (3)**			**0.39 (3)**	**0.82 (3)**	**0.17 (3)**			**0.39 (3)**	**0.82 (3)**	**0.17 (3)**		
	Hexane	1.9	1.86 (3)	1.71 (3)	0.45 (3)	1.47	6.91	**1.5 (3)**	1.42 (3)	0.43 (3)	1.11	17.03	**0.48 (3)**	0.79 (3)	0.06 (3)	0.09	1.923
	Toluene	2.4	1.94 (3)	1.53 (3)	0.5 (3)	1.55	7.67	**1.82 (3)**	1.3 (3)	0.4 (3)	1.43	21.94	**0.42 (3)**	0.89 (3)	0.03 (3)	0.03	0.962
	DCM	9.1	1.39 (3)	1.39 (3)	0.33 (3)	1.00	5.06	**1.12 (3)**	1.33 (3)	0.28 (3)	0.73	11.20	**1.89 (3)**	0.93 (3)	0.23 (3)	1.50	7.373
	Acetone	21.0	1.96 (3)	1.36 (3)	0.55 (3)	1.57	8.44	**1.73 (3)**	1.46 (3)	0.4 (3)	1.34	20.56	**0.99 (3)**	1.32 (3)	0.19 (3)	0.60	6.091
	Ethanol	24.6	1.61 (3)	0.98 (3)	0.12 (3)	1.22	1.84	**0.88 (3)**	2.57 (3)	0.19 (3)	0.49	7.52	**0.44 (3)**	1.13 (3)	0.04 (3)	0.05	1.282
	Methanol	32.7	0.53 (3)	1.16 (3)	0.08 (3)	0.14	1.23	**0.5 (3)**	1.59 (3)	0.12 (3)	0.11	1.69	**0.68 (3)**	0.8 (3)	0.04 (3)	0.29	1.282
	Water	80.0											**0.53 (3)**	0.67 (3)	0.06 (3)	0.14	1.923
KAO	unreacted		**0.07 (3)**	**0.53 (3)**	**0.03 (3)**			**0.07 (3)**	**0.53 (3)**	**0.03 (3)**			**0.07 (3)**	**0.53 (3)**	**0.03 (3)**		
	Hexane	1.9	0.72 (3)	1.31 (3)	0.3 (3)	0.65	4.60	**1.09 (3)**	1.35 (3)	0.42 (3)	1.02	15.65	**0.22 (3)**	1.08 (3)	0.02 (3)	0.15	0.641
	Toluene	2.4	1.22 (3)	1.41 (3)	0.4 (3)	1.15	6.14	**1.72 (3)**	1.54 (3)	0.6 (3)	1.65	25.32	**0.21 (3)**	1 (3)	0.11 (3)	0.14	3.526
	DCM	9.1	0.44 (3)	1.34 (3)	0.14 (3)	0.37	2.15	**1.03 (3)**	1.27 (3)	0.31 (3)	0.96	14.73	**0.23 (3)**	0.94 (3)	0.02 (3)	0.16	0.641

Acetone	21.0	1.17 (3)	1.46 (3)	0.32 (3)	1.10	4.91	**2.25 (3)**	1.51 (3)	0.62 (3)	2.18	33.45	**1.46 (3)**	1.14 (3)	0.25 (3)	1.39	8.014
Ethanol	24.6	1.12 (3)	1.39 (3)	0.42 (3)	1.05	6.45	**1.02 (3)**	1.35 (3)	0.23 (3)	0.95	14.58	**0.23 (3)**	0.96 (3)	0.04 (3)	0.16	1.282
Methanol	32.7	0.55 (3)	1.25 (3)	0.22 (3)	0.48	3.38	**1.12 (3)**	1.43 (3)	0.27	1.05	16.11	**0.83 (3)**	1.16 (3)	0.04 (3)	0.76	1.282
Water	80.0											**0.41 (3)**	1.31 (3)	0.1 (3)	0.34	3.206
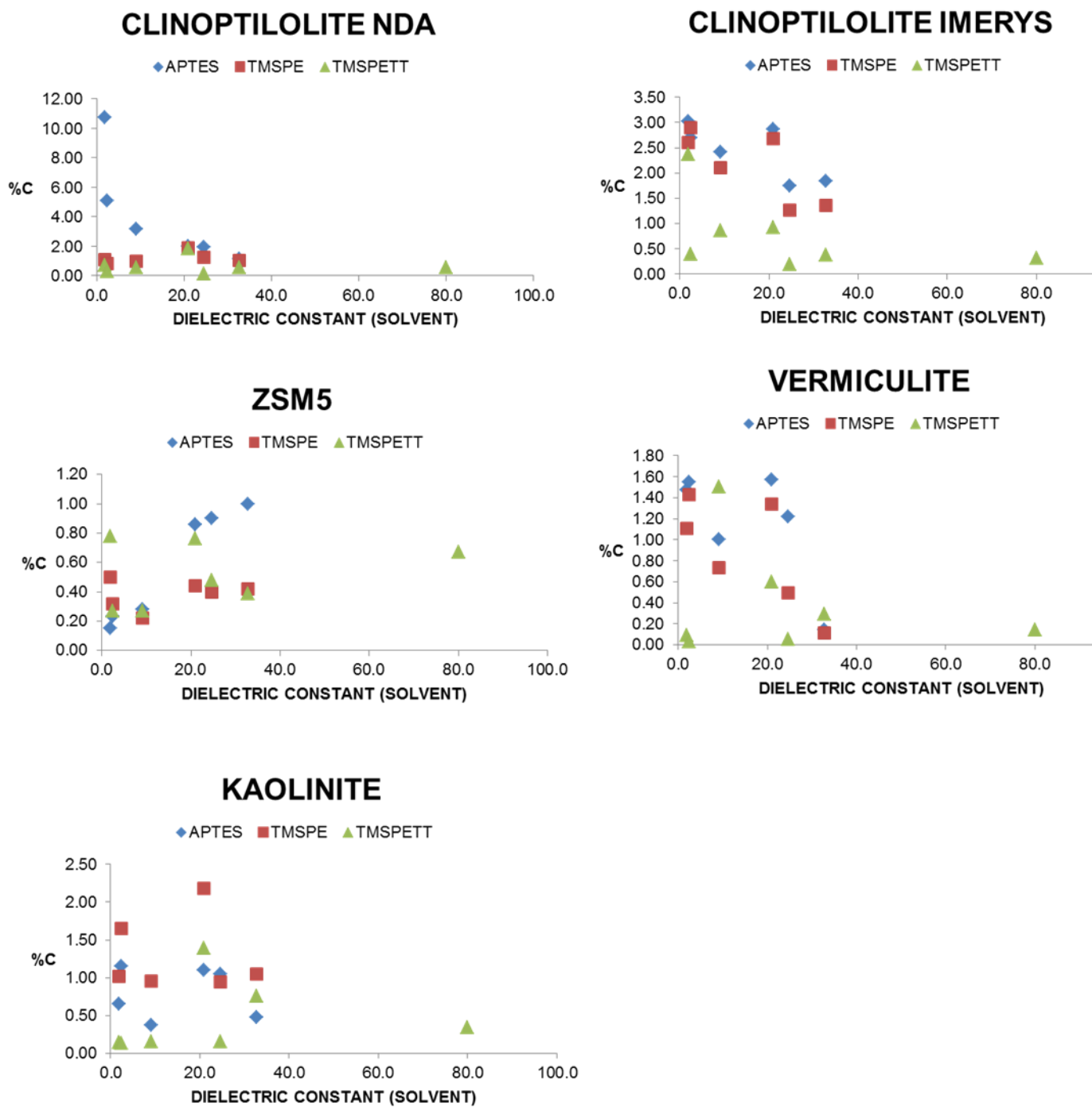
Figure 3.30: Change in carbon content with ligand in solvents with varying dielectric constants

The material most affected by solvent appears to be clinoptilolite, where low polarity solvents manage to improve the grafting levels to an extent beyond the scope of need of this project; where the graft

is exceeding 10%, well above that needed for removal of all the plutonium and uranium in the waste stream. Since these ligands are expensive, and scaling up any process involving them needs to consider the costs associated with operating the SIXEP plant itself, these higher level grafting levels were not explored extensively in this project. However a short programme of work was employed to investigate the effect of acid leaching which has been shown to improve the take up capability of crystalline materials for grafting. Due to the sensitivity of zeolites to concentrated mineral acids, a group of milder acids were chosen as well to roughen the surface rather than breakdown the material.[161–164]
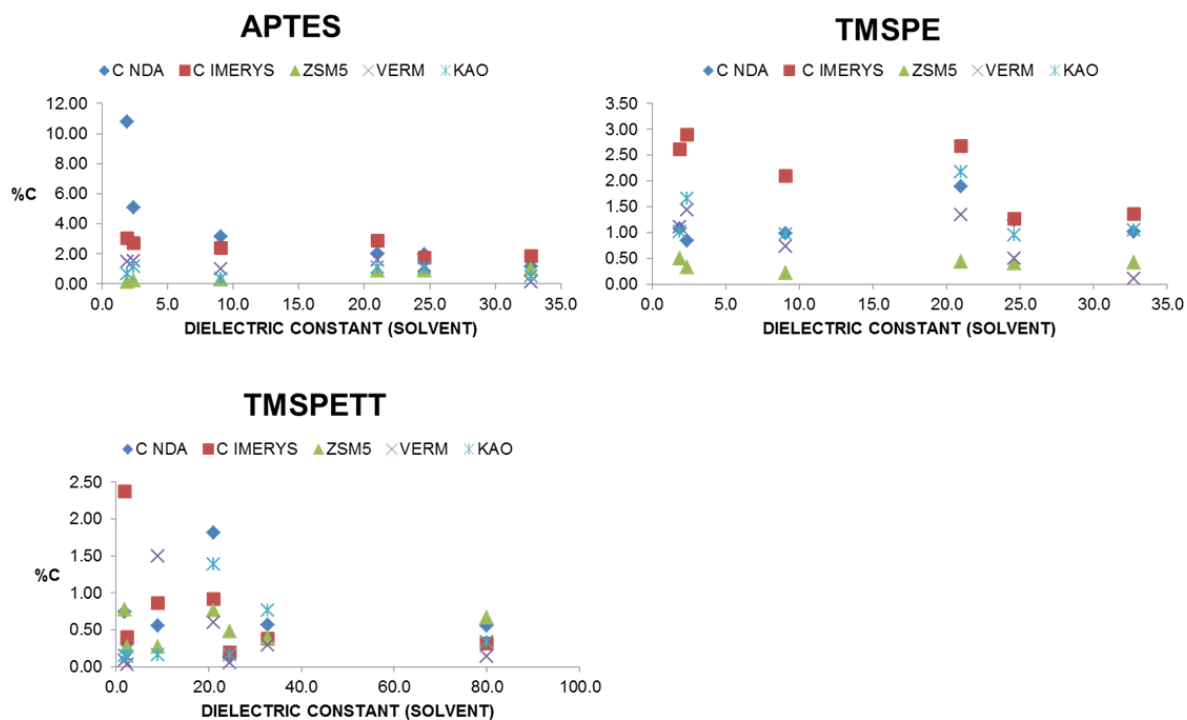
Figure 3.31: Change in carbon content with dielectric constant of the solvent for APTES, TMSPE and TMSPETT.

3.4.4 Morphology and particle size by SEM

Particle size analysis carried by on the SEM images utilising Image J software are tabulated and shown below in table 3.28.

Table 3.28: Particle size analysis from SEM images

Sample	Average size / μm	Error ±/ μm
Clino NDA	2.46	0.93
Clino NDA - Aptes	0.61	0.56
Clino NDA - TMSPE	0.50	0.26
Clino NDA - TMSPETT	0.17	0.09
Clino Imerys	0.64	0.29
Clino Imerys - Aptes	0.42	0.26
Clino Imerys - TMSPE	2.46	1.23
Clino Imerys - TMSPETT	0.55	0.17
ZSM-5	2.55	0.92
ZSM-5 - Aptes	4.61	0.75
Zsm-5 TMSPE	2.28	0.75
zsm5- TMSPETT	5.61	0.87
Vermiculite	17.64	12.95
vermiculite-Aptes	6.61	8.42
Vermicultie - TMSPE	3.75	1.54
vermiculite - TMSPETT	7.61	2.57
Kaolinite	5.61	0.66
Kaolinite - aptes	0.85	0.40
kaolinite - TMSPE	2.47	1.26
Kaolinite - TMSPETT	1.25	0.38

The results show that in all cases the particle size is decreased after the reaction has occurred, this is attributed to the particles breaking down under mechanical stirring, with the exception of ZSM-5. This can be explained by the low reaction yield observed previously. The NDA clinoptilolite is shown to be larger than that of the clinoptilolite from Imerys minerals which is in agreement with the results

previously discussed in this section. The analysis on the clays shows that vermiculite is formed of fairly large plates with a wide distribution of particle sizes and is reflected in the large error associated with the measurement. In the case of the kaolinite the particles are smaller but are still plate like in nature.

SEM micrographs of the materials before and after grafting with ligands are shown in Figure 3.32 to 3.36. As expected, very little change to the particles is seen as a result of grafting as the proportion of ligand on the surface is low. None of the solvents used will be expected to change the supports used to any significant degree as they are all inorganic with very high stability in these media. Similarly the low temperatures used for the reactions are well below the decomposition temperatures for these materials which are all well in excess of 100°C
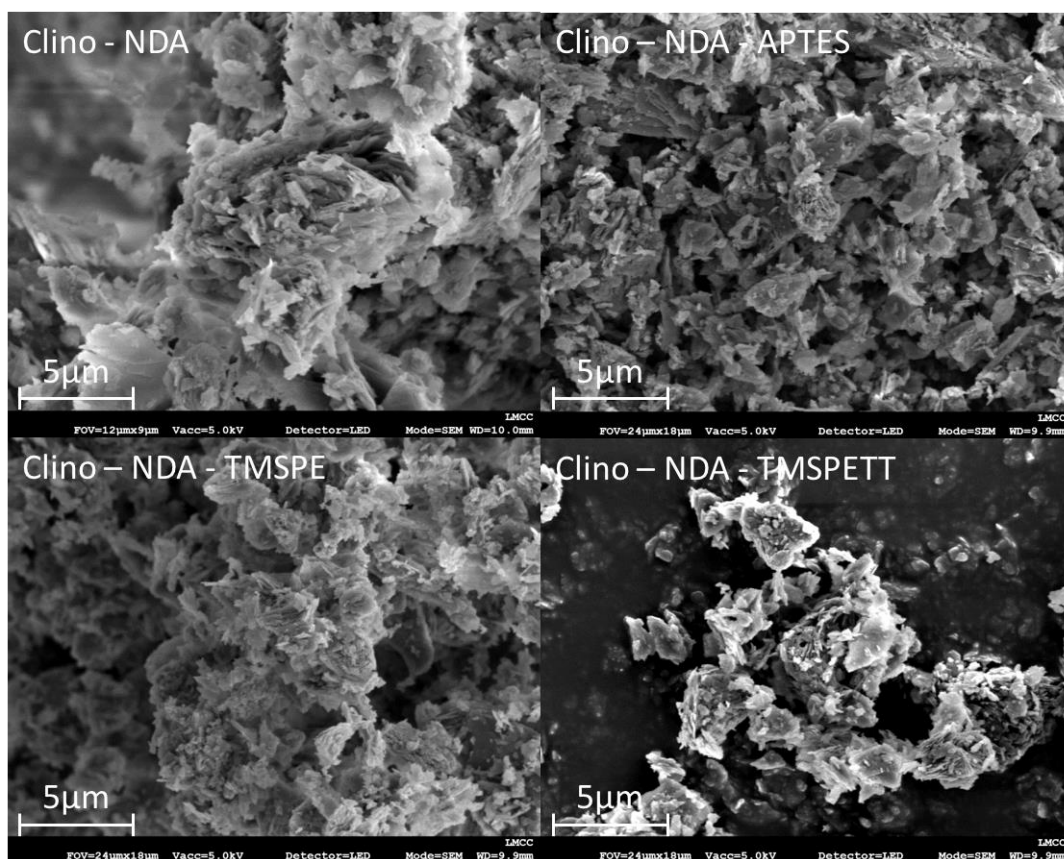
Figure 3.32: SEM images for clinoptilolite (NDA) modified with APTES, TMSPE and TMSPETT.
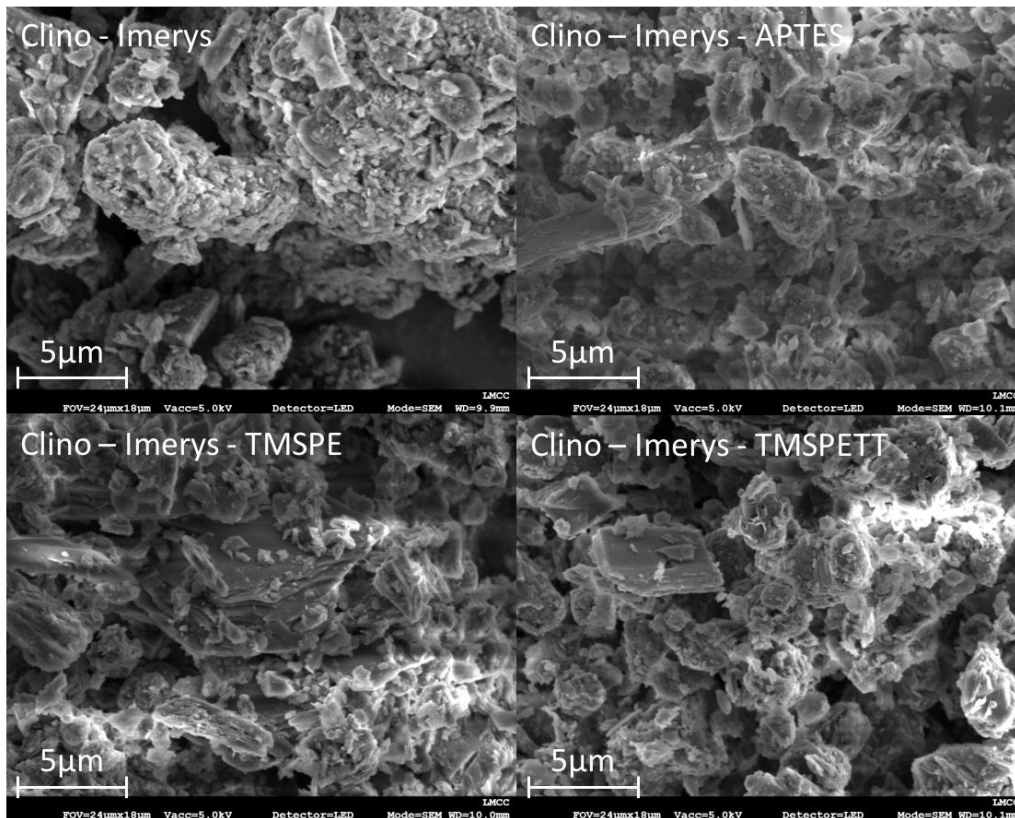
Figure 3.33: SEM images for clinoptilolite (Imerys) modified with APTES, TMSPE and TMSPETT.
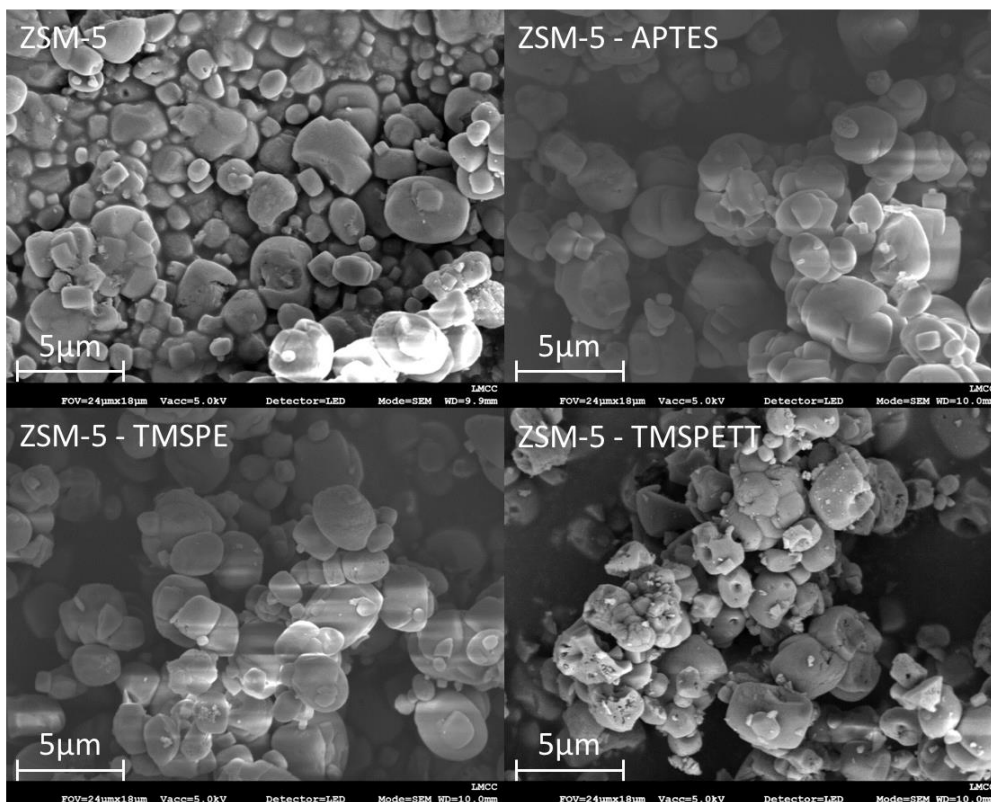
Figure 3.34: SEM images for ZSM-5 modified with APTES, TMSPE and TMSPETT
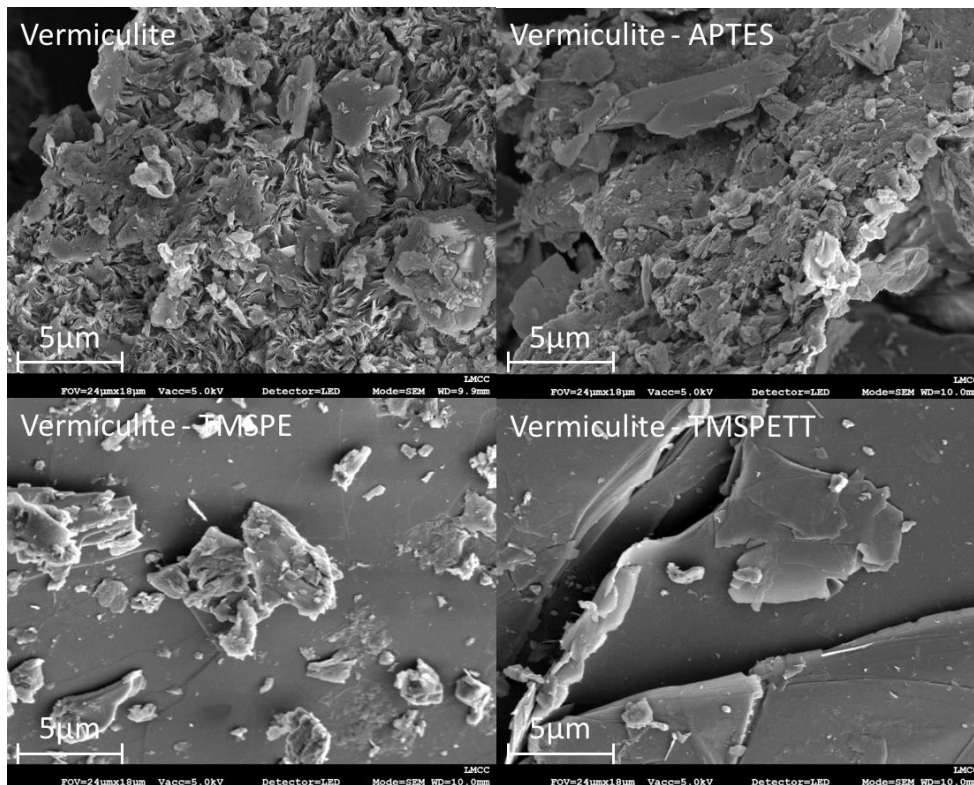
Figure 3.35: SEM images for vermiculite modified with APTES, TMSPE and TMSPETT
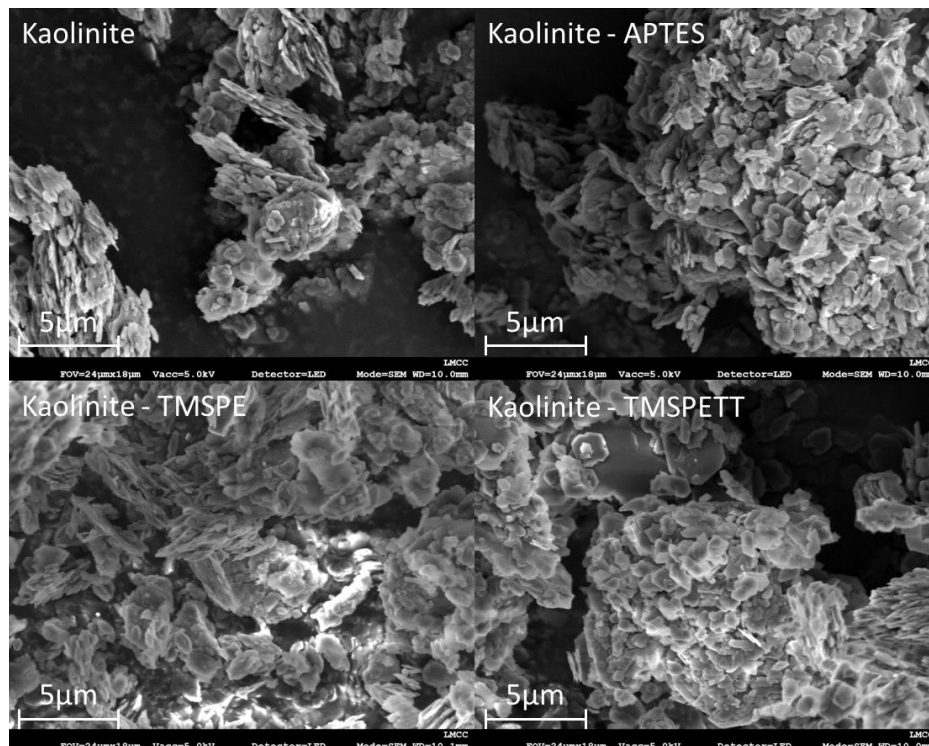
Figure 3.36: SEM images for kaolinite modified with APTES, TMSPE and TMSPETT

3.4.5 Structure by SSNMR of functionalised materials

SSNMR was carried out on clinoptilolite (NDA) and ZSM-5 after reaction with all three ligands. Where liquid NMR produces sharp resonances which can be used to determine structural information, SSNMR produces broad line peaks in the spectra due to incomplete averaging of anisotropic interactions in the static magnetic field. To produce conditions that mimic the tumbling of molecules in solution, the sample is spun rapidly at the magic angle as described in section 2.1.3.1. In the study of clinoptilolite and ZSM-5 both cross polarisation and direct polarisation measurements were used to investigate the grafting of the ligand by ^{13}C SSNMR measurements. Cross polarisation has been used in this thesis to enhance the ^{13}C signals. Since this NMR active nucleus has a low abundance of 1.1%, it can take a long time to produce a useable spectrum. By using a pulse program and observing ^{13}C through transferring of the spin from ^{1}H, which has a higher abundance of approximately 100%, the amount of time needed for the nuclides to relax is reduced and more scans can be completed reducing signal to noise and producing enhanced spectra. All ^{29}Si spectra shown in this thesis were collected using a CP pulse sequence.[135-139]

^{29}Si SSNMR was run to allow comparison of the spectra before and after grafting and monitor any changes that may have occurred within the sample during the grafing process. This can be seen below in figures 3.37 and 3.38.

Clino ^{29}Si MAS

Clino + APTES ^{29}Si MAS

Clino + TMSPE ^{29}Si MAS

Clino + TMSPE ^{29}Si MAS
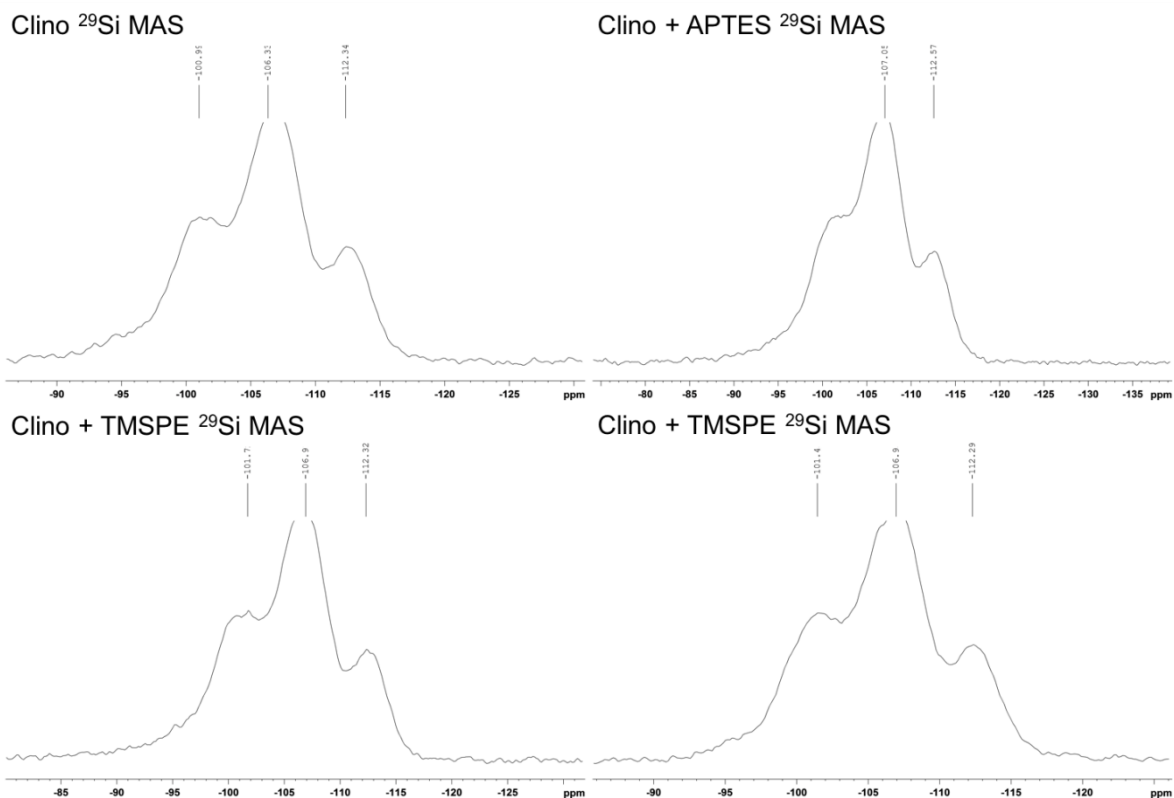
Figure 3.37: ^{29}Si SSNMR spectra for clinoptilolite (NDA) before modification and after modification with APTES, TMSPE and TMSPETT

ZSM-5 ^{29}Si MAS

ZSM-5 + APTES ^{29}Si MAS

ZSM-5 + TMSPE ^{29}Si MAS

ZSM-5 + TMSPE ^{29}Si MAS
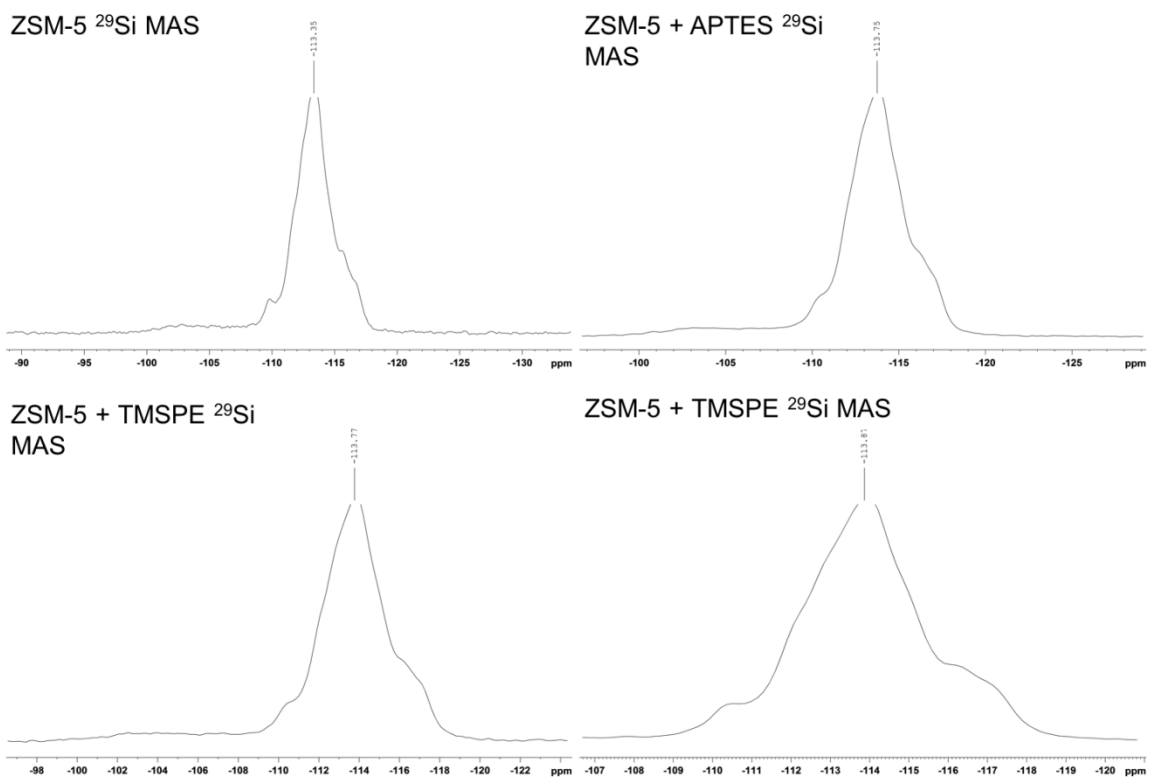
Figure 3.38 ^{29}Si SSNMR spectra for.ZSM-5 before modification and after modification with APTES, TMSPE and TMSPETT:

+

The ^{29}Si SSNMR spectra show that there is no noticeable change in the long-range order of the structure in both cases. This supports the results seen in the PXRD and FTIR which is expected as the ligand is expected to graft to a small number of surface sites due to the rigid framework structure of the zeolites and size of the ligand preventing any disruption of long-range order.

^{13}C SSNMR was run in both direct polarisation and cross polarisation mode to determine if the ligand was present as a solid in the sample and if it was attached to the surface of the solid supports. The ^{13}C SSNMR for clinoptilolite (NDA) can be seen in figure 3.39 and ZSM-5 in figure 3.40.
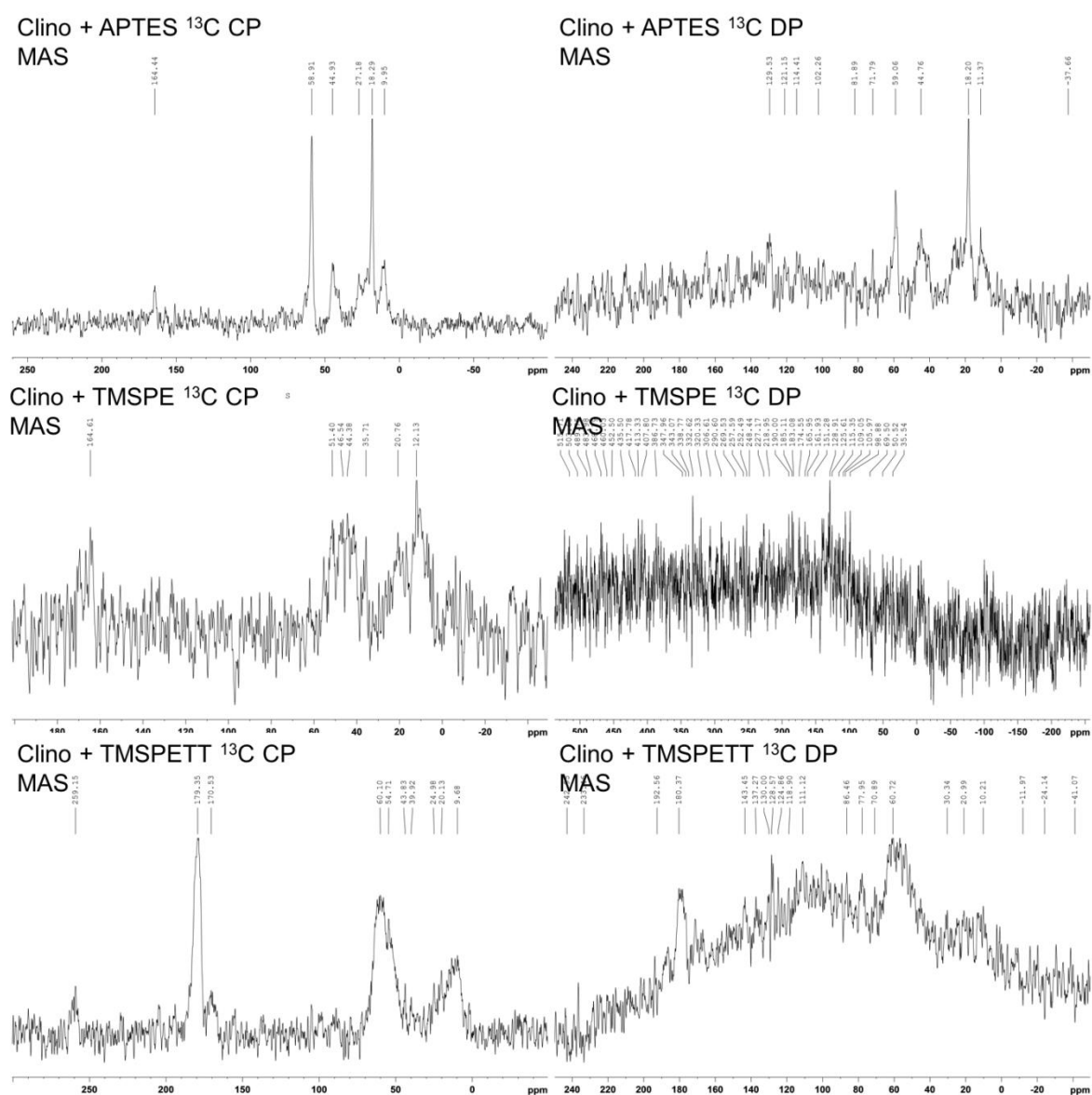
Figure 3.39: ^{13}C CP and DP SSNMR spectra for clinoptilolite (NDA) after modification with APTES, TMSPE and TMSPETT

In all cases it can be seen that the ligands have shown some grafting to the surface. The CP ^{13}C spectra show that the ligand is present in the samples. DP was also carried out with varying success. The noise of the spectra is due to the low levels of grafting seen and the time the samples were analysed for.
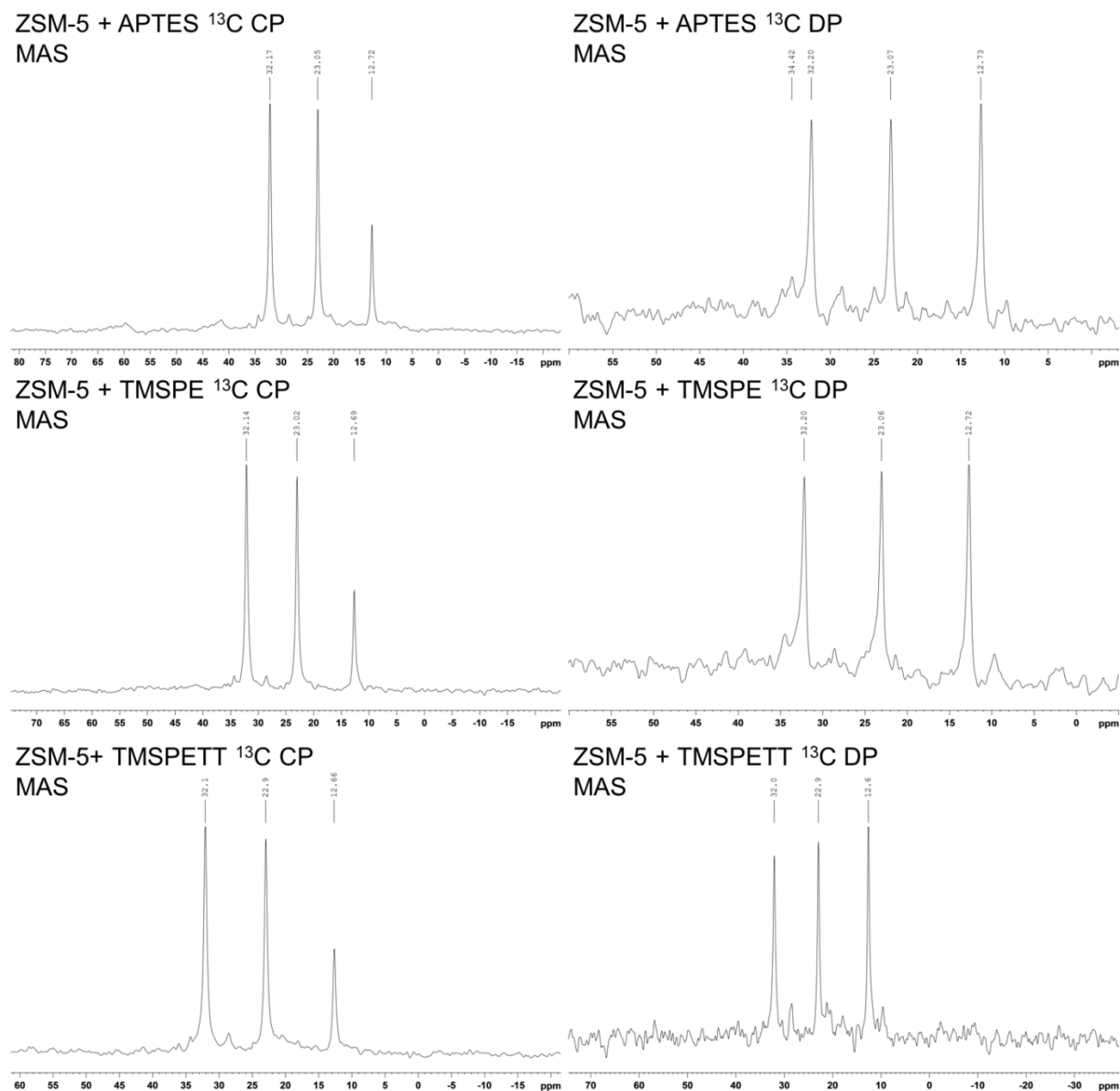
Figure 3.40 ^{13}C CP and DP SSNMR spectra for ZSM-5 after modification with APTES, TMSPE and TMSPETT:

The ^{13}C SSNMR of ZSM-5 gives spectra with greater signal to noise than clinoptilolite (NDA) even with the lower grafting seen due to the fine nature of the particles. The smaller particles allow the solid to similarly to a liquid resulting in sharp lines even with the lower amount of grafting seen in ZSM-5. In

all cases it can be seen that the ligands have shown some grafting to the surface. The CP ^{13}C spectra shows that the ligand is present in the samples and the DP was also carried with the higher signal to noise supporting the sample behaving like a liquid.

3.4.5 Acid pre-treatment experiments

Although the ligand substitution levels reached in the initial experiments described above are suitable for removal of all the actinide species in the solution during the lifetime of the clinoptilolite beds, it was decided to investigate whether the grafting levels could be increased. As clinoptilolite has found uses in other areas of water treatment such as permeable ion exchange walls in ground water, there is a possibility that these grafted materials might have utility elsewhere. By treating the surface with acid to roughen the surface by chemical reaction by essentially breaking it down, more hydroxyl groups should be available to enable greater functionalisation of the supports.   As the sample of clinoptilolite from the NDA was plentiful and had shown good grafting capability, it was selected for these experiments along with the APTES ligand.

2 g of Clinoptilolite (NDA) was placed in 10 mL of either citric or nitric acid of varying concentration ranging from 1 - 5 mol L^{-1} for 30 mins at 25°C. Material was then filtered via sintered glass crucible under suction and washed with 100 mL of deionised water. The material was then placed in 20 mL of acetone in a 100 mL round bottom flask. The methodology for ligand grafting was then followed as previously described in section 3.4.1.1 using 8 ml (3.42×10^{-2} moles) of APTES for a period of 24h. Samples were analysed by CHN analysis to determine the effect of the pre-treatments and are summarised in Table 3.29.

Table 3.29 – Change in carbon content with acid treatment on clinoptilolite (NDA)

Clinoptilolite (NDA)				
Acid	%C	%N	% difference in C	Mmol of ligand / g
No acid	0.03(3)	0.01(3)		
1M Nitric	4.59(3)	1.45(3)	4.56	69.98
3M Nitric	4.22(3)	1.31(3)	4.19	64.30
5M Nitric	5.19(3)	1.47(3)	5.16	79.18
5M Citric	7.05(3)	1.66(3)	7.03	107.73
3M Citric	4.39(3)	1.00(3)	4.36	66.91
1M Citric	5.80(3)	1.58(3)	5.77	88.54

In these preliminary experiments, the data indicate that there is some variation in the carbon content with concentration of acid, although the results are not conclusive. The variability of the natural samples always leads to some variation in the level of grafting due to the mineralogical origins.

The citric acid appears to be having a greater effect than the mineral acid on increasing the grafting capability. This is a curious result as the acid with the higher pKa (nitric) is expected to be stronger and perhaps cause more damage to the surface of the material and hence provide more surface area for the functionalisation to take place. After reaction, the citric acid treated samples were examined in more detail and had gone brown in colour as shown in Figure 3.41. The acid solution was yellow in colour which when tested with potassium hexcyanoferrate (II) went blue indicating the presence of iron (III) through the formation of Prussian blue. It therefore appears that the citric acid is highly effective in removing poorly crystalline iron compounds from the solid; they are poorly crystalline as no identifiable iron phases appeared in the diffraction pattern. This extraction process is well-known in the extraction of iron minerals where ferrihydrite can be removed from goethite by citric acid washing.[161,162]

Figure 3.41: Sample of clinoptilolite after pre-treatment with citric acid.

A third pre-treatment acid with a pka between that of the very strong nitric acid and the much weaker citric acid was then added. Phosphoric acid was therefore chosen with the concentration being fixed at 3 M following the same pre-treatment procedure. Table 3.30 shows the effect of acid pre-treatment on the carbon content of the support. The changing content of the citric acid samples implies that some residual acid is left trapped in the pores and/or coordinated to the framework.

Clinoptilolite NDA					
Acid	Time	%C	%N	% difference in C	Filtrate
No acid		0.03(3)	0.01(3)	3.16	
Citric	1Hr	2.61(3)	0.03(3)	3.75	V. Pale yellow
Citric	2Hr	1.04(3)	0.02(3)	4.78	Pale yellow
Citric	4Hr	0.75(3)	0.02(3)	3.58	Pale yellow
Citric	8Hr	2.18(3)	0.00(3)	8.01	Pale Yellow
Citric	16Hr	1.33(3)	0.02(3)	8.28	Yellow
Citric	24Hr	1.63(3)	0.03(3)	2.51	Deep Yellow
Phosphoric	1Hr	0.00(3)	0.02(3)	2.64	Clear
Phosphoric	2Hr	0.00(3)	0.02(3)	3.34	"oily"
Phosphoric	4Hr	0.02(3)	0.02(3)	6.39	"oily"
Phosphoric	8Hr	0.00(3)	0.06(3)	3.75	"oily"
Phosphoric	16Hr	0.01(3)	0.03(3)	9.43	"oily"
Phosphoric	24Hr	0.03(3)	0.02(3)	3.00	"oily"
Nitric	1Hr	0.00(3)	0.25(3)	2.58	Clear
Nitric	2Hr	0.00(3)	0.60(3)	7.33	"oily"
Nitric	4Hr	0.00(3)	0.40(3)	11.55	"oily"
Nitric	8Hr	0.05(3)	0.28(3)	6.02	"oily"
Nitric	16Hr	0.01(3)	0.18(3)	3.34	"oily"
Nitric	24Hr	0.01(3)	0.29(3)	3.16	"oily"

Filtrates from each sample were collected and showed significant change with increasing acid treatment time. The yellow colour of the solution is likely to be due to the presence of iron (III) citrate which has been isolated from similar washing experiments before on goethite. Formation of other acid salts was also thought to be the cause of material with a different refractive index to the initial

aqueous acid, causing an "oily" streaked appearance within phosphoric and nitric samples. Further dot testing was carried out on filtrates using potassium hexacyanoferrate(II) solution. The presence of iron(III) salts was confirmed in both the citric filtrates and nitric filtrates. However where the citric filtrate was positive with immediate effect (Colour change orange to blue), nitric filtrates required a much longer reaction times to produce a positive result, suggesting that nitric acid is less effective at removing the poor crystalline iron impurities from the clinoptilolite. The washing solutions from the phosphoric acid experiments were not positive for iron salts. The citric acid filtrate was crystallised out from solution and further analysed by FT-IR as detailed below. All filtrate samples showed a decrease from initial molarity as confirmed by titration with 1M KOH indicating that all acids had taken part in a chemical reaction.

The effect of the pre-treatment reactions on grafting were further investigated by carrying out additional experiments over a varying grafting period of 1, 2, 4, 8, 16, 24 h. The samples were then analysed to determine the change in CHN content of the material after reaction with APTES. Quantity of ligand grafted (mmols) was calculated via total %C the RMM of the ligand (APTES, 221.37 g/mol), and the quantity of material used during CHN analysis.

Table 3.31 - CHN data for modified, acid treated samples

Acid	Acid reaction time	%C	%N	mmol of ligand / g)
Citric	1Hr	3.19(3)	0.57	103.67
Citric	2Hr	3.78(3)	0.78	130.35
Citric	4Hr	4.81(3)	0.85	155.20
Citric	8Hr	3.61(3)	0.62	64.46
Citric	16Hr	8.04(3)	2.3(3)	196.32
Citric	24Hr	8.31(3)	2.15(3)	166.10
Phosphoric	1Hr	2.54(3)	0.69(3)	72.16
Phosphoric	2Hr	2.67(3)	0.66(3)	64.16
Phosphoric	4Hr	3.37(3)	0.54(3)	44.77
Phosphoric	8Hr	6.42(3)	1.91(3)	176.84
Phosphoric	16Hr	3.78(3)	0.86(3)	90.35
Phosphoric	24Hr	9.46(3)	3.04(3)	156.53
Nitric	1Hr	3.03(3)	0.83(3)	66.44
Nitric	2Hr	2.61(3)	0.58(3)	79.66
Nitric	4Hr	7.36(3)	1.77(3)	163.78
Nitric	8Hr	11.58(3)	3.85(3)	253.93
Nitric	16Hr	6.05(3)	1.41(3)	155.28
Nitric	24Hr	3.37(3)	0.65(3)	46.13

Within the limits of error generated by using samples from a natural origin, acids do appear to affect the grafting capability of the clinoptilolite with APTES. Changes in carbon content appear to indicate that it is not simply acid strength that matters, as phosphoric acid appears to show a greater change in carbon content than nitric acid. Stronger acids may perhaps cause a breakdown of the material entirely rather than just a roughening of the surface resulting in worse uptake. Citric acid remains a curiosity as the citric acid itself seems to possibly graft to the surface or at least be occluded into it. A proportion of further work in this area, but beyond the scope of this thesis, might involve looking at how citric acid could be a cheaper alternative to APTES for actinide binding as the oxide groups make act in a sequestration capacity once bound (or occluded) by the framework.

3.5 Chapter conclusions

The organic ligands APTES, TMSPE and TMSPETT were successfully grafted onto the surfaces of Clinoptilolite (NDA), clinoptilolite (Imerys), ZSM-5, vermiculite and kaolinite with a maximum increase in carbon of 10.76% equating to 56.16 mmol of ligand grafted in the case of APTES to clinoptilolite (NDA).

Various elements of the reaction were investigated with emphasis on reaction time, solvent polarity and ligand concentration. The results indicate that extent of ligand grafted increases with reaction time until a saturation point is reached which varies for each material and ligand combination. The effect of solvent polarity varies with the material investigated. The most significant result was clinoptilolite with a non-polar solvent showing the greatest effect on amount of ligand grafted. In the case of the ligand concentration the clinoptilolite samples show an increased graft with increased ligand concentration however no discernible difference is seen in the cases of ZSM-5, vermiculite and kaolinite.

The effect of surface roughening with selected acids was studied. The experiments indicate that after treatment there is an increase in ligand grafted, which appears to be independent of acid strength and concentration.

The analysis by PXRD, SSNMR and FTIR show that there is no change in the long range order of the material and so the structure unchanged which should not prevent ion exchange from occurring. This hypothesis was investigated in chapter 4.

Chapter 4-Radionuclide sequestration experiments

4.0 Introduction to Chapter 4

The ability of the two clinoptilolite samples, ZSM-5, vermiculite and kaolinite are investigated in this chapter for their ability to remove caesium and strontium from solution before and after modification with APTES, TMSPE and TMSPETT. Clinoptilolite is already used in the nuclear industry in SIXEP to remove caesium and strontium cations from aqueous waste streams where they are in high concentration, therefore it is important to investigate if the modification of these materials influences their sequestering ability for these species deleteriously. All investigations were conducted using a radiotracer to monitor the ability of the solids to remove both cations from solution. The ability of the two clinoptilolite samples, ZSM-5, vermiculite and kaolinite are then investigated for their ability to remove uranium and plutonium from solution before and after modification with the sequestering ligands. Uranium and plutonium are present in fuel rods; when the fuel rod cladding deteriorates some uranium and plutonium species become soluble and are present in the storage pond liquor. These ions need to be removed from the waste stream before discharge of the solution from the SIXEP process into the sea.

4.1 Experimental methodology for caesium and strontium experiments

The sequestration capacity of the materials used has been investigated radiometrically using batch sorption studies at varying concentrations of metal ions. The sorption experiments were conducted in 15 mL plastic sample tubes with approximately 0.05 g of solid and 10 mL of metal nitrate solution ranging from 10^{-2} to 10^{-10} mol L^{-1} in increments of 10^{-2} mol L^{-1}. The solution was then spiked with the relevant radio tracer. The samples were then shaken for 7 days to allow equilibrium between the solid and liquid to be reached. After this time period had elapsed, 2 mL of the supernatant were then filtered through a 0.22 μm Teflon pore filter to remove any solid particulate. The amount of metal ions removed from solution was calculated using mass balance calculations relative to a control sample. This allows the activities of the solutions before and after being exposed to the solid surface to be compared talking into account wall sorption effects. All experiments were carried out in triplicate to show reproducibility and under ambient conditions.[144,165]

The activity in solution is determined by ratio of the final activity and the initial activity, multiplied by the concentration as shown in the Equation 4.1.
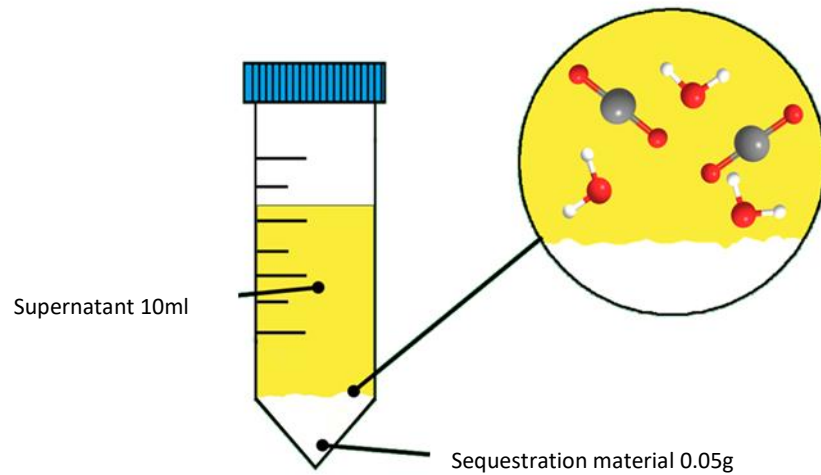
Figure 4.1: Schematic Diagram of Batch Experiment

If the initial concentration of the cation in solution is

$$= [Z^{x+}]_0$$

and the initial radioactivity added to this solution is

$$= A_o(RN)$$

and the final radioactivity remaining in solution after addition of a solid sorbent and after equilibration is

$$= A(RN)$$

Then the final concentration of cation remaining in solution after addition of a solid sorbent and after equilibration is

$$[Z^{X+}]_f = \frac{[Z^{X+}]_0 \; x \; A(RN)}{A_0(RN)}$$

The concentration of cation sorbed to the solid material is

$$= [Z^{x+}]_0 - [Z^{x+}]_f$$

$$= [Z^{x+}]_0 - [Z^{x+}]_0 \times \frac{A(RN))}{A_o(RN)}$$

Most of the results of the sorption experiments shown in this thesis are shown as percentages of the initial cation concentration removed from solution by sorption onto a solid material and the equation below shows the calculation of these results:

% of initial solution concentration removed by solid

$$= \frac{[Z^{x+}]_0 - \left([Z^{x+}]_0 \ X \ \frac{A(RN)}{Ao(RN)}\right) X \ 100}{[Z^{x+}]_0}$$

Equation 4.1

An example calculation   for caesium on unmodified clinoptilolite (NDA)

Where:

$[Z^{x+}]_0 = 1 \times 10^{-2}$ mol L^{-1}

$[Z^{x+}]_f = 4.14 \times 10^{-3}$ mol L^{-1}

$A_o(RN) = 34064$ cpm

$A(RN) = 14100$ cpm

Then the final % of initial solution concentration removed by solid

$$= \frac{1 \times 10^{-2} - \left(1 \times 10^{-2} \ X \ \frac{14100}{34064}\right) X \ 100}{1 \times 10^{-2}}$$

$= 58.6\ \%$

The tables of results show the average value for three measurements e.g

$$\frac{58.6 + 37.8 + 59.5}{3}$$

$= 51.7\ \%$

The error in the percentage of solution removed was given to one σ deviation using the equation below.

$$\sigma = \sqrt{\sum \frac{(x - \bar{x})^2}{n}}$$

Where:

σ = standard deviation

x = average counts

x̄ = replicate value

n = number of replicates

e.g

x-x̄		(x-x̄)²
Calculation	Value	
51.7 - 58.6	-6.9	47.61
51.7 - 37.8	13.9	193.21
51.7 - 59.5	-7.8	60.84

Therefore

$$\sigma = \sqrt{\sum \frac{301.66}{3}}$$

= 10.02 %

The kinetic experiments were carried out using the same experimental methodology and calculations for different time periods. The kinetic experiments were carried out using a 1×10^{-3} mol L^{-1} solution which was shown by the batch sorption experiments to be sufficient concentration allow saturation of the materials. Desorption experiments were carried out using the solid from the sorption experiments with 10 mL of deionised water added with an assumed concentration of ions of zero to determine if the cations are ion exchanged or simply physisorbed on the surface.

Although the results in this thesis are presented as percentage sorbed, it is common practice in the nuclear industry to present results as the distribuition ratio R_d, sometimes refered to as K_d, results are presented as R_d in appendix 8.3.

4.1 Batch sorption experiments

0.05 g of solid was weighed out in to a 15 mL plastic centrifuge tube; to this 10 ml of an inactive metal nitrate solution with concentrations ranging from 10^{-2} to 10^{-10} mol L^{-1}. A 50 µl spike of 0.3kBq of either ^{137}Cs or ^{85}Sr radiotracer was added. Samples were then placed on to a flatbed shaker and gently agitated for a period of 7 days. The supernatant was then decanted, and a 2 ml aliquot removed and filtered through a 0.22 µm Teflon pore filter to remove any solid particulate and transferred to a 4 mL plastic gamma vial. Samples were then analysed by either gamma counting using a Cobra II auto gamma counter. All measurements were conducted in triplicate and measured relative to a control sample to take into account wall sorption effects. The experimental set- up used for sorption, desorption and kinetic experiments can be seen in Figure 4.1.

4.3 Desorption experiments

The samples from the sorption experiment were used to carry out the desorption experiments of the materials. The sorption experiment solution was decanted from the centrifuge tube leaving the solid. 10 mL of distilled water was added to the solid. The samples were then shaken for 28 days, and a 2 mL aliquot was taken and filtered using a 0.22 µm filter to remove any solids. The samples were counted using a Cobra gamma counter. 28 days was selected to show stability of the binding when applied to plant process. The percentage desorbed is calculated using Equation 4.3.[113]

$$\frac{A_D(RN)}{A_0(RN) - A(RN)} = \% \, desorbed$$

where $A_0(RN)$ is the initial concentration of activity in solution (cpm)

$A(RN)$ is the activity in solution after contact with the solid (cpm)

$A_D(RN)$ is the activity in solution after contact with fresh solution (cpm)

4.4 Kinetic experiments

0.05 g of solid was weighed out in to a 15 mL plastic centrifuge tube; to this 10 ml of a 1 x 10^{-3} mol L^{-1} carrier solution was added. A 50 µl spike of 0.3 kBq was then added as a radiotracer. The kinetic experiments were set up in replicates of three. Metal nitrate was used as the carrier solutions, ^{137}Cs or ^{85}Sr were used as radiotracers; concentration was determined using batch sorption experimental isotherm results. Times of one hour, one day, one week, two weeks and four weeks were used to investigate the speed of the sequestration of the materials before and after modification. The samples

were shaken and at the set time intervals a 2 mL aliquot was taken and filtered using a 0.22 µm filter to remove any solids. The samples were counted using a Cobra gamma counter.

The uptake of caesium to clinoptilolite, ZSM-5, vermiculite and kaolinite was investigated using the batch sorption methodology discussed in section 4.3. The results are shown in Figure 4.2 and Table 4.1.
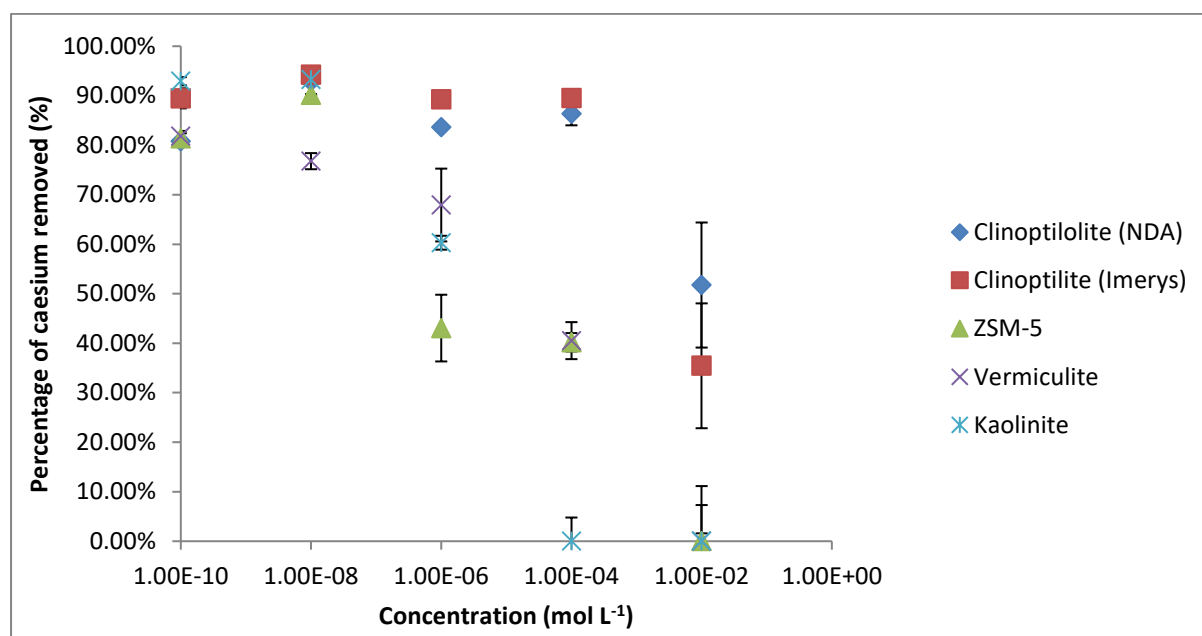
Figure 4.2: Batch sorption experiments for caesium using on the ungrafted solid supports

The results show that all materials successfully remove caesium to varying degrees of effectiveness. The greatest extent of removal can be seen by the clinoptilolite samples followed by the vermiculite, ZSM-5 and then finally kaolinite. This can be attributed to the sites in clinoptilolite cages being of the appropriate size and coordination number for the caesium cation. Due to the much lower aluminium content of ZSM5 compared to clinoptilolite and hence concomitant lower numbers of exchangeable sodium cations, it is expected that ZSM-5 will not be as efficient an ion-exchanger as clinoptilolite. Vermiculite and kaolinite are both clay minerals and so the method of sequestration is slightly different to that of the zeolites. In clay minerals, the ions are sequestered between layers not within cages as they are in the zeolites. The clays show different efficacies for caesium removal, where vermiculite is more efficient than kaolinite. Vermiculite has exchangeable cations within the layers and can extrude to allow different size cations to enter the layers to replace them, but for kaolinite, the layers are neutral and there are none. Any interaction with the actinide is expected to be basic physisorption rather than ion exchange for kaolinite.

Concentration	Clinoptilolite (NDA)		Clinoptilolite (Imerys)		ZSM-5		Vermiculite		Kaolinite	
	% removed	Error (+/-)	% removed	Error (+/-)	% removed	Error (+/-)	% removed	Error (+/-)	% removed	Error (+/-)
1×10^{-2}	51.8%	12.6%	35.4%	12.6%	0.0%	1.6%	0.0%	7.3%	0.0%	11.1%
1×10^{-4}	86.3%	2.3%	89.5%	0.8%	40.2%	1.9%	40.5%	3.7%	0.0%	4.8%
1×10^{-6}	83.6%	0.6%	89.2%	1.2%	43.1%	6.7%	67.9%	7.4%	60.3%	1.4%
1×10^{-8}	92.9%	0.3%	94.2%	0.8%	90.2%	0.2%	76.8%	1.6%	93.2%	0.7%
1×10^{-10}	80.8%	2.4%	89.5%	2.0%	81.3%	1.1%	81.8%	1.1%	92.9%	0.8%

4.5 Uptake of caesium by APTES modified materials

The uptake of caesium to the APTES modified materials clinoptilolite, ZSM-5, vermiculite and kaolinite was investigated using the batch sorption methodology discussed in section 4.3. The results are shown in Figure 4.3 and Table 4.2.
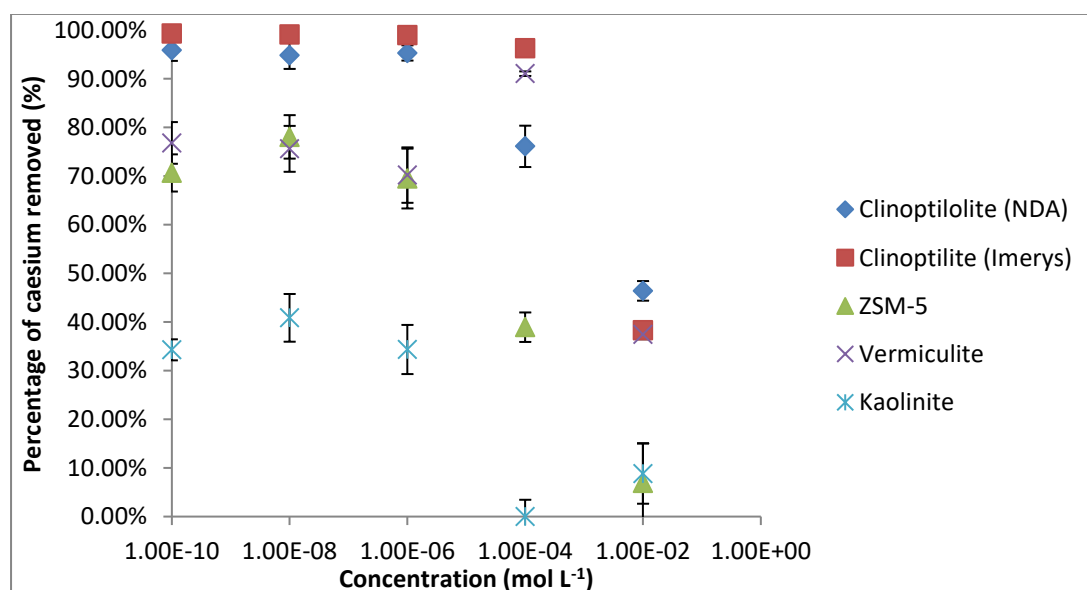
Figure 4.3: Uptake of caesium by APTES modified clinoptilolite at varying caesium concentration

 The uptake of caesium by the APTES modified clinoptilolite samples shows that the cages of the zeolite are still accessible by the cation in solution and ion exchange still occurs. Overall, the APTES modified clinoptilolite samples remove more caesium at lower concentrations after modification than before. The synthetic zeolite ZSM-5 and the clay vermiculite are marginally improved at the higher concentration end but remain significantly poorer than clinoptilolite overall. The greater extraction of the caesium can be attributed to some of the caesium cations binding to the ligand.

Material	Clinoptilolite (NDA)		Clinoptilolite (Imerys)		ZSM-5		Vermiculite		Kaolinite	
Concentration	% removed	Error (+/-)	% removed	Error (+/-)	% removed	Error (+/-)	% removed	Error (+/-)	% removed	Error (+/-)
1×10^{-2}	46.4%	2.0%	38.3%	0.8%	6.9%	8.2%	37.5%	1.0%	8.83%	6.2%
1×10^{-4}	76.1%	4.3%	96.3%	0.4%	38.9%	3.0%	91.1%	0.5%	0.0%	3.5%
1×10^{-6}	95.3%	1.6%	99.0%	0.3%	65.5%	6.2%	70.2%	5.7%	34.4%	5.0%
1×10^{-8}	94.8%	2.8%	99.1%	0.2%	78.0%	4.5%	75.6%	4.7%	40.9%	4.9%
1×10^{-10}	95.9%	2.2%	99.3%	0.2%	70.7%	3.8%	76.8%	4.3%	34.3%	2.6%

4.6 Uptake of caesium by TMSPE modified materials

The uptake of caesium to the TMSPE modified minerals clinoptilolite, ZSM-5, vermiculite and kaolinite was investigated using the batch sorption methodology discussed in section 4.2. The results are shown in Figure 4.4 and Table 4.3.

Figure 4.4: Effect of TMPSE complexation on uptake of caesium cations by the substrates.

Material	Clinoptilolite (NDA)		Clinoptilolite (Imerys)		ZSM-5		Vermiculite		Kaolinite	
Concentration	% removed	Error (+/-)	% removed	Error (+/-)	% removed	Error (+/-)	% removed	Error (+/-)	% removed	Error (+/-)
1×10^{-2}	60.3%	4.0%	36.6%	3.7%	0.4%	4.6%	39.3%	5.4%	3.6%	4.6%
1×10^{-4}	95.2%	4.5%	92.2%	8.6%	39.6%	1.9%	96.8%	2.8%	18.2%	1.3%
1×10^{-6}	99.4%	0.9%	100.0%	0.0%	70.0%	6.1%	96.5%	3.9%	41.0%	5.9%
1×10^{-8}	100.0%	0.0%	100.0%	0.0%	78.6%	8.0%	96.2%	1.1%	46.1%	3.8%
1×10^{-10}	100.0%	0.0%	99.9%	0.0%	86.7%	15.7%	100.0%	0.0%	70.8%	7.3%

The uptake of caesium by the TMSPE modified clinoptilolite samples shows similar behaviour to APTES, with improved uptake of the caesium cations at low concentration and no real loss in ion exchange capacity of the zeolite. There is also a noticeable improvement in the take up of caesium cations at high concentrations in the case of vermiculite.

4.7 Uptake of caesium by TMSPETT modified materials

The uptake of caesium to the TMSPETT modified minerals clinoptilolite, ZSM-5, vermiculite and kaolinite was investigated using the batch sorption methodology discussed in section 4.2. The results are shown in Figure 4.5 and Table 4.4.
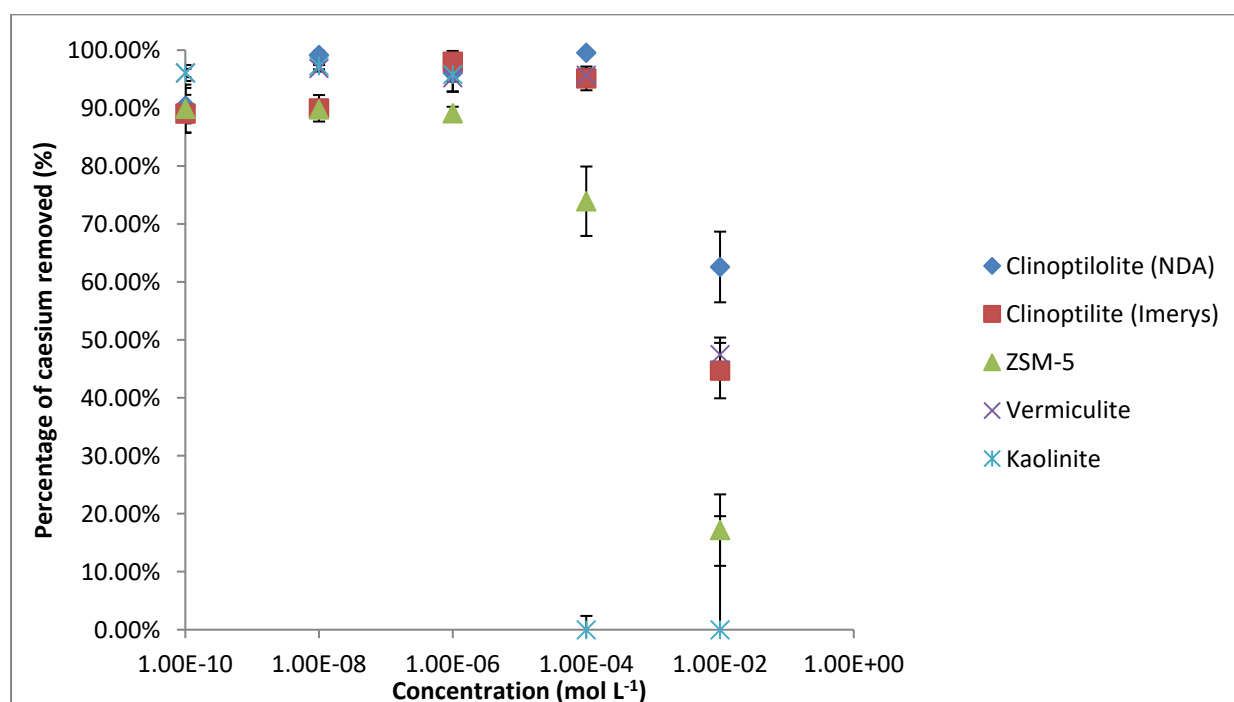

Figure 4.5 Effect of TMPSETT complexation on uptake of caesium cations by the substrates

The trend observed for the first two ligands is replicated for TMSPETT. The uptake of caesium by the TMSPETT modified clinoptilolite samples shows that the cages of the zeolites are still accessible by the cation and ion exchange still occurs despite the bulky nature of this ligand. Kaolinite does not show any improvement at high concentrations with practically zero take up. Vermiculite shows a significant increase in its capacity to sequester caesium after grafting, particular at higher concentrations. The synthetic zeolite, ZSM-5, shows some improvement, albeit at much lower levels than vermiculite. This can be attributed to caesium binding to the ligand. The TMSPETT ligand contains twice the number of binding sites as APTES or TMSPE per ligand grafted.

Table 4.4: Change in caesium uptake of minerals after grafting with TMSPETT

Material	Clinoptilolite (NDA)		Clinoptilolite (Imerys)		ZSM-5		Vermiculite		Kaolinite	
Concentration	% removed	Error (+/-)	% removed	Error (+/-)	% removed	Error (+/-)	% removed	Error (+/-)	% removed	Error (+/-)
1×10^{-2}	62.6%	6.1%	44.7%	4.8%	17.2%	6.2%	47.5%	2.9%	0.0%	19.6%
1×10^{-4}	99.6%	0.1%	95.1%	2.1%	73.9%	6.0%	95.7%	1.1%	0.0%	2.4%
1×10^{-6}	96.1%	3.3%	98.0%	1.9%	89.1%	1.1%	95.2%	0.7%	95.8%	2.9%
1×10^{-8}	99.2%	0.7%	90.0%	2.3%	89.8%	1.0%	96.9%	0.6%	97.3%	0.6%
1×10^{-10}	90.4%	3.1%	89.1%	3.2%	89.9%	4.2%	96.1%	1.4%	96.0%	0.7%

4.8 Comparison of caesium cation uptake by grafted and non-grafted clinoptilolite (NDA) materials

The uptake of caesium cations to the unmodified and modified mineral clinoptilolite was investigated using the batch sorption methodology discussed in section 4.2. The results are shown in Figure 4.6.
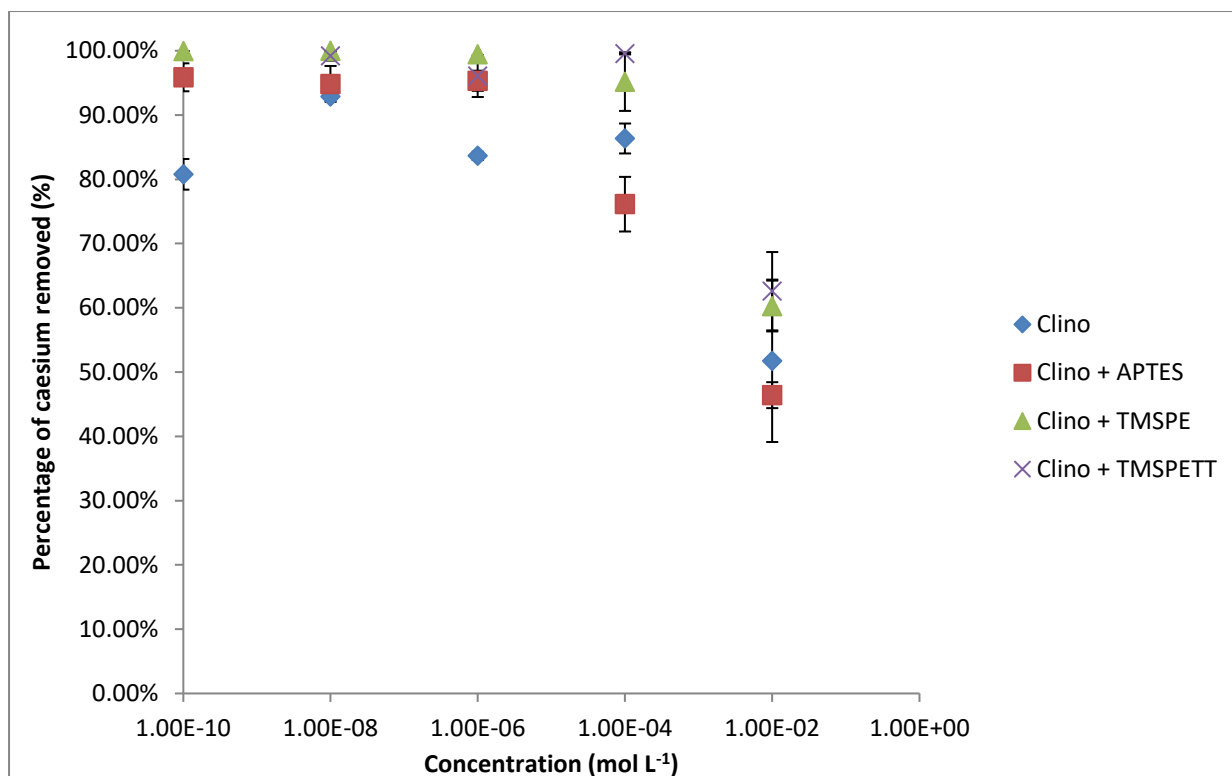
**Figure 4.6 Comparison between clinoptilolite NDA with and without ligand grafts**

The removal of caesium is still observed in the modified materials, leading to the conclusion that the ligands are not affecting the ability of the material to ion exchange. The ligand TMSPETT shows the greatest enhancement in caesium removal, probably due to the multiple binding sites.

4.9 Comparison of caesium uptake by grafted and non-grafted clinoptilolite (Imerys) materials

The uptake of caesium to the unmodified and modified mineral clinoptilolite was investigated using the batch sorption methodology discussed in section 4.2. The results are shown in figure 4.7.
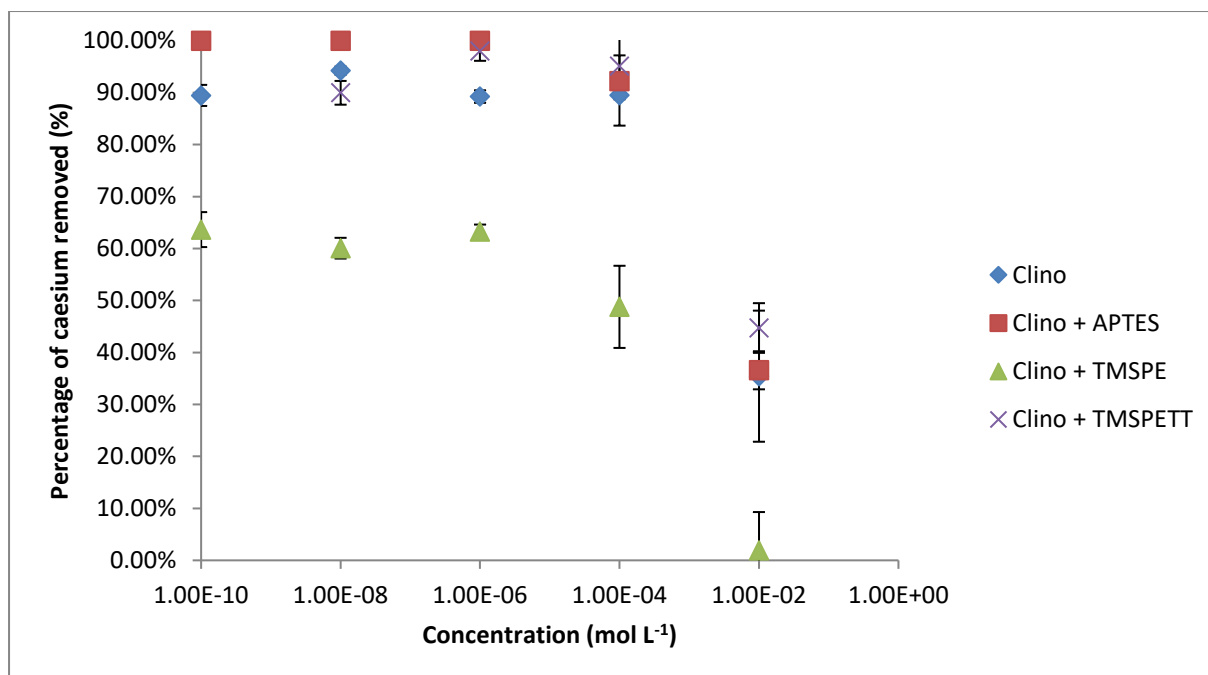
Figure 4.7 Comparison between clinoptilolite Imerys with and without ligand grafts

The removal of caesium is still observed in the modified materials, leading to the conclusion that the ligands are not effecting the ability of clinoptilolite Imerys to undertake caesium cation exchange. The ligand TMSPE shows a reduction in the removal of caesium cations over the raw material. This is attributed to the size of the particles of the clinoptilolite and the size of the ligand. The clinoptilolite (Imerys) particle size is smaller than the clinoptilolite (NDA) sample; the increased size of the TMSPE ligand compared to the APTES ligand could be affecting the access to the channels reducing the uptake of the material. Another factor in the reduction of the uptake of the TMSPE modified clinoptilolite (Imerys) is the atoms available for binding. The TMSPETT ligand contains more binding sites and therefore can remove more ions than APTES or TMSPE.

4.10 Comparison of caesium uptake by grafted and non-grafted ZSM-5 materials

The uptake of caesium to the unmodified and modified ZSM-5 was investigated using the batch sorption methodology discussed in section 4.2. The results are shown in Figure 4.8.
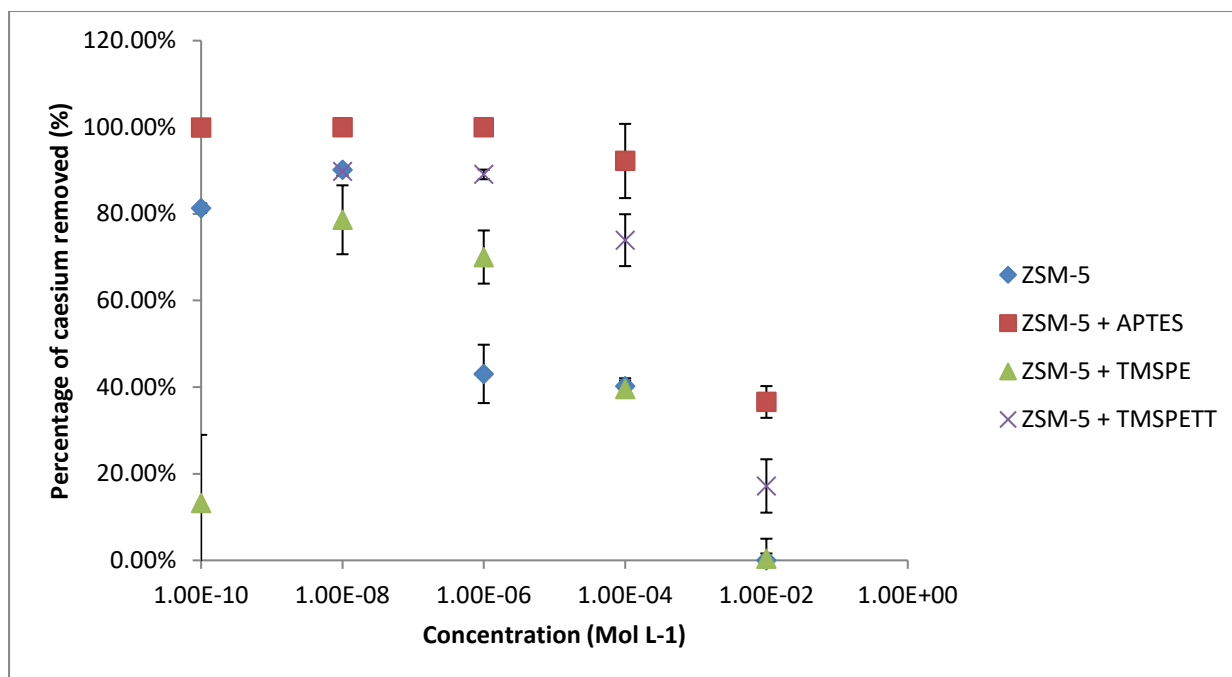
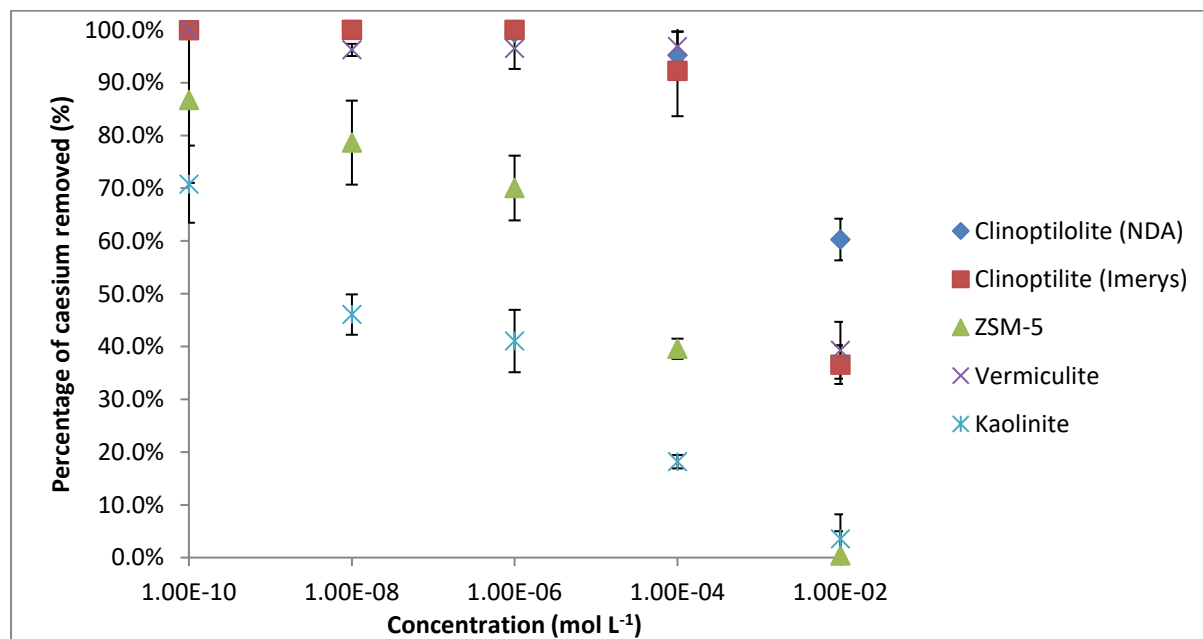**Figure 4.8 Comparison between ZSM5 with and without ligand grafts**

The APTES and TMSPETT modified ZSM-5 samples show some improvement in the removal of caesium cations but here the ion exchange capability is significantly less than that of clinoptilolite due to much fewer exchangeable cations and exchange sites of less suitable size. Clinopilolite was chosen as an ion exchange material for SIXEP after considerable testing as it is the best material for caesium and strontium uptake available anywhere; of all deposits in the World, the Mojave desert deposits used for SIXEP were the best of all clinoptilolite deposits found in the World for ion exchange of caesium and strontium cations. It is therefore unsurprising that no other material tested shows better caesium cation exchange capability than the clinoptilolite provided by the NDA. As the APTES ligand is smaller than the other two ligands, it is less likely to hinder access to the channels than TMSPE. TMSPETT has more donor atoms available for bonding than the other two ligands and hence is likely to show better take up even at the lower grafting levels observed.

4.11 Comparison of vermiculite materials

The uptake of caesium to the unmodified and modified vermiculite was investigated using the batch sorption methodology discussed in section 4.2. The results are shown in Figure4.9
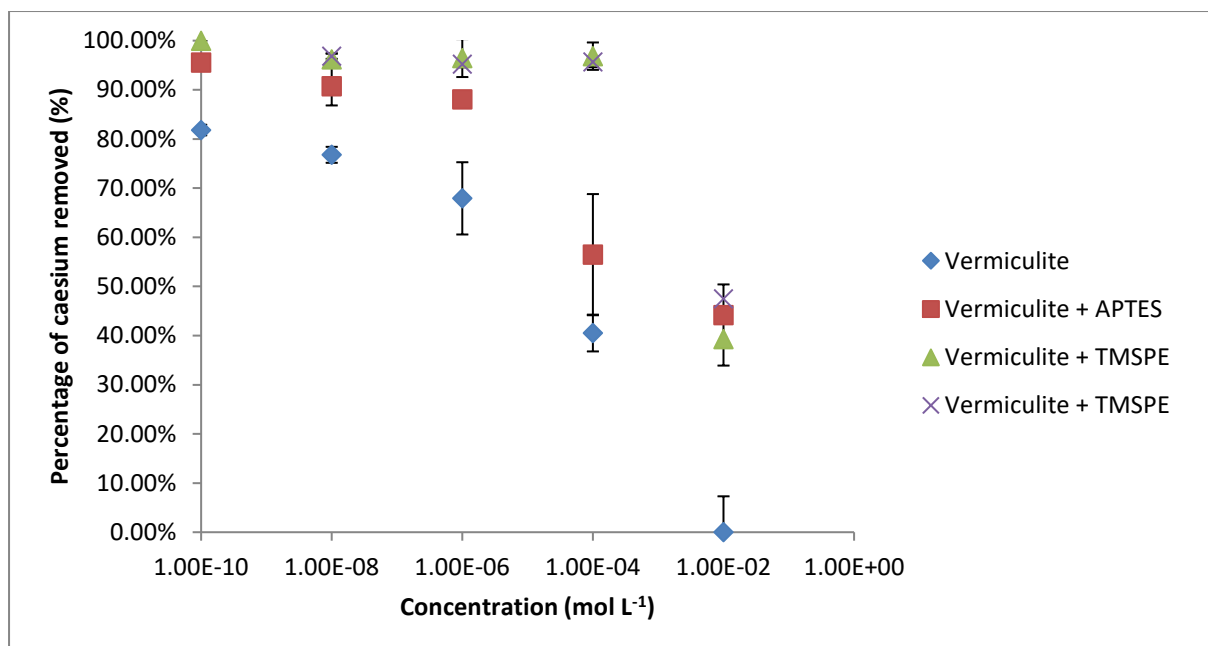
Figure 4.9 Comparison of caesium cation uptake between vermiculite with and without ligand grafts

All the modified materials show an improved caesium removal over the unmodified material at all concentrations. This can be explained by the ligands binding between the layers of the clay causing the layers to expand making them more accessible to the cation and/or surface binding giving additional capacity for ion removal. Vermiculite shows better caesium removal capability than ZSM-5 as the clay possesses exchangeable cations between the layers.

4.12 Comparison of kaolinite materials

The uptake of caesium to the unmodified and modified kaolinite was investigated using the batch sorption methodology discussed in section 4.2. The results are shown in Figure 4.10.
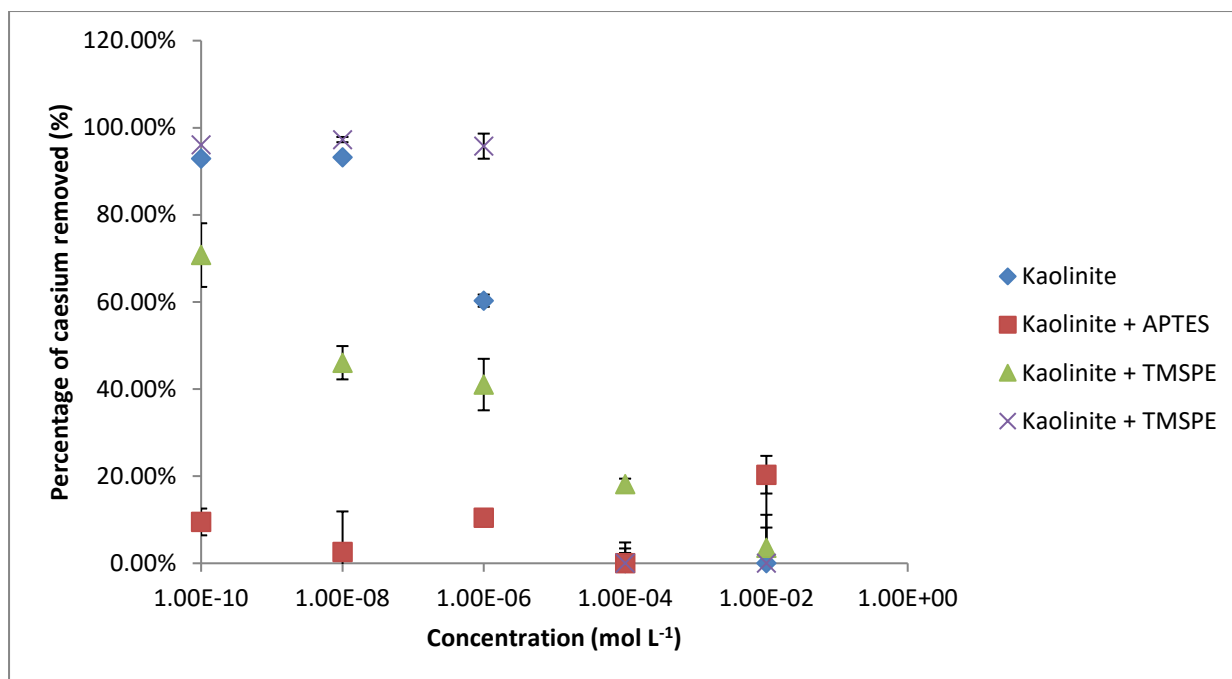
Figure 4.10 Comparison of caesium cation uptake between kaolinite with and without ligand grafts

Kaolinite is not capable of ion exchange as it has no exchangeable cations. The layers are neutral and no cations lie between the layers. As a result the unaltered clay does not undergo ion exchange, but can only physisorb caesium cations to the surface. As a result, these species would readily desorb as they are not bonded in or held by cation/anion electrostatic interactions. Due to the low amount of graft, the grafted materials also show relatively poor take up after grafting. The removal of caesium by the modified and unmodified kaolinite samples shows some removal at low concentrations but very little removal at higher concentrations.

4. 13 Batch desorption sorption experimental results

4.13.1 Desorption of caesium by unmodified materials

The desorption of caesium cations from the unmodified materials was investigated using the batch sorption methodology discussed in section 4.3. The results are shown in Table 4.5.

Table 4.5 Caesium cation desorption experiments on unmodified support material

Material	Clinoptilolite (NDA)		Clinoptilolite (Imerys)		ZSM-5		Vermiculite		Kaolinite	
Concentration	% desorbed	Error (+/-)	% desorbed	Error (+/-)	% desorbed	Error (+/-)	% desorbed	Error (+/-)	% desorbed	Error (+/-)
1×10^{-2}	0.0%	0.0%	0.0%	0.1%	0.0%	0.7%	11.5%	0.7%	0.0%	1.2%
1×10^{-4}	0.0%	0.1%	0.0%	0.0%	0.0%	0.0%	2.7%	0.5%	2.4%	0.8%
1×10^{-6}	0.0%	0.1%	0.0%	0.5%	0.0%	0.8%	5.1%	4.2%	4.1%	0.6%
1×10^{-8}	0.0%	0.1%	0.0%	0.1%	0.0%	0.1%	3.6%	0.5%	0.3%	0.1%
1×10^{-10}	0.0%	0.0%	0.0%	0.0%	0.0%	0.0%	4.4%	0.3%	0.6%	0.0%

The results from the desorption tests show that in the case of all zeolitic materials, the caesium cations are entirely retained. This is expected due to the metal cation being trapped in the zeolite cages. Both clays show a small degree of desorption, much more notably in the case of vermiculite. This can be attributed to vermiculite having a greater shrink/swell capacity, therefore allowing ions to travel in and out of the layers more easily.

4. 13.2 Desorption of caesium cations by APTES modified materials

The desorption of caesium to APTES modified materials was investigated using the batch sorption methodology discussed in section 4.3 the results are shown in Table 4.6.

Table 4.6 Desorption experiment on APTES modified support materials

Material	Clinoptilolite (NDA)		Clinoptilolite (Imerys)		ZSM-5		Vermiculite		Kaolinite	
Concentration	% desorbed	Error (+/-)	% desorbed	Error (+/-)	% desorbed	Error (+/-)	% desorbed	Error (+/-)	% desorbed	Error (+/-)
1×10^{-2}	0.0%	0.3%	1.1%	0.4%	10.3%	0.9%	1.5%	0.2%	8.7%	0.8%
1×10^{-4}	0.0%	0.1%	0.0%	0.1%	3.1%	0.8%	0.6%	0.1%	7.3%	1.1%
1×10^{-6}	0.0%	0.0%	0.0%	0.0%	4.1%	0.0%	4.0%	0.3%	3.5%	0.2%
1×10^{-8}	0.0%	0.2%	0.0%	0.0%	3.9%	0.3%	2.3%	0.1%	1.9%	0.4%
1×10^{-10}	0.0%	0.1%	0.0%	0.0%	4.0%	0.3%	2.3%	0.0%	3.0%	0.2%

The results from the desorption tests show that in the case of the clinoptilolite materials they retain the caesium as expected due to the metal cations being trapped in the zeolite cages as seen in the unmodified samples. In the case of ZSM-5 and kaolinite an increase in the extent of desorption is

observed, this can be attributed to some of the metal being associated with the ligand, due to HSAB predicting poor interaction between the hard ligand and soft metal cation. The vermiculite shows a decrease in desorption after modification, one possible explanation is the ligand preventing the vermiculite from shrinking to gain better coordination to the cation and so the metal cations become more difficult to remove from the layers.

4.13.3 Desorption of caesium cations by TMSPE modified materials

The desorption of caesium cations from the unmodified and modified materials was investigated using the batch sorption methodology discussed in section 4.3. The results are shown in Table 4.7.

Table 4.7 Caesium desorption experiments on TMSPE modified grafted materials

Material	Clinoptilolite (NDA)		Clinoptilolite (Imerys)		ZSM-5		Vermiculite		Kaolinite	
Concentration	% desorbed	Error (+/-)	% desorbed	Error (+/-)	% desorbed	Error (+/-)	% desorbed	Error (+/-)	% desorbed	Error (+/-)
1×10^{-2}	45.0%	0.2%	71.9%	0.4%	44.5%	0.1%	27.1%	0.2%	41.9%	0.3%
1×10^{-4}	5.7%	0.1%	9.2%	0.3%	28.3%	0.1%	1.5%	0.0%	35.5%	0.7%
1×10^{-6}	0.7%	0.2%	0.0%	2.2%	13.8%	0.1%	1.6%	0.4%	26.5%	0.1%
1×10^{-8}	0.0%	0.5%	0.0%	0.1%	9.7%	0.4%	1.0%	0.2%	16.7%	0.1%
1×10^{-10}	0.0%	0.1%	0.0%	0.0%	10.8%	0.7%	0.0%	0.0%	3.9%	0.0%

Desorption is seen in all materials with the most desorption seen at the highest caesium cation concentration, indicating that the ligand maybe preventing access to the pores and more metal ions are interacting with the ligand.

4.13.4 Desorption of caesium by TMSPETT modified materials

The desorption of caesium cations from TMSPETT modified materials was investigated using the batch sorption methodology discussed in section 4.3. The results are shown in Table 4.8.

Material	Clinoptilolite (NDA)		Clinoptilolite (Imerys)		ZSM-5		Vermiculite		Kaolinite	
Concentration	% desorbed	Error (+/-)	% desorbed	Error (+/-)	% desorbed	Error (+/-)	% desorbed	Error (+/-)	% desorbed	Error (+/-)
1×10^{-2}	37.6%	0.2%	55.6%	0.1%	10.2%	0.1%	6.5%	0.0%	10.3%	0.2%
1×10^{-4}	0.4%	0.1%	4.8%	0.1%	3.1%	0.0%	0.5%	0.1%	1.6%	0.1%
1×10^{-6}	3.9%	0.3%	2.0%	0.2%	1.3%	0.0%	0.6%	0.0%	0.3%	0.0%
1×10^{-8}	0.8%	0.1%	10.0%	0.1%	1.2%	0.0%	0.3%	0.0%	0.4%	0.0%
1×10^{-10}	9.6%	0.0%	11.0%	0.3%	1.3%	0.1%	0.6%	0.0%	0.5%	0.0%

As with the previous ligand desorption experiments, desorption is seen in all materials with the most desorption seen at the highest concentration, indicating that the ligand maybe preventing access to the pores and more metal ions are interacting with the ligand.

4.14 Kinetic experiments on uptake of caesium

4.14.1 Rate of uptake of caesium by unmodified materials

The rate of uptake of caesium to the unmodified and modified materials was investigated using the kinetic batch sorption methodology discussed in section 4.4. The results are shown in Figure 4.11 and tabulated in Table 4.9.

Figure 4.11 Kinetic experiments to examine caesium uptake by unmodified materials.

Material	Clinoptilolite (NDA)		Clinoptilolite (Imerys)		ZSM-5		Vermiculite		Kaolinite	
Time (days)	% removed	Error (+/-)	% removed	Error (+/-)	% removed	Error (+/-)	% removed	Error (+/-)	% removed	Error (+/-)
0.04	12.6%	3.5%	94.5%	0.8%	15.1%	4.3%	32.5%	1.5%	36.3%	0.7%
1	42.2%	4.7%	94.0%	1.1%	17.6%	9.7%	52.9%	3.0%	16.1%	5.5%
7	92.0%	1.2%	94.9%	0.8%	15.3%	5.3%	89.3%	0.2%	32.5%	11.2%
14	99.4%	0.1%	98.3%	0.2%	26.1%	5.1%	96.5%	0.7%	29.3%	2.8%
28	100.0%	0.0%	100.0%	0.0%	72.1%	4.3%	98.5%	0.1%	30.8%	5.0%

The removal of caesium by the clinoptilolite (Imerys) sample is quicker than the clinoptilolite (NDA) sample. This is due to the smaller particle size of the clinoptilolite (Imerys) sample creating a larger surface area allowing more of the caesium cations to be in contact with the sample. Both clinoptilolite samples reach complete removal after 28 days with the majority of the caesium cations being removed within 7 days. Vermiculite shows a similar trend to the clinoptilolite samples suggesting that the process of removing the caesium ions is ion exchange. ZSM-5 does not show much removal of caesium until 28 days which would suggest that ion exchange is not the main process of removal but physisorption occurs at the surface after prolonged contact. Kaolinite shows no ion exchange but physisorption occurs on the surface even after one hour of contact time.

4.14.2 Rate of uptake of caesium by APTES modified materials

The rate of uptake of caesium to the APTES modified materials was investigated using the kinetic batch sorption methodology discussed in section 4.4. The results are shown in Figure 4.12 and tabulated in Table 4.10.

Figure 4.12 Kinetic experiment for the removal of caesium using APTES modified materials.

Table 4.10: Kinetic experiments for the removal of caesium using APTES modified materials

Material	Clinoptilolite (NDA)		Clinoptilolite (Imerys)		ZSM-5		Vermiculite		Kaolinite	
Time (days)	% removed	Error (+/-)	% removed	Error (+/-)	% removed	Error (+/-)	% removed	Error (+/-)	% removed	Error (+/-)
0.04	19.8%	9.2%	38.3%	2.7%	25.1%	1.1%	44.2%	0.8%	20.3%	4.3%
1	4.8%	4.2%	25.7%	11.0%	9.0%	6.0%	56.5%	12.3%	0.0%	3.4%
7	27.9%	6.7%	46.3%	6.8%	25.9%	7.9%	88.1%	1.6%	10.5%	1.9%
14	40.0%	12.8%	62.2%	3.7%	13.3%	2.0%	90.7%	3.9%	2.6%	9.3%
28	79.5%	0.7%	84.4%	3.6%	14.7%	4.0%	95.6%	0.3%	9.5%	3.1%

The removal of caesium in all cases of the APTES modified zeolites is slower. This is attributed to the ligand restricting access to the channels of the zeolites. The removal of caesium is quicker in the case of the vermiculite due to the ligand expanding layers increasing the interlayer space removing the extrusion step therefore increasing the speed of ion removal. The removal of caesium by kaolinite is reduced as discussed previously, probably due the ligand preventing access to the surface of the solid.

4.14.3 Rate of uptake of caesium by TMSPE modified materials

The rate of uptake of caesium to the TMSPE modified materials was investigated using the kinetic batch sorption methodology discussed in section 4.4. The results are shown in Figure 4.13 and tabulated in Table 4.10.
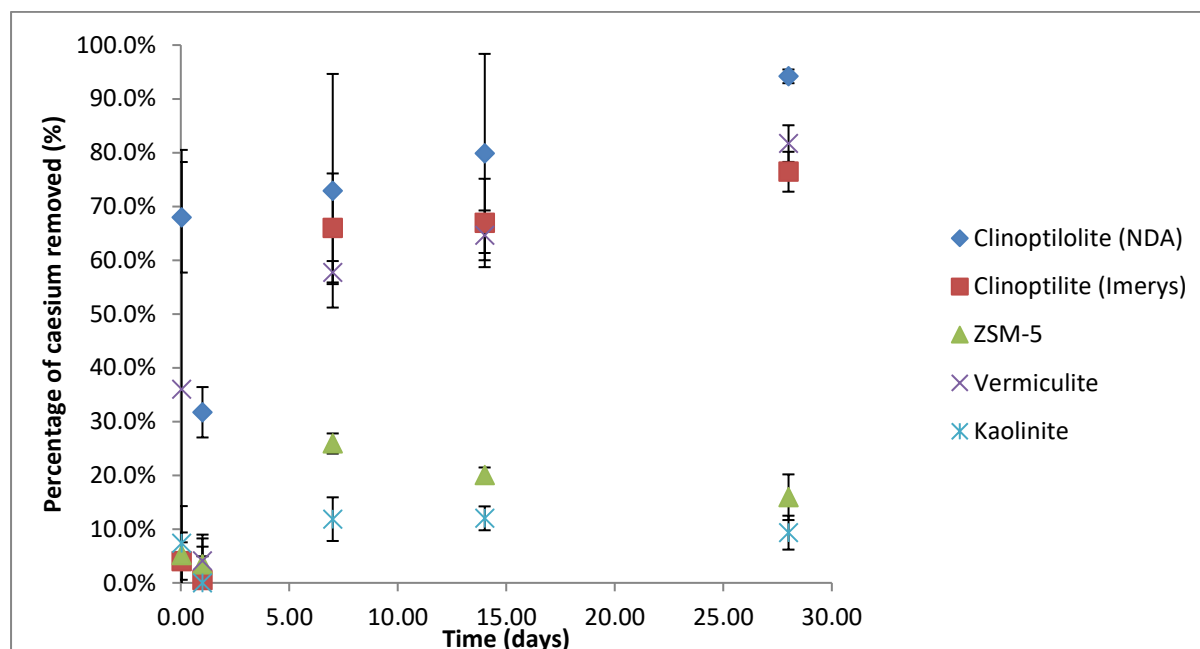
Figure 4.13 Kinetic experiment for the removal of caesium using TMSPE modified materials.

The removal of caesium in all cases of the TMSPE modified zeolites is slower than for the unmodified species as discussed before this is attributed to the ligand restricting access to the channels of the zeolites. The removal of caesium is quicker in the case of the vermiculite due to the ligand expanding layers increasing the interlayer space removing the extrusion step therefore increasing the speed of ion removal. The removal of caesium by kaoilinte is reduced as discussed previously due the ligand preventing access to the surface of the solid.

Material	Clinoptilolite (NDA)		Clinoptilolite (Imerys)		ZSM-5		Vermiculite		Kaolinite	
Time (days)	% removed	Error (+/-)	% removed	Error (+/-)	% removed	Error (+/-)	% removed	Error (+/-)	% removed	Error (+/-)
0.04	68.0%	10.3%	4.1%	3.5%	5.2%	9.1%	36.0%	14.5%	7.4%	2.0%
1	31.7%	4.7%	0.5%	6.2%	3.4%	1.5%	4.1%	4.2%	0.0%	9.0%
7	72.9%	21.7%	66.0%	10.1%	25.9%	1.9%	57.7%	2.1%	11.8%	4.1%
14	79.9%	18.5%	66.9%	8.2%	20.0%	1.4%	64.6%	4.6%	12.0%	2.2%
28	94.2%	1.3%	76.4%	3.7%	15.9%	4.2%	81.7%	3.4%	9.3%	3.2%

4.14.4 Rate of uptake of caesium by TMSPETT modified materials

The rate of uptake of caesium to the TMSPETT modified materials was investigated using the kinetic batch sorption methodology discussed in section 4.4 the results are shown in figure 4.14 and tabulated in table 4.11.
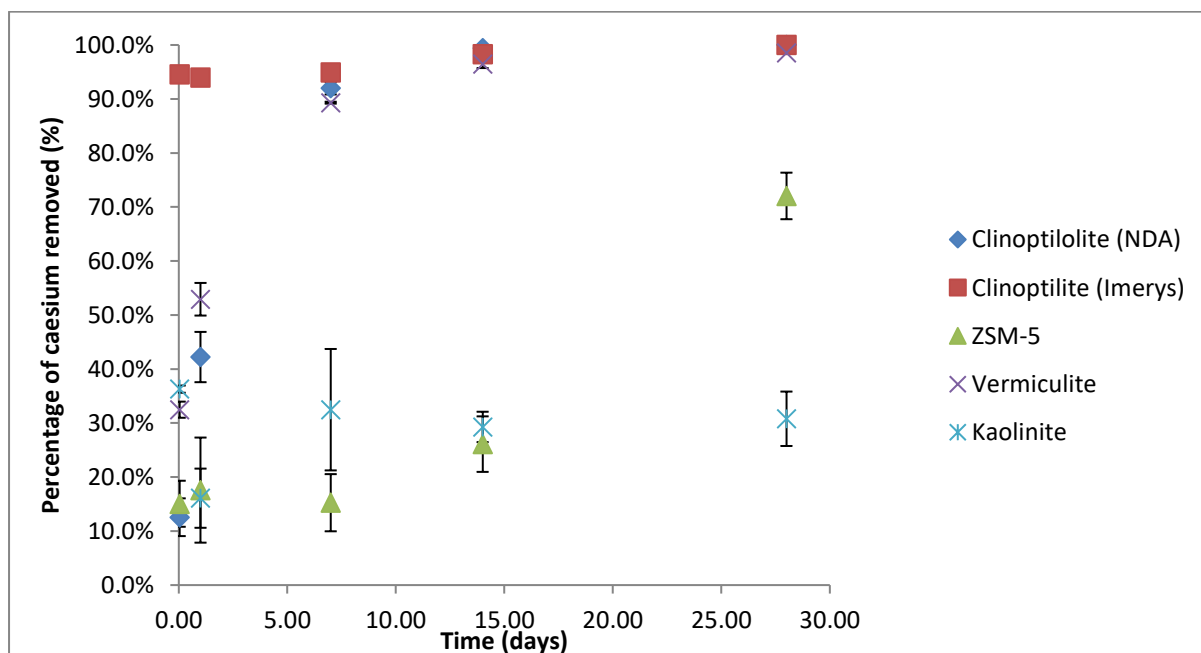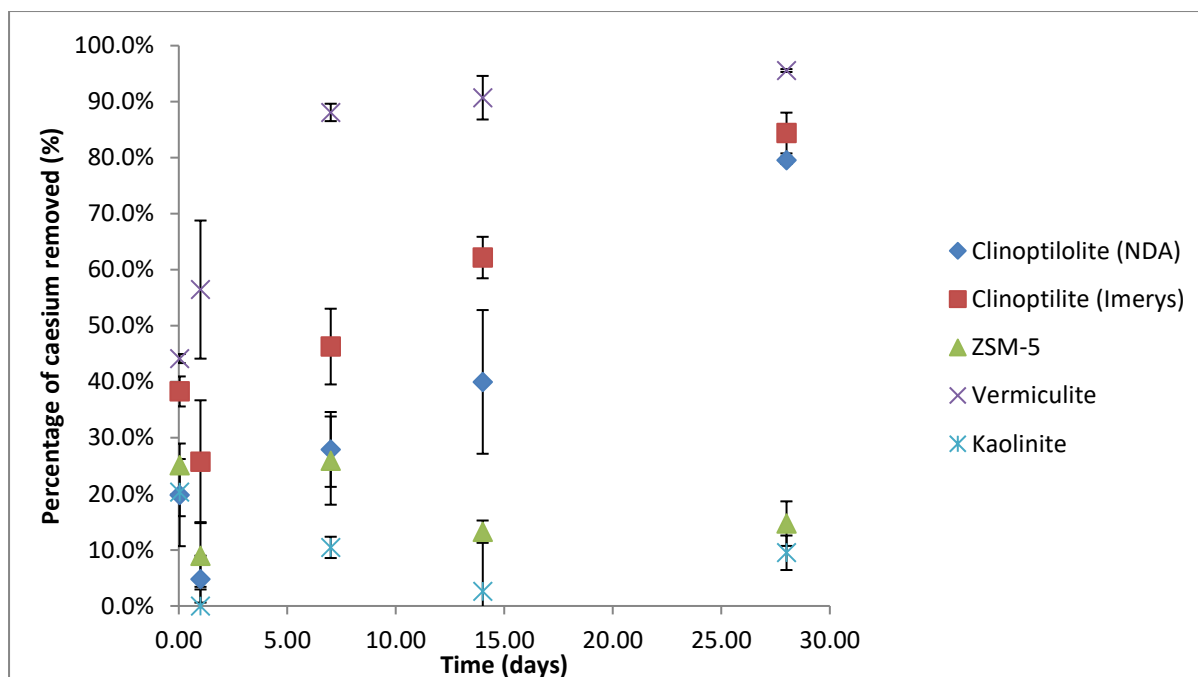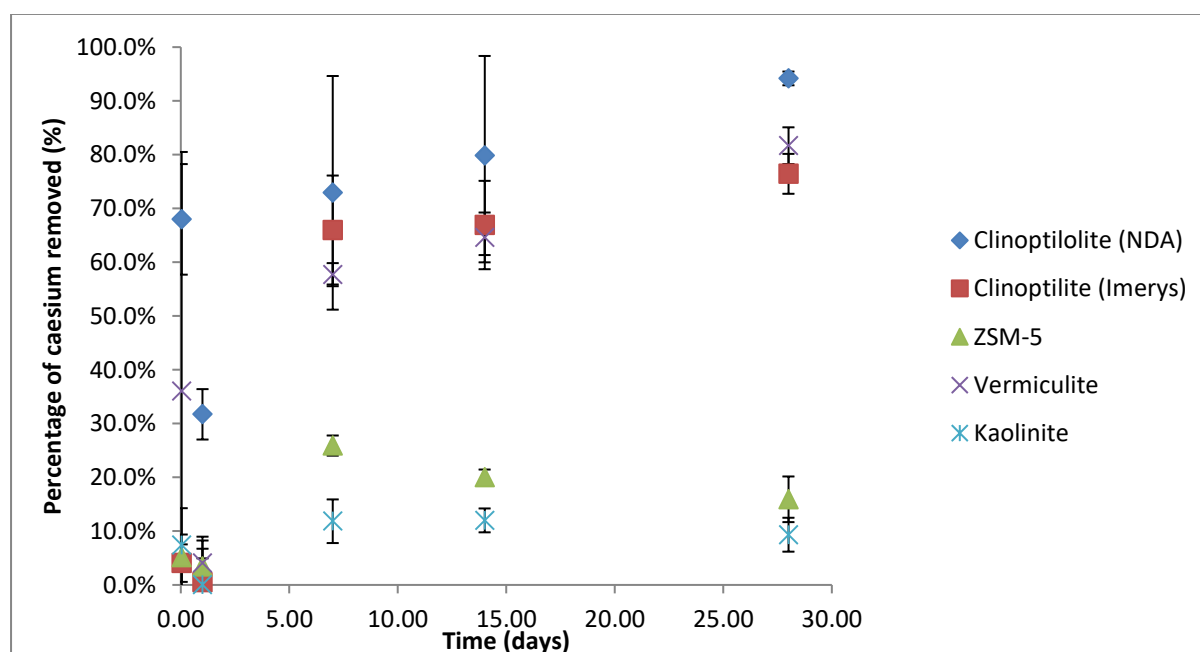

Figure 4.14: Kinetic Experiments for the removal of caesium using TMSPETT modified clinoptilolite.

Material	Clinoptilolite (NDA)		Clinoptilolite (Imerys)		ZSM-5		Vermiculite		Kaolinite	
Time (days)	% removed	Error (+/-)	% removed	Error (+/-)	% removed	Error (+/-)	% removed	Error (+/-)	% removed	Error (+/-)
0.04	5.0%	7.2%	1.9%	7.4%	0.0%	2.6%	11.0%	6.0%	4.3%	9.6%
1	59.1%	7.0%	48.8%	7.9%	13.4%	5.2%	53.0%	3.6%	0.0%	8.0%
7	70.1%	2.6%	63.3%	1.4%	21.0%	4.1%	64.5%	2.0%	11.0%	0.4%
14	78.2%	1.9%	60.1%	2.0%	8.7%	5.7%	71.2%	1.7%	9.0%	2.1%
28	85.8%	1.6%	63.6%	3.4%	8.4%	3.9%	78.2%	1.7%	7.6%	1.6%

The same trend in the rate of removal is also seen in the TMSPETT modified materials as in the APTES and TMSPE modified materials.

4. 15 Comparison of clinoptilolite (NDA) materials

The rate of uptake of caesium to the unmodified and modified mineral clinoptilolite was investigated using the kinetic batch sorption methodology discussed in section 4.4. The results are shown in Figure 4.15.

Figure 4.15 Comparison of uptake of caesium by clinoptilolite NDA before and after ligand grafting

The removal of caesium is still observed in the modified materials; however the uptake is slower in the grafted materials. Leading to the conclusion that the ligands are affecting the accessibility of the pores. An alternative hypothesis maybe that the caesium is more easily removed from the coordinated ligand compared with the zeolite pores where the ions are in cation sites which are highly selective for caesium.

4.16 Comparison of clinoptilolite (Imerys) materials

A comparison of the uptake of caesium to the modified and unmodified materials using the kinetic batch sorption methodology is shown in Figure 4.16
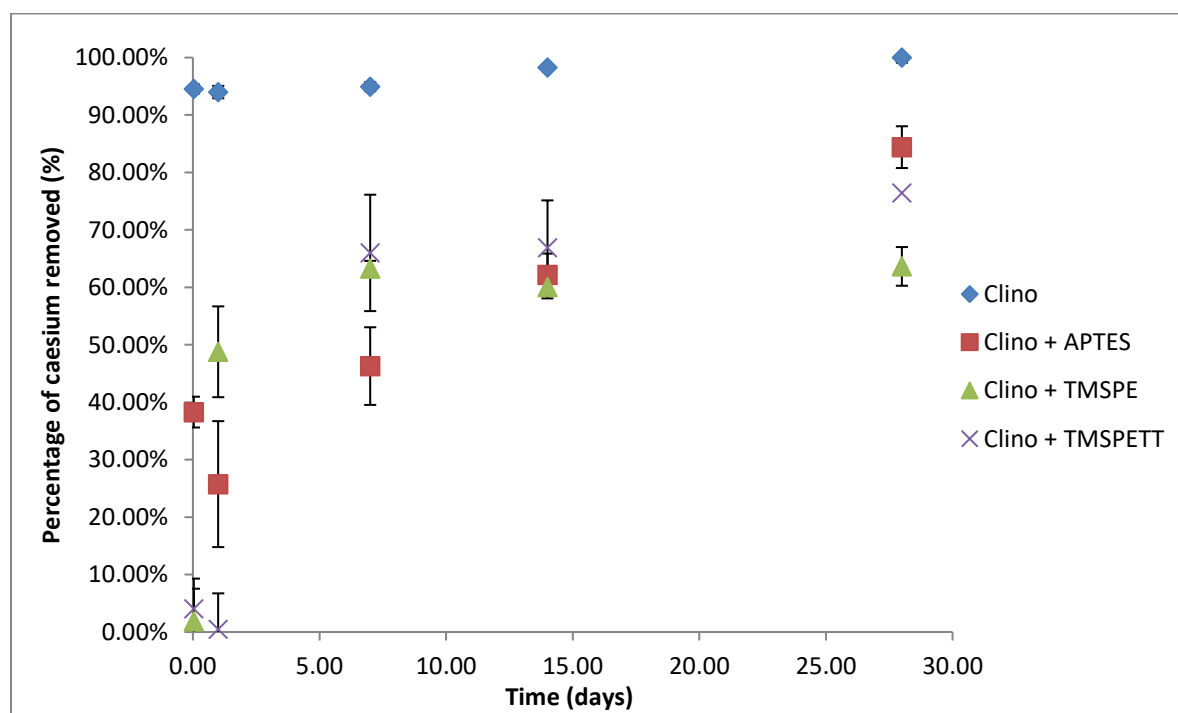
Figure 4.16 Comparison of uptake of caesium by clinoptilolite NDA before and after ligand grafting

In a similar way to the NDA clinoptilolite, the caesium uptake is slowed in the Imerys clinoptilolite by the grafted material. This could be due to the ligand being less able to retain the ligand and releasing it back into solution or the ligands blocking the zeolite pores making it more difficult for the caesium cation to move to the ion exchange sites within the pores. This is again to do with the lack of selectivity of the ligand for caesium compared to the zeolite material itself.

4.17 Comparison of ZSM-5 materials

The rate of uptake of caesium to the unmodified and modified material ZSM-5 was investigated using the kinetic batch sorption methodology discussed in section 4.4. The results are shown in Figure 4.17.
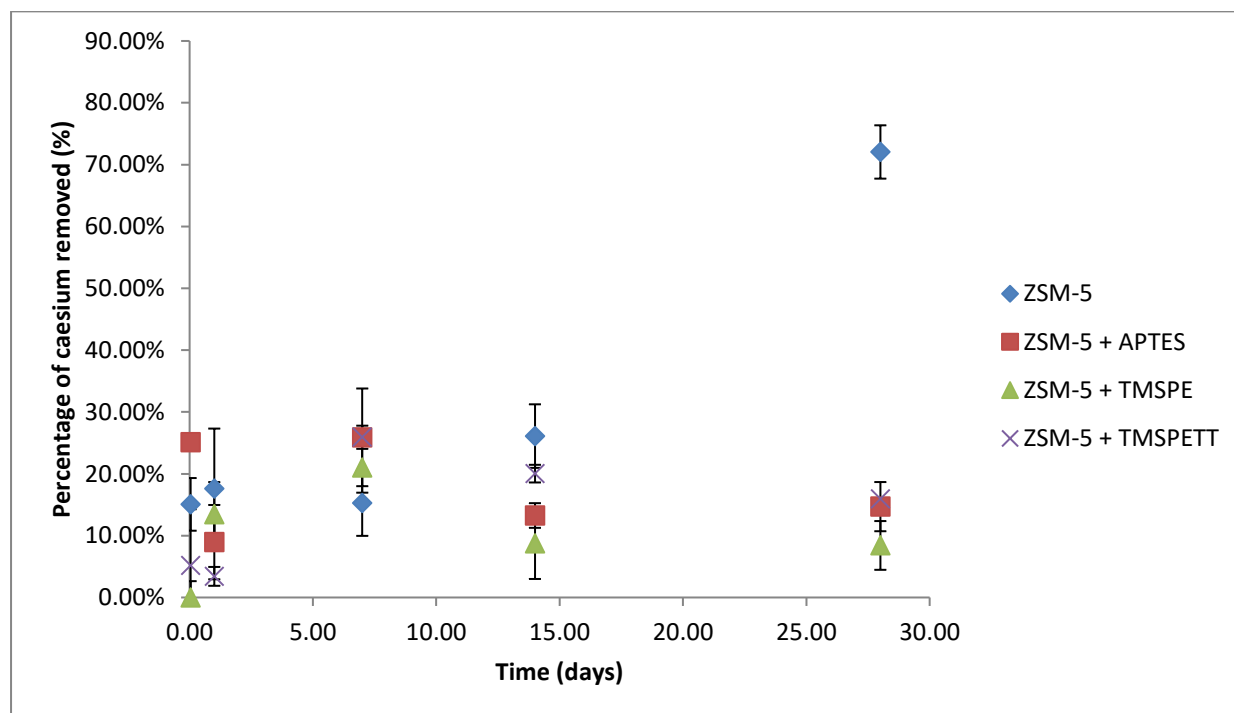

Figure 4.17 Comparison of uptake of caesium by ZSM-5 before and after ligand grafting

The removal of caesium is still observed in the modified materials, with little change in the rate of uptake of the un-grafted and grafted materials. The presence of the ligand appears to reduce the capability of the substrate for physisorption and the caesium uptake is poor compared to clinoptilolite. ZSM-5 is not selective for caesium cations and has few exchangeable cations.

4.18 Comparison of vermiculite materials

The rate of uptake of caesium to the unmodified and modified mineral vermiculite was investigated using the kinetic batch sorption methodology discussed in section 4.4. The results are shown in Figure 4.18.
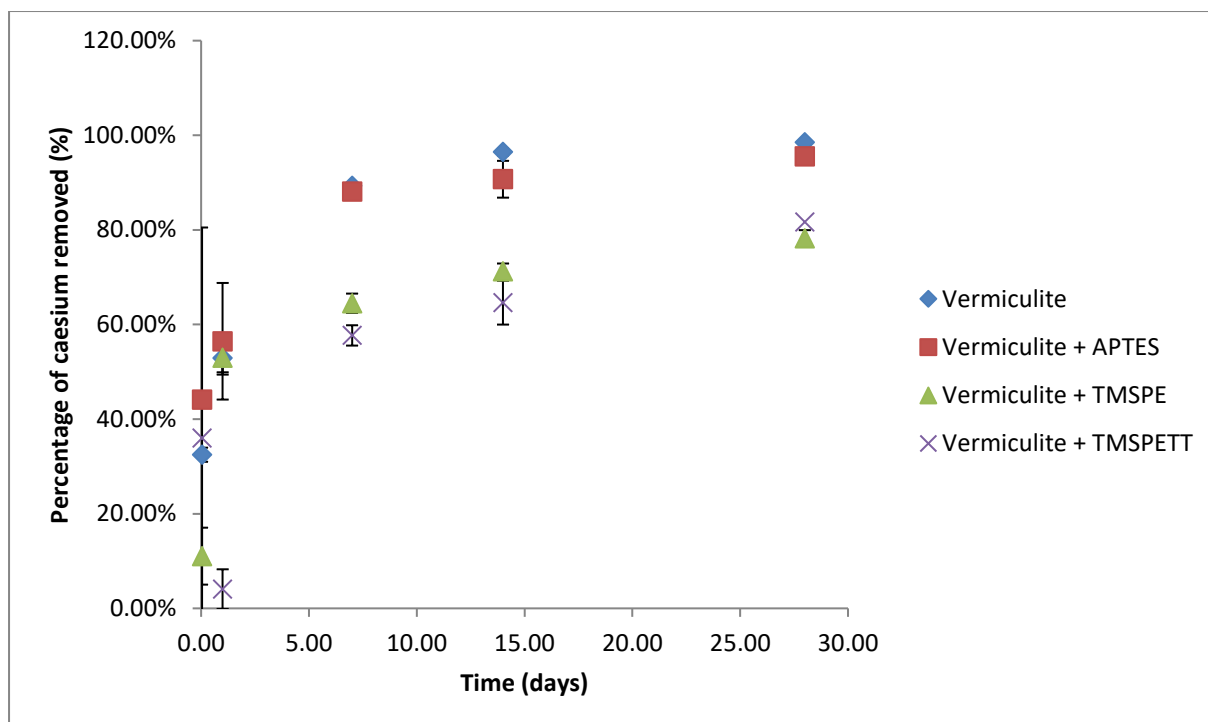
Figure 4.18 Comparison of uptake of caesium by vermiculite before and after ligand grafting

The removal of caesium is still observed in the modified materials, with little difference observed between the unmodified and materials modified with APTES. TMSPE and TMSPETT cause a fall in the uptake of caesium cations on vermiculite compared to the ungrafted species.

4.19 Comparison of kaolinite materials

The rate of uptake of caesium to the unmodified and modified mineral kaolinite was investigated using the kinetic batch sorption methodology discussed in section 4.4. The results are shown in Figure 4.19.
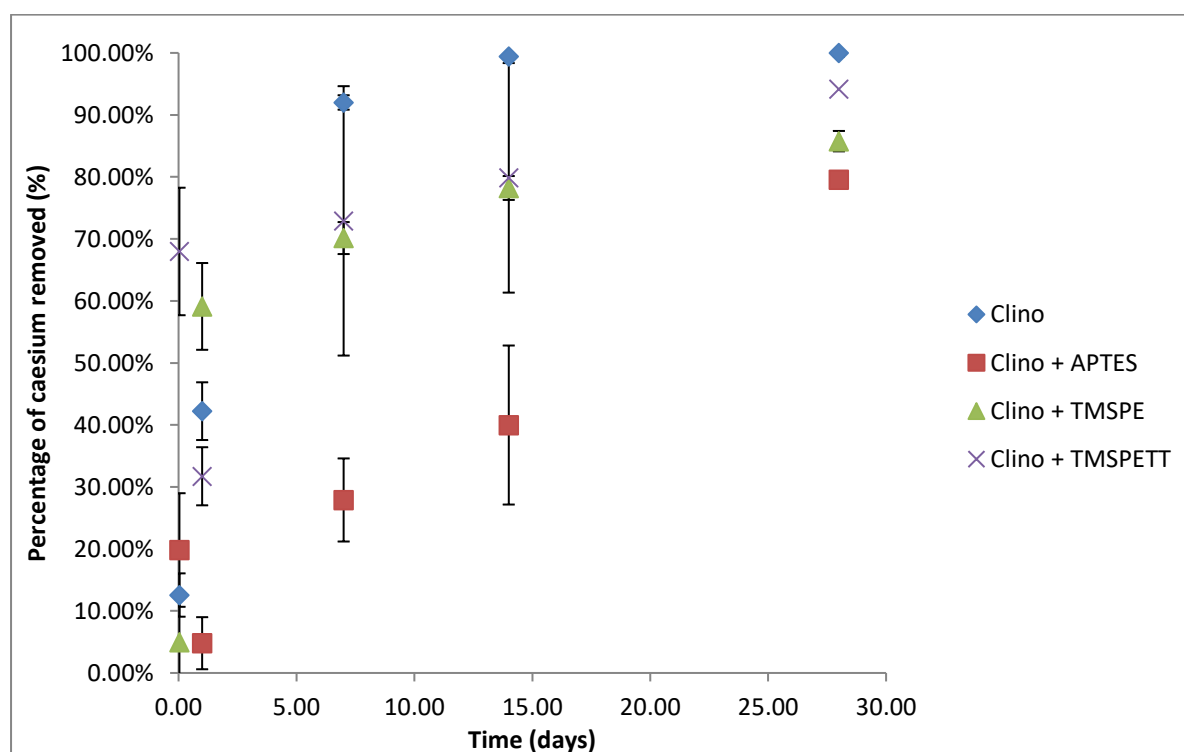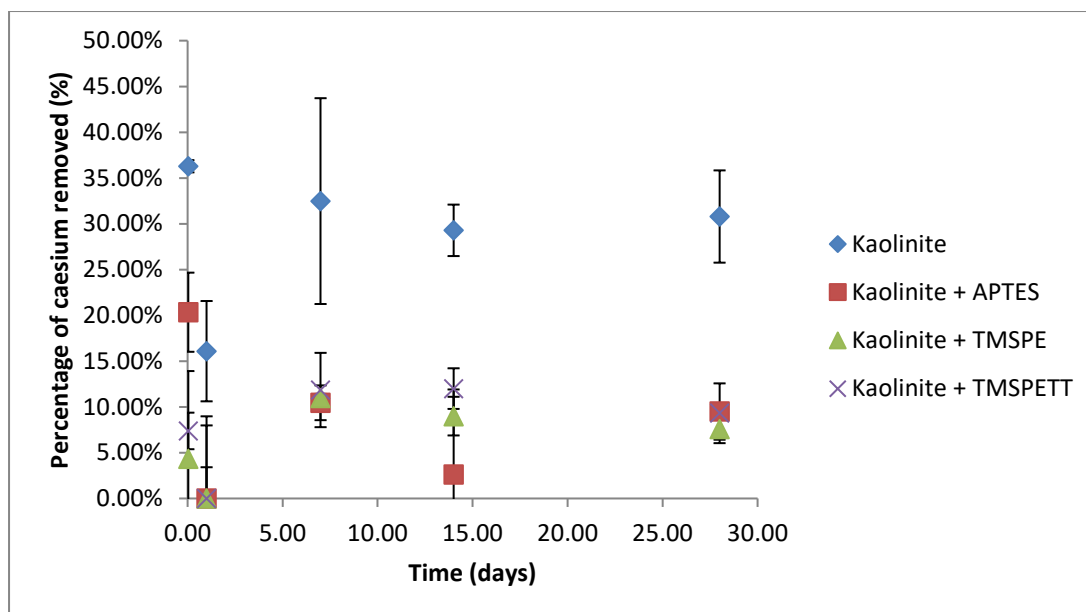
Figure 4.19 Comparison of uptake of caesium by kaolinite before and after ligand grafting

The removal of caesium is still observed in the modified materials. The amount of uptake is less in the modified materials but the rate of uptake to capacity occurs at the same speed. This suggests that the mechanism of uptake remains the same but the modification of the material has decreased the capacity by reducing the surface available for physisorption. Kaolinite remains the least effective of all materials studied at removing caesium cations from solution.

4.20 Caesium sorption summary

The effect of caesium uptake by the materials Clinoptilolite (NDA), clinoptilolite (Imerys), ZSM-5, vermiculite and kaolinite before and after modification with the organic ligands APTES, TMSPE and TMSPETT were investigated. Experiments were conducted to study the amount and rate of caesium uptake by the materials.

The amount of caesium uptake remained consistent for the modified and unmodified materials except for vermiculite which significant increase in uptake after modification. The rate uptake shows a decrease for the modified materials which can be contributed to the ligand restricting access to the exchange sites, this is most noticeable for the larger ligands.

4.21 Strontium experimental results

4.21. 1 Batch sorption experimental results

4.21.1.1 Uptake of strontium by unmodified materials

The uptake of strontium to the minerals clinoptilolite, ZSM-5, vermiculite and kaolinite was investigated using the batch sorption methodology discussed in section 4.2. The results are shown in Figure 4.20 and Table 4.12.

Figure 4.20: Removal of strontium cations by unmodified substrates as a function of concentration

The results show that all materials successfully remove strontium to varying degrees of effectiveness. The greatest extent of removal can be seen by the clinoptilolite samples followed by the vermiculite, kaolinite and finally ZSM-5. This can be attributed to the clinoptilolite cages being correctly sized for the strontium cation. Similar to the caesium experiments, the ZSM-5 shows poor take up of aqueous cation. The highly silaceous framework has very low numbers of exchangeable cations and since strontium is a divalent cation, two sodium ions need to be removed for every one strontium cation replacing them. Therefore in comparison to caesium, it is expected that strontium will exchange to a lesser level in ZSM-5

Vermiculite and kaolinite are both clay minerals and so the method of sequestration is slightly different to that of the zeolites. In clay minerals, the ions are sequestered between layers not cages as the zeolites. The clays show different efficacies for caesium removal, where vermiculite is more efficient than kaolinite. Vermiculite has exchangeable cations within the layers and can extrude to

allow different size cations to enter the layers, whereas kaolinite has no exchangeable cations and removes the ions via surface physisorption and reaches capacity at low concentrations.

Table 4.12: Removal of strontium cations by unmodified materials as a function of concentration.

Material	Clinoptilolite (NDA)		Clinoptilolite (Imerys)		ZSM-5		Vermiculite		Kaolinite	
Concentration	% removed	Error (+/-)	% removed	Error (+/-)	% removed	Error (+/-)	% removed	Error (+/-)	% removed	Error (+/-)
1×10^{-2}	60.3%	1.4%	52.8%	0.7%	45.9%	3.0%	0.0%	2.0%	0.0%	4.8%
1×10^{-4}	92.3%	2.7%	100.0%	0.4%	45.4%	1.4%	89.5%	7.8%	0.0%	5.7%
1×10^{-6}	94.1%	1.3%	100.0%	0.0%	42.0%	2.2%	85.0%	0.4%	95.9%	0.5%
1×10^{-8}	98.4%	1.0%	100.0%	0.0%	73.1%	0.5%	87.3%	1.0%	96.1%	0.3%
1×10^{-10}	98.6%	0.6%	100.0%	0.0%	42.6%	1.3%	85.8%	0.7%	95.9%	0.4%

4. 21.2 Uptake of strontium by APTES modified materials

The uptake of strontium to the APTES modified minerals clinoptilolite, ZSM-5, vermiculite and kaolinite was investigated using the batch sorption methodology discussed in section 4.2. The results are shown in Figure 4.21 and Table 4.13.

The uptake of strontium by the APTES modified clinoptilolite samples shows that the cages of the zeolite are still accessible by the cation and ion exchange still occurs. Overall less strontium is removed by the modified clinoptilolite, ZSM-5 and vermiculite samples which can be attributed to the ligand blocking some of the exchange sites. The increased removal seen in kaolinite could be due to the ligand removing some of the cations.

Table 4.13 Removal of strontium cations as a function of cation concentration for APTES modified substrates

Material	Clinoptilolite (NDA)		Clinoptilolite (Imerys)		ZSM-5		Vermiculite		Kaolinite	
Concentration	% removed	Error (+/-)	% removed	Error (+/-)	% removed	Error (+/-)	% removed	Error (+/-)	% removed	Error (+/-)
1×10^{-2}	60.3%	1.4%	52.8%	0.7%	45.9%	3.0%	0.0%	2.0%	0.0%	4.8%
1×10^{-4}	92.3%	2.7%	100.0%	0.4%	45.4%	1.4%	89.5%	7.8%	0.0%	5.7%
1×10^{-6}	94.1%	1.3%	100.0%	0.0%	42.0%	2.2%	85.0%	0.4%	95.9%	0.5%
1×10^{-8}	98.4%	1.0%	100.0%	0.0%	73.1%	0.5%	87.3%	1.0%	96.1%	0.3%
1×10^{-10}	98.6%	0.6%	100.0%	0.0%	42.6%	1.3%	85.8%	0.7%	95.9%	0.4%

4.21.3 Uptake of strontium by TMSPE modified materials

The uptake of strontium to the TMSPE modified minerals clinoptilolite, ZSM-5, vermiculite and kaolinite was investigated using the batch sorption methodology discussed in section 4.1. The results are shown in Figure 4.22 and Table 4.14.
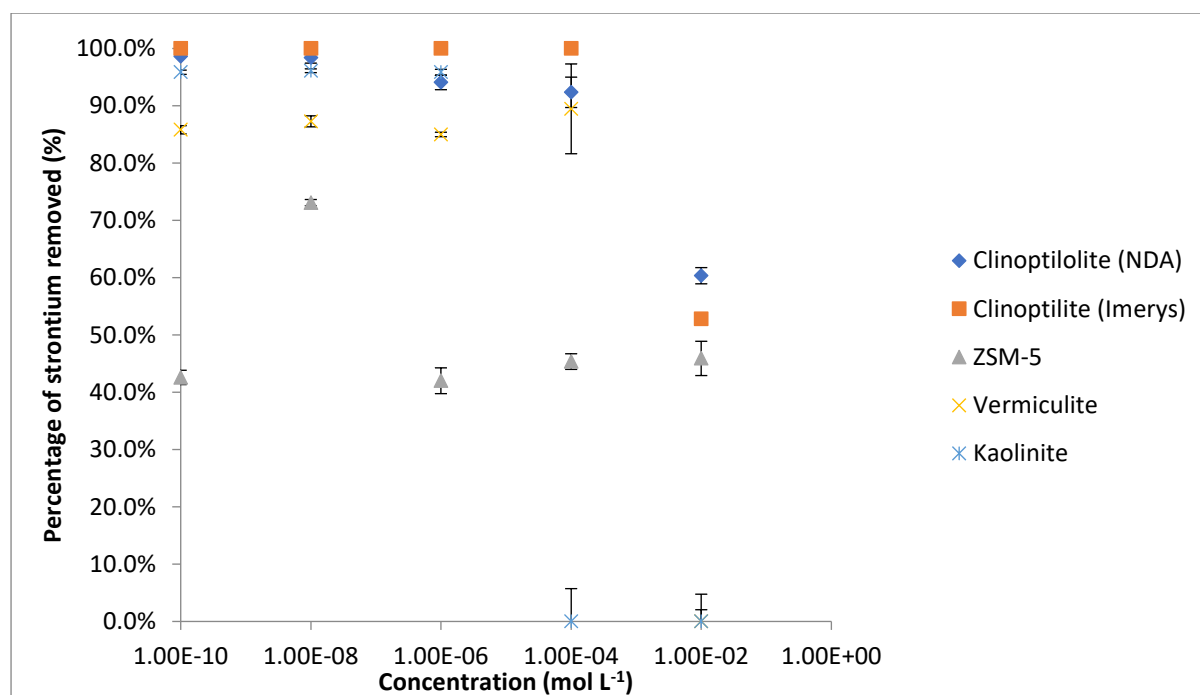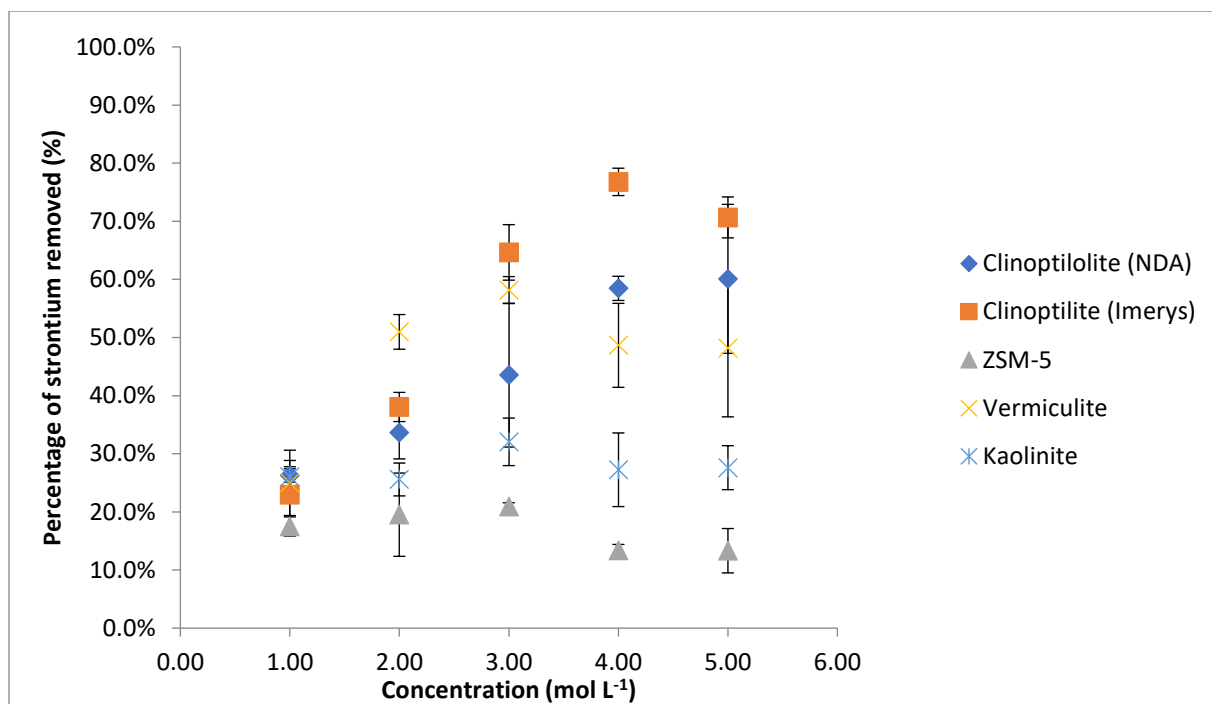
Figure 4.22: Strontium removal as a function of strontium cation concentration for TMSPE modified materials.

As discussed previously for caesium, the uptake of strontium by the TMSPE modified samples show that the exchangeable ions are still accessible by the ions and ion exchange still occurs. Overall less strontium is removed by the modified clinoptilolite, ZSM-5 and vermiculite samples, mirroring the results previously observed for APTES. In comparison to APTES, TMSPE seems to have a greater effect on reducing the absolute uptake of strontium by the clinoptilolite. Since two exchangeable monovalent cations must be removed for every divalent strontium cation inserted, the likelihood of the ligand affecting the exchange process is increased.

Table 4.14: Removal of strontium cations by TMSPE grafted materials as a function of strontium concentration

Material	Clinoptilolite (NDA)		Clinoptilolite (Imerys)		ZSM-5		Vermiculite		Kaolinite	
Concentration	% removed	Error (+/-)	% removed	Error (+/-)	% removed	Error (+/-)	% removed	Error (+/-)	% removed	Error (+/-)
1×10^{-2}	36.3%	1.5%	26.4%	0.9%	19.9%	2.1%	36.9%	3.2%	26.2%	4.4%
1×10^{-4}	55.0%	8.0%	52.5%	5.6%	20.6%	2.9%	61.9%	1.2%	28.3%	2.7%
1×10^{-6}	70.9%	10.2%	91.1%	2.2%	23.1%	1.0%	66.7%	0.4%	33.8%	4.6%
1×10^{-8}	87.2%	10.3%	94.8%	1.4%	23.8%	4.7%	72.2%	7.6%	36.8%	4.9%
1×10^{-10}	82.3%	2.2%	95.5%	1.1%	28.1%	4.5%	66.0%	3.8%	49.9%	3.0%

4.21.4 Uptake of strontium by TMSPETT modified materials

The uptake of strontium to the TMSPETT modified minerals clinoptilolite, ZSM-5, vermiculite and kaolinite was investigated using the batch sorption methodology discussed in section 4.2. The results are shown in Figure 4.23 and Table 4.15.
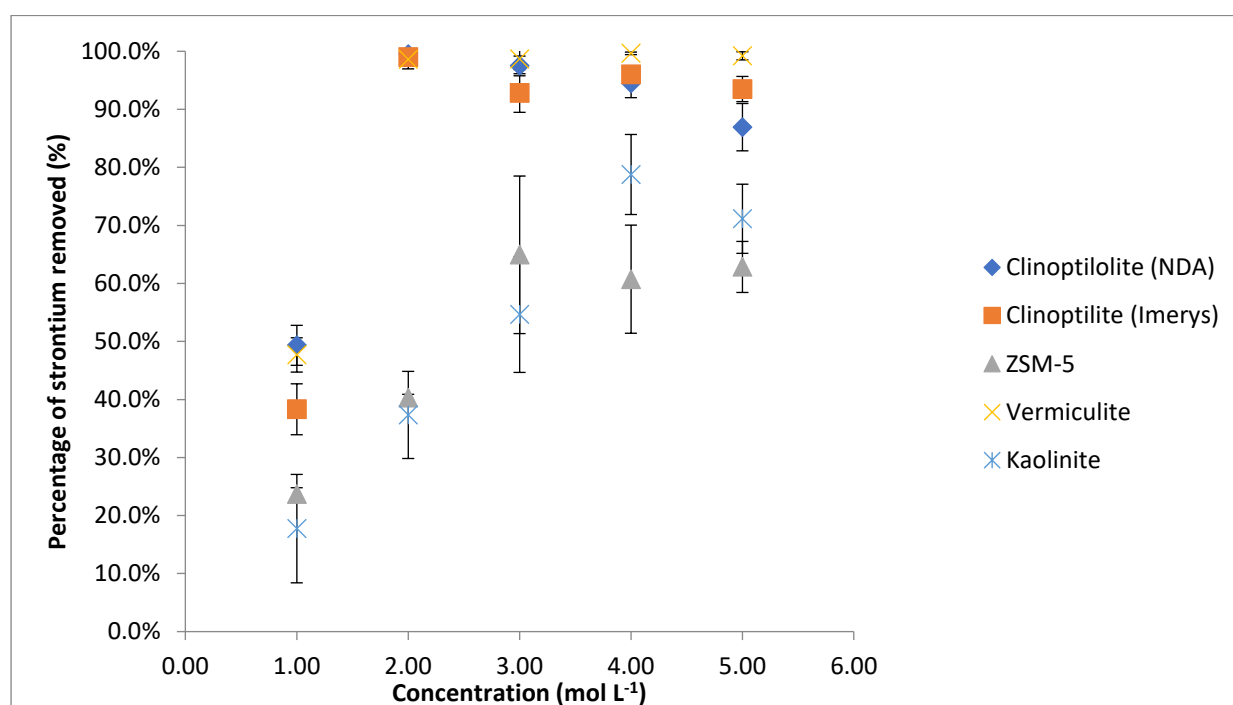
Figure 4.23: Strontium caption uptake by TMSPETT modified materials as a function of concentration

The uptake of strontium by the TMSPETT modified samples show exchangeable ions are still accessible and ion exchange still occurs as observed with the other ligands. Overall more strontium is removed by the TMSPETT modified samples when compared to the APTES and TMSPE ligands which can be attributed more donor sites on the TMPSETT ligand.

Table 4.15: Strontium caption uptake by TMSPETT modified materials as a function of concentration

Concentration	Clinoptilolite (NDA)		Clinoptilolite (Imerys)		ZSM-5		Vermiculite		Kaolinite	
	% removed	Error (+/-)	% removed	Error (+/-)	% removed	Error (+/-)	% removed	Error (+/-)	% removed	Error (+/-)
1×10^{-2}	49.3%	3.4%	38.3%	4.4%	23.7%	1.1%	47.7%	3.0%	17.7%	9.3%
1×10^{-4}	99.5%	0.2%	99.0%	0.2%	40.3%	0.6%	98.6%	1.6%	37.3%	7.5%
1×10^{-6}	97.5%	1.7%	92.8%	3.3%	64.9%	13.6%	98.7%	1.8%	54.6%	10.0%
1×10^{-8}	94.4%	2.4%	96.0%	0.5%	60.7%	9.3%	99.6%	0.2%	78.8%	6.9%
1×10^{-10}	86.9%	4.1%	93.5%	2.2%	62.8%	4.4%	99.2%	0.7%	71.1%	6.0%

4.22 Comparison of clinoptilolite (NDA) materials before and after ligand modification

The rate of uptake of strontium to the unmodified and modified mineral clinoptilolite was investigated using the batch sorption methodology discussed in section 4.2. The results are shown in Figure 4.24.
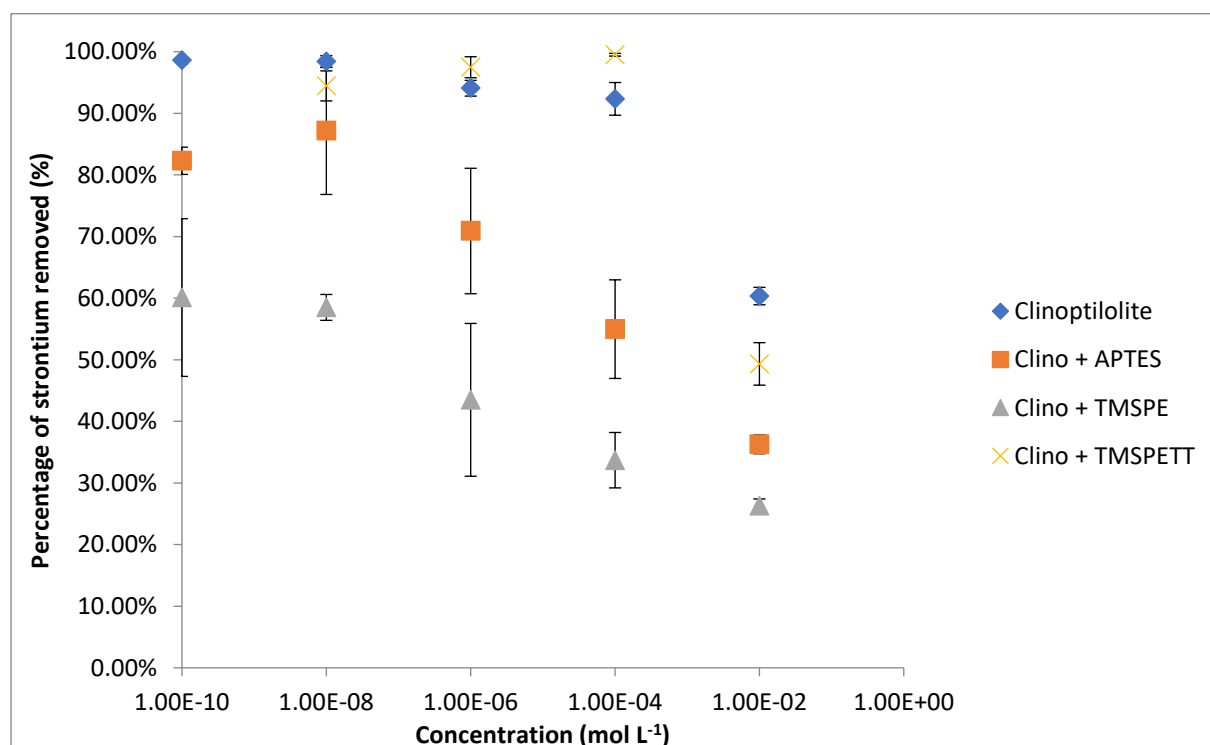
Figure 4.24: Comparison of strontium cation removal capability of clinoptilolite NDA materials before and after grafting with ligands.

Strontium cations are still removed by the grafted clinoptilolite, but the capacity is reduced. This suggests that the graft is effecting the movement of the ions into and out of the zeolite.

4.23 Comparison of clinoptilolite (Imerys) materials

The rate of uptake of strontium to the unmodified and modified mineral clinoptilolite was investigated using the batch sorption methodology discussed in section 4.2. The results are shown in Figure 4.25.
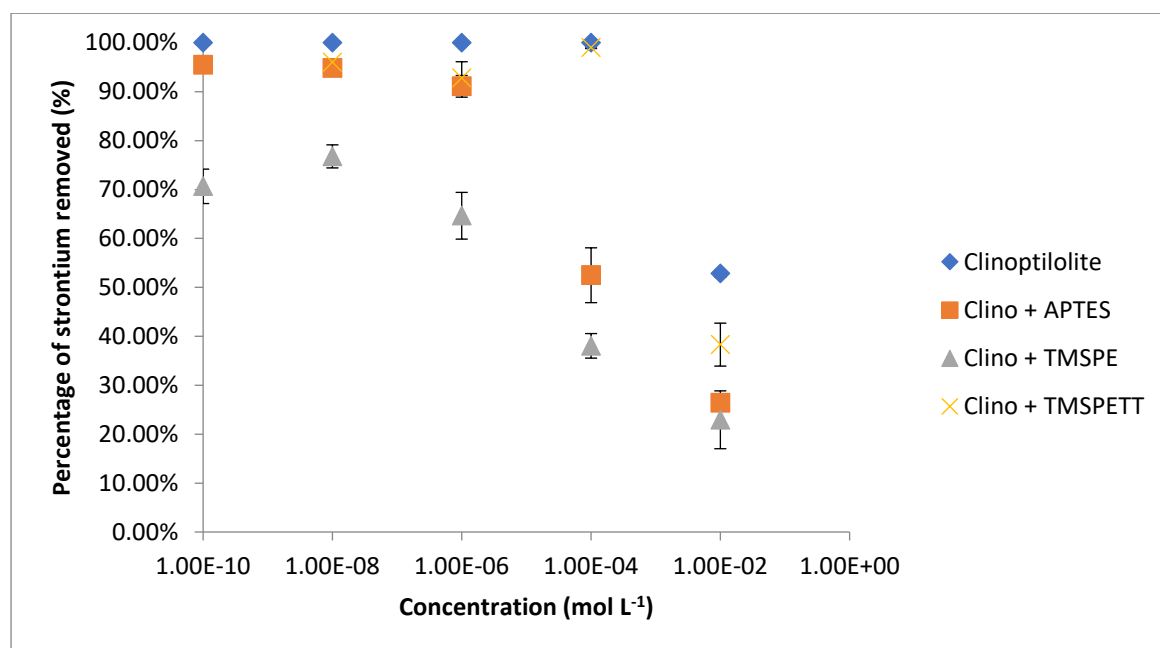
**Figure 4.25: Comparison of strontium cation removal capability of clinoptilolite Imerys materials before and after grafting with ligands.**

The removal of strontium is still observed in the modified materials; however the uptake is lower in the grafted materials. Leading to the conclusion that the ligands are affecting the accessibility of the exchangeable ions in the pores.   In comparison to clinoptilolite NDA, the clinoptilolite Imerys is less affected by the graft.

4.24 Comparison of ZSM-5 materials

The rate of uptake of strontium to the unmodified and modified material ZSM-5 was investigated using the batch sorption methodology discussed in section 4.2. The results are shown in Figure 4.26.
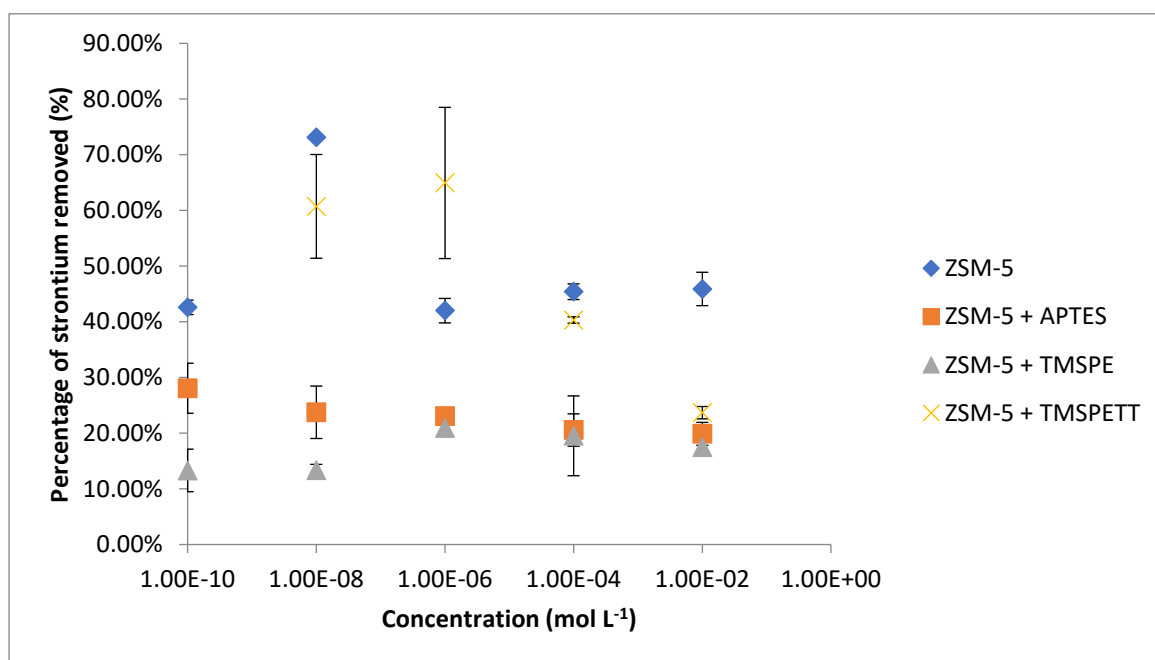
Figure 4.26: Comparison of strontium cation removal capability of ZSM-5 materials before and after grafting with ligands.

The removal of strontium is still observed in the modified materials, with little change in the amount of uptake of the un-grafted, APTES grafted and TMSPE grafted materials. The TMSPETT grafted   ZSM-5 does show an improvement in the removal of strontium at lower concentrations but with a significant estimated standard deviation due to the low concentration.

4.25 Comparison of vermiculite materials

The rate of uptake of strontium to the unmodified and modified mineral vermiculite was investigated using the kinetic batch sorption methodology discussed in section 4.2. The results are shown in Figure 4.27.
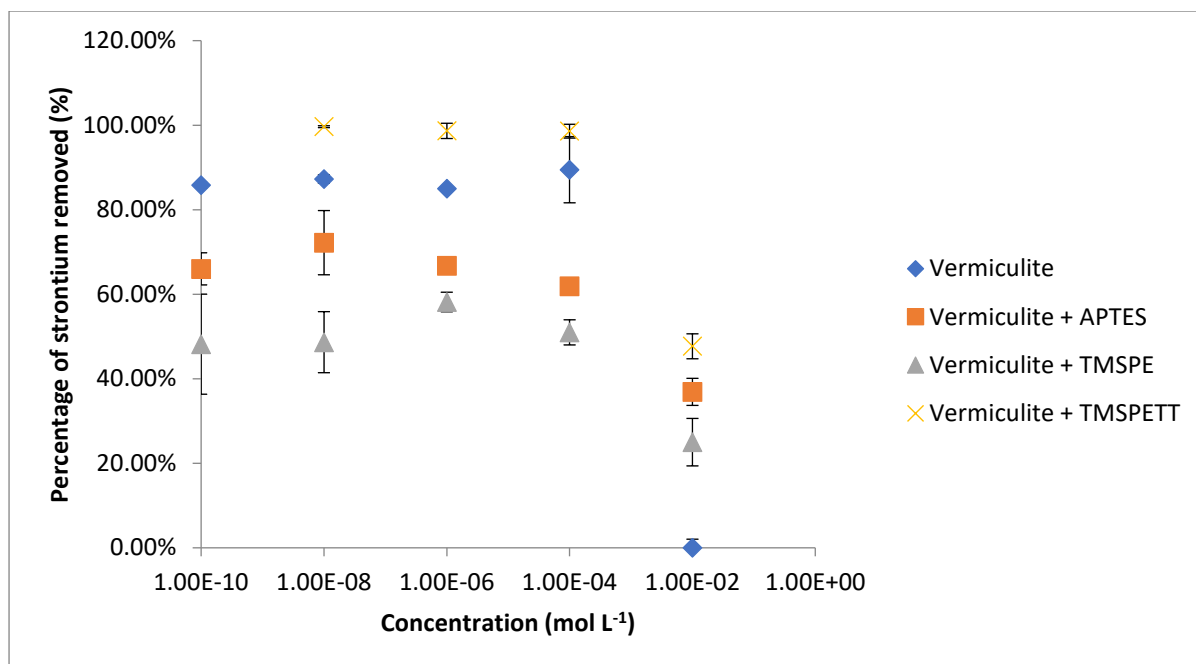
Figure 4.27: Comparison of strontium cation removal capability of vermiculite materials before and after grafting with ligands.

The removal of strontium is still observed in the modified materials, with less strontium removed in the APTES grafted and TMSPE grafted materials when compared to the unmodified materials. The TMSPETT grafted vermiculite shows an improvement in the removal of strontium. These observations are attributed to the exchangeable cations not being as accessible and the amount of donor atoms on the ligands.

4.26 Comparison of kaolinite materials

The rate of uptake of strontium to the unmodified and modified mineral kaolinite was investigated using the kinetic batch sorption methodology discussed in section 4.2. The results are shown in Figure 4.28.
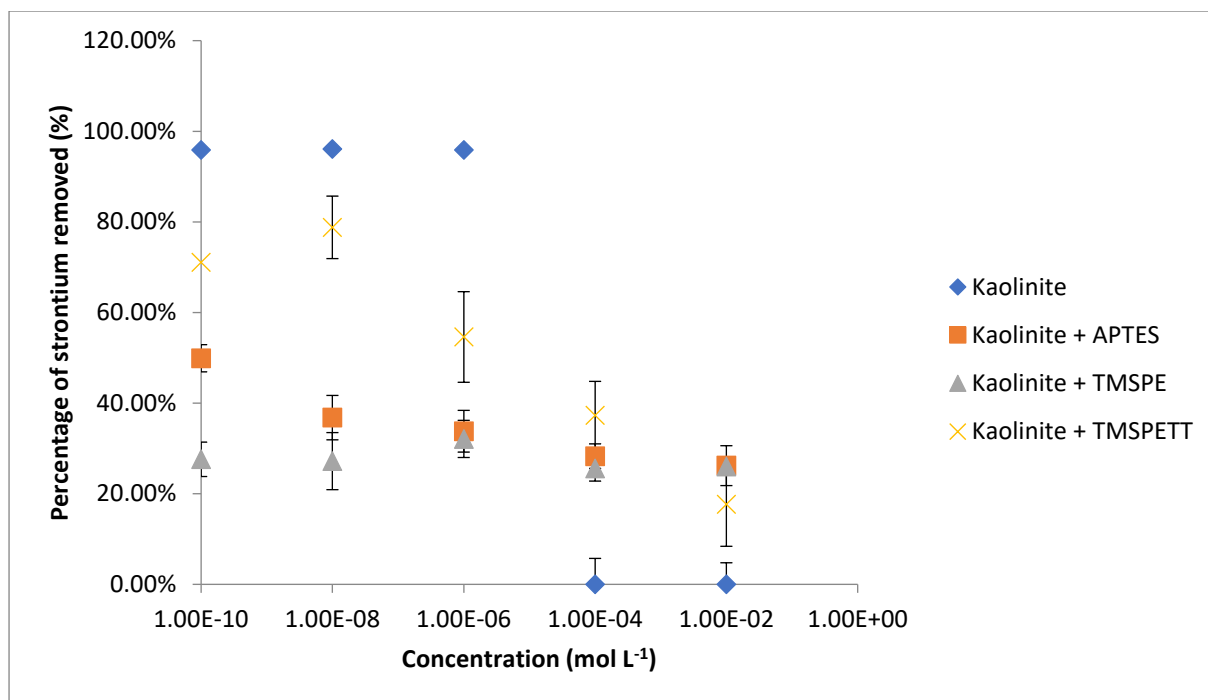
**Figure 4.28: Comparison of strontium cation removal capability of kaolinite materials before and after grafting with ligands.**

The removal of strontium is still observed in the modified materials. At low concentrations the amount removed is less which is attributed to the surface of the material being blocked by the ligand. At higher concentrations the amount removed is higher which is thought to be due to the donor atoms on the ligand.

4.27 Batch desorption sorption experimental results

4.27.1 Desorption of strontium by unmodified materials

The desorption of strontium to the unmodified materials was investigated using the batch sorption methodology discussed in section 4.3. The results are shown in Table 4.16

Table 4.16: Desorption experiments for strontium cations on ungrafted materials as a function of concentration.

Material	Clinoptilolite (NDA)		Clinoptilolite (Imerys)		ZSM-5		Vermiculite		Kaolinite	
Concentration	% desorbed	Error (+/-)	% desorbed	Error (+/-)	% desorbed	Error (+/-)	% desorbed	Error (+/-)	% desorbed	Error (+/-)
1×10^{-2}	0.0%	0.3%	0.0%	0.1%	0.0%	0.5%	0.3%	0.4%	0.1%	0.3%
1×10^{-4}	0.0%	0.2%	0.0%	0.3%	0.0%	0.1%	0.7%	1.6%	0.6%	0.1%
1×10^{-6}	0.0%	0.1%	0.0%	0.0%	0.0%	0.1%	2.0%	0.0%	0.2%	0.6%
1×10^{-8}	1.1%	2.3%	0.0%	0.2%	0.0%	0.1%	1.6%	0.4%	0.4%	0.1%
1×10^{-10}	0.0%	0.1%	0.0%	0.1%	0.1%	0.1%	2.0%	0.4%	0.8%	0.4%

The results from the desorption tests show that in the case of all zeolitic materials retain the strontium as expected due to the metal being trapped in the zeolite cages. Both clays show a small degree of desorption, but less than was seen for caesium, suggesting the clays have a higher affinity for strontium, probably as a result of the higher charge on strontium compared to caesium.

4.27.2 Desorption of strontium by APTES modified materials

The desorption of strontium to the APTES modified materials was investigated using the batch sorption methodology discussed in section 4.3. The results are shown in Table 4.17.

Table 4.17: Desorption experiments for strontium cations on APTES materials as a function of concentration.

Material	Clinoptilolite (NDA)		Clinoptilolite (Imerys)		ZSM-5		Vermiculite		Kaolinite	
Concentration	% desorbed	Error (+/-)	% desorbed	Error (+/-)	% desorbed	Error (+/-)	% desorbed	Error (+/-)	% desorbed	Error (+/-)
1×10^{-2}	4.3%	1.1%	1.3%	5.4%	3.7%	0.3%	4.5%	1.4%	2.9%	0.7%
1×10^{-4}	0.0%	0.5%	0.0%	0.2%	1.9%	5.5%	8.4%	2.5%	3.3%	1.7%
1×10^{-6}	0.0%	0.8%	0.0%	1.3%	1.7%	6.9%	16.0%	1.3%	1.6%	0.2%
1×10^{-8}	0.0%	0.7%	0.0%	0.4%	0.0%	4.7%	9.6%	4.9%	4.8%	0.5%
1×10^{-10}	6.5%	1.2%	6.3%	0.4%	3.2%	4.2%	25.3%	0.6%	8.8%	1.9%

All materials show an increase in desorption, indicating that the ligand is interacting with some of the sorped metal cations and are more easier released from the ligand than the host. HSAB theory would suggest a weak interaction of the hard ligand donors and soft metal cation. This is also seen in the caesium results to a greater degree, this can be attributed to the caesium ion being +1 and the

strontium ion being +2 making strontium harder than caesium due to ions being of similar charge by the ionic potential (charge/radius) being larger for strontium.

4.27.3 Desorption of strontium by TMSPE modified materials

The desorption of strontium to the TMSPE modified materials was investigated using the batch sorption methodology discussed in section 4.3. The results are shown in Table 4.18.

Table 4.18: Desorption experiments for strontium cations on TMSPE materials as a function of concentration.

Material	Clinoptilolite (NDA)		Clinoptilolite (Imerys)		ZSM-5		Vermiculite		Kaolinite	
Concentration	% desorbed	Error (+/-)	% desorbed	Error (+/-)	% desorbed	Error (+/-)	% desorbed	Error (+/-)	% desorbed	Error (+/-)
1×10^{-2}	0.1%	4.3%	0.4%	2.5%	1.2%	4.2%	1.6%	1.5%	1.0%	3.7%
1×10^{-4}	0.0%	2.9%	0.0%	2.2%	0.8%	0.7%	7.6%	1.4%	0.8%	4.5%
1×10^{-6}	0.0%	1.5%	0.0%	0.8%	0.0%	3.8%	8.7%	2.2%	0.0%	2.3%
1×10^{-8}	0.0%	1.0%	2.1%	1.5%	0.0%	2.0%	11.4%	2.3%	2.4%	1.2%
1×10^{-10}	0.0%	2.2%	0.0%	1.4%	0.0%	2.5%	7.5%	4.3%	1.0%	0.5%

Retention of the strontium during the desorption experiments is good for the majority of the materials with vermiculite showing the worst retention. In the case of clinoptilolite, the retention is close to 100% across the concentration scale.

4.27.4 Desorption of strontium by TMSPETT modified materials

The desorption of strontium to the TMSPETT modified materials was investigated using the batch sorption methodology discussed in section 4.3. The results are shown in Table 4.19.

Table 4.19: Desorption experiments for strontium cations on TMSPETT materials as a function of concentration.

Material	Clinoptilolite (NDA)		Clinoptilolite (Imerys)		ZSM-5		Vermiculite		Kaolinite	
Concentration	% desorbed	Error (+/-)	% desorbed	Error (+/-)	% desorbed	Error (+/-)	% desorbed	Error (+/-)	% desorbed	Error (+/-)
1×10^{-2}	0.0%	0.9%	0.7%	0.8%	2.5%	8.2%	0.0%	2.4%	0.0%	2.2%
1×10^{-4}	0.0%	0.7%	0.0%	0.8%	0.0%	2.0%	0.0%	2.0%	0.7%	1.9%
1×10^{-6}	0.0%	0.7%	0.0%	0.5%	0.0%	1.2%	0.0%	0.7%	0.0%	2.9%
1×10^{-8}	0.0%	0.3%	0.0%	1.1%	0.0%	1.1%	0.0%	0.0%	0.0%	0.4%
1×10^{-10}	0.0%	0.8%	0.0%	1.8%	0.0%	1.4%	0.0%	0.5%	0.0%	1.1%

Very little desorption is seen in all cases except at the higher concentrations, there are more sites for the metal ions to interact with in the TMSPETT. Since the ligand has chelating properties and multiple coordination sites per molecule, it is expected that desorption would be low and prevent the release of the metal ion back into solution.

4.28 Kinetic batch sorption experimental results

4.27.1 Rate of uptake of strontium by unmodified materials

The rate of uptake of strontium to the unmodified and modified materials was investigated using the kinetic batch sorption methodology discussed in section 4.4. The results are shown in Figure 4.29 and tabulated in Table 4.20.

Figure 4.29 Kinetic experiments to measure the strontium take up by unmodified materials as a function of time

The removal of strontium by the clinoptilolite (Imerys) sample is quicker than the clinoptilolite (NDA) sample. This is due to the smaller particle size of the clinoptilolite (Imerys) sample creating a larger surface area allowing more of the strontium to be in contact with the sample. Both clinoptilolite samples reach complete removal after 28 days with the majority of the strontium being removed within 7 days. Vermiculite shows a similar trend to the clinoptilolite samples suggesting that the process removing the strontium ions is ion exchange. ZSM-5 does not show as much removal of strontium but the rate of uptake is consistent with ion exchange. Kaolinite shows no ion exchange but chemisorption to the surface even after one hour of contact time.

Table 4.20 Kinetic batch absorption experiments for strontium on unmodified substrates

Material	Clinoptilolite (NDA)		Clinoptilolite (Imerys)		ZSM-5		Vermiculite		Kaolinite	
Time (days)	% removed	Error (+/-)	% removed	Error (+/-)	% removed	Error (+/-)	% removed	Error (+/-)	% removed	Error (+/-)
0.04	12.6%	3.5%	47.5%	2.4%	17.1%	3.3%	24.1%	2.8%	26.7%	3.8%
1	42.2%	4.7%	54.5%	1.7%	17.2%	8.7%	37.6%	3.6%	29.6%	2.6%
7	92.0%	1.2%	86.5%	1.1%	19.7%	4.9%	46.9%	4.4%	22.1%	7.2%
14	99.4%	0.1%	91.2%	0.7%	31.8%	11.9%	54.6%	4.0%	30.2%	8.7%
28	100.0%	0.0%	100.0%	2.5%	33.1%	4.3%	73.0%	2.6%	59.4%	2.2%

4.28.2 Rate of uptake of strontium by APTES modified materials

The rate of uptake of strontium to the APTES modified materials was investigated using the kinetic batch sorption methodology discussed in section 4.4. The results are shown in figure 4.30 and tabulated in table 4.21.

Figure 4.30: Kinetic experiments to measure the strontium take up by APTES modified materials as a function of time

Material	Clinoptilolite (NDA)		Clinoptilolite (Imerys)		ZSM-5		Vermiculite		Kaolinite	
Time (days)	% removed	Error (+/-)	% removed	Error (+/-)	% removed	Error (+/-)	% removed	Error (+/-)	% removed	Error (+/-)
0.04	16.7%	1.0%	18.1%	2.0%	15.2%	4.5%	20.8%	3.2%	14.8%	2.5%
1	21.8%	2.0%	21.1%	4.3%	17.0%	0.4%	35.5%	1.0%	18.3%	3.8%
7	41.4%	5.0%	29.0%	4.8%	18.5%	3.3%	42.6%	4.7%	17.3%	3.6%
14	59.9%	9.6%	41.0%	3.8%	18.1%	1.7%	45.0%	1.2%	22.8%	5.4%
28	85.2%	2.9%	58.0%	1.2%	20.8%	3.7%	52.8%	3.8%	24.9%	0.4%

The removal of strontium in all cases of the APTES modified zeolites and vermiculite is slower with the total amount of strontium removed less than for the unmodified materials. This is attributed to the ligand restricting access to the exchangeable cations of the materials. The removal of strontium by kaolinite is reduced as discussed previously due the ligand preventing access to the surface of the solid but the rate of uptake to capacity occurs at the same speed. Suggesting that the mechanism of uptake remains the same but the modification of the material has decreased the capacity by reducing the surface available for physisorption.

4.28.3 Rate of uptake of strontium by TMSPE modified materials

The rate of uptake of strontium to the TMSPE modified materials was investigated using the kinetic batch sorption methodology discussed in section 4.4. The results are shown in Figure 4.31 and tabulated in table 4.22.
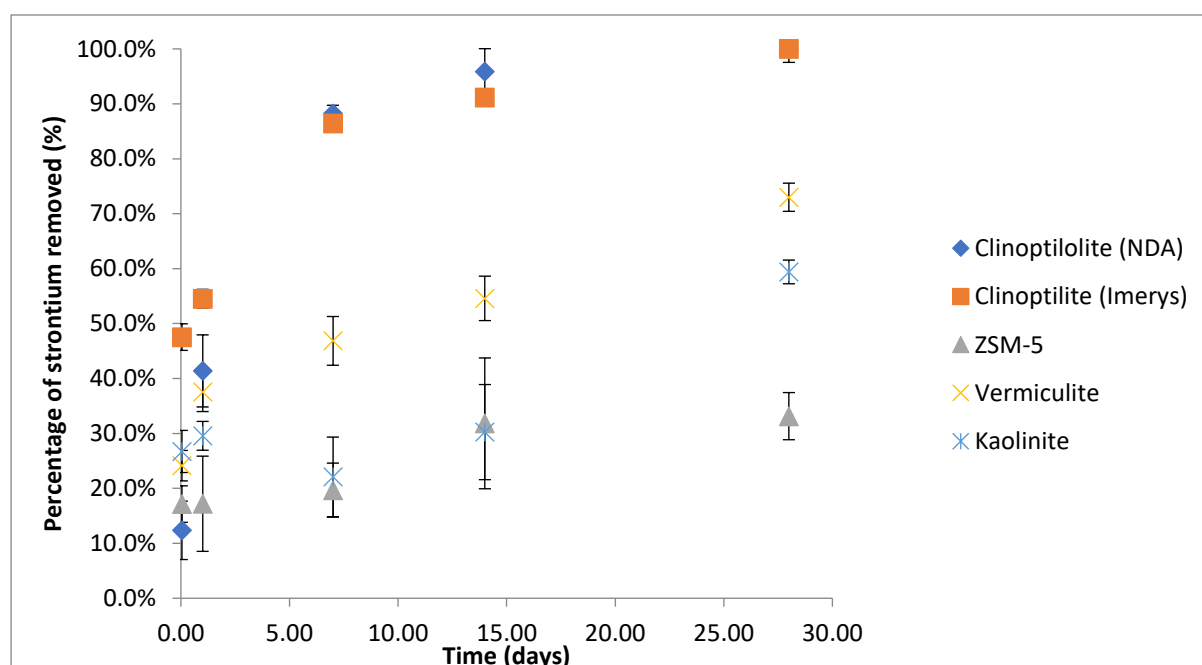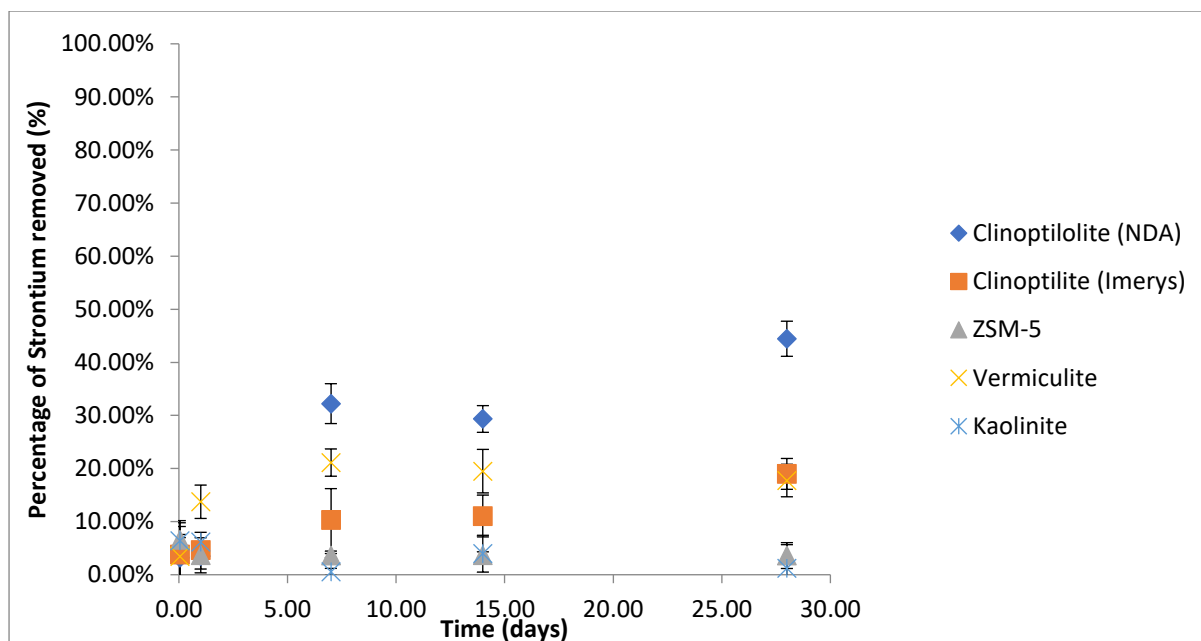
Figure 4.31: Kinetic experiments to measure the strontium take up by TMSPE modified materials as a function of time

Table 4.22: Kinetic batch absorption experiments for strontium on TMSPE modified substrates

Material	Clinoptilolite (NDA)		Clinoptilolite (Imerys)		ZSM-5		Vermiculite		Kaolinite	
Time (days)	% removed	Error (+/-)	% removed	Error (+/-)	% removed	Error (+/-)	% removed	Error (+/-)	% removed	Error (+/-)
0.04	3.21%	3.78%	3.80%	6.39%	6.57%	3.21%	3.41%	5.67%	6.42%	1.16%
1	3.50%	2.43%	4.66%	1.52%	3.66%	3.31%	13.74%	3.14%	6.14%	1.85%
7	32.22%	3.76%	10.34%	5.88%	3.61%	0.38%	21.12%	2.56%	0.52%	0.67%
14	29.34%	2.51%	11.06%	3.94%	3.66%	0.65%	19.50%	4.10%	3.96%	3.46%
28	44.45%	3.30%	18.99%	2.91%	3.61%	2.43%	17.74%	3.07%	1.20%	4.46%

The removal of strontium in all cases of the TMSPE modified zeolites is much slower with this ligand compared to the unmodified material and APTES modified substrates. This can be attributed to the ligand restricting access to the exchangeable cations being lost from the substrate via the channels of the materials. The removal of strontium by kaolinite is reduced as discussed previously due the ligand preventing access and hence to the surface of the solid.

4.28.4 Rate of uptake of strontium by TMSPETT modified materials

The rate of uptake of strontium to the TMSPETT modified materials was investigated using the kinetic batch sorption methodology discussed in section 4.4. The results are shown in figure 4.32 and tabulated in table 4.23.
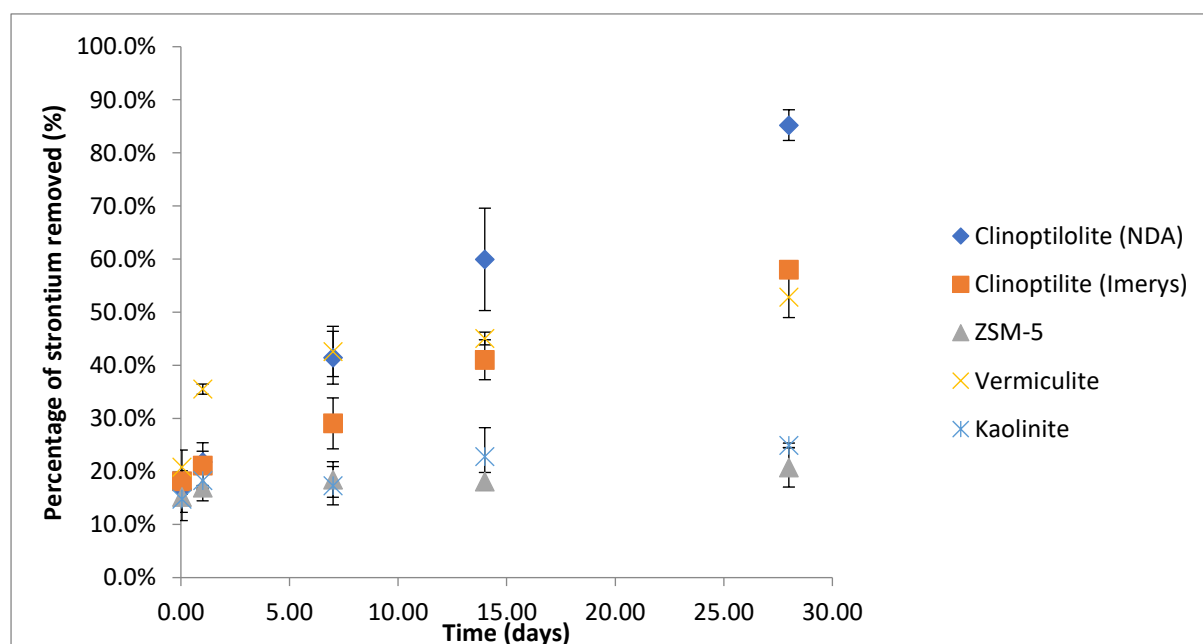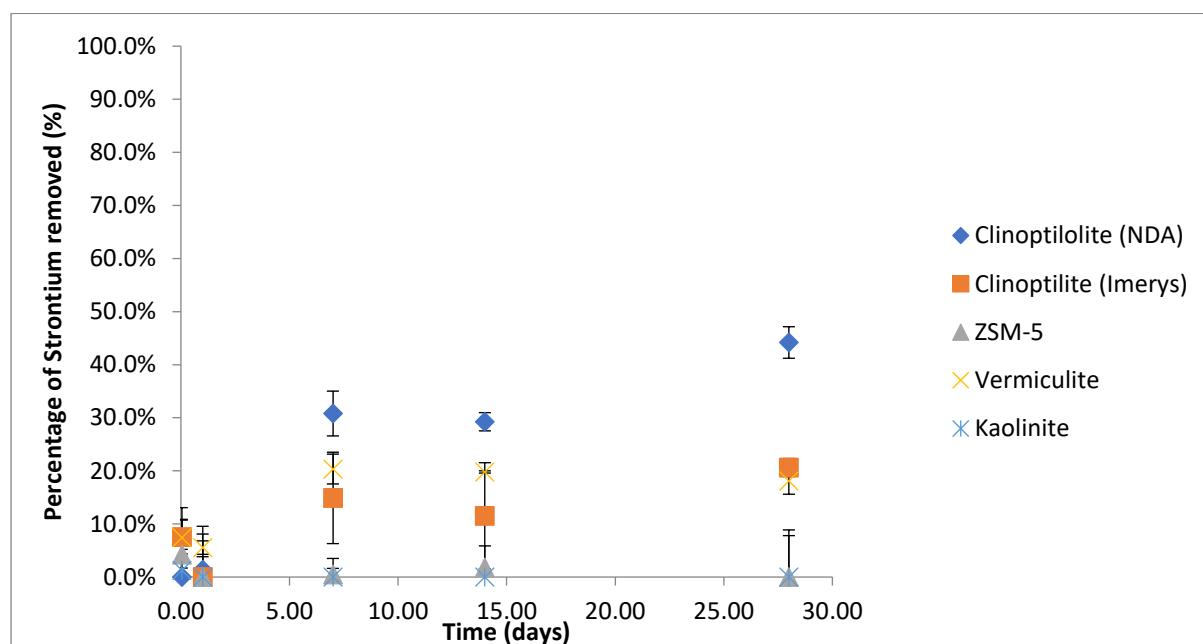

Figure 4.32: Kinetic experiments to measure the strontium take up by TMSPETT modified materials as a function of time

Table 4.22: Kinetic batch absorption experiments for strontium on TMSPETT modified substrates

Material	Clinoptilolite (NDA)		Clinoptilolite (Imerys)		ZSM-5		Vermiculite		Kaolinite	
Time (days)	% removed	Error (+/-)	% removed	Error (+/-)	% removed	Error (+/-)	% removed	Error (+/-)	% removed	Error (+/-)
0.04	0.0%	5.2%	7.5%	3.2%	9.55%	14.0%	7.4%	5.7%	1.2%	2.4%
1	1.4%	2.5%	0.0%	8.1%	1.0%	22.2%	5.5%	1.3%	0.0%	2.0%
7	30.8%	4.2%	14.9%	8.6%	1.2%	6.1%	20.3%	2.8%	0.0%	1.6%
14	29.3%	1.7%	11.5%	10.0%	0.0%	8.5%	19.8%	0.2%	0.0%	1.5%
28	44.2%	3.0%	20.6%	1.7%	0.0%	15.6%	18.1%	2.5%	0.0%	8.9%

The TMSPETT modification appears to have slowed the uptake of the cations from solution compared to the ungrafted clinoptilolite materials.

4.29 Comparison of clinoptilolite (NDA) materials

The rate of uptake of strontium to the unmodified and modified mineral clinoptilolite was investigated using the kinetic batch sorption methodology discussed in section 4.4. The results are shown in figure 4.33.

**Figure 4.33: Comparison of kinetic experiments for strontium uptake of clinoptilolite NDA**

The removal of strontium is still observed in the modified materials, however the uptake capacity is reduced. Leading to the conclusion that the ligands are effecting the accessibility of the pores and exchangeable cations but that the mechanism of uptake remains the same.

4.30 Comparison of clinoptilolite (Imerys) materials

The rate of uptake of strontium to the unmodified and modified mineral clinoptilolite was investigated using the kinetic batch sorption methodology discussed in section 4.4. The results are shown in figure 4.34.

Figure 4.34: Comparison of kinetic experiments for strontium uptake of clinoptilolite Imerys

Similar results are observed for the clinoptilolite received from Imerys to that received from the NDA. The smaller particle size appears to have a greater effect on the retardation of the uptake of the strontium after grafting.

4.31 Comparison of ZSM-5 materials

The rate of uptake of strontium to the unmodified and modified material ZSM-5 was investigated using the kinetic batch sorption methodology discussed in section 4.4. The results are shown in Figure 4.35.
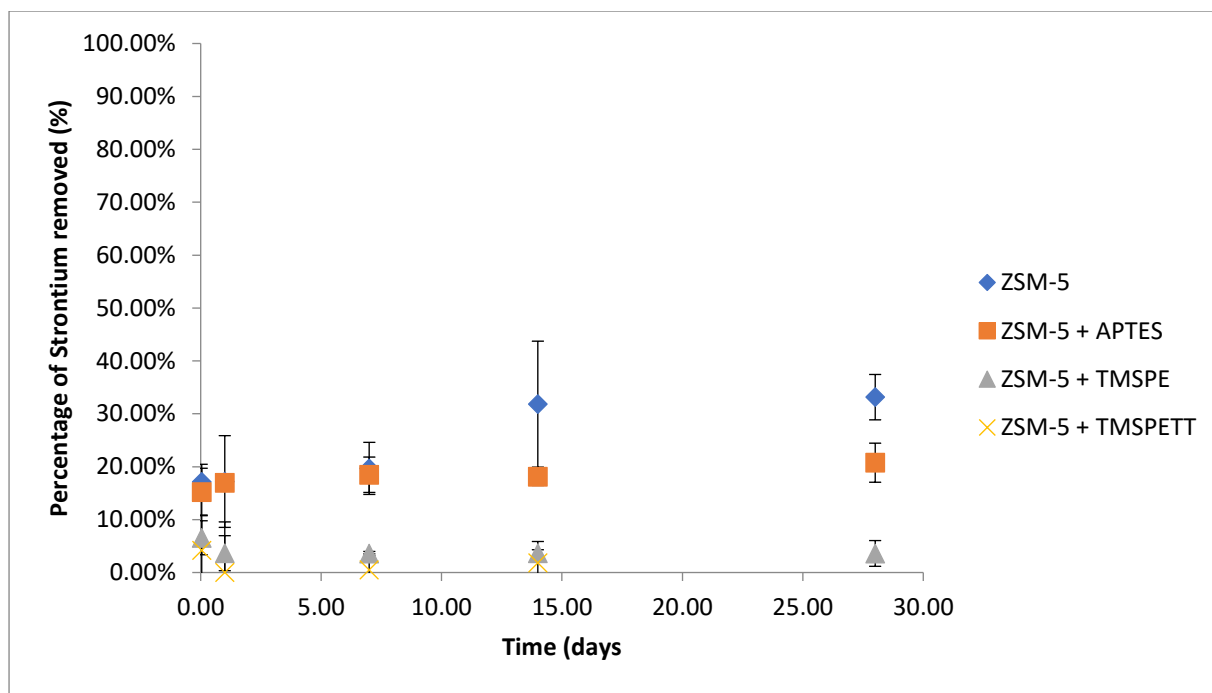
Figure 4.35: Comparison of kinetic experiments for strontium uptake of ZSM5

Grafting of the ligands does not appear to have made a marked difference to the strontium uptake by ZSM5. The low number of cations available for exchange due to the small numbers of aluminium tetrahedra in the framework making the ion exchange capacity poor and the ligand does not show particular selectivity for strontium as it is a low charged, large ion.

4.32 Comparison of vermiculite materials

The rate of uptake of strontium to the unmodified and modified mineral vermiculite was investigated using the kinetic batch sorption methodology discussed in section 4.4. The results are shown in figure 4.36.
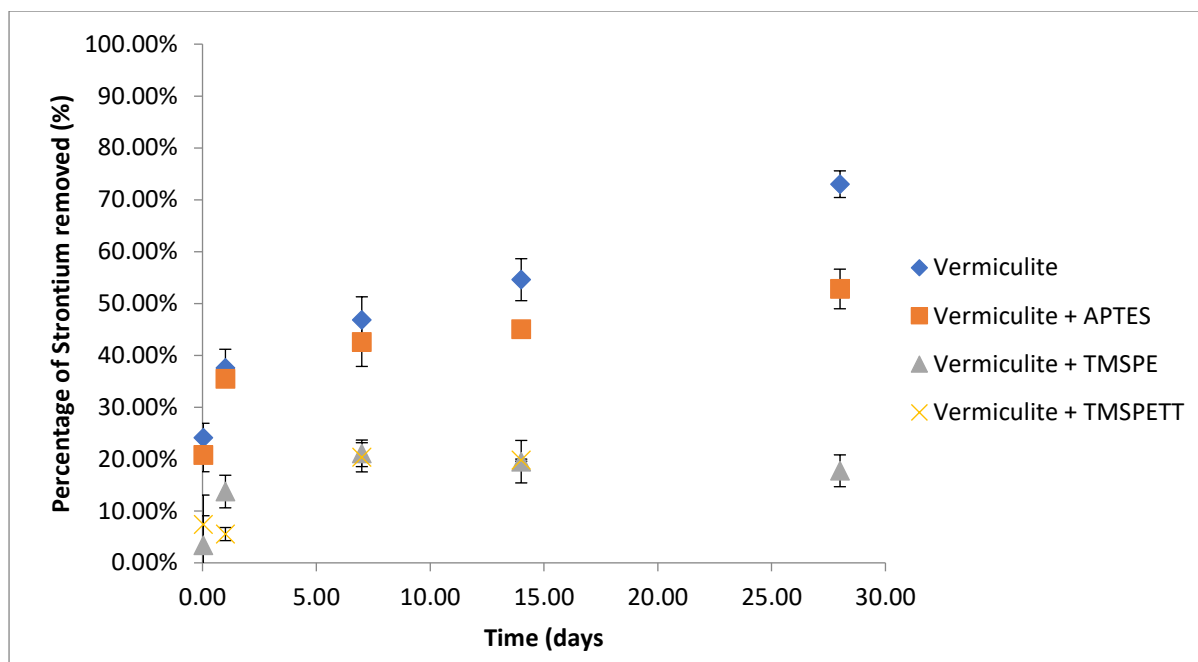
Figure 4.36: Comparison of kinetic experiments for strontium uptake of vermiculite

The removal of strontium is still observed in the modified materials; however the uptake capacity is reduced. Leading to the conclusion that the ligands are affecting the accessibility of the layers and exchangeable cations therein but that the mechanism of uptake remains the same.

4.33 Comparison of kaolinite materials

The rate of uptake of strontium to the unmodified and modified mineral kaolinite was investigated using the kinetic batch sorption methodology discussed in section 4.4. The results are shown in figure 4.37.
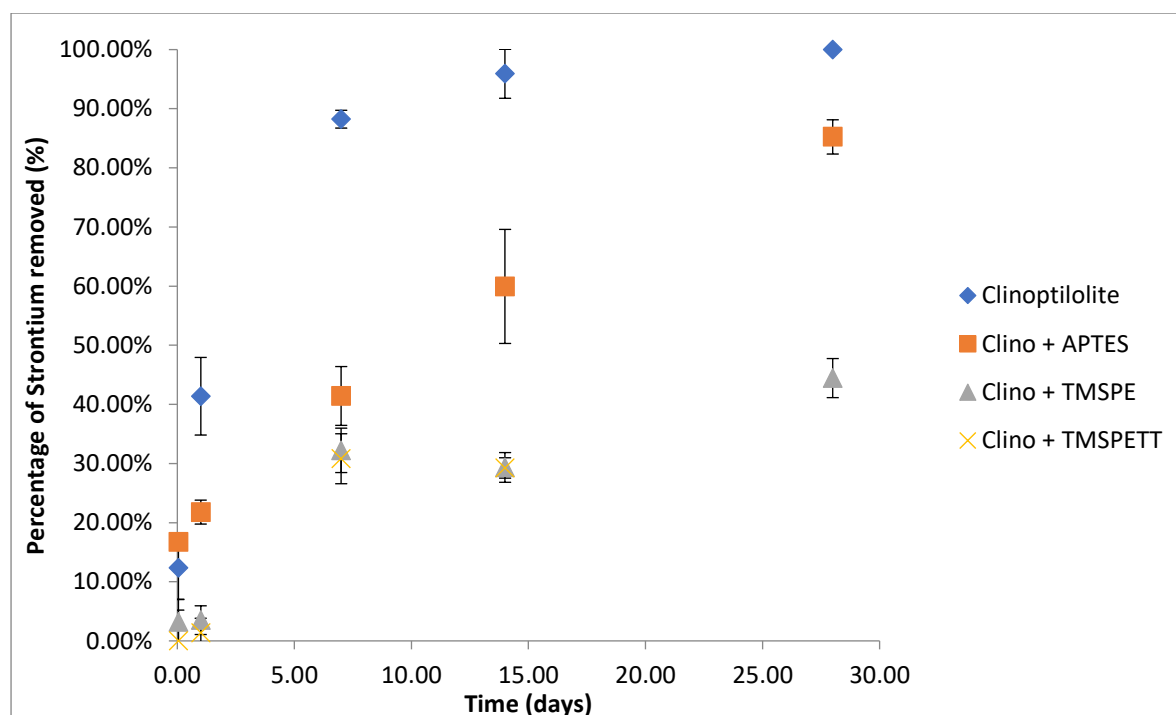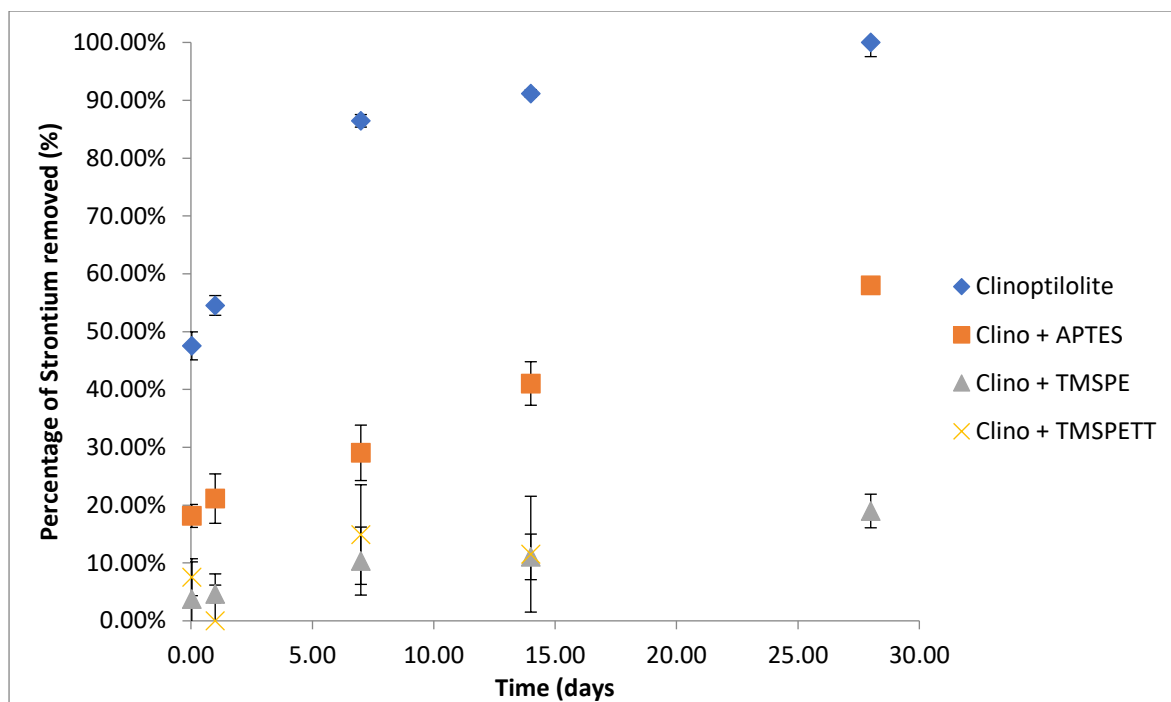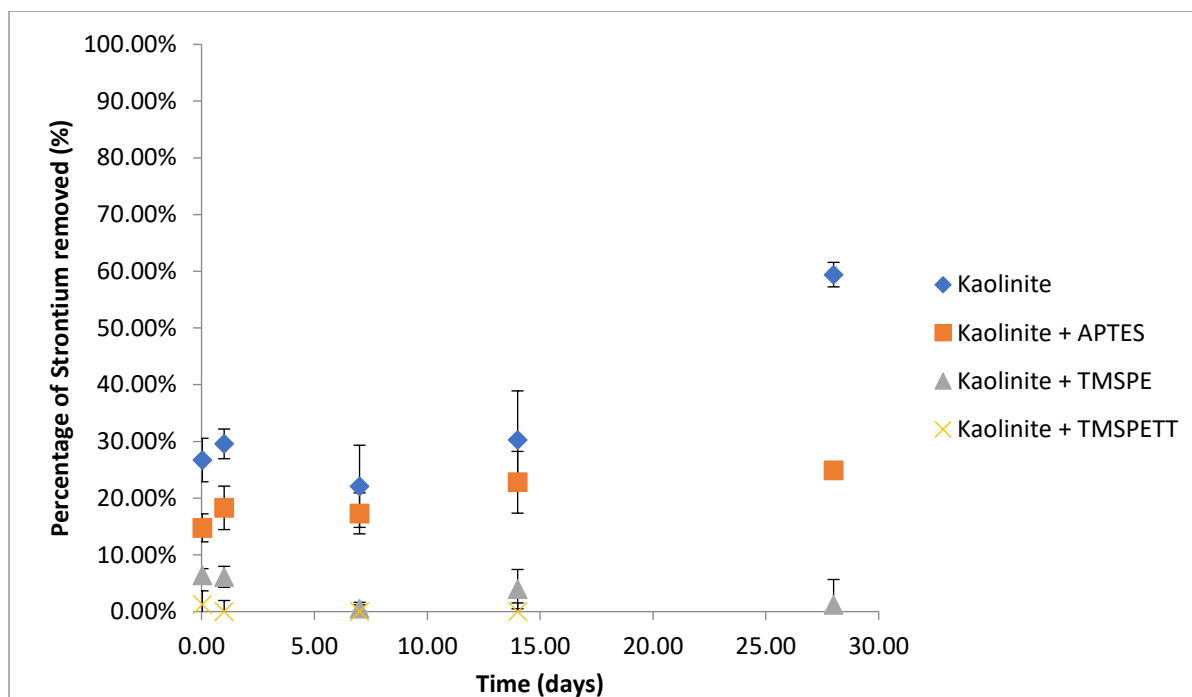
Figure 4.37: Comparison of kinetic experiments for strontium uptake of kaolinite

The removal of strontium is still observed in the modified materials. The amount of uptake is less in the modified materials but the rate of uptake to capacity occurs at the same speed. This suggests that the mechanism of uptake remains the same but the modification of the material has decreased the capacity by reducing the surface available for physisorption.

4.34 Strontium uptake summary

The effect of strontium uptake by the materials Clinoptilolite (NDA), clinoptilolite (Imerys), ZSM-5, vermiculite and kaolinite before and after modification with the organic ligands APTES, TMSPE and TMSPETT were investigated. Experiments were conducted to study the amount and rate of strontium uptake by the materials.

Strontium uptake is still observed in all modified materials, although the modified materials show less strontium uptake than their unmodified counterparts. This can be attributed to the exchangeable cations not being as accessible. The rate of strontium uptake is slower in all cases which again can be attributed to restricted access to the exchange sites.

4.35 Experimental methodology for uranium experiments

The sequestration capacity of the materials used has been investigated radiometrically for the sequestration of uranium using batch sorption studies at varying concentrations of metal ions. The sorption experiments were conducted in 15 mL plastic sample tubes with approximately 0.05 g of solid and 10 mL of metal nitrate solution. The solution was then spiked with ^{233}U radio tracer. The samples were then shaken to encourage equilibrium between the solid and liquid to be reached. After this 2 mL of the supernatant was filtered through a 0.22 µm pore filter to remove any solid particulate and ^{233}U was measured using liquid scintillation counting. The amount of metal ions removed from solution was calculated using mass balance calculations to compare the activities of the solutions before and after being exposed to the solid surface. All experiments were carried out in triplicate to show reproducibility and under ambient conditions. Method used for determining percentage sorbed same as previously mentioned in section 4.1.

The kinetic experiments were carried out using the same experimental methodology and calculations for different time periods. The kinetic experiments were carried out using a 1×10^{-3} mol L^{-1} solution which was determined from the batch sorption experiments as it was shown to allow saturation of the materials. Desorption experiments were carried out using the solid from the sorption experiments with 10 mL of deionised water added with an assumed concentration of ions of zero.

4.35.1 Batch sorption experiments

0.05 g of solid was weighed into a 15 mL plastic centrifuge tube. To this 10 mL of uranyl nitrate solution were added. A range of uranyl nitrate concentrations from 10^{-2} to 10^{-10} mol L^{-1} were used to investigate the sequestration capacity of the base materials before and after modification. A 0.16 kBq spike of ^{233}U was added to the centrifuge tube. Samples were then placed on to a flatbed shaker and agitated for 7 days. After this time period the solution was decanted and filtered using a 0.22 µm Teflon filter, a 2 mL aliquot was taken and analysed for ^{233}U by liquid scintillation counting using a Packard TRI-carb 2100tr liquid scintillation counter. All samples were conducted in triplicate and percentage sorption calculated relative to a control to take into account wall sorption.

4.35.2 Desorption experiments

The samples from the sorption experiment were used to carry out the desorption experiments of the materials. The sorption experiment solution was decanted from the centrifuge tube leaving the solid. 10 mL of distilled water was added to the solid. The samples were then shaken for 28 days, and a 2 mL aliquot was taken and filtered using a 0.22 µm filter to remove any solids. The samples were

counted using a Packard TRI-carb 2100tr liquid scintillation counter. 28 days was selected to show stability of the binding when applied to plant process.

4.35.3 Kinetic experiments

0.05 g of solid was weighed out in to a 15 mL plastic centrifuge tube; to this 10 ml of a 1 x 10^{-3} M natural uranium carrier solution was added. A spike of 0.16 kBq was then added as a radiotracer. The kinetic experiments were set up in replicates of three, to show reproducibility. Natural uranium metal nitrate was used as the carrier solutions, U^{233} was used as a radiotracer, concentration was determined using batch sorption experimental isotherm data. Times of one hour, one day, one week, two weeks and four weeks were used to investigate the speed of the sequestration of the materials before and after modification. The samples were shaken and at the set time intervals a 2 mL aliquot was taken and filtered using a 0.22 μm filter to remove any solids. The samples were counted using a Packard TRI-carb 2100tr liquid scintillation counter.

4.36 Preliminary experiments with ^{233}U

Preliminary work was carried out to look at feasibility of counting ^{233}U by liquid scintillation counting, interference of natural uranium with the counting, the linear dynamic range of ^{233}U counting and the viability of sequestration experiments.

As discussed in sections 4.33 the experimental methodology is similar to the caesium and strontium experimental sections 4.1. In the caesium and strontium experiments an inactive carrier is used, in the case of uranium there are no inactive isotopes available and natural uranium is used as the carrier solution. The influence of the activity of the carrier solution on the samples being counted was investigated to ensure this would not affect the results. Higher concentrations of natural uranium are coloured, this can cause colour quenching of the sample and this needed to be investigated. The linear dynamic range was also investigated to determine the concentration window for ^{233}U.

4.36.1 ^{233}U analysis by liquid scintillation counting

The ^{233}U stock used was determined to have an activity of 366 Bq μl^{-1}. This was determined by placing 50 μl of ^{233}U into a scintillation vial with 10 mL of scintillation fluid and analysis by liquid scintillation counting.

The resulting spectrum shown in figure 4.38 shows that ^{233}U is detectable using liquid scintillation counting and a single peak was observed at 272 keV.
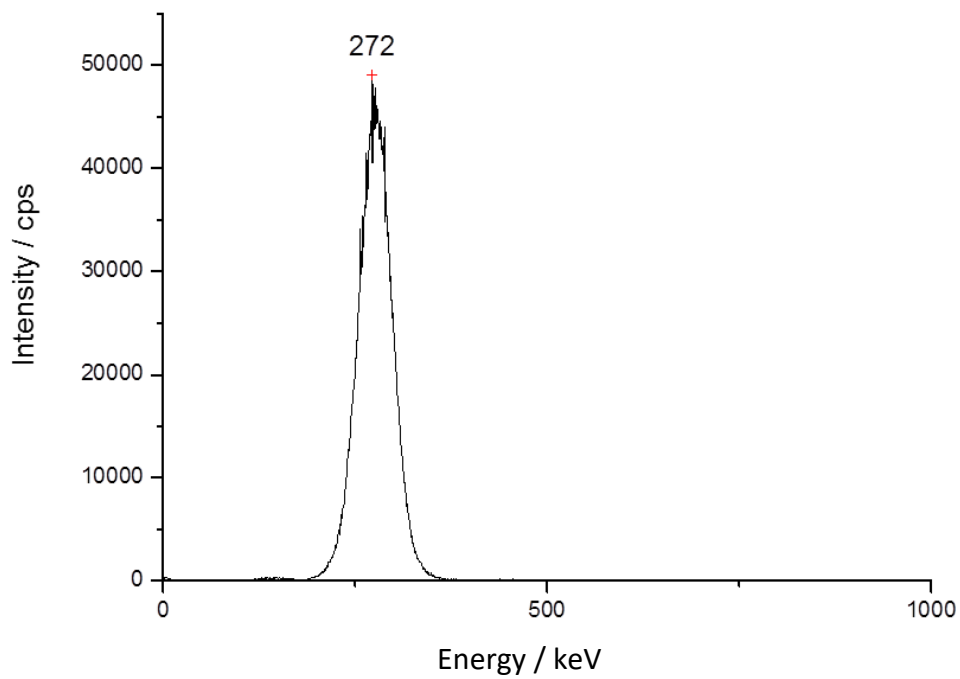
Figure 4.38: Liquid scintillation spectrum for ^{233}U standard.

2 mL of $1x10^{-3}$ mol L^{-1} uranyl nitrate were added to the previous scintillation vial with 10 mL of liquid scintillation fluid and analysed by liquid scintillation counting.

The resulting spectrum is shown in figure 4.39 The results show an additional peak was observed at 160 keV.
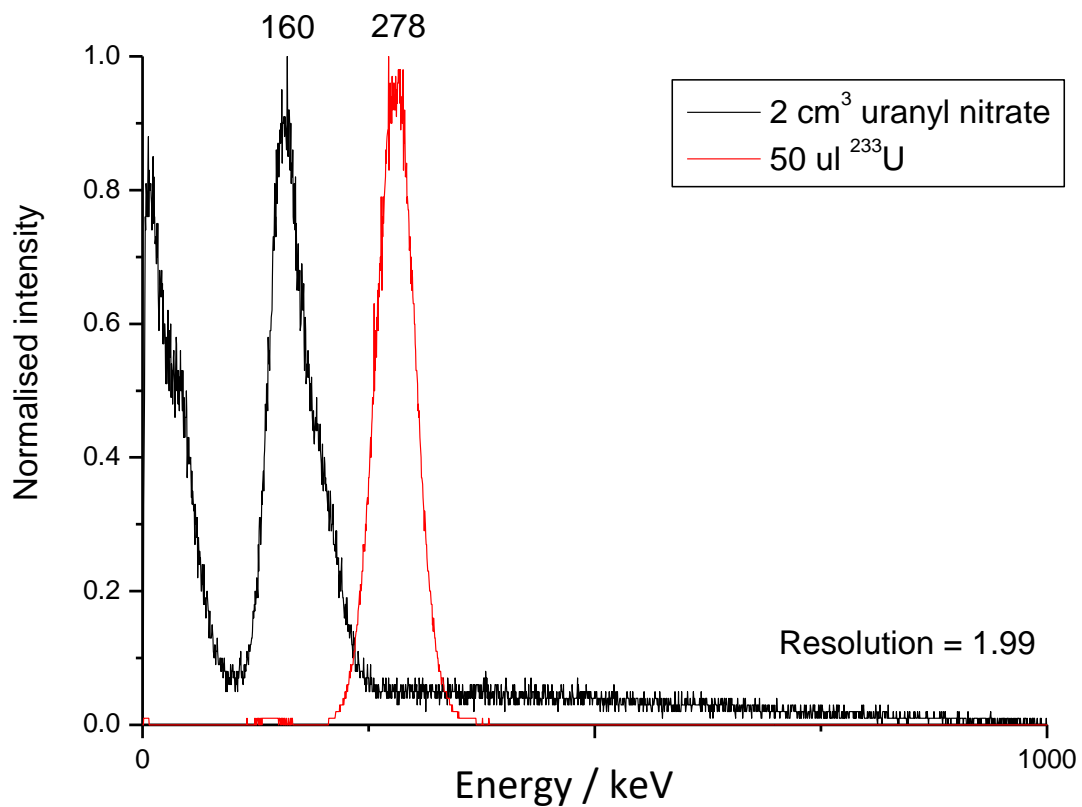
Figure 4.39 Liquid scintillation spectra for ^{233}U with the addition of natural uranium

$$R_s \ = \ \left(\frac{2DZ}{w_i \ + \ w_j} \right)$$

Where ΔZ = Separation between peaks

$W_i + W_j$ = peak width at half height of the respective peaks

$$\frac{238}{(62.7 + 56.9)} = 1.99$$

The overlay of the natural uranium and the ^{233}U spike spectra shown above were normalised relative to the maximum intensity. The resolution was determined to be 1.99 suggesting that the two peaks are fully resolved. The natural uranium is a mixture of isotopes ^{234}U, ^{235}U and ^{238}U this causes the natural uranium peak to have a non-symmetrical shape due to the overlap of the emissions from the

- 214 -

isotopes. A counting window was established between 250 – 400 keV to only count the ^{233}U signal and exclude any counts from the natural uranium.

4.36.2 Linear dynamic range of ^{233}U

The linear dynamic range was investigated by adding increasing volumes of U^{233}, ranging from 5-50 µl. and is depicted in Figure 4.40 and 4.41

Figure 4.40(top) linear dynamic range plots for ^{233}U Figure 4.41 (bottom) linear dynamic range plot for ^{233}U + natural

uranium
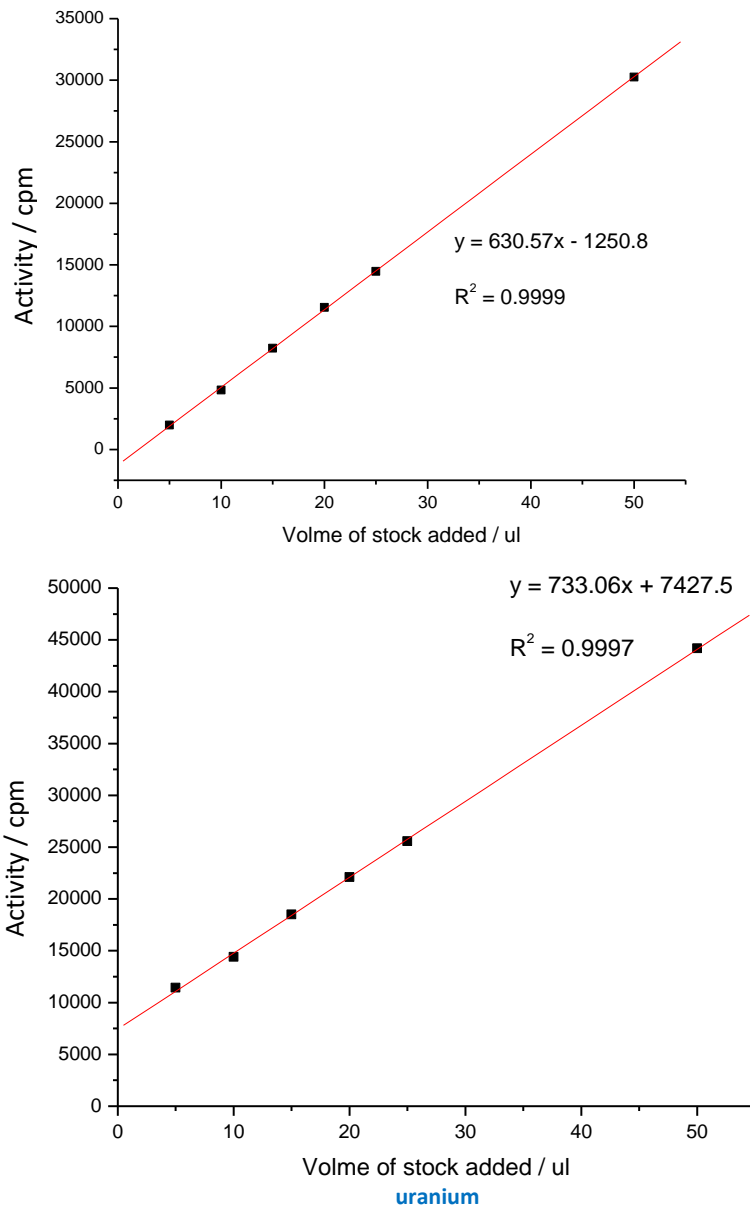
The calibration graph shown in figure 4.40 shows a linear response over an order of magnitude. From the equation of the line the limit of detection and quantification were determined to be 5.95 and 59.52 cpm respectively, this was calculated from the equation of the line shown in figures 4.40 and 4.41.

The experiment was repeated with the addition of 2 mL of 1×10^{-3} mol L^{-1} natural uranium. The same linear response was observed figure 4.41. The linear response suggests that any concentration in this window can be used.

4.36.2 Sequestration of experiment

0.05g of unmodified and APTES modified clinoptilolite samples were added to 15 mL centrifuge tubes with 10 mL of deionised water added, a U^{233} spike was then added and left for a period of one hour. A 2 mL aliquot was then taken and analysed by liquid scintillation counting as discussed in section 4.34. Experimental results for the triplicate studies are shown in table 4.23.

Table 4.23: Preliminary batch absorption experiments on clinoptilolite (NDA) grafted with APTES.

Sample	cpm	cpm removed	Mols removed	Mass ^{233}U removed / g	g/g of zeolite	% removed
Clinoptilolite NO carrier	2466	2473	4.96E-10	1.16E-07	2.31E-06	16.71%
Clinoptilolite NO carrier	2475	2428	4.87E-10	1.13E-07	2.27E-06	16.40%
Clinoptilolite NO carrier	2372	2943	5.90E-10	1.37E-07	2.75E-06	19.88%
Clinoptilolite + APTES no carrier	587	11868	2.38E-09	5.54E-07	1.11E-05	80.17%
Clinoptilolite + APTES no carrier	663	11488	2.30E-09	5.37E-07	1.07E-05	77.61%
Clinoptilolite + APTES no carrier	731	11148	2.24E-09	5.21E-07	1.04E-05	75.31%

The unmodified clinoptilolite saw an uptake of approximately $17.6 \pm 2.3\%$ compared to $77.7 \pm 2.4\%$ for the modified material. This suggests that the modified clinoptilolite does remove the actinide species from solution and the good agreement within the results suggests the methodology is sound. Further experimental result were then attempted on all the grafted materials

4.37 Uranium experimental results

4.37.1 Batch sorption experimental results of unmodified materials

The uptake of uranium to the minerals clinoptilolite, ZSM-5, vermiculite and kaolinite was investigated using the batch sorption methodology discussed in section 4.33.1. The results are shown in figure 4.42 and table 4.24.
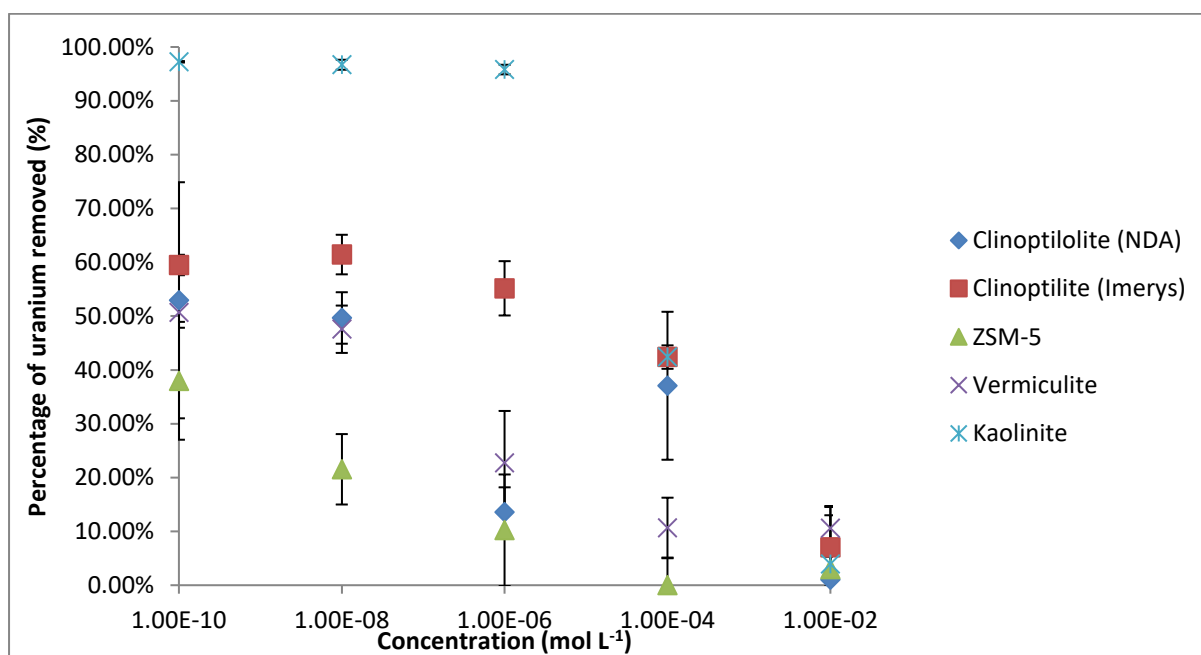
Figure 4.42: Batch absorption experiments for uranium on unmodified materials.

Material	Clinoptilolite (NDA)		Clinoptilolite (Imerys)		ZSM-5		Vermiculite		Kaolinite	
Concentration	% removed	Error (+/-)	% removed	Error (+/-)	% removed	Error (+/-)	% removed	Error (+/-)	% removed	Error (+/-)
1×10^{-2}	1.0%	13.5%	7.0%	6.0%	3.0%	2.3%	10.6%	4.1%	3.9%	4.1%
1×10^{-4}	37.1%	13.7%	42.4%	2.2%	0.0%	5.1%	10.6%	5.6%	42.4%	1.3%
1×10^{-6}	13.6%	4.6%	55.2%	5.0%	10.2%	10.4%	22.7%	9.6%	95.8%	0.9%
1×10^{-8}	49.7%	4.8%	61.4%	3.7%	21.5%	6.5%	47.6%	4.4%	96.7%	0.9%
1×10^{-10}	52.9%	21.9%	59.5%	1.9%	38.0%	10.9%	50.7%	2.8%	97.3%	0.1%

Table 4.24: Uranium absorption by ungrafted materials as a function of uranium concentration

All materials show uptake of uranium with the highest percentage removed by kaolinite of approximately 96% at concentrations below 1×10^{-6} mol L^{-1} with saturation being reached, whilst ZSM-5 shows the lowest affinity for uranium. The very different results presented here compared to those for strontium and caesium cations show the differences between the type of ions in solution; the zeolites and vermiculite demonstrate poorer utility as the size and charge of the actinide does not favour ion exchange which is greater for ions with lower ionic potential.

4.37.2 Uptake of uranium by APTES modified materials

The uptake of uranium to the APTES modified minerals clinoptilolite, ZSM-5, vermiculite and kaolinite was investigated using the batch sorption methodology discussed in section 4.33.1. The results are shown in figure 4.43 and table 4.25.

Figure 4.43 Uranium species uptake as a function of concentration on APTES grafted materials

Table 4.25: Uranium species uptake as a function of concentration on APTES grafted materials

Material	Clinoptilolite (NDA)		Clinoptilolite (Imerys)		ZSM-5		Vermiculite		Kaolinite	
Concentration	% removed	Error (+/-)	% removed	Error (+/-)	% removed	Error (+/-)	% removed	Error (+/-)	% removed	Error (+/-)
1×10^{-2}	8.5%	6.8%	31.6%	2.3%	6.1%	5.2%	35.9%	8.0%	20.2%	10.7%
1×10^{-4}	91.6%	2.4%	94.8%	0.6%	55.3%	5.1%	94.2%	0.9%	97.1%	0.3%
1×10^{-6}	61.1%	6.9%	98.5%	0.1%	97.2%	0.9%	98.8%	0.1%	91.7%	0.1%
1×10^{-8}	76.5%	1.5%	98.6%	0.2%	98.8%	0.2%	98.8%	0.2%	87.3%	3.2%
1×10^{-10}	78.6%	5.0%	98.5%	0.1%	98.6%	0.1%	98.6%	0.2%	89.0%	1.6%

After modification with APTES all materials show a significant increase in the removal of uranium from solution. This is attributed to the ligand as all materials show the same behaviour. Saturation appears to be reached between a concentration of 1×10^{-2} and 1×10^{-4} mol L^{-1}. It is noteworthy this is much lower than the concentration of uranium species observed in the SIXEP liquor.

4.37.3 Uptake of uranium by TMSPE modified materials

The uptake of uranium to the TMSPE modified minerals clinoptilolite, ZSM-5, vermiculite and kaolinite was investigated using the batch sorption methodology discussed in section 4.33.1. The results are shown in figure 4.44 and table 4.26.

Table 4.26 Uranium species uptake as a function of concentration on TMSPE grafted materials

Material	Clinoptilolite (NDA)		Clinoptilolite (Imerys)		ZSM-5		Vermiculite		Kaolinite	
Concentration	% removed	Error (+/-)	% removed	Error (+/-)	% removed	Error (+/-)	% removed	Error (+/-)	% removed	Error (+/-)
1×10^{-2}	12.0%	7.4%	50.9%	36.5%	7.1%	3.4%	36.1%	4.1%	28.0%	4.1%
1×10^{-4}	51.8%	1.8%	73.0%	4.6%	10.0%	4.2%	83.1%	2.0%	25.9%	2.9%
1×10^{-6}	91.0%	1.8%	92.3%	1.2%	65.8%	5.0%	91.1%	1.8%	77.9%	11.2%
1×10^{-8}	92.5%	2.3%	93.7%	0.9%	92.9%	3.0%	95.5%	0.1%	23.2%	3.1%
1×10^{-10}	94.3%	1.3%	96.0%	0.3%	93.3%	1.7%	96.0%	0.6%	29.7%	8.7%
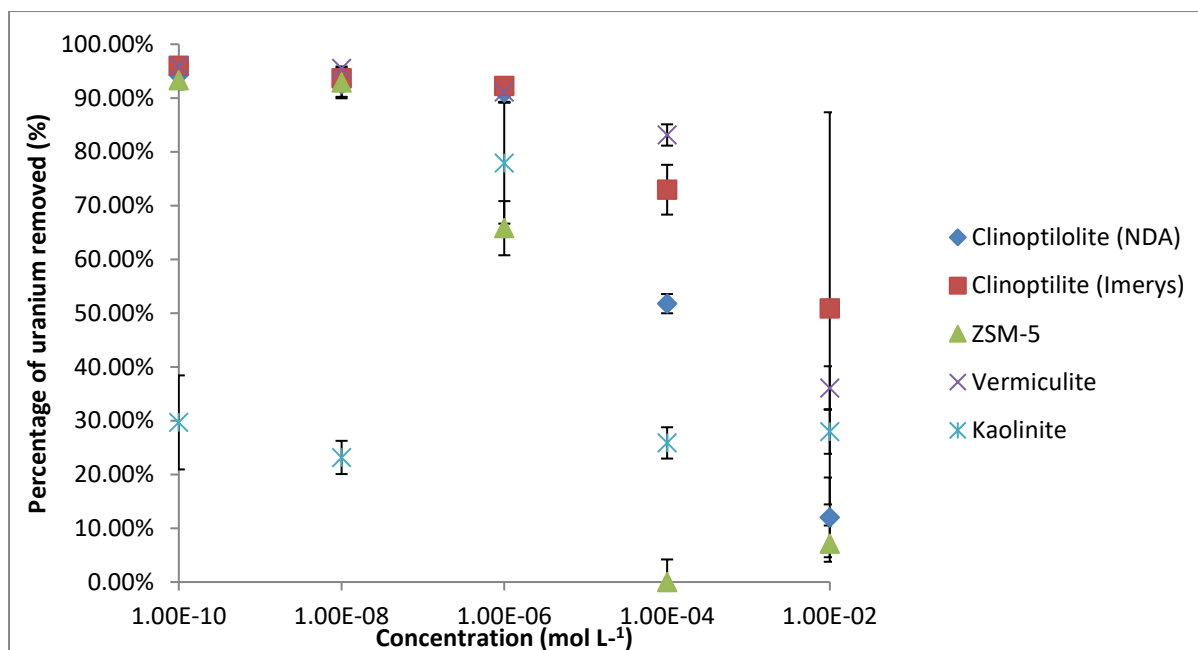
Figure 4.44 Uranium species uptake as a function of concentration on TMSPE grafted materials

The materials clinoptilolite (NDA), clinoptilolite (IMERYS), ZSM-5 and vermiculite all show an improvement after modification with TMSPE with saturation being seen between 1×10^{-4} and 1×10^{-6} mol L^{-1}. The kaolinite sample shows a decrease in the uptake of uranium, this could be due to the ligand from the modification hindering the removal of the uranium by the modified kaolinite.

4.37.4 Uptake of uranium by TMSPETT modified materials

The uptake of uranium to the TMSPETT modified minerals clinoptilolite, ZSM-5, vermiculite and kaolinite was investigated using the batch sorption methodology discussed in section 4.33.1. The results are shown in figure 4.45 and table 4.27.
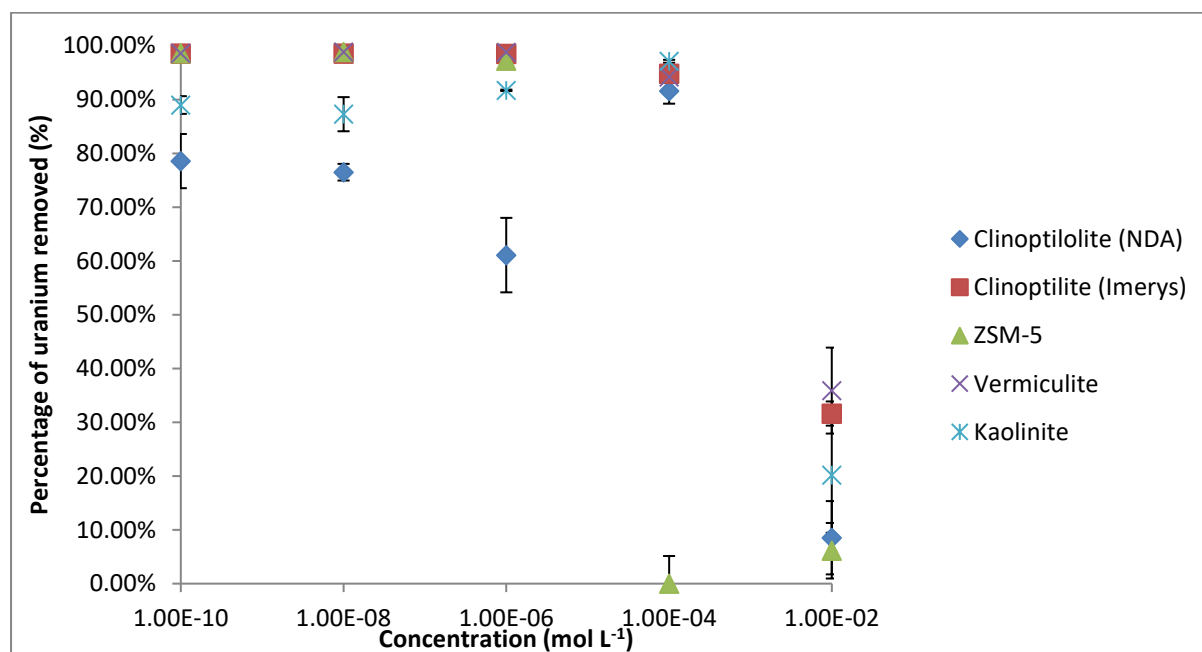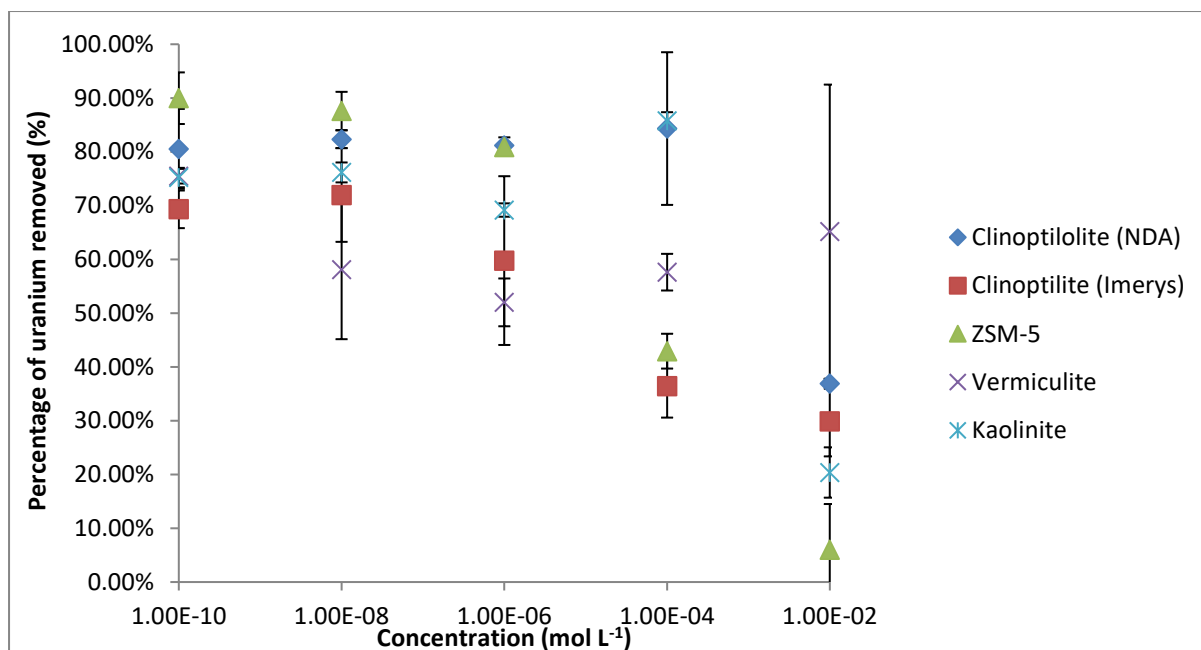
Figure 4.45: Uranium species uptake as a function of concentration on TMSPETT grafted materials

All materials show removal of uranium but to a lesser extent than the previous two ligands except in the case of kaolinite. TMSPETT modified kaolinite shows an increased removal of uranium at higher concentrations than the unmodified sample. Less grafting is seen with the TMSPETT ligand due to its size. Due to the chelating nature of the ligand more donor atoms are present per molecule and it is expected to very effective at retaining the species once bound.

Table 4.27: Uranium species uptake as a function of concentration on TMSPETT grafted materials.

Material	Clinoptilolite (NDA)		Clinoptilolite (Imerys)		ZSM-5		Vermiculite		Kaolinite	
Concentration	% removed	Error (+/-)	% removed	Error (+/-)	% removed	Error (+/-)	% removed	Error (+/-)	% removed	Error (+/-)
1×10^{-2}	36.9%	0.9%	29.9%	6.5%	29.9%	6.5%	65.1%	27.4%	20.4%	4.7%
1×10^{-4}	84.3%	14.2%	36.4%	5.8%	36.4%	5.8%	57.6%	3.4%	85.8%	1.6%
1×10^{-6}	81.1%	1.5%	59.8%	15.7%	59.8%	15.7%	52.0%	4.4%	69.2%	1.2%
1×10^{-8}	82.3%	1.6%	72.0%	8.7%	72.0%	8.7%	58.1%	12.9%	76.2%	1.9%
1×10^{-10}	80.5%	7.4%	69.3%	3.5%	69.3%	3.5%	75.5%	1.4%	75.2%	1.8%

4.38 Comparison of clinoptilolite (NDA) materials

The uptake of uranium to the unmodified and modified mineral clinoptilolite was investigated using the batch sorption methodology discussed in section 4.33.1. The results are shown in figure 4.46.

Figure 4.46: Uptake of uranium onto modified and unmodified clinoptilolite substrate with concentration

The modified materials show an increase in the removal of uranium with the TMSPE modified material showing the largest increase.

4.39 Comparison of clinoptilolite (Imerys) materials

The uptake of uranium to the unmodified and modified mineral clinoptilolite was investigated using the batch sorption methodology discussed in section 4.33.1. The results are shown in figure 4.47.

Figure 4.47: Uptake of uranium onto modified and unmodified clinoptilolite Imerys substrate with concentration

It can be seen from the above graph that the APTES modified clinoptilolite (IMERYS) shows the highest percentage removal of uranium. All ligands show an increase in the removal of uranium over the original ungrafted material.

4.40 Comparison of ZSM-5 materials

The uptake of uranium to the unmodified and modified ZSM-5 was investigated using the batch sorption methodology discussed in section 4.33.1. The results are shown in figure 4.48.
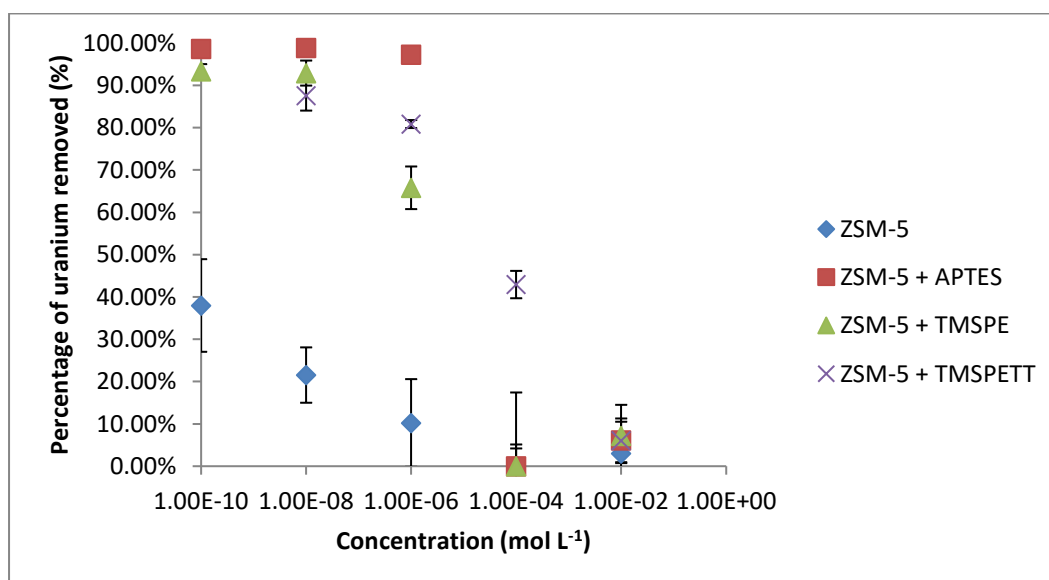
Figure 4.48: Uptake of uranium onto modified and unmodified ZSM5 substrate with concentration

It can be seen from the above graph that the APTES modified ZSM-5 shows the highest percentage removal of uranium. All ligands show an increase in the removal of uranium below 1×10^{-4} mol L^{-1}. This contrasts with the caesium and strontium uptake and demonstrates the difference between ion exchange and ligand sequestration.

4.41 Comparison of vermiculite materials

The uptake of uranium to the unmodified and modified vermiculite was investigated using the batch sorption methodology discussed in section 4.33.1. The results are shown in figure 4.49.
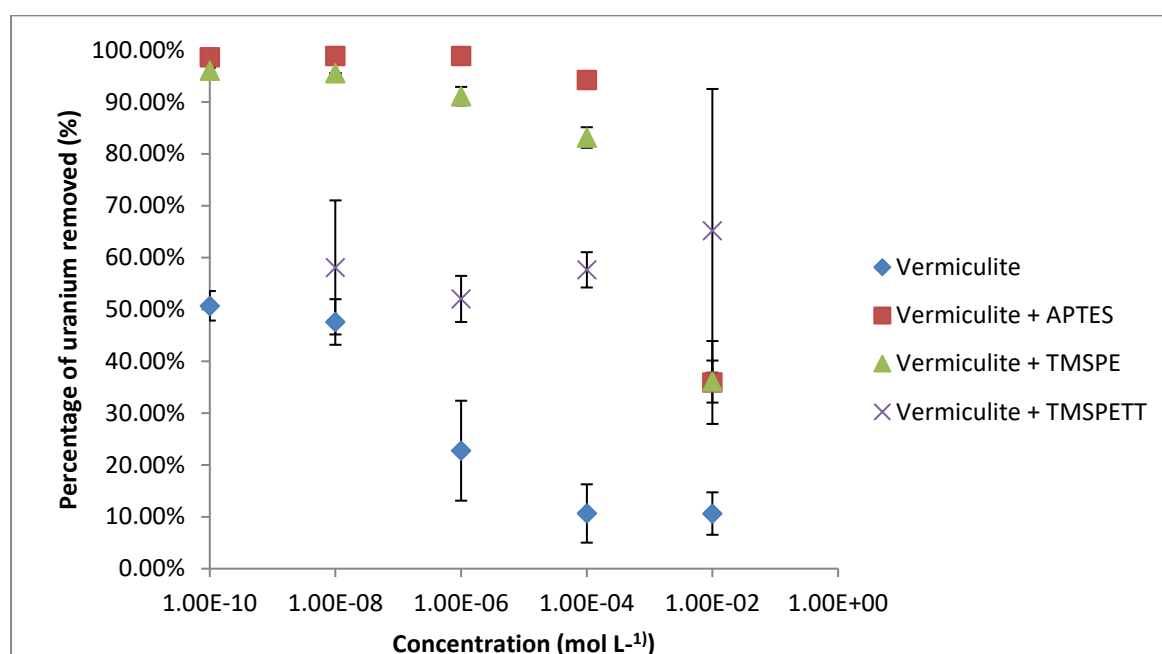

Figure 4.49: Uptake of uranium onto modified and unmodified vermiculite substrate with concentration

All the modified materials show an increase in uranium removal with the largest increase being seen in the APTES modified vermiculite.

4.42 Comparison of kaolinite materials

The uptake of uranium to the unmodified and modified kaolinite was investigated using the batch sorption methodology discussed in section 4.33.1. The results are shown in figure 4.50.
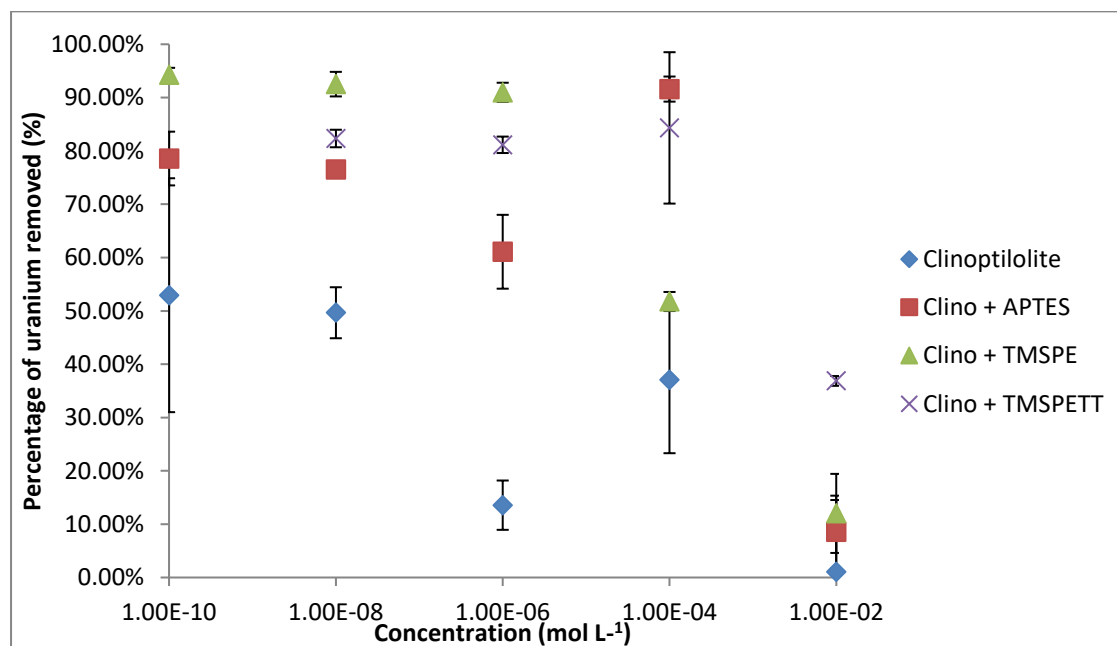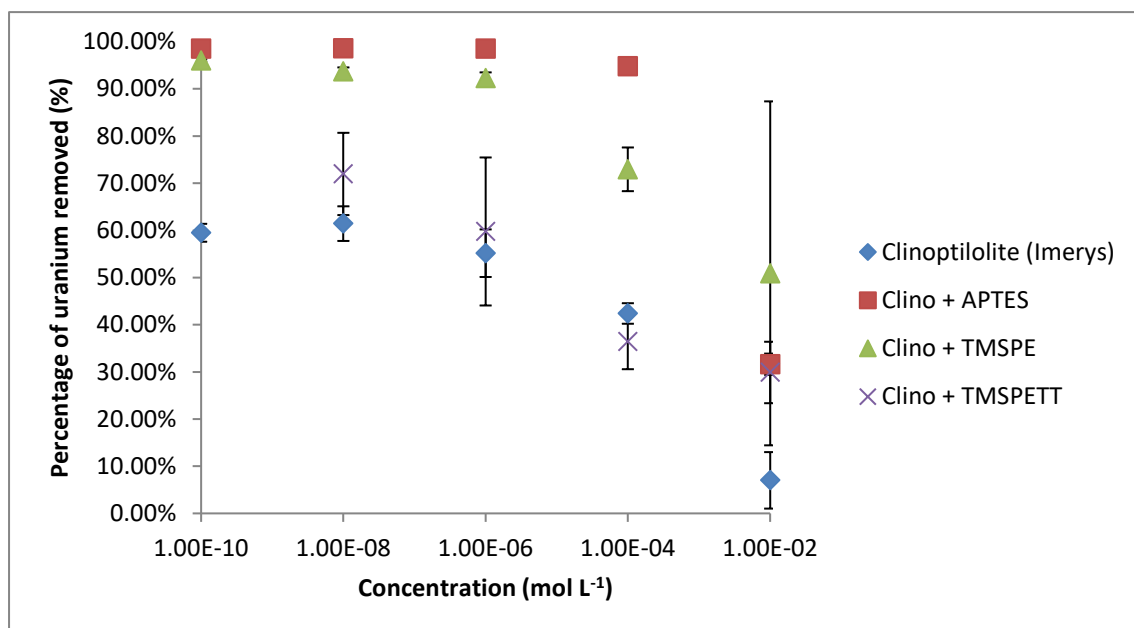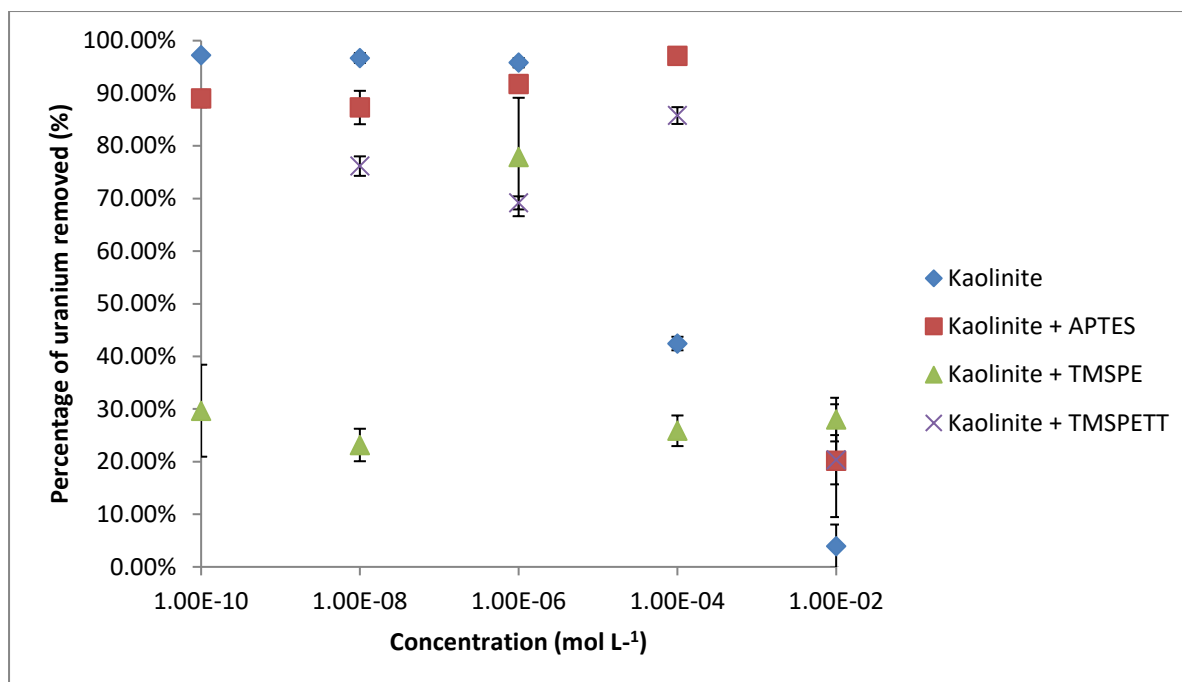
Figure 4.50: Uptake of uranium onto modified and unmodified kaolinite substrate with concentration

Kaolinite shows a decrease in uranium removal after modification. This may be due to the ligand blocking access to the surface. It is clear from these set of experiments that grafting improves the utility of the kaolinite. Kaolinite has no ion exchange capacity due to the absence of exchangeable, therefore the graft can only vehicle for the uranium removal.

4.43 Uranium desorption experiments

4.43.1 Desorption of uranium by unmodified materials

The desorption of uranium to the unmodified and modified materials was investigated using the batch sorption methodology discussed in section 4.33.2. The results are shown in table 4.28

Table 4.28: Desorption of uranium from the unmodified materials as a function of uranium concentration

Material	Clinoptilolite (NDA)		Clinoptilolite (Imerys)		ZSM-5		Vermiculite		Kaolinite	
Concentration	% desorbed	Error (+/-)	% desorbed	Error (+/-)	% desorbed	Error (+/-)	% desorbed	Error (+/-)	% desorbed	Error (+/-)
1×10^{-2}	63.3%	3.3%	15.8%	0.7%	8.1%	18.5%	1.6%	1.1%	32.5%	8.3%
1×10^{-4}	3.1%	2.1%	3.5%	4.5%	23.3%	29.8%	7.7%	2.6%	0.8%	0.3%
1×10^{-6}	1.6%	8.6%	1.5%	1.8%	10.7%	19.6%	2.3%	14.3%	0.8%	0.4%
1×10^{-8}	1.4%	1.1%	1.9%	0.9%	2.3%	0.9%	4.4%	1.3%	1.0%	0.2%

| 1 x 10⁻¹⁰ | 0.7% | 0.6% | 1.4% | 0.4% | 2.4% | 0.6% | 5.1% | 1.3% | 1.1% | 0.0% |

| **1 x 10⁻¹⁰** | 0.7% | 0.6% | 1.4% | 0.4% | 2.4% | 0.6% | 5.1% | 1.3% | 1.1% | 0.0% |

Higher levels of desorption are seen at the higher concentrations, this is due to there being more metal ions for desorption.

4.43.2 Desorption of uranium by APTES modified materials

The desorption of uranium to APTES modified materials was investigated using the batch sorption methodology discussed in section 4.33.2. The results are shown in table 4.29.

Table 4.29: Desorption of uranium from the materials modified with APTES as a function of uranium concentration

Material	Clinoptilolite (NDA)		Clinoptilolite (Imerys)		ZSM-5		Vermiculite		Kaolinite	
Concentration	% desorbed	Error (+/-)	% desorbed	Error (+/-)	% desorbed	Error (+/-)	% desorbed	Error (+/-)	% desorbed	Error (+/-)
1 x 10⁻²	8.5%	1.2%	8.00%	0.7%	13.7%	2.5%	11.2%	3.6%	11.8%	1.9%
1 x 10⁻⁴	0.1%	0.1%	0.2%	0.1%	0.5%	0.2%	0.0%	0.1%	0.1%	0.0%
1 x 10⁻⁶	0.0%	0.1%	0.1%	0.0%	0.1%	0.0%	0.1%	0.1%	0.0%	0.0%
1 x 10⁻⁸	0.1%	0.1%	0.2%	0.0%	0.2%	0.0%	0.2%	0.0%	0.1%	0.0%
1 x 10⁻¹⁰	0.1%	0.1%	0.2%	0.0%	0.2%	0.0%	0.2%	0.0%	0.2%	0.0%

Less desorption is seen in the APTES modified samples indicating that the ligand is removing metal ions and the interaction of the ligand and metal ions is stronger than the unmodified samples.

4.43.3 Desorption of uranium by TMSPE modified materials

The desorption of uranium to TMSPE modified materials was investigated using the batch sorption methodology discussed in section 4.33.2. The results are shown in table 4.30.

**Table 4.30: Desorption of uranium from the TMSPE modified materials as a function of uranium concentration**

Material	Clinoptilolite (NDA)		Clinoptilolite (Imerys)		ZSM-5		Vermiculite		Kaolinite	
Concentration	% desorbed	Error (+/-)	% desorbed	Error (+/-)	% desorbed	Error (+/-)	% desorbed	Error (+/-)	% desorbed	Error (+/-)
1 x 10⁻²	1.4%	0.2%	2.8%	0.6%	1.5%	0.5%	2.7%	1.0%	3.2%	0.3%
1 x 10⁻⁴	0.2%	0.0%	0.1%	0.1%	0.2%	0.2%	0.1%	0.2%	0.3%	0.1%
1 x 10⁻⁶	1.7%	0.8%	0.6%	0.1%	0.0%	0.1%	0.0%	0.2%	0.4%	0.1%
1 x 10⁻⁸	0.3%	0.1%	0.5%	0.0%	0.5%	0.0%	0.4%	0.0%	0.5%	0.0%

| 1 x 10^{-10} | 2.8% | 0.4% | 3.2% | 0.3% | 4.6% | 0.6% | 3.2% | 0.2% | 2.6% | 1.1% |

Less desorption is seen in the TMSPE modified samples compared to the unmodified species indicating that the ligand is removing metal ions and the interaction of the ligand and metal ions is stronger than with the unmodified samples. Furthermore TMSPE seems more successful in holding on to the uranium species than APTES, with much lower levels of desorption in all cases.

4.43.4 Desorption of uranium by TMSPETT modified materials

The desorption of uranium to TMSPETT modified materials was investigated using the batch sorption methodology discussed in section 4.33.2. The results are shown in table 4.31

Table 4.31: Desorption of uranium from the TMSPETT modified materials as a function of uranium concentration

Material	Clinoptilolite (NDA)		Clinoptilolite (Imerys)		ZSM-5		Vermiculite		Kaolinite	
Concentration	% desorbed	Error (+/-)	% desorbed	Error (+/-)	% desorbed	Error (+/-)	% desorbed	Error (+/-)	% desorbed	Error (+/-)
1 x 10^{-2}	0.8%	0.1%	1.6%	0.3%	0.9%	0.3%	1.4%	0.5%	1.8%	0.2%
1 x 10^{-4}	0.5%	0.1%	0.9%	1.0%	4.0%	5.7%	5.4%	8.7%	2.3%	0.9%
1 x 10^{-6}	1.0%	3.3%	3.2%	0.4%	0.3%	2.9%	0.2%	1.8%	1.4%	0.3%
1 x 10^{-8}	0.3%	0.7%	2.9%	0.2%	4.0%	0.3%	2.5%	0.3%	1.8%	0.1%
1 x 10^{-10}	0.7%	0.4%	3.1%	0.3%	4.5%	0.6%	3.0%	0.2%	2.5%	1.1%

TMSPETT seems even more effective at retaining the uranium than the previous two ligands. The chelating nature of the ligand with multiple donors means it is more difficult to remove the uranium from this ligand once it is sequesterd.

4.44 Kinetic experimental results

4.44.1 Rate of uptake of uranium by unmodified materials

The rate of uptake of uranium to the unmodified and modified materials was investigated using the kinetic batch sorption methodology discussed in section 4.33.3. The results are shown in figure 4.51 and tabulated in table 4.32.

Figure 4.51 Kinetic experiment showing uptake of uranium as a function of time for unmodified materials

The rate of uptake of the samples shows that both clinoptilolite samples and ZSM-5 reach saturation at about 7 days where as the clay samples see an increase in removal up to the 28 days. This is due to the layered nature of the clays, vermiculite has a large shrink/swell capacity and therefore swells to accommodate the ions whereas the rigid zeolite structure does not need this step due to the channel structure. The delay may be a result of the layers needing to swell before large ions can be accommodated between the layers.

Table 4.32 Kinetic experiment showing uptake of uranium as a function of time for unmodified materials

Material	Clinoptilolite (NDA)		Clinoptilolite (Imerys)		ZSM-5		Vermiculite		Kaolinite	
Time (days)	% removed	Error (+/-)	% removed	Error (+/-)	% removed	Error (+/-)	% removed	Error (+/-)	% removed	Error (+/-)
0.04	23.9%	6.8%	39.9%	5.2%	14.7%	9.8%	54.6%	10.4%	12.2%	14.0%
1	14.5%	4.8%	59.8%	6.7%	6.0%	8.1%	92.0%	0.4%	20.7%	3.8%
7	18.4%	1.0%	93.7%	5.1%	0.9%	3.2%	96.3%	1.0%	30.2%	0.3%
14	35.2%	4.6%	98.8%	0.2%	2.3%	1.5%	96.2%	0.5%	38.2%	9.8%
28	40.9%	2.7%	98.0%	0.4%	7.5%	8.5%	96.9%	0.7%	31.5%	5.1%

4.44.2 Rate of uptake of uranium by APTES modified materials

The rate of uptake of uranium to the APTES modified materials was investigated using the kinetic batch sorption methodology discussed in section 4.33.3. The results are shown in figure 4.52 and tabulated in table 4.33.

Figure 4.52 Kinetic experiment showing uptake of uranium as a function of time for APTES modified materials

Table 4.33 Kinetic experiment showing uptake of uranium as a function of time for APTES modified materials

Material	Clinoptilolite (NDA)		Clinoptilolite (Imerys)		ZSM-5		Vermiculite		Kaolinite	
Time (days)	% removed	Error (+/-)	% removed	Error (+/-)	% removed	Error (+/-)	% removed	Error (+/-)	% removed	Error (+/-)
0.04	56.4%	5.1%	56.9%	3.2%	10.3%	1.7%	66.9%	6.3%	26.4%	4.0%
1	49.2%	3.6%	53.5%	7.1%	5.8%	2.5%	68.7%	2.0%	0.0%	2.0%
7	63.7%	2.4%	70.8%	1.4%	25.7%	6.3%	68.7%	2.4%	30.8%	3.9%
14	59.5%	3.2%	74.3%	0.5%	17.4%	2.7%	73.3%	3.6%	23.2%	2.3%
28	62.0%	4.0%	73.5%	2.6%	11.2%	4.7%	59.8%	3.4%	14.8%	2.4%

The modified samples show a quicker uptake than the unmodified samples, suggesting that the ligand is interacting with the uranium species. Clinoptilolite (IMERYS) and vermiculite show the quickest uptake reaching saturation at one and seven days respectively.

4.44.3 Rate of uptake of uranium by TMSPE modified materials

The rate of uptake of uranium to the TMSPE modified materials was investigated using the kinetic batch sorption methodology discussed in section 4.33.3. The results are shown in figure 4.53 and tabulated in table 4.34
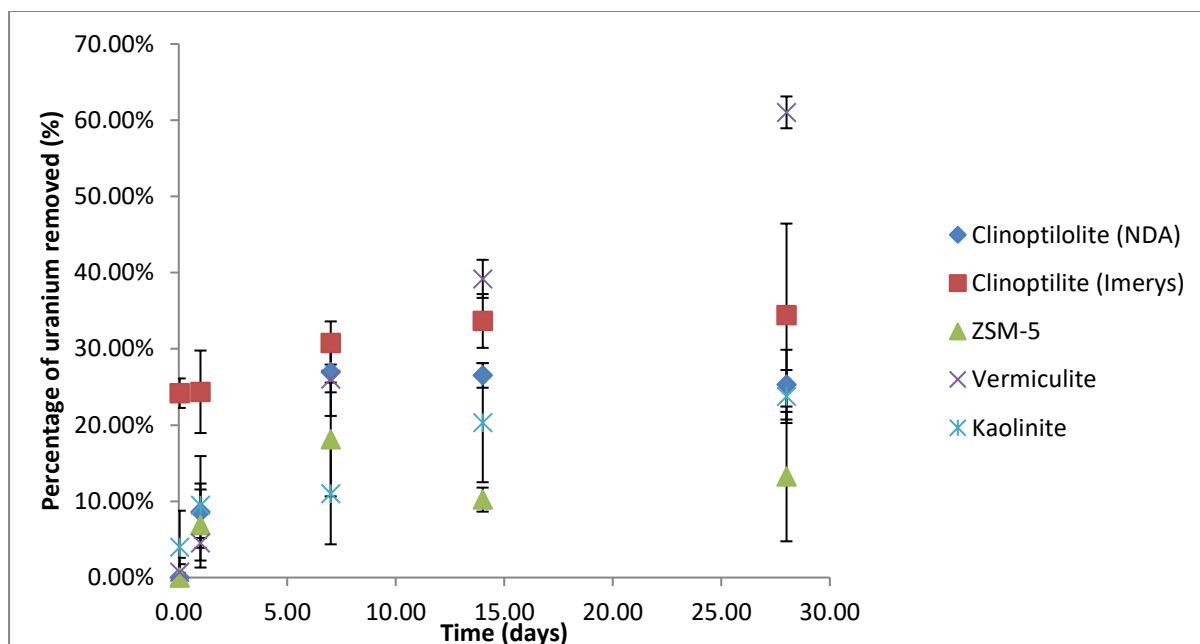
.

Figure 4.53 Kinetic experiment showing uptake of uranium as a function of time for TMSPE modified materials

Table 4.34 Kinetic experiment showing uptake of uranium as a function of time for TMSPE modified materials

Time (days)	% removed	Error (+/-)	% removed	Error (+/-)	% removed	Error (+/-)	% removed	Error (+/-)	% removed	Error (+/-)
0.04	7.2%	7.2%	14.9%	7.4%	0.0%	2.6%	9.4%	6.0%	4.5%	3.1%
1	18.7%	7.0%	22.6%	7.9%	3.3%	5.2%	40.5%	3.6%	11.7%	2.5%
7	31.7%	2.6%	40.2%	1.4%	0.3%	4.1%	89.0%	2.0%	18.0%	2.6%
14	30.3%	1.9%	35.9%	2.0%	0.0%	5.7%	95.3%	1.7%	17.7%	4.4%
28	44.0%	1.6%	43.5%	3.4%	0.5%	3.9%	97.5%	1.7%	15.0%	3.0%

The TMSPE modified materials show the least affect in the rate of uptake with time, but show the largest increase in the removal of uranium in the case of clinoptilolite (IMERYS).

4.44.4 Rate of uptake of uranium by TMSPETT modified materials

The rate of uptake of uranium to the TMSPETT modified materials was investigated using the kinetic batch sorption methodology discussed in section 4.33.3. The results are shown in figure 4.54 and tabulated in table 4.35.
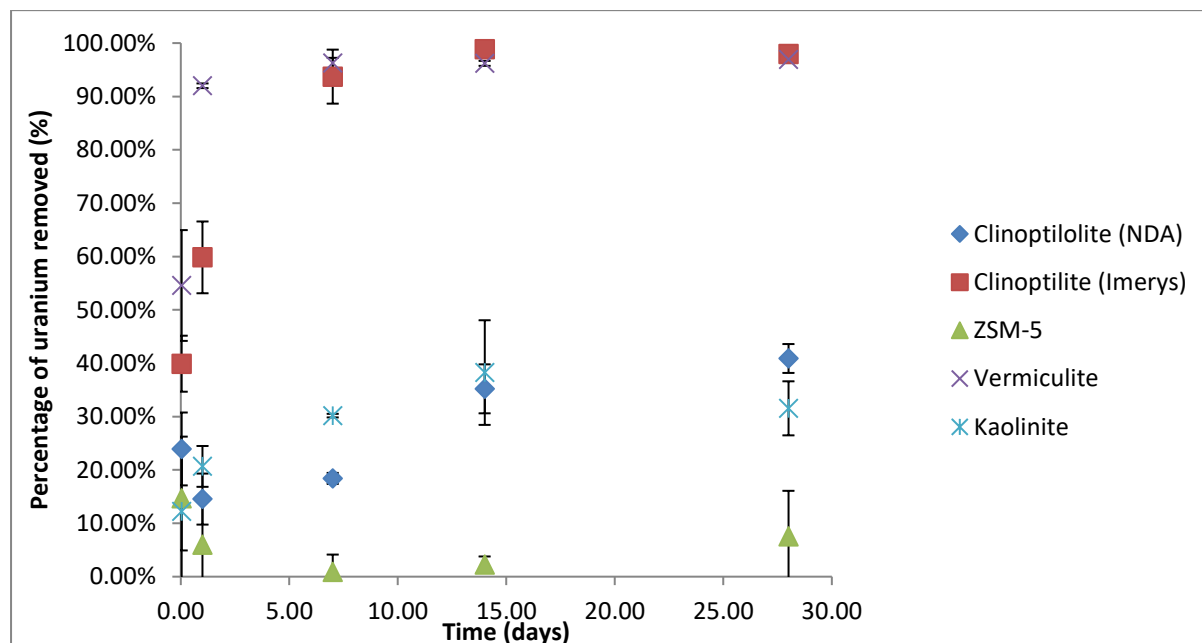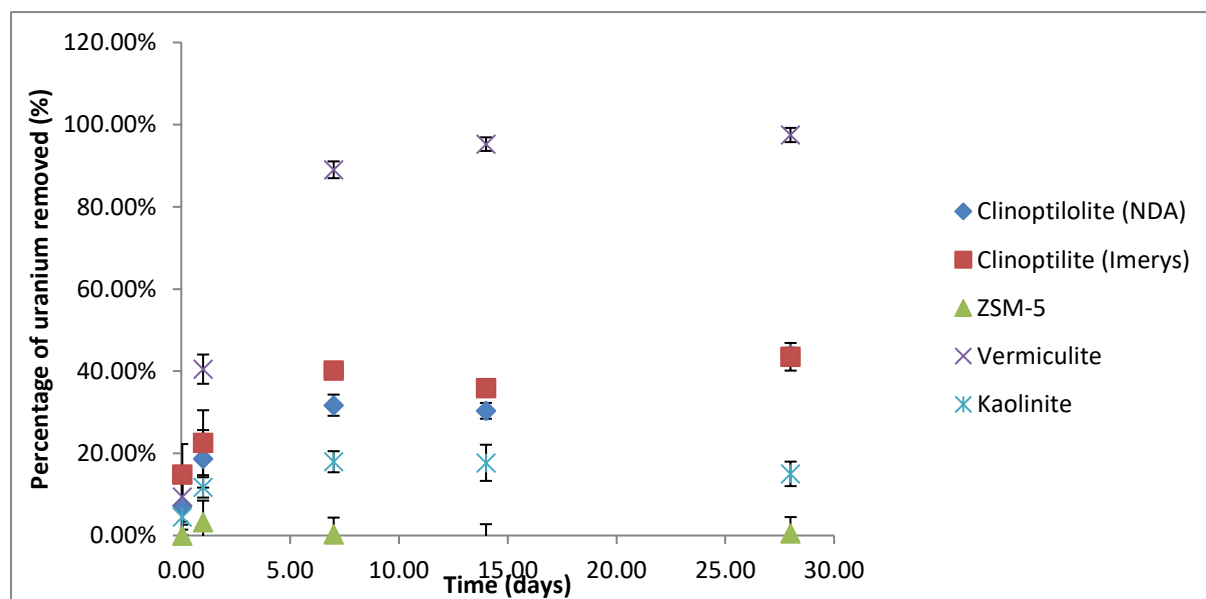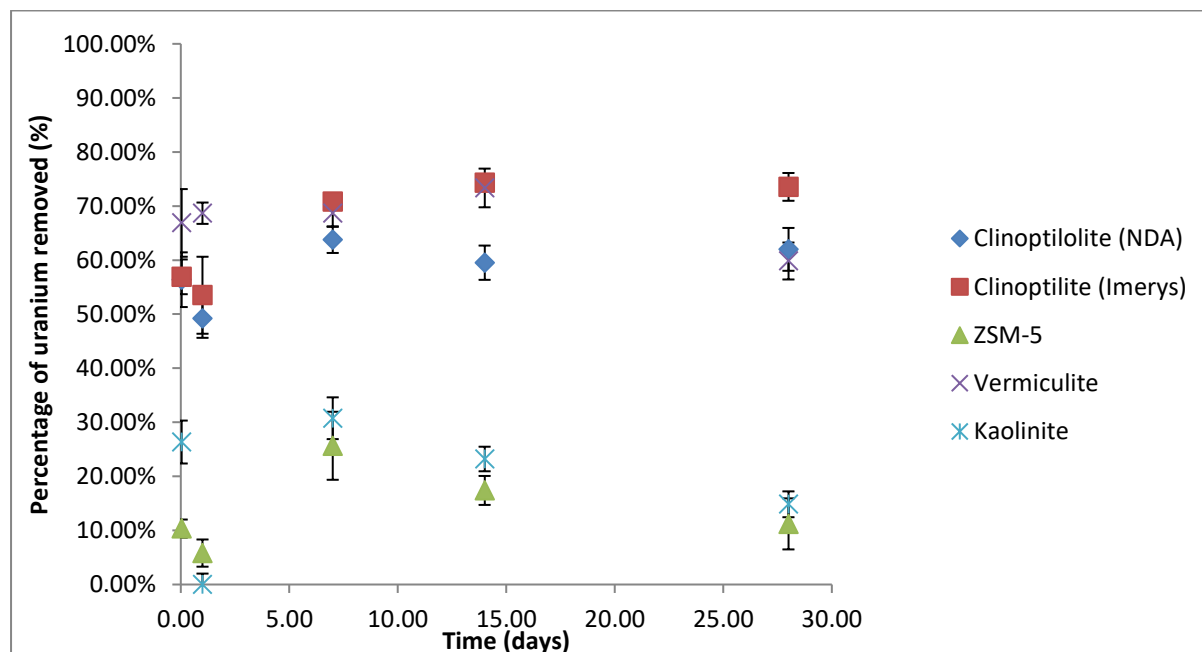

Figure 4.54 Kinetic experiment showing uptake of uranium as a function of time for TMSPETT modified materials

Table 4.35 Kinetic experiment showing uptake of uranium as a function of time for TMSPETT modified materials

Material	Clinoptilolite (NDA)		Clinoptilolite (Imerys)		ZSM-5		Vermiculite		Kaolinite	
Time (days)	% removed	Error (+/-)	% removed	Error (+/-)	% removed	Error (+/-)	% removed	Error (+/-)	% removed	Error (+/-)
0.04	56.4%	5.1%	56.9%	3.2%	10.3%	1.7%	66.9%	6.3%	26.4%	4.0%
1	49.2%	3.6%	53.5%	7.1%	5.8%	2.5%	68.7%	2.0%	0.0%	2.0%
7	63.7%	2.4%	70.8%	1.4%	25.7%	6.3%	68.7%	2.4%	30.8%	3.9%
14	59.5%	3.2%	74.3%	0.5%	17.4%	2.7%	73.3%	3.6%	23.2%	2.3%
28	62.0%	4.0%	73.5%	2.6%	11.2%	4.7%	59.8%	3.4%	14.8%	2.4%

An increased rate of removal is seen in the TMSPETT modified materials, with the greatest increase seen in the modified vermiculite.

4.45 Comparison of clinoptilolite (NDA) materials

The rate of uptake of uranium to the unmodified and modified mineral clinoptilolite was investigated using the kinetic batch sorption methodology discussed in section 4.33.3. The results are shown in figure 4.55.

Figure 4.55: Comparison of uranium removal by unmodified and modified clinoptilolite (NDA) over time

It can be seen that in most cases the rate of uptake of the metal ion increases with the modification of the materials. With the TMSPETT modified sample showing the largest increase in the rate of removal reaching the saturation point within one hour. This indicated that the ligands are removing the metal ions from solution.

4.46 Comparison of clinoptilolite (Imery) materials

The rate of uptake of uranium to the unmodified and modified mineral clinoptilolite was investigated using the kinetic batch sorption methodology discussed in section 4.33.3. The results are shown in figure 4.56.

**Figure 4.56: Comparison of uranium removal by unmodified and modified clinoptilolite (Imerys) over time**

As seen with the clinoptilolite (NDA) materials the modified materials show an increase in the rate of uranium removal. APTES modified clinoptilolite shows the largest removal reaching saturation in 7 days, with the TMSPETT ligand again showing the largest change in the rate of uptake after one hour.

4.47 Comparison of ZSM-5 materials

The rate of uptake of uranium to the unmodified and modified material ZSM-5 was investigated using the kinetic batch sorption methodology discussed in section 4.33.3. The results are shown in figure 4.57.
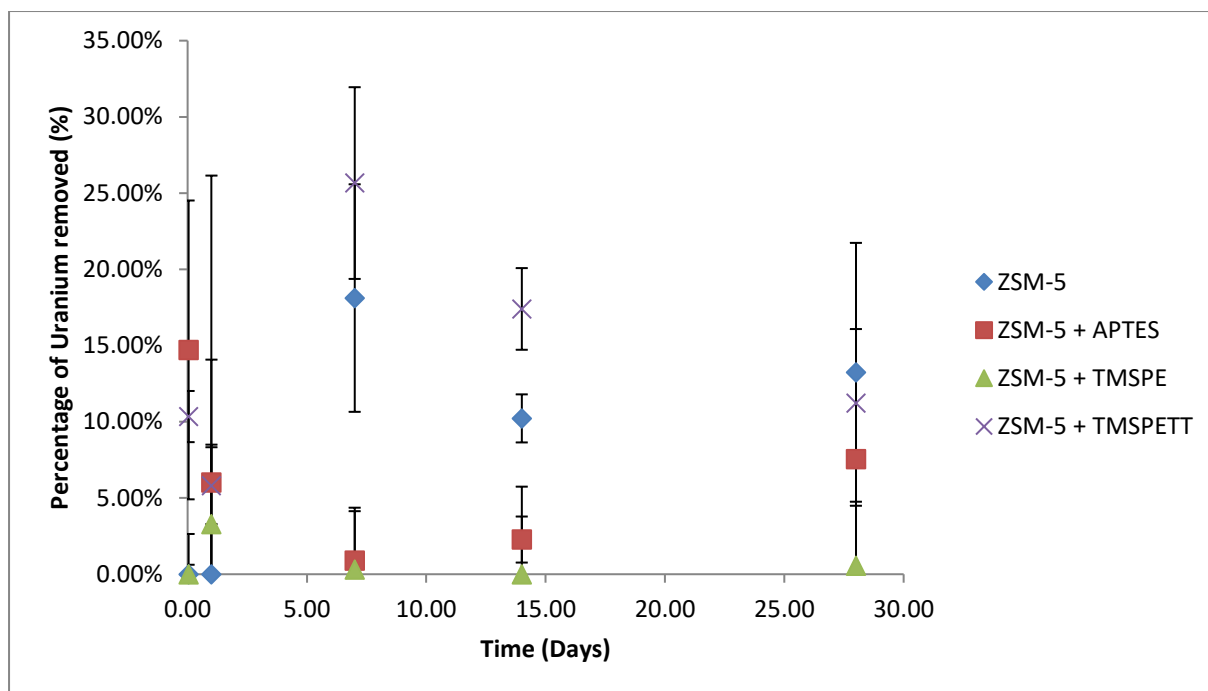
Figure 4.57: Comparison of uranium removal by unmodified and modified ZSM5 over time

The modified samples show quicker uptake to begin with but due to the low amount of graft the overall amount removed remains low.

4.48 Comparison of vermiculite materials

The rate of uptake of uranium to the unmodified and modified mineral vermiculite was investigated using the kinetic batch sorption methodology discussed in section 4.33.3. The results are shown in figure 4.58.
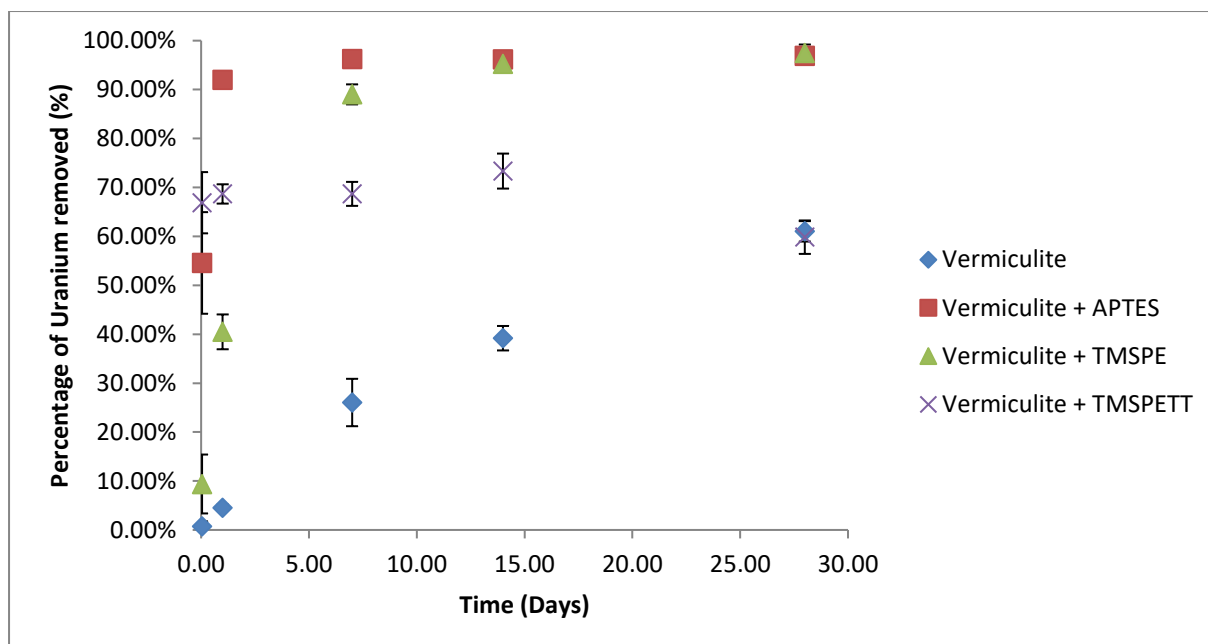
Figure 4.58: Comparison of uranium removal by unmodified and modified vermiculite over time

The modified samples show a quicker uptake in all cases with the percentage removed increased as well. This shows that the ligand is removing the uranium from solution with APTES and TMSPETT reaching saturation within 24 hours.

4.49 Comparison of kaolinite materials

The rate of uptake of uranium to the unmodified and modified mineral kaolinite was investigated using the kinetic batch sorption methodology discussed in section 4.33.3. The results are shown in figure 4.59.

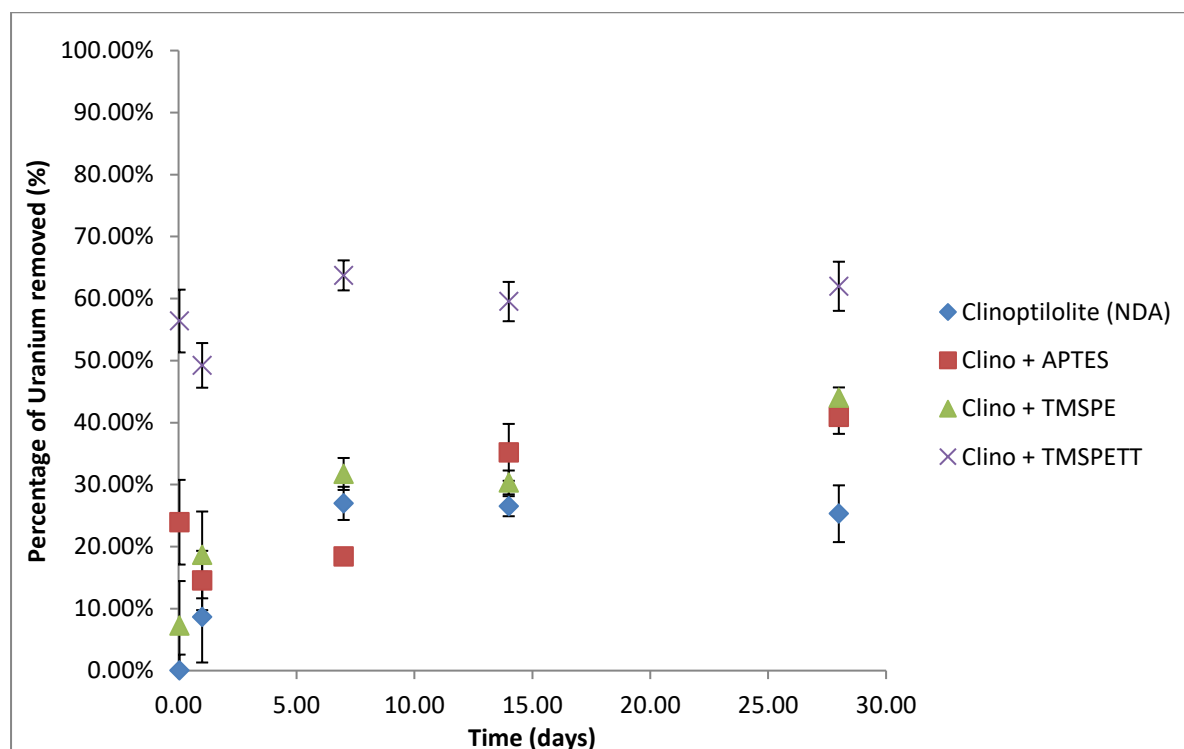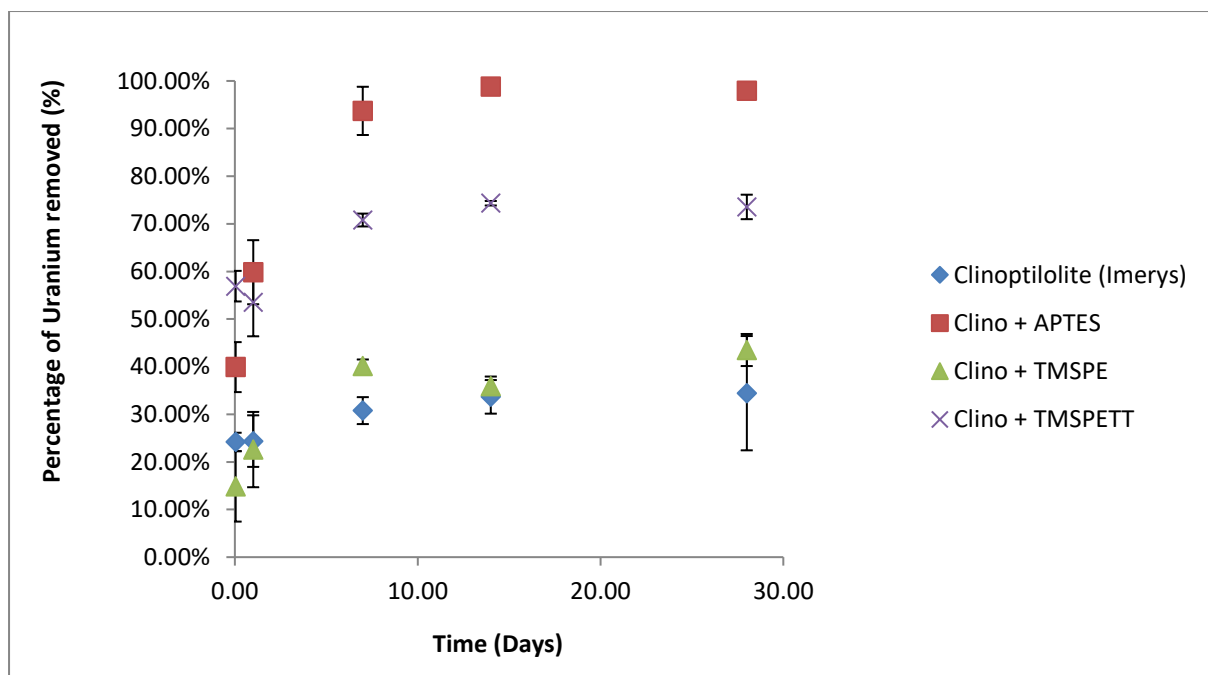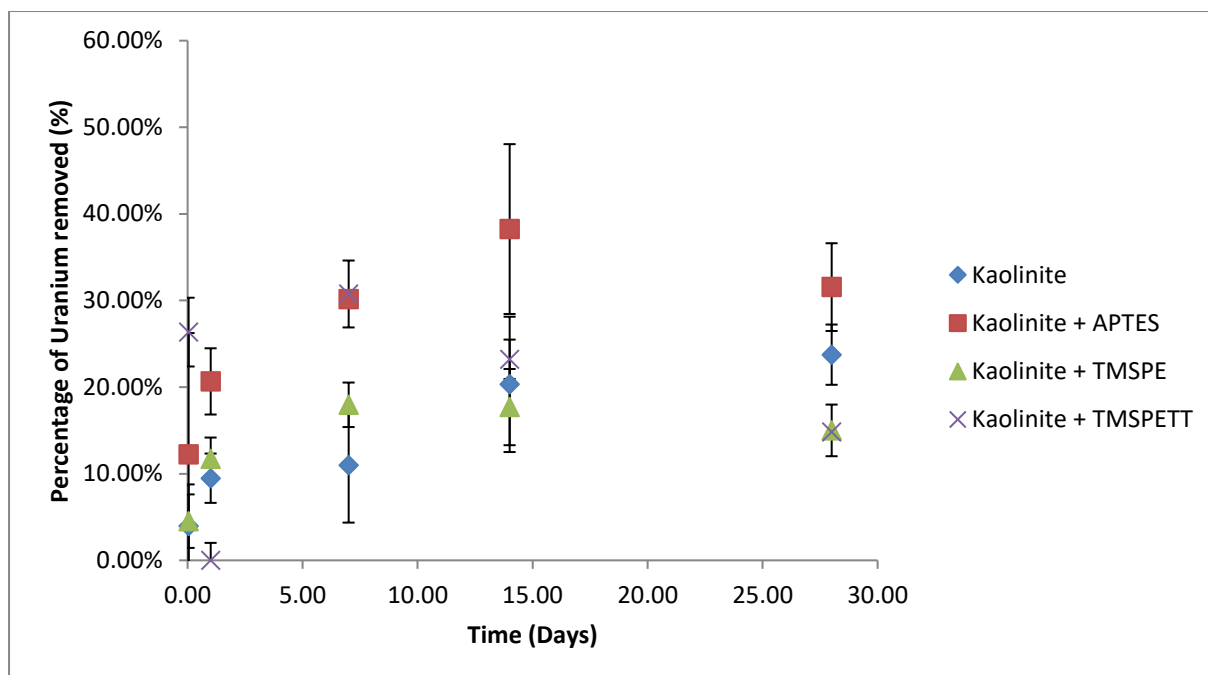**Figure 4.59: Comparison of uranium removal by unmodified and modified kaolinite over time**

The modified materials show a quicker uptake of the uranium ion with the TMSPETT modified material showing the quickest uptake. This again suggests the ligand is removing the uranium species.

4.50 Uranium sorption summary

The effect of uranium uptake by the materials Clinoptilolite (NDA), clinoptilolite (Imerys), ZSM-5, vermiculite and kaolinite before and after modification with the organic ligands APTES, TMSPE and TMSPETT were investigated. Experiments were conducted to study the amount and rate of uranium uptake by the materials.

An increase in uranium sorption was observed for all materials apart from kaolinite. This can be attributed to the mechanism of sorption to kaolinite where the process is physisorption and not ion exchange. The greatest increase in sorption was seen for APTES grated materials, the sorption was not readily reversible, suggesting a strong chemical interaction between the ligand and the ion. The rate of uptake increased in all cases which suggests that the mechanism is chemisorption by the ligand and not ion exchange.

4.51 Experimental methodology for plutonium experiments

The sequestration capacity of the materials used has been investigated radiometrically using batch sorption studies at varying amounts of solid and carrier solution taking care to keep the same solid to liquid ratio. The sorption experiments were conducted in 15 mL plastic sample tubes with ^{239}Pu as the radioactive species. The samples were shaken to encourage equilibrium between the solid and liquid to be reached, the samples were separated by centrifugation at 6000 rpm for 10 minutes and a 2 mL aliquot taken. The samples were counted using a Packard TRI-carb 2100tr liquid scintillation counter. The amount of metal ions removed from solution was calculated using mass balance calculations to compare the activities of the solutions before and after being exposed to the solid surface. All experiments were carried out in triplicate and under ambient conditions. Method used for determining percentage sorbed same as previously mentioned in section 4.1.

The kinetic experiments were carried out using the same experimental methodology and calculations for different time periods. The kinetic experiments were carried out using 2 mL of a plutonium stock solution, with an activity of 4 kBq mL^{-1}.

4.51.1 Batch sorption experiments

0.01, 0.025, 0.05, 0.075 or 0.1 g of solid was weighed out in to a 15 mL plastic centrifuge tube; to this 9, 7.5, 5, 2.5 or 1ml of carrier solution was added and 8 kBq of ^{239}Pu was added. The batch sorption experiments were set up in replicates of three. A range of concentrations from 10^{-2} to 10^{-10} mol L^{-1} were used to investigate the sequestration capacity of the materials before and after modification. The experimental set- up used for sorption, desorption and kinetic experiments can be seen in figure 4.1. The samples were shaken for 7 days then separated by centrifugation at 6000 rpm for 10 minutes and a 2 mL aliquot taken. The samples were counted using a Packard TRI-carb 2100tr liquid scintillation counter.

4.51.2 Kinetic experiments

0.025 g of solid was weighed out in to a plastic tube; to this 2 mL of a plutonium stock solution, with an activity of 4 kBq mL^{-1} was added. The kinetic experiments were set up in replicates of three. Times of one hour, one day, one week, two weeks and four weeks were used to investigate the speed of the sequestration of the materials before and after modification. The samples were shaken and at the set time intervals. The samples were separated by centrifugation at 6000 rpm for 10 minutes and a 2 mL aliquot taken. The samples were counted using a Packard TRI-carb 2100tr liquid scintillation counter.

4.52 Preliminary work

The ^{239}Pu stock used was determined to have an activity of 515 Bq µl^{-1}. This was determined by placing 50 µl of ^{239}Pu into a scintillation vial with 10 mL of scintillation fluid and measuring by liquid scintillation counting.

The possibility of using natural uranium as a carrier solution was investigated; the spectrum is shown below in figure 4.60.
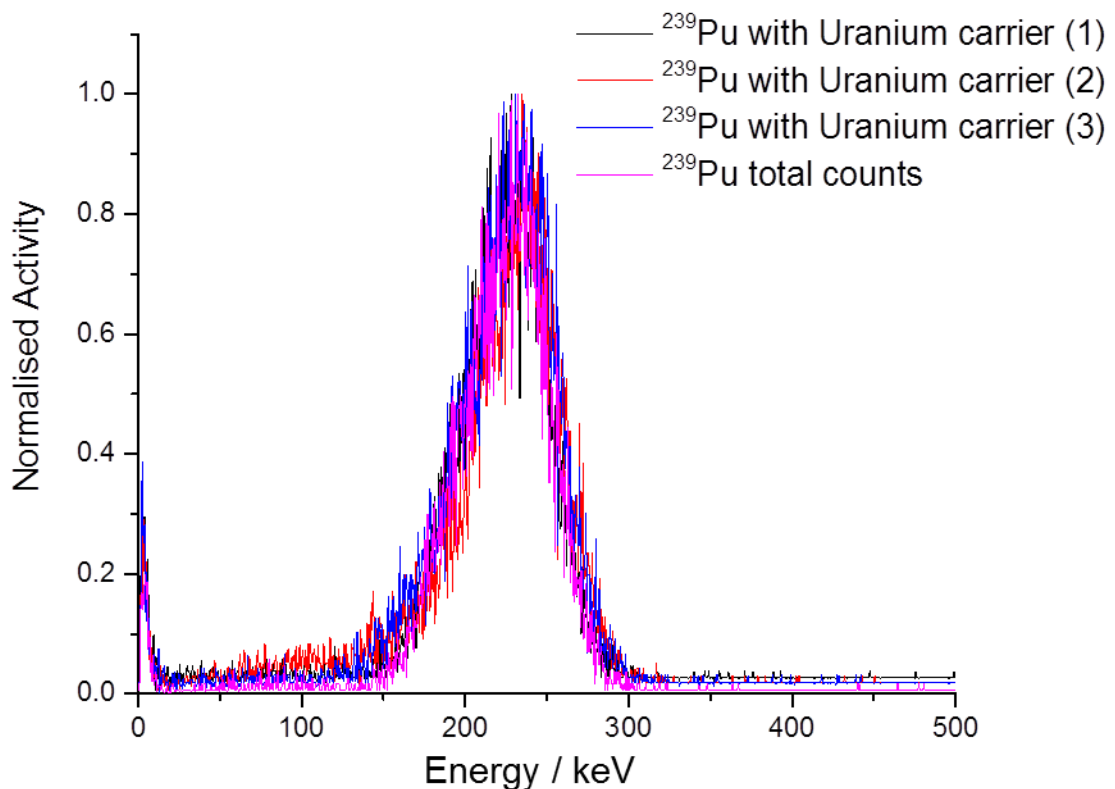
Figure 4.60 Liquid scintillation counting spectrum of Pu

The spectrum shown in figure 4.60 shows that ^{239}Pu is detectable using liquid scintillation counting and a single peak was observed at 291 keV. The ability of natural uranium to act as a carrier was investigated as there is no plutonium isotope that is viable to use as a carrier solution.

$$R_s = \left(\frac{2DZ}{w_i + w_j} \right),$$

Where ΔZ = Separation between peaks

W_i + W_j = peak width at half height of the respective peaks

$$\frac{2 * 35}{(41.0 + 34.5)} = 0.93$$

To be fully resolved R must be greater than 1.5 as shown above in equation 4.5 this is not the case and therefore natural uranium cannot be used as a carrier solution. Sodium perchlorate ($NaClO_4$) was selected as a carrier solution as the sodium ions are expected to block the sites the plutonium may stick to and perchlorate is a non-complexing counter ion.

The linearity of plutonium counting by liquid scintillation counting over the range of plutonium concentrations expected in the experiments was studied. A plot of which is shown below in figure 4.61.
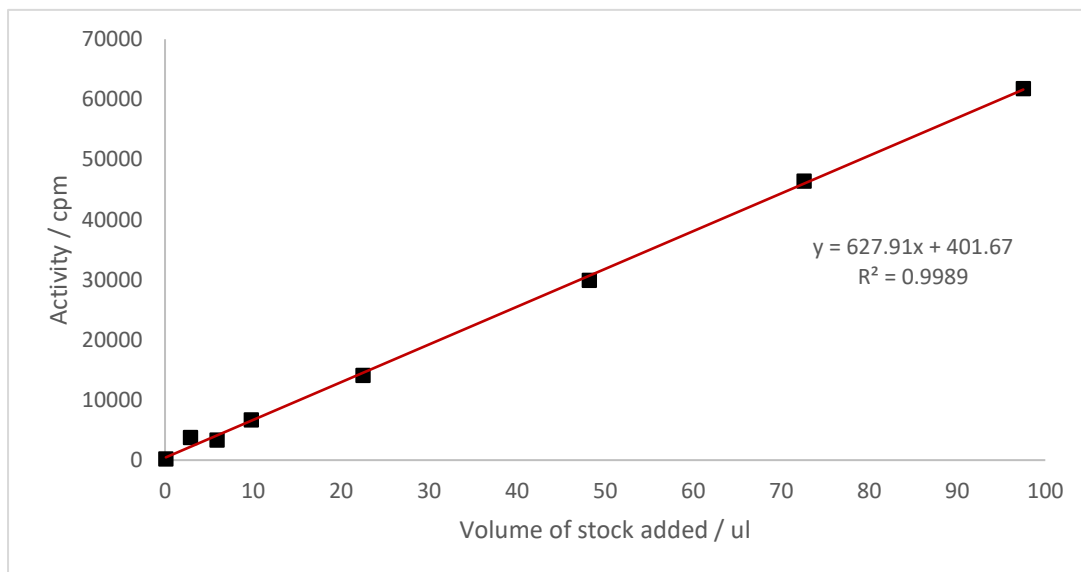
Figure 4.61 linear dynamic range of plutonium by liquid scintillation counting

The plot shows that the concentration range is within the linear dynamic range of the instrument for the activity range required. The effect of quenching was investigated and determined not to be of significance through analysis of the pulse height spectra.

4.53 Plutonium experimental results

4.53.1 Batch sorption experimental results

The uptake of plutonium to unmodified and modified clinoptilolite (NDA) and vermiculite was investigated using the batch sorption methodology using sodium perchlorate as a carrier discussed in section 4.48.1. The results are shown in figure 4.62 and table 4.33.
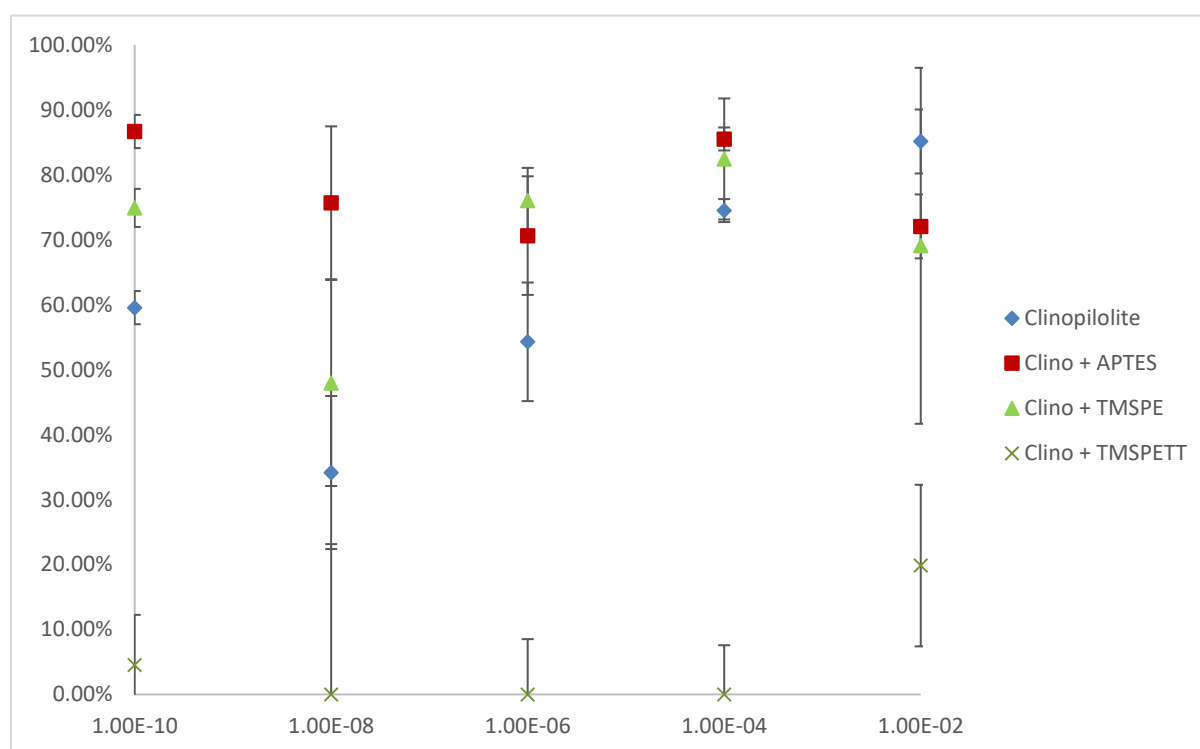
Figure 4.62 Batch sorption experiments on grafted and ungrafted clinoptilolite NDA

It can be seen from the results above that the APTES and TMSPE modified samples show an increase in the uptake of plutonium suggesting that the ligand is interacting with the plutonium species.

Concentration	Clinoptilolite (NDA)		Clinoptilolite + APTES		Clinoptilolite + TMSPE		Clinoptilolite + TMSPETT	
	% removed	Error (+/-)	% removed	Error (+/-)	% removed	Error (+/-)	% removed	Error (+/-)
1×10^{-2}	85.1%	4.9%	72.1%	18.5%	69.1%	27.4%	19.8%	12.4%
1×10^{-4}	74.5%	1.8%	85.5%	1.1%	82.4%	9.3%	0.0%	7.6%
1×10^{-6}	54.3%	9.1%	70.6%	3.0%	76.0%	5.0%	0.0%	199.9%
1×10^{-8}	34.2%	11.8%	75.7%	6.6%	48.0%	15.9%	0.0%	23.1%
1×10^{-10}	59.6%	2.6%	86.7%	4.6%	74.9%	2.9%	4.5%	71.7%
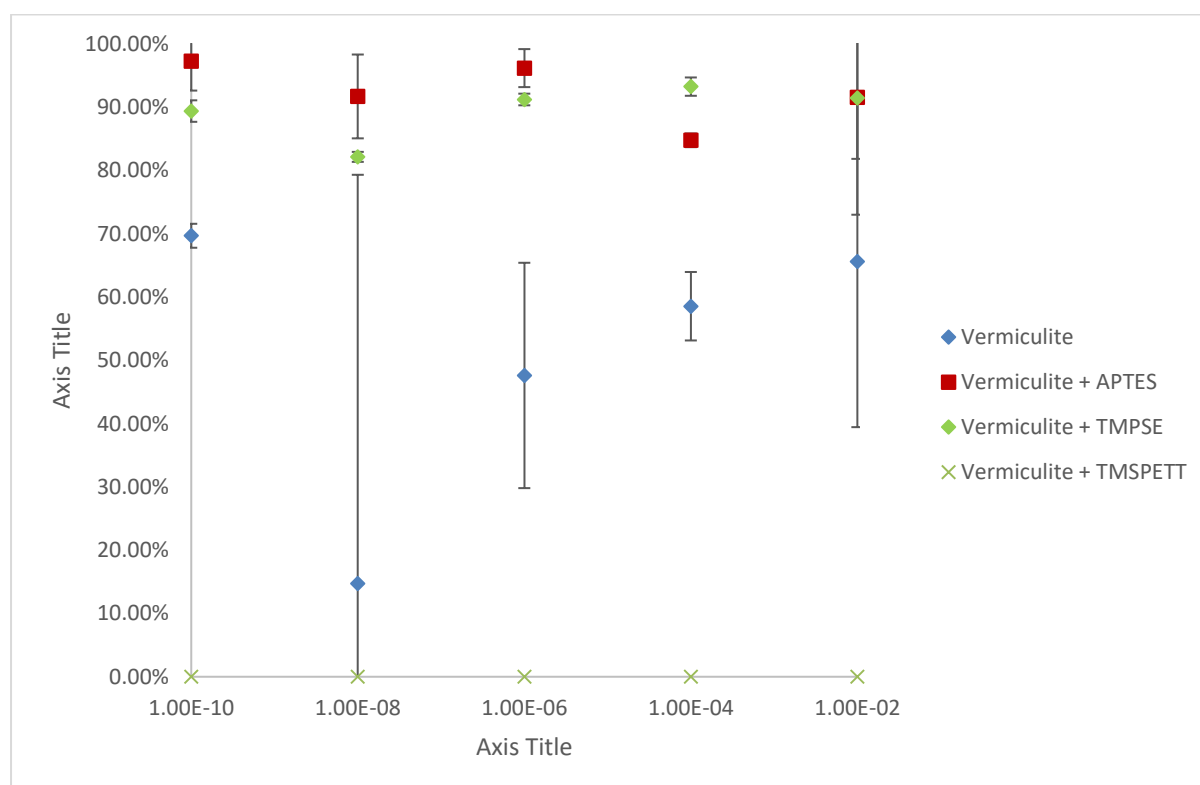
Figure 4.63: Batch sorption experiments on grafted and ungrafted vermiculite

As seen previously with the clinoptilolite (NDA), the vermiculite samples modified with APTES and TMSPE modified show an increase in the uptake of plutonium supporting that the ligand is interacting with the plutonium.

Table 4.34: Batch sorption experiments on grafted and ungrafted vermiculite

Concentration	Vermiculite		Vermiculite + APTES		Vermiculite + TMSPE		Vermiculite + TMSPETT	
	% removed	Error (+/-)	% removed	Error (+/-)	% removed	Error (+/-)	% removed	Error (+/-)
1×10^{-2}	65.6%	26.2%	91.5%	4.7%	91.5%	9.6%	0.0%	298.5%
1×10^{-4}	58.5%	5.4%	84.8%	8.8%	93.2%	1.4%	0.0%	27.4%
1×10^{-6}	47.6%	17.8%	96.2%	1.6%	91.2%	0.9%	0.0%	37.4%
1×10^{-8}	14.7%	64.6%	91.7%	6.6%	82.1%	0.8%	0.0%	7.5%
1×10^{-10}	69.7%	1.9%	97.2%	1.8%	89.4%	1.7%	0.0%	8.2%

4.53.2 Using sodium hydroxide as a carrier

The uptake of plutonium to unmodified and modified clinoptilolite (NDA) and vermiculte was investigated using the batch sorption methodology as discussed in section 4.48.1. in order to experiment closer to the conditions of the SIXEP plant 0.01 mol L^{-1} sodium hydroxide solution at a pH of 11.5 was purged with carbon dioxide to the reduce the pH of the solution to pH7. This solution was then used in place of the sodium perchlorate discussed in section 4.50.1. Determination of the percentage sorbed was calculated relative to a control where no solid was present to check for precipitation and wall sorption. The results are shown in table 4.35.

Table 4.35 Grafting of clinoptilolite and vermiculite using a sodium hydroxide solution.

Ligand	Clinoptilolite (NDA)		Vermiculite	
	% removed	error (+ / -)	% removed	error (+ / -)
unmodified	87.81%	6.80%	92.93%	0.96%
APTES	99.29%	0.23%	99.51%	0.62%
TMSPE	99.33%	0.62%	99.46%	0.13%

The results show that the modified samples show an increase in the removal of plutonium in the presence of sodium hydroxide. This supports that the plutonium is being removed by the ligands.

4.54 Plutonium kinetic experimental results

4.54.1 Rate of uptake of plutonium by unmodified materials

The rate of uptake of plutonium to the unmodified and modified materials was investigated using the kinetic batch sorption methodology discussed in section 4.48.1. The results are shown in figure 4.64 and tabulated in table 4.36.

Table 4.36: Uptake of plutonium as a function time for unmodified materials

Material	Clinoptilolite (NDA)		Clinoptilolite (Imerys)		ZSM-5		Vermiculite		Kaolinite	
Time (days)	% removed	Error (+/-)	% removed	Error (+/-)	% removed	Error (+/-)	% removed	Error (+/-)	% removed	Error (+/-)
0.04	71.5%	2.7%	88.3%	0.5%	85.9%	3.4%	83.5%	1.1%	93.3%	1.0%
1	75.9%	5.1%	83.9%	2.3%	57.8%	3.6%	96.5%	0.5%	73.7%	4.1%
7	93.1%	0.5%	56.3%	0.4%	90.5%	0.5%	93.8%	0.7%	89.0%	14.7%
14	94.8%	2.2%	55.2%	2.5%	90.2%	1.9%	97.5%	1.5%	99.3%	0.2%
28	97.6%	0.9%	56.6%	1.5%	88.7%	0.2%	99.2%	0.4%	88.3%	19.5%
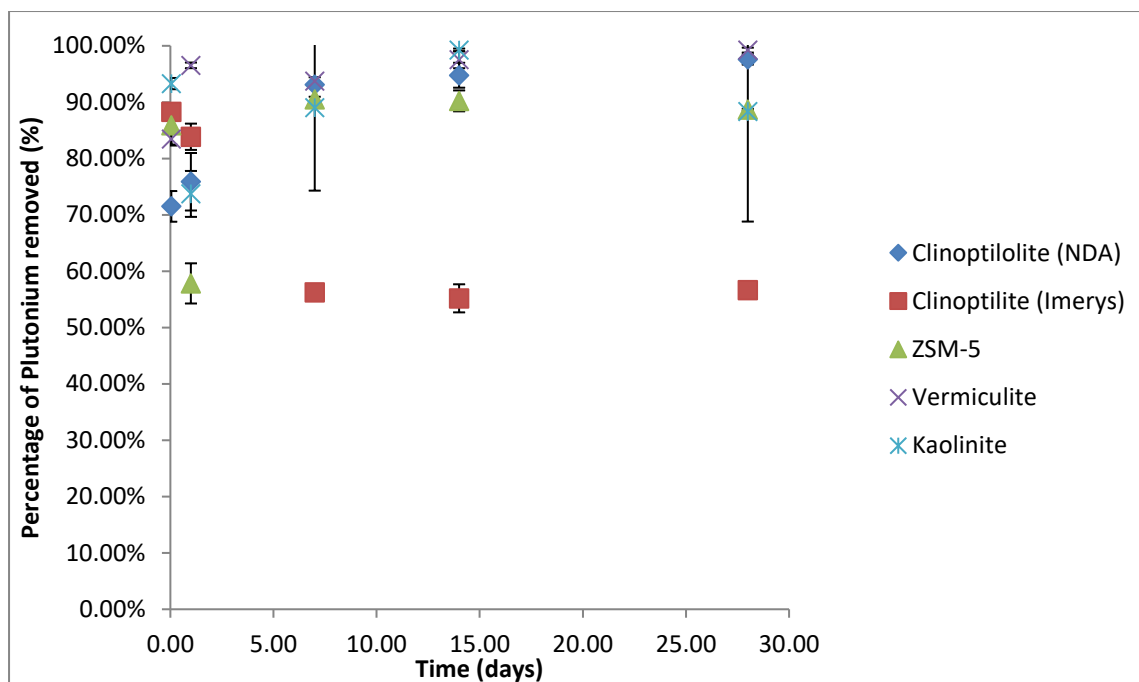
Figure 4.64 Uptake of plutonium as a function of time for unmodified materials

The rate of uptake seen by all materials is rapid due to the low concentration of plutonium in solution. All samples show some removal suggesting that physisorption is playing a role if compared with the other sequestration experiments.

Table 4.36 Uptake of plutonium as a function of time for ungrafted materials.

Material	Clinoptilolite (NDA)		Clinoptilolite (Imerys)		ZSM-5		Vermiculite		Kaolinite	
Time (days)	% removed	Error (+/-)	% removed	Error (+/-)	% removed	Error (+/-)	% removed	Error (+/-)	% removed	Error (+/-)
0.04	0.0%	2.8%	54.2%	18.4%	15.0%	4.0%	62.4%	6.5%	28.5%	8.1%
1	49.7%	11.2%	83.7%	3.8%	21.1%	4.0%	97.8%	0.2%	64.6%	5.0%
7	63.2%	2.1%	98.4%	0.7%	5.1%	3.9%	98.2%	0.3%	97.8%	2.7%
14	74.8%	6.6%	99.0%	0.5%	1.3%	5.6%	98.8%	0.5%	99.0%	0.4%
28	88.3%	2.0%	99.3%	0.5%	41.8%	45.1%	98.0%	1.6%	99.5%	0.2%

4.54.2 Rate of uptake of plutonium by APTES modified materials

The rate of uptake of plutonium to the APTES modified materials was investigated using the kinetic batch sorption methodology discussed in section 4.48.1. The results are shown in figure 4.65 and tabulated in table 4.37.

Figure 4.65: Removal of plutonium as a function of time for APTES grafted materials.

Table 4.37 Removal of plutonium as a function of time for APTES grafted materials

Time (days)	% removed	Error (+/-)	% removed	Error (+/-)	% removed	Error (+/-)	% removed	Error (+/-)	% removed	Error (+/-)
0.04	0.0%	2.8%	54.2%	18.4%	15.0%	4.0%	62.4%	6.5%	28.5%	8.1%
1	49.7%	11.2%	83.7%	3.8%	21.1%	4.0%	97.8%	0.2%	64.6%	5.0%
7	63.2%	2.1%	98.4%	0.7%	5.1%	3.9%	98.2%	0.3%	97.8%	2.7%
14	74.8%	6.6%	99.0%	0.5%	1.3%	5.6%	98.8%	0.5%	99.0%	0.4%
28	88.3%	2.0%	99.3%	0.5%	41.8%	45.1%	98.0%	1.6%	99.5%	0.2%

The addition of the ligand slows the uptake of the plutonium which would suggest that the removal seen by the unmodified materials is being hindered by the ligand. This supports the hypothesis that

the metal ion is interacting with the ligand. ZSM-5 shows a decrease in the overall removal which could be due to the low amount of ligand grafted compared with the other materials.

4.54.3 Rate of uptake of plutonium by TMSPE modified materials

The rate of uptake of plutonium to the TMSPE modified materials was investigated using the kinetic batch sorption methodology discussed in section 4.48.1. The results are shown in figure 4.66 and tabulated in table 4.38.

Figure 4.66. Removal of plutonium as a function of time for TMSPE grafted materials.

The results show an overall increase of removal of plutonium, the rate of removal is not greatly affected by the modification.

Table 4.38 Removal of plutonium as a function of time for TMSPE grafted materials

Material	Clinoptilolite (NDA)		Clinoptilolite (Imerys)		ZSM-5		Vermiculite		Kaolinite	
Time (days)	% removed	Error (+/-)	% removed	Error (+/-)	% removed	Error (+/-)	% removed	Error (+/-)	% removed	Error (+/-)
0.04	81.6%	1.2%	50.7%	7.1%	88.1%	0.6%	87.2%	3.9%	93.4%	0.1%
1	66.0%	1.8%	74.4%	6.3%	62.3%	3.2%	71.7%	0.3%	97.2%	0.2%
7	98.8%	0.4%	83.7%	25.7%	55.0%	5.2%	97.0%	3.4%	73.2%	4.6%
14	99.5%	0.1%	99.4%	0.3%	66.7%	8.0%	99.4%	0.1%	88.5%	3.1%
28	99.3%	0.4%	99.6%	0.1%	74.4%	8.5%	99.3%	0.3%	95.5%	0.9%

4.54.4 Rate of uptake of plutonium by TMSPETT modified materials

The rate of uptake of plutonium to the TMSPETT modified materials was investigated using the kinetic batch sorption methodology discussed in section 4.48.1. The results are shown in figure 4.67 and tabulated in table 4.39.
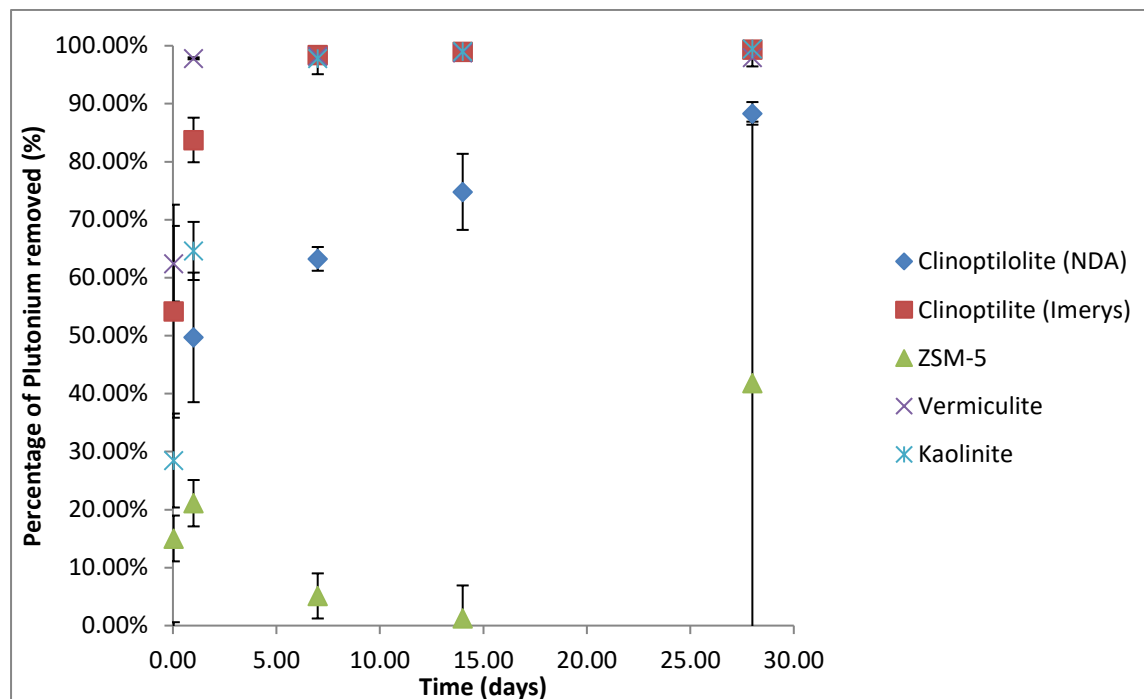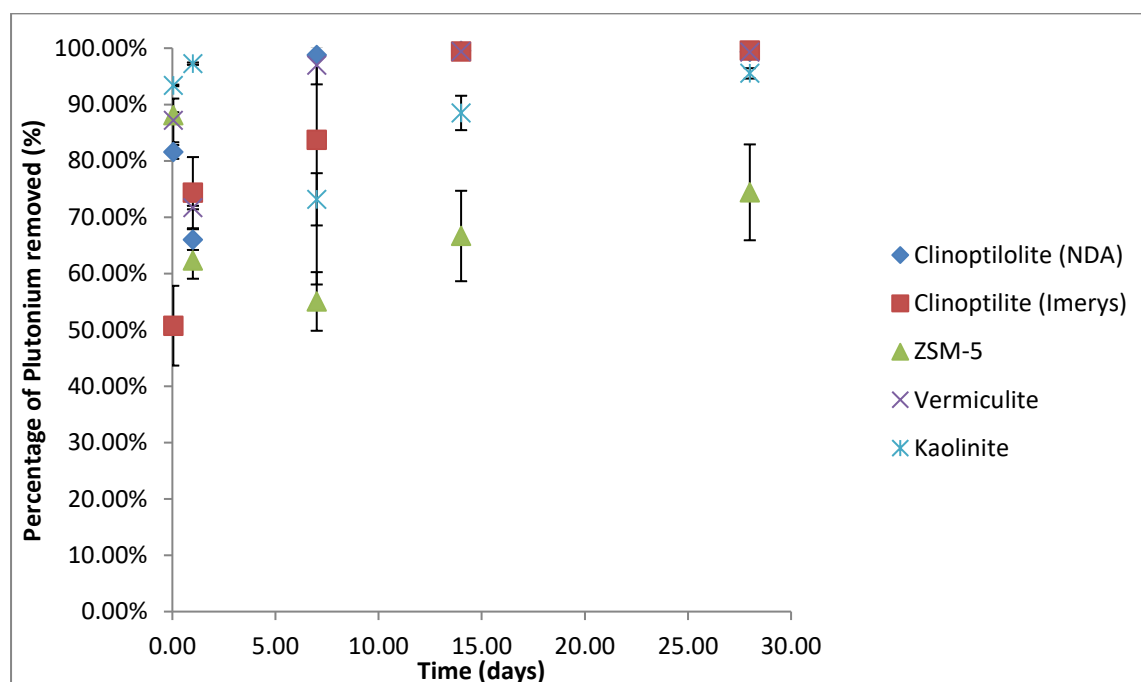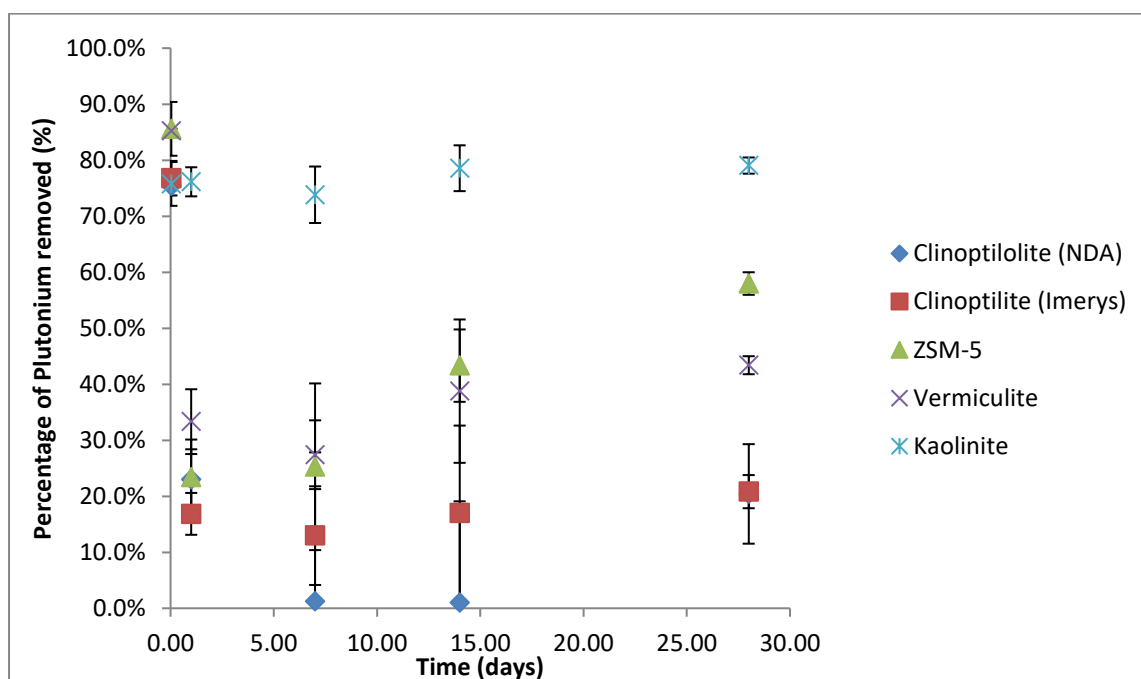

Figure 4.67. Removal of plutonium as a function of time for TMSPETT grafted materials

Table 4.39:. Removal of plutonium as a function of time for TMSPETT grafted materials

Material	Clinoptilolite (NDA)		Clinoptilolite (Imerys)		ZSM-5		Vermiculite		Kaolinite	
Time (days)	% removed	Error (+/-)	% removed	Error (+/-)	% removed	Error (+/-)	% removed	Error (+/-)	% removed	Error (+/-)
0.04	75.4%	0.8%	76.8%	3.1%	85.6%	4.8%	85.3%	0.4%	75.8%	3.9%
1	23.0%	5.4%	16.9%	3.7%	23.4%	6.7%	33.3%	5.8%	76.1%	2.6%
7	1.2%	26.6%	13.0%	8.8%	25.3%	14.9%	27.4%	6.1%	73.8%	5.0%
14	1.0%	18.1%	17.0%	15.6%	43.3%	6.5%	38.8%	12.8%	78.6%	4.1%
28	20.4%	8.9%	20.8%	3.0%	58.0%	2.0%	43.4%	1.6%	79.0%	1.4%

The overall removal of plutonium is lower, and the rate of removal of the metal ion is also slower. This suggests that the ligand is not aiding in the removal of plutonium.

4.55 Comparison of clinoptilolite (NDA) materials

The rate of uptake of plutonium to the unmodified and modified mineral clinoptilolite was investigated using the kinetic batch sorption methodology discussed in section 4.48.1. The results are shown in figure 4.68.

Figure 4.68: Comparison of the rate uptake of plutonium by grafted and ungrafted clinoptilolite NDA

The rate of uptake is increased with the TMSPE modified materials and the overall uptake of plutonium is higher. The APTES and TMSPETT modified samples show a decrease in rate.

4.56 Comparison of clinoptilolite (Imerys) materials

The rate of uptake of plutonium to the unmodified and modified mineral clinoptilolite was investigated using the kinetic batch sorption methodology discussed in section 4.48.1. The results are shown in figure 4.69.


Figure 4.69: Comparison of the rate uptake of plutonium by grafted and ungrafted clinoptilolite (Imerys)

The rate of uptake is slower for the modified materials as the ligand may be blocking access to the material. The overall uptake of plutonium is higher in the APTES and TMSPE modified samples.

4.57 Comparison of ZSM-5 materials

The rate of uptake of plutonium to the unmodified and modified material ZSM-5 was investigated using the kinetic batch sorption methodology discussed in section 4.48.1. The results are shown in figure 4.70.

Figure 4.70: Comparison of the rate uptake of plutonium by grafted and ungrafted ZSM-5

The rate of uptake is increased with the TMSPE and TMSPETT modified materials and the overall uptake of plutonium is higher. The APTES modified samples show a decrease in rate.

4.58 Comparison of vermiculite materials

The rate of uptake of plutonium to the unmodified and modified mineral vermiculite was investigated using the kinetic batch sorption methodology discussed in section 4.48.1. The results are shown in figure 4.71.
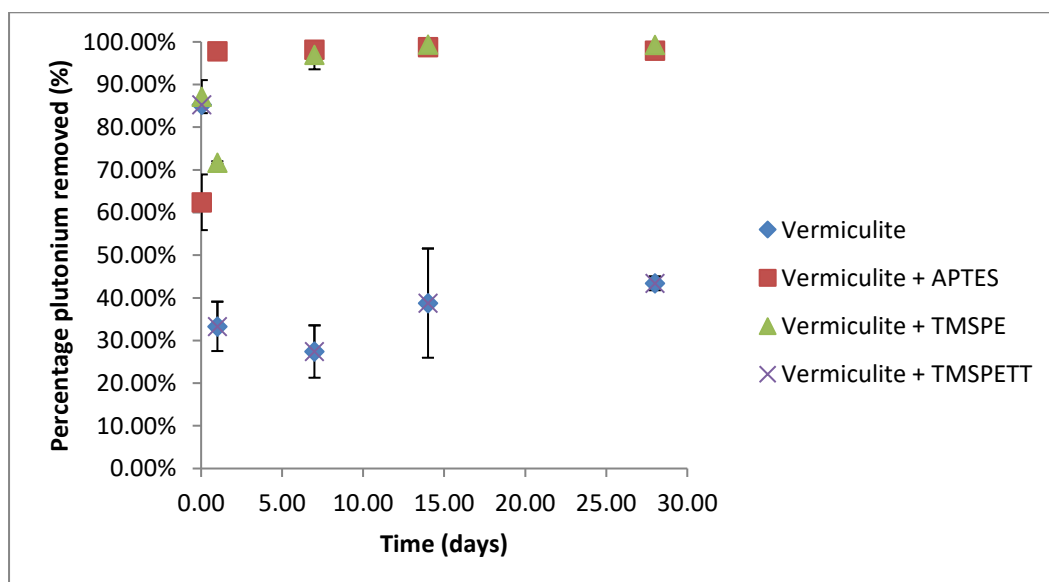
Figure 4.71: Comparison of the rate uptake of plutonium by grafted and ungrafted vermiculite

The rate of uptake is quicker for the APTES modified materials. The overall uptake of plutonium is higher in the APTES and TMSPE modified samples.

4.59 Comparison of kaolinite materials

The rate of uptake of plutonium to the unmodified and modified mineral kaolinite was investigated using the kinetic batch sorption methodology discussed in section 4.48.1 The results are shown in figure 4.72.

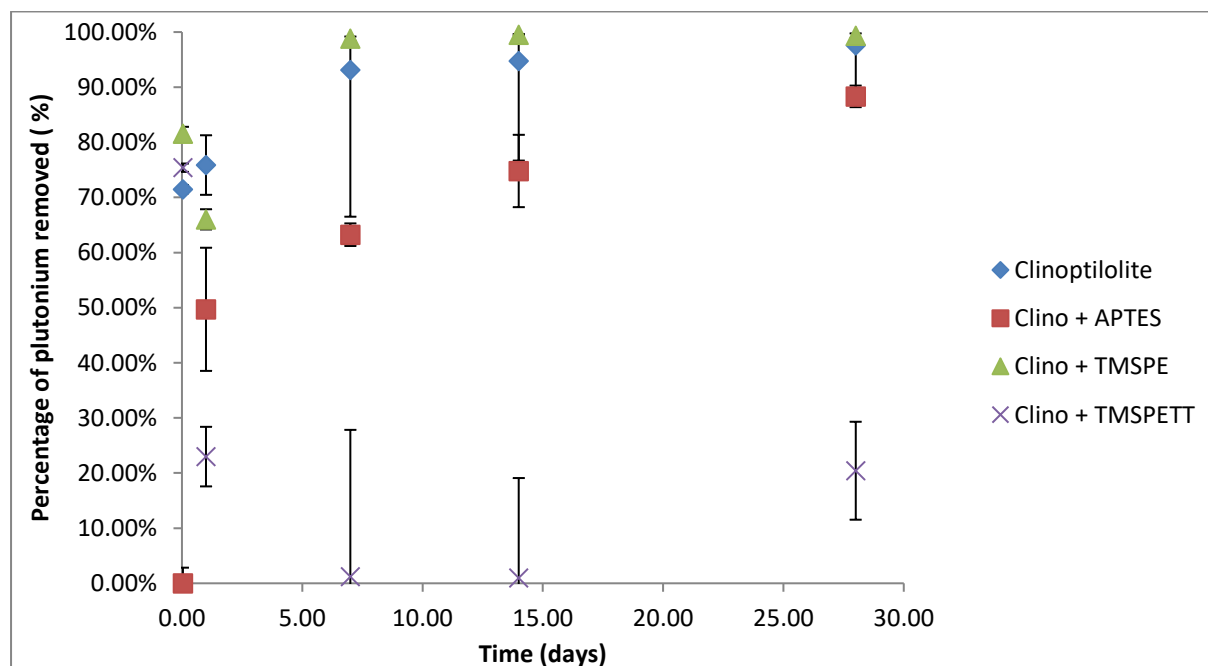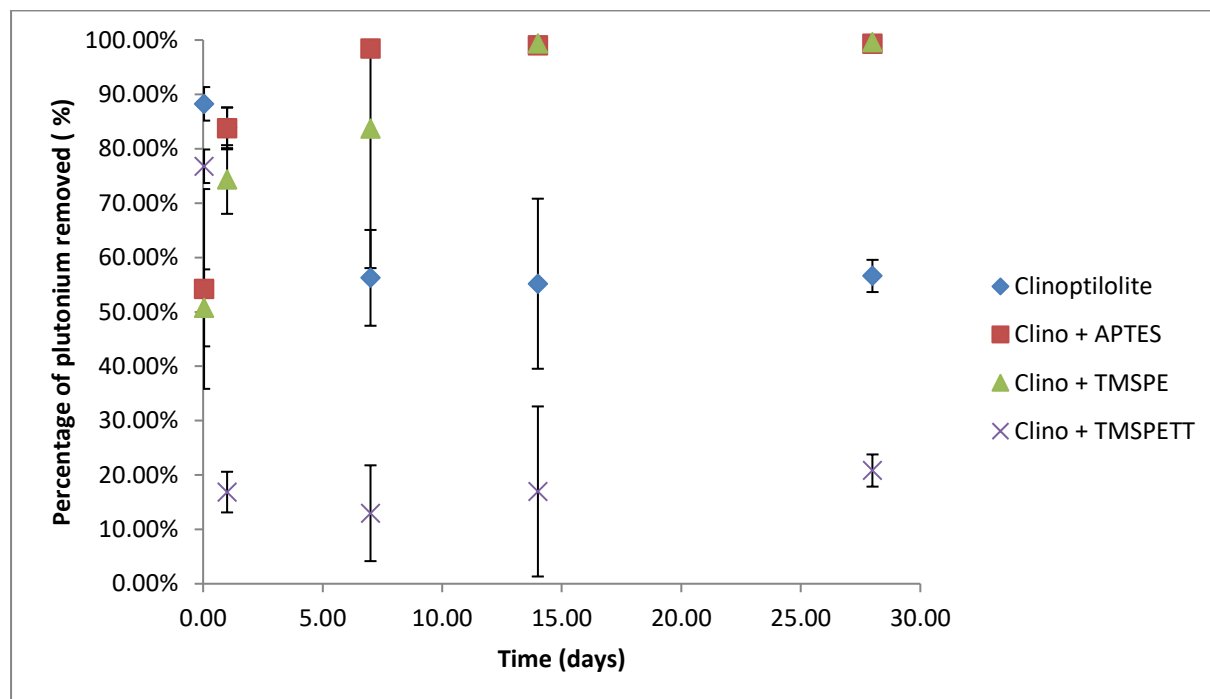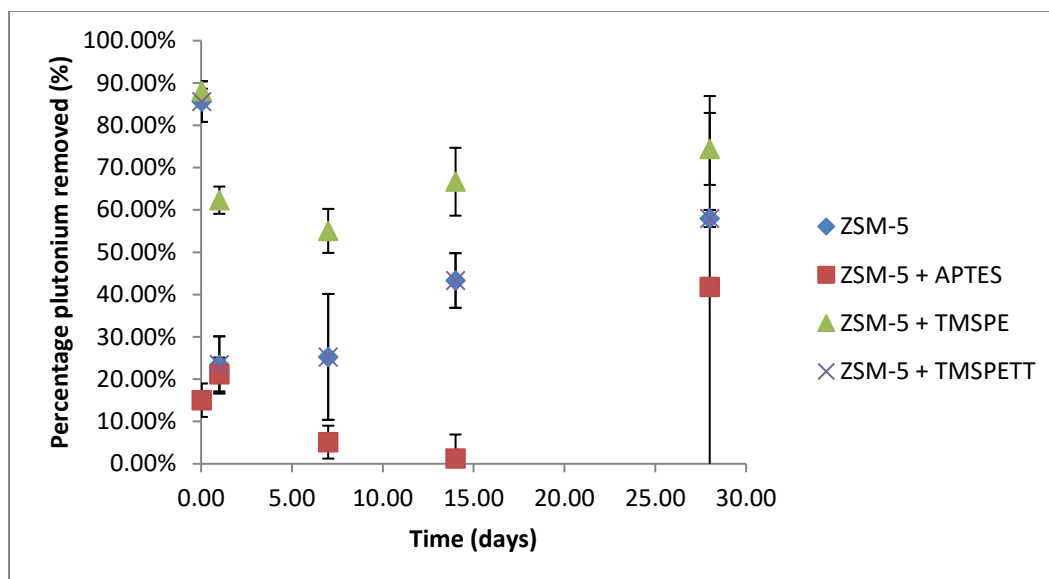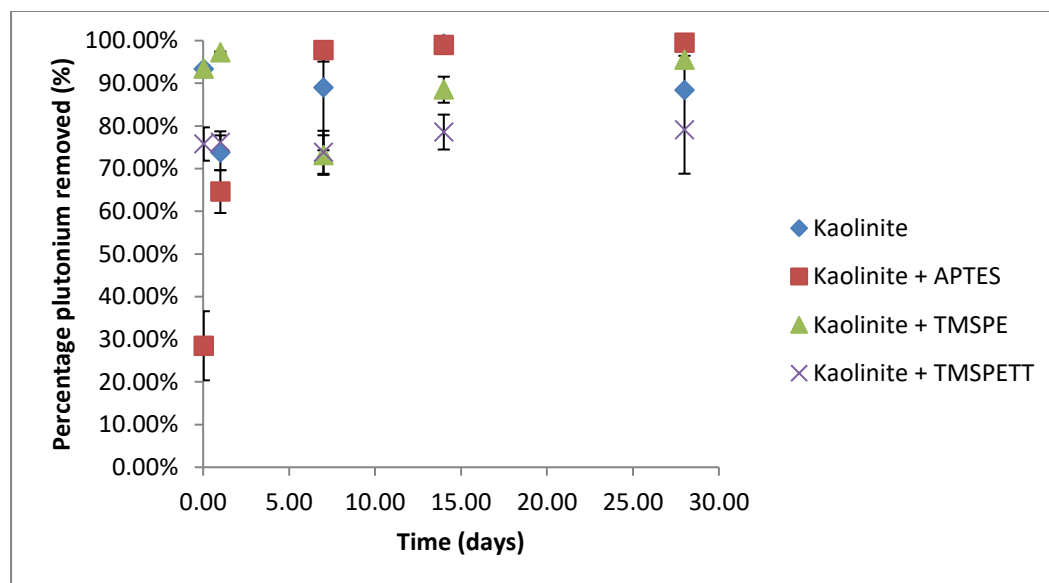**Figure 4.72: Comparison of the rate uptake of plutonium by grafted and ungrafted kaolinite**

The above plot shows no significant effect in the rate of uptake of plutonium by the modified materials with saturation being observed after 5 days in all cases.

4.60 Plutonium sorption Summary

The effect of plutonium uptake by the materials Clinoptilolite (NDA), clinoptilolite (Imerys), ZSM-5, vermiculite and kaolinite before and after modification with the organic ligands APTES, TMSPE and TMSPETT were investigated. Experiments were conducted to study the amount and rate of plutonium uptake by the materials.

An increase in plutonium uptake was observed for the modified materials however the rate of uptake was slower than the unmodified materials. This could be attributed to the low concentration of plutonium ions ion exchanging with the unmodified materials but interacting preferentially with the ligand when present. Competing ion experiments were conducted using sodium, this showed that little effect was seen in the extent of plutonium uptake even under alkaline conditions.

4.61 Chapter conclusions

The results of the caesium and strontium work is entirely in context of previous work on uptake within zeolites and clays. Clinoptilolite crystallises with the heulandite structure with channels running through the framework made up of rings of TO_4 tetrahedra (T= Si or Al). The silicon to aluminium ratio dictates which ions will be most easily extracted by the zeolite. The higher the Al:Si ratio the greater the negative charge on the framework as each vertex-sharing aluminium tetrahedron carries a negative charge. The NDA selected the clinoptilolite used in SIXEP for its high selectively for caesium and strontium cations. As the Si:Al ratio is greater than 5:1, the charge is low and hence large lowly charged ions are favoured for ion exchange. Although there is a mixture of group 1 and group 2 ions in the liquor, caesium and strontium are the most abundant and are both large species. There has been some discussion in the literature previously[10] about why the divalent strontium cation and the monovalent caesium cation should both be selectively absorbed. The strontium cation is smaller at 1.18A than the caesium cation at 1.67A but authors (NNL pub)[22] suggest that it maybe present in the liquor as $[Sr(OH)]^+$ or $Sr[HCO_3]^+$ making it larger and more likely to fit in the same ion exchange site.

Structure refinements on clinoptilolite suggest there are 4 caesium sites in the structure each with six bond lengths between 2.9 and 3.1 A. [166] Bond valence calculations on these sites using an Ro for Cs^+ as 2.42 gives 1.1(1) as the bond valence indicating a highly suitable environment for caesium. Strontium with Ro of 2.68, gives 1.6(1) indicating underbonding in the site, so it is likely that additional species are coordinated as perhaps suggested previously.[167] Once bonded in these sites, it is easy to see why the environment is stable and that practically no desorption occurs. In contrast, vermiculite has a layer structure and can swell and adjust the distance between the layers freely to absorb many species. In nature, the cation sites between the layers are normally filled with sodium, potassium or calcium cations but these are held weakly by electrostatic interactions compared to three-dimensional arrangement of the zeolite. A greater desorption of caesium and strontium is expected in this compound as a result of the much less rigid structure and the less 'perfect' arrangement of the caesium and strontium cations. As expected the worst take up of the caesium and strontium cations by ungrafted products is by kaolinite and ZSM-5, which have zero and few exchangeable cations respectively. Surface physisorption is expected to dominate in these compounds and as a result these weak intermolecular forces are easily overcome and the species are seen to desorb during standing in water as a result of entropic considerations. After grafting with the ligands, there is general increase in the amount of caesium and strontium being absorbed and desorbed. This can be attributed to the ligands competing with the substrates to take up the cations. While it is expected that the cations sites inside the zeolite would be most likely to retain the ions due to the perfect geometric arrangement, the grafted ligands chosen contain nitrogen and/or oxygen donors that would be

suitable to pick up the group 1 and 2 cations from solution. However, due to their large size and low charge, these ions are not easily retained by the small number of donors and can be released back into solution. In terms of HSAB theory, these ligands were chosen to target uranium (VI) and plutonium (V) which are much harder acids due to their higher charge.

In terms of the uranium and plutonium speciation, PHREEQC has been used to predict the likely species in solution.

Post carbonation, the following tables show the input for the calculations and the results of the calculations.

Table 4.40. Inputs for PHREEQC calculations.

Calculation	Temperature C	pH	ρE	Eh/ mV	Moles Na+	Moles U	Total alkalinity Eq/kg
1	25	7.0	5.06	295	1.037×10^{-3}	1.0×10^{-12}	1.029×10^{-3}
2	25	7.0	6.75	398	1.037×10^{-3}	1.0×10^{-12}	1.029×10^{-3}

The following Table shows the PHREEQC calculation results of the number of moles of each possible oxidation state of uranium for an input of 1×10^{-12} moles of uranium.

Table 4.41 Oxidation states of uranium in carbonated sodium hydroxide solution.

U(III)	U(IV)	U(V)	U(VI)
0	5.285×10^{-28}	1.7592×10^{-20}	1.0×10^{-12}

The results show that 100% of uranium exists as U(VI) species.

The following Table shows the major species of uranium present as U(VI).

Table 4.42 Major U species in solution as calculated using PHREEQC.

Major species	U Oxidation State	Percentage of U species in solution at Eh 300 mV	Percentage of U species in solution at Eh 400 mV
$UO_2(CO_3)_2^{2-}$	U (VI)	65.2	65.2
$UO_2(CO_3)$	U (VI)	26.0	26.0
$UO_2)_2(CO_3)^{4-}$	U(VI)	7.9	7.9

These species would not be expected to be removed by cation exchangers such as clinoptilolite as the species are anions rather than cations and these species are also far too large to enter the cages and move into the appropriate sites; ion exchange involves both species being present with the cage simultaneously and this would not be possible in such as small T-O-T channel.[168]

The experiments carried out in this thesis on uranium were to use uranium (VI) as a surrogate for plutonium (V) before carrying out a limited number of experiments on the more hazardous ion. In order to do this effectively, it was necessary to use an acidic solution where mobile cationic species dominate and this mirrors the work of Camacho who investigated Sweetwater clinoptilolite for removing uranium (VI) from water. Experiments were conducted using uranium (IV) nitrate solutions and the measured pH was between 4.5 and 6, which was the optimum range for remediation according to Camacho *et al*.[20] Preliminary experiments on the ungrafted clinoptilolite samples showed relatively low take up ca 20% which improved dramatically to greater than 80% after grafting. As discussed previously, the ungrafted material is not likely to undergo ion exchange due to size of the cavity being unsuitable for the UO_2^{2+} ion. The method of sequestration could be physisorption onto the surface of the zeolite and/or impurities in the mineral undertaking ion exchange/physisorption. Since clay minerals and quartz are often present in clinoptilolite due to its geological origins, it is difficult to determine which method of take up is most likely. However, the dramatic increase after grafting implies that the ligands are having a major effect on the removal of the uranium species and its retention whatever sequestration method was occurring in the raw material. This suggested that using the grafted to remove plutonium was a possibility, so further experiments were conducted on uranium over the full range of absorption and desorption experiments carried out for caesium and strontium cations previously. It should be noted however, as the impurities in clinoptilolite also contain silanol groups that could be grafted, it will never be clear whether it is the zeolite or the phases cocrystallised with it that is truly undertaking the removal of the species.

The Pu Porbaix diagram given in chapter 1 indicates that the major Pu species at pH 7 are $Pu(OH)_4$ and PuO_2^+ i.e. Pu(IV) and Pu(V). Only the latter species would be removed by ligands such as APTES as it specifically targets cations due to a concentration of hard base donor atoms. Previous work on surface modified silica by Holt et al showed that APTES was able to remove a whole range of ions from solution, albeit unselectively[135].

The following Table, which shows the approximate redox potential of some solutions, is shown in In Water Structure and Science by Martin Chaplin. [169]

Table 4.43. Eh of some common waters.

Aqueous material	Redox potential (mV)
Water saturated with H_2	-600
Degassed pure water	+200
Distilled water	+250
Mineral water	+300 ~ +400
Tap water	+300 ~ +400
Swimming pool	+400 ~ +475
Water saturated with O_2	+600

The Eh of mineral water (+300 - +400 mV) calculates to a pE of approximately 5 to 7. Both Porbaix diagrams shown above indicate that the speciation of Pu at pH 7 and Eh of between 0.3 – 0.4 V and pE of between 5 and 7 is $Pu(OH)_4$ and is therefore unlikely to be extracted from solution by a cation exchange material. Only water at pH 7 and saturated with O_2 (Eh 0.6 V and pE = 10.1) would contain Pu (V) species as PuO_2^+. More likely is that the carbonated pH 7 water would contain a mixture of both Pu(IV) and Pu(V) species and thus clino or a modified clino material is unlikely to extract 100% of the Pu from the SIXEP carbonated Main Pond liquor without further chemical treatment e.g. with the addition of H_2O_2. However, the experimental results presented in this thesis, which were obtained from the extraction of plutonium from the carbonated sodium hydroxide, show that almost 100% of plutonium was removed from solution.

To further understand the extraction of plutonium, Dr Nick Bryan at NNL was asked to carry out speciation modelling using the PREEQC computer program to model plutonium and uranium solution speciation in sodium hydroxide solution after bubbling carbon dioxide through it to bring its pH down to pH 7. The following inputs to PHREEQC were used:

Table 4.44. Inputs for PHREEQC calculations.

Calculation	Temperature C	pH	ρE	Eh mV	Moles Na+	Moles Pu	Total alkalinity Eq/kg
1	25	7.0	5.06	295	1.037×10^{-3}	1.0×10^{-12}	1.029×10^{-3}
2	25	7.0	6.75	398	1.037×10^{-3}	1.0×10^{-12}	1.029×10^{-3}

The following Table shows the PHREEQC calculation results of the number of moles of each possible oxidation state of plutonium for an input of 1×10^{-12} moles of plutonium.

Table 4.45. Oxidation states of plutonium in carbonated sodium hydroxide solution.

Pu(III)	Pu(IV)	Pu(V)	Pu(VI)
2.696×10^{-18}	9.999×10^{-13}	1.192×10^{-16}	3.122×10^{-24}

The results show that almost 100% of plutonium exists as Pu(IV) species.

The following Table shows the species of plutonium present as Pu(IV).

Table 4.46. Major Pu species as calculated using PHREEQC

Major species	Pu Oxidation State	Percentage of Pu species in solution at Eh 300 mV	Percentage of Pu species in solution at Eh 400 mV
$Pu(OH)_4$	Pu (IV)	82.7	82.2
$Pu(OH)_3^+$	Pu (IV)	13.6	13.7
$Pu(CO_3)_2(OH)^{2-}$	PU (IV)	3.7	3.7
PuO_2^+	Pu(V)	0.55	0.01

To explain the experimental results shown in section 4.57.3, that almost 100% of Pu was extracted even though only approximately 13.5% of the Pu was present as a cationic species, the following diagram shows the species involved

Solid Extractant
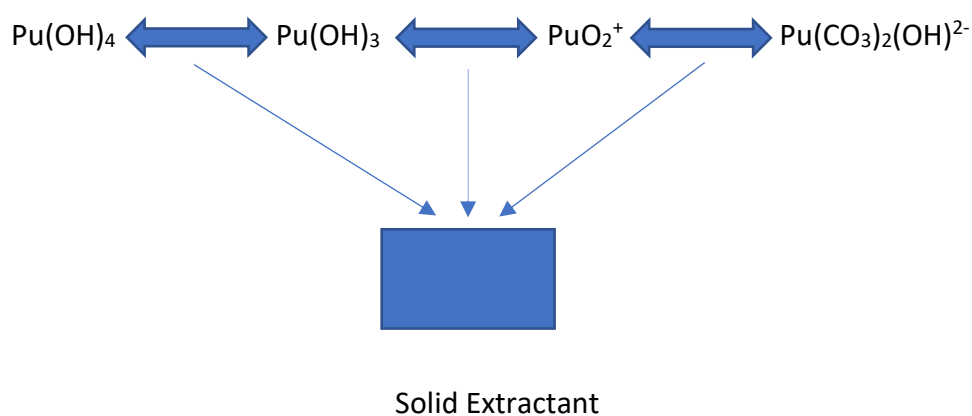
If only cationic species are extracted by the solid material, then as these species are removed from solution, the other species which are neutral and negative re-establish equilibrium (Le Chatelier's principle) and therefore form more cationic species which are then extracted by the solid. The re-arrangement of Pu species and removal of cationic species continues until almost all of the Pu is removed from solution. This hypothesis has potential for further work.

Chapter 5- Conclusions

5.0 Conclusions

Five materials that are known sorbents clinoptilolite (NDA), clinoptilolite (Imerys), ZSM-5, vermiculite and kaolinite) were chosen for grafting experiments to produce inorganic-organic hybrids for the removal of actinides of interest in the SIXEP process namely uranium and plutonium. The materials were fully characterised before and after ligand modification experiments were conducted. The characterisation techniques used were PXRD, FTIR, Raman, SEM, CHN and XRF.

The materials chosen were modified by grafting organic ligands to the surface of the material with the objective of not reducing any ion exchange capacity that the materials exhibit; for example in the case of clinoptilolite, the ability to selectively remove caesium and strontium in the presence of other ions such as group 1 and group 2 cations that are more abundant in the SIXEP liquor. The three ligands chosen were APTES, TMSPE and TMSPETT which had a range of donor atoms and chelation abilities.

Preliminary grafting experiments to determine the viability of the technique were carried out by grafting APTES to the two clinoptilolite samples. Analysis by CHN, FTIR and ^{13}C SSNMR showed that the grafting technique was viable and the ligand had grafted to the surface.

From the preliminary experiments, optimisation of the grafting process was investigated using reaction time, ligand concentration and solvent polarity as the experimental parameters. A range of 1–24 hours reaction time, 1-3 mmol of ligand and solvent polarity with a dielectric constant range from 1.9– 80.0 were considered. All materials were investigated with all ligands under all conditions.

In the case of APTES, all the zeolitic materials and kaolinite retained their long-range order as shown in the PXRD and FTIR. An increase in carbon content was seen by the CHN and confirmed by FTIR. Vermiculite did however show a broadening of the reflections at half maximum height in the PXRD meaning that the preferred orientation is less pronounced, suggesting a disruption of the layer structure after grafting. Vermiculite is the only material that has a large shrink/swell capacity and the ligand may be grafting between layers. The general trend seen in all materials except kaolinite with regards to time was an overall increase of the grafting with reaction time. Clinoptilolite (NDA) showed an increase of grafting with the increased concentration of the ligand. No other materials followed this trend with the concentration of ligand showing no discernible influence on the grafted amount. For both clinoptilolite samples the non-polar solvents saw the greatest grafting, whereas the opposite is true for ZSM-5. The solvent polarity had no noticeable influence on the grafting of vermiculite and kaolinite. For the APTES grafting the material that showed the highest graft achieved was clinoptilolite (NDA) under the reaction conditions of 24 h reflux in hexane, with 3.41 x 10^{-2} mols of ligand giving a 56.16 mmol/g graft.

For TMSPE and TMSPETT ligands a similar trend was seen with reaction time increasing the graft in most cases and the ligand concentration and solvent polarity having less effect. The grafting levels of the ligands follow the order APTES>TMSPE>TMSPETT which indicates that the size of the ligand which also follows the order APTES>TMSPE>TMSPETT is influencing the grafting ability. The long-range order of the zeolitic materials and kaolinite remained consistent which was shown in the PXRD and FTIR, with a carbon content increase was seen in the CHN and FTIR. The overall grafting ability of the materials is clinoptilolite (NDA)=clinoptilolite (Imerys)>vermiculite>kaolinite>ZSM-5.

The clinoptilolite (NDA) sample was selected to investigate the effect of acid pre-treatment. Three acids were selected for investigation these were citric acid, nitric acid and phosphoric acid. A range of concentrations of 1, 3 and 5 M were investigated and different time windows from 1 to 24 hours. The results suggest that the strength of the acid has less effect than the acid selected. The stronger acids may show less grafting as they are perhaps breaking down the surface rather than just roughening the surface.

Experiments were carried out on the materials before and after grafting to examine the sequestration ability of each of the materials. As expected, both clinoptilolite samples demonstrated rapid and substantial ion exchange for both strontium and caesium cations; this is afterall what the clinoptilolite was selected for specifically in SIXEP. Neither sample showed significant desorption behaviour indicating the high affinity of the zeolite for these two large, lowly charged ions where the ion lies in a site with perfect bond lengths and coordination geometry for the caesium cation. The high silicon to aluminium ratio and the narrow channels are expected to favour low charged, large ions with a small hydration sphere. While vermiculite also showed some ability to remove these cations, more desorption was shown than for clinoptilolite samples, reflecting the less 'locked in' nature of a layer structure over a cage arrangement. The very low levels of aluminium in ZSM5 and concomitant exchangeable cations meant that the structure performed poorly in comparison to the other zeolites but better than kaolinite, where there were no exchangeable cations available. After grafting, all ligand grafted materials showed improved uptake of caesium and strontium but also increased desorption, probably as a result of competition for the cations in the case of clinoptilolite. Overall, only a very minor reduction in the caesium and strontium take up is observed for clinoptilolite even with significant quantities of graft. Major differences were seen between the take up of plutonium and uranium before and after grafting on all materials, indicating that the grafts are successful in improving the utility of all materials and enabling the removal of actinides from solution. This is expected as the small highly charged actinide species are not ideal for ion exchange purposes due to highly polarising nature of the ion resulting in very large polyatomic species in solution making ion

exchange difficult. In contrast, the grafts with hard oxygen and nitrogen donors, should be highly effective in removing both uranium and plutonium from solution as they are hard cations and according to HSAB theory, like species attract and hard acids prefer hard bases. Uranium is not expected to be present in high concentrations in SIXEP once the liquor reaches the clinoptilolite beds as a result of a drop in the solubility of the uranium species with increasing pH. In the case of plutonium, where plutonium remains in the liquor in the clinoptilolite beds in SIXEP (around pH 7), the ligands remained effective at removing the plutonium species in synthetic liquor suggesting the partition of species predicted by PHREEQC is altered by the ligand removing cationic species from solution. This fortuitous application of Le Chatelier's principle means that all plutonium is rapidly removed from solution.

Chapter 6- Future work

6.0 Future work

6.1 Modification experiments efficiency

Investigating the efficiency of the modification reaction would be of interest, as this work is based on an ongoing process any up scaled modification would be cost driven with the ligands used being one of the most expensive items. Therefore carrying out work to determine how much ligand is left unreacted in solution using techniques such as gas chromatography wold allow the minimum amount of ligand to be used in the reaction to allow the optimal amount of ligand grafted for sequestration properties.

6.2 Investigation of other ligands

This work has focussed on three available ligands with differing donor atoms and chelation techniques in order to determine the viability of the modified materials as sequestration agents. While the ligands studied in this work were success in removal of uranium and plutonium there are other ligands available that may be more efficient.

This also leads onto the fact that due to the varied nature of the waste in the ponds there are other radionuclides / applications where the materials used in this work could be applied elsewhere.

6.3 Investigation of support materials

The materials in this work largely focus on natural clinoptilolite, as this is used currently in the SIXEP process. However there are a range of applications both within the industrial and nuclear sectors where this technology could be of use. Therefore looking at a range of other zeolitic and clay materials which may have better stability in these applications would be of interest.

This work has focussed on one source of clinoptilolite, however there are many tuffs located in different geological locations. This will affect the composition of the material which will alter the ion exchange capacity of the material as well as its ability to be grafted.

6.3.2 Surface roughening experiments

Preliminary experiments discussed in this work to roughen the surface using acid to increase ligand grafting capacity showed some promise. Future work would use a wider range of acids and also investigate the roughening ability of other materials of interest.

6.4 Study the interaction between the ligand and radionuclides of interest

This work has assumed that the radionuclides studies interact with the donor atoms associated with the ligand, and while this is likely to be the case there has been no conclusive experimental results obtained. The strength of the interaction between the radionuclides and the ligand could be studied by means on an NMR titration. Where the ligand would be kept at a fixed concentration and the radionuclide doped in. By observing the changes in the NMR spectrum the binding site can be identified, as well as an estimation of the binding constant. These results could further be used to tune selected ligands for the removal of the radionuclides of interest. .

6.5 Further batch experiments

As previously mentioned this work has focussed on allowing the removal of uranium and plutonium as they are the two species of concern in the SIXEP process. However there are many other radionuclides that this work could be applied to and so investigating the interaction between other actinides.

6.5.1 Simulated pond liquor

The majority of the work discussed focuses on simple systems with no competing ions to determine a base line for the selectivity of the modified materials with no interferences present. This is obviously far from what is expected in the real world applications where there materials could potentially be used. Therefore investigating the effects of competing ions and conducting experiments with conditions more closely related to those found in the SIXEP plant would determine how viable the materials are in real world applications, identifying areas where they could be further improved.

6.5.2 pH dependence

The experiments in this work have focused on near neutral pH as these are the conditions that the materials will be subjected to in the SIXEP plant. However there is potential to use the materials in

other applications where the pH is likely to be either acidic or alkaline. This will affect the ligands ability to remove the ions of interest and may also have detrimental effects on the substrates used.

6.6 Column experiments

Static batch experiments have been used in this work, while they allow a good overview of the effectiveness of the materials they are not representative of how the materials are used in the SIXEP plant. The plant uses columns where the sequestration material is encapsulated; this means that any laboratory test will have to consider the hydrodynamic flow of the waste solution through the substrate which may change the distribution ratio as the equilibrium of the system will be altered. Looking at small scale column experiments and observing the breakthrough and saturation point of the material would gain insight into how the materials may work in an industrial application.

6.6.1 Up scaled experiments

6.6.1.1 Modification of materials
The largest amount of material used in the modification experiments has currently been 2 g. For use on a larger scale the material would need to be made on a significantly larger scale. The extent of grafting may not scale up linearly and so experimental work to determine the efficiency of the grafting reaction at larger scales needs to be investigated.

6.6.1.2 Sequestration experiments
All batch tests have used a very small amount of material where the radionuclide and solution have been in vast excess to allow saturation to be achieved. Further testing investigating larger volumes of solid and varying solid/liquid ratios is of importance.

6.7 Retrieval of immobilised radionuclides

Currently the SIXEP process results in large amounts of spent ion exchanger being stored which leads to large volumes of radioactive waste being stored awaiting disposal. It would be advantageous to be able to concentrate the radioactivity into a smaller volume to make final disposal more cost effective. This could be done by changing the pH or passing some other solution through the ion exchangers when they become spent to remove and concentrate the radioactive material.

6.8 Ligand stability experiments

Before the materials could be used in an industrial application the stability of the ligand needs to be investigated. The chemical stability could be investigated by exposing the material to different chemical environments and analysing the material before and after. The other area for study is stability to radiolysis, in its final application the material is subjected to a large radiation dose which may result in the ligand becoming detached from the solid support, or altering the nature of the ligand. This work would need to be carried out at a facility with a large chemical irradiator, where the material would be subjected to a large dose of radioactivity for a known time.

6.9 Waste form stability

Once the ion exchange materials are spent they will need to be packaged into a final waste form ready for disposal. There are several options that are available encapsulation in a cementitious grout. This is problematic as due to the hydration of the zeolites it prevents the cement from curing properly leaving the waste unsupported. The other options are more expensive and involve encapsulation in a borosilicate glass or being immobilised in a ceramic and sealed using hot isostatic pressing. The viability of these options would need to be investigated due to the organic content of the material and the stability of the ligand under the conditions mentioned.

Chapter 7- References

1.   https://www.theguardian.com/environment/2013/oct/21/nuclear-power-in-the-uk-a-history accessed 6/4/2016

2.   http://www.atomicarchive.com/History/british/index.shtml accessed 6/4/2016

3.   Chapman, N. & Hooper, A. The disposal of radioactive wastes underground. *Proc. Geol. Assoc.* **123,** 46–63 (2012).

4.   Calvin, T. *WM2011 Conference, February 27 – March 3 2011, Phoenix, AZ Decommissioning Sellafield's First Fuel Storage Pond - 11125 Tony Calvin, Sellafield Ltd, Sellafield, Cumbria, UK*. (2011).

5.   http://unfccc.int/paris_agreement/items/9485.php accessed 6/4/2016

6.   Engelder, T., Howarth, R. & Ingraffea, A. Should fracking stop? *Nature* **477,** 271–275 (2011).

7.   *DTI White Paper July 2002: managing the Nuclear Legacy – A Strategy for action*.

8.   Poyry Energy Ltd. *The 2010 UK Radioactive Waste Inventory:* (2010).

9.   Kingdom, U. & Limited, N. United Kingdom Nirex Limited Nirex Report no. N/085 July 2003. *Management* (2003).

10.   International Atomic Energy Agency. Application of Ion Exchange Processes for the Treatment of Radioactive Waste and Management of Spent Ion Exchangers. *Tech. Rep. Ser. No. 408* (2002).

11.   Haszeldine, S. & Smythe, D. Sellafield. *Geoscientist* **7,** 18–20 (1997).

12.   International Atomic Energy Agency IAEA-TECDOC-1340. *Manual for reactor produced radioisotopes*. (2003). at <http://www.isotopes.gov/outreach/reports/Reactor_Isotopes.pdf>

13.   Aragonne National Laboratory EVS. Neptunium. *Hum. Heal. Fact Sheet* **238,** 238–239 (2005).

14.   Parry, S. a. *et al.* Plutonium behaviour in nuclear fuel storage pond effluents. *Energy Environ. Sci.* **4,** 1457 (2011).

15.   *https://www.nda.gov.uk/ accessed 2/4/2012*.

16.   Sellafield Ltd. *Novel Processes for the Treatment of ILW*. (2010).

17.   Szabó, Z., Toraishi, T., Vallet, V. & Grenthe, I. Solution coordination chemistry of actinides: Thermodynamics, structure and reaction mechanisms. *Coordination Chemistry Reviews* **250,** 784–815 (2006).

18.   Takeno, N. Atlas of Eh-pH diagrams Intercomparison of thermodynamic databases. *Natl. Inst. Adv. Ind. Sci. Technol.* **285,** 1–287 (2005).

19.   Knope, K. E. & Soderholm, L. Solution and solid-state structural chemistry of actinide hydrates and their hydrolysis and condensation products. *Chem. Rev.* **113,** 944–994 (2013).

20.   Camacho, lucy mar, Deng, S. & Parra, R. R. Uranium removal from groundwater by natural clinoptilolite zeolite: Effects of pH and initial feed concentration. *J. Hazard. Mater.* **175,** 393–398 (2010).

21.   Misaelides, P., Godelitsas, A., Filippidis, A., Charistos, D. & Anousis, I. Thorium and uranium uptake by natural zeolitic materials. *Sci. Total Environ.* **173–174,** 237–246 (1995).

22.	Maher, Z. *et al.* Actanide Abatment in SIXEP. *Tech. Conf.* (2012).

23.	Gregson, C. & Taylor, R. Plutonium Speciaction in a Sellafield Legacy Feul storage Pond. *NNL* 9–12 (2013).

24.	Owens, S., Higgins-Bos, M., Bankhead, M. & Austin, J. USING CHEMICAL AND PROCESS MODELLING TO DESIGN, UNDERSTAND AND IMPROVE AN EFFLUENT TREATMENT PLANT. *NNL Sci.* 4–13 (2013).

25.	R.C.EWing. Long-term storage of spent nuclear fuel. *Nat. Mater.* **14,** 25698421 (2015).

26.	*http://www.nda.gov.uk/ukinventory/documents/Reports/upload/2010-UK-Radioactive-Waste-Inventory-Main-Report.pdf*. accessed 2/4/2012

27.	*The 2010 UK Radioactive Waste Inventory, Main Report, Report prepared for the Department of Energy of Climate Change (DECC) and the Nuclear Decommissioning Authority (NDA) by Pöyry Energy Limited, (URN 10D/985 NDA/ST/STY(11)0004 February 2011)*.

28.	*Nirex Report N/034 June 2001: Why a cementitious repository?*

29.	*The scientific foundations of deep geological disposal Nirex Report N/016 2001*.

30.	http://davidsmythe.lafontenille.org/nuclear/jrc_reference_report_2009_10_geol_disposal.pdf accessed 2/4/2016

31.	Faghihian, H., Marageh, M. G. & Kazemian, H. The use of clinoptilolite and its sodium form for removal of radioactive cesium , and strontium from nuclear. *Appl. Radiat. Isot.* **50,** 1–6 (1999).

32.	Gallen, D Frysinger, R. Caesium-sodium ion exchange on clinoptilolite. *Nature* **194,** 351–353 (1962).

33.	Humelnicu, D., Dinu, M. V. & Drăgan, E. S. Adsorption characteristics of UO(2)(2+) and Th(4+) ions from simulated radioactive solutions onto chitosan/clinoptilolite sorbents. *J. Hazard. Mater.* **185,** 447–55 (2011).

34.	Wani, P. P. & Thorat, S. R. Heavy metal adsorption by clinoptilolite from aqueous solutions. *Curr. World Env.* **3,** 135–141 (2008).

35.	Hulbert, M. H. Sodium, Calcium, and Ammonium Exchange on Clinoptilolite from the Fort Laclede Deposit, Sweetwater County, Wyoming. *Clays Clay Miner.* **35,** 458–462 (1987).

36.	Valkov, M. & Simha, G. Vermiculite: Structural Properties and Examples of the Use. *Clay Miner. Nat. - Their Charact. Modif. Appl.* (2012). doi:10.5772/51237

37.	Akai, J. *et al.* Mineralogical and geomicrobial examination of soil contamination by radioactive Cs due to 2011 Fukushima Daiichi Nuclear Power Plant accident. *Phys. Chem. Earth* **58–60,** 57–67 (2013).

38.	Baerlocher, C., McCusker, L. B., Olson, D. & International, Z. A. *Atlas of zeolite framework types*. (Amsterdam ; Oxford : Elsevier, 2007).

39.	*http://www.iza-structure.org/databases accessed 27/10/12*.

40.	Dutta, P. K., Shieh, D. C. & Purl, M. Raman spectroscopic study of the synthesis of zeolite Y. *J.*

Phys. Chem. **91,** 2332 (1987).

41.   Karami, D. & Rohani, S. Synthesis of pure zeolite Y using soluble silicate, a two-level factorial experimental design. *Chem. Eng. Process. Process Intensif.* **48,** 1288–1292 (2009).

42.   Georgiev, D., Bogdanov, B., Angelova, K., Markovska, I. & Hristov, Y. SYNTHETIC ZEOLITES - STRUCTURE, CLASIFICATION, CURRENT TRENDS IN ZEOLITE SYNTHESIS REVIEW. *Int. Sci. Conf. 4th - 5th June 2009, Stara Zagor. Bulg.* **VII,** 1–5 (2009).

43.   Muhammad, S. & Munawar, E. Nanocrystalline Zeolite Y : Synthesis and Heavy Metal Removal. *J. Rekayasa Kim. dan Lingkung.* **6,** 55–62 (2007).

44.   Kovo, a. S. & Holmes, S. M. Effect of Aging on the Synthesis of Kaolin-Based Zeolite Y from Ahoko Nigeria Using a Novel Metakaolinization Technique. *J. Dispers. Sci. Technol.* **31,** 442–448 (2010).

45.   Azizi, S. N. & Ehsani Tilami, S. Recrystallization of Zeolite Y to Analcime and Zeolite P with D-Methionine as Structure-Directing Agent (SDA). *Zeitschrift für Anorg. und Allg. Chemie* NA-NA (2009). doi:10.1002/zaac.200900297

46.   Yin, H., Zhou, T., Liu, Y., Chai, Y. & Liu, C. Synthesis of high-quality nanocrystalline zeolite Y using pseudoboehmite as aluminum source. *J. Porous Mater.* **19,** 277–281 (2011).

47.   Htay, M. M. & Oo, M. M. Preparation of Zeolite Y Catalyst for Petroleum Cracking. *World Acad. Sci. Eng. Technol.* **24,** 114–120 (2008).

48.   Corporation, J. M. H., Division, C. & Grace, H. De. *Factors Influencing the Synthesis of Zeolites A, X, and Y*. **21078,** (1983).

49.   Barrer, R. M. Molecular sieves. *Nature* **249,** 783 (1964).

50.   Breck, D. W. *Zeolite molecular sieves : structure, chemistry, and use*. (New York ; London etc. : Wiley-Interscience, 1974).

51.   Occelli, M. I. & Kressler, H. *Synthesis of Porous Meterials: Zeolites, Clays and Nanostructures*. (CRC Press, 1997).

52.   http://www.bza.org/zeolites.html accessed 27/10/2012

53.   van Koningsveld, H. *Compendium of Zeolite Framework Types, 1st Edition, Building Schemes and Type Characteristics*. (Elsevier Science, 2007).

54.   Kerr, G. T. Chemistry of Crystalline Aluminosilicates. I. Factors Affecting the Formation of Zeolite A. *J. Phys. Chem.* **70,** 1047–1050 (1966).

55.   First, E. L., Gounaris, C. E., Wei, J. & Floudas, C. a. Computational characterization of zeolite porous networks: an automated approach. *Phys. Chem. Chem. Phys.* **13,** 17339–58 (2011).

56.   Clearfield, A., Abm, T. & College, U. Role of Ion Exchange in Solid-state Chemistry. *Chem. Rev.* 125–148 (1988).

57.   Erdem, E., Karapinar, N. & Donat, R. The removal of heavy metal cations by natural zeolites. *J. Colloid Interface Sci.* **280,** 309–314 (2004).

58.   Mon, J., Deng, Y., Flury, M. & Harsh, J. B. Cesium incorporation and diffusion in cancrinite, sodalite, zeolite, and allophane. *Microporous Mesoporous Mater.* **86,** 277–286 (2005).

59. Curkovic, L., Cerjan-Stefanovic, S. & Filipan, T. e r g a m o n. *Wat. Res.* **31,** 3–6 (1997).

60. Dyer, A. (A. *An introduction to zeolite molecular sieves*. (Chichester : Wiley, 1988).

61. Szostak, R. *Molecular Sieves*. (Thompson Science, 1989).

62. Trindade, F. J., Rey, J. F. Q. & Brochsztain, S. Modification of molecular sieves MCM-41 and SBA-15 with covalently grafted pyromellitimide and 1,4,5,8-naphthalenediimide. *J. Colloid Interface Sci.* **368,** 34–40 (2012).

63. Mumpton, F. A. La roca magica: Uses of natural zeolites in agriculture and industry. *Proc. Natl. Acad. Sci.* **96,** 3463–3470 (1999).

64. Lowenstein, W. No Title. *Am. Miner.* **39,** 92 (1954).

65. Mumpton, F. A. *Minerology and Geology of Natural Zeolites, M.S.A. Short Course Notes,*. **4,** (Mineralogical Society of America, 1977).

66. Misaelides, P., Macásek, F., Pinnavaia, T. J. & Colella, C. *Natural Microporous Materials in Environmental Technology: Proceedings of the NATO Advanced Research Workshop on the Application of Natural ... 1998 (Nato Science Series E: (closed))*. (Springer, 1999).

67. Mumpton, F. A. & Sand, L. B. *Natural Zeolites: Occurences, Properties, use*. (Pergamon Press, 1978).

68. Motsi, T., Rowson, N. A. & Simmons, M. J. H. Adsorption of heavy metals from acid mine drainage by natural zeolite. *Int. J. Miner. Process.* **92,** 42–48 (2009).

69. Mitchell, S., Bonilla, A. & Pérez-Ramírez, J. Preparation of organic-functionalized mesoporous ZSM-5 zeolites by consecutive desilication and silanization. *Mater. Chem. Phys.* **127,** 278–284 (2011).

70. Ríos, C. A., Williams, C. D. & Roberts, C. L. Removal of heavy metals from acid mine drainage (AMD) using coal fly ash, natural clinker and synthetic zeolites. *J. Hazard. Mater.* **156,** 23–35 (2008).

71. Gaag, F. J. Van Der. ZSM-5 type zeolites : Synthesis and use in gasphase reactions with amonia. *Disertation* 1–112 (1987).

72. Kusakabe, K., Kuroda, T., Murata, A. & Morooka, S. Formation of a Y-Type Zeolite Membrane on a Porous r-Alumina Tube for Gas Separation. *Ind. Eng. Chem. Res.* **36,** 649–655 (1997).

73. Chen, X. Y., Nik, O. G., Rodrigue, D. & Kaliaguine, S. Mixed matrix membranes of aminosilanes grafted FAU/EMT zeolite and cross-linked polyimide for CO2/CH4 separation. *Polymer (Guildf).* **53,** 3269–3280 (2012).

74. Chen, X. Y., Nik, O. G., Rodrigue, D. & Kaliaguine, S. Mixed matrix membranes of aminosilanes grafted FAU/EMT zeolite and cross-linked polyimide for CO2/CH4 separation. *Polymer (Guildf).* **53,** 3269–3280 (2012).

75. Nik, O. G., Nohair, B. & Kaliaguine, S. Aminosilanes grafting on FAU/EMT zeolite: Effect on CO2 adsorptive properties. *Microporous Mesoporous Mater.* **143,** 221–229 (2011).

76. J, W. Interation of U(VI) with CHA-type zeolitic materials. *Microporous Mesoporous Mater.* **153,** 63–69 (2012).

77.   Sayari, A., Belmabkhout, Y. & Da'na, E. CO2 deactivation of supported amines: does the nature of amine matter? *Langmuir* **28,** 4241–7 (2012).

78.   Mendoza-Barron, J. *et al.* No Title. *Adsorption* **17,** 489 (2011).

79.   Gil, M., Tiscornia, I., de la Iglesia, Ó., Mallada, R. & Santamaría, J. Monoamine-grafted MCM-48: An efficient material for CO2 removal at low partial pressures. *Chem. Eng. J.* **175,** 291–297 (2011).

80.   Sobczak, I. *et al.* Efficient isomerization of safrole by amino-grafted MCM-41 materials as basic catalysts. *Catal. Today* **179,** 159–163 (2012).

81.   Yang, S.-T., Kim, J.-Y., Kim, J. & Ahn, W.-S. CO2 capture over amine-functionalized MCM-22, MCM-36 and ITQ-2. *Fuel* **97,** 435–442 (2012).

82.   Nik, O. G., Sadrzadeh, M. & Kaliaguine, S. Surface grafting of FAU/EMT zeolite with (3-aminopropyl)methyldiethoxysilane optimized using Taguchi experimental design. *Chem. Eng. Res. Des.* **90,** 1313–1321 (2012).

83.   Liu, G., Xiangli, F., Wei, W., Liu, S. & Jin, W. Improved performance of PDMS/ceramic composite pervaporation membranes by ZSM-5 homogeneously dispersed in PDMS via a surface graft/coating approach. *Chem. Eng. J.* **174,** 495–503 (2011).

84.   *http://www.epa.gov/rpdweb00/radionuclides/strontium.html accessed 7/8/12*.

85.   Mola, M., Palomo, M., Peñalver, a, Borrull, F. & Aguilar, C. Comparative study of different analytical methods for the determination of 238U, 234U, 235U, 230Th and 232Th in NORM samples (Southern Catalonia). *J. Environ. Radioact.* **115,** 207–13 (2013).

86.   Maggi, R., Piscopo, C. G., Sartori, G., Storaro, L. & Moretti, E. Supported sulfonic acids: Metal-free catalysts for the oxidation of hydroquinones to benzoquinones with hydrogen peroxide. *Appl. Catal. A Gen.* **411–412,** 146–152 (2012).

87.   Bao, S., Liu, G., Wang, L. & Zhang, X. Quasi-homogeneous catalytic activities of hydrocarbon dispersible HZSM-5 nanocrystals grafted with different alkyl groups. *Appl. Catal. A Gen.* **405,** 61–68 (2011).

88.   Mitchell, S., Bonilla, A. & Pérez-Ramírez, J. Preparation of organic-functionalized mesoporous ZSM-5 zeolites by consecutive desilication and silanization. *Mater. Chem. Phys.* **127,** 278–284 (2011).

89.   http://www.iza-online.org/natural/Datasheets/clinoptilolite/clinoptilolite.html accessed 27/10/2012

90.   Dowty, E. ATOMS. Shape Software, Kingsport, Tennessee, USA. (2006).

91.   *http://www.britannica.com/EBchecked/topic/121782/clinoptilolite accessed 25/4/2012*

92.   Johnson, M. *et al.* Cation exchange, dehydration, and calcination in clinoptilolite: In situ x-ray diffraction and computer modeling. *J. Phys. Chem. B* **107,** 942–951 (2003).

93.   Depmeier, W. The sodalite family - A simple but versatile framework structure. *Micro-Mesoporous Miner. Phases* **57,** (2005).

94.   Douglas, G., Shackleton, M. & Woods, P. Hydrotalcite formation facilitates effective contaminant and radionuclide removal from acidic uranium mine barren lixiviant. *Appl.*

Geochemistry **42,** 27–37 (2014).

95. Wiles, D. R. *The Chemistry of Nuclear Fuel Waste Disposal*. (Polytechnic International Press, Canada, 2002).

96. Technology, E. & Litter, C. Clay Minerals Clay Minerals Clay Minerals Clay Minerals are Phyllosilicates. 1–22

97. King, R. S. P., Dann, S. E., Elsegood, M. R. J., Kelly, P. F. & Mortimer, R. J. The synthesis, full characterisation and utilisation of template-free silica sodalite, a novel polymorph of silica. *Chemistry* **15,** 5441–3 (2009).

98. Kogel, J. E., Trivedi, N. C. & Barker, J. M. *Industrial Minerals and Rocks, 7th Ed*. (Society for Mining, Metallurgy, and Exploration, 2006).

99. Jillavenkatesa, A., Dapkunas, S. J. & Lum, L. H. practice guide Particle size caracterization. *Nist* **Special pu,** 164 (2001).

100. Wang, J. F., Lin, F. & Pang, W. Q. Ammonium exchange in aqueous solution using Chinese natural clinoptillolite and modified zeolite. *J. Hazard. Mater.* **142,** 160 (2007).

101. Kerr, P. F. *Formation and occurrence of clay minerals. Proceedings of the first national conference on clays and clay technology*. (1955).

102. Madejová, J. FTIR techniques in clay mineral studies. *Vib. Spectrosc.* **31,** 1–10 (2003).

103. KISHK FM & BARSHAD. Morphology of Vermiculite Clay Particles As Affected By Their Genesi. *Am. Mineral.* **54,** 849–857 (1969).

104. Deer, W. A. W. *Rock forming minerals. Vol. 4B, Framework silicates : silica minerals, feldspathoids and zeolites*. (London : Geological Society, 2004).

105. Deer, W. A., Howie, R. A. & Zussman, J. *An Introduction to the Rock forming minerals 2 ed.* (Longman, 1992).

106. Deer, W. A., Howie, R. A. & Zussman, J. *Rock Forming Minerals Vol.3, Sheet Silicates*. (Longman, 1963).

107. *http://webmineral.com/data/Vermiculite.shtml accessed 4/9/12*.

108. *http://rruff.geo.arizona.edu/doclib/hom/vermiculite.pdf accessed 4/9/12*

109. Donat, R. The removal of uranium (VI) from aqueous solutions onto natural sepiolite. *J. Chem. Thermodyn.* **41,** 829–835 (2009).

110. Matherson, A. & Walker, G. F. Crystal structure of magnesium vermiculite. *Am. Mineral.* **38,** 231–256 (1953).

111. *http://www.webmineral.com/data/Kaolinite.shtml acessed 3/9/12*

112. *http://rruff.geo.arizona.edu/doclib/hom/kaolinite.pdf acessed 3/9/12*

113. Willms, C., Li, Z., Allen, L. & Evans, C. V. Desorption of cesium from kaolinite and illite using alkylammonium salts. *Appl. Clay Sci.* **25,** 125–133 (2004).

114. Avila, L. R. *et al.* Journal of Colloid and Interface Science New synthesis strategies for effective functionalization of kaolinite and saponite with silylating agents. *J. Colloid Interface Sci.* **341,**

186–193 (2010).

115. Che, C., Glotch, T. D., Bish, D. L., Michalski, J. R. & Xu, W. Spectroscopic study of the dehydration and/or dehydroxylation of phyllosilicate and zeolite minerals. *J. Geophys. Res. E Planets* **116,** 1–23 (2011).

116. Zou, Q., Zou, L. & Tian, H. Detection and adsorption of Hg2+ by new mesoporous silica and membrane material grafted with a chemodosimeter. *J. Mater. Chem.* **21,** 14441 (2011).

117. Agarande, M., Schmidt, S. & Bouisset, P. Plutonium , protactinium , uranium and thorium isotopes determination in environmental samples by SF ICP-MS. *Radioprotection* **40,** 727–731 (2005).

118. Cozzella, R. Pettirossi, M. L. *Use of ICP-MS with different analytical techniques to investigate uranium, thorium and plutonium in urine in case of radiological emergency*. (2005).

119. A. S. Knox, D. I. Kaplan, D. C. Adriano, T. G. Hinton, M. D. W. Apatite and Phillipsite as Seqestering Agents for Metals and Radionuclides. *J. Environ. Qual.* **32,** 515 (2003).

120. Omar, H., Arida, H. & Daifullah, A. Adsorption of 60Co radionuclides from aqueous solution by raw and modified bentonite. *Appl. Clay Sci.* **44,** 21–26 (2009).

121. Van Hoof, V., Dotremont, C. & Buekenhoudt, A. Performance of Mitsui NaA type zeolite membranes for the dehydration of organic solvents in comparison with commercial polymeric pervaporation membranes. *Sep. Purif. Technol.* **48,** 304–309 (2006).

122. Lemoine, G. Comparison of Different Types of Zeolites Used As Solid Acid Catalysts in Jatropha-Type Oil for Biodiesel. 1–183 (2013).

123. Savannah, W. & Company, R. Uranium co-precipitation with iron oxide minerals. *Geochim. Cosmochim. Acta* **66,** 3533–3547 (2002).

124. Orechovska, J. & P, R. Sorption of cesium on composite sorbents based on nickel ferrocyanide. *j radioanal nucl ch* **242,** 387–390 (1999).

125. Sharma, P., Singh, G. & Tomar, R. Synthesis and charachterisation of an analogue of heulandite. *J. Colloid Interface Sci.* **332,** 289 (2009).

126. Knops-Gerrits, P.-P., De Vos, D. E., Feijen, E. J. P. & Jacobs, P. a. Raman spectroscopy on zeolites. *Microporous Mater.* **8,** 3–17 (1997).

127. Suc, V. N. & Ly, H. T. Y. Adsorption of U (Vi) From Aqueous Solution Onto Modified Chitosan. *Uranium* **4,** 286–299 (2012).

128. Zou, W., Zhao, L. & Han, R. Absorption characteristics of uranyl ions by manganesse oxide coated sand in batch mode. *J RADIOANAL NUCL CH* **288,** 239–249 (2011).

129. Vasiliev, A. N., Golovko, L. V., Trachevsky, V. V., Hall, G. S. & Khinast, J. G. Adsorption of heavy metal cations by organic ligands grafted on porous materials. *Microporous Mesoporous Mater.* **118,** 251–257 (2009).

130. Jones, C. Organic functionlised molecular sieves as shape selective catalysts. *Nature* **393,** 52–54 (1998).

131. Creyghton, E. Organic groups cling to the pores. *Nature* **393,** 21–22 (1998).

132.   Gopalan, A. *et al.* No Title. in *5th An. WERC Tech. Devel. Conf.* 123–132 (1995).

133.   Bisset, W., Jacobs, H., Koshti, N., Stark, P. & Gopalan, A. Synthesis and metal ion complexation properties of a novel polyethyleneimine N-methylhydroxamic acid water soluble polymer. *React. Funct. Polym.* **55,** 109–119 (2003).

134.   Panahi, H. A., Mehmandost, N., Moniri, E. & Galaev, I. Y. Iminodiacetic Acid-Containing Polymer Brushes Grafted onto Silica Gel for Preconcentration and Determination of Copper(II) in Environmental Samples. *J. Appl. Polym. Sci.* **126,** 480–489 (2012).

135.   Holt, J. Thesis. (Loughborough University, 2014).

136.   Bakhmutov, V. I. NMR spectroscopy in liquids and solids. (2015).

137.   Abraham, J. L., Fisher, J. & Loftus, P. *Introduction to NMR spectroscopy*. (John Wiley and sons, 1988).

138.   Crisp, J. Thesis. (Loughborough University, 2011).

139.   Duer, M. J. *Solid-State NMR Spectroscopy Principles and Applications*. (Blackwell Science Ltd, 2001). doi:10.1002/9780470999394

140.   Exeter Analytical. CHN Micro-analysis: A comparative review of the instrument design on analytical performance

141.   Dann, S. E. & of Chemistry Royal Society. *Reactions and characterization of solids*. (Cambridge : Royal Society of Chemistry, 2000).

142.   https://www.jeol.co.jp/en/applications/pdf/sm/sem_atoz_all.pdf accessed 2/4/16

143.   Carpenter, B. & Longworth, G. *The Radiochemical Manual*. (1998).

144.   Malcolme-Lawes, D. J. *Introduction into radiochemistry*. (1979).

145.   *http://webmineral.com/data/Clinoptilolite-Na.shtml accessed 11/6/2012*

146.   *Nirex Technical Note July 2003: Site selection and investigations for a deep geological repository, preliminary technical planning in support of the stepwise process.*

147.   Rocha, J. & Klinowski, J. Solid-State NMR Studies of the Structure and Reactivity of Metakaolinite. *Angew. Chemie Int. Ed. English* **29,** 553–554 (1990).

148.   Chan, K. L. A. & Kazarian, S. G. Detection of trace materials with Fourier transform infrared spectroscopy using a multi-channel detector. *Analyst* **131,** 126–131 (2006).

149.   Amarasinghe, P. M., Katti, K. S. & Katti, D. R. Nature of organic fluid-montmorillonite interactions: An FTIR spectroscopic study. *J. Colloid Interface Sci.* **337,** 97–105 (2009).

150.   Joseph, J. K. & Glenn, T. S *The chemistry of the actinide elements*. (Methuen, 1957).

151.   Housecroft, C. E. & Sharpe, A. G. *Inorganic chemistry*. (Harlow : Pearson Prentice Hall, 2007).

152.   Diaz-Nava, C., Olguin, M. T., Alarcon-Herrera, M. T. & Aguilar-Elguezabal, A. Effects of preparation and experimental conditions on removal of phenol by surfactant-modified zeolites. *Environ. Technol.* **29,** 1229 (2005).

153.   Kneuer, C. *et al.* Silica nanoparticles modified with aminosilanes as carriers for plasmid DNA.

Int. J. Pharm. **196,** 257–261 (2000).

154. Guo, C., Zhou, L. & Lv, J. Effects of expandable graphite and modified ammonium polyphosphate on the flame-retardant and mechanical properties of wood flour-polypropylene composites. *Polym. Polym. Compos.* **21,** 449–456 (2013).

155. Djomgoue, P. & Njopwouo, D. FT-IR Spectroscopy Applied for Surface Clays Characterization. *J. Surf. Eng. Mater. Adv. Technol.* **3,** 275–282 (2013).

156. Birger Anspach, F. Silica-based metal chelate affinity sorbents I. Preparation and characterization of iminodiacetic acid affinity sorbents prepared via different immobilization techniques. *J. Chromatogr. A* **672,** 35–49 (1994).

157. Sarangi, A. K. Uranium and its measurment in ore by radiometric method. *J. Mines, Met. Fuels, Annu. Rev.* 1–8 (2000).

158. Beatty, S. T., Fischer, R. J., Hagers, D. L. & Rosenberg, E. SEPARATIONS A Comparative Study of the Removal of Heavy Metal Ions from Water Using a Silica - Polyamine Composite and a Polystyrene Chelator Resin. *Ind. Eng. Chem. Res.* **38,** 4402–4408 (1999).

159. Deka, R. C. ChemInform Abstract: Acidity in Zeolites and Their Characterization by Different Spectroscopic Methods. *ChemInform* **30,** no-no (2010).

160. Lin, Y. *et al.* Incorporation of hydroxypyridinone ligands into self-assembled monolayers on mesoporous supports for selective actinide sequestration. *Environ. Sci. Technol.* **39,** 1332–1337 (2005).

161. Alves, A. P. M., Fonseca, M. G. & Wanderley, A. F. Inorganic-organic hybrids originating from organosilane anchored onto leached vermiculite. *Mater. Res.* **16,** 891–897 (2013).

162. Sánchez, F., Iglesias, M., Corma, A. & del Pino, C. New rhodium complexes anchored on silica and modified Y-zeolite as efficient catalysts for hydrogenation of olefins. *J. Mol. Catal.* **70,** 369–379 (1991).

163. Corma, A., Iglesias, M., del Pino, C. & Sanchez, F. New Rhodium Complexes anchored on Modified USY Zeolites. A Remarkable Effect of the Support on the Enantioselectivity of Catalytic Hydrogenation of Prochiral Alkenes. *J. Am. Chem. Soc.* 1253–1255 (1991). doi:10.1039/c39910001253

164. Carmona, A., Corma, A., Iglesias, M., San José, A. & Sánchez, F. Synthesis and characterization of new chiral Rh(I) complexes with N, N'-, and N, P-ligands. A study of anchoring on the moodified zeolites and catalytic properties of heterogenized complexes. *J. Organomet. Chem.* **492,** 11–21 (1995).

165. Preedy, O. *et al.* Uranium and technetium interactions with wüstite surfaces under geological disposal facility conditions. *Mineral. Mag.* **78,** 1097–1113 (2014).

166. Yang, P. & Armbruster, T. Na, K, Rb, and Cs Exchange in Heulandite Single-Crystals: X-Ray Structure Refinements at 100 K. *J. Solid State Chem.* **123,** 140–149 (1996).

167. Aldermatt, D. & Brown, I. D. Bond valence calculations. *Acta Crystallogr. A* **43,** 125–130 (1987).

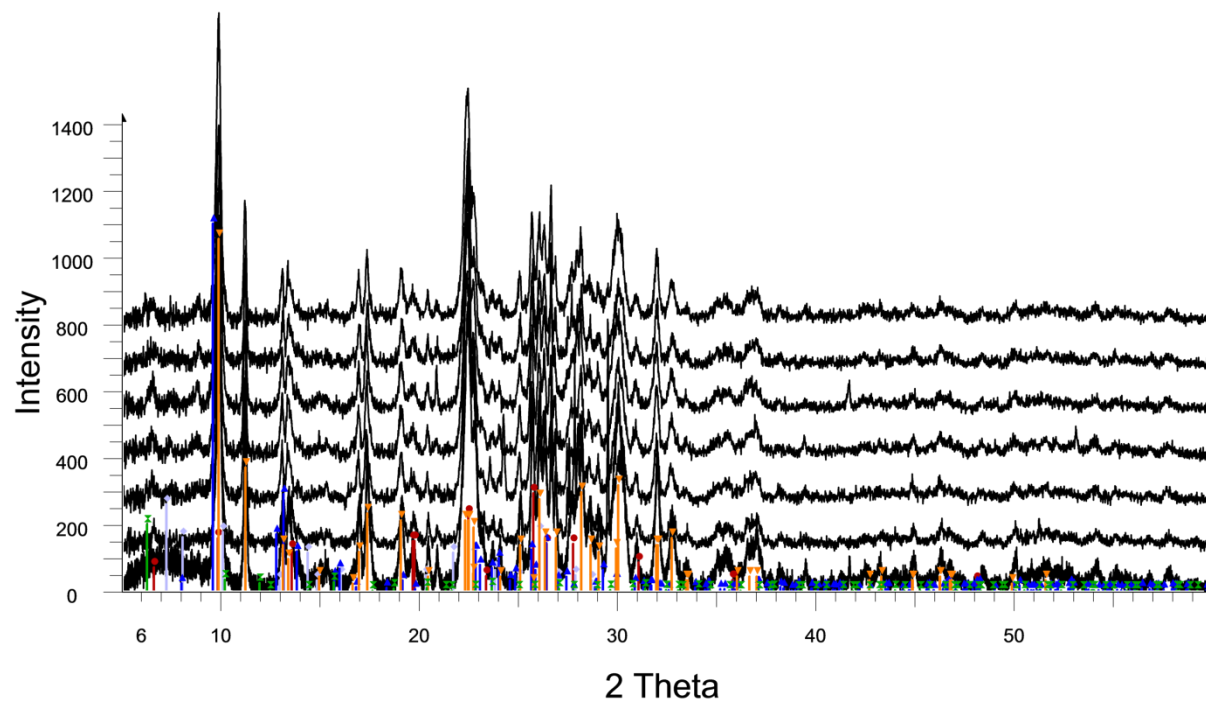168. Howery D. G. & Thomas H. C. Ion Exchange on the mineral clinoptilolite. J. Phys. Chem. **69,**

531-537 (1965)

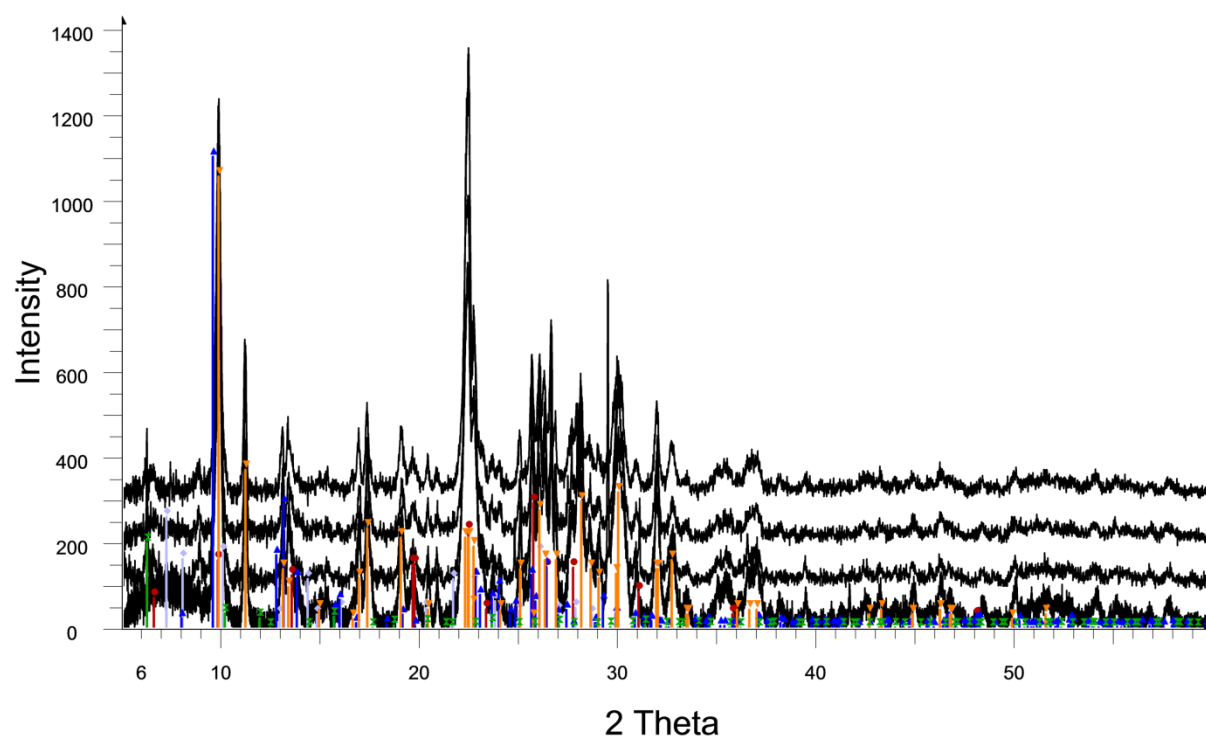169.   http://www1.lsbu.ac.uk/water/water_redox.html accessed 2/2/2012

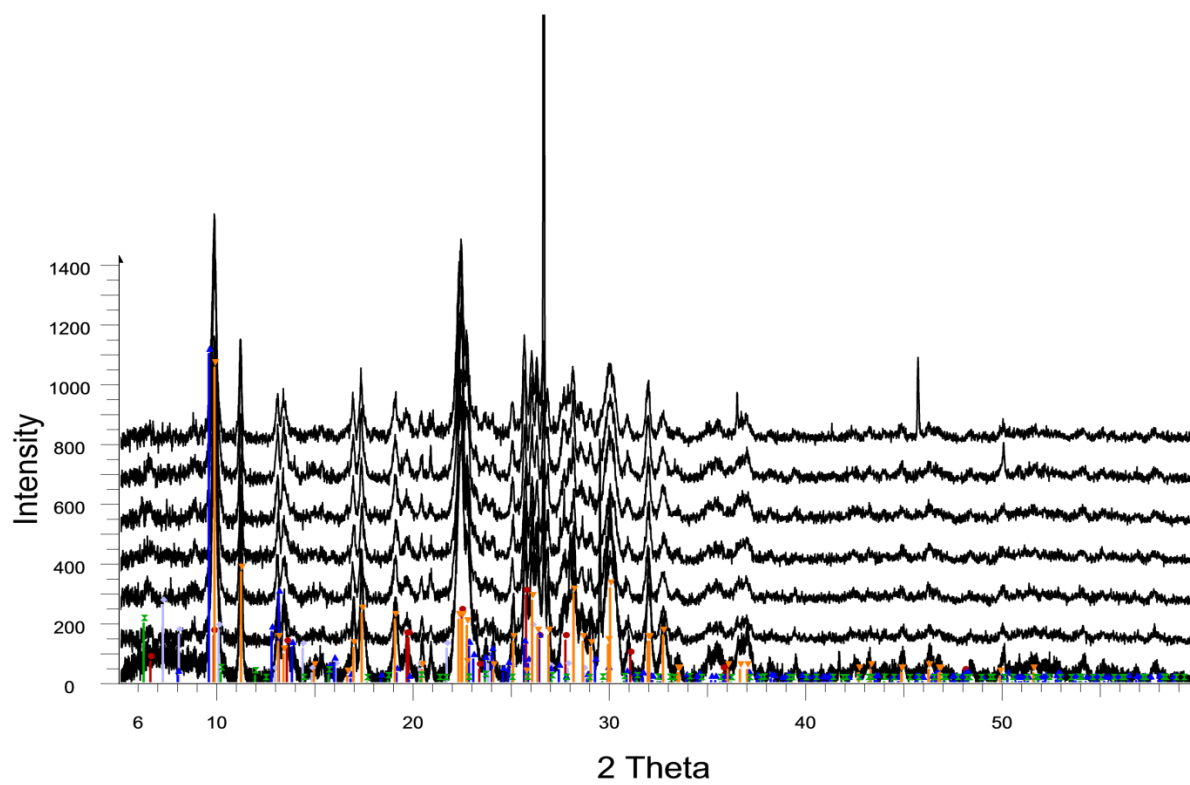# Chapter 8 – Appendices

8.1 PXRD patterns

Clinoptilolite (NDA) and TMSPE grafting PXRD patterns for reaction time layered from bottom to top, unmodified, 1, 2, 4, 8, 16 and 24 hours

Clinoptilolite (NDA) and TMSPE grafting PXRD patterns for ligand concentration layered from bottom to top, unmodified, 1, 3, 8 mL.
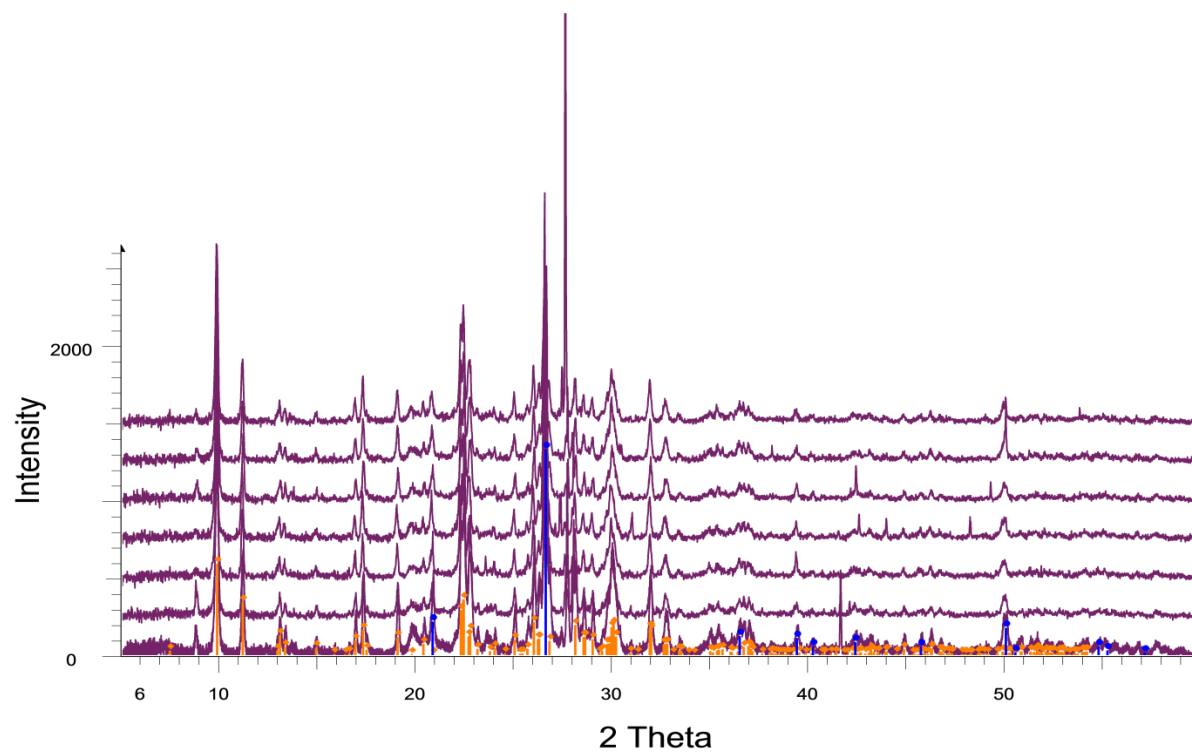
Clinoptilolite (NDA) and TMSPE grafting PXRD patterns for reaction time layered from bottom to top, unmodified, methanol, ethanol, dichloromethane, acetone, toluene and hexane.
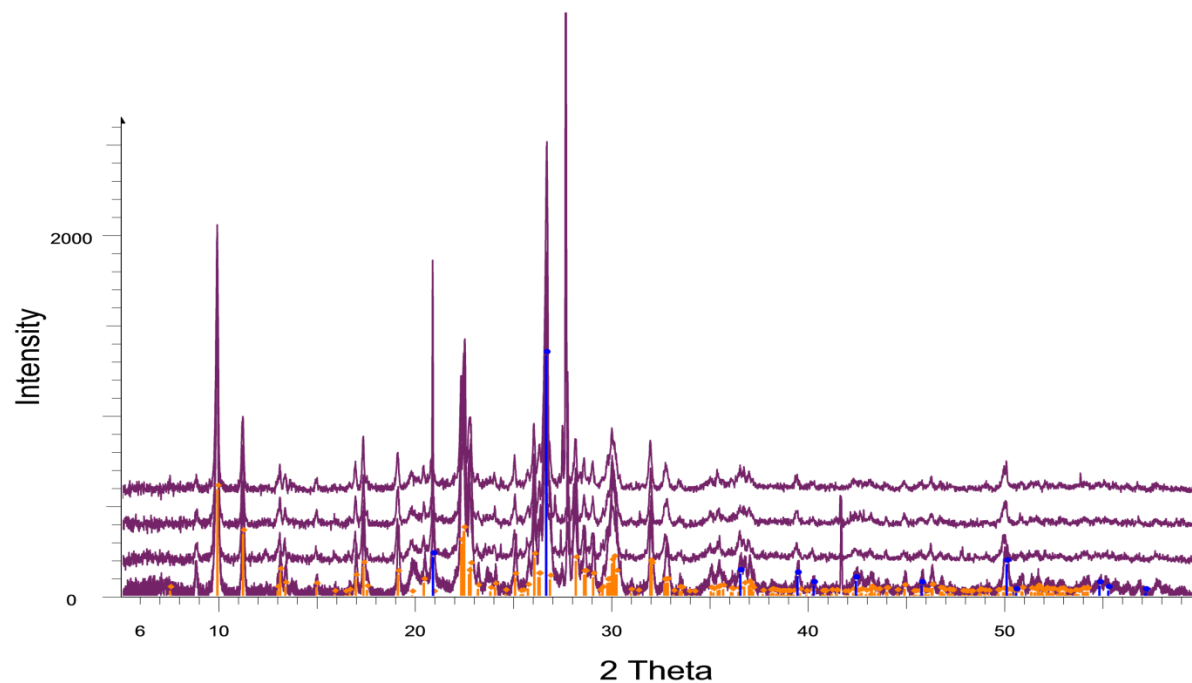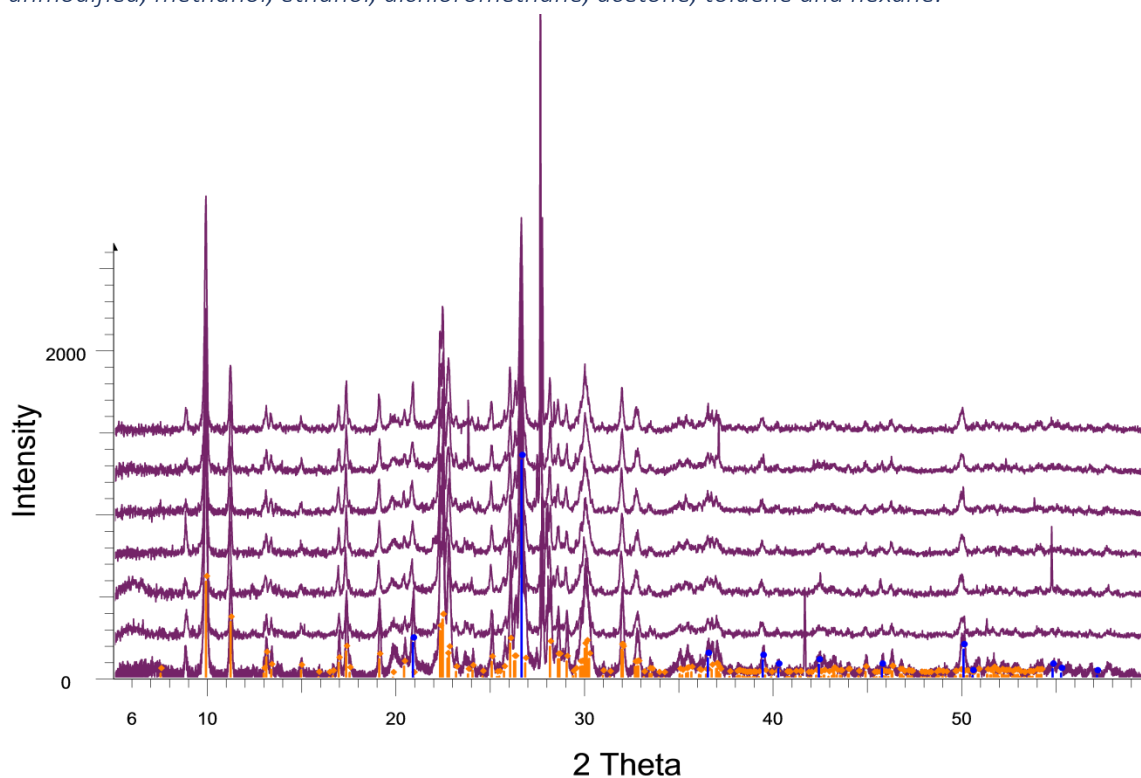
Clinoptilolite (Imerys) and TMSPE grafting PXRD patterns for reaction time layered from bottom to top, unmodified, 1, 2, 4, 8, 16 and 24 hours
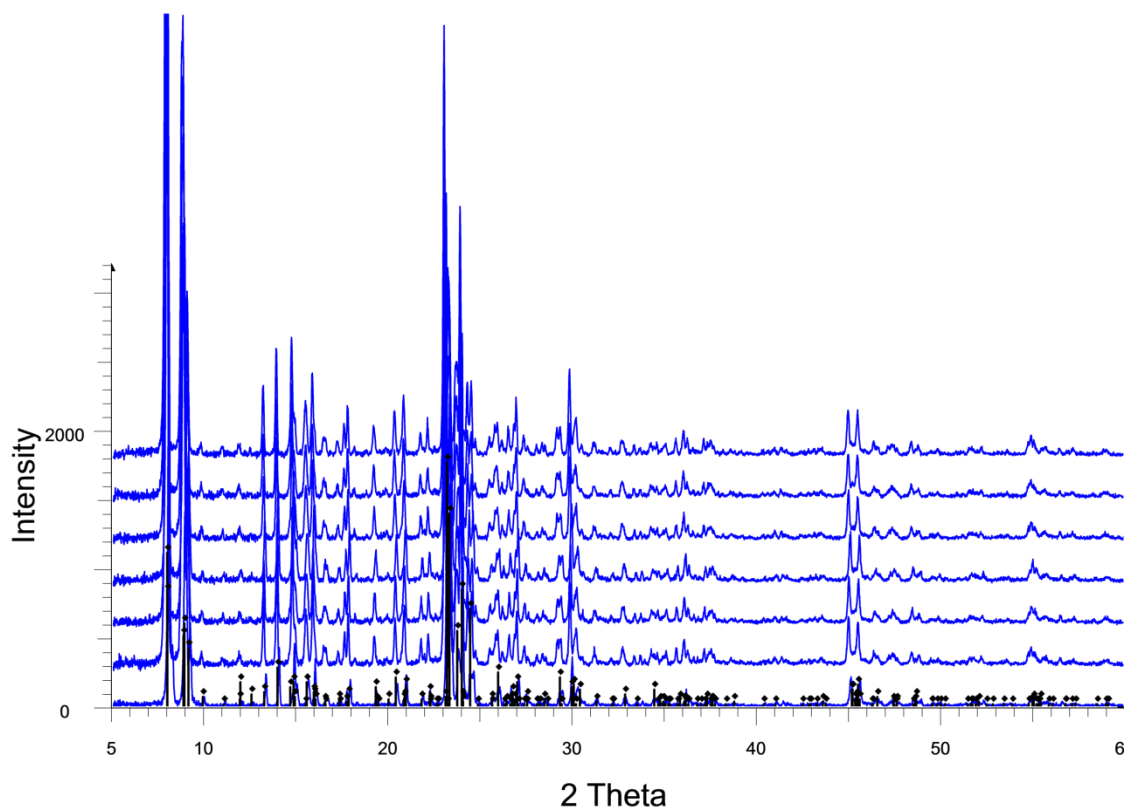

Clinoptilolite (Imerys) and TMSPE grafting PXRD patterns for ligand concentration layered from bottom to top, unmodified, 1, 3, 8 mL.
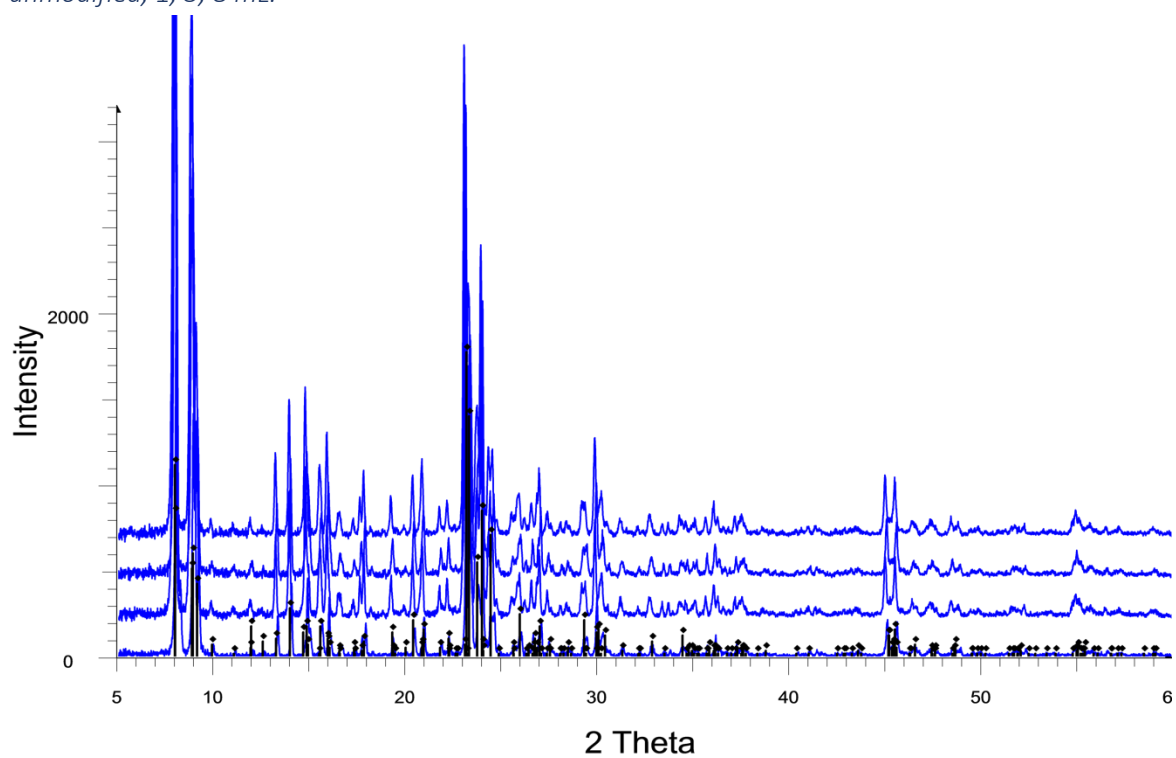
Clinoptilolite (Imerys) and TMSPE grafting PXRD patterns for reaction time layered from bottom to top, unmodified, methanol, ethanol, dichloromethane, acetone, toluene and hexane.

ZSM-5 and TMSPE grafting PXRD patterns for reaction time layered from bottom to top, unmodified, 1, 2, 4, 8, 16 and 24 hours

ZSM-5 and TMSPE grafting PXRD patterns for ligand concentration layered from bottom to top, unmodified, 1, 3, 8 mL.

ZSM-5 and TMSPE grafting PXRD patterns for reaction time layered from bottom to top, unmodified, methanol, ethanol, dichloromethane, acetone, toluene and hexane.

Vermiculite and TMSPE grafting PXRD patterns for reaction time layered from bottom to top, unmodified, 1, 2, 4, 8, 16 and 24 hours

Vermiculite and TMSPE grafting PXRD patterns for ligand concentration layered from bottom to top, unmodified, 1, 3, 8 mL.

Vermiculite and TMSPE grafting PXRD patterns for reaction time layered from bottom to top, unmodified, methanol, ethanol, dichloromethane, acetone, toluene and hexane.
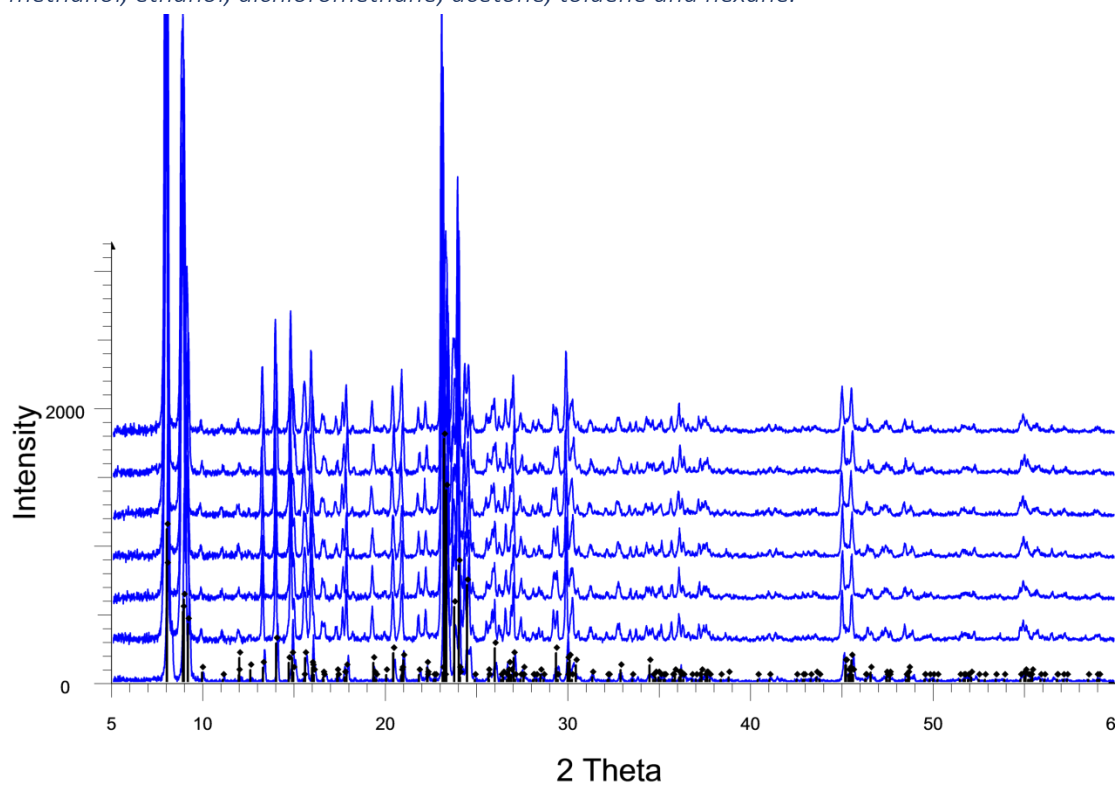
Kaolinite and TMSPE grafting PXRD patterns for reaction time layered from bottom to top, unmodified, 1, 2, 4, 8, 16 and 24 hours
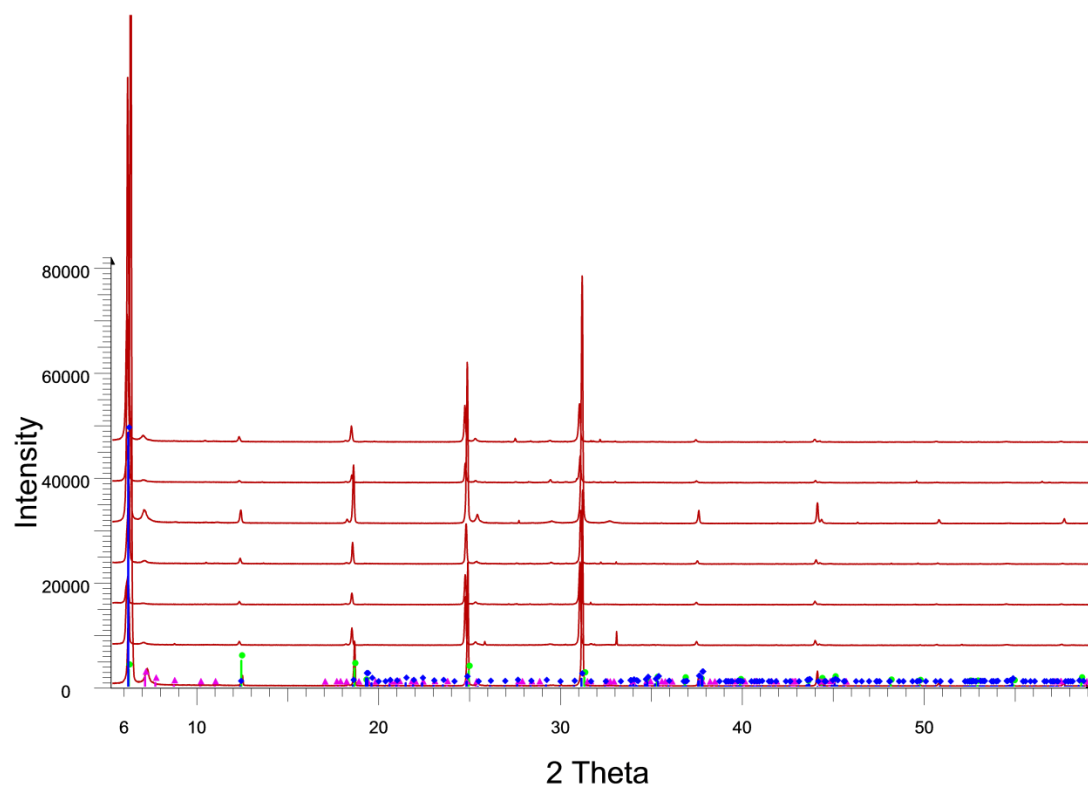

Kaolinite and TMSPE grafting PXRD patterns for ligand concentration layered from bottom to top, unmodified, 1, 3, 8 mL.
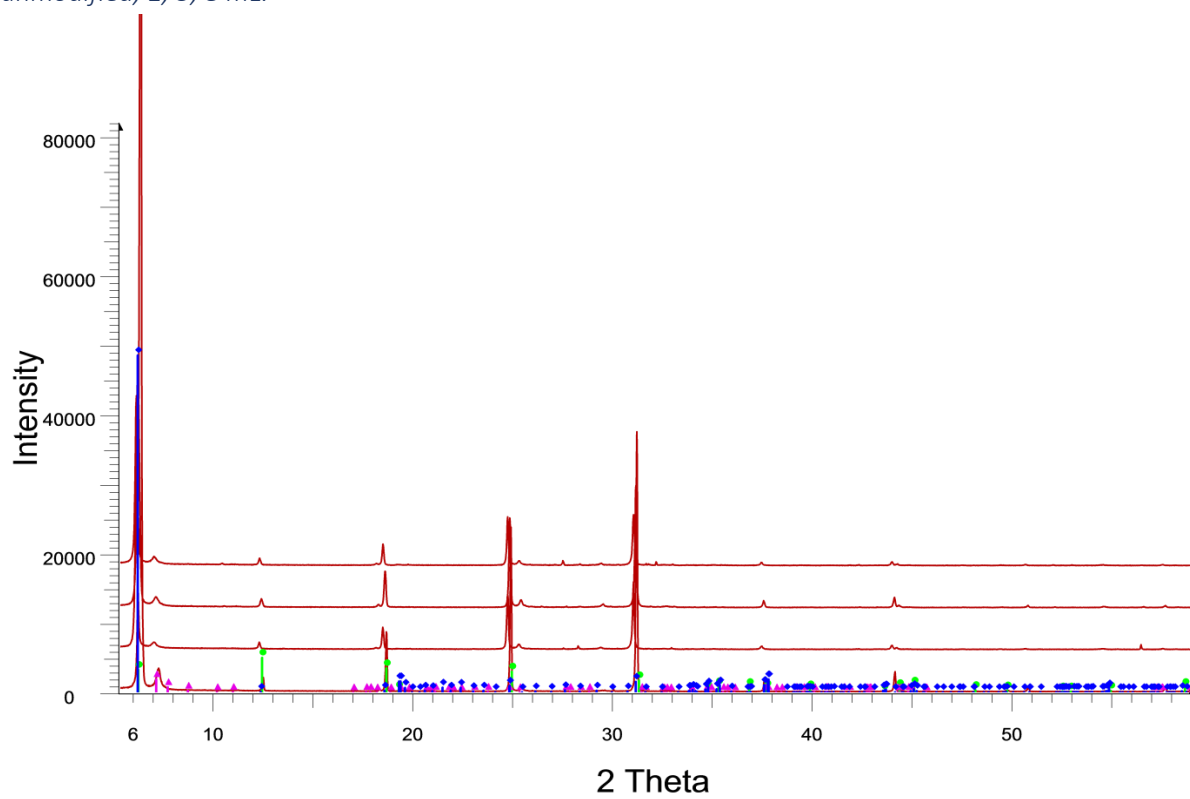
Kaolinite and TMSPE grafting PXRD patterns for reaction time layered from bottom to top, unmodified, methanol, ethanol, dichloromethane, acetone, toluene and hexane.

Clinoptilolite (NDA) and TMSPETT grafting PXRD patterns for reaction time layered from bottom to top, unmodified, 1, 2, 4, 8, 16 and 24 hours

Clinoptilolite (NDA) and TMSPETT grafting PXRD patterns for ligand concentration layered from bottom to top, unmodified, 1, 3, 8 mL.

Clinoptilolite (NDA) and TMSPETT grafting PXRD patterns for reaction time layered from bottom to top, unmodified, methanol, ethanol, dichloromethane, acetone, toluene and hexane.
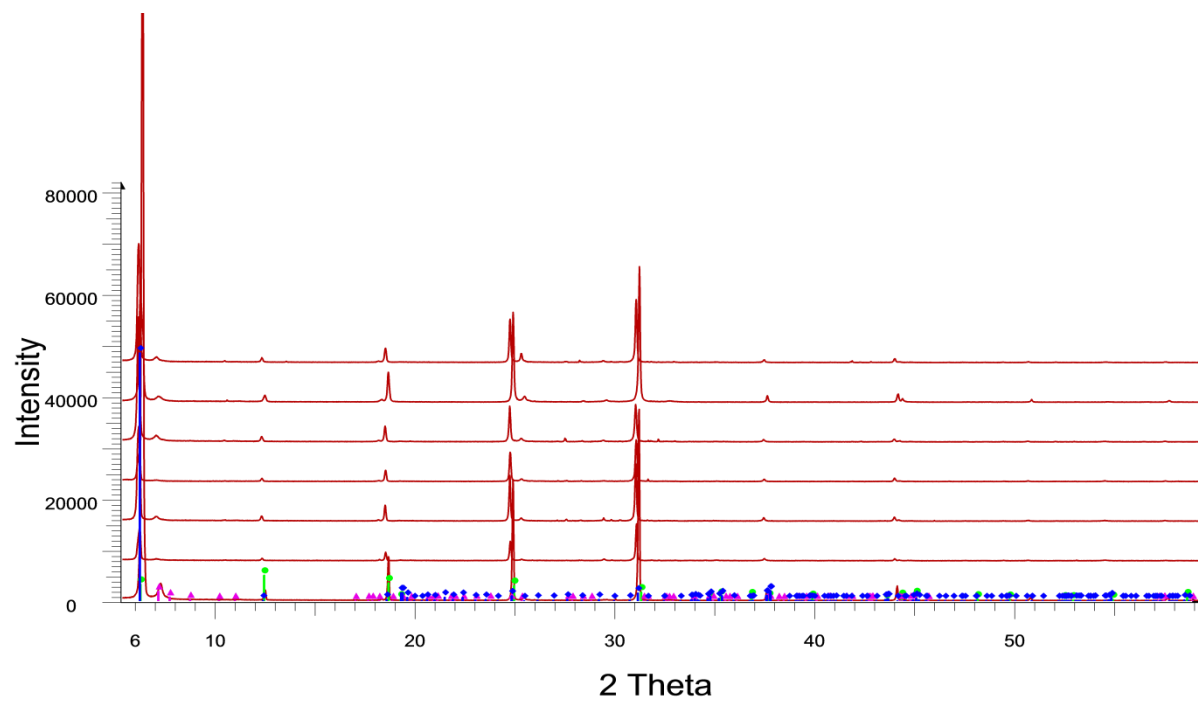

Clinoptilolite (Imerys) and TMSPETT grafting PXRD patterns for reaction time layered from bottom to top, unmodified, 1, 2, 4, 8, 16 and 24 hours

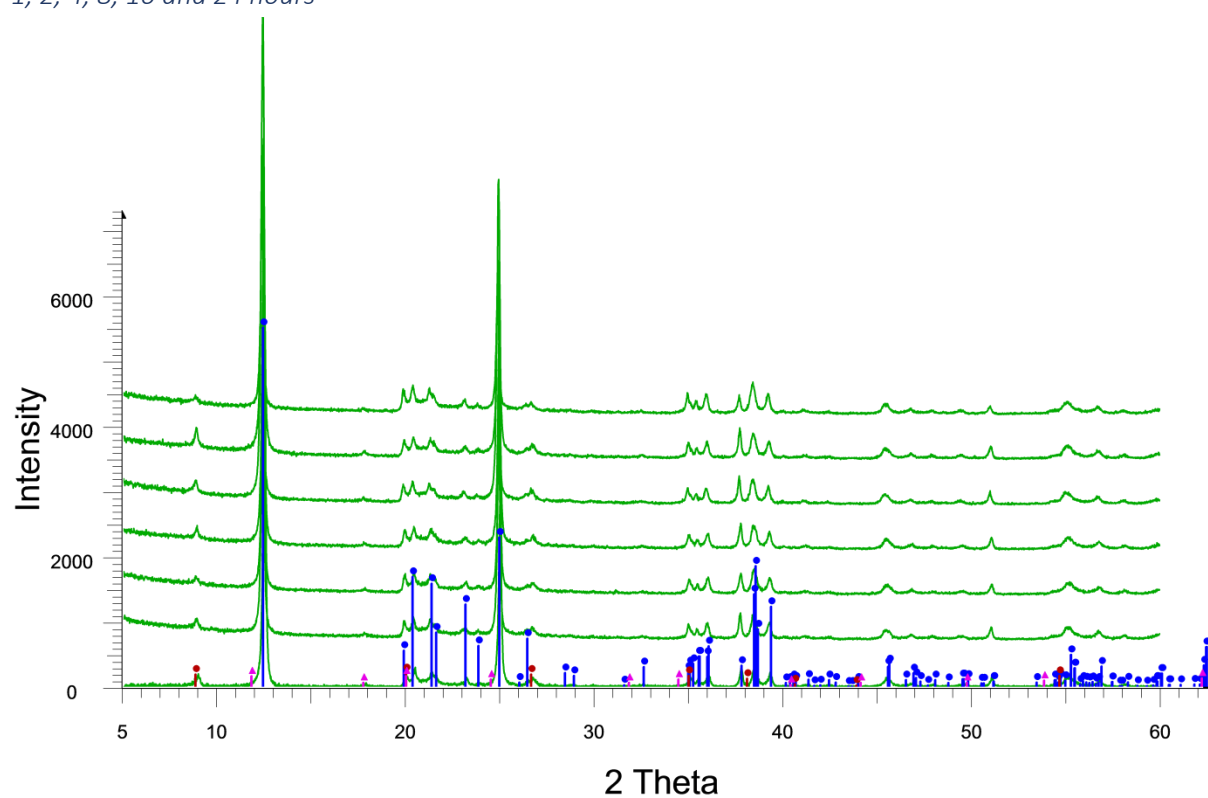*Clinoptilolite (Imerys) and TMSPETT grafting PXRD patterns for ligand concentration layered from bottom to top, unmodified, 1, 3, 8 mL.*

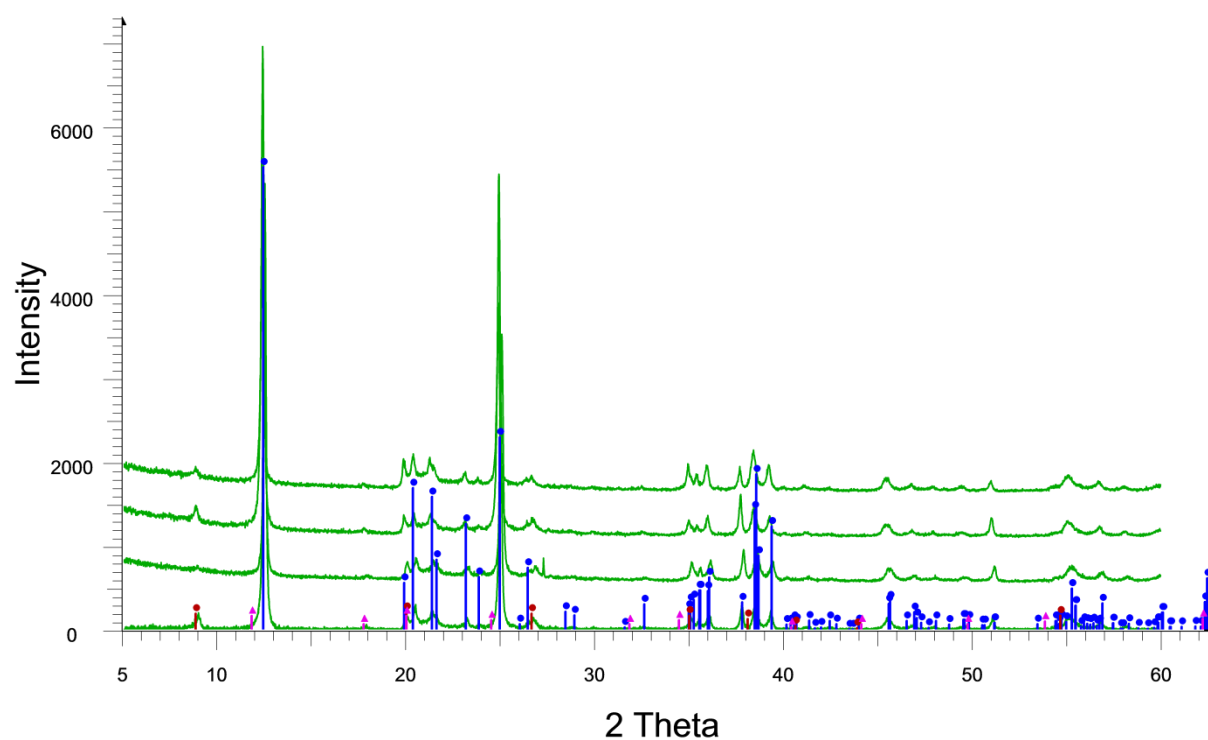*Clinoptilolite (Imerys) and TMSPETT grafting PXRD patterns for reaction time layered from bottom to top, unmodified, methanol, ethanol, dichloromethane, acetone, toluene and hexane.*

ZSM-5 and TMSPETT grafting PXRD patterns for reaction time layered from bottom to top, unmodified, 1, 2, 4, 8, 16 and 24 hours

ZSM-5 and TMSPETT grafting PXRD patterns for ligand concentration layered from bottom to top, unmodified, 1, 3, 8 mL.

ZSM-5 and TMSPETT grafting PXRD patterns for reaction time layered from bottom to top, unmodified, methanol, ethanol, dichloromethane, acetone, toluene and hexane.
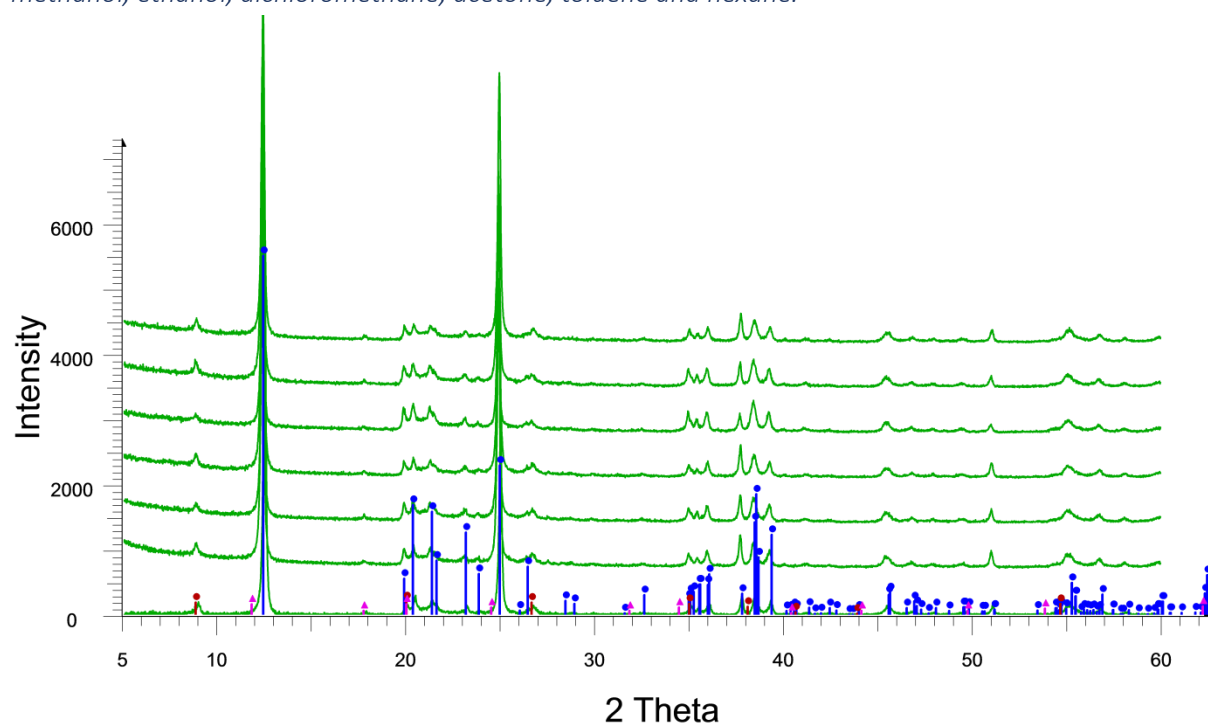
Vermiculite and TMSPETT grafting PXRD patterns for reaction time layered from bottom to top, unmodified, 1, 2, 4, 8, 16 and 24 hours

Vermiculite and TMSPETT grafting PXRD patterns for ligand concentration layered from bottom to top, unmodified, 1, 3, 8 mL.

Vermiculite and TMSPETT grafting PXRD patterns for reaction time layered from bottom to top, unmodified, methanol, ethanol, dichloromethane, acetone, toluene and hexane.

Kaolinite and TMSPETT grafting PXRD patterns for reaction time layered from bottom to top, unmodified, 1, 2, 4, 8, 16 and 24 hours
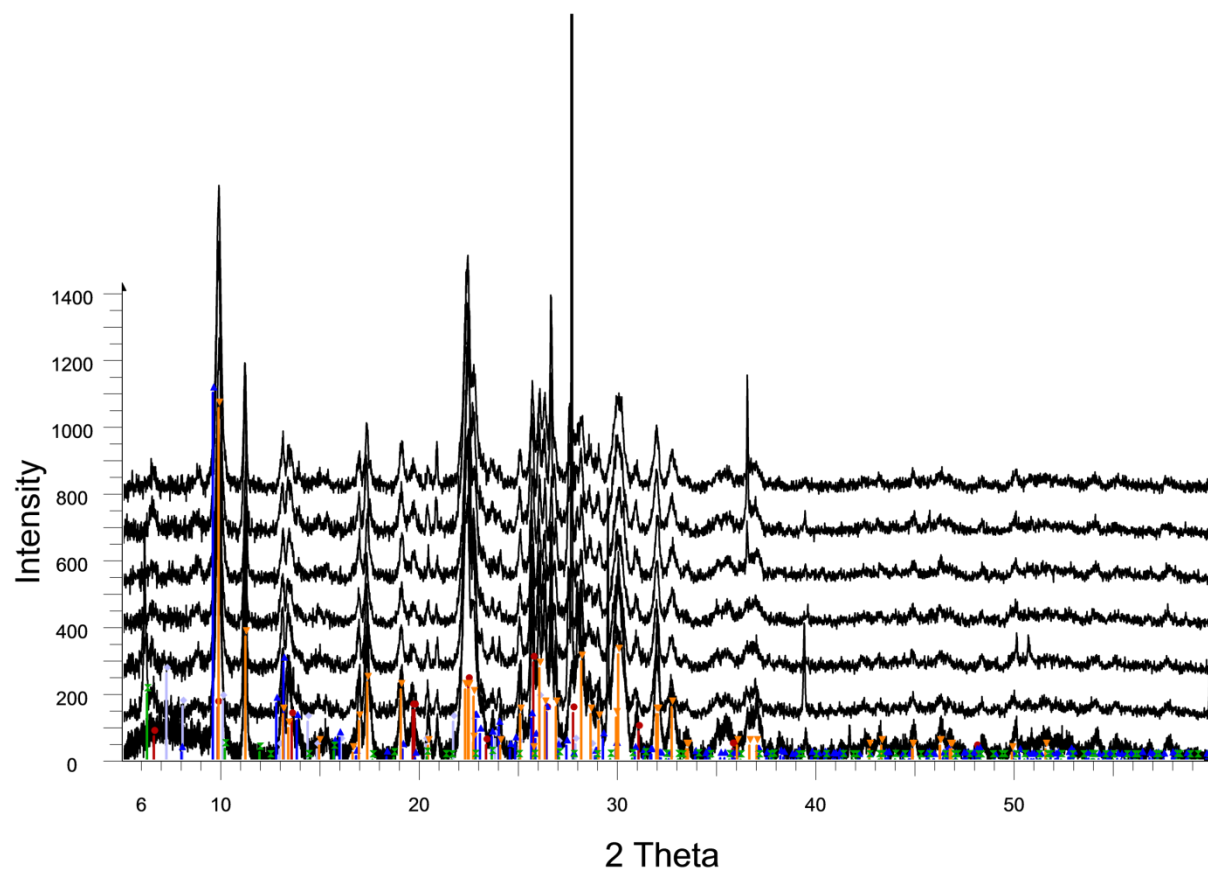
Kaolinite and TMSPETT grafting PXRD patterns for ligand concentration layered from bottom to top, unmodified, 1, 3, 8 mL.
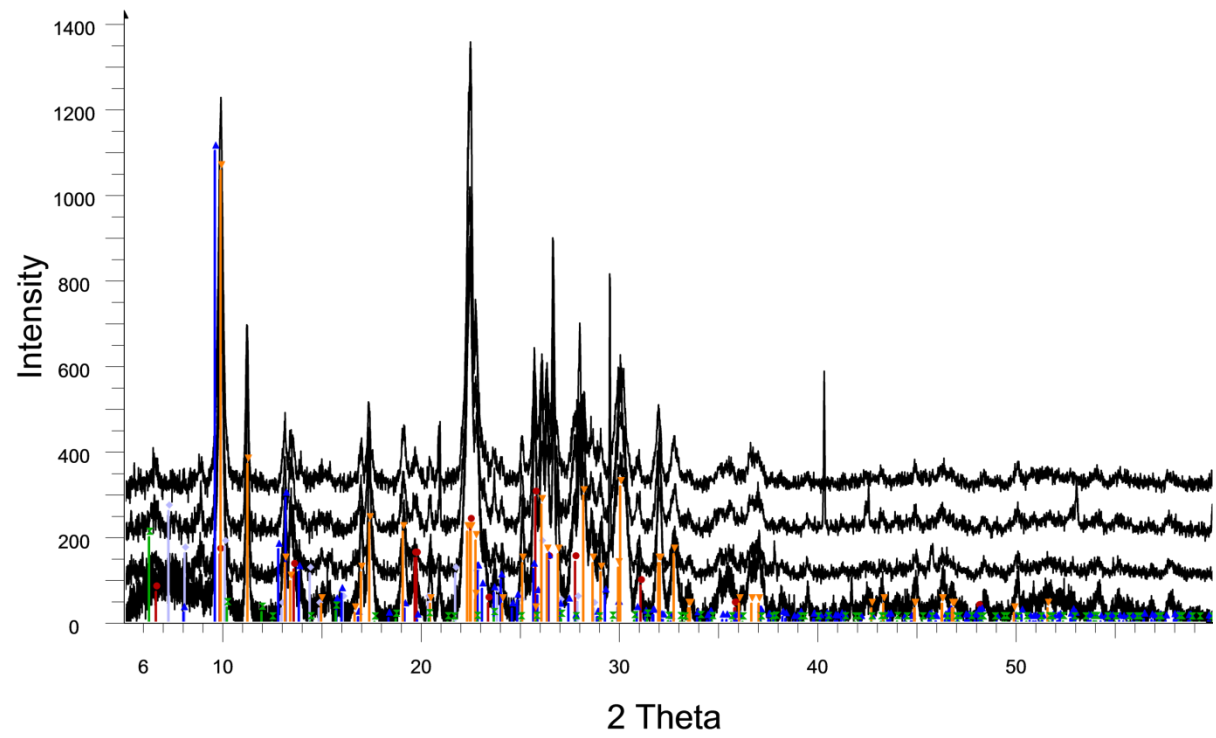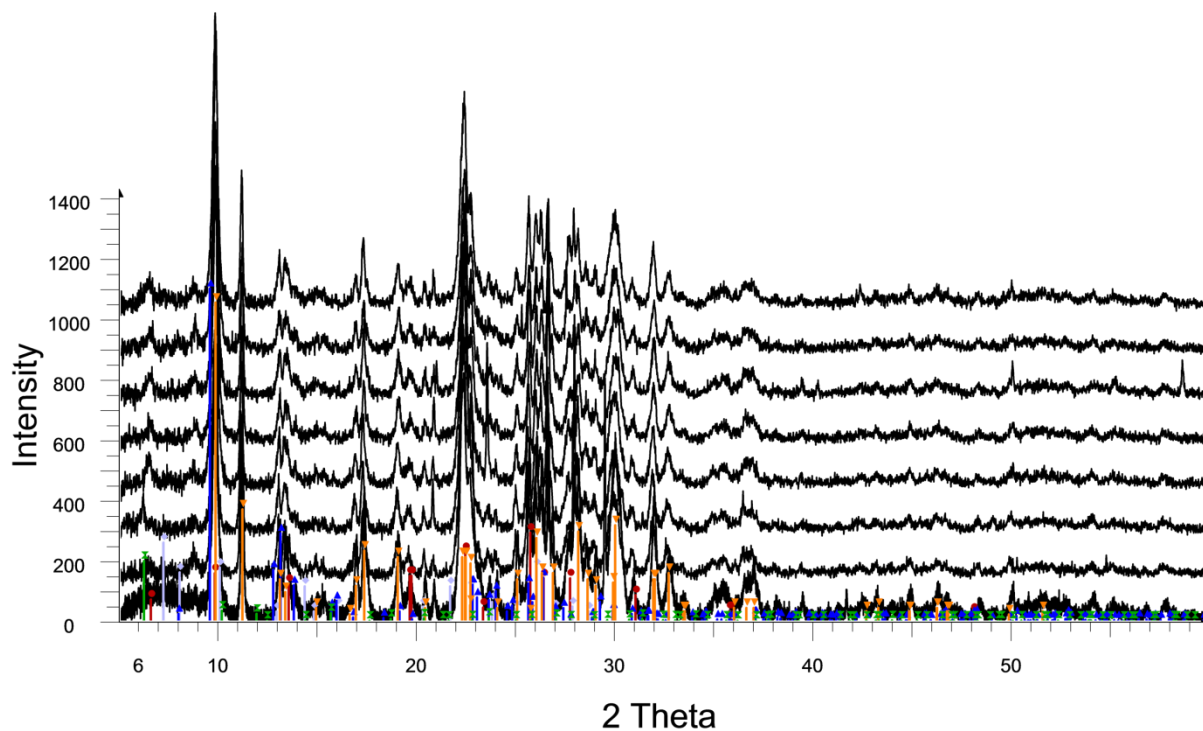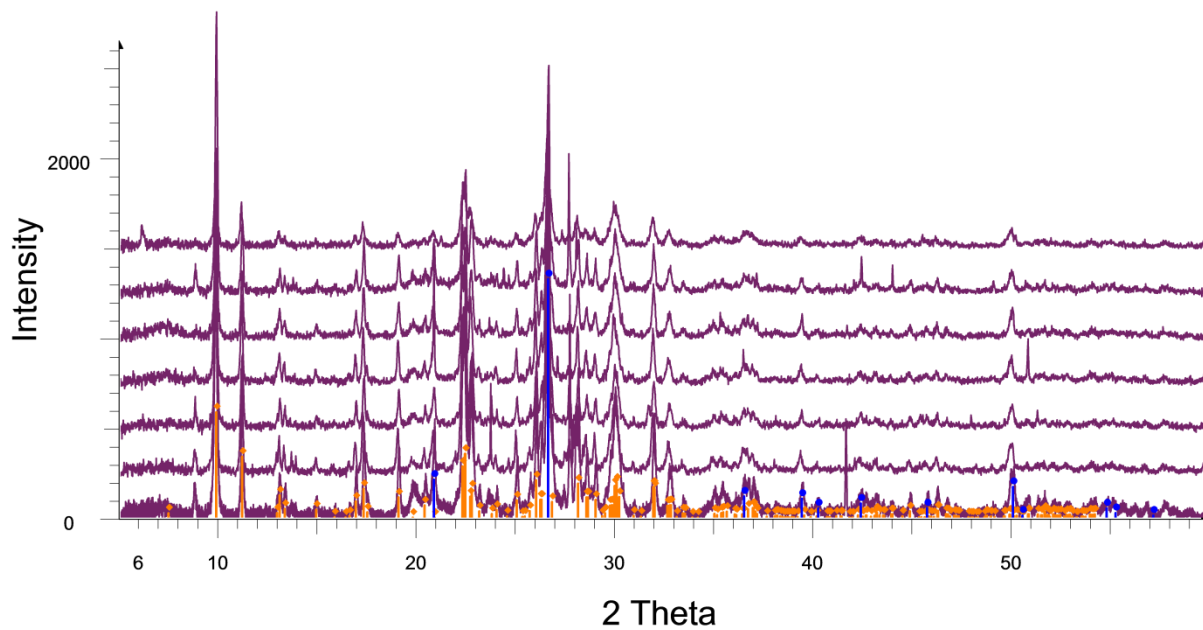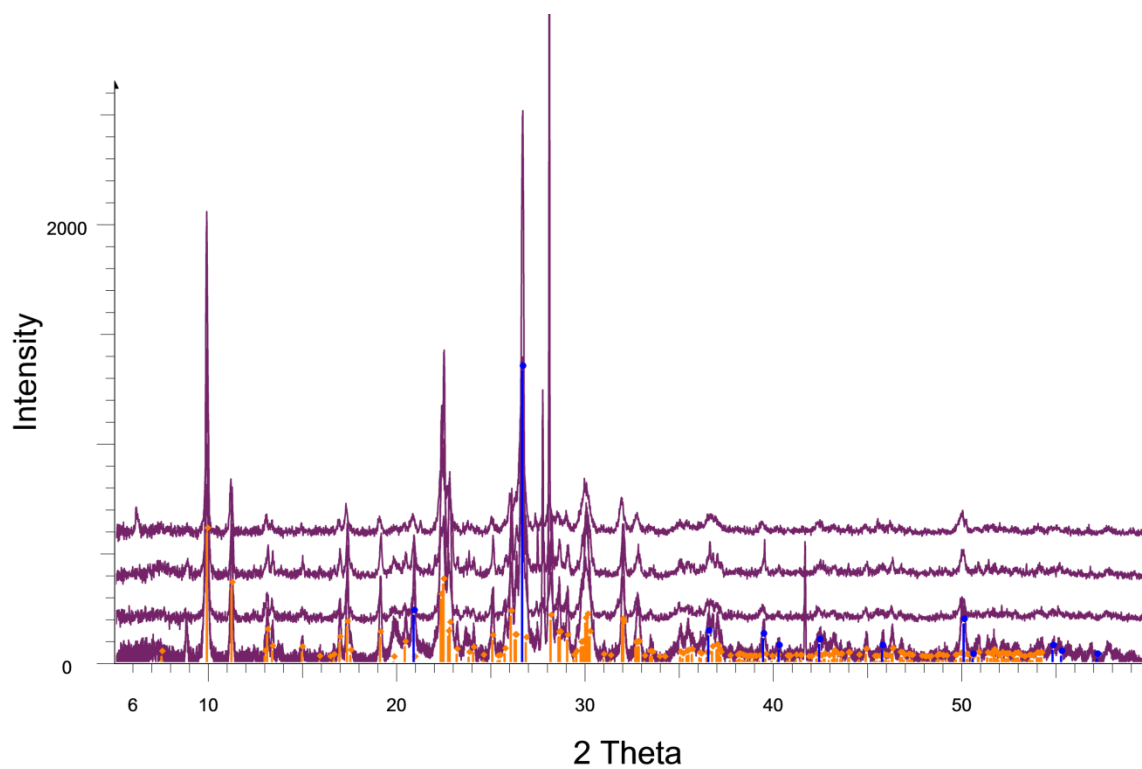

Kaolinite and TMSPETT grafting PXRD patterns for reaction time layered from bottom to top, unmodified, methanol, ethanol, dichloromethane, acetone, toluene and hexane.
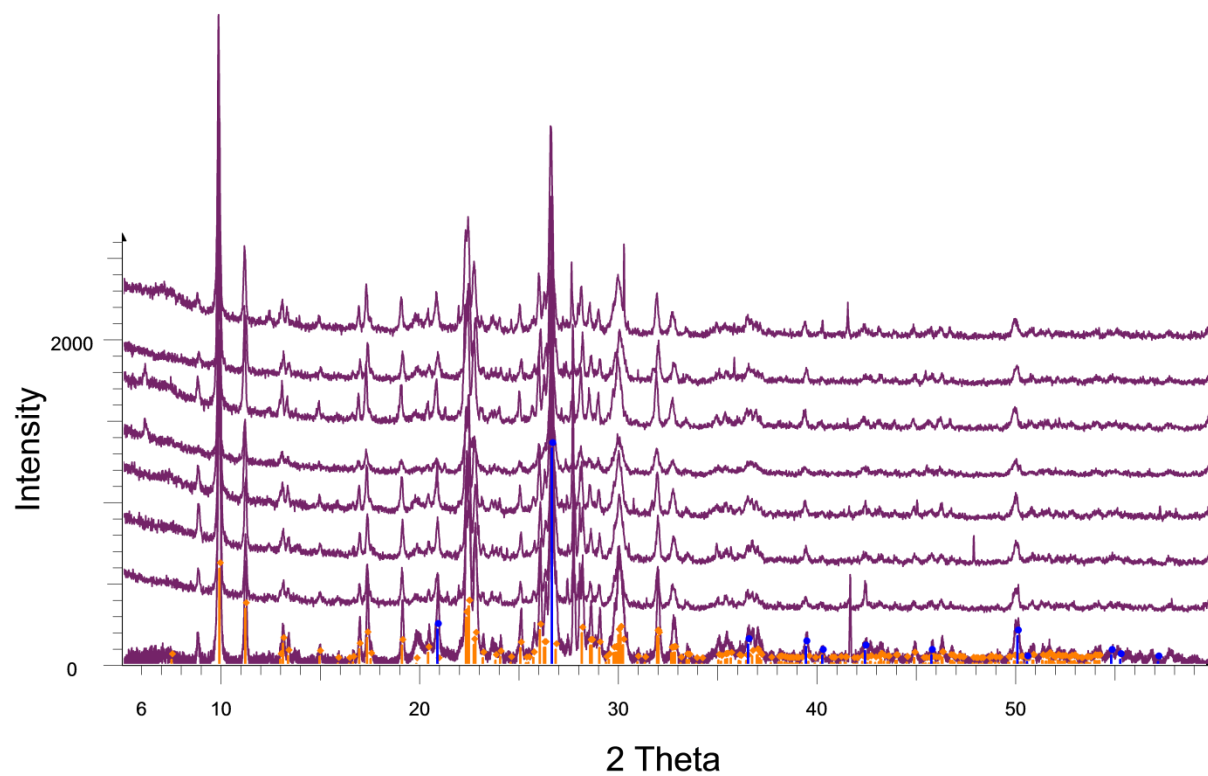
8.1 Functional group identification by FTIR

Clinoptilolite (NDA) and APTES grafting FTIR table for reaction time

Reaction time / h	NH$_2$ Stretch	O-H Asymmetric stretch	CH$_2$ Stretch	Si-O Stretch / NH2 bend / H$_2$O	Si - O Asymmetric stretch	T- O Symmetric stretch	Double rings	T-O bend
				Observations / cm^{-1}				
Literature values	3300-3500	3200-3400	2900-3100	1600-1700	1250-950	820-650	650-500	500-420
1		3417		1627	1010	671	601	432
2		3402		1627	1026	786	601	432
4		3356		1628	1010	786	601	432
8		3410		1627	1018	752	601	432
16		3471	3001	1627	1010	671	601	432
24		3394	2931	1627	1026	786	601	432

Clinoptilolite (NDA) and APTES grafting FTIR table for ligand concentration

Reaction amount / mL	NH$_2$ Stretch	O-H Asymmetric stretch	CH$_2$ Stretch	Si-O Stretch / NH$_2$ bend / H$_2$O	Si - O Asymmetric stretch	T- O Symmetric stretch	Double rings	T-O bend
	Observations / cm^{-1}							
Literature values	3300-3500	3200-3400	2900-3100	1600-1700	1250-950	820-650	650-500	500-420
3		3394	3001	1627	1026	756	601	432
5		3325	3001	1627	1018	756	601	432
8		3394	2931	1627	1026	786	601	432

Clinoptilolite (NDA) and APTES grafting FTIR table for solvent polarity

Reaction solvent	NH$_2$ Stretch	O-H Asymmetric stretch	CH$_2$ Stretch	Si-O Stretch / NH$_2$ bend/ H$_2$O	Si - O Asymmetric stretch	T- O Symmetric stretch	Double rings	T-O bend
	Observations / cm^{-1}							
Literature values	3300-3500	3200-3400	2900-3100	1600-1700	1250-950	820-650	650-500	500-420
Methanol		3372	3001	1627	1265	756	601	432
Ethanol		3371	3001	1627	1018	756	601	432
DCM		3394	2931	1627	1026	786	601	432
Acetone		3387	3008	1627	1049	756	601	432
Toluene		3371	3001	1627	1033	756	601	432
Hexane		3348	3078	1627	1026	786	601	432

Clinoptilolite (Imerys) and APTES grafting FTIR table for reaction time

Reaction time / h	Observation / cm^{-1}							
	NH$_2$ Stretch	O-H Asymmetric stretch	CH$_2$ Stretch	Si-O Stretch / NH$_2$ bend / H$_2$O	Si - O Asymmetric stretch	T- O Symmetric stretch	Double rings	T-O bend
Literature values	3300-3500	3200-3400	2900-3100	1600-1700	1250-950	820-650	650-500	500-420
1		3256	2956	1627	1010	756	601	432
2		3187	2932	1627	1010	756	601	432
4		3271	3008	1627	1010	756	601	432
8		3288	3111	1627	1010	756	601	432
16		3211	2948	1627	1010	756	601	432
24		3394	3001	1627	1018	756	601	432

Clinoptilolite (Imerys) and APTES grafting FTIR table for ligand concentration

Reaction amount / mL	Observation / cm^{-1}							
	NH$_2$ Stretch	O-H Asymmetric stretch	CH$_2$ Stretch	Si-O Stretch / NH$_2$ bend / H$_2$O	Si - O Asymmetric stretch	T- O Symmetric stretch	Double rings	T-O bend
Literature values	3300-3500	3200-3400	2900-3100	1600-1700	1250-950	820-650	650-500	500-420
3		3394	3008	1627	1010	756	594	432
5		3325	3001	1627	1018	756	601	432
8		3394	3001	1627	1018	756	601	432

Clinoptilolite (Imerys) and APTES grafting FTIR table for solvent polarity

Reaction solvent	Observation / cm^{-1}							
	NH$_2$ Stretch	O-H Asymmetric stretch	CH$_2$ Stretch	Si-O Stretch / NH$_2$ bend / H$_2$O	Si - O Asymmetric stretch	T- O Symmetric stretch	Double rings	T-O bend
Literature values	3300-3500	3200-3400	2900-3100	1600-1700	1250-950	820-650	650-500	500-420
Methanol		3387	3001	1635	1026	756	601	432
Ethanol		3294	3001	1627	1026	756	594	432
DCM		3394	3001	1627	1018	756	601	432
Acetone		3387	3008	1627	1033	756	601	432
Toluene		3371	3001	1627	1018	756	601	432
Hexane		3323	3001	1627	1018	756	601	432

ZSM-5 and APTES grafting FTIR table for reaction time

Reaction time / h	Observation / cm^{-1}							
	NH$_2$ Stretch	O-H Asymmetric stretch	CH$_2$ Stretch	Si-O Stretch / NH$_2$ bend / H$_2$O	Si - O Asymmetric stretch	T- O Symmetric stretch	Double rings	T-O bend
Literature values	3300-3500	3200-3400	2900-3100	1600-1700	1250-950	820-650	650-500	500-420
1			2993	1635	1064	756	547	432
2			2993	1651	1064	756	547	432
4			3008	1651	1064	756	547	432
8			3001	1581	1002	756	532	432
16			3008	1634	1064	756	547	432
24			3008	1635	1064	756	547	432

ZSM-5 and APTES grafting FTIR table for ligand concentration

Reaction amount / mL	Observation/ cm^{-1}							
	NH$_2$ Stretch	O-H Asymmetric stretch	CH$_2$ Stretch	Si-O Stretch / NH$_2$ bend / H$_2$O	Si - O Asymmetric stretch	T- O Symmetric stretch	Double rings	T-O bend
Literature values	3300-3500	3200-3400	2900-3100	1600-1700	1250-950	820-650	650-500	500-420
3			3008	1651	1064	802	547	432
5			3008	1635	1064	756	547	432
8			3008	1635	1064	756	547	432

ZSM-5 and APTES grafting FTIR table for solvent polarity

Reaction solvent	NH₂ Stretch	O-H Asymmetric stretch	CH₂ Stretch	Si-O Stretch / NH₂ bend / H₂O	Si - O Asymmetric stretch	T- O Symmetric stretch	Double rings	T-O bend
	Observation / cm⁻¹							
Literature values	3300-3500	3200-3400	2900-3100	1600-1700	1250-950	820-650	650-500	500-420
Methanol			3001	1651	1064	756	547	432
Ethanol			3008	1635	1064	756	547	432
DCM			3008	1635	1064	756	547	432
Acetone			3008	1635	1064	756	547	432
Toluene			3001	1651	1064	756	547	432
Hexane			3001	1627	1064	756	547	432

Vermiculite and APTES grafting FTIR table for reaction time

Reaction time / h	Observation / cm^{-1}							
	Si-O-Si stretch	OH Stretch	CH2 Stretch	Si-O Stretch / NH2 bend / H$_2$O	Si-O Symmetric stretch	Si-O-Si stretch	Al-OH bend	Si-O-Al /Si-O-Si bend
Literature values	3600-3700	3620-3550	2900-3100	1600-1700	1200-1400	1150-1050	950-600	550-500
1		3654		1651	1273	972	748	532
2		3564		1651	1273	972	748	524
4				1651	1273	956	756	532
8		3564		1651	1273	964	756	532
16				1643	1265	972	756	524
24		3564	3016	1643	1265	972	748	532

Vermiculite and APTES grafting FTIR table for ligand concentration

Reaction amount / mL	Observations / cm^{-1}							
	Si-O-Si stretch	OH Stretch	CH$_2$ Stretch	Si-O Stretch / NH$_2$ bend / H$_2$O	Si-O Symmetric stretch	Si-O-Si stretch	Al-OH bend	Si-O-Al /Si-O-Si bend
Literature values	3600-3700	3620-3550	2900-3100	1600-1700	1200-1400	1150-1050	950-600	550-500
3		3564	3001	1651	1273	972	756	532
5			3008	1651	1273	964	748	532
8		3564	3016	1643	1265	972	748	532

Vermiculite and APTES grafting FTIR table for solvent polarity

Reaction solvent	Observation / cm^{-1}							
	Si-O-Si stretch	OH Stretch	CH$_2$ Stretch	Si-O Stretch / NH$_2$ bend / H$_2$O	Si-O Symmetric stretch	Si-O-Si stretch	Al-OH bend	Si-O-Al /Si-O-Si bend
Literature values	3600-3700	3620-3550	2900-3100	1600-1700	1200-1400	1150-1050	950-600	550-500
Methanol				1651	1273	956	748	532
Ethanol				1643	1273	972	655	532
DCM			3008	1651	1273	972	756	532
Acetone		3564	3016	1643	1265	972	748	532
Toluene		3654	2954	1635	1211	979	817	524
Hexane			931	1635	1254	972	810	524

Kaolinite and APTES grafting FTIR table for reaction time

Reaction time / h	Observation / cm^{-1}							
	Si-O-Si stretch	OH Stretch	CH$_2$ Stretch	Si-O Stretch / NH$_2$ bend / H$_2$O	Si-O Symmetric stretch	Si-O-Si stretch	Al-OH bend	Si-O-Al /Si-O-Si bend
Literature values	3600-3700	3620-3550	2900-3100	1600-1700	1200-1400	1150-1050	950-600	550-500
1	3687	3618		1627	1273	1002	756	532
2	3687	3618		1627	1265	1002	756	532
4	3687	3618		1635	1273	1002	756	532
8	3687	3618	3001	1651	1273	995	756	532
16	3687	3618		1635	1265	1002	756	532
24	3687	3618	2978	1627	1273	1002	756	532

Kaolinite and APTES grafting FTIR table for ligand concentration

Reaction amount / mL	Observation/ cm^{-1}							
	Si-O-Si stretch	OH Stretch	CH$_2$ Stretch	Si-O Stretch / NH$_2$ bend / H$_2$O	Si-O Symmetric stretch	Si-O-Si stretch	Al-OH bend	Si-O-Al /Si-O-Si bend
Literature values	3600-3700	3620-3550	2900-3100	1600-1700	1200-1400	1150-1050	950-600	550-500
3	3687	3618	3008	1635	1265	1002	756	523
5	3687	3618	3001	1651	1265	995	756	524
8	3687	3618	2978	1627	1273	1002	756	532

Kaolinite and APTES grafting FTIR table for solvent polarity

Reaction solvent	Observations / cm^{-1}							
	Si-O-Si stretch	OH Stretch	CH$_2$ Stretch	Si-O Stretch / NH$_2$ bend / H$_2$O	Si-O Symmetric stretch	Si-O-Si stretch	Al-OH bend	Si-O-Al /Si-O-Si bend
Literature values	3600-3700	3620-3550	2900-3100	1600-1700	1200-1400	1150-1050	950-600	550-500
Methanol	3867	3618	3001	1627	1273	1002	756	532
Ethanol	3587	3618		1627	1273	1002	748	524
DCM	3687	3618	3008	1651	1273	1002	756	532
Acetone	3687	3618	2978	1627	1273	1002	756	532
Toluene	3687	3618	3008	1627	1273	1002	756	532
Hexane	3687	3618	2954	1651	1273	995	748	524

Clinoptilolite (NDA) and TMSPE grafting FTIR table for reaction time

Reaction time / h	NH$_2$ Stretch	O-H Asymmetric stretch	CH$_2$ Stretch	Si-O Stretch / NH$_2$ bend / H$_2$O	Si - O Asymmetric stretch	T- O Symmetric stretch	Double rings	T-O bend
				Observation / cm^{-1}				
Literature values	3300-3500	3200-3400	2900-3100	1600-1700	1250-950	820-650	650-500	500-420
1		3363	3001	1635	1041	756	601	432
2		3325	3008	1627	1026	756	601	432
4		3325	3001	1635	1041	756	601	432
8		3332		1627	1033	756	601	432
16		3332	3001	1627	1026	756	601	432
24		3402	3001	1627	1018	756	601	432

Clinoptilolite (NDA) and TMSPE grafting FTIR table for ligand concentration

Reaction amount / mL	Observations / cm^{-1}							
	NH$_2$ Stretch	O-H Asymmetric stretch	CH$_2$ Stretch	Si-O Stretch / NH$_2$ bend / H$_2$O	Si - O Asymmetric stretch	T- O Symmetric stretch	Double rings	T-O bend
Literature values	3300-3500	3200-3400	2900-3100	1600-1700	1250-950	820-650	650-500	500-420
3		3255	3001	1627	1018	756	601	432
5		3394	3008	1643	1026	756	601	432
8		3402	3001	1627	1018	756	601	432

Clinoptilolite (NDA) and TMSPE grafting FTIR table for solvent polarity

Reaction solvent	Observations / cm^{-1}							
	NH$_2$ Stretch	O-H Asymmetric stretch	CH$_2$ Stretch	Si-O Stretch / NH$_2$ bend / H$_2$O	Si - O Asymmetric stretch	T- O Symmetric stretch	Double rings	T-O bend
Literature values	3300-3500	3200-3400	2900-3100	1600-1700	1250-950	820-650	650-500	500-420
Methanol		3356		1627	1026	786	601	432
Ethanol		3325	3001	1627	1026	756	601	432
DCM		3325	3008	1635	1026	756	601	432
Acetone		3402	3001	1627	1018	756	601	432
Toluene		3394	3008	1627	1026	756	601	432
Hexane		3394	3008	1635	1033	756	601	432

Clinoptilolite (Imerys) and TMSPE grafting FTIR table for reaction time

Reaction time / h			Observations / cm-1					
	NH$_2$ Stretch	O-H Asymmetric stretch	CH$_2$ Stretch	Si-O Stretch / NH$_2$ bend / H$_2$O	Si - O Asymmetric stretch	T- O Symmetric stretch	Double rings	T-O bend
Literature values	3300-3500	3200-3400	2900-3100	1600-1700	1250-950	820-650	650-500	500-420
1		3248	3001	1651	1026	756	594	432
2		3363		1651	1010	756	594	432
4		3325	3001	1635	1018	756	594	432
8		3387	3008	1627	1018	756	594	432
16		3309		1627	1010	756	594	432
24		3379	3008	1635	1018	756	594	432

Clinoptilolite (Imerys) and TMSPE grafting FTIR table for ligand concentration

Reaction amount / mL			Observations / cm^{-1}					
	NH$_2$ Stretch	O-H Asymmetric stretch	CH$_2$ Stretch	Si-O Stretch / NH$_2$ bend / H$_2$O	Si - O Asymmetric stretch	T- O Symmetric stretch	Double rings	T-O bend
Literature values	3300-3500	3200-3400	2900-3100	1600-1700	1250-950	820-650	650-500	500-420
3		3309	3008	1635	1026	756	594	432
5		3327	3001	1651	1026	756	594	432
8		3379	3008	1635	1018	756	594	432

Clinoptilolite (Imerys) and TMSPE grafting FTIR table for solvent polarity

Reaction solvent	Observations / cm^{-1}							
	NH$_2$ Stretch	O-H Asymmetric stretch	CH$_2$ Stretch	Si-O Stretch / NH$_2$ bend / H$_2$O	Si - O Asymmetric stretch	T- O Symmetric stretch	Double rings	T-O bend
Literature values	3300-3500	3200-3400	2900-3100	1600-1700	1250-950	820-650	650-500	500-420
Methanol		3317	3001	1635	1010	756	594	432
Ethanol		3394	3001	1627	1010	756	594	432
DCM		3379	3001	1627	1018	756	594	432
Acetone		3371	3008	1635	1018	756	594	432
Toluene		3387	3001	1635	1026	756	594	432
Hexane		3379	3001	1635	1026	756	594	432

ZSM-5 and TMSPE grafting FTIR table for reaction time

	Observation / cm^{-1}							
Reaction time / h	NH$_2$ Stretch	O-H Asymmetric stretch	CH$_2$ Stretch	Si-O Stretch / NH$_2$ bend / H$_2$O	Si - O Asymmetric stretch	T- O Symmetric stretch	Double rings	T-O bend
Literature values	3300-3500	3200-3400	2900-3100	1600-1700	1250-950	820-650	650-500	500-420
1				1612	1064	802	547	432
2			3001	1674	1064	756	547	432
4		3363	3001	1643	1064	756	547	432
8			2993	1627	1064	756	547	432
16		3332	3008	1651	1064	756	547	432
24		3224	3008	1629	1064	756	547	432

ZSM-5 and TMSPE grafting FTIR table for ligand concentration

	Observation / cm^{-1}							
Reaction amount / mL	NH$_2$ Stretch	O-H Asymmetric stretch	CH$_2$ Stretch	Si-O Stretch / NH$_2$ bend / H$_2$O	Si - O Asymmetric stretch	T- O Symmetric stretch	Double rings	T-O bend
Literature values	3300-3500	3200-3400	2900-3100	1600-1700	1250-950	820-650	650-500	500-420
3		3323	3008	1651	1064	756	547	432
5				1651	1064	794	547	432
8		3224	3008	1629	1064	756	547	432

ZSM-5 and TMSPE grafting FTIR table for solvent polarity

Reaction solvent	Observation / cm^{-1}							
	NH$_2$ Stretch	O-H Asymmetric stretch	CH$_2$ Stretch	Si-O Stretch / NH$_2$ bend / H$_2$O	Si - O Asymmetric stretch	T- O Symmetric stretch	Double rings	T-O bend
Literature values	3300-3500	3200-3400	2900-3100	1600-1700	1250-950	820-650	650-500	500-420
Methanol			3001	1620	1064	756	547	432
Ethanol			3001	1664	1064	756	547	432
DCM			3001	1620	1064	756	547	432
Acetone		3224	3008	1629	1064	756	547	432
Toluene		3325	3001	1635	1064	756	547	432
Hexane		3315	3001	1627	1064	756	547	432

Vermiculite and TMSPE grafting FTIR table for reaction time

	Observation / cm^{-1}							
Reaction time / h	Si-O-Si stretch	OH Stretch	CH$_2$ Stretch	Si-O Stretch / NH$_2$ bend / H$_2$O	Si-O Symmetric stretch	Si-O-Si stretch	Al-OH bend	Si-O-Al /Si-O-Si bend
Literature values	3600-3700	3620-3550	2900-3100	1600-1700	1200-1400	1150-1050	950-600	550-500
1			3008	1643	1273	979	756	532
2				1643	1273	972	748	532
4			3008	1651	1273	972	756	532
8			3008	1651	1273	972	748	532
16		3525	3008	1651	1273	964	756	532
24		3541		1651	1265	964	748	532

Vermiculite and TMSPE grafting FTIR table for ligand concentration

	Observation / cm^{-1}							
Reaction amount / mL	Si-O-Si stretch	OH Stretch	CH$_2$ Stretch	Si-O Stretch / NH$_2$ bend / H$_2$O	Si-O Symmetric stretch	Si-O-Si stretch	Al-OH bend	Si-O-Al /Si-O-Si bend
Literature values	3600-3700	3620-3550	2900-3100	1600-1700	1200-1400	1150-1050	950-600	550-500
3			3008	1651	1273	964	756	532
5			3008	1651	1273	964	756	532
8		3541	0	1651	1265	964	748	532

Vermiculite and TMSPE grafting FTIR table for solvent polarity

Reaction solvent	Observation / cm^{-1}							
	Si-O-Si stretch	OH Stretch	CH2 Stretch	Si-O Stretch / NH2 bend / H$_2$O	Si-O Symmetric stretch	Si-O-Si stretch	Al-OH bend	Si-O-Al /Si-O-Si bend
Literature values	3600-3700	3620-3550	2900-3100	1600-1700	1200-1400	1150-1050	950-600	550-500
Methanol			3008	1651	1273	964	756	532
Ethanol			3008	1643	1273	964	756	532
DCM				1643	1265	972	748	532
Acetone		3541		1651	1265	964	748	532
Toluene	3687			1643	1280	972	740	532
Hexane			3008	1651	1273	972	756	532

Kaolinite and TMSPE grafting FTIR table for reaction time

Reaction time / h	Observation / cm^{-1}							
	Si-O-Si stretch	OH Stretch	CH$_2$ Stretch	Si-O Stretch / NH$_2$ bend / H$_2$O	Si-O Symmetric stretch	Si-O-Si stretch	Al-OH bend	Si-O-Al /Si-O-Si bend
Literature values	3600-3700	3620-3550	2900-3100	1600-1700	1200-1400	1150-1050	950-600	550-500
1	3687	3618	3008	1651	1273	1002	756	532
2	3687	3618		1651	1273	1002	748	524
4	3687	3618		1658	1265	1002	748	532
8	3687	3618		1651	1265	1002	756	532
16	3687	3618	3001	1651	1273	1002	756	532
24	3687	3618		1651	1273	1002	756	532

Kaolinite and TMSPE grafting FTIR table for ligand concentration

Reaction amount / mL	Observation / cm^{-1}							
	Si-O-Si stretch	OH Stretch	CH$_2$ Stretch	Si-O Stretch / NH$_2$ bend/ H$_2$O	Si-O Symmetric stretch	Si-O-Si stretch	Al-OH bend	Si-O-Al /Si-O-Si bend
Literature values	3600-3700	3620-3550	2900-3100	1600-1700	1200-1400	1150-1050	950-600	550-500
3	3687	3618	2931	1651	1373	1002	748	542
5	3687	3618		1627	1319	1010	794	532
8	3687	3618	0	1651	1273	1002	756	532

Kaolinite and TMSPE grafting FTIR table for solvent polarity

Reaction solvent	Observation / cm^{-1}							
	Si-O-Si stretch	OH Stretch	CH$_2$ Stretch	Si-O Stretch / NH$_2$ bend / H$_2$O	Si-O Symmetric stretch	Si-O-Si stretch	Al-OH bend	Si-O-Al /Si-O-Si bend
Literature values	3600-3700	3620-3550	2900-3100	1600-1700	1200-1400	1150-1050	950-600	550-500
Methanol	3687	3618	3008	1651	1273	1002	748	524
Ethanol	3687	3618	2924	1651	1273	1002	748	524
DCM	3687	3618		1651	1273	1002	748	532
Acetone	3687	3618	0	1651	1273	1002	756	532
Toluene	3687	3618		1627	1273	1002	756	532
Hexane	3687	3618		1651	1273	1002	748	52

Clinoptilolite (NDA) and TMSPETT grafting FTIR table for reaction time

Reaction time / h	Observation / cm^{-1}						
	O-H Asymmetric stretch	CH$_2$ Stretch	Si-O Stretch / H$_2$O	Si - O Asymmetric stretch	T- O Symmetric stretch	Double rings	T-O bend
Literature values	3200-3400	2900-3100	1600-1700	1250-950	820-650	650-500	500-420
1	3371		1627	1033	740	601	432
2	3371	3001	1627	1026	756	601	432
4	3255	2993	1627	1033	756	601	432
8	3417	3008	1627	1026	756	601	432
16	3402	3001	1627	1026	756	601	432
24	3348	3008	1627	1026	756	601	432

Clinoptilolite (NDA) and TMSPETT grafting FTIR table for ligand concentration

Reaction amount / mL	Observation / cm^{-1}						
	O-H Asymmetric stretch	CH$_2$ Stretch	Si-O Stretch / H$_2$O	Si - O Asymmetric stretch	T- O Symmetric stretch	Double rings	T-O bend
Literature values	3200-3400	2900-3100	1600-1700	1250-950	820-650	650-500	500-420
3	3325	3008	1627	1026	756	601	431
5	3294		1627	1018	717	601	432
8	3348	3008	1627	1026	756	601	432

Clinoptilolite (NDA) and TMSPETT grafting FTIR table for solvent polarity

Reaction solvent	Observation / cm^{-1}						
	O-H Asymmetric stretch	CH$_2$ Stretch	Si-O Stretch / H$_2$O	Si - O Asymmetric stretch	T- O Symmetric stretch	Double rings	T-O bend
Literature values	3200-3400	2900-3100	1600-1700	1250-950	820-650	650-500	500-420
Methanol	3394	3001	1627	1041	756	601	432
Ethanol	3394	3001	1635	1056	756	609	432
DCM	3410	3001	1627	1026	756	601	432
Acetone	3348	3008	1627	1026	756	601	432
Toluene	3433	3001	1627	1026	756	601	432
Hexane	327	3008	1627	1026	756	601	432
Water	3387	3008	1627	1026	756	601	432

Clinoptilolite (Imerys) and TMSPETT grafting FTIR table for reaction time

Reaction time / h	Observation / cm^{-1}						
	O-H Asymmetric stretch	CH$_2$ Stretch	Si-O Stretch / H$_2$O	Si - O Asymmetric stretch	T- O Symmetric stretch	Double rings	T-O bend
Literature values	3200-3400	2900-3100	1600-1700	1250-950	820-650	650-500	500-420
1	3371	3008	1627	1010	756	594	432
2	3325		1620	1018	756	594	432
4	3356	2893	1627	1018	786	594	432
8	3387	2954	1627	1010	786	594	432
16	3325	3001	1627	1010	756	594	432
24	3332	3001	1627	1010	756	594	432

Clinoptilolite (Imerys) and TMSPETT grafting FTIR table for ligand concentration

Reaction amount / mL	Observation / cm^{-1}						
	O-H Asymmetric stretch	CH$_2$ Stretch	Si-O Stretch / H$_2$O	Si - O Asymmetric stretch	T- O Symmetric stretch	Double rings	T-O bend
Literature values	3200-3400	2900-3100	1600-1700	1250-950	820-650	650-500	500-420
3	3278	3008	1627	1010	756	594	432
5	3356		1627	1018	786	594	432
8	3332	3001	1627	1010	756	594	432

Clinoptilolite (Imerys) and TMSPETT grafting FTIR table for solvent polarity

Reaction solvent	Observations / cm^{-1}						
	O-H Asymmetric stretch	CH$_2$ Stretch	Si-O Stretch / H$_2$O	Si - O Asymmetric stretch	T- O Symmetric stretch	Double rings	T-O bend
Literature values	3200-3400	2900-3100	1600-1700	1250-950	820-650	650-500	500-420
Methanol	3371	3008	1627	1010	756	594	432
Ethanol	3332	3008	1627	1018	756	594	432
DCM	3402	3001	1627	1010	756	594	432
Acetone	3332	3001	1627	1010	756	594	432
Toluene	3394	3001	1627	1010	756	594	432
Hexane	3387	3008	1627	1010	756	594	432
Water	3394	3008	1627	1010	756	594	432

ZSM-5 and TMSPETT grafting FTIR table for reaction time

Reaction time / h	Observations / cm⁻¹						
	O-H Asymmetric stretch	CH₂ Stretch	Si-O Stretch / H₂O	Si - O Asymmetric stretch	T- O Symmetric stretch	Double rings	T-O bend
Literature values	3200-3400	2900-3100	1600-1700	1250-950	820-650	650-500	500-420
1	3309	3001	1620	1064	756	547	432
2	3371	3001	1627	1064	756	547	432
4	3302	3008	1627	1064	756	547	432
8	3417	3008	1620	1064	756	547	432
16	3306	3001	1627	1072	794	547	432
24	3321	3001	1635	1064	756	547	432

ZSM-5 and TMSPETT grafting FTIR table for ligand concentration

Reaction amount / mL	Observation / cm⁻¹						
	O-H Asymmetric stretch	CH₂ Stretch	Si-O Stretch/ H₂O	Si - O Asymmetric stretch	T- O Symmetric stretch	Double rings	T-O bend
Literature values	3200-3400	2900-3100	1600-1700	1250-950	820-650	650-500	500-420
3	3394	3008	1620	1064	756	547	432
5	3357	3001	1620	1064	756	547	432
8	3321	3001	1635	1064	756	547	432

ZSM-5 and TMSPETT grafting FTIR table for solvent polarity

	Observation / cm^{-1}						
Reaction solvent	O-H Asymmetric stretch	CH$_2$ Stretch	Si-O Stretch / H$_2$O	Si - O Asymmetric stretch	T- O Symmetric stretch	Double rings	T-O bend
Literature values	3200-3400	2900-3100	1600-1700	1250-950	820-650	650-500	500-420
Methanol	3294	3001	1627	1064	756	547	432
Ethanol	3309	2993	1635	1064	756	547	432
DCM	3232	3008	1651	1064	756	547	432
Acetone	3321	3001	1635	1064	756	547	432
Toluene	3317	3008	1627	1064	756	547	432
Hexane	3379	3001	1627	1064	756	547	432
Water	3394	3008	1635	1064	756	547	432

Vermiculite and TMSPETT grafting FTIR table for reaction time

Reaction time / h	Observation / cm^{-1}							
	Si-O-Si stretch	OH Stretch	CH$_2$ Stretch	Si-O Stretch / H$_2$O	Si-O Symmetric stretch	Si-O-Si stretch	Al-OH bend	Si-O-Al /Si-O-Si bend
Literature values	3600-3700	3620-3550	2900-3100	1600-1700	1200-1400	1150-1050	950-600	550-500
1		3564	3008	1651	1273	972	756	532
2			3008	1651	1273	972	756	532
4			3008	1651	1273	964	756	532
8		3564	3008	1651	1273	964	756	532
16			3008	1651	1273	964	756	532
24		3564	3008	1643	1273	964	748	523

Vermiculite and TMSPETT grafting FTIR table for ligand concentration

Reaction amount / mL	Observations / cm^{-1}							
	Si-O-Si stretch	OH Stretch	CH$_2$ Stretch	Si-O Stretch/ H$_2$O	Si-O Symmetric stretch	Si-O-Si stretch	Al-OH bend	Si-O-Al /Si-O-Si bend
Literature values	3600-3700	3620-3550	2900-3100	1600-1700	1200-1400	1150-1050	950-600	550-500
3		3533		1635	1273	964	817	532
5			2924	1643	1273	956	748	532
8		3564	3008	1643	1273	964	748	523

Vermiculite and TMSPETT grafting FTIR table for solvent polarity

	Observation / cm^{-1}							
Reaction solvent	Si-O-Si stretch	OH Stretch	CH$_2$ Stretch	Si-O Stretch / H$_2$O	Si-O Symmetric stretch	Si-O-Si stretch	Al-OH bend	Si-O-Al /Si-O-Si bend
Literature values	3600-3700	3620-3550	2900-3100	1600-1700	1200-1400	1150-1050	950-600	550-500
Methanol		3564	3008	1651	1273	964	756	532
Ethanol		3564	3008	1651	1273	964	756	532
DCM		3564	3008	1651	1273	956	756	532
Acetone		3564	3008	1643	1273	964	748	523
Toluene		3564	3008	1643	1273	964	756	532
Hexane		3525	3008	1651	1273	964	748	532
Water		3564	3008	1651	1273	956	756	532

Kaolinite and TMSPETT grafting FTIR table for reaction time

Reaction time / h	Observation / cm^{-1}							
	Si-O-Si stretch	OH Stretch	CH$_2$ Stretch	Si-O Stretch / H$_2$O	Si-O Symmetric stretch	Si-O-Si stretch	Al-OH bend	Si-O-Al /Si-O-Si bend
Literature values	3650-3695	3620-3550	2900-3100	1600-1700	1200-1400	1150-1050	950-600	550-500
1	3687	3618	3008	1627	1273	995	748	524
2	3687	3618	3001	1654	1273	1002	748	524
4	3687	3618	3008	1651	1273	995	756	524
8	3687	3618	3008	1689	1265	995	748	524
16	3687	3618	3008	1651	1273	1002	748	524
24	3687	3618	3008	1620	1273	1002	756	532

Kaolinite and TMSPETT grafting FTIR table for ligand concentration

Reaction amount / mL	Observations / cm^{-1}							
	Si-O-Si stretch	OH Stretch	CH$_2$ Stretch	Si-O Stretch / H$_2$O	Si-O Symmetric stretch	Si-O-Si stretch	Al-OH bend	Si-O-Al /Si-O-Si bend
Literature values	3650-3695	3620-3550	2900-3100	1600-1700	1200-1400	1150-1050	950-600	550-500
3	3687	3618	3008	1651	1265	995	748	524
5	687	3618	3008	1651	1273	995	756	524
8	3687	3618	3008	1620	1273	1002	756	532

Kaolinite and TMSPETT grafting FTIR table for solvent polarity

Reaction solvent	Observation / cm^{-1}							
	Si-O-Si stretch	OH Stretch	CH$_2$ Stretch	Si-O Stretch / H$_2$O	Si-O Symmetric stretch	Si-O-Si stretch	Al-OH bend	Si-O-Al /Si-O-Si bend
Literature values	3650-3695	3620-3550	2900-3100	1600-1700	1200-1400	1150-1050	950-600	550-500
Methanol	3687	3618		1689	1273	1002	756	532
Ethanol	3687	3618	3008	1673	1265	1002	756	524
DCM	3687	3618	3008	1651	1273	995	748	524
Acetone	3687	3618	3008	1620	1273	1002	756	532
Toluene	3687	3618	3008	1627	1273	1002	748	524
Hexane	3687	3618		1651	1273	995	748	524
Water	3687	3618	3008	1643	1273	995	748	524

8.3 R$_d$ plots for batch tests

Caesium experimental results

Batch sorption experimental results

Uptake of caesium by unmodified materials

Material	Clinoptilolite (NDA)		Clinoptilolite (Imerys)		ZSM-5		Vermiculite		Kaolinite	
Concentration	Rd	Error (+/-)	Rd	Error (+/-)	Rd	Error (+/-)	Rd	Error (+/-)	Rd	Error (+/-)
1 x 10-2	231.7	98.3	118.6	67.8	0.1	3.1	0.0	12.2	0.0	5.5
1 x 10-4	1292.7	249.2	1713.5	146.0	134.6	10.3	137.1	20.8	0.0	5.5
1 x 10-6	1023.8	47.9	1674.4	200.5	154.5	41.2	449.2	169.3	304.2	17.7
1 x 10-8	1134.5	58.4	3306.1	457.2	1836.3	31.6	664.1	63.0	2780.1	296.0
1 x 10-10	850.5	126.1	1742.6	344.2	874.3	62.4	902.4	66.5	2652.7	356.5

Uptake of caesium by APTES modified materials

Material	Clinoptilolite (NDA)		Clinoptilolite (Imerys)		ZSM-5		Vermiculite		Kaolinite	
Concentration	Rd	Error (+/-)	Rd	Error (+/-)	Rd	Error (+/-)	Rd	Error (+/-)	Rd	Error (+/-)
1 x 10-2	231.7	98.3	118.6	67.8	0.1	3.1	0.0	12.2	0.0	5.5
1 x 10-4	1292.7	249.2	1713.5	146.0	134.6	10.3	137.1	20.8	0.0	5.5
1 x 10-6	1023.8	47.9	1674.4	200.5	154.5	41.2	449.2	169.3	304.2	17.7
1 x 10-8	1134.5	58.4	3306.1	457.2	1836.3	31.6	664.1	63.0	2780.1	296.0
1 x 10-10	850.5	126.1	1742.6	344.2	874.3	62.4	902.4	66.5	2652.7	356.5

Material	Clinoptilolite (NDA)		Clinoptilolite (Imerys)		ZSM-5		Vermiculite		Kaolinite	
Concentration	Rd	Error (+/-)	Rd	Error (+/-)	Rd	Error (+/-)	Rd	Error (+/-)	Rd	Error (+/-)
1 x 10-2	231.7	98.3	118.6	67.8	1.0	9.2	131.1	28.0	0.0	5.5
1 x 10-4	1292.7	249.2	1713.5	146.0	131.2	10.3	1.0	6860.0	0.0	5.5
1 x 10-6	1023.8	47.9	1674.4	200.5	486.0	136.3	474522.8	814112.3	304.2	17.7
1 x 10-8	1134.5	58.4	3306.1	457.2	815.8	322.6	5384.7	1579.8	2780.1	296.0
1 x 10-10	850.5	126.1	1742.6	344.2	36.4	47.5	410951.7	49860.5	2652.7	356.5

Uptake of caesium by TMSPE modified materials
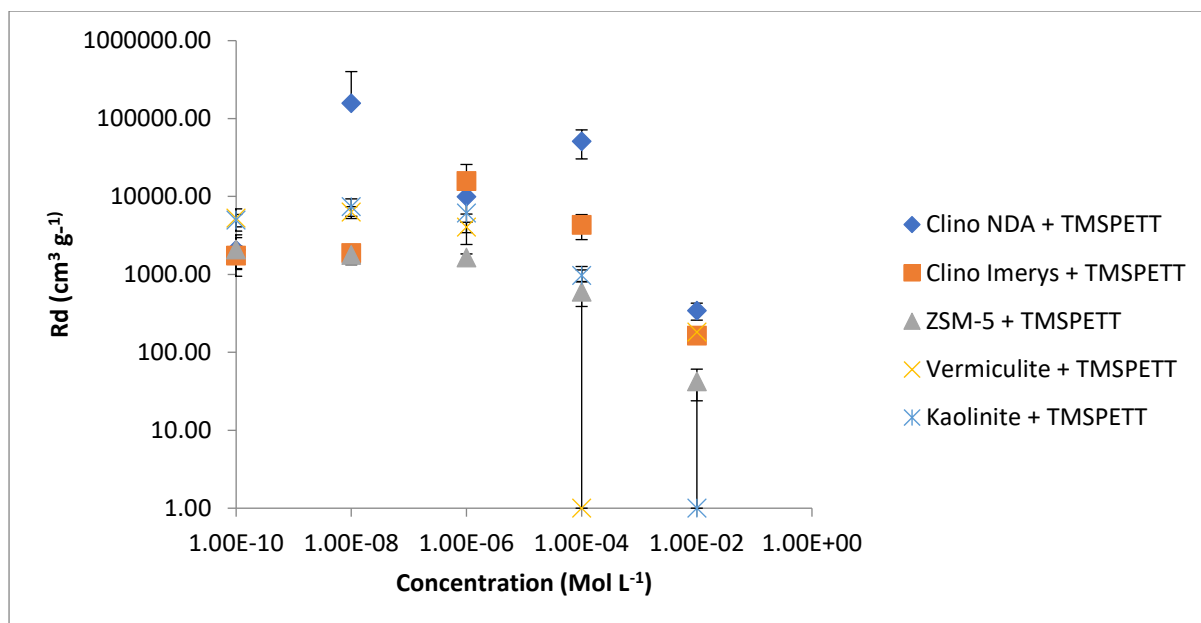
Material	Clinoptilolite (NDA)		Clinoptilolite (Imerys)		ZSM-5		Vermiculite		Kaolinite	
Concentration	Rd	Error (+/-)	Rd	Error (+/-)	Rd	Error (+/-)	Rd	Error (+/-)	Rd	Error (+/-)
1 x 10-2	343.7	84.6	163.5	30.4	42.4	18.5	181.6	21.4	1.0	32.7
1 x 10-4	50921.9	20587.0	4329.4	1530.4	599.6	211.5	1.0	1263.8	972.0	169.7
1 x 10-6	9909.6	10312.5	15865.9	9904.4	1649.8	179.9	4055.2	618.7	6130.4	3707.8
1 x 10-8	157515.6	243458.2	1875.7	544.0	1774.2	199.3	6304.6	1090.0	7443.4	1872.1
1 x 10-10	2077.3	888.7	1738.8	581.9	2084.4	1136.0	5266.4	1665.6	4981.5	902.1

Comparison of clinoptilolite (NDA) materials
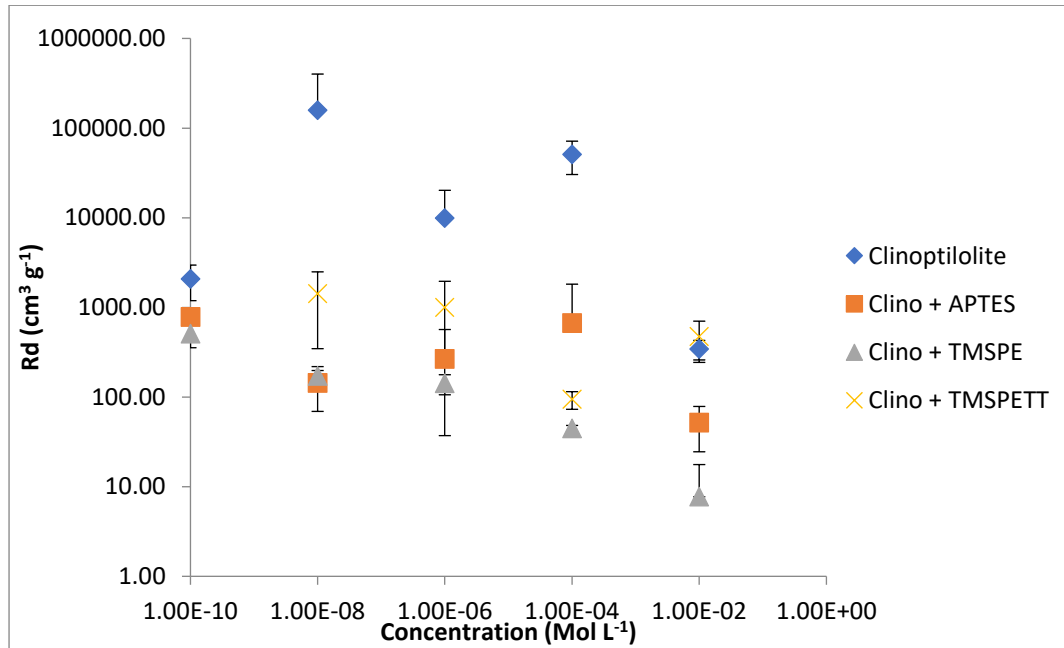
Comparison of clinoptilolite (Imerys) materials
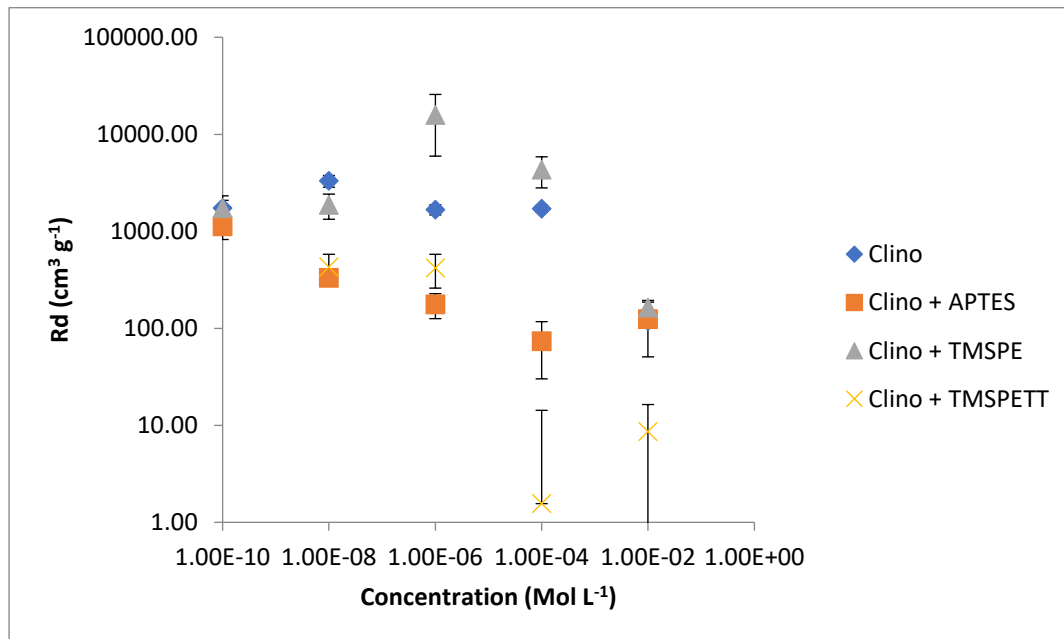
Comparison of ZSM-5 materials
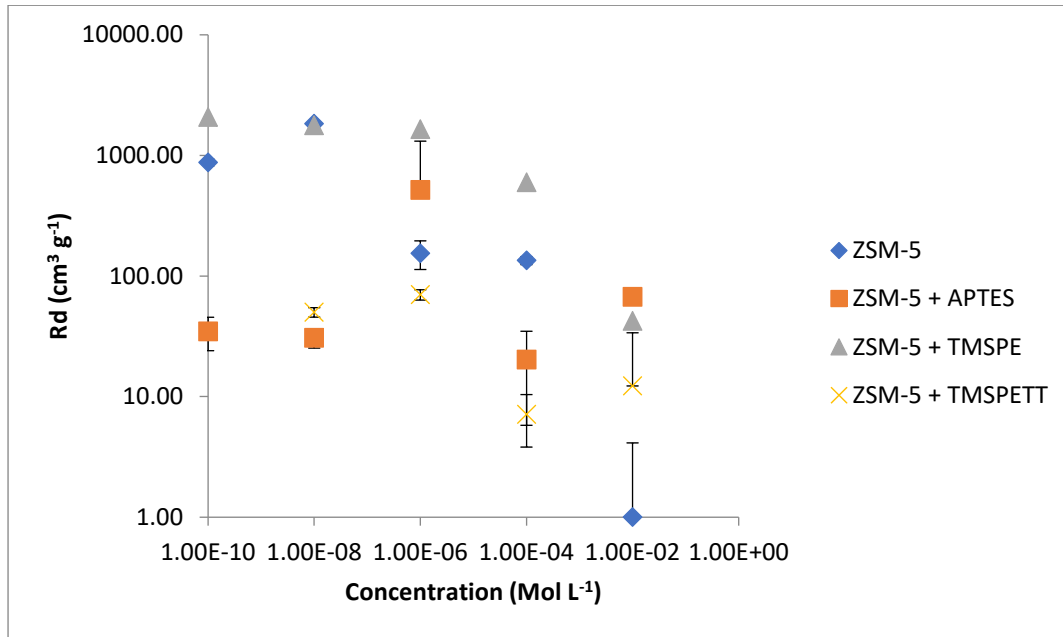
Comparison of vermiculite materials
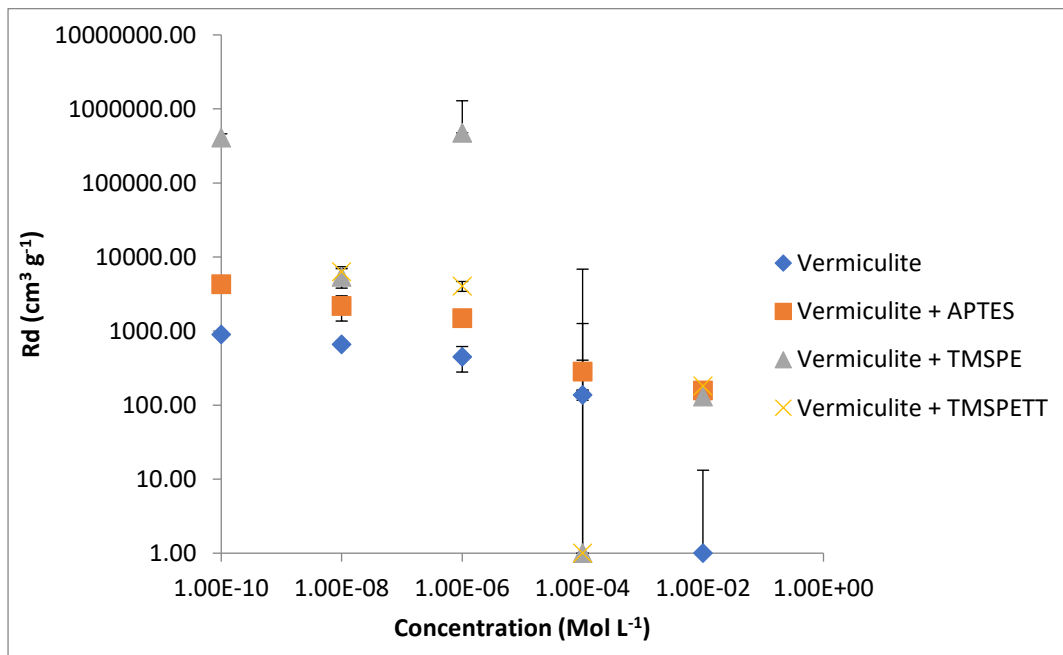
Comparison of kaolinite materials
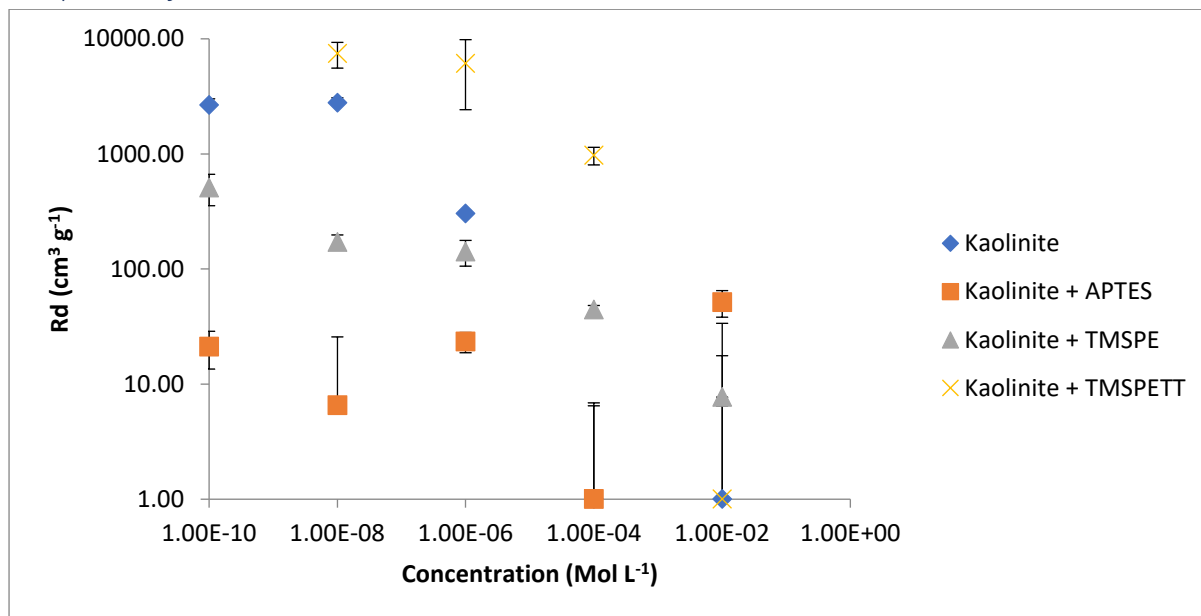
Strontium experimental results

Batch sorption experimental results
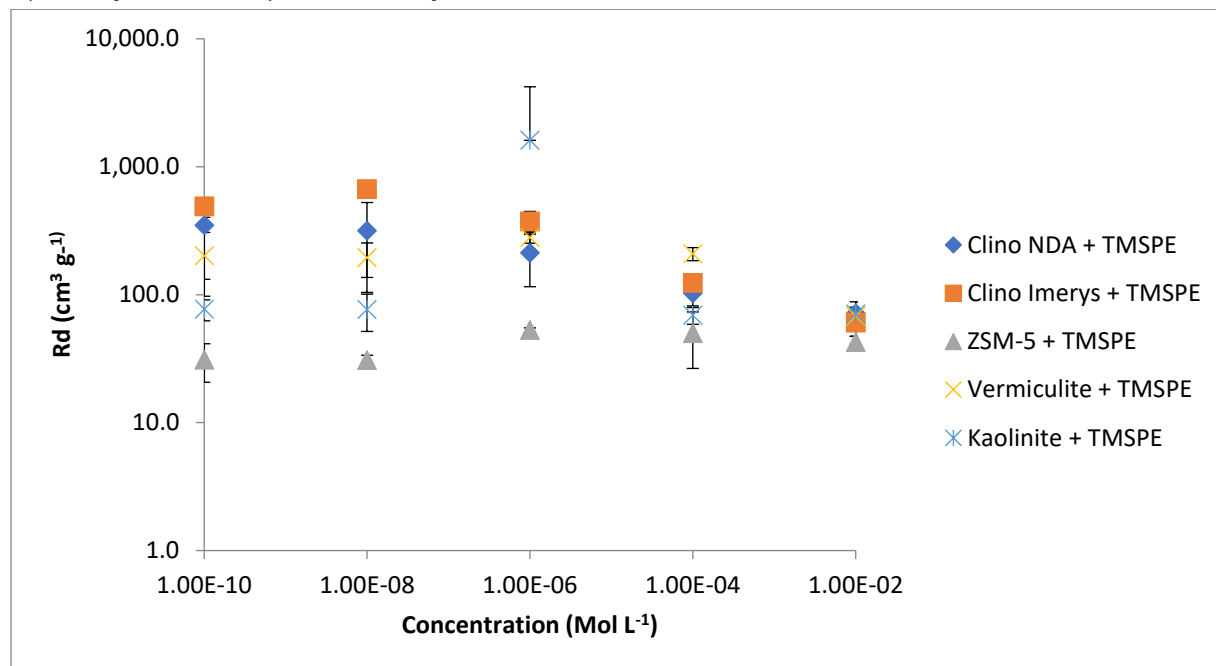
Uptake of strontium by unmodified materials
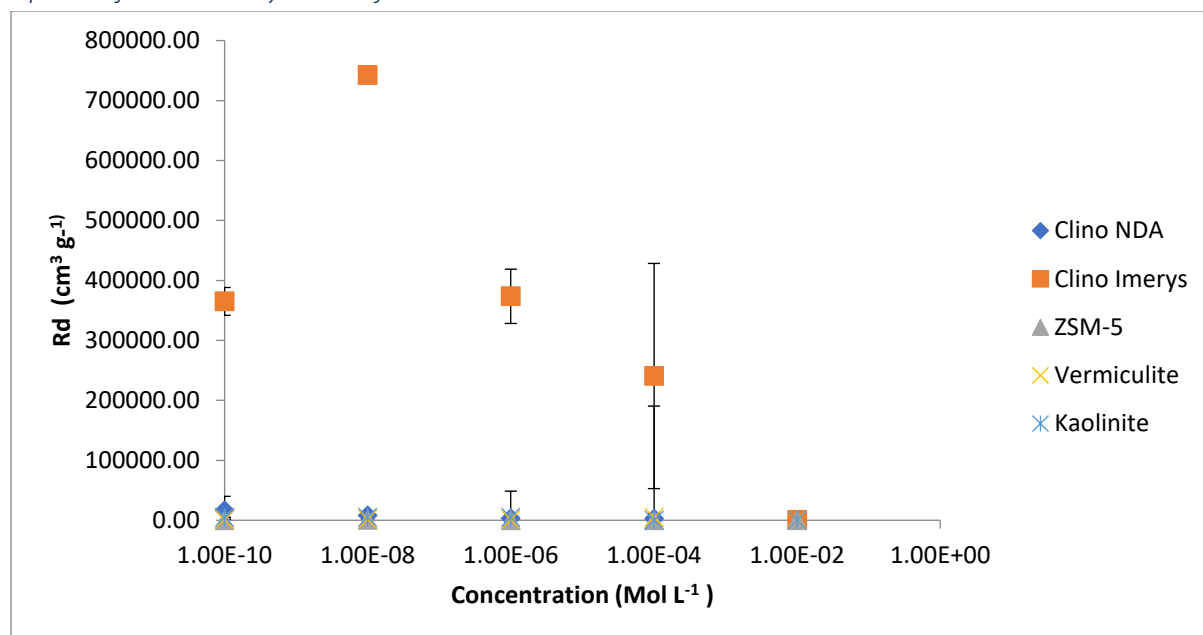
Material	Clinoptilolite (NDA)		Clinoptilolite (Imerys)		ZSM-5		Vermiculite		Kaolinite	
Concentration	Rd	Error (+/-)	Rd	Error (+/-)	Rd	Error (+/-)	Rd	Error (+/-)	Rd	Error (+/-)
1 x 10-2	304.7	17.8	223.6	6.2	170.5	20.3	1.0	78.3	1.0	198.4
1 x 10-4	2690.3	1204.4	240579.7	187765.0	166.2	9.0	4757.4	6255.3	1.0	245.9
1 x 10-6	3297.5	844.8	373463.2	45286.5	145.2	13.5	1133.2	34.8	4670.3	558.5
1 x 10-8	7838.8	5465.6	742271.4	1654.3	543.6	15.0	1378.6	123.1	4966.4	424.6
1 x 10-10	16733.6	9466.4	365026.1	23157.8	148.5	7.7	1211.3	73.2	4647.7	452.3

Uptake of strontium by APTES modified materials
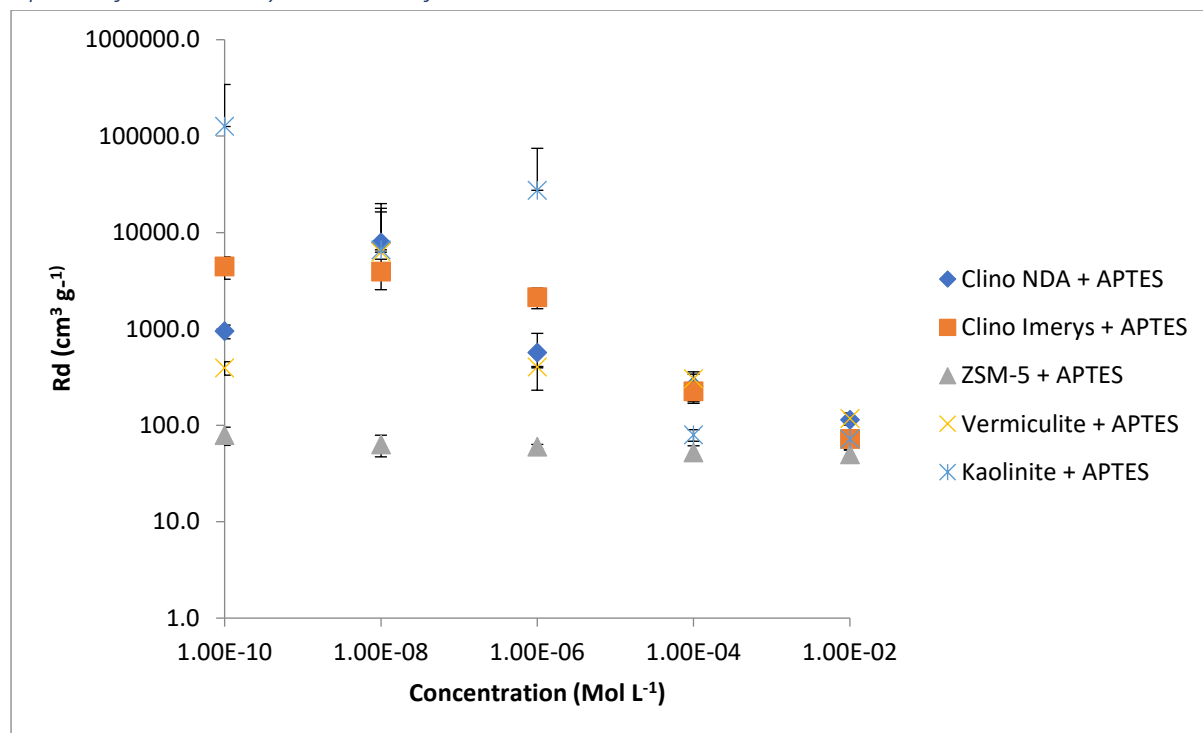
Material	Clinoptilolite (NDA)		Clinoptilolite (Imerys)		ZSM-5		Vermiculite		Kaolinite	
Concentration	Rd	Error (+/-)	Rd	Error (+/-)	Rd	Error (+/-)	Rd	Error (+/-)	Rd	Error (+/-)
1×10^{-2}	114.0	7.7	71.7	3.5	49.7	6.4	117.4	16.7	71.7	16.5
1×10^{-4}	254.2	85.3	224.8	49.2	52.0	9.2	303.0	55.4	79.2	10.8
1×10^{-6}	565.2	333.9	2135.2	515.4	60.0	3.4	400.9	6.7	27403.8	47307.6
1×10^{-8}	7849.0	12098.4	3917.5	1366.2	63.0	15.9	6256.3	175.4	6606.3	11219.6
1×10^{-10}	942.8	153.6	4432.1	1155.6	78.8	16.9	393.6	62.3	125754.1	217447.5

Uptake of strontium by TMSPE modified materials

Material	Clinoptilolite (NDA)		Clinoptilolite (Imerys)		ZSM-5		Vermiculite		Kaolinite	
Concentration	Rd	Error (+/-)	Rd	Error (+/-)	Rd	Error (+/-)	Rd	Error (+/-)	Rd	Error (+/-)
1 x 10-2	71.3	4.2	60.5	19.4	42.5	4.8	67.7	20.3	70.5	6.4
1 x 10-4	102.4	20.8	123.2	13.1	49.9	23.4	208.9	24.4	69.0	10.3
1 x 10-6	212.7	97.3	372.5	75.2	53.0	2.0	279.0	26.3	1610.4	2609.3
1 x 10-8	314.8	210.6	667.5	92.3	30.8	2.8	195.0	58.6	76.3	24.7
1 x 10-10	347.3	215.3	488.6	86.2	31.0	10.3	201.9	104.6	76.8	14.3

Uptake of strontium by TMSPETT modified materials
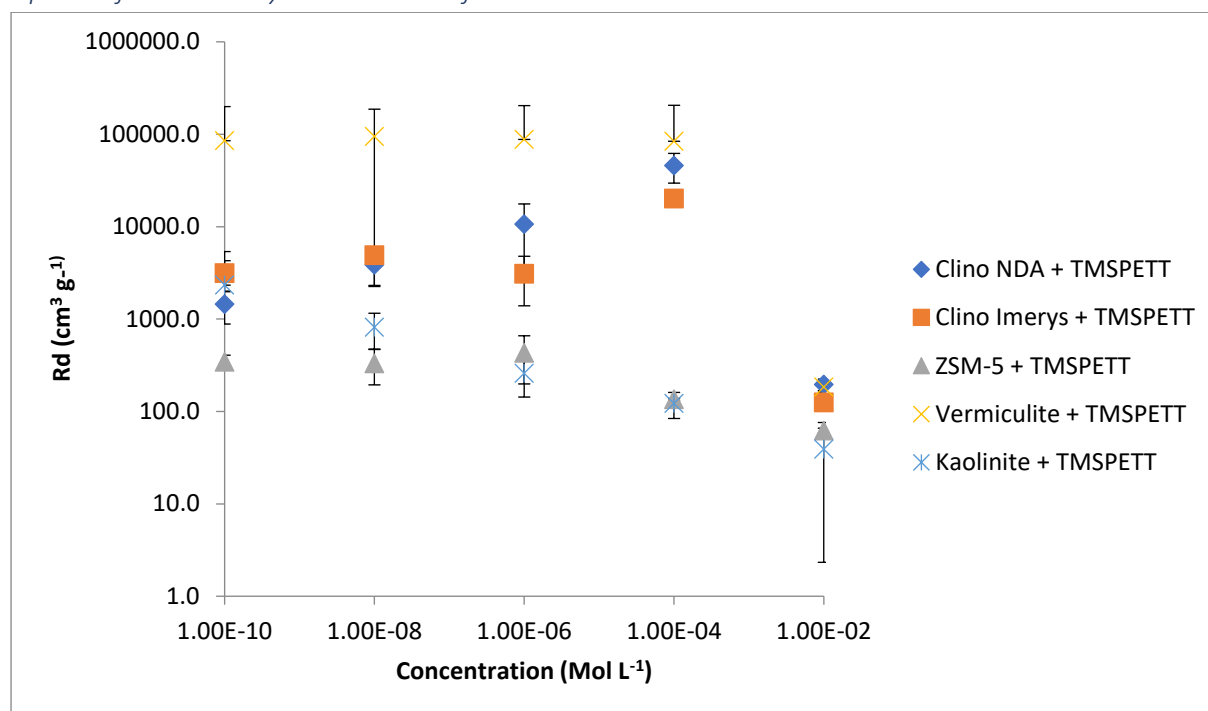
Material	Clinoptilolite (NDA)		Clinoptilolite (Imerys)		ZSM-5		Vermiculite		Kaolinite	
Concentration	Rd	Error (+/-)	Rd	Error (+/-)	Rd	Error (+/-)	Rd	Error (+/-)	Rd	Error (+/-)
1 x 10-2	196.0	28.0	125.3	22.4	62.1	3.9	183.0	21.2	39.1	36.8
1 x 10-4	45803.8	16214.4	20132.9	3223.2	135.2	3.2	84009.8	121742.3	122.2	38.3
1 x 10-6	10645.6	6937.0	3084.6	1694.6	428.5	230.2	87846.8	116226.8	257.8	114.5
1 x 10-8	3843.0	1532.1	4885.1	660.6	330.9	137.2	94575.8	92326.2	814.6	341.2
1 x 10-10	1444.8	561.7	3127.4	1153.4	343.2	63.0	85033.4	114180.7	2328.4	3045.6

Comparison of clinoptilolite (NDA) materials
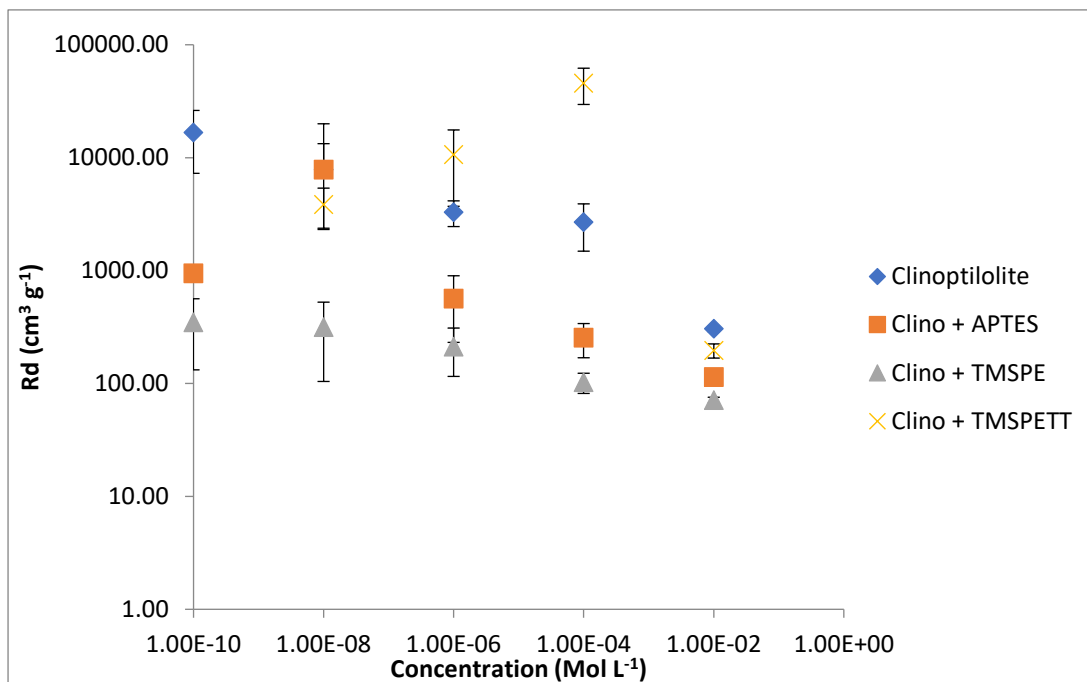
Comparison of clinoptilolite (Imerys) materials
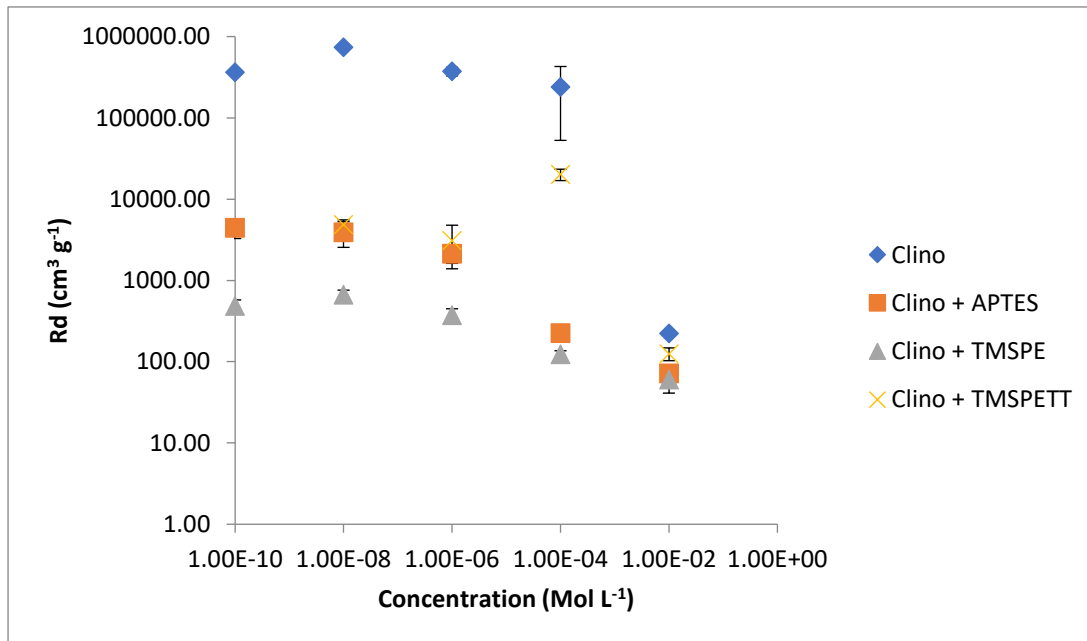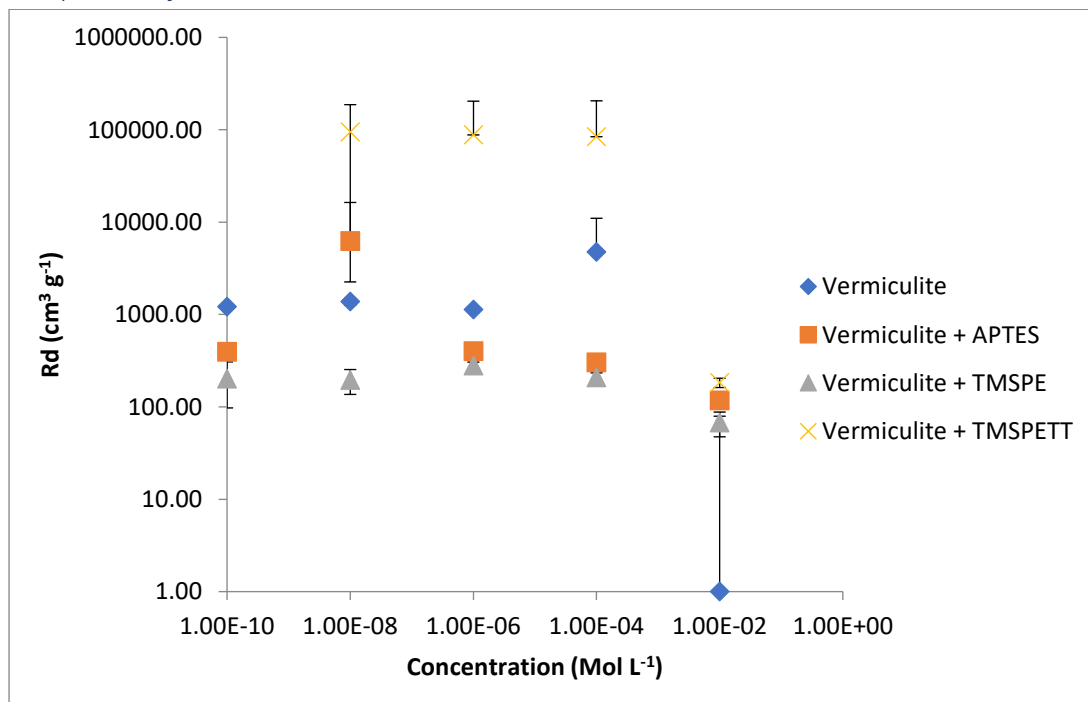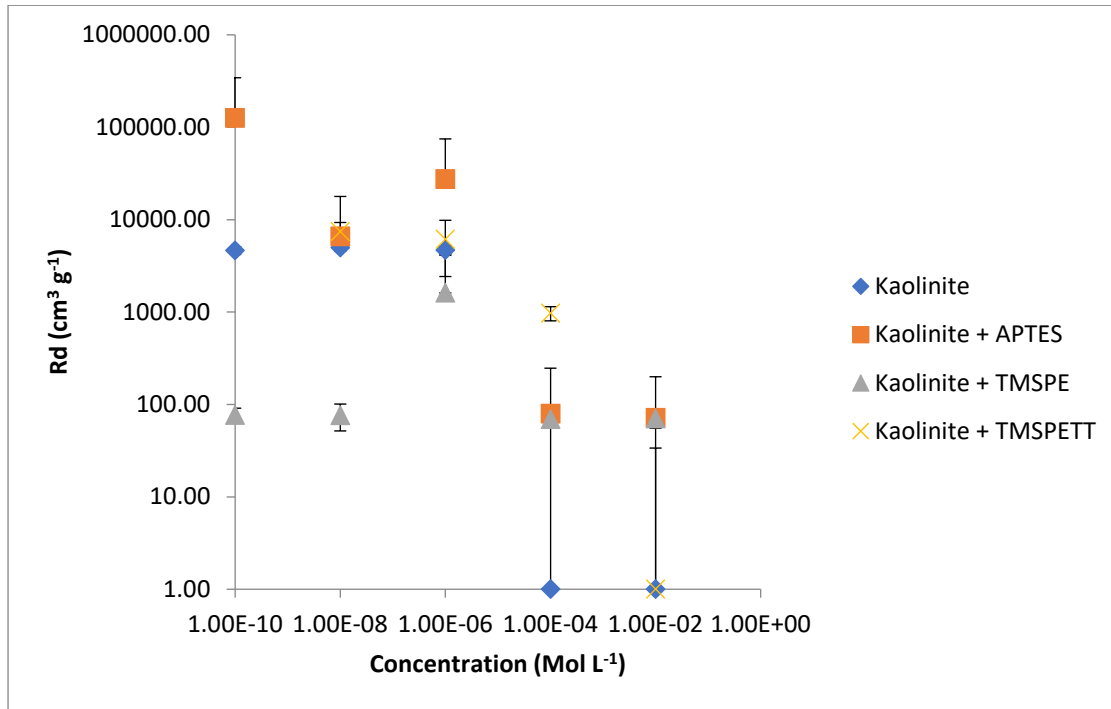
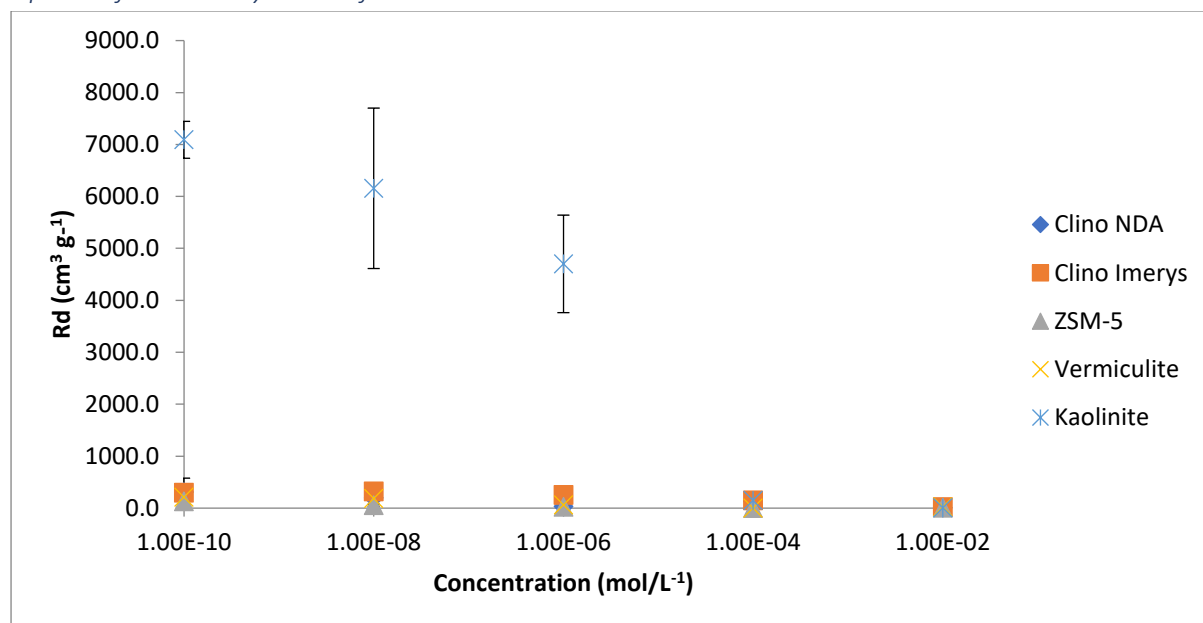*Comparison of ZSM-5 materials*
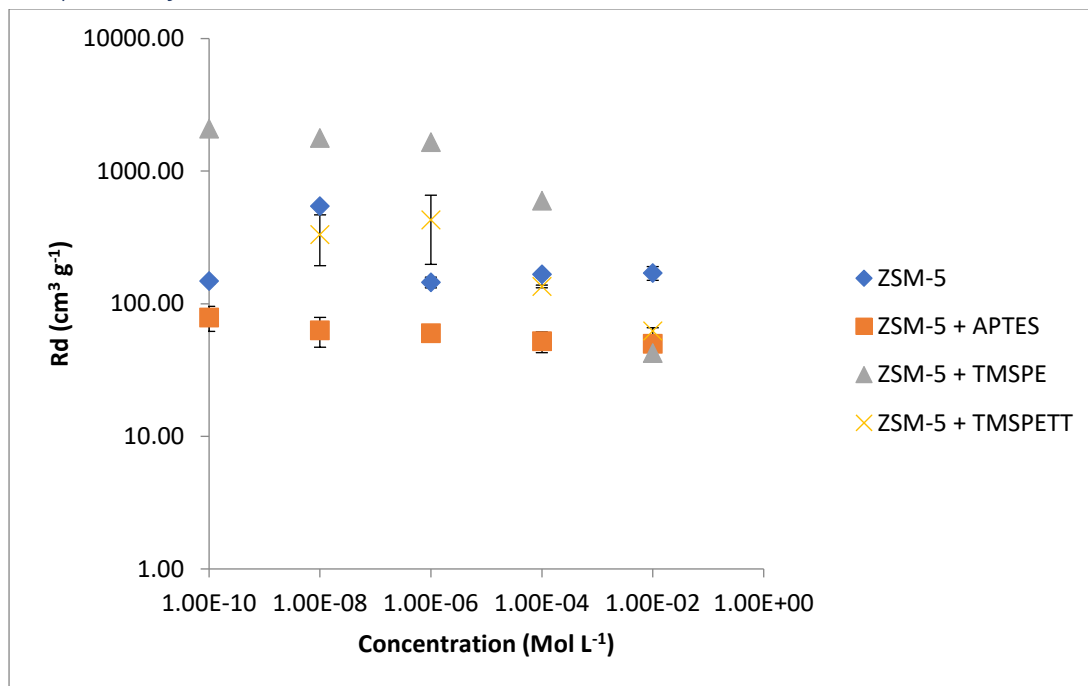
Comparison of vermiculite materials

*Comparison of kaolinite materials*

Uranium experimental results

*Batch sorption experimental results*

Uptake of uranium by unmodified materials

Material	Clinoptilolite (NDA)		Clinoptilolite (Imerys)		ZSM-5		Vermiculite		Kaolinite	
Concentration	Rd	Error (+/-)	Rd	Error (+/-)	Rd	Error (+/-)	Rd	Error (+/-)	Rd	Error (+/-)
1 x 10-2	4.5	26.1	15.7	14.2	6.3	4.9	24.1	10.4	8.5	8.8
1 x 10-4	127.0	63.5	147.5	13.1	0.0	9.7	0.0	14.5	147.6	7.7
1 x 10-6	31.8	12.6	250.1	53.7	24.6	24.4	61.7	33.9	4701.8	938.8
1 x 10-8	199.6	37.8	321.9	52.5	56.0	20.4	183.2	32.5	6156.5	1544.6
1 x 10-10	306.5	271.0	294.5	22.9	129.2	57.4	206.4	22.7	7089.7	355.3

Uptake of uranium by APTES modified materials
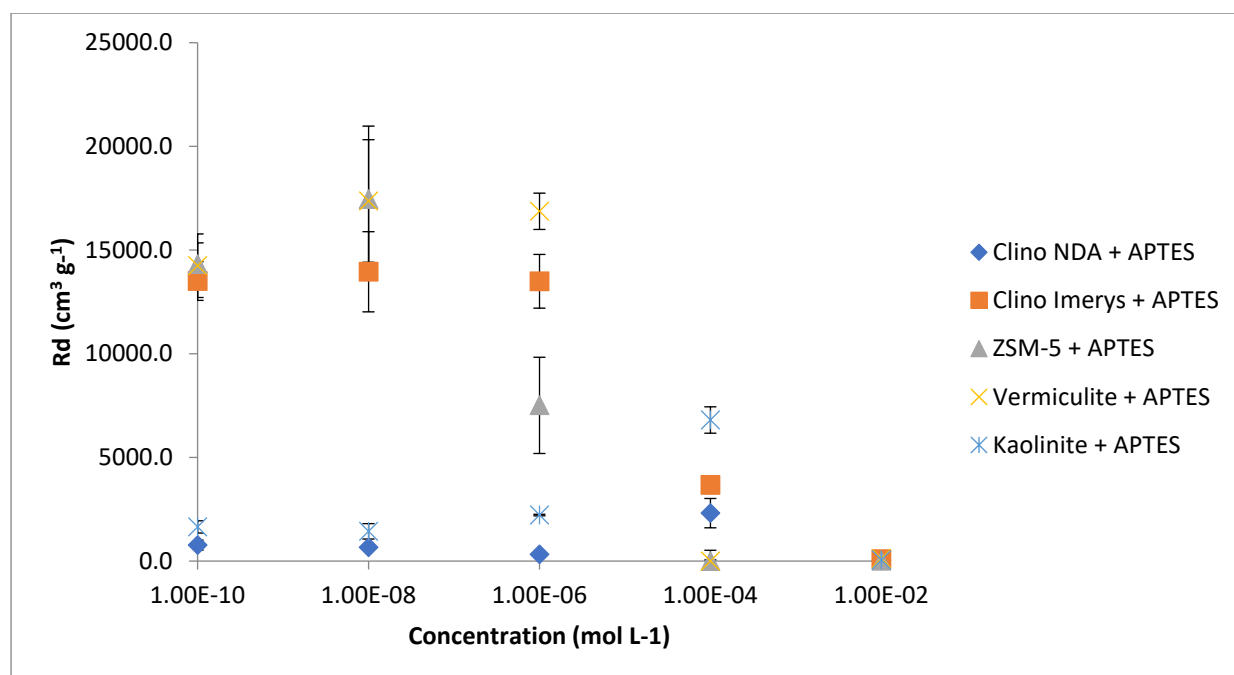
Material	Clinoptilolite (NDA)		Clinoptilolite (Imerys)		ZSM-5		Vermiculite		Kaolinite	
Concentration	Rd	Error (+/-)	Rd	Error (+/-)	Rd	Error (+/-)	Rd	Error (+/-)	Rd	Error (+/-)
1 x 10-2	19.4	15.7	92.7	9.8	13.5	11.5	115.5	42.2	53.9	36.8
1 x 10-4	2311.3	707.3	3675.6	414.2	0.0	55.2	3318.2	522.3	6803.2	635.8
1 x 10-6	326.3	103.6	13494.0	1295.6	7509.4	2320.8	16869.7	875.9	2218.6	38.4
1 x 10-8	653.8	56.5	13952.3	1933.5	17459.8	3519.6	17368.1	2954.1	1435.2	370.0
1 x 10-10	770.8	240.7	13505.1	932.5	14322.3	1022.7	14243.3	1530.9	1647.0	293.2

Uptake of uranium by TMSPE modified materials
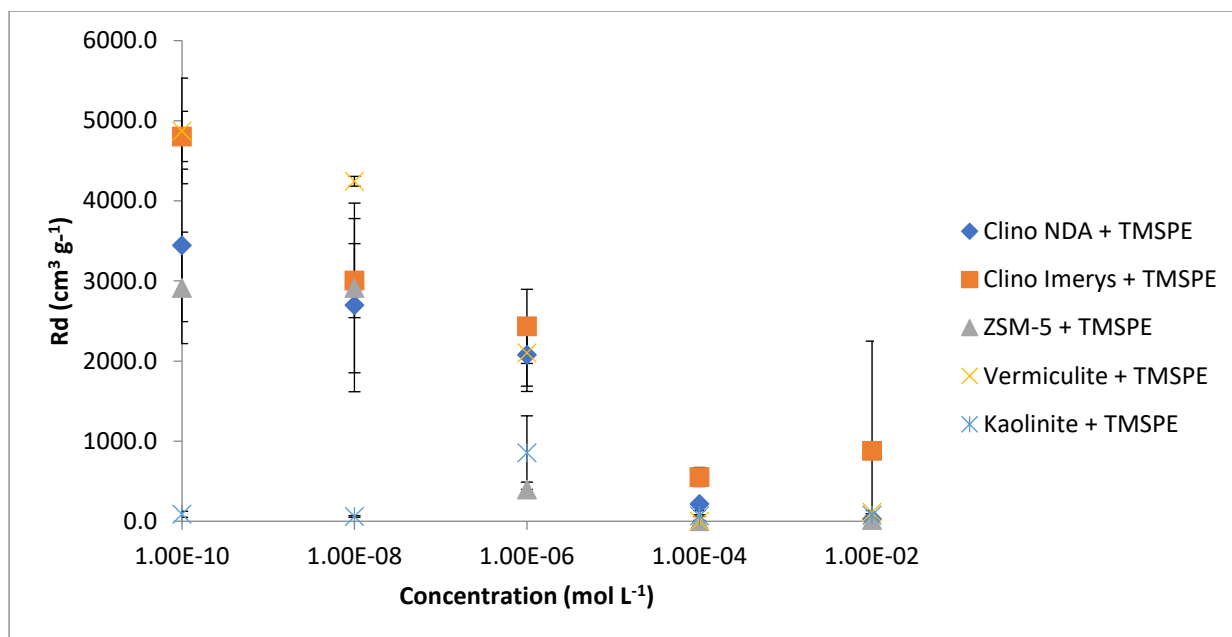
Material	Clinoptilolite (NDA)		Clinoptilolite (Imerys)		ZSM-5		Vermiculite		Kaolinite	
Concentration	Rd	Error (+/-)	Rd	Error (+/-)	Rd	Error (+/-)	Rd	Error (+/-)	Rd	Error (+/-)
1 x 10-2	28.5	20.2	879.0	1370.3	15.6	8.0	113.7	20.1	78.4	16.1
1 x 10-4	215.0	15.3	552.9	118.9	1.0	10.4	1.0	131.5	70.1	10.4
1 x 10-6	2080.1	459.4	2433.4	462.7	394.1	95.3	2102.6	415.5	856.8	459.3
1 x 10-8	2697.9	1081.0	3004.2	461.9	2913.1	1059.4	4245.0	60.9	60.6	10.3
1 x 10-10	3444.5	952.0	4804.5	313.5	2914.2	695.9	4873.2	659.6	87.5	37.4

Uptake of uranium by TMSPETT modified materials
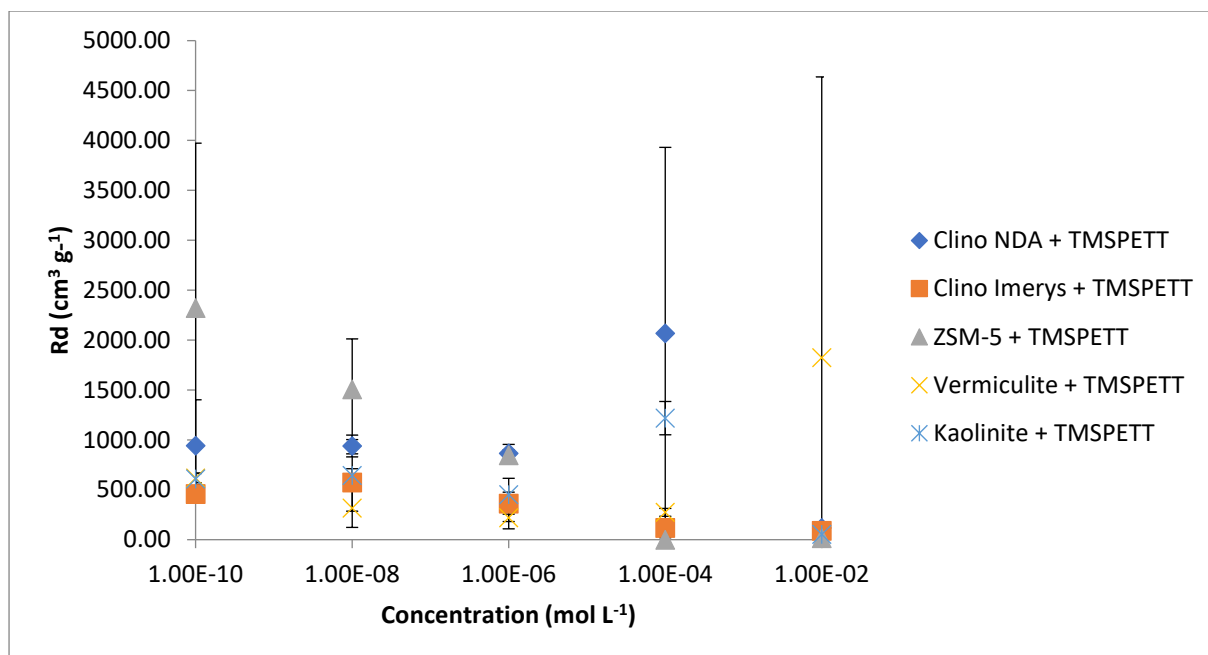
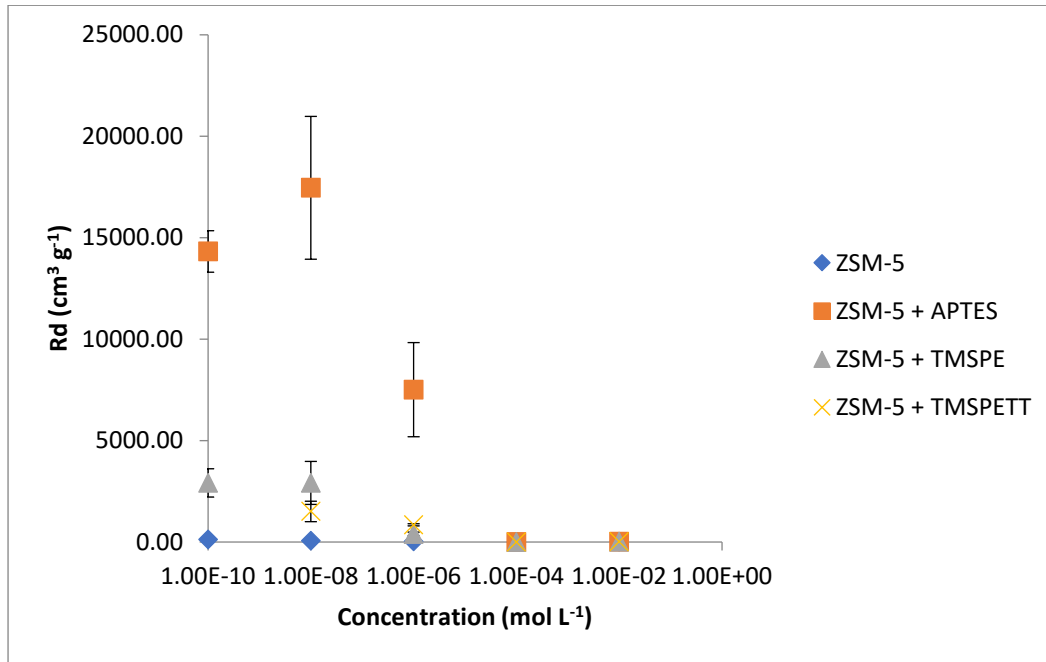| Material	Clinoptilolite (NDA)		Clinoptilolite (Imerys)		ZSM-5		Vermiculite		Kaolinite	
Concentration	Rd	Error (+/-)	Rd	Error (+/-)	Rd	Error (+/-)	Rd	Error (+/-)	Rd	Error (+/-)
1 x 10-2	116.8	4.6	87.0	28.0	14.0	20.3	1824.2	2812.2	51.7	15.3
1 x 10-4	2066.8	1864.7	116.2	27.6	0.0	19.4	274.0	39.2	1217.8	167.0
1 x 10-6	865.8	89.1	361.8	253.3	846.9	53.2	219.0	37.1	449.5	26.8
1 x 10-8	938.8	109.5	572.8	287.0	1507.2	504.1	317.0	193.9	642.5	68.6
1 x 10-10	942.4	459.3	456.9	70.3	2319.9	1653.1	616.7	45.8	609.6	57.2

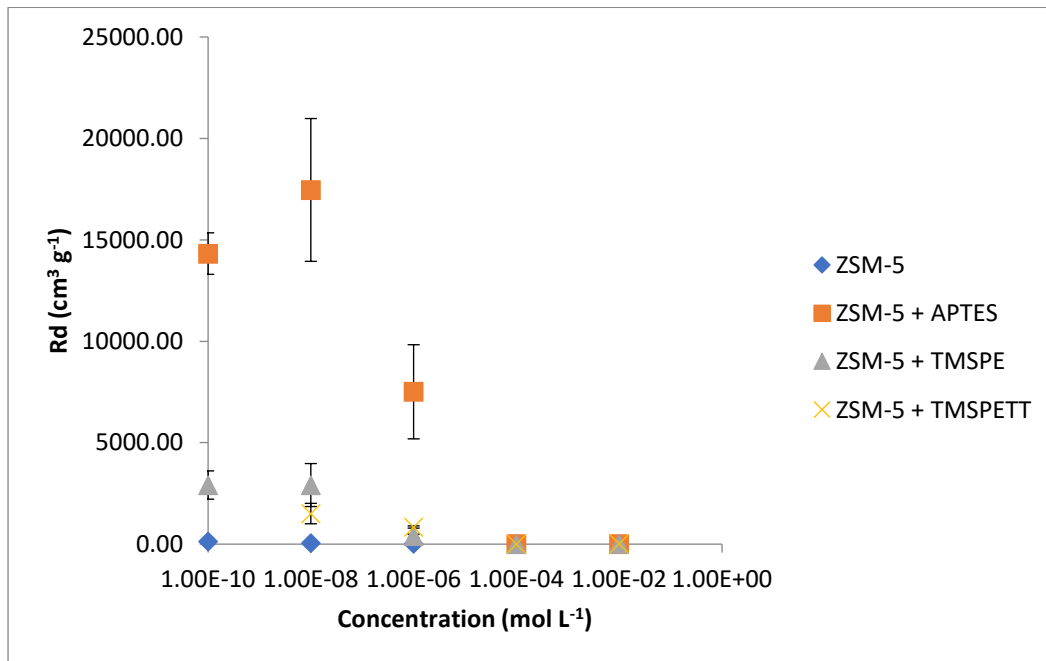## Comparison of clinoptilolite (NDA) materials

Comparison of clinoptilolite (Imerys) materials

Comparison of ZSM-5 materials

Comparison of vermiculite materials

Comparison of kaolinite materials